Trinity College Dublin
Coláiste na Tríonóide, Baile Átha Cliath
The University of Dublin

Quantum Thermodynamics with Nonequilibrium Steady States

PhD thesis

by

Artur Machado Lacerda

A document submitted in partial fulfillment of the requirements for the degree of

Doctor of Philosophy

at

Trinity College Dublin, the University of Dublin

2026

Abstract

This thesis investigates the thermodynamics of quantum systems far from equilibrium, with particular emphasis on nonequilibrium steady states (NESS). Its central contributions are twofold: a methodological development of the mesoscopic leads technique for modeling open quantum systems, and a geometric framework for understanding entropy production in slow transitions between NESS.

The first part of the thesis refines the mesoscopic leads approach, providing a consistent thermodynamic description within this formalism. By treating each lead as a finite quantum system weakly coupled to an external Markovian reservoir, the method enables a Markovian embedding of the extended system, even when the central system itself exhibits non-Markovian dynamics. Within this framework, we derive expressions for heat currents and entropy production, recovering the Landauer–Büttiker formula in the limit of large leads. As an application, the method is used to study thermal rectification in a periodically driven double quantum dot.

The second part focuses on entropy production in slow, quasistatic transitions between nonequilibrium steady states. Using the Hatano–Sasa decomposition, we separate the total entropy production into adiabatic and non-adiabatic contributions, where the latter quantifies deviations from instantaneous steady states. In the slow-driving limit, this non-adiabatic entropy production is shown to be governed by a Riemannian metric on the space of control parameters, allowing the use of geometric techniques to derive thermodynamic bounds.

In addition to these original results, the thesis offers pedagogical reviews of foundational topics in quantum thermodynamics, including a comprehensive introduction to Gaussian fermionic systems without pairing terms and a modern exposition of the Hatano–Sasa framework for both classical Markov chains and Lindblad master equations.

Declaration

I declare that this thesis has not been submitted as an exercise for a degree at this or any other university and it is entirely my own work.

I agree to deposit this thesis in the University's open access institutional repository or allow the library to do so on my behalf, subject to Irish Copyright Legislation and Trinity College Library conditions of use and acknowledgment.

Artur Machado Lacerda

February 27, 2026

List of Publications

The results discussed in this thesis appeared in the following publications:

1. A. M. Lacerda, A. Purkayastha, M. Kewming, G. T. Landi, and J. Goold. "Quantum thermodynamics with fast driving and strong coupling via the mesoscopic leads approach". *Physical Review B* 107:19, 2023. ISSN: 2469-9969. DOI: 10.1103/physrevb.107.195117. URL: http://dx.doi.org/10.1103/PhysRevB.107.195117.
2. A. M. Lacerda, M. J. Kewming, M. Brenes, C. Jackson, S. R. Clark, M. T. Mitchison, and J. Goold. "Entropy production in the mesoscopic-leads formulation of quantum thermodynamics". *Physical Review E* 110:1, 2024. ISSN: 2470-0053. DOI: 10.1103/physreve.110.014125. URL: http://dx.doi.org/10.1103/PhysRevE.110.014125.
3. S. L. Jacob, L. P. Bettmann, A. M. Lacerda, K. Zawadzki, S. R. Clark, J. Goold, and J. J. Mendoza-Arenas. "Dephasing-assisted transport in a tight-binding chain with a linear potential". *Frontiers in Physics* 12, 22, 2024. Publisher: Frontiers. ISSN: 2296-424X. DOI: 10.3389/fphy.2024.1474018. URL: https://www.frontiersin.org/journals/physics/articles/10.3389/fphy.2024.1474018/full.
4. A. M. Lacerda, L. P. Bettmann, and J. Goold. "Information geometry of transitions between quantum nonequilibrium steady states". *Physical Review E* 112:2, 2025. ISSN: 2470-0053. DOI: 10.1103/9f6l-d766. URL: http://dx.doi.org/10.1103/9f6l-d766.

The following work, although not discussed in this thesis, was completed and published during the course of the PhD:

1. S. L. Jacob, A. M. Lacerda, Y. Dubi, and J. Goold. "Thermodynamics of photoelectric devices". *Physical Review Research* 7:1, 2025. ISSN: 2643-1564. DOI: 10.1103/physrevresearch.7.013252. URL: http://dx.doi.org/10.1103/PhysRevResearch.7.013252.

Acknowledgements

First and foremost, I would like to express my gratitude to my supervisor, Professor John Goold, for his invaluable guidance, support and patience throughout my PhD. John has been incredibly supportive, and I would not have reached the end of this journey without him. His ability to quickly grasp the core of a problem and know the direction of a project will always be an inspiration. His mentorship has shaped not only the course of this research but also my growth as a researcher. John will continue to be a role model in my career as a Physicist.

I would like to thank Prof. Felix Binder and Prof. François Damanet for serving as examiners, for their careful reading of this thesis, and for their constructive and insightful comments.

I am profoundly grateful to my parents, Wilza and Joel, for their unwavering love and support over the years. Their belief in me made this journey possible. This thesis is dedicated to you. To my brothers, Tomás and Otávio: thank you for always being there. Your encouragement and good humor helped keep me grounded.

A heartfelt thanks to all my friends in QuSys and ToQCS. I'm lucky to have been surrounded by such a bright and supportive group of peers. Thank you for the stimulating discussions, the shared frustrations, and a few too many pints. To Oisín, Alessandro, Cecilia, Marlon, Krissia, Leonard, Mattia, Sindre, Nathan, Maria, Ivan, Samuel, Marco, Peter, Magdalini, Mark and Gabriel: thank you for being part of the journey.

A special thanks to my friend Laetitia, who read most of this thesis and made sure I did not drop a stitch.

To my dear friends Luisa, Magda, and Eoin, your friendship, understanding, and constant support meant more to me than words can say. You helped me through the hardest times and celebrated the best ones with me.

To all my friends in Brazil and across other time zones, thank you for the endless conversations, the late-night laughs, and the support that knows no distance. You are the secret tram that always pushes me uphill.

To my parents

Contents

1 Introduction 1
1.1 Structure of the Thesis . . . 8

I Theorical Background 11

2 Open quantum systems 13
2.1 Dynamical map . . . 14
2.2 Lindblad master equation . . . 16
2.2.1 Example: Single qubit coupled to a thermal bath . . . 17
2.3 Example: single qubit under pure dephasing . . . 18
2.4 Adjoint master equation . . . 19
2.5 Single fermionic mode . . . 20
2.6 Microscopic Derivations . . . 21
2.7 A note on fermions . . . 27
2.8 Example: microscopic derivation for a single fermionic mode . . . 28
2.9 Local vs global master equations: transport in a double quantum dot . . . 31
2.9.1 Local approach . . . 33
2.9.2 Global approach . . . 36

3 Quantum thermodynamics 41
3.1 Setup: microscopic description of open quantum systems . . . 42
3.2 First Law of Thermodynamics . . . 43
3.3 Second Law of Thermodynamics . . . 47
3.3.1 Classical Clausius inequality . . . 47
3.3.2 Von Neumann and relative entropies . . . 47
3.3.3 Validity of the Global Energy Approach . . . 51
3.4 Generalized Setup: Multiple Baths, Chemical Potential and Currents . . . 52
3.4.1 Second law . . . 53
3.4.2 Particle and energy currents . . . 54
3.5 Example: Entropy Production in a Single Fermionic Mode . . . 55
3.5.1 Finite-Size Bath Approximation . . . 56
3.5.2 Time evolution . . . 57
3.5.3 Currents and Entropy Production: Numerical Results . . . 58
3.5.4 Second law violation with the bare Hamiltonian approach . . . 60
3.6 Quantum Thermodynamics in the Markovian Regime . . . 61
3.6.1 Alicki's Framework: Energy Balance and the First Law . . . 62
3.6.2 Spohn's framework: Entropy Production and the Second Law . . . 64

3.6.3 Multiple Reservoirs . . . 67

II Gaussian Fermionic Systems 69

4 Gaussian fermionic systems 71
4.1 Quadratic Hamiltonians . . . 71
4.2 Diagonalization . . . 73
4.2.1 Canonical Transformations . . . 74
4.3 Gaussian states . . . 75
4.3.1 Diagonal Form of the Density Matrix . . . 76
4.3.2 Covariance Matrix in the Energy Basis . . . 77
4.3.3 Wick's Theorem . . . 78
4.3.4 Reduced and product states . . . 79
4.3.5 Von Neumann Entropy . . . 80
4.3.6 Covariance matrix of a thermal state . . . 81
4.4 Time evolution . . . 82
4.4.1 Unitary time evolution . . . 82
4.4.2 Quadratic Lindblad Master Equation . . . 83
4.4.3 The Lyapunov equation . . . 84
4.4.4 Efficient steady-state solution . . . 86
4.5 Spin-chains and the Jordan–Wigner transformation . . . 87
4.6 Dephasing noise . . . 91
4.7 Case study: dephasing enhanced transport in a tilted-lattice . . . 93
4.7.1 Dephasing-assisted Transport . . . 96
4.8 Quantum information with Gaussian states . . . 99
4.8.1 Relative entropy . . . 100
4.8.2 Rényi entropy . . . 100
4.8.3 Rényi relative entropy . . . 101
4.8.4 Fidelity . . . 102

III Mesoscopic Leads 105

5 The mesoscopic approach to quantum thermodynamics 107
5.1 The Target Problem: Fermionic System Coupled to Thermal Reservoirs . . . 109
5.2 The Mesoscopic Leads Approach . . . 111
5.2.1 Unitary description . . . 111
5.2.2 Markovian embedding . . . 114
5.2.3 Time Resolution . . . 116
5.3 Mesoscopic Leads and Reaction Coordinate Mapping . . . 118
5.3.1 The Reaction Coordinate Transformation . . . 118
5.3.2 Connection to the Mesoscopic Leads Approach . . . 124
5.3.3 Chain Mapping . . . 127

5.4 Thermodynamics in the Mesoscopic Leads Approach . . . 129
5.4.1 Steady-State Currents . . . 130
5.4.2 Internal Currents . . . 132
5.5 Mesoscopic Leads with Non-Interacting Systems . . . 135
5.5.1 Single-Particle Hamiltonian . . . 135
5.5.2 Covariance Matrix . . . 136
5.5.3 Dynamics: Lyapunov Equation . . . 138
5.5.4 Floquet Solution of the Periodically-Driven Lyapunov Equation . . . 139
5.6 Example: Thermodynamics of a Driven Resonant-Level . . . 141
5.6.1 Model and Implementation . . . 141
5.6.2 Entropy production . . . 142
5.6.3 High-Temperature Limit . . . 143
5.7 Case Study: Rectification in a Driven Double Dot . . . 144

6 Entropy production in the mesoscopic-leads formalism 149
6.1 Entropy production in Markovian systems . . . 150
6.2 Model and Setup . . . 150
6.3 Thermalization of the extended system steady state . . . 152
6.3.1 Non-interacting systems ($U = 0$) . . . 152
6.3.2 Interacting systems ($U \neq 0$) . . . 153
6.4 Entropy production . . . 155
6.4.1 Entropic discrepancy with a single bath . . . 157
6.4.2 Entropic differences with multiple baths . . . 159

IV Information Geometry 163

7 Information Geometry in Thermodynamics 165
7.1 Classical Fisher Information . . . 166
7.1.1 Single Parameter Case . . . 166
7.1.2 Classical Fisher Information from the Relative Entropy . . . 167
7.1.3 Multiparameter Generalization . . . 169
7.2 Quantum Fisher Information . . . 169
7.3 Quantum Fisher Information from Relative Entropy . . . 173
7.3.1 Multiparameter Generalization . . . 174
7.4 Historical Development of Thermodynamic Geometry . . . 174
7.4.1 Weinhold: Geometric Structure from Thermodynamic Potentials (1975) 174
7.4.2 Ruppeiner: Metric from Fluctuation Theory (1979) . . . 175
7.4.3 Salamon and Berry: Thermodynamic Length (1983) . . . 176
7.4.4 Crooks: Thermodynamic Divergence and Information Geometry (2007) 176
7.4.5 Scandi and Perarnau-Llobet: Thermodynamic Length in Open Quantum Systems (2019) . . . 178
7.4.6 Summary . . . 179

8 Entropy production in nonequilibrium steady states 181
8.1 Entropy Production in Classical Markovian Systems . . . 182
8.1.1 Local vs. Global Detailed Balance . . . 183
8.1.2 Schnakenberg Entropy Production . . . 185
8.1.3 Time-Dependent Driving and the Adiabatic/Nonadiabatic Decomposition . . . 188
8.1.4 The Nonequilibrium Potential and the Housekeeping/Excess Decomposition . . . 191
8.1.5 Trajectory-Level Description of Markov Dynamics . . . 194
8.1.6 Trajectory-Level Entropy Production . . . 195
8.1.7 Trajectory-Level Adiabatic and Nonadiabatic Contributions . . . 197
8.2 Three Fluctuation Theorems: the Dual and Dual-Reversed Processes . . . 198
8.3 Entropy Production in Time-Dependent Lindblad Dynamics . . . 202
8.3.1 Entropy Production and Entropy Flux . . . 203
8.3.2 Ensemble-Level Adiabatic/nonadiabatic Splitting . . . 204
8.3.3 Ensemble-Level Housekeeping/Excess Decomposition . . . 205
8.3.4 Quantum Trajectories and Jump Unraveling . . . 207
8.3.5 Trajectory-Level Entropy Production . . . 209
8.3.6 The Dual Dynamics . . . 213
8.3.7 Dual and Dual-Reverse Processes . . . 215
8.3.8 Fluctuation Theorems for the Adiabatic and nonadiabatic Components 217

9 Information geometry of transitions between quantum nonequilibrium steady states 221
9.1 Housekeeping/excess decomposition . . . 222
9.2 Geometry of Slow NESS-to-NESS Transitions . . . 223
9.2.1 Protocol . . . 223
9.2.2 Slow-driving Expansion . . . 225
9.2.3 Quasistatic Limit . . . 227
9.2.4 Geometric Structure and the Friction Tensor . . . 229
9.3 Positivity of the friction tensor . . . 230
9.3.1 Green-Kubo Relations and the Quantum Fisher Information . . . 232
9.3.2 Optimization: Geodesics in Parameter Space . . . 234
9.4 Example: Three-Level Maser . . . 236
9.5 Beyond Slow Driving: Arbitrary-Speed Transitions . . . 238

10 Conclusion 241

Appendix 245
A.1 Time Derivative of the von Neumann . . . 247
A.2 Vectorization . . . 247
A.3 Trace-Determinant Identities for Fermionic Quadratic Forms . . . 248
A.3.1 Basic Trace-Determinant Formula . . . 249
A.3.2 Generalized Trace-Determinant Formula . . . 249

A.4 Action of the Inverse Kubo–Mori Operator on the Steady State 250
A.5 Superfermion formalism and TDVP implementation 251
A.5.1 Superfermion formalism 251
A.5.2 Vectorized Liouvillian and TDVP thermal-state preparation 253
A.6 Uncertainty estimate for the variability 254

Bibliography 257

1 Introduction

The foundations of thermodynamics were established with a primary focus on systems in *equilibrium* and *quasistatic* processes. The pioneering work of Carnot, Clausius and Kelvin, centered on idealized cyclic engine protocols involving transformations between well-defined equilibrium states [1, 2, 3]. Central to this framework was the second law of thermodynamics, formalized via the Clausius inequality,

$$\Delta S \geq \int \frac{\delta Q}{T}, \tag{1.1}$$

which states that the total change in entropy ΔS of a system is greater than or equal to the reversible heat exchange, with equality holding only for reversible processes. While the second law imposes fundamental constraints on all thermodynamic processes—including those that pass through nonequilibrium states, the dominant theoretical focus at the time—shaped by the technological demands of the industrial era—remained on *stroke-based* thermodynamic cycles operating between equilibrium states.

The emergence of statistical mechanics, particularly through the work of Boltzmann, offered a complete microscopic understanding of equilibrium thermodynamics. The *H-theorem* offered a statistical interpretation of the second law, providing a bridge between macroscopic irreversibility and an underlying microscopic dynamics [4, 5]. Yet even within this framework, nonequilibrium states appeared only as *transient stages*—intermediate steps in processes connecting equilibrium points.

In contrast, a *nonequilibrium steady state* (NESS) represents a fundamentally different regime: one in which macroscopic observables remain stationary over time, despite ongoing dissipation and exchange with the environment. A canonical example is a system connected to two heat baths at different temperatures. For instance, a metal rod in thermal contact with a hot and a cold bath will, after sufficient time, exhibit a stable temperature profile—indicative of stationarity—yet will sustain a nonzero heat current, reflecting its nonequilibrium nature.

Such systems are characterized by persistent *entropy production*. This can be made explicit by rearranging the Clausius inequality to define the *entropy production* Σ as the discrepancy between the total entropy change and the entropy flow due to heat exchange:

$$\Sigma = \Delta S - \int \frac{\delta Q}{T} \geq 0. \tag{1.2}$$

In a NESS, while the system's state remains unchanged in time ($\Delta S = 0$), entropy is continuously produced due to maintained fluxes. This is quantified by the *entropy production rate*,

$$\sigma = \frac{\mathrm{d}\Sigma}{\mathrm{d}t} > 0, \tag{1.3}$$

which remains strictly positive in steady-state conditions. Persistent entropy production is thus a hallmark of NESS, distinguishing them from equilibrium configurations.

A major milestone in the theoretical understanding of nonequilibrium phenomena was the development of *linear response theory*, particularly through the work of Lars Onsager in the 1930s. Onsager's reciprocity relations formalized the behavior of systems near equilibrium, describing how small perturbations give rise to proportional responses [6, 7]. But it was Ilya Prigogine, in the mid-20th century, who pushed thermodynamics beyond linearity. His work on *dissipative structures* and *far-from-equilibrium systems* laid the groundwork for describing self-organization in systems subject to continuous driving [8, 9, 10].

Not coincidentally, Prigogine had a background in chemistry, for which he was awarded the Nobel Prize in 1977. Chemical reaction networks served as prototypical examples demonstrating how far-from-equilibrium systems can exhibit complex and self-organized behavior. Canonical models such as the *Brusselator*—a chemical *oscillator* developed in the Free University of *Brussels*—exemplify how chemical systems can give rise to NESS with structured dynamics [11].

This connection between thermodynamics and chemical networks has since inspired a wide range of interdisciplinary applications. In biology, for example, cellular processes such as ATP synthesis and ion transport operate in NESS, sustaining order through continuous dissipation [12, 13]. In chemistry, autocatalytic cycles and oscillatory reactions, such as the Belousov–Zhabotinsky reaction, illustrate robust far-from-equilibrium behavior [14]. In engineering, continuously operating thermal devices—unlike traditional cyclic engines—are designed to function in NESS, with sustained fluxes of heat or particles [15].

As noted by Schrödinger in his seminal book *What is Life?*, based on a series of public lectures given at Trinity College Dublin, "it is by avoiding the rapid decay into the inert state of 'equilibrium' that an organism appears so enigmatic; [...] it feeds on negative entropy" [16]. This metaphor captures the essential insight that living systems must operate in nonequilibrium steady states. In nature, equilibrium is the exception, not the rule.

As attention turned to microscopic and mesoscopic systems, the need for a thermodynamic theory incorporating fluctuations became increasingly apparent. This led to the development of *stochastic thermodynamics* [17], a framework in which thermodynamic quantities—such as work, heat, and entropy production—are defined at the level of individual stochastic trajectories. Central to this theory are the *fluctuation theorems* [18, 19, 20, 21], which quantify the statistical weight of entropy-reducing events and extend the second law beyond its traditional, macroscopic limits. Stochastic thermodynamics has become a foundational tool in describing systems where noise and fluctuations are essential—such as molecular motors, colloidal particles, and other microscale systems operating far from equilibrium.

The late 20^{th} and early 21^{st} centuries brought new challenges—and opportunities—with miniaturization of technology. As devices have scaled down to the nanoscale and coherence times have increased, the need for a quantum formulation of thermodynamic principles has become increasingly pressing. These developments gave rise to *quantum thermodynamics*—a field that seeks to generalize thermodynamic laws and concepts to the quantum regime [22, 23, 24, 25].

This thesis presents a set of theoretical tools and results that advance our understanding of thermodynamics in quantum systems far from equilibrium, with a focus on *nonequilibrium steady states*, *entropy production*, and *quantum transport*.

The contributions of this thesis are in two fronts: methodological and theoretical. From a methodological perspective, we formulate a thermodynamic framework for open quantum systems coupled to *mesoscopic leads*, enabling a consistent description of energy exchange and entropy production under time-dependent driving. From a conceptual perspective, we analyze *transitions between NESS* using tools from information geometry.

Beyond Markovianity: The Mesoscopic Leads Framework

The natural setting for quantum thermodynamics is the theory of open quantum systems, which deals with quantum systems interacting with external environments. One of the pillars of this theory is the Gorini–Kossakowski–Sudarshan–Lindblad (GKSL) master equation [26, 27], often referred to simply as the *Lindblad equation*. This equation describes the effective dynamics of a system that is weakly coupled to an environment, along with other suitable conditions, and characterizes the most general form of Markovian quantum dynamics that is completely positive and trace-preserving (CPTP).

The Lindblad formalism offers substantial advantages for both analytical and numerical treatments. From a computational perspective, the Markovian and time-local structure of the equation facilitates scalable simulations. In particular, the quantum trajectories or *quantum jump* method enables efficient stochastic unravelings of the dynamics, substantially reducing memory requirements compared to full density matrix evolution [28, 29].

From a theoretical point of view, the Lindblad framework has been the subject of extensive mathematical and physical investigation, resulting in a vast library of results. In particular, entropy production in Markovian systems—especially those with a thermal steady state—is well understood through Spohn's framework [30].

The Lindblad equation has found widespread application across many different fields, both phenomenologically or grounded in a microscopic derivation. It has been successfully used to describe many experimental setups, particularly in quantum optics [31, 32]. However, despite its success, the Lindblad paradigm has important limitations. The Markovian approximation that underlies most derivations of the Lindblad equation amounts to neglecting memory effects and assuming a clear separation of time scales between the system dynamics and the decay of bath correlations. In many textbook treatments this is justified by assuming that the environmental spectral density is smooth on the scale of the system's transition frequencies, so that bath correlation functions decay rapidly in time [31, 33, 34]. Crucially, however, a flat (or nearly flat) spectral density is neither necessary nor sufficient for Markovianity: structured environments can still give rise to effectively memoryless dynamics on appropriate time scales, and conversely, deviations from the weak-coupling or secular approximations may lead to non-Markovian behaviour even for relatively featureless spectra [33, 34]. What ultimately characterizes Markovianity is therefore a property of the dynamical map (e.g. semigroup or divisibility properties), not of the spectral density alone.

At this point it is useful to clarify the terminology that will be used throughout this thesis. In the mathematical theory of open quantum systems, a prototypical notion of *quantum*

Markovian dynamics is provided by *quantum dynamical semigroups*, whose generators have the Lindblad form [26, 27]. More generally, modern discussions of quantum (non-)Markovianity emphasise properties such as complete-positive divisibility of the dynamical map or the absence of information backflow, which allow for time-local master equations with time-dependent (but still Lindblad-like) generators that need not form a strict semigroup [33]. Different, partly inequivalent, definitions of quantum Markovianity coexist in the literature; see, for example, Refs. [35, 34, 36] for detailed discussions.

In this thesis, unless explicitly stated otherwise, we will adopt the common but somewhat narrower convention of using the term *Markovian dynamics* synonymously with dynamics generated by a time-homogeneous Lindblad master equation, i.e. by a completely positive, trace-preserving quantum dynamical semigroup. When we wish to refer to more general notions of Markovianity (such as CP-divisible time-local evolutions) we will state this explicitly. Likewise, when we speak of *non-Markovian* dynamics we will simply mean dynamics that cannot be described within this semigroup / Lindblad framework.

A promising strategy to overcome these challenges is the *mesoscopic leads approach*. This method replaces the infinite-dimensional macroscopic bath with a finite subsystem—the *lead*—which is itself weakly coupled to an idealized thermal reservoir. The resulting composite system evolves according to a Lindblad master equation, effectively restoring a Markovian description. This is an example of a *Markovian embedding*: the system of interest is enlarged to include part of the environment, and the composite dynamics is Markovian.

The concept of substituting the environment with a damped finite subsystem dates back to seminal work by İmamoğlu in the 1990s [37, 38], initially devised to extend quantum jump methods—which was then a promising new technique—to non-Markovian systems. Around the same time, the idea was further extended by the works of Garraway, under the name of *pseudomodes* [39, 40].

The central idea underpinning mesoscopic leads is to approximate the environmental *spectral density*—a crucial function characterizing environment-system interactions—with a finite sum of Lorentzians:

$$\mathcal{J}(\omega) \approx \sum_{i=1}^{L} c_i L_i(\omega), \quad \text{where} \quad L_i(\omega) = \frac{\Delta_i^2}{(\omega - \epsilon_i)^2 + \Delta_i^2}. \tag{1.4}$$

If the spectral density is well approximated, the original dynamics is also recovered.

While this can be seen as a mathematical construction, the mesoscopic leads formulation bears close resemblance to actual experimental setups, particularly in mesoscopic transport scenarios [41], such as molecular junctions [42].

Moreover, recent experiments have demonstrated the ability to directly implement the setup. A compelling illustration is provided by a recent trapped-ion quantum simulation of spin-boson models with structured baths [43]. As summarized in Fig. 1.1, the experiment uses a chain of seven $^{171}Yb^{+}$ ions, where a central spin qubit is coupled to selected motional modes that serve as a controllable bosonic environment. By applying laser-induced amplitude and phase noise to these modes, the environment's spectral density can be finely tuned, approximating complex target functions through a sum of damped Lorentzian components.

The ability to experimentally realize such environments with programmable structure underscores the need for thermodynamic tools that remain valid beyond idealized reservoirs—precisely the setting addressed in this thesis.

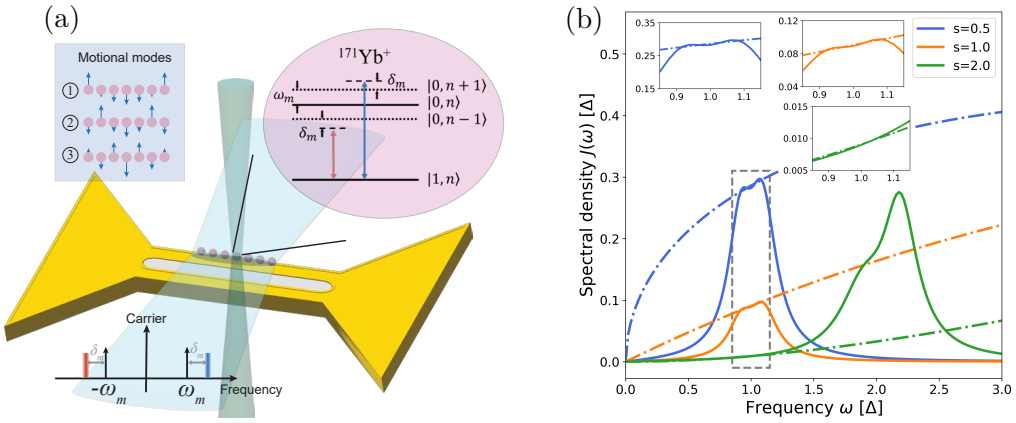

Figure 1.1: **Quantum simulation of a spin-boson model with structured bath.** (a) Schematic of the experimental setup: a chain of seven $^{171}Yb^+$ ions in a linear Paul trap, where a single ion encodes the spin qubit and selected motional modes serve as the bosonic bath. The spectral properties of the environment are engineered via laser-induced amplitude and phase noise, allowing programmable damping and coupling. (b) Engineered spectral densities for the spin–boson setup. Solid lines show the spectral densities realized using only two bath modes. For each curve, the mode parameters are chosen so that the resulting spectral density approximates, within the relevant frequency window indicated by the grey rectangle, a Leggett spectral density $\mathcal{J}_{\text{Legg}}(\omega) = A\omega^s\omega_c^{1-s}e^{-\omega/\omega_c}$ in one of three regimes: sub-Ohmic ($s = 0.5$), Ohmic ($s = 1.0$), and super-Ohmic ($s = 2.0$). The corresponding target densities are indicated by dot–dashed lines. The insets show a magnified view inside the relevant window. Adapted from Ref. [43].

Thus, the mesoscopic leads framework emerges as a versatile methodology for analyzing quantum systems strongly coupled to structured environments. This naturally raises the question of how quantum thermodynamics can be studied within the approach.

Previous work [44] has presented a detailed thermodynamic analysis in steady-state regimes, alongside an exploration of implementations for interacting systems using tensor-network methods.

A key methodological advancement of this thesis lies in extending this thermodynamic analysis to time-dependent scenarios, with arbitrarily fast driving. This work, presented in [45], establishes a consistent and rigorous quantum thermodynamic framework for strongly coupled driven systems within the mesoscopic leads formalism. The analysis includes a rigorous derivation of energy flows, entropy balances, and the identification of thermodynamically consistent definitions of work and heat within the mesoscopic leads framework.

This thesis also provides a pedagogically structured introduction to the mesoscopic leads method, with a particular focus on its thermodynamic foundations, along with practical implementation details for non-interacting systems. In addition, it provides a formal justification of the technique via the reaction coordinate mapping. While this connection is acknowledged in the literature, the derivation is presented here in full detail and with pedagogical clarity.

An important feature of the mesoscopic leads approach is that it opens access to the rich toolbox of Markovian quantum theory. Notably, it enables the use of the quantum jump

method for memory-efficient numerical simulation, which was originally one of the main motivations for the framework [37, 46]. Importantly, however, these tools only apply directly to the *extended* system, comprising both system and lead. For example, applying Spohn's results for entropy production [30] to make predictions about the central system requires careful interpretation.

Another central contribution of this thesis, detailed in Ref. [47], is to establish how Spohn's framework can be consistently adapted to the mesoscopic leads setting. We provide a detailed comparison between the entropy production in the extended and central systems, interpreting each term from an information-theoretical perspective. This result offers valuable insights into the challenging problem of characterizing entropy production under strong coupling and non-Markovianity [34, 48].

Finally, the thesis introduces a detailed and practical prescription for implementing the mesoscopic leads method in non-interacting systems using the formalism of fermionic Gaussian states. A comprehensive and pedagogically guided introduction to these systems is provided, with particular emphasis on their role in efficient numerical simulations.

In summary, this thesis provides a detailed and rigorous thermodynamic exploration of the mesoscopic leads approach, demonstrating its utility as a flexible platform for quantum thermodynamics under strong coupling and fast driving.

Having outlined the methodological contributions, we now turn to the theoretical results concerning transitions between nonequilibrium steady states.

Transitions between NESS

The thermodynamics of nonequilibrium processes, particularly in quantum systems, remains one of the most intriguing and actively investigated frontiers in statistical physics. Among the most striking phenomena in this domain are *dissipative phase transitions* [49], characterized by the closing of the Liouvillian gap and abrupt qualitative changes in the steady state. Such transitions are fundamentally distinct from equilibrium or zero-temperature quantum phase transitions, where the energy gap of the Hamiltonian itself closes.

A paradigmatic example is the *open Dicke model* [50, 51, 52], in which a large ensemble of atoms interacts with a single mode of an optical cavity. As the atom-light coupling strength is tuned, the system transitions from a normal phase, with negligible photon occupation, to a superradiant phase, where the cavity population becomes extensive.

Brunelli *et al.* (2018) demonstrated that the irreversible entropy production diverges as the critical point is approached [53]. Their experiment, which combined optomechanical systems with ultracold atoms in a cavity QED setup, employed full state tomography to dynamically monitor entropy production, revealing its singular behavior at criticality (see Fig. 1.2).

This experiment suggests that dissipative phase transitions exhibit a distinct thermodynamic signature, which initially motivated our investigation.

While compelling, this question also revealed that a general understanding of the thermodynamics of transitions between quantum NESS, irrespective of criticality, is still absent. In particular, the divergence of the irreversible entropy production in Ref. [53] signals a breakdown of adiabaticity near the critical point, where the system fails to track the instantaneous

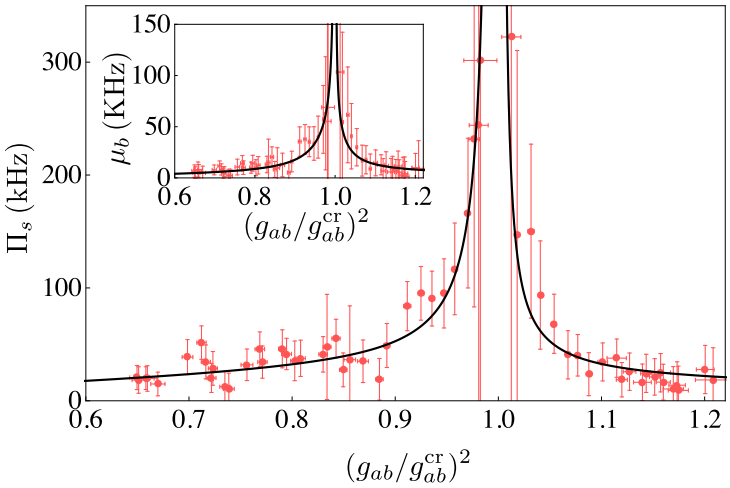

Figure 1.2: **Irreversible entropy production near the critical point in the Dicke model.** Experimental measurement of the irreversible entropy production rate Π_s in a two-mode cavity–BEC setup, as a function of the coupling strength between the modes. The system realizes a Dicke model in an open quantum setting, and the entropy production is seen to diverge as the critical point is approached, highlighting its role as a dynamical indicator of criticality. Inset: contribution μ_b from the atomic (BEC) subsystem. Adapted from Ref. [53].

steady state and becomes dynamically "frozen". This led us to consider the important question: *What is the thermodynamic cost of slow transitions between nonequilibrium steady states?*

Addressing this broader question naturally invokes the powerful framework of *thermodynamic length*, originally introduced within classical equilibrium thermodynamics. Crooks (2007) established that entropy production during slow transitions between thermal states in classical systems can be interpreted geometrically through a metric defined on parameter space [54]. This geometric perspective enables the use of geometric tools to obtain bounds of thermodynamic quantities. Subsequently, Sivak and Crooks (2012) explicitly connected this metric to dissipative work, demonstrating that minimal dissipation can be achieved by following geodesic paths in parameter space [55].

This idea was extended to classical nonequilibrium steady states by Jarzynski and Mandal [56]. They considered a slow protocol between two NESS of a classical continuous-time Markov chain. However, a slow transition between NESS is fundamentally different than that between thermal states.

In a quasistatic transition between equilibrium states, in which the state remains arbitrarily close to a thermal state, the entropy production is zero at all times. In contrast, even in a quasistatic transition between NESS, there is a non-zero entropy production at each point in time, due to baseline steady-state currents. For this reason, in order to apply the formalism of Ref. [54, 55], it is necessary to isolate the entropy production coming from the baseline NESS dissipation and the entropy production associated with the protocol itself.

A suitable framework for such decomposition is the Hatano–Sasa formalism [57, 58]. In this formalism, the heat exchange with the environment is split into two contributions: the *housekeeping heat*—which is the heat supplied by the environment to sustain the NESS—and the *excess* heat, reflecting deviations from the steady state induced by the protocol.

Employing this formalism, Mandal and Jarzynski established a metric structure governing excess heat during slow transitions between classical NESS.

The quantum extension began with Scandi and Perarnau-Llobet (2019), who considered slow transitions between thermal states within Lindblad dynamics, showing a deep connection between the resulting metric and the Kubo-Mori Fisher information [59].

Building upon this foundation, our primary contribution is the generalization of Mandal and Jarzynski's framework to quantum systems undergoing slow NESS transitions governed by Lindblad master equations. Utilizing the Hatano–Sasa decomposition [57, 60, 61], we emphasize the splitting of entropy production into adiabatic and non-adiabatic contributions. Analogous to Scandi and Perarnau-Llobet, our results reveal a close relationship between the derived metric and modified quantum Fisher information.

Our work thereby completes a critical conceptual framework, summarized in the following table:

	Classical	***Quantum***
Equilibrium	Sivak & Crooks(2007) [55]	Scandi & Perarnau-Llobet (2019) [59]
NESS	Mandal & Jarzynski (2016) [56]	***Present work*** (2025) [62]

This contribution represents a significant advancement in understanding the thermodynamics of quantum nonequilibrium processes.

1.1 Structure of the Thesis

The thesis is organized into ten chapters, each building on the previous ones to develop a comprehensive framework for the study of thermodynamics in nonequilibrium quantum systems. What follows is a brief overview of each chapter and its role in the overall narrative.

- **Chapter 1: Introduction**
  Introduces the field of quantum thermodynamics, the motivating questions behind this work, and an overview of the experimental and theoretical landscape. It presents the scope, goals, and structure of the thesis.

- **Chapter 2: Open Quantum Systems**
  Reviews the foundational tools used to model quantum systems coupled to environments. It introduces the Lindblad master equation, including its microscopic derivation, and discusses the issue of local versus global master equations. It also provides the basic mathematical tools used throughout the thesis.

- **Chapter 3: Quantum Thermodynamics**
  Provides definitions of work, heat, and entropy production, and discusses the first and second laws in the context of open quantum systems. It examines conceptual challenges that arise in the strong coupling regime and introduces key quantities such as the von Neumann entropy and the relative entropy. The chapter concludes with a treatment of quantum thermodynamics in the Markovian regime, focusing on the frameworks developed by Alicki and Spohn.

- **Chapter 4: Gaussian Systems**
  Provides a comprehensive overview of Gaussian fermionic systems described by quadratic Hamiltonians. It introduces the covariance matrix formalism and the Lyapunov equation, which serve as essential technical tools for the mesoscopic leads framework developed in the following chapter.

- **Chapter 5: Mesoscopic Leads**
  Develops the mesoscopic leads framework and provides a consistent formulation of thermodynamics within this approach, with a focus on time-dependent driving. It presents a formal justification of the method via the reaction coordinate mapping and illustrates its application through two example systems.

- **Chapter 6: Entropy Production in Mesoscopic Leads**
  Discusses the application of Spohn's framework for entropy production within the mesoscopic leads formalism, demonstrating how the method can be used to analyze entropy production in the strong coupling regime.

- **Chapter 7: Information Geometry**
  Provides a pedagogical introduction to quantum Fisher information and its role in information geometry. It then presents a historical overview of the concept of thermodynamic length.

- **Chapter 8: Entropy Production in Nonequilibrium Steady States**
  Provides a modern and comprehensive review of entropy production in nonequilibrium steady states using the Hatano–Sasa decomposition. The first part focuses on classical continuous-time Markov chains, introducing the concepts of adiabatic and non-adiabatic entropy production and deriving the corresponding fluctuation theorems. The second part extends these ideas to the quantum regime, highlighting the technical difficulties that emerge in formulating consistent quantum analogues.

- **Chapter 9: Slow Transitions**
  Investigates entropy production in slow transitions between quantum nonequilibrium steady states, linking irreversible entropy production to a metric in parameter space. It discusses how this connection can be used to optimize finite-time driving protocols.

- **Chapter 10: Conclusion**
  Summarizes the main results and contributions of the thesis and outlines future directions for theoretical and experimental development in quantum thermodynamics.

Part I

Open Quantum Systems & Quantum Thermodynamics

2 Open quantum systems

Open quantum systems are, in a nutshell, quantum systems that interact with an external quantum environment. No physical system is perfectly isolated. Any realistic quantum system interacts, to some extent, with its surrounding environment, whether due to thermal fluctuations, electromagnetic noise, or coupling to measurement devices. While this coupling may be detrimental for certain quantum technologies—e.g., in quantum computing—it also enables a wide range of applications in quantum thermodynamics and transport. The theory of open quantum systems provides the tools to describe and understand these processes, and it will play a central role in this thesis.

In the open quantum systems framework, the dynamics of the joint state is unitary, but the dynamics of the reduced state of the system—obtained by tracing out the environment—is generally non-unitary and often highly non-trivial. The environment is typically modeled as a large reservoir with an effectively infinite number of degrees of freedom. As a result, exact solutions of the full dynamics are rarely accessible. Much of open quantum systems theory revolves around developing controlled approximations to derive an effective equation of motion for the system.

One of the central approximations in this context is the *Markovian assumption*. Although multiple definitions of Markovianity exist in the literature (see, e.g., the review by Breuer *et al.* [63]), they all share the same spirit of the memorylessness property in classical stochastic processes: conditioned on the present, the future of the evolution is independent of the past. In this chapter, we adopt the widely used definition based on divisibility of the dynamical map: if the evolution can be described by a quantum dynamical semigroup, then the dynamics is said to be Markovian.

The structure of the most general Markovian dynamics was independently established by Lindblad [27] and by Gorini, Kossakowski, and Sudarshan [26]. In their seminal work, they show that any Markovian and completely-positive trace-preserving (CPTP) evolution must take the form of a *Lindblad master equation*, which is one of the pillars of open quantum systems theory.

Lindblad master equations offer several practical advantages, especially for numerical simulations. The Lindblad structure opens the way for the quantum jumps method, which is a powerful tool for simulating large systems. For non-interacting systems, methods based on the Lyapunov equation [64] or the third quantization formalism [65] can reach very large system sizes. Moreover, there is growing effort in combining Lindblad dynamics with tensor network methods to simulate open many-body systems [66, 67, 68]. From a theoretical perspective, Lindblad master equations have been extensively studied and there is a wide library of results available.

Nevertheless, the Lindblad formalism has limitations. The derivation of a Lindblad equation usually assumes weak coupling and a structureless (memoryless) environment, and

that the initial state of the system is uncorrelated from the bath. When these assumptions break down—such as in the strong-coupling regime or in the presence of structured or finite reservoirs—the Markovian approximation may fail. In such cases, non-Markovian methods are needed. Notable examples include the Hierarchical Equations of Motion (HEOM) [69, 70], path integral approaches [71] such as QUAPI (Quasi-Adiabatic Path Integral) [72], TEMPO (Time-Evolving Matrix Product Operator) [73] and TEDOPA (Time-Evolving Density matrix using Orthogonal Polynomials Algorithm) [74], and the Nakajima–Zwanzig and Time-Convolutionless master equation [31]. These methods are typically numerically demanding, but they allow for accurate simulations of strongly coupled and/or structured environments far beyond the reach of Lindblad-based descriptions.

Another important class of methods is based on embedding techniques. These approaches simulate non-Markovian dynamics by embedding the system of interest into an enlarged, effectively Markovian system. For instance, in the *Mesoscopic Leads* formalism [44, 45], which will be the theme of Chapter 5, the system is coupled to finite-sized auxiliary reservoirs that are themselves coupled to larger baths. The evolution of the extended system is Markovian, but the original system exhibits memory effects.

In this Chapter, we review some important aspects of open quantum systems theory. This Chapter is structured as follows. in Section 2.1, we introduce the concept of dynamical map and discuss the Markov assumption. Then, in Section 2.2, we introduce the Lindblad master equation and discuss some of its formal properties. From Sections 2.2.1 to 2.5, we apply the formalism to two simple examples: a single qubit and a single fermionic mode, each subject to dissipation. In Sections 2.6, we discuss a method for performing a microscopic derivation and in Section 2.8 we discuss an example. Finally, in Section 2.9.1, we discuss the dichotomy between local and global master equations through an instructive example: transport in a double quantum dot.

◆

2.1 Dynamical map

We begin by introducing the general framework of open quantum systems and the concept of a *dynamical map*. Consider a quantum system S with Hilbert space $\mathcal{H}_S$ interacting with an environment E with Hilbert space $\mathcal{H}_E$. The Hilbert space of the total system is $\mathcal{H}_S \otimes \mathcal{H}_E$, and its Hamiltonian takes the general form

$$\hat{H} = \hat{H}_S \otimes \hat{\mathbb{1}}_E + \hat{\mathbb{1}}_S \otimes \hat{H}_E + \hat{H}_{SE}, \tag{2.1}$$

where $\hat{H}_S$ and $\hat{H}_E$ are the Hamiltonians of the system and environment, respectively, and $\hat{H}_{SE}$ is the interaction term, which acts on both Hilbert spaces. A schematic representation of an open quantum system is shown in Fig. 2.1 (a).

The joint state of the system and environment $\hat{\rho}$ evolves unitarily under the total Hamiltonian (2.1), according to the von Neumann equation $\dot{\hat{\rho}} = -i[\hat{H}, \hat{\rho}]$. The formal solution is given by

$$\hat{\rho}(t) = \hat{U}_t \hat{\rho}(0) \hat{U}_t^\dagger, \tag{2.2}$$

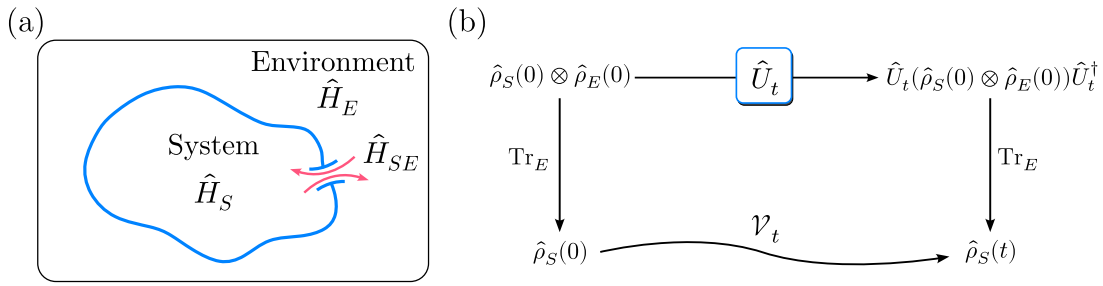

Figure 2.1: (a) Schematic representation of an open quantum system. (b) Diagram describing the action of the dynamical map. Adapted from [31].

where $\hat{U}_t = \mathcal{T} e^{-i \int_0^t \mathrm{d}t' \, \hat{H}(t')}$ is the time-evolution operator and $\mathcal{T}$ denotes the time ordering operator.

To obtain the dynamics of the system alone, we trace over the environment:

$$\hat{\rho}_S(t) = \mathrm{Tr}_E[\hat{\rho}(t)], \tag{2.3}$$

where $\mathrm{Tr}_E[\cdot]$ denotes the partial trace over $\mathcal{H}_E$. This reduced state contains all the expectation values of observables acting only on the system, i.e., those of the form $\hat{A} \otimes \hat{\mathbb{1}}_E$.

Assuming that the system and environment are initially uncorrelated, we write the initial state as $\hat{\rho}(0) = \hat{\rho}_S(0) \otimes \hat{\rho}_E(0)$. The state of the system at time t is then given by

$$\hat{\rho}_S(t) = \mathrm{Tr}_E\left[\hat{U}_t(\hat{\rho}_S(0) \otimes \hat{\rho}_E(0))\hat{U}_t^\dagger\right]. \tag{2.4}$$

This motivates the definition of the *dynamical map*, a linear superoperator $\mathcal{V}_t$ that takes the system from the initial time to t:

$$\hat{\rho}_S(t) = \mathcal{V}_t \hat{\rho}_S(0) \equiv \mathrm{Tr}_E\left[\hat{U}_t(\hat{\rho}_S(0) \otimes \hat{\rho}_E(0))\hat{U}_t^\dagger\right]. \tag{2.5}$$

Without further assumptions, the map $\mathcal{V}_t$ can be highly nontrivial. However, to be physically consistent, it must preserve the defining properties of a density matrix. This leads to the requirement that $\mathcal{V}_t$ be a completely positive trace-preserving (CPTP) map.

A map $\mathcal{E}$ is CPTP if it satisfies the following:

(i) **Linearity:** $\mathcal{E}(\alpha\hat{\rho}_1 + \beta\hat{\rho}_2) = \alpha\mathcal{E}(\hat{\rho}_1) + \beta\mathcal{E}(\hat{\rho}_2)$,

(ii) **Trace preservation:** $\mathrm{Tr}[\mathcal{E}(\hat{\rho})] = \mathrm{Tr}[\hat{\rho}]$,

(iii) **Complete positivity:** $\mathcal{E} \otimes \mathcal{I}_n$ maps positive operators to positive operators for all $n \geq 1$, where $\mathcal{I}_n$ is the identity map on an n-dimensional ancillary space.

Property (iii) is stronger than simply requiring $\mathcal{E}(\hat{\rho})$ to be positive. It ensures that the map behaves properly even when the system is entangled with an ancillary system.

Any CPTP map admits an operator-sum (Kraus) representation [75, 31]:

$$\mathcal{E}(\hat{\rho}) = \sum_k \hat{M}_k \hat{\rho} \hat{M}_k^\dagger, \quad \text{with} \quad \sum_k \hat{M}_k^\dagger \hat{M}_k = \hat{\mathbb{1}}. \tag{2.6}$$

The operators $\{\hat{M}_k\}$ are known as Kraus operators. To obtain them for $\mathcal{V}_t$, we expand $\hat{\rho}_E(0)$ in its eigenbasis:

$$\hat{\rho}_E(0) = \sum_j p_j |e_j\rangle\langle e_j|. \tag{2.7}$$

Inserting this into Eq. (2.5) and tracing over the environment yields

$$\mathcal{V}_t \hat{\rho}_S(0) = \sum_{j,k} \hat{M}_{jk} \hat{\rho}_S(0) \hat{M}_{jk}^\dagger, \quad \text{where} \quad \hat{M}_{jk} = \sqrt{p_j}\langle e_k|\hat{U}_t|e_j\rangle. \tag{2.8}$$

2.2 Lindblad master equation

The dynamical map [(2.5)] is a formal object but may not be particularly useful for practical calculations. Without further assumptions, the dynamics of the reduced state can be as complicated as the global one, as it requires keeping track of the environment at all times. Moreover, it is often more convenient to work with a differential equation for $\hat{\rho}$.

To derive such an equation, we must make simplifying assumptions. One of the most important is the *Markov assumption*. As mentioned in the introduction of this chapter, Markovianity in open quantum systems can be characterized in several ways [63]. Here, we adopt the definition based on the divisibility of the dynamical map. Specifically, the dynamics is Markovian if the evolution satisfies the semigroup property:

$$\mathcal{V}_{t_1} \circ \mathcal{V}_{t_2} = \mathcal{V}_{t_1+t_2}, \quad \forall t_1, t_2 \geq 0. \tag{2.9}$$

This is analogous to the Markov property in classical stochastic processes: the future evolution depends only on the present state, not on the system's history. The approximation is well justified when the environment correlation time is much shorter than the system's characteristic timescale. In such cases, the environment cannot retain or return information to the system, resulting in memoryless dynamics. We will revisit the validity of this assumption in the context of microscopic derivations in Section 2.6.

A map satisfying Eq. (2.9) is known as a quantum dynamical semigroup [31]. For time-independent and finite $\hat{H}_S$, such a map can be written in the exponential form $\mathcal{V}_t(\cdot) = e^{\mathcal{L}t}(\cdot)$ [31, 76], where the linear map $\mathcal{L}$ is the generator of the semigroup. The reduced state then satisfies a linear differential equation

$$\frac{\mathrm{d}\hat{\rho}_S}{\mathrm{d}t} = \mathcal{L}\hat{\rho}_S. \tag{2.10}$$

Lindblad's theorem [27, 26] states that the most general form of $\mathcal{L}$ that generates a CPTP semigroup is

$$\frac{\mathrm{d}\hat{\rho}_S}{\mathrm{d}t} = \mathcal{L}\hat{\rho}_S \equiv -i[\hat{H}', \hat{\rho}_S] + \sum_k \gamma_k \left(\hat{L}_k \hat{\rho}_S \hat{L}_k^\dagger - \frac{1}{2}\{\hat{L}_k^\dagger \hat{L}_k, \hat{\rho}_S\} \right), \tag{2.11}$$

where $\hat{H}'$ is a Hermitian operator, the $\hat{L}_k$ are the so-called *jump operators*, and $\gamma_k > 0$ are rates associated with different dissipative channels. This equation is known as the Gorini–Kossakowski–Sudarshan–Lindblad (GKSL) master equation [26, 27].

The term in Eq. (2.11) involving $\hat{H}'$ generates unitary evolution, while the remaining term, referred to as the *dissipator*, accounts for decoherence and dissipation due to the environment. We define

$$\mathcal{D}(\hat{\rho}_S) = \sum_k \gamma_k \left(\hat{L}_k \hat{\rho}_S \hat{L}_k^\dagger - \frac{1}{2}\{\hat{L}_k^\dagger \hat{L}_k, \hat{\rho}_S\} \right), \tag{2.12}$$

and introduce the shorthand

$$\mathbb{D}[\hat{L}_k] = \hat{L}_k \hat{\rho}_S \hat{L}_k^\dagger - \frac{1}{2}\{\hat{L}_k^\dagger \hat{L}_k, \hat{\rho}_S\}, \tag{2.13}$$

so that $\mathcal{D}(\hat{\rho}_S) = \sum_k \gamma_k \mathbb{D}[\hat{L}_k]$.

Lindblad's theorem guarantees that any Markovian master equation must take the form of Eq. (2.11), but it does not specify the explicit forms of $\hat{H}'$ and $\{\hat{L}_k\}$. In many cases, $\hat{H}'$ coincides with the system Hamiltonian $\hat{H}_S$, but this is not true in general. Moreover, the representation is not unique: one can perform unitary transformations on the jump operators without changing the dynamics [31].

There are two main approaches to obtaining Eq. (2.11). The first is *phenomenological*: one posits a Lindblad equation based on symmetry arguments and physical intuition, selecting jump operators that model the observed behavior. This approach is widely used across many areas of quantum physics and provides excellent agreement with experiments.

The second is the *microscopic* approach, in which one begins with the full system–bath Hamiltonian and derives an effective equation for the reduced state via a sequence of approximations and partial tracing over the environment. This derivation is discussed in detail in Section 2.6.

In the next sections, we explore the Lindblad master equation through two illustrative examples: a single qubit and a single fermionic mode, each subject to dissipation.

2.2.1 Example: Single qubit coupled to a thermal bath

In this first example, we consider a single qubit (a two-level system) coupled to a thermal reservoir at inverse temperature β. The Hamiltonian of the system is given by

$$\hat{H} = \frac{\Omega}{2}\hat{\sigma}^z, \tag{2.14}$$

where Ω is the energy difference between the two energy levels and

$$\hat{\sigma}^z = \begin{pmatrix} 1 & 0 \\ 0 & -1 \end{pmatrix}. \tag{2.15}$$

The interaction with the bath is described by the following master equation:

$$\frac{\mathrm{d}\hat{\rho}}{\mathrm{d}t} = -\frac{i\Omega}{2}[\hat{\sigma}^z, \hat{\rho}] + \gamma(1-f)\mathbb{D}[\hat{\sigma}^-](\hat{\rho}) + \gamma f \mathbb{D}[\hat{\sigma}^+](\hat{\rho}), \tag{2.16}$$

where $\gamma > 0$ is the strength and $f = (e^{\beta\Omega} + 1)^{-1}$ is the Fermi-Dirac distribution of the bath. A schematic representation of the model is shown in Fig. 2.2 (a).

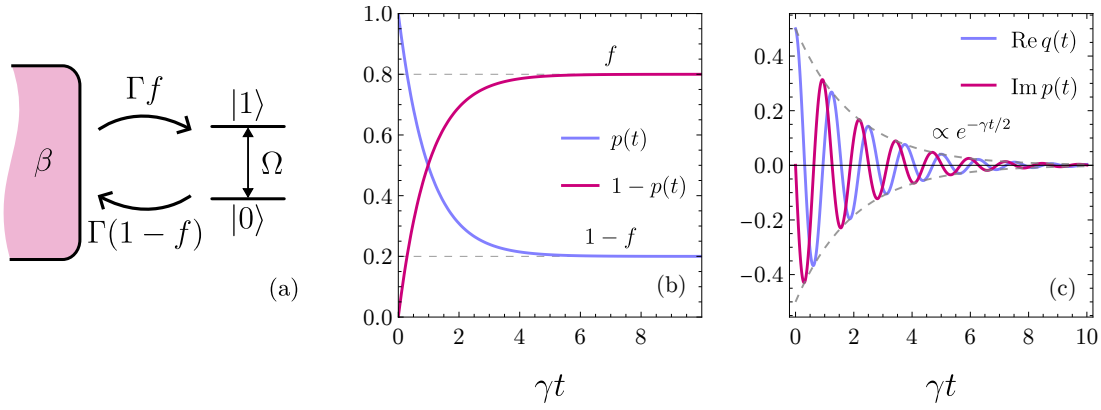

Figure 2.2: (a) Schematic representation of a qubit coupled to a thermal bath. (b) Dynamics of the populations in the single qubit model starting at the excited state. (c) Dynamics of the coherence $q(t)$ in the single qubit model, with $p(0) = 0.5$ and $q(0) = 0.5$. In both plots, we used $\Omega = 5$, $\gamma = 1$ and $f = 0.2$.

A general density matrix of a two-level system can be parametrized as

$$\hat{\rho} = \begin{pmatrix} p & q \\ q^* & 1-p \end{pmatrix}, \tag{2.17}$$

where $0 < p < 1$, by $\mathrm{Tr}[\hat{\rho}] = 1$ is the population of the excited state and q represents the coherence, with $|q| < \sqrt{p(1-p)}$ by positivity. We insert this parametrization into Eq. (2.16), resulting in the following set of equations:

$$\begin{aligned} \dot{p} &= \gamma(f - p), \\ \dot{q} &= -(i\Omega + \tfrac{\gamma}{2})q. \end{aligned} \tag{2.18}$$

The solutions to these equations are

$$\begin{aligned} p(t) &= p(0)e^{-\gamma t} + f(1 - e^{-\gamma t}), \\ q(t) &= e^{-(i\Omega + \frac{\gamma}{2})t} q(0). \end{aligned} \tag{2.19}$$

An example of the dynamics of the population and the coherence for a particular choice of parameters is shown in Figs. 2.2 (b) and (c). Taking the limit $t \to \infty$, we see that the system relaxes to a thermal state:

$$\hat{\rho}_{\mathrm{ss}} = \lim_{t\to\infty} \hat{\rho} = \begin{pmatrix} f & 0 \\ 0 & 1-f \end{pmatrix} = \frac{e^{-\beta \hat{H}}}{Z} \tag{2.20}$$

where $Z = \mathrm{Tr}[e^{-\beta \hat{H}}]$. Therefore, we see that the dissipator in Eq. (2.16) simultaneously kills the coherences and thermalizes the populations.

2.3 Example: single qubit under pure dephasing

Consider again the single qubit Hamiltonian, but it is now subject to a dissipator of the form:

$$\mathcal{D}(\hat{\rho}) = \frac{\Gamma}{2}\mathbb{D}[\hat{\sigma}^z] = \frac{\Gamma}{2}(\hat{\sigma}^z \hat{\rho} \hat{\sigma}^z - \hat{\rho}). \tag{2.21}$$

This dissipator models a dephasing environment. The master equation under pure dephasing is given by

$$\frac{\mathrm{d}\hat{\rho}}{\mathrm{d}t} = -\frac{i\omega}{2}[\hat{\sigma}^z, \hat{\rho}] + \frac{\Gamma}{2}(\hat{\sigma}^z\hat{\rho}\hat{\sigma}^z - \hat{\rho}). \tag{2.22}$$

Using the parametrization (2.17), we obtain the equations

$$\begin{aligned} \dot{p} &= 0, \\ \dot{q} &= -(\Gamma + i\omega)q, \end{aligned} \tag{2.23}$$

from which we see that the dephasing environment does not affect the populations, while the coherences decay as

$$q(t) = e^{-(\Gamma+i\omega)t}q(0). \tag{2.24}$$

Therefore, in the long time limit, the off-diagonal elements vanish, and the system reaches the steady state:

$$\hat{\rho}_{\mathrm{ss}} = \lim_{t\to\infty}\hat{\rho} = \begin{pmatrix} p(0) & 0 \\ 0 & 1-p(0) \end{pmatrix} \tag{2.25}$$

2.4 Adjoint master equation

In this section, we discuss how the Lindblad master equation [(2.11)] can be recast in the Heisenberg picture, which is very useful for the computation of expectation values. We start by assuming that the Liouvillian $\mathcal{L}$ is time-independent, so that the density matrix evolves as $\hat{\rho}(t) = e^{\mathcal{L}t}\hat{\rho}(0)$. For a general operator $\hat{\mathcal{O}}$, we define its Heisenberg-picture evolution $\hat{\mathcal{O}}(t)$ by imposing that its expectation is the same in the Schrödinger and Heisenberg pictures:

$$\langle\hat{\mathcal{O}}\rangle_t = \mathrm{Tr}\left[\hat{\mathcal{O}}(t)\hat{\rho}(0)\right] = \mathrm{Tr}\left[\hat{\mathcal{O}}\hat{\rho}(t)\right] = \mathrm{Tr}[\mathcal{O}e^{\mathcal{L}t}[\hat{\rho}(0)]]. \tag{2.26}$$

This motivates the introduction of the *adjoint Liouvillian*, formally defined by the identity

$$\mathrm{Tr}\left[\hat{A}\mathcal{L}[\hat{B}]\right] = \mathrm{Tr}\left[\mathcal{L}^\dagger[\hat{A}]\hat{B}\right]. \tag{2.27}$$

From this definition, it follows that $\mathrm{Tr}[\hat{A}e^{\mathcal{L}t}[\hat{B}]] = \mathrm{Tr}[e^{\mathcal{L}^\dagger t}[\hat{A}]\hat{B}]$, which can be seen by expanding $e^{\mathcal{L}t}$ in a power series and using the identity $\mathrm{Tr}[\hat{A}\mathcal{L}^n[\hat{B}]] = \mathrm{Tr}[(\mathcal{L}^\dagger)^n[\hat{A}]\hat{B}]$.

Substituting into Eq. (2.26), we find:

$$\langle\mathcal{O}\rangle_t = \mathrm{Tr}\left[e^{\mathcal{L}^\dagger t}[\mathcal{O}]\hat{\rho}(0)\right], \tag{2.28}$$

which implies that the Heisenberg-picture operator evolves as $\hat{\mathcal{O}}(t) = e^{\mathcal{L}^\dagger t}\hat{\mathcal{O}}$. Therefore, in the Heisenberg picture, operators satisfy the differential equation

$$\frac{\mathrm{d}\hat{\mathcal{O}}}{\mathrm{d}t} = \mathcal{L}^\dagger\hat{\mathcal{O}}, \tag{2.29}$$

with $\mathcal{L}^\dagger$ acting as the generator of time evolution. For a time-dependent Liouvillian, the generalization is given by the time-ordered exponential:

$$\hat{\mathcal{O}}(t) = \mathcal{T}\exp\left(\int_0^t \mathrm{d}\tau\mathcal{L}^\dagger\tau\right)\hat{\mathcal{O}}(0). \tag{2.30}$$

The explicit form of $\mathcal{L}^\dagger$ can be derived from the Lindblad master equation. For an arbitrary operator $\hat{\mathcal{O}}$ and state $\hat{\rho}$, the definition (2.27) yields:

$$\begin{aligned}\operatorname{Tr}\left[\mathcal{L}^\dagger\hat{\mathcal{O}}\hat{\rho}\right] &= \operatorname{Tr}\left[\hat{\mathcal{O}}\mathcal{L}\hat{\rho}\right] \\ &= -i\operatorname{Tr}\left[\hat{\mathcal{O}}[\hat{H},\hat{\rho}]\right] + \sum_k \operatorname{Tr}\left[\hat{\mathcal{O}}\left(\hat{L}_k\hat{\rho}\hat{L}_k^\dagger + \frac{1}{2}\left\{\hat{L}_k^\dagger\hat{L}_k,\hat{\rho}\right\}\right)\right] \\ &= i\operatorname{Tr}\left[\hat{\rho}[\hat{H},\hat{\mathcal{O}}]\right] + \sum_k \operatorname{Tr}\left[\hat{\rho}\left(\hat{L}_k^\dagger\hat{\mathcal{O}}\hat{L}_k + \frac{1}{2}\left\{\hat{L}_k^\dagger\hat{L}_k,\hat{\mathcal{O}}\right\}\right)\right],\end{aligned} \tag{2.31}$$

where the final equality uses the cyclic property of the trace. Since this holds for arbitrary $\hat{\rho}$, we identify:

$$\mathcal{L}^\dagger[\bullet] = i[\hat{H},\bullet] + \sum_k\left(\hat{L}_k^\dagger\bullet\hat{L}_k + \frac{1}{2}\left\{\hat{L}_k^\dagger\hat{L}_k,\bullet\right\}\right). \tag{2.32}$$

The non-unitary contribution in this equation is referred to as the adjoint dissipator, which we will often write compactly as

$$\mathcal{L}^\dagger[\bullet] = i[\hat{H},\bullet] + \sum_k \mathbb{D}^\dagger[\hat{L}_k](\bullet) \tag{2.33}$$

where

$$\mathbb{D}^\dagger[\hat{L}_k](\bullet) = \hat{L}_k^\dagger\bullet\hat{L}_k + \frac{1}{2}\{\hat{L}_k^\dagger\hat{L}_k,\bullet\}. \tag{2.34}$$

Alternatively, using cyclic property of the trace, this can also be expressed in the symmetrized form

$$\mathbb{D}^\dagger[\hat{L}](\bullet) = \frac{1}{2}\hat{L}^\dagger[\bullet,\hat{L}] + \frac{1}{2}[\hat{L}^\dagger,\bullet]\hat{L}. \tag{2.35}$$

2.5 Single fermionic mode

We now consider a system consisting of a single fermionic mode coupled to a thermal bath at inverse temperature β. This system is fully equivalent to the single qubit analyzed in Section 2.2.1, since both are two-level systems. Nevertheless, the fermionic formulation is particularly convenient for time-evolution analysis using the adjoint master equation. It will also serve as the fundamental building block for the Lyapunov equation formalism discussed in Chapter 4.

The Hamiltonian of the system is given by

$$\hat{H} = \Omega\hat{c}^\dagger\hat{c}, \tag{2.36}$$

where $\hat{c}$ is a fermionic annihilation operator satisfying $\{\hat{c},\hat{c}^\dagger\} = \hat{1}$ and Ω is the energy of the mode. The coupling to the thermal bath is modeled by a Lindblad master equation:

$$\frac{\mathrm{d}\rho}{\mathrm{d}t} = -i[\hat{H},\hat{\rho}] + \gamma(1-f)\mathbb{D}[\hat{c}] + \gamma f\mathbb{D}[\hat{c}^\dagger], \tag{2.37}$$

where $f = (e^{\beta\Omega} + 1)^{-1}$ is the Fermi-Dirac distribution of the bath and $\gamma > 0$ is the coupling strength. Let $p(t) = \langle \hat{c}^\dagger \hat{c} \rangle$ be the occupation number of the dot. Using the adjoint master equation formalism, we obtain:

$$\frac{\mathrm{d}\langle \hat{c}^\dagger \hat{c} \rangle}{\mathrm{d}t} = i\langle [\hat{H}, \hat{c}^\dagger \hat{c}] \rangle + \langle \gamma(1-f)\mathbb{D}^\dagger[\hat{c}](\hat{c}^\dagger \hat{c}) \rangle + \langle \gamma f \mathbb{D}^\dagger[\hat{c}^\dagger](\hat{c}^\dagger \hat{c}) \rangle. \tag{2.38}$$

Using the identity $[\hat{A}\hat{B}, \hat{C}] = \hat{A}\{\hat{B}, \hat{C}\} - \{\hat{A}, \hat{C}\}\hat{B}$, we find

$$[\hat{c}^\dagger \hat{c}, \hat{c}] = -\hat{c} \quad \text{and} \quad [\hat{c}^\dagger \hat{c}, \hat{c}^\dagger] = \hat{c}^\dagger. \tag{2.39}$$

The first adjoint dissipator is given by

$$\mathbb{D}^\dagger[\hat{c}](\hat{c}^\dagger \hat{c}) = \frac{1}{2}\hat{c}^\dagger [\hat{c}^\dagger \hat{c}, \hat{c}] + \frac{1}{2}[\hat{c}^\dagger, \hat{c}^\dagger \hat{c}]\hat{c} = -\hat{c}^\dagger \hat{c} \tag{2.40}$$

Similarly, we obtain $\mathbb{D}^\dagger[\hat{c}^\dagger](\hat{c}^\dagger \hat{c}) = \hat{1} - \hat{c}^\dagger \hat{c}$. Combining these results in Eq. (2.38), we obtain

$$\frac{\mathrm{d}\langle \hat{c}^\dagger \hat{c} \rangle}{\mathrm{d}t} = \gamma(f - \langle \hat{c}^\dagger \hat{c} \rangle). \tag{2.41}$$

Solving the differential equation yields:

$$p(t) = p(0)e^{-\gamma t} + f(1 - e^{-\gamma t}). \tag{2.42}$$

Therefore, the population of the mode relaxes exponentially to the thermal value f with a rate γ. In the spin formulation, $\langle \hat{c}^\dagger \hat{c} \rangle$ corresponds to the excited-state population $p(t)$, in agreement with Eq. (2.19).

2.6 Microscopic Derivations

A microscopic derivation of a Lindblad equation involves starting from a unitary description of the system and its environment, and deriving an effective master equation for the system by tracing out the environmental degrees of freedom. This process relies on a series of key approximations that render the equations tractable. The three main ingredients are:

1. **The Born approximation**: assumes weak system-bath coupling, such that the total density matrix factorizes as $\hat{\rho}(t) \approx \hat{\rho}_S(t) \otimes \hat{\rho}_E$.

2. **The Markov approximation**: neglects memory effects by assuming a fast-decaying environment.

3. **The Secular approximation**: eliminates fast-oscillating terms and ensures the resulting equation has a proper Lindblad form.

Different approaches to microscopic derivations can be found in the literature, including the Nakajima–Zwanzig projection method and the quantum Langevin formalism. In this chapter, we primarily follow the eigenoperator approach of Ref. [31]. Our main interest lies in a specific example: a fermionic system coupled to a non-interacting fermionic bath. For completeness, we begin with a general setup and later specialize to this case.

While this derivation is standard and can be found in many references [31, 35, 77, 32, 78], it introduces several useful tools for later chapters. In particular, the spectral density—naturally arising in the derivation—will play a central role in the mesoscopic leads framework discussed in Chapter 5. Moreover, upon completing the derivation, we will have all the necessary tools to discuss the dichotomy between local and global master equations, which will be important in Chapter 6.

We consider an open quantum system described by the total Hamiltonian

$$\hat{H} = \hat{H}_S + \hat{H}_E + \hat{H}_{SE}, \tag{2.43}$$

where $\hat{H}_S$ is the system Hamiltonian, $\hat{H}_E$ describes the environment, and $\hat{H}_{SE}$ encodes the interaction between the two. We assume the environment is initially in a thermal state:

$$\hat{\rho}_E \equiv \hat{\rho}_E(0) = \frac{e^{-\beta \hat{H}_E}}{Z}, \quad Z = \mathrm{tr}\left[e^{-\beta \hat{H}_E}\right]. \tag{2.44}$$

We also assume, without loss of generality, that the interaction Hamiltonian satisfies [1]

$$\mathrm{Tr}\left[\hat{H}_{SE}\hat{\rho}_E(0)\right] = 0. \tag{2.45}$$

We now move to the interaction picture with respect to the free Hamiltonian $\hat{H}_0 = \hat{H}_S + \hat{H}_E$, where the time evolution of the full density matrix is governed by

$$\frac{\mathrm{d}\tilde{\rho}}{\mathrm{d}t} = -i[\tilde{H}_{SE}(t), \tilde{\rho}(t)], \tag{2.46}$$

where $\tilde{\rho}(t) = e^{-i\hat{H}_0 t}\hat{\rho}(t)e^{i\hat{H}_0 t}$, $\tilde{H}_{SE} = e^{-i\hat{H}_0 t}\hat{H}_{SE}(t)e^{i\hat{H}_0 t}$. Here, the tilde notation denotes operators in the interaction picture. Formally integrating Eq. (2.46), we obtain

$$\tilde{\rho}(t) = \tilde{\rho}(0) - i\int_0^t \mathrm{d}s\,[\tilde{H}_{SE}(s), \tilde{\rho}(s)] \tag{2.47}$$

Substituting this result back into Eq. (2.46), we find

$$\frac{\mathrm{d}}{\mathrm{d}t}\tilde{\rho}_S(t) = -i[\tilde{H}_{SE}(t)\tilde{\rho}(0)] - \int_0^t \mathrm{d}s\,[\tilde{H}_{SE}(t), [\tilde{H}_{SE}(s), \tilde{\rho}(s)]]. \tag{2.48}$$

Taking the partial trace over the environment and using assumption Eq. (2.45), we obtain the equation

$$\frac{\mathrm{d}}{\mathrm{d}t}\tilde{\rho}_S(t) = -\int_0^t \mathrm{d}s\,\mathrm{Tr}_E[\tilde{H}_{SE}(t), [\tilde{H}_{SE}(s), \tilde{\rho}(s)]]. \tag{2.49}$$

Born approximation—At this point, Eq. (2.49) is formally exact, but typically intractable due to the dependence on the full system-environment density matrix. To make progress, we employ the first main ingredient of the derivation: the Born approximation which assumes

[1] If this condition is not satisfied, one can always redefine $\hat{H}'_S = \hat{H}_S + \mathrm{Tr}\left[\hat{H}_{SE}\hat{\rho}_E(0)\right]$ and $\hat{H}'_{SE} = \hat{H}_{SE} - \mathrm{Tr}\left[\hat{H}_{SE}\hat{\rho}_E(0)\right]$ [79].

weak coupling between system and bath. This allows us to neglect system- environment correlations and write

$$\frac{\mathrm{d}}{\mathrm{d}t}\tilde{\rho}_{SE}(t) \approx \tilde{\rho}_S(s) \otimes \hat{\rho}_E(0). \tag{2.50}$$

Substituting this into Eq. (2.49) and performing the change of variables $\tau = t - s$, we obtain the non-Markovian master equation:

$$\frac{\mathrm{d}}{\mathrm{d}t}\tilde{\rho}_S(t) = -\int_0^t \mathrm{d}s\, \mathrm{Tr}_E[\tilde{H}_{SE}(t), [\tilde{H}_{SE}(t-\tau), \tilde{\rho}_S(t-\tau) \otimes \hat{\rho}_E]]. \tag{2.51}$$

We now express the interaction Hamiltonian in the general form:

$$\hat{H}_{SE} = \sum_\alpha \hat{A}_\alpha \otimes \hat{B}_\alpha, \tag{2.52}$$

where $\{\hat{A}_\alpha\}$ are operators acting on the system and $\{\hat{B}_\alpha\}$ act on the environment. The Hermiticity of $\hat{H}_{SE}$ implies that $\sum_\alpha \hat{A}_\alpha \otimes \hat{B}_\alpha = \sum_\alpha \hat{A}_\alpha^\dagger \otimes \hat{B}_\alpha^\dagger$, but the operators $\hat{A}_\alpha$ and $\hat{B}_\alpha$ are not necessarily Hermitian. Under this decomposition, condition (2.45) becomes $\mathrm{Tr}_E\{\hat{B}_\alpha\} = \langle \hat{B}_\alpha \rangle = 0$.

In the interaction picture, the interaction Hamiltonian evolves as

$$\tilde{H}_{SE}(t) = \sum_\alpha \tilde{A}_\alpha(t) \otimes \tilde{B}_\alpha(t), \tag{2.53}$$

with

$$\tilde{A}_\alpha(t) = e^{i\hat{H}_S t}\hat{A}_\alpha e^{-i\hat{H}_S t} \quad \text{and} \quad \tilde{B}_\alpha(t) = e^{i\hat{H}_E t}\hat{B}_\alpha e^{-i\hat{H}_E t}. \tag{2.54}$$

Before substituting Eq. (2.53) into Eq. (2.51), it is helpful to expand the nested commutators explicitly:

$$\begin{aligned}\frac{\mathrm{d}}{\mathrm{d}t}\tilde{\rho}_S(t) = \int_0^t \mathrm{d}\tau \mathrm{Tr}_E\Big\{&\tilde{H}_{SE}(t-\tau)\tilde{\rho}_S(t-\tau)\hat{\rho}_E\tilde{H}_{SE}(t) - \tilde{H}_{SE}(t)\tilde{H}_{SE}(t-\tau)\hat{\rho}_S(t-\tau)\hat{\rho}_E\Big\} \\ &+ \text{h.c.},\end{aligned} \tag{2.55}$$

Here, h.c. denotes the Hermitian conjugate of the preceding terms, which compactly accounts for the remaining two terms.

Substituting Eq. (2.53) in the expression above, we obtain:

$$\begin{aligned}\tilde{H}_{SE}(t-\tau)\tilde{\rho}_S(t-\tau)\hat{\rho}_E\tilde{H}_{SE}(t) &= \\ &= \left[\sum_\beta \tilde{A}_\beta(t-\tau)\tilde{B}_\beta(t-\tau)\right]\tilde{\rho}_S(t-\tau)\hat{\rho}_E\left[\sum_\alpha \tilde{A}_\alpha^\dagger(t)\tilde{B}_\alpha^\dagger(t)\right] \\ &= \sum_{\alpha\beta} \tilde{A}_\beta(t-\tau)\tilde{\rho}_S(t-\tau)\tilde{A}_\alpha^\dagger(t)\, \tilde{B}_\beta(t-\tau)\hat{\rho}_E\tilde{B}_\alpha^\dagger(t).\end{aligned} \tag{2.56}$$

where we used the fact that $\tilde{\rho}(t)$ is a product state to push all the bath operators to the right. Then, tracing out the environment and using the cyclic property of the trace, we obtain

$$\mathrm{Tr}_E\Big\{\tilde{H}_{SE}(t-\tau)\tilde{\rho}_S(t-\tau)\hat{\rho}_E\tilde{H}_{SE}(t)\Big\} = \sum_{\alpha\beta} g_{\alpha\beta}(\tau)\tilde{A}_\beta(t-\tau)\tilde{\rho}_S(t-\tau)\tilde{A}_\alpha^\dagger(t), \tag{2.57}$$

where we introduced *bath correlation functions*:

$$g_{\alpha\beta}(\tau) = \mathrm{Tr}_E[\tilde{B}_\alpha^\dagger(t)\tilde{B}_\beta(t-\tau)\tilde{\rho}_E] = \langle\tilde{B}_\alpha^\dagger(t)\tilde{B}_\beta(t-\tau)\rangle. \tag{2.58}$$

Because the environment is in a thermal state, $[\hat{H}_E, \hat{\rho}_E] = 0$, thus the bath correlation functions are time translation invariant:

$$\langle\tilde{B}_\alpha^\dagger(t)\tilde{B}_\beta(t-\tau)\rangle = \langle\tilde{B}_\alpha^\dagger(\tau)\tilde{B}_\beta(0)\rangle. \tag{2.59}$$

Consequently, the correlation functions satisfy

$$g_{\alpha\beta}^*(\tau) = g_{\beta\alpha}(-\tau). \tag{2.60}$$

Repeating the same procedure for the second term in Eq. (2.55), we finally obtain the master equation under the Born approximation:

$$\frac{\mathrm{d}}{\mathrm{d}t}\tilde{\rho}_S(t) = \sum_{\alpha\beta}\int_0^t \mathrm{d}\tau\, g_{\alpha\beta}(\tau)\Big[\tilde{A}_\beta(t-\tau)\tilde{\rho}_S(t-\tau)\tilde{A}_\alpha^\dagger(t) - \tilde{A}_\alpha^\dagger(t)\tilde{A}_\beta(t-\tau)\tilde{\rho}_S(t-\tau)\Big] + \text{h.c.}, \tag{2.61}$$

This equation is starting to resemble the Lindblad form, but further steps are still required. In particular, Eq. (2.61) is not time-local, and the solution depends on the whole history of the evolution.

Markovian approximation—In order to convert Eq. (2.51) into a Markovian master equation, we want to replace $\tilde{\rho}_S(t-\tau)$ with $\tilde{\rho}_S(t)$, so that the right-hand side becomes local in time, and extend the upper limit of the integral to ∞, eliminating dependence on the initial condition. This approximation is justified if the integrand in Eq. (2.61) decays very quickly with τ, so that the change in $\tilde{\rho}_S(t-\tau)$ from its value at $t = 0$ is negligible. This is the case if the bath operators have a very short correlation time τ_E compared to the system's relaxation time τ_R, for instance if the correlation functions decay as $g_\alpha(\tau) \sim e^{-\tau/\tau_E}$, with $\tau_E \ll \tau_R$ [80]. Therefore, performing the approximation in Eq. (2.51), we get the equation

$$\frac{\mathrm{d}}{\mathrm{d}t}\tilde{\rho}_S(t) = -\int_0^\infty \mathrm{d}\tau\,\mathrm{Tr}_E[\tilde{H}_{SE}(t), [\tilde{H}_{SE}(t-\tau), \tilde{\rho}_S(t)\otimes\tilde{\rho}_E]], \tag{2.62}$$

which is known as the Born–Markov master equation. In terms of the operators $\{\hat{A}_\alpha\}$, this becomes

$$\frac{\mathrm{d}}{\mathrm{d}t}\tilde{\rho}_S(t) = \sum_{\alpha\beta}\int_0^\infty \mathrm{d}\tau\, g_{\alpha\beta}(\tau)\Big[\tilde{A}_\beta(t-\tau)\tilde{\rho}_S(t)\tilde{A}_\alpha^\dagger(t) - \tilde{A}_\alpha^\dagger(t)\tilde{A}_\beta(t-\tau)\tilde{\rho}_S(t)\Big] + \text{h.c.}. \tag{2.63}$$

Unfortunately, however, Eq. (2.63) is not guaranteed to be in Lindblad form [31, 35]. To enforce a Lindblad structure, it is often necessary to perform a further approximation, which will be the last main ingredient of this derivation: the *secular approximation*, also known as *rotating wave approximation* (RWA).

The approximation consists, essentially, in averaging out fast oscillating terms. To do this, we need to make the time dependence of the operators $\tilde{A}_\alpha(t)$ explicit, which can be achieved by expanding them in the eigenbasis of $\hat{H}_S$. We define the *jump operators* $\hat{A}_\alpha(\omega)$ via

$$\hat{A}_\alpha(\omega) = \sum_{\epsilon'-\epsilon=\omega} |\epsilon\rangle\langle\epsilon|\hat{A}_\alpha|\epsilon'\rangle\langle\epsilon'|, \tag{2.64}$$

where $\{|\epsilon\rangle\}$ is the eigenbasis of $\hat{H}_S$, defined via $\hat{H}_S|\epsilon\rangle = \epsilon|\epsilon\rangle$. Notice that, in general, the construction of the operators $\hat{A}_\alpha(\omega)$ requires the diagonalization of $\hat{H}_S$. The operators $\hat{A}_\alpha(\omega)$ connect eigenstates with energy difference ω, These operators will later give rise to the jump operators in the Lindblad equation. From the completeness of the basis $\{\epsilon\}$, it follows that $\hat{A}_\alpha$ can be recovered by summing over all frequencies, i.e., $\hat{A}_\alpha = \sum_\omega \hat{A}_\alpha(\omega)$.

The key property of the jump operators is the fact that they satisfy the properties

$$[\hat{H}_S, \hat{A}_\alpha(\omega)] = -\omega\hat{A}_\alpha(\omega) \quad \text{and} \quad [\hat{H}_S, \hat{A}^\dagger_\alpha(\omega)] = \omega\hat{A}^\dagger_\alpha(\omega), \tag{2.65}$$

which can be seen from the definition (2.64):

$$\begin{aligned}
[\hat{H}_S, \hat{A}_\alpha(\omega)] &= \sum_{\epsilon'-\epsilon=\omega} \left(\hat{H}_S|\epsilon\rangle\langle\epsilon|\hat{A}_\alpha|\epsilon'\rangle\langle\epsilon'| - |\epsilon\rangle\langle\epsilon|\hat{A}_\alpha|\epsilon'\rangle\langle\epsilon'|\hat{H}_S\right) \\
&= \sum_{\epsilon'-\epsilon=\omega} (\epsilon - \epsilon')|\epsilon\rangle\langle\epsilon|\hat{A}_\alpha|\epsilon'\rangle\langle\epsilon'| \\
&= -\omega\hat{A}_\alpha(\omega),
\end{aligned} \tag{2.66}$$

and similarly for $\hat{A}^\dagger(\omega)$. For this reason, $\hat{A}_\alpha(\omega)$ and $\hat{A}^\dagger_\alpha(\omega)$ are said to be eigenoperators of $\hat{H}_S$ Bohr frequencies $\pm\omega$. As a consequence, their time evolution in the interaction picture becomes:

$$\begin{aligned}
e^{i\hat{H}_S t}\hat{A}_\alpha(\omega)e^{-i\hat{H}_S t} &= \sum_{\epsilon'-\epsilon=\omega} e^{i\hat{H}_S t}|\epsilon\rangle\langle\epsilon|\hat{A}_\alpha|\epsilon'\rangle\langle\epsilon'|e^{-i\hat{H}_S} \\
&= \sum_{\epsilon'-\epsilon=\omega} e^{i\epsilon t}|\epsilon\rangle\langle\epsilon|\hat{A}_\alpha|\epsilon'\rangle\langle\epsilon'|e^{-i\epsilon t} \\
&= e^{-i\omega t}\hat{A}_\alpha(\omega).
\end{aligned} \tag{2.67}$$

Summing over all frequencies, we obtain $\tilde{A}_\alpha(t) = \sum_\omega e^{-i\omega t}\hat{A}_\alpha(\omega)$. Inserting this result in Eq. (2.62) and computing the integral over τ, we arrive at

$$\frac{\mathrm{d}}{\mathrm{d}t}\tilde{\rho}_S(t) = \sum_{\omega,\omega'}\sum_{\alpha\beta} e^{i(\omega-\omega')t}\Gamma_{\alpha\beta}(\omega)\left[\hat{A}_\beta(\omega)\tilde{\rho}_S(t)\hat{A}^\dagger_\alpha(\omega') - \hat{A}^\dagger_\alpha(\omega)\hat{A}_\beta(\omega')\tilde{\rho}_S(t)\right] + \text{h.c.} \tag{2.68}$$

where we introduced the one-sided Fourier transform of the bath correlation functions:

$$\Gamma_{\alpha\beta}(\omega) = \int_0^\infty \mathrm{d}\tau e^{i\omega\tau} g_{\alpha\beta}(\tau). \tag{2.69}$$

Secular approximation—Eq. (2.68) contains terms oscillating with $e^{i(\omega-\omega')t}$. If $\omega \neq \omega'$, these terms oscillate rapidly in time. The solution $\tilde{\rho}_S(t)$ at some given time t is found by integrating Eq. (2.68). The secular approximation consists in neglecting the rapidly oscillating terms assuming that their contribution averages out to zero when integrated over the relevant timescales of the system's dynamics. To see this explicitly, consider the rescaled time $s = t/\tau_R$. Integrating Eq. (2.68) and using this change of variables, we find

$$\tilde{\rho}(t) = \hat{\rho}(0) - \frac{1}{\tau_R}\sum_{\omega,\omega'}\sum_{\alpha\beta}\int_0^{t/\tau_R} \mathrm{d}s\, e^{i\tau_R(\omega-\omega')s}\Gamma_{\alpha\beta}(\omega)[\,\dots\,]. \tag{2.70}$$

We can now apply the Riemann–Lebesgue lemma [81, 35], an important result in real and complex analysis which states that

$$\lim_{\xi\to 0}\int_a^b \mathrm{d}t\, e^{i\xi t} f(t) = 0, \tag{2.71}$$

where $f(t)$ is an integrable function. Applying this lemma to Eq. (2.70), we see that if the Bohr frequencies satisfy

$$|\omega - \omega'| \ll \frac{1}{\tau_R}, \quad \forall \omega, \omega', \tag{2.72}$$

then the time integral of these oscillatory terms over timescales $\sim \tau_R$ vanishes. Under this assumption, we can remove all the terms with $\omega \neq \omega'$ in Eq. (2.68), which yields

$$\frac{\mathrm{d}}{\mathrm{d}t}\tilde{\rho}_S(t) = \sum_{\omega}\sum_{\alpha\beta}\Gamma_{\alpha\beta}(\omega)\left[\hat{A}_\beta(\omega)\tilde{\rho}_S(t)\hat{A}_\alpha^\dagger(\omega) - \hat{A}_\alpha^\dagger(\omega)\hat{A}_\beta(\omega)\tilde{\rho}_S(t)\right] + \text{h.c.} \tag{2.73}$$

To cast this into Lindblad form, we decompose $\Gamma_{\alpha\beta}(\omega)$ into its Hermitian and anti-Hermitian parts:

$$\gamma_{\alpha\beta}(\omega) = \Gamma_{\alpha\beta}(\omega) + \Gamma_{\alpha\beta}^*(\omega) \quad \text{and} \quad \Delta_{\alpha\beta}(\omega) = \frac{1}{2i}(\Gamma_{\alpha\beta}(\omega) - \Gamma_{\alpha\beta}^*(\omega)). \tag{2.74}$$

By construction, both matrices are Hermitian, and we can write:

$$\Gamma_{\alpha\beta}(\omega) = \frac{1}{2}\gamma_{\alpha\beta}(\omega) + i\Delta_{\alpha\beta}(\omega). \tag{2.75}$$

Moreover, it can be shown that the matrix $\boldsymbol{\gamma}(\omega)$ is positive semi-definite [31, 35].

Inserting this decomposition back into Eq. (2.73) and adding the Hermitian conjugate term, we obtain:

$$\begin{aligned}\frac{\mathrm{d}}{\mathrm{d}t}\tilde{\rho}_S(t) = \sum_{\omega}\sum_{\alpha\beta}\Big\{ &-i\Delta_{\alpha\beta}(\omega)[\hat{A}_\alpha^\dagger(\omega)\hat{A}_\beta(\omega), \tilde{\rho}_S] \\ &+ \gamma_{\alpha\beta}(\omega)\Big(\hat{A}_\beta(\omega)\hat{\rho}_S(t)\hat{A}_\alpha^\dagger(\omega) - \{\hat{A}_\alpha^\dagger(\omega)\hat{A}_\beta(\omega), \tilde{\rho}_S(t)\}\Big)\Big\}.\end{aligned} \tag{2.76}$$

This equation can be now written as

$$\frac{\mathrm{d}\tilde{\rho}_S}{\mathrm{d}t} = -i[\hat{H}_{LS}, \tilde{\rho}_S] + \mathcal{D}(\tilde{\rho}), \tag{2.77}$$

where the dissipative term is given by

$$\mathcal{D}(\tilde{\rho}) = \sum_{\omega} \sum_{\alpha\beta} \gamma_{\alpha\beta}(\omega)\Big(\hat{A}_{\beta}(\omega)\tilde{\rho}_S\hat{A}^{\dagger}_{\alpha}(\omega) - \{\hat{A}^{\dagger}_{\alpha}(\omega)\hat{A}_{\beta}(\omega), \tilde{\rho}_S\}\Big) \tag{2.78}$$

and the unitary term is generated by the so called Lamb-Shift Hamiltonian:

$$\hat{H}_{LS} = \sum_{\omega} \sum_{\alpha\beta} \Delta_{\alpha\beta}(\omega)\hat{A}^{\dagger}_{\alpha}(\omega)\hat{A}_{\beta}(\omega). \tag{2.79}$$

It can be verified from the definition of the operators $\hat{A}_{\alpha}(\omega)$, Eq. (2.64), that they also satisfy the property

$$[\hat{H}_S, \hat{A}^{\dagger}_{\alpha}(\omega)\hat{A}_{\alpha}(\omega)] = 0. \tag{2.80}$$

Consequently, the Lamb-Shift Hamiltonian commutes with $\hat{H}_S$, which means they can be diagonalized in the same basis. Therefore, the presence of $\hat{H}_{LS}$ only induces energy level shifts without affecting the eigenstates of $\hat{H}_S$. In many systems of interest, the energy shifts $\Delta_{\alpha\beta}(\omega)$ are typically very small and are often neglected.

Finally, to express the master equation in the diagonal Lindblad form of Eq. (2.11), we diagonalize the matrix $\boldsymbol{\gamma}(\omega)$. Being Hermitian and positive semi-definite, $\boldsymbol{\gamma}(\omega)$ has non-negative eigenvalues $\kappa_k(\omega)$ and can be diagonalized via a unitary matrix $\boldsymbol{S}(\omega)$, yielding $\gamma_{\alpha\beta}(\omega) = \sum_k \kappa_k(\omega) S_{\alpha k}(\omega) S^*_{\beta k}(\omega)$.

Therefore, by defining a new set of jump operators $\hat{\mathcal{A}}_k(\omega) = \sum_{\alpha} S^*_{\alpha k}(\omega)\hat{A}_{\alpha}(\omega)$ and substituting back in Eq. (2.78) we obtain:

$$\frac{\mathrm{d}\hat{\rho}_S}{\mathrm{d}t} = -i[\hat{H}_S + \hat{H}_{LS}, \hat{\rho}_S] + \sum_{\omega} \sum_{k} \kappa_k(\omega)\Big(\hat{\mathcal{A}}_k(\omega)\hat{\rho}_S\hat{\mathcal{A}}^{\dagger}_k(\omega) - \{\hat{\mathcal{A}}^{\dagger}_k(\omega)\hat{\mathcal{A}}_k(\omega), \hat{\rho}_S\}\Big). \tag{2.81}$$

2.7 A note on fermions

A key step in the microscopic derivation of the Born–Markov master equation is expressing the system-bath interaction as

$$\hat{H}_{SE} = \sum_{\alpha} \hat{A}_{\alpha} \otimes \hat{B}_{\alpha}, \tag{2.82}$$

which assumes a tensor product structure between system and environment operators. While this formulation works naturally for bosonic systems or spins, it becomes problematic when applied to fermionic systems.

To see this, consider a simple model where a single fermionic mode, represented by the annihilation operator $\hat{c}$, is linearly coupled to a continuum of fermionic bath modes $\hat{b}_k$:

$$\hat{H}_{SE} = \sum_{k} \lambda_k\Big(\hat{c}^{\dagger}\hat{b}_k + \hat{b}^{\dagger}_k\hat{c}\Big) \tag{2.83}$$

$$= \hat{c}^{\dagger}\sum_{k} \lambda_k\hat{b}_k - \hat{c}\sum_{k} \lambda_k\hat{b}^{\dagger}_k. \tag{2.84}$$

Here, the minus sign in the second line arises due to the fermionic anti-commutation relations between $\hat{c}$ and $\hat{b}_k$. Crucially, this Hamiltonian is *not* of the form in Eq. (2.82), since fermionic operators do not admit a simple tensor product decomposition. That is,

$$\hat{c}^\dagger \hat{b}_k \neq \hat{c}^\dagger \otimes \hat{b}_k. \tag{2.85}$$

As a result, the standard microscopic derivation, such as the one outlined in Section 2.8, cannot be directly applied to fermionic systems in the second quantization language.

One approach to resolving this issue is to use the Jordan-Wigner transformation to map the fermionic operators onto spin operators, which exhibit a tensor product structure. After tracing out the environment and evaluating the bath correlation functions, the resulting master equation can be mapped back into the fermionic picture. As noted in Refs. [77, 82] this procedure yields the same result if one replaces the tensor product in Eq. (2.52) with an ordinary product between operators.

2.8 Example: microscopic derivation for a single fermionic mode

We now apply the general procedure to a concrete example: a single fermionic mode coupled to a fermionic thermal bath. We consider a system described by a single fermionic mode, with Hamiltonian

$$\hat{H}_S = \epsilon \hat{c}^\dagger \hat{c}, \tag{2.86}$$

where ϵ is the energy gap of the level. The system is coupled to a non-interacting fermionic environment via a linear interaction. The environment Hamiltonian and the interaction term are given by

$$\hat{H}_E = \sum_k \omega_k \hat{b}_k^\dagger \hat{b}_k \tag{2.87}$$

$$\hat{H}_{SE} = \sum_k \lambda_k \left(\hat{c}^\dagger \hat{b}_k + \hat{b}_k^\dagger \hat{c} \right) \tag{2.88}$$

The total Hamiltonian is then

$$\hat{H} = \hat{H}_S + \hat{H}_E + \hat{H}_{SE} \tag{2.89}$$

$$= \epsilon \hat{c}^\dagger \hat{c} + \sum_k \omega_k \hat{b}_k^\dagger \hat{b}_k + \sum_k \left(\lambda_k \hat{c}^\dagger b_k + \lambda_k^* \hat{b}_k^\dagger \hat{c} \right). \tag{2.90}$$

We assume the environment is initially in a thermal state at inverse temperature β:

$$\hat{\rho}_E \equiv \hat{\rho}_E(0) = \frac{1}{Z} e^{-\beta \hat{H}_E} \quad \text{with} \quad Z = \mathrm{Tr}\left[e^{-\beta \hat{H}_E} \right]. \tag{2.91}$$

For a non-interacting environment, the thermal averages of the bath operators satisfy

$$\begin{aligned}\langle \hat{b}_k \hat{b}_q \rangle &= \langle \hat{b}_k^\dagger \hat{b}_q^\dagger \rangle = 0 \\ \langle \hat{b}_k^\dagger \hat{b}_q \rangle &= f(\omega_k)\delta_{kq} \\ \langle \hat{b}_k \hat{b}_q^\dagger \rangle &= [1 - f(\omega_k)]\delta_{kq},\end{aligned} \tag{2.92}$$

where $f(\omega_k) = (1 + e^{-\beta\omega_k})^{-1}$ is the Fermi function. Following the prescription of Ref. [77], we decompose the interaction Hamiltonian into the form $\hat{H}_{SE} = \hat{A}_0\hat{B}_0 + \hat{A}_1\hat{B}_1$, where

$$\hat{A}_0 = \hat{c}, \quad \hat{A}_1 = \hat{c}^\dagger, \quad \hat{B}_0 = \sum_k \lambda_k \hat{b}_k^\dagger \quad \text{and} \quad \hat{B}_1 = -\sum_k \lambda_k \hat{b}_k. \tag{2.93}$$

As in the general case, we need to express these operators in the interaction picture with respect to the free Hamiltonian $\hat{H}_0 = \hat{H}_S + \hat{H}_E$. In this case, the system operators $\hat{A}_0 = \hat{c}$ and $\hat{A}_1 = \hat{c}^\dagger$ are already eigenoperators of $\hat{H}_S$, satisfying the required commutation relations:

$$[\hat{H}, \hat{c}] = -\epsilon\hat{c} \quad \text{and} \quad [\hat{H}, \hat{c}^\dagger] = \epsilon\hat{c}^\dagger \tag{2.94}$$

Therefore, using the BCH expansion, we find that

$$\tilde{c}(t) = e^{-i\epsilon t}\hat{c} \quad \text{and} \quad \tilde{c}^\dagger(t) = e^{i\epsilon t}\hat{c}^\dagger. \tag{2.95}$$

Similarly, since the environment is non-interacting, the bath operators evolve as

$$\tilde{B}_0(t) = \sum_k \lambda_k e^{i\omega_k t}\hat{b}_k^\dagger \quad \text{and} \quad \tilde{B}_1(t) = -\sum_k \lambda_k^* e^{-i\omega_k t}\hat{b}_k. \tag{2.96}$$

We will now compute the bath correlation functions. Using the thermal correlation relations in Eq. (2.92), we see that the off-diagonal bath correlation functions vanish:

$$\begin{aligned}g_{0,1}(\tau) &= \langle \tilde{B}_0^\dagger(\tau)\hat{B}_1 \rangle = 0, \\ g_{1,0}(\tau) &= \langle \tilde{B}_1^\dagger(\tau)\hat{B}_0 \rangle = 0,\end{aligned} \tag{2.97}$$

while the diagonal correlation functions read

$$g_{0,0}(\tau) = \sum_k |\lambda_k|^2 e^{-i\omega_k\tau}[1 - f(\omega_k)], \tag{2.98}$$

$$g_{1,1}(\tau) = \sum_k |\lambda_k|^2 e^{i\omega_k\tau} f(\omega_k). \tag{2.99}$$

As expected, the bath correlation functions decay exponentially with τ, supporting the Markov approximation.

The bath correlation functions can be expressed in terms of the *spectral density*, which is a central quantity in open quantum systems, defined as

$$\mathcal{J}(\omega) = 2\pi \sum_k |\lambda_k|^2 \delta(\omega - \omega_k). \tag{2.100}$$

This function quantifies the effective coupling strength between the system and the environment at each frequency ω. In this discrete form, $\mathcal{J}(\omega)$ corresponds to a series of Dirac

delta peaks located at frequencies ω_k—a so-called Dirac comb. However, in the continuum limit of the bath modes, it becomes a smooth function of ω and the sum can be replaced by an integral. With this definition, the bath correlation functions become

$$g_{0,0}(\tau) = \int \frac{\mathrm{d}\omega}{2\pi} e^{-i\omega\tau} \mathcal{J}(\omega)[1 - f(\omega)], \tag{2.101}$$

$$g_{1,1}(\tau) = \int \frac{\mathrm{d}\omega}{2\pi} e^{i\omega\tau} \mathcal{J}(\omega) f(\omega). \tag{2.102}$$

Note that due to the assumption that the environment is thermal, which gets rid of the non-diagonal elements in $g_{\alpha\beta}(\tau)$, the bath correlation functions are fully specified by $\mathcal{J}(\omega)$. According to the Eq. (2.61), which only required the Born approximation, the dynamics of the system is completely characterized by the knowledge of $g_{\alpha\beta}(\tau)$ and $\hat{H}_S$, which dictates how $\hat{A}_\alpha$ evolve in the interaction picture. Therefore, we conclude that, under the Born assumption, the spectral density fully characterizes the action of the environment on the system, even before the Markovian approximation (although the resulting master equation might be intractable).

Substituting the bath correlation functions in the Born–Markov master equation (2.63), we obtain

$$\begin{aligned} \frac{\mathrm{d}\tilde{\rho}_S}{\mathrm{d}t} &= \int_0^\infty \mathrm{d}\tau \left\{ e^{i\epsilon\tau} g_{0,0}(\tau)[\hat{c}\tilde{\rho}_S\hat{c}^\dagger - \hat{c}^\dagger\hat{c}\tilde{\rho}_S] + e^{-i\epsilon\tau} g_{1,1}(\tau)[\hat{c}^\dagger\tilde{\rho}_S\hat{c} - \hat{c}\hat{c}^\dagger\tilde{\rho}_S] \right\} + \text{h.c.} \\ &= \Gamma_{0,0}[\hat{c}\tilde{\rho}_S\hat{c}^\dagger - \hat{c}^\dagger\hat{c}\tilde{\rho}_S] + \Gamma_{1,1}[\hat{c}^\dagger\tilde{\rho}_S\hat{c} - \hat{c}\hat{c}^\dagger\tilde{\rho}_S] + \text{h.c.}, \end{aligned} \tag{2.103}$$

where we defined

$$\Gamma_{0,0} = \int_0^\infty \mathrm{d}\tau e^{-i\epsilon\tau} g_{0,0}(\tau) \quad \text{and} \quad \Gamma_{1,1} = \int_0^\infty \mathrm{d}\tau e^{i\epsilon\tau} g_{1,1}(\tau). \tag{2.104}$$

Since $\hat{A}_0$ and $\hat{A}_1$ are eigenoperators of $\hat{H}_S$, this equation is already in the form (2.68) and no further expansion is necessary. Consquently, there are no fast-oscillating terms, and the secular approximation is not required. Therefore, to obtain the Lindblad form, all we need is to add the Hermitian conjugate term and perform the integrals in τ. To do so, we split the complex coefficients $\Gamma_{0,0}$ and $\Gamma_{1,1}$ in real and imaginary parts:

$$\Gamma_{0,0} = \frac{1}{2}\gamma_- + i\Delta_0 \quad \text{and} \quad \Gamma_{1,1} = \frac{1}{2}\gamma_+ + i\Delta_1 \tag{2.105}$$

Finally, including the Hermitian conjugate in Eq. (2.103), we obtain

$$\frac{\mathrm{d}\tilde{\rho}_S}{\mathrm{d}t} = -i[\hat{H}_{LS}, \tilde{\rho}_S] + \gamma_- \mathbb{D}[\hat{c}](\hat{\rho}_S) + \gamma_+ \mathbb{D}[\hat{c}^\dagger](\hat{\rho}_S), \tag{2.106}$$

where the Lamb-Shift Hamiltonian is given by

$$\hat{H}_{LS} = \Delta_0 \hat{c}\hat{c}^\dagger + \Delta_1 \hat{c}^\dagger\hat{c} = (\Delta_1 - \Delta_0)\hat{c}^\dagger\hat{c} - \Delta_0. \tag{2.107}$$

To evaluate the rates and the Lamb-Shift term, we can use the identity [35]

$$\int_0^\infty \frac{\mathrm{d}\tau}{2\pi} e^{i(\epsilon-\omega)\tau} = \frac{1}{2}\delta(\epsilon-\omega) - \frac{i}{2}\mathcal{P}\frac{1}{\epsilon-\omega}, \tag{2.108}$$

where $\mathcal{P}$ denotes the Cauchy principal value. Using this identity in Eq. (2.104), we find

$$\begin{aligned}\Gamma_{0,0} &= \frac{1}{2}\mathcal{J}(\epsilon)[1-f(\epsilon)] - \frac{i}{2}\mathcal{P}\int \frac{\mathrm{d}\omega}{2\pi}\frac{\mathcal{J}(\omega)}{\epsilon-\omega},\\ \Gamma_{1,1} &= \frac{1}{2}\mathcal{J}(\epsilon)f(\epsilon) + \frac{i}{2}\mathcal{P}\int \frac{\mathrm{d}\omega}{2\pi}\frac{\mathcal{J}(\omega)}{\epsilon-\omega}.\end{aligned} \tag{2.109}$$

Therefore, by comparison with Eq. (2.105), we obtain

$$\gamma_- = \mathcal{J}(\epsilon)f(\epsilon) \quad \text{and} \quad \Delta_0 = -\frac{1}{2}\mathcal{P}\int \mathrm{d}\omega\,\frac{\mathcal{J}(\omega)}{\epsilon-\omega} \tag{2.110}$$

and similarly

$$\gamma_+ = \mathcal{J}(\epsilon)[1-f(\epsilon)] \quad \text{and} \quad \Delta_1 = \frac{1}{2}\mathcal{P}\int \frac{\mathrm{d}\omega}{2\pi}\frac{\mathcal{J}(\omega)}{\epsilon-\omega}. \tag{2.111}$$

The energy of the level is thus renormalized as

$$\epsilon' = \epsilon + \frac{1}{2}\mathcal{P}\int \mathrm{d}\omega\,\frac{\mathcal{J}(\omega)}{\epsilon-\omega}. \tag{2.112}$$

Again, we see that the rates can be directly computed from $\mathcal{J}(\omega)$, which shows that it completely characterizes the environment.

As an example, consider a spectral density that is constant in some frequency window $[-W, W]$ that contains ϵ:

$$\mathcal{J}(\omega) = \begin{cases}\Gamma, & \omega \in [-W, W]\\ 0, & \text{otherwise.}\end{cases} \tag{2.113}$$

In this case, the master equation in the Schrödinger picture takes the familiar form

$$\frac{\mathrm{d}\hat{\rho}_S}{\mathrm{d}t} = -i[\hat{H}_S, \hat{\rho}_S] + \Gamma[1-f(\epsilon)]\mathbb{D}[\hat{c}](\hat{\rho}_S) + \Gamma f(\epsilon)\mathbb{D}[\hat{c}^\dagger](\hat{\rho}_S). \tag{2.114}$$

2.9 Local vs global master equations: transport in a double quantum dot

To address the issue of local versus global master equations, we analyze transport in a chain of two coupled fermionic modes under both approaches. The system Hamiltonian is given by

$$\hat{H}_S = \epsilon_1\hat{c}_1^\dagger\hat{c}_1 + \epsilon_2\hat{c}_2^\dagger\hat{c}_2 + g\big(\hat{c}_1^\dagger\hat{c}_2 + \hat{c}_2^\dagger\hat{c}_1\big), \tag{2.115}$$

where $\epsilon_{1,2}$ are the on-site energies of each mode and g is the inter-mode coupling strength. Note that this Hamiltonian can be decomposed as $\hat{H}_S = \hat{H}_A + \hat{H}_B + \hat{H}_{AB}$, where $\hat{H}_A = \epsilon_1\hat{c}_1^\dagger\hat{c}_1$, $\hat{H}_B = \epsilon_2\hat{c}_2^\dagger\hat{c}_2$, and $\hat{H}_{AB} = g(\hat{c}_1^\dagger\hat{c}_2 + \hat{c}_2^\dagger\hat{c}_1)$. Additionally, each mode is coupled to an independent non-interacting fermionic environment.

The total Hamiltonian of the setup is

$$\hat{H} = \hat{H}_S + \sum_{\alpha=1,2} \big(\hat{H}_\alpha + \hat{H}_{S\alpha}\big), \tag{2.116}$$

with bath and interaction Hamiltonians defined as

$$\begin{aligned} \hat{H}_\alpha &= \sum_k \omega_{k\alpha} \hat{b}^\dagger_{k\alpha} \hat{b}_{k\alpha} \\ \hat{H}_{S\alpha} &= \sum_k \lambda_{k\alpha} \big(\hat{c}^\dagger_\alpha \hat{b}_{k\alpha} + \hat{b}^\dagger_{k\alpha} \hat{c}_\alpha\big). \end{aligned} \tag{2.117}$$

For the microscopic derivation, it is convenient to define a collective environment E, so that $\hat{H} = \hat{H}_S + \hat{H}_E + \hat{H}_{SE}$, where $\hat{H}_E = \sum_\alpha \hat{H}_\alpha$ and $\hat{H}_{SE} = \sum_\alpha \hat{H}_{S\alpha}$.

We assume each reservoir has a flat spectral density within a bandwidth:

$$\mathcal{J}_\alpha(\omega) = \begin{cases} \Gamma_\alpha, & \omega \in [-W, W] \\ 0, & \text{otherwise.} \end{cases} \tag{2.118}$$

We allow Γ_1 and Γ_2 to take arbitrary values, which enables us to selectively couple or decouple each mode from its respective bath.

We assume that, at $t = 0$, each environment is in a thermal state with inverse temperature β_α and that the global state is factorized:

$$\hat{\rho}(0) = \hat{\rho}_S(0) \otimes \hat{\rho}_{E_1} \otimes \hat{\rho}_{E_1}, \quad \text{with} \quad \hat{\rho}_{E_\alpha} = \frac{1}{Z_\alpha} e^{-\beta_\alpha \hat{H}_\alpha}. \tag{2.119}$$

Under this assumption, the initial two-point correlations for each bath satisfy:

$$\begin{aligned} \langle \hat{b}_{k\alpha} \hat{b}_{q\alpha} \rangle &= \langle \hat{b}^\dagger_{k\alpha} \hat{b}^\dagger_{k\alpha} \rangle = 0 \\ \langle \hat{b}^\dagger_{k\alpha} \hat{b}_{q\alpha} \rangle &= f(\omega_{k\alpha}) \delta_{kq} \\ \langle \hat{b}_{k\alpha} \hat{b}^\dagger_{q\alpha} \rangle &= [1 - f(\omega_{k\alpha})] \delta_{kq}. \end{aligned} \tag{2.120}$$

Furthermore, the factorized initial state ensures that inter-bath correlations vanish:

$$\langle \hat{b}_{k,1} \hat{b}_{k,2} \rangle = \langle \hat{b}^\dagger_{k,1} \hat{b}_{k,2} \rangle = \langle \hat{b}^\dagger_{k,2} \hat{b}_{k,1} \rangle = 0. \tag{2.121}$$

To proceed with the derivation, we rewrite the interaction Hamiltonian in the canonical form $\hat{H}_{SE} = \sum_i \hat{A}_i \hat{B}_i$. Grouping terms, we obtain

$$\begin{aligned} \hat{H}_{SE} &= \hat{c}^\dagger_1 \Big(\sum_k \lambda_{k,1} \hat{b}_{k,1} \Big) + \hat{c}_1 \Big(- \sum_k \lambda_{k,1} \hat{b}^\dagger_{k,1} \Big) + \hat{c}^\dagger_2 \Big(\sum_k \lambda_{k,2} \hat{b}_{k,2} \Big) + \hat{c}_2 \Big(- \sum_k \lambda_{k,2} \hat{b}^\dagger_{k,2} \Big) \\ &= \hat{A}^{(0)}_1 \hat{B}^{(1)}_1 + \hat{A}^{(1)}_1 \hat{B}^{(0)}_1 + \hat{A}^{(0)}_2 \hat{B}^{(1)}_2 + \hat{A}^{(1)}_2 \hat{B}^{(0)}_2. \end{aligned} \tag{2.122}$$

where we defined

$$\begin{aligned}
\hat{A}_1^{(0)} &= \hat{c}_1, \qquad \hat{B}_1^{(0)} = \sum_k \lambda_{k,1} \hat{b}_{k,1}, \\
\hat{A}_1^{(1)} &= \hat{c}_1^\dagger, \qquad \hat{B}_1^{(1)} = -\sum_k \lambda_{k,1} \hat{b}_{k,1}^\dagger \\
\hat{A}_2^{(0)} &= \hat{c}_2, \qquad \hat{B}_2^{(0)} = \sum_k \lambda_{k,2} \hat{b}_{k,2}, \\
\hat{A}_2^{(1)} &= \hat{c}_2^\dagger, \qquad \hat{B}_2^{(1)} = -\sum_k \lambda_{k,2} \hat{b}_{k,2}^\dagger.
\end{aligned} \tag{2.123}$$

Although the operators could be labeled with a single index, the use of double indices $\hat{A}\alpha^{(\sigma)}$ and $\hat{B}\alpha^{(\sigma)}$ proves more convenient for expressing general results. Here, the index α denotes the subsystem or bath, and σ indicates whether the operator is Hermitian-conjugated.

2.9.1 Local approach

The next step in our microscopic derivation involves expanding the system operators $\hat{A}_\alpha^{(\sigma)}$ in terms of eigenoperators of the system Hamiltonian and computing their evolution in the interaction picture. In the *local approach*, we neglect the coupling between the modes and instead expand $\hat{A}_\alpha^{(\sigma)}$ in terms of the eigenoperators of the local version of the Hamiltonian, $\hat{H}_S^{\text{local}} = \hat{H}_A + \hat{H}_B$. The time evolution in the interaction picture will be generated by $\hat{H}_S^{\text{local}}$, but the full system Hamiltonian $\hat{H}_S$ still contributes to a unitary term in the Schrödinger picture.

Since $\hat{H}_S^{\text{local}} = \epsilon_1 \hat{c}_1^\dagger \hat{c}_1 + \epsilon_2 \hat{c}_2^\dagger \hat{c}_2$ is already in diagonal form, the operators $\hat{c}_\alpha$ and $\hat{c}_\alpha^\dagger$ are its eigenoperators, satisfying

$$[\hat{H}_S^{\text{local}}, \hat{c}_\alpha] = -\epsilon_\alpha \hat{c}_\alpha \quad \text{and} \quad [\hat{H}_S^{\text{local}}, \hat{c}_\alpha^\dagger] = \epsilon_\alpha \hat{c}_\alpha^\dagger, \quad \alpha = 1, 2. \tag{2.124}$$

Therefore, as in the single-mode case, no additional expansion is needed, and the interaction-picture evolution is straightforward:

$$\tilde{c}_\alpha(t) = e^{-i\epsilon_\alpha t} \hat{c} \quad \text{and} \quad \tilde{c}_\alpha^\dagger(t) = e^{i\epsilon_\alpha t} \hat{c}^\dagger. \tag{2.125}$$

Additionally, since each bath is non-interacting, the bath operators evolve according to

$$\tilde{B}_\alpha^{(0)}(t) = \sum_k \lambda_{k\alpha} e^{i\omega_{k\alpha} t} \hat{b}_{k\alpha}^\dagger \quad \text{and} \quad \tilde{B}_\alpha^{(1)}(t) = -\sum_k \lambda_{k\alpha}^* e^{-i\omega_{k\alpha} t} \hat{b}_{k\alpha}. \tag{2.126}$$

Next, we calculate the bath correlation functions, defined as

$$g_{\alpha\beta}^{(\sigma,\sigma')}(\tau) = \langle \tilde{B}_\alpha^{(\sigma)}(t)^\dagger \hat{B}_\beta^{(\sigma')} \rangle. \tag{2.127}$$

Due to the assumption that the initial state is uncorrelated, correlation functions involving different baths vanish:

$$g_{\alpha\beta}^{(\sigma,\sigma')}(\tau) = 0 \quad \text{for} \quad \alpha \neq \beta. \tag{2.128}$$

For example,

$$\begin{aligned} g_{1,2}^{(0,0)}(\tau) &= \langle \tilde{B}_1^{(1)}(t)^\dagger \hat{B}_2^{(0)} \rangle \\ &= \sum_{kq} \lambda_{k,1}\lambda_{q,2} e^{i\omega_{k,1}\tau} \langle \hat{b}_{k,1}^\dagger \hat{b}_{q,2} \rangle \\ &= 0. \end{aligned} \tag{2.129}$$

Additionally, within each individual bath, only correlations with $\sigma = \sigma'$ survive, making the correlation matrix diagonal—mirroring the single-mode case discussed earlier. Consequently, the two baths act independently, and each generates its own dissipator. This leads to a master equation of the form

$$\frac{\mathrm{d}\tilde{\rho}_S}{\mathrm{d}t} = \sum_\alpha \left\{ \gamma_\alpha^- \mathbb{D}[\hat{c}_\alpha](\tilde{\rho}_S) + \gamma_\alpha^+ \mathbb{D}[\hat{c}_\alpha^\dagger](\tilde{\rho}_S) \right\}, \tag{2.130}$$

where the rates $\gamma_\alpha^\pm$ are obtained from the spectral densities as

$$\gamma_\alpha^+ = \mathcal{J}_\alpha(\epsilon) f_\alpha(\epsilon) \quad \text{and} \quad \gamma_\alpha^- = \mathcal{J}_\alpha(\epsilon)[1 - f_\alpha(\epsilon)], \tag{2.131}$$

with $f_\alpha(\epsilon) = (1 + e^{-\beta_\alpha \epsilon_\alpha})^{-1}$.

Finally, returning to the Schrödinger picture and restoring the full Hamiltonian $\hat{H}_S$, we arrive at

$$\frac{\mathrm{d}\hat{\rho}_S}{\mathrm{d}t} = -i[\hat{H}_S, \hat{\rho}_S] + \mathcal{D}_1(\hat{\rho}_S) + \mathcal{D}_2(\hat{\rho}_S), \tag{2.132}$$

where each dissipator is given explicitly by

$$\mathcal{D}_\alpha(\hat{\rho}_S) = \Gamma_\alpha f_\alpha(\epsilon) \mathbb{D}[\hat{c}_\alpha^\dagger] + \Gamma_\alpha [1 - f_\alpha(\epsilon)] \mathbb{D}[\hat{c}_\alpha]. \tag{2.133}$$

The Liouvillian in Eq. (2.132) is a simple example of a quadratic system, as it includes only terms up to second order in fermionic operators. In Chapter 4, we present a thorough discussion of such systems. In particular, we show that the steady state of Eq. (2.132) is completely characterized by the covariance matrix

$$C_{ji} = \langle \hat{c}_j^\dagger \hat{c}_i \rangle. \tag{2.134}$$

As detailed in Section 4.4.4, the steady-state covariance matrix can be obtained by solving a corresponding Lyapunov equation:

$$\boldsymbol{W}\boldsymbol{C}_{\mathrm{ss}} + \boldsymbol{C}_{\mathrm{ss}}\boldsymbol{W}^\dagger = \boldsymbol{F}, \tag{2.135}$$

where $\boldsymbol{W} = i\boldsymbol{H} + \boldsymbol{\Gamma}/2$. The matrices $\boldsymbol{H}$, $\boldsymbol{\Gamma}$ and$\boldsymbol{F}$ are given by

$$\boldsymbol{H} = \begin{pmatrix} \epsilon_1 & g \\ g & \epsilon_2 \end{pmatrix}, \quad \boldsymbol{\Gamma} = \begin{pmatrix} \Gamma_1 & 0 \\ 0 & \Gamma_2 \end{pmatrix}, \quad \boldsymbol{F} = \begin{pmatrix} f_1\Gamma_1 & 0 \\ 0 & f_2\Gamma_2 \end{pmatrix}. \tag{2.136}$$

Here, $\boldsymbol{H}$ is the single-particle Hamiltonian corresponding to $\hat{H}_S$.

Let us first consider the case where only the first mode is coupled to a reservoir, i.e., $\Gamma_1 = \Gamma$ and $\Gamma_2 = 0$. Solving the Lyapunov equation yields the steady-state covariance matrix:

$$\boldsymbol{C}_{\text{ss}} = \begin{pmatrix} f_1(\epsilon_1) & 0 \\ 0 & f_1(\epsilon_1) \end{pmatrix} \qquad [\Gamma_2 = 0]. \tag{2.137}$$

We observe that both modes acquire the same occupation $f_1(\epsilon_1)$, despite only one of them being directly coupled to a bath. This covariance matrix does not correspond to a thermal state, which would take the form

$$\boldsymbol{C}_\beta = (\mathbb{1} + e^{-\beta \boldsymbol{H}})^{-1}, \tag{2.138}$$

as discussed in Chapter 4. We thus conclude that the local bath fails to properly thermalize the system.

Next, we examine a non-equilibrium scenario in which both modes are coupled to reservoirs at different temperatures, setting $\Gamma_1 = \Gamma_2 = \Gamma$. To study transport in this setting, we consider the dynamics of the local occupations $n_i = \langle \hat{c}_i^\dagger \hat{c}_i \rangle$. From the master equation, we obtain the following continuity equations:

$$\begin{aligned} \frac{\mathrm{d}n_1}{\mathrm{d}t} &= -J_{1\to 2} + J_1^{\text{bath}}, \\ \frac{\mathrm{d}n_2}{\mathrm{d}t} &= +J_{1\to 2} + J_2^{\text{bath}}, \end{aligned} \tag{2.139}$$

where the edge currents J_α^{bath} describe the flow of particles between bath α and site α,

$$J_\alpha^{\text{bath}} = \mathrm{Tr}[\hat{c}_\alpha^\dagger \hat{c}_\alpha \mathcal{D}_\alpha(\hat{\rho})] = \Gamma(f_\alpha - n_\alpha). \tag{2.140}$$

and the bulk current $J_{1\to 2}$ accounts for coherent hopping between the two sites,

$$J_{1\to 2} = ig\langle \hat{c}_2^\dagger \hat{c}_1 - \hat{c}_1^\dagger \hat{c}_2 \rangle = 2g\,\mathrm{Im}\langle \hat{c}_2^\dagger \hat{c}_1 \rangle \tag{2.141}$$

In the steady state, both time derivatives vanish, so all the currents must coincide. We can then define a single steady-state current flowing through the system:

$$J_{\text{ss}} \equiv J_1^{\text{bath}} = J_{1\to 2} = -J_2^{\text{bath}}. \tag{2.142}$$

Solving the Lyapunov equation, we find the steady-state covariance matrix:

$$\boldsymbol{C}_{\text{ss}} = \frac{1}{4g^2 + \Gamma^2 + \Delta\epsilon^2} \begin{pmatrix} f_1(\Gamma^2 + \Delta\epsilon^2) + 2g^2(f_1 + f_2) & g\,\Delta f(\Delta\epsilon - i\Gamma) \\ g\,\Delta f(\Delta\epsilon + i\Gamma) & f_2(\Gamma^2 + \Delta\epsilon^2) + 2g^2(f_1 + f_2) \end{pmatrix}, \tag{2.143}$$

where $\Delta f = f_2 - f_1$ and $\Delta\epsilon = \epsilon_2 - \epsilon_1$. From this expression, the steady-state current is readily obtained:

$$J_{\text{ss}} = \frac{2\Gamma g\,\Delta f}{4g^2 + \Gamma^2 + \Delta\epsilon^2}. \tag{2.144}$$

This shows that the local master equation, despite failing to yield thermal equilibrium in the single-bath case, supports non-equilibrium steady states with finite currents, making it a useful tool for modeling quantum transport.

2.9.2 Global approach

In the global approach, the full system Hamiltonian $\hat{H}_S$ is retained throughout the microscopic derivation. Unlike the local case, the operators $\hat{c}_\alpha$ and $\hat{c}_\alpha^\dagger$ are no longer eigenoperators of $\hat{H}_S$, and must be expanded in terms of the true energy eigenmodes. Since the Hamiltonian is quadratic, this diagonalization can be performed analytically, as described in Chapter 4.

We begin by diagonalizing the single-particle Hamiltonian $\boldsymbol{H}$, which is a real symmetric 2×2 matrix. It can be diagonalized by an orthogonal transformation $\boldsymbol{S}$:

$$\boldsymbol{S}^\top \boldsymbol{H} \boldsymbol{S} = \begin{pmatrix} \Omega_1 & 0 \\ 0 & \Omega_2 \end{pmatrix}, \quad \text{with} \quad \boldsymbol{S} = \begin{pmatrix} \cos\theta & -\sin\theta \\ \sin\theta & \cos\theta \end{pmatrix}, \quad \tan\theta = \frac{2g}{\epsilon_2 - \epsilon_1}, \tag{2.145}$$

where the eigenvalues are given by

$$\Omega_{1,2} = \frac{1}{2}(\epsilon_1 + \epsilon_2) \pm \sqrt{4g^2 + (\epsilon_1 - \epsilon_2)^2}, \tag{2.146}$$

and $\boldsymbol{S}$ satisfies $\boldsymbol{S}\boldsymbol{S}^\top = \boldsymbol{S}^\top \boldsymbol{S} = \mathbb{1}$. The system Hamiltonian then takes the diagonal form

$$\hat{H}_S = \Omega_1 \hat{\eta}_1^\dagger \hat{\eta}_1 + \Omega_2 \hat{\eta}_2^\dagger \hat{\eta}_2, \tag{2.147}$$

where the energy eigenmodes are defined by

$$\hat{\eta}_1 = \cos\theta \hat{c}_1 + \sin\theta \hat{c}_2 \quad \text{and} \quad \hat{\eta}_2 = \sin\theta \hat{c}_1 - \cos\theta \hat{c}_2. \tag{2.148}$$

These new modes are eigenoperators of $\hat{H}_S$, since they satisfy the properties

$$[\hat{H}_S, \hat{\eta}_k] = \Omega_k \hat{\eta}_k \quad \text{and} \quad [\hat{H}_S, \hat{\eta}_k^\dagger] = -\Omega_k \hat{\eta}_k^\dagger, \quad k = 1, 2. \tag{2.149}$$

By inverting Eq. (2.148), we express $\hat{c}_\alpha$ in terms of eigenoperators and obtain their interaction-picture evolution:

$$\tilde{c}_\alpha(t) = \sum_{k=1}^{2} e^{-i\Omega_k t} S_{\alpha k} \hat{\eta}_k. \tag{2.150}$$

Substituting this into the general interaction-picture master equation [Eq. (2.68)], and using the fact that inter-bath correlation functions vanish, we find

$$\begin{aligned} \frac{\mathrm{d}\tilde{\rho}_S}{\mathrm{d}t} = &\sum_{k,q,\alpha} e^{i(\Omega_k - \Omega_q)t} S_{\alpha k} \Gamma_\alpha^-(\Omega_k) S_{\alpha q} \left[\hat{\eta}_k \tilde{\rho}_S \hat{\eta}_q^\dagger - \hat{\eta}_q^\dagger \hat{\eta}_k \tilde{\rho}_S\right] \\ &+ \sum_{k,q,\alpha} e^{i(\Omega_k - \Omega_q)t} S_{\alpha k} \Gamma_\alpha^+(\Omega_k) S_{\alpha q} \left[\hat{\eta}_k^\dagger \tilde{\rho}_S \hat{\eta}_q - \hat{\eta}_q \hat{\eta}_k^\dagger \tilde{\rho}_S\right] + \text{h.c.}, \end{aligned} \tag{2.151}$$

with frequency-dependent complex rates

$$\Gamma_\alpha^-(\Omega_k) = \int_0^\infty \mathrm{d}\tau e^{-i\Omega_k \tau} g_{\alpha\alpha}^{(0,0)}(\tau) \quad \text{and} \quad \Gamma_\alpha^+(\Omega_k) = \int_0^\infty \mathrm{d}\tau e^{i\Omega_k \tau} g_{\alpha\alpha}^{(1,1)}(\tau). \tag{2.152}$$

Applying the secular approximation, we retain only terms with $\Omega_k = \Omega_q$, yielding

$$\frac{\mathrm{d}\tilde{\rho}_S}{\mathrm{d}t} = \sum_{n,\alpha}(S_{\alpha n})^2\Gamma_\alpha^-(\Omega_n)\left[\hat{\eta}_n\hat{\rho}_S\hat{\eta}_n^\dagger - \hat{\eta}_n^\dagger\hat{\eta}_n\hat{\rho}_S\right] + \sum_{n,\alpha}(S_{\alpha n})\Gamma_\alpha^+(\Omega_n)\left[\hat{\eta}_n^\dagger\hat{\rho}_S\hat{\eta}_n - \hat{\eta}_n\hat{\eta}_n^\dagger\hat{\rho}_S\right] + \text{h.c.} \tag{2.153}$$

Finally, including the Hermitian conjugate term and neglecting the Lamb-Shift term, we obtain

$$\frac{\mathrm{d}\tilde{\rho}_S}{\mathrm{d}t} = \sum_{k,\alpha}\Big\{\gamma_{\alpha k}^+\mathbb{D}[\hat{\eta}_k^\dagger](\tilde{\rho}_S) + \gamma_{\alpha k}^-\mathbb{D}[\hat{\eta}_k](\tilde{\rho}_S)\Big\}, \tag{2.154}$$

where the rates are

$$\gamma_{\alpha k}^+ = (S_{\alpha k})^2\mathcal{J}_\alpha(\Omega_k)f_\alpha(\Omega_k), \quad \gamma_{\alpha k}^- = (S_{\alpha k})^2\mathcal{J}_\alpha(\Omega_k)[1 - f_\alpha(\Omega_k)]. \tag{2.155}$$

Transforming back to the Schrödinger picture and assuming flat spectral densities, we obtain the global master equation:

$$\frac{\mathrm{d}\hat{\rho}_S}{\mathrm{d}t} = -i[\hat{H}_S, \hat{\rho}_S] + \mathcal{D}_1(\hat{\rho}_S) + \mathcal{D}_2(\hat{\rho}_S), \tag{2.156}$$

where the dissipator corresponding to the first bath is

$$\begin{aligned}\mathcal{D}_1(\hat{\rho}_S) = \Gamma_1\cos^2\theta\{f_1(\Omega_1)\mathbb{D}[\hat{\eta}_1^\dagger] + [1 - f_1(\Omega_1)]\mathbb{D}[\hat{\eta}_1]\} \\ + \Gamma_1\sin^2\theta\Big\{f_1(\Omega_2)\mathbb{D}[\hat{\eta}_2^\dagger] + [1 - f_1(\Omega_2)]\mathbb{D}[\hat{\eta}_2]\Big\}\end{aligned} \tag{2.157}$$

and the dissipation corresponding to the second bath is given by

$$\begin{aligned}\mathcal{D}_2(\hat{\rho}_S) = \Gamma_2\sin^2\theta\{f_2(\Omega_1)\mathbb{D}[\hat{\eta}_1^\dagger] + [1 - f_2(\Omega_1)]\mathbb{D}[\hat{\eta}_1]\} \\ + \Gamma_2\cos^2\theta\Big\{f_2(\Omega_2)\mathbb{D}[\hat{\eta}_2^\dagger] + [1 - f_2(\Omega_2)]\mathbb{D}[\hat{\eta}_2]\Big\}.\end{aligned} \tag{2.158}$$

As in the local case, we first consider equilibrium by setting $\Gamma_2 = 0$ and $\beta_1 = \beta$, so only the dissipator $\mathcal{D}_1$ is active. Despite the local nature of the system-bath coupling, the dissipator acts globally on delocalized eigenmodes. Since $\hat{H}_S$ is diagonal in the $\hat{\eta}_k$ basis, each eigenmode evolves independently and thermalizes individually.

Thus, the steady-state covariance matrix in the energy eigenbasis, defined by $B_{kq} = \langle\hat{\eta}_q^\dagger\hat{\eta}_k\rangle$, becomes diagonal:

$$\boldsymbol{B} = \begin{pmatrix} f_1(\Omega_1) & 0 \\ 0 & f_1(\Omega_2)\end{pmatrix} \qquad [\Gamma_2 = 0]. \tag{2.159}$$

To find the covariance matrix in terms of the original fermionic modes $\hat{c}_1$ and $\hat{c}_2$, we rotate back using $\boldsymbol{S}$:

$$\boldsymbol{C} = \boldsymbol{S}(\mathbb{1} + e^{\beta\boldsymbol{\Omega}})^{-1}\boldsymbol{S}^\top \tag{2.160}$$

$$= (\mathbb{1} + e^{\beta\boldsymbol{S}\boldsymbol{\Omega}\boldsymbol{S}^\top})^{-1} \tag{2.161}$$

$$= (1 + e^{\beta\boldsymbol{H}})^{-1}. \tag{2.162}$$

This coincides exactly with the thermal covariance matrix of $\hat{H}_S$, confirming that the global master equation under the secular approximation yields the correct thermal equilibrium.

We now consider the non-equilibrium case, with two baths at different temperatures and symmetric coupling $\Gamma_1 = \Gamma_2 = \Gamma$. The equation of motion for each population now includes terms coming from both baths:

$$\begin{aligned} \frac{\mathrm{d}n_1}{\mathrm{d}t} &= -J_{1\to2} + \sum_{\alpha=1,2} \mathrm{Tr}[\hat{n}_1 \mathcal{D}_\alpha(\hat{\rho})], \\ \frac{\mathrm{d}n_2}{\mathrm{d}t} &= +J_{1\to2} + \sum_{\alpha=1,2} \mathrm{Tr}[\hat{n}_2 \mathcal{D}_\alpha(\hat{\rho})], \end{aligned} \tag{2.163}$$

Combining the dissipators from Eqs. (2.157) and (2.158), we obtain the total dissipator:

$$\mathcal{D}(\hat{\rho}_S) = \mathcal{D}_(_1(\hat{\rho}_S) + \mathcal{D}_(_2(\hat{\rho}_S) \tag{2.164}$$

$$= \Gamma\tilde{f}_1\mathbb{D}[\hat{\eta}_1^\dagger] + \Gamma(1-\tilde{f}_1)\mathbb{D}[\hat{\eta}_1] + \Gamma\tilde{f}_2\mathbb{D}[\hat{\eta}_2^\dagger] + \Gamma(1-\tilde{f}_2)\mathbb{D}[\hat{\eta}_2] \tag{2.165}$$

where we defined the effective occupations

$$\tilde{f}_1 = \cos^2\theta f_1(\Omega_1) + \sin^2\theta f_2(\Omega_1), \quad \tilde{f}_2 = \sin^2\theta f_1(\Omega_2) + \cos^2\theta f_2(\Omega_2). \tag{2.166}$$

As before, the dynamics of the energy modes remain uncoupled, and the total dissipator (2.164) can be interpreted as two fictitious baths with Fermi functions $\tilde{f}_1$ and $\tilde{f}_2$ acting individually on modes $\hat{\eta}_1$ and $\hat{\eta}_2$, respectively. Consequently, the steady-state covariance matrix in the energy eigenbasis remains diagonal:

$$\boldsymbol{B} = \begin{pmatrix} \tilde{f}_1 & 0 \\ 0 & \tilde{f}_2 \end{pmatrix}, \tag{2.167}$$

and the corresponding density matrix is diagonal in the energy eigenbasis:

$$\hat{\rho} = \bigotimes_k [f_k\,\hat{\eta}_k^\dagger\hat{\eta}_k + (1-f_k)(\hat{\mathbb{1}} - \hat{\eta}_k^\dagger\hat{\eta}_k)]. \tag{2.168}$$

A key implication is that, because $\langle \hat{\eta}_j^\dagger \hat{\eta}_k \rangle = 0$ for $j \neq k$, the current in the bulk of the chain vanishes:

$$\begin{aligned} J_{1\to 2} &= ig\langle \hat{c}_2^\dagger \hat{c}_1 - \hat{c}_1^\dagger \hat{c}_2 \rangle \\ &= ig\,\langle (\sin\theta\,\hat{\eta}_1^\dagger - \cos\theta\,\hat{\eta}_2^\dagger)(\cos\theta\,\hat{\eta}_1 + \sin\theta\,\hat{\eta}_2) - \text{h.c.} \rangle \\ &= ig\sin(2\theta)\,\langle \hat{\eta}_1^\dagger \hat{\eta}_2 - \hat{\eta}_2^\dagger \hat{\eta}_1 \rangle \\ &= 0 \end{aligned} \tag{2.169}$$

Therefore, although the dissipative contributions at each site are locally balanced—i.e., $\mathrm{Tr}[\hat{n}_i \mathcal{D}_1(\hat{\rho})] = \mathrm{Tr}[\hat{n}_i \mathcal{D}_2(\hat{\rho})]$—there is no coherent particle current flowing through the system.

Nevertheless, one can define a global current based on particle number conservation. Letting $\hat{N} = \hat{n}_1 + \hat{n}_2$, we write:

$$J = \mathrm{Tr}[\hat{N}\mathcal{D}_1(\hat{\rho})] = \Gamma(\tilde{f}_1 - \langle \hat{\eta}_1^\dagger \hat{\eta}_1 \rangle) + \Gamma(\tilde{f}_2 - \langle \hat{\eta}_2^\dagger \hat{\eta}_2 \rangle). \tag{2.170}$$

However, this current reflects the total particle exchange between the system and the reservoir and does not correspond to a locally conserved current flowing through the chain.

This observation is consistent with the general result of Ref. [83], which shows that the global master equation under the secular approximation always yields a steady state that is diagonal in the energy eigenbasis, even when the system is coupled to baths at different temperatures. As a result, no coherent steady-state current can be sustained within this framework.

In summary, both the local and global approaches offer limited descriptions of open quantum systems. The local approach, while numerically advantageous, fails to reproduce thermalization in equilibrium scenarios. Nevertheless, it naturally supports nonequilibrium steady states with finite currents, making it suitable for studying transport.

In contrast, the global approach correctly enforces thermalization in the case of a single bath. Yet, due to the secular approximation, the resulting steady states are diagonal in the energy eigenbasis, leading to the suppression of coherent currents.

These complementary limitations are some of the motivations of the mesoscopic leads approach, where the system is coupled to an auxiliary leads that are, in turn, damped by local Markovian baths. This hybrid method retains the numerical advantages of local Markovian master equations, while preserving the capability to sustain steady-state currents, offering a consistent and computationally efficient framework for quantum transport and thermodynamics.

3 Quantum thermodynamics

Thermodynamics is one of the most universal frameworks in physics, governing the flow of energy and entropy in systems across vastly different scales—from steam engines to black holes. Traditionally formulated for macroscopic systems, it provides a powerful description of energy exchanges through heat and work. Rooted in empirical laws, classical thermodynamics has been remarkably successful in predicting the behavior of thermal devices such as heat engines and refrigerators—regardless of the microscopic details of their working medium [84, 85].

However, with the advent of quantum technologies and the ability to isolate and control individual quantum systems, such as superconducting qubits, trapped ions and ultracold atoms, a natural question arises: How do thermodynamic laws manifest at the quantum scale?

Quantum thermodynamics is the field that seeks to answer this question by merging the principles of thermodynamics with the formalism of quantum mechanics [24, 23]. It aims to understand how thermodynamic concepts such as heat, work, and entropy emerge and behave in quantum systems, where phenomena like coherence, entanglement, and measurement backaction play a fundamental role.

One of the central challenges in quantum thermodynamics is to formulate consistent thermodynamic quantities in the strong coupling regime. When a system interacts strongly with its environment, the boundary between them becomes blurred, and assigning a clear meaning to quantities such as heat and internal energy becomes subtle. This challenge sparked an active area of research aimed at extending thermodynamic concepts beyond the weak coupling limit [86, 87, 88, 89]. Establishing consistent definitions in this regime remains an open problem and a central focus of ongoing efforts in the field.

In this chapter, we examine the challenge of defining thermodynamic quantities in quantum systems, particularly in the strong coupling regime. After introducing a general system-bath setup and the underlying assumptions, we discuss different approaches from the literature [90, 87], highlighting the ambiguities that arise at strong coupling. We then focus on one of such proposals, which we refer to as the global energy approach.

This chapter is structured as follows. In Section 1, we introduce a general microscopic description of open quantum systems, which serves as the foundation for our thermodynamic analysis. Section 2 focuses on the first law of thermodynamics and the definition of work and heat at the quantum level. In Section 3, we turn to the second law and discuss entropy production in quantum systems. Finally, in Section 4, we extend the framework to multiple baths and nonzero chemical potentials, allowing for the treatment of energy and particle currents.

◆

3.1 Setup: microscopic description of open quantum systems

The starting point for our discussion of thermodynamics is a microscopic description of open quantum systems—a global Hamiltonian describing system and environment. Specifically, we consider a composite system consisting of a finite-dimensional quantum system S interacting with an environment E. The dynamics of the total system is governed by a time-dependent Hamiltonian of the form

$$\hat{H}(t) = \hat{H}_S(t) + \hat{H}_E + \hat{H}_{SE}, \tag{3.1}$$

where $\hat{H}_S(t)$ is the Hamiltonian of the system, $\hat{H}_E$ is the Hamiltonian of the environment, and H_{SE} describes their interaction. Importantly, we assume that only $H_S(t)$ has an explicit time dependence, corresponding to an externally controlled driving protocol. Moreover, we assume that $[\hat{H}_E, \hat{N}_E] = 0$, where $\hat{N}_E$ is the particle number operator of the environment. These assumptions imply that all energy and particle changes in the environment are mediated through the system-bath couplings $\hat{H}_{SE}$.

The environment is assumed to be initially uncorrelated with the system and prepared in a thermal state at inverse temperature β

$$\hat{\rho}(0) = \hat{\rho}_S(0) \otimes \hat{\omega}_\beta, \quad \text{where} \quad \hat{\omega}_\beta = \frac{e^{-\beta \hat{H}_E}}{Z_E}, \tag{3.2}$$

and $Z_E = \mathrm{Tr}_E[e^{-\beta \hat{H}_E}]$ is the corresponding partition function.

For simplicity, we begin by considering the case of vanishing chemical potential, $\mu = 0$, where only energy is exchanged between system and environment. The generalization to multiple baths and nonzero chemical potentials will be addressed later in the chapter.

The total state $\hat{\rho}(t)$ evolves unitarily under the von Neumann equation,

$$\frac{\mathrm{d}}{\mathrm{d}t}\hat{\rho}(t) = -i[\hat{H}(t), \hat{\rho}(t)], \tag{3.3}$$

so that at time t the total state is

$$\hat{\rho}(t) = \hat{U}(t)\hat{\rho}(0)\hat{U}^\dagger(t), \quad \text{where} \quad \hat{U}(t) = \mathcal{T} \exp\left(-i \int_0^t \mathrm{d}t'\, \hat{H}(t')\right), \tag{3.4}$$

and $\mathcal{T}$ denotes time-ordering. From this total state, one obtains the reduced state of the system via partial tracing:

$$\hat{\rho}_S(t) = \mathrm{Tr}_E[\hat{\rho}(t)]. \tag{3.5}$$

This framework will serve as the foundation for the definitions of work, heat, internal energy, and entropy production.

3.2 First Law of Thermodynamics

With the system-bath framework in place, we now turn to the fundamental thermodynamic quantities: work, heat, internal energy, and entropy. Throughout this chapter, we focus on a thermodynamic description based on average quantities. That is, we consider average work and heat, without addressing fluctuations or trajectory-level formulations.

Work—Among these quantities, work is the most straightforward to define. Since the global system is isolated and does not participate in any heat exchange, any energy change must be attributed to work:

$$\dot{W}(t) \equiv \frac{\mathrm{d}}{\mathrm{d}t}\langle \hat{H}(t)\rangle, \tag{3.6}$$

where $\dot{W}(t)$ denotes the instantaneous work. Computing the derivative, we find

$$\frac{\mathrm{d}}{\mathrm{d}t}\langle \hat{H}(t)\rangle = \mathrm{Tr}\left[\frac{\mathrm{d}\hat{\rho}(t)}{\mathrm{d}t}\hat{H}(t)\right] + \mathrm{Tr}\left[\hat{\rho}(t)\frac{\mathrm{d}\hat{H}(t)}{\mathrm{d}t}\right]. \tag{3.7}$$

Since the total evolution is unitary, the first term vanishes. In our setting, only the system Hamiltonian $\hat{H}_S(t)$ varies with time, so that $\partial_t \hat{H} = \partial_t \hat{H}_S$. We are then left with

$$\dot{W}(t) = \mathrm{Tr}\left[\hat{\rho}_S(t)\frac{\mathrm{d}\hat{H}_S(t)}{\mathrm{d}t}\right], \tag{3.8}$$

where we used that $\mathrm{Tr}[\hat{\rho}\hat{H}_S] = \mathrm{Tr}_S[\hat{\rho}_S\hat{H}_S]$. The total work performed on the system up to time t is then

$$\begin{aligned} W(t) &= \langle \hat{H}(t)\rangle - \langle \hat{H}(0)\rangle \\ &= \int_0^t \mathrm{d}\tau\, \mathrm{Tr}\left[\hat{\rho}(\tau)\frac{\partial \hat{H}(\tau)}{\partial \tau}\right]. \end{aligned} \tag{3.9}$$

Therefore, the work associated with the external protocol can be interpreted as the work performed on the system alone.

Internal energy and heat—The definitions of internal energy and heat are more subtle, particularly in the presence of strong coupling. In thermodynamics, one way of defining heat is via the first law, as the component of energy exchange not accounted for by work. To understand the energy balance in our setup, let us examine the time evolution of the total average energy:

$$\frac{\mathrm{d}}{\mathrm{d}t}\langle \hat{H}(t)\rangle = \frac{\mathrm{d}}{\mathrm{d}t}\langle \hat{H}_S(t)\rangle + \frac{\mathrm{d}}{\mathrm{d}t}\langle \hat{H}_E\rangle + \frac{\mathrm{d}}{\mathrm{d}t}\langle \hat{H}_{SE}\rangle. \tag{3.10}$$

The interaction energy $\langle \hat{H}_{SE}(t)\rangle$ contributes to the total energy of the composite system, but it is unclear whether this term should be attributed to the system, the environment, or treated as a separate entity. Moreover, since $\hat{H}_{SE}$ acts on both Hilbert spaces, its expectation value cannot be computed from the reduced states $\hat{\rho}_S$ and $\hat{\rho}_E$ alone, as it may depend on the correlations. As a result, defining internal energy solely in terms of system observables becomes problematic.

This ambiguity disappears in the weak coupling regime, where the energy stored in the interaction becomes negligible:

$$\langle \hat{H} \rangle \approx \langle \hat{H}_S \rangle + \langle \hat{H}_E \rangle \qquad \textit{(weak coupling)}. \tag{3.11}$$

In that case, the internal energy can be identified unambiguously as

$$U(t) = \langle \hat{H}_S \rangle = \mathrm{Tr}_S \left[\hat{\rho}_S(t) \hat{H}_S(t) \right]. \tag{3.12}$$

Substituting into Eq. (3.10) and neglecting the contribution from $\hat{H}_{SE}$, we obtain

$$\dot{U}(t) = \dot{W}(t) - \frac{\mathrm{d}}{\mathrm{d}t} \langle \hat{H}_E \rangle, \tag{3.13}$$

where we used Eq. (3.8) for the work rate. This implies that the heat rate should be defined as

$$\dot{Q}(t) = -\frac{\mathrm{d}}{\mathrm{d}t} \langle \hat{H}_E \rangle, \tag{3.14}$$

which is aligned with the intuition: since $\hat{H}_E$ is time-independent, any change in the environment's energy must result from heat exchanges with the system.

Together, these definitions satisfy the first law of thermodynamics in differential form:

$$\frac{\mathrm{d}U(t)}{\mathrm{d}t} = \dot{W}(t) + \dot{Q}(t). \tag{3.15}$$

However, computing $\langle \hat{H}_E \rangle$ requires access to the full environment state, which is generally not experimentally accessible. To obtain an expression in terms of system observables alone, we take the derivative of $U(t)$:

$$\frac{\mathrm{d}\langle \hat{H}_S(t) \rangle}{\mathrm{d}t} = \mathrm{Tr}_S \left[\hat{\rho}_S(t) \frac{\mathrm{d}\hat{H}_S(t)}{\mathrm{d}t} \right] + \mathrm{Tr}_S \left[\frac{\mathrm{d}\hat{\rho}_S(t)}{\mathrm{d}t} \hat{H}_S(t) \right], \tag{3.16}$$

Comparing with Eq. (3.8), we identify the first term as work, so the second term must be attributed to heat. Therefore, in the weak coupling regime, the heat rate admits two equivalent expressions:

$$\dot{Q}(t) = -\frac{\mathrm{d}}{\mathrm{d}t} \langle \hat{H}_E \rangle = \mathrm{Tr}_S \left[\frac{\mathrm{d}\hat{\rho}_S(t)}{\mathrm{d}t} \hat{H}_S(t) \right], \tag{3.17}$$

with the second form having the advantage of being accessible through system operators alone. This approach yields a consistent thermodynamic description in the weak coupling limit, where the contribution of $\langle \hat{H}_{SE} \rangle$ can be safely ignored.

However, this clean separation breaks down in the strong coupling regime. When the interaction Hamiltonian $\hat{H}_{SE}$ is non-negligible, the splitting of total energy into system and environment contributions becomes ambiguous. The system may be strongly correlated with the environment, and the interaction energy $\langle \hat{H}_{SE} \rangle$ can no longer be ignored. Crucially, this quantity depends on the full system-environment state and cannot be reconstructed from the reduced states $\hat{\rho}_S(t)$ or $\hat{\rho}_E(t)$ alone. As a result, internal energy and heat can no longer

be defined purely in terms of system observables. Several alternative definitions have been proposed in the literature to ensure thermodynamic consistency in this regime [89].

One possible route—referred to here as the *bare Hamiltonian approach*—is to retain the weak-coupling definition and define the internal energy as

$$U^{\text{bare}}(t) = \langle \hat{H}_S(t) \rangle. \tag{3.18}$$

This choice is appealing for its simplicity. However, if heat is defined as the change in the energy of the environment [(3.14)], the first law is no longer satisfied. Substituting the definitions of internal energy and heat in the global energy balance [(3.10)] yields

$$\dot{U}^{\text{bare}}(t) = \dot{W}(t) + \dot{Q}(t) - \frac{\mathrm{d}}{\mathrm{d}t}\langle \hat{H}_{SE} \rangle, \tag{3.19}$$

which clearly violates the first law.

To restore consistency with the first law, one might instead define heat via the time derivative of the internal energy, as in Eq. (3.16), leading to

$$\dot{Q}^{\text{bare}}(t) = \mathrm{Tr}\left[\frac{\mathrm{d}\hat{\rho}_S(t)}{\mathrm{d}t} \hat{H}_S(t) \right]. \tag{3.20}$$

With this choice, the first law is automatically satisfied, provided work is defined via Eq. (3.8). However, from the global energy balance, it follows that

$$\dot{Q}^{\text{bare}}(t) = -\frac{\mathrm{d}}{\mathrm{d}t}\langle \hat{H}_E \rangle + \frac{\mathrm{d}}{\mathrm{d}t}\langle \hat{H}_{SE} \rangle, \tag{3.21}$$

indicating that this definition implicitly includes changes in the interaction energy into the heat flow. As a result, although the first law is satisfied, the physical interpretation of heat becomes ambiguous. Furthermore, as we will see in the next section, this definition can lead to apparent violations of the second law.

To address some of these ambiguities, particularly in equilibrium scenarios with strong coupling, an alternative framework has been proposed based on the Hamiltonian of Mean Force (HMF) [91, 89]. Here, we briefly outline the formalism and its main properties.

The HMF formalism is originally formulated under the assumption that the system Hamiltonian $\hat{H}_S$ is time-independent and that the global system—including the environment—reaches thermal equilibrium at long times:

$$\hat{\rho} \overset{t\to\infty}{\longrightarrow} \frac{e^{-\beta \hat{H}}}{Z}, \tag{3.22}$$

where $Z = \mathrm{Tr}[e^{-\beta \hat{H}}]$ is the global partition function. As discussed in Ref. [89], this assumption is expected to hold in the long-time limit under suitable conditions.

The central idea is to express the reduced equilibrium state as a thermal state with respect to an effective, temperature-dependent Hamiltonian $\hat{H}^*_S(\beta)$, known as the *Hamiltonian of mean force*:

$$\hat{\rho}_S = \frac{e^{-\beta \hat{H}^*_S(\beta)}}{Z^*_S(\beta)}. \tag{3.23}$$

where $Z_S^*(\beta) = \mathrm{Tr}_S[e^{-\beta\hat{H}^*(\beta)}]$ is the corresponding partition function. The operator $\hat{H}^*(\beta)$ is then implicitly defined by Eq. (3.23).

An explicit expression for the HMF can be obtained by tracing out the environment in the global equilibrium state (3.22) and equating the result with Eq. (3.23), leading to

$$\hat{H}_S^*(\beta) = -\frac{1}{\beta}\log\left(\frac{\mathrm{Tr}_E[e^{-\beta\hat{H}}]}{Z_E}\right) \tag{3.24}$$

where $Z_E = \mathrm{Tr}_E[e^{-\beta\hat{H}_E}]$. Although $\hat{H}_S^*(\beta)$ acts only on the system, it encapsulates the influence of both the environment and interaction on the system. Importantly, the HMF explicitly depends on the temperature.

Once $\hat{H}_S^*(\beta)$ is defined, all the thermodynamic quantities follow from the partition function using standard relations [84]. For example, the internal energy is defined via $U^*(\beta) = -\partial_\beta \log Z_S^*(\beta)$ [89]. The expressions obtained this way are thermodynamically consistent, reduce to the weak-coupling form in the appropriate limit, and correctly reproduce equilibrium properties.

Despite these appealing features, the HMF approach is not without limitations. Its definition relies on the global equilibrium state (3.22), and as such, it lacks a natural extension to nonequilibrium situations. In particular, there is no clear prescription for defining a time-dependent HMF during a general dynamical process. Moreover, because the HMF depends on temperature in a nontrivial way, the identification of thermodynamic quantities such as internal energy or heat becomes less transparent outside of equilibrium. These issues have been highlighted in previous work [92, 89, 88], which emphasize that, while the HMF provides a useful tool for strong-coupling equilibrium thermodynamics, it does not readily generalize to nonequilibrium processes.

The final approach we consider, which we adopt throughout the remainder of this chapter, will be referred to as the *global energy approach*. It defines the internal energy by explicitly including the interaction term:

$$U(t) = \langle\hat{H}_S(t)\rangle + \langle\hat{H}_{SE}(t)\rangle. \tag{3.25}$$

This choice is paired with the natural definition of heat as the change in the environment's energy:

$$\dot{Q}(t) = -\frac{\mathrm{d}}{\mathrm{d}t}\langle\hat{H}_E(t)\rangle. \tag{3.26}$$

With these definitions, the first law of thermodynamics is satisfied, as can be verified by substituting into the global energy balance equation (3.10).

It is important to emphasize, however, that the heat rate in this formulation cannot be expressed solely in terms of system observables. In particular,

$$\dot{Q}(t) = -\frac{\mathrm{d}}{\mathrm{d}t}\langle\hat{H}_E(t)\rangle \neq \mathrm{Tr}_S\left[\frac{\mathrm{d}\hat{\rho}_S(t)}{\mathrm{d}t}\hat{H}_S(t)\right], \tag{3.27}$$

which reflects the fact that the heat flow requires knowledge of the environment's energy. While this might appear to conflict with the goal of a thermodynamic description based solely on system observables—especially given that the environment's degrees of freedom

are generally inaccessible experimentally—we will show in later sections that all relevant thermodynamic quantities, including the heat rate, can be re-expressed in terms of the particle and energy currents, which are typically accessible. This resolves the apparent issue and ensures that the global energy approach remains both thermodynamically consistent and operationally meaningful.

3.3 Second Law of Thermodynamics

3.3.1 Classical Clausius inequality

With internal energy, work, and heat now defined, we turn to the second law of thermodynamics. To motivate our discussion, let us briefly recall one of its classical formulations. Consider a system in contact with a thermal reservoir at temperature T. According to the Clausius formulation, the second law states that the change in entropy of the system satisfies the inequality

$$\Delta S \geq \frac{Q}{T}, \tag{3.28}$$

where Q is the heat absorbed by the system, and equality holds only for reversible processes.

This bound naturally motivates the definition of the *entropy production* as

$$\Sigma = \Delta S - \frac{Q}{T}, \tag{3.29}$$

which quantifies the irreversibility of the process. The second law then takes the form

$$\Sigma \geq 0, \tag{3.30}$$

with $\Sigma = 0$ characterizing reversible transformations.

It is sometimes convenient to refer to the quantity $\Phi = Q/T$ as the *entropy flow*, representing the entropy change associated with reversible heat exchange. In this case, the second law can be expressed as

$$\Delta S = \Phi - \Sigma, \tag{3.31}$$

emphasizing that the system's entropy change can be decomposed into two contributions: one arising from heat exchange with the environment, and another from irreversible effects such as internal dissipation or correlation buildup.

3.3.2 Von Neumann and relative entropies

Motivated by this classical picture, we now seek to formulate the second law in the quantum regime. We begin by introducing the *von Neumann entropy*, the natural quantum generalization of the classical Shannon entropy. For a given state $\hat{\rho}$, it is defined as

$$S(\hat{\rho}) = -\operatorname{Tr}[\hat{\rho}\log\hat{\rho}] = -\sum_i p_i \log p_i, \tag{3.32}$$

where $p_i \geq 0$ are the eigenvalues of $\hat{\rho}$.

It will also be useful to introduce the *quantum relative entropy*, which plays a central role in quantum information and quantum thermodynamics. Given two density matrices $\hat{\rho}$ and $\hat{\sigma}$, it is defined as

$$D(\hat{\rho}\|\hat{\sigma}) = \mathrm{Tr}[\hat{\rho}\log\hat{\rho} - \hat{\rho}\log\hat{\sigma}], \tag{3.33}$$

and satisfies the non-negativity condition

$$D(\hat{\rho}\|\hat{\sigma}) \geq 0, \tag{3.34}$$

with equality if and only if $\hat{\rho} = \hat{\sigma}$ [93]. The relative entropy can be interpreted as a measure of distinguishability between quantum states. It will be key in our formulation of entropy production.

We also note the alternative form,

$$D(\hat{\rho}\|\hat{\sigma}) = -S(\hat{\rho}) - \mathrm{Tr}[\hat{\rho}\log\hat{\sigma}], \tag{3.35}$$

which will prove useful in later calculations.

Let us now recall some properties of the von Neumann and relative entropies. Consider a bipartite state $\hat{\rho}_{AB}$ with marginals $\hat{\rho}_A = \mathrm{Tr}_B\,\hat{\rho}_{AB}$ and $\hat{\rho}_B = \mathrm{Tr}_A\,\hat{\rho}_{AB}$. If the joint state is a product, $\hat{\rho}_{AB} = \hat{\rho}_A \otimes \hat{\rho}_B$, then the entropy is additive:

$$S(\hat{\rho}_A \otimes \hat{\rho}_B) = S(\hat{\rho}_A) + S(\hat{\rho}_B). \tag{3.36}$$

This follows from the identity

$$\log(\hat{\rho}_A \otimes \hat{\rho}_B) = \log\hat{\rho}_A \otimes \hat{\mathbb{1}}_B + \hat{\mathbb{1}}_A \otimes \log\hat{\rho}_B. \tag{3.37}$$

which, when substituted into the definition of entropy, yields:

$$\begin{aligned} S(\hat{\rho}_A \otimes \hat{\rho}_B) &= -\mathrm{Tr}[(\hat{\rho}_A \otimes \hat{\rho}_B)\log(\hat{\rho}_A \otimes \hat{\rho}_B)] \\ &= -\mathrm{Tr}[\hat{\rho}_A\log\hat{\rho}_A] - \mathrm{Tr}[\hat{\rho}_B\log\hat{\rho}_B] \\ &= S(\hat{\rho}_A) + S(\hat{\rho}_B). \end{aligned} \tag{3.38}$$

In the general case, where $\hat{\rho}_{AB}$ may be correlated, the entropy satisfies the subadditivity inequality:

$$S(\hat{\rho}_{AB}) \leq S(\hat{\rho}_A) + S(\hat{\rho}_B). \tag{3.39}$$

To see this, we will show that

$$D(\hat{\rho}_{AB}\|\hat{\rho}_A \otimes \hat{\rho}_B) = S(\hat{\rho}_A) + S(\hat{\rho}_B) - S(\hat{\rho}_{AB}) \geq 0, \tag{3.40}$$

where the inequality holds because relative entropy is non-negative. To verify this identity, we use the relation Eq. (3.35):

$$\begin{aligned} D(\hat{\rho}_{AB}\|\hat{\rho}_A \otimes \hat{\rho}_B) &= -\operatorname{Tr}[\hat{\rho}_{AB} \log(\hat{\rho}_A \otimes \hat{\rho}_B)] - S(\hat{\rho}_{AB}) \\ &= -\operatorname{Tr}[\hat{\rho}_{AB} \log \hat{\rho}_A] - \operatorname{Tr}[\hat{\rho}_{AB} \log \hat{\rho}_B] - S(\hat{\rho}_{AB}) \\ &= -\operatorname{Tr}_A[\hat{\rho}_A \log \hat{\rho}_A] - \operatorname{Tr}_B[\hat{\rho}_B \log \hat{\rho}_B] - S(\hat{\rho}_{AB}) \\ &= S(\hat{\rho}_A) + S(\hat{\rho}_B) - S(\hat{\rho}_{AB}), \end{aligned} \tag{3.41}$$

The subadditivity property motivates the definition of the *mutual information*:

$$I_{AB} = S(\hat{\rho}_A) + S(\hat{\rho}_B) - S(\hat{\rho}_{AB}) = D(\hat{\rho}_{AB}\|\hat{\rho}_A \otimes \hat{\rho}_B), \tag{3.42}$$

which quantifies the total (classical and quantum) correlations between subsystems A and B.

Second law in the quantum regime

Having established these formal properties, we now turn to the dynamics of entropy in our setup. The global state evolves unitarily according to $\hat{\rho}(t) = \hat{U}(t)\hat{\rho}(0)\hat{U}^\dagger(t)$. Since unitary evolution preserves the eigenvalues of the density matrix, the von Neumann entropy of the global state is conserved:

$$S(\hat{\rho}(t)) = S(\hat{\rho}(0)). \tag{3.43}$$

In contrast, the entropy of the reduced system, which we denote by

$$S(t) = -\operatorname{Tr}_S[\hat{\rho}_S(t) \log \hat{\rho}_S(t)], \tag{3.44}$$

generally evolves with time, since the reduced dynamics of $\hat{\rho}_S(t)$ is non-unitary.

Motivated by the classical second law, our aim is to derive a quantum analogue of the splitting $\Delta S = \Phi - \Sigma$. To this end, we follow the approach of Ref. [94], deriving this decomposition from first principles using the global conservation of entropy and the properties of the initial state.

To begin, recall that the system and environment are initially uncorrelated:

$$\hat{\rho}(0) = \hat{\rho}_S(0) \otimes \hat{\rho}_E(0), \tag{3.45}$$

with the environment prepared in a thermal state, $\hat{\rho}_E(0) = \hat{\omega}_\beta$. Since the von Neumann entropy is additive for product states, the initial global entropy is

$$S(\hat{\rho}(0)) = S(\hat{\rho}_S(0)) + S(\hat{\rho}_E(0)). \tag{3.46}$$

As the system and environment evolve, they typically become correlated, and this additivity no longer holds. However, using the definition of mutual information, the global entropy at time t can be expressed as

$$S(\hat{\rho}(t)) = S(\hat{\rho}_S(t)) + S(\hat{\rho}_E(t)) - I_{SE}(t). \tag{3.47}$$

Combining this with the conservation of global entropy,$S(\hat{\rho}(t)) = S(\hat{\rho}(0))$, we find

$$\Delta S = S(\hat{\rho}_E(0)) - S(\hat{\rho}_E(t)) + I_{SE}(t), \tag{3.48}$$

where $\Delta S = S(\hat{\rho}_S(t)) - S(\hat{\rho}_S(0))$ is the change in the system's entropy.

To evaluate the change in the environment's entropy, we first note that the initial entropy can be computed using the fact that $\hat{\rho}_E(0) = \hat{\omega}_\beta$ is a thermal state:

$$\log \hat{\omega}_\beta = -\beta \hat{H}_E - \log Z_E \quad \Rightarrow \quad S(\hat{\rho}_E(0)) = \beta \langle \hat{H}_E \rangle_0 + \log Z_E. \tag{3.49}$$

At later times, the environment is generally no longer thermal. Nevertheless, using Eq. (3.35), its entropy can be written as

$$\begin{aligned} S(\hat{\rho}_E(t)) &= -D(\hat{\rho}_E(t) \| \hat{\omega}_\beta) - \operatorname{Tr}\left[\hat{\rho}_E(t) \log \hat{\omega}_\beta\right] \\ &= -D(\hat{\rho}_E(t) \| \hat{\omega}_\beta) + \beta \langle \hat{H}_E \rangle_t + \log Z_E. \end{aligned} \tag{3.50}$$

Substituting this into Eq. (3.48), we obtain

$$\begin{aligned} \Delta S &= D(\hat{\rho}_E(t) \| \hat{\omega}_\beta) + I_{SE}(t) - \beta \left(\langle \hat{H}_E \rangle_t - \langle \hat{H}_E \rangle_0 \right) \\ &= \Sigma + \beta Q, \end{aligned} \tag{3.51}$$

where we identified the heat as

$$Q = \langle \hat{H}_E \rangle_t - \langle \hat{H}_E \rangle_0, \tag{3.52}$$

and defined the entropy production as

$$\Sigma = D(\hat{\rho}_E(t) \| \hat{\omega}_\beta) + I_{SE}(t) \geq 0, \tag{3.53}$$

with the inequality following from the non-negativity of both relative entropy and mutual information.

Therefore, the second law can be stated as

$$\Sigma = \Delta S - \beta Q \geq 0 \tag{3.54}$$

The decomposition of the entropy production in Eq. (3.53) provides an interesting interpretation of the sources of irreversibility in quantum thermodynamics. The term $D(\hat{\rho}_E(t) \| \hat{\omega}_\beta)$ quantifies how much the environment has deviated from its initial thermal equilibrium, while $I_{SE}(t)$ captures the total correlations generated between the system and its environment during the evolution.

The entropy production can also be expressed in a more compact and widely used form, which highlights a different physical interpretation. Specifically, Σ can be written as the relative entropy between the actual global state and the uncorrelated reference state $\hat{\rho}_S(t) \otimes \hat{\omega}_\beta$:

$$\Sigma = D(\hat{\rho}(t) \| \hat{\rho}_S(t) \otimes \hat{\omega}_\beta). \tag{3.55}$$

This expression emphasizes that irreversibility arises from how distinguishable the true joint state of the system and environment is from an idealized scenario where the two remain uncorrelated and the environment stays thermal.

To verify the equivalence with the earlier decomposition, we expand the relative entropy using Eq. (3.35):

$$\begin{aligned} D(\hat{\rho}(t)\|\hat{\rho}_S(t)\otimes\hat{\omega}_\beta) &= -S(\hat{\rho}(t)) - \mathrm{Tr}\big[\hat{\rho}(t)\log\big(\hat{\rho}_S(t)\otimes\hat{\omega}_\beta\big)\big] \\ &= -S(\hat{\rho}(t)) - \mathrm{Tr}_S[\hat{\rho}_S(t)\log\hat{\rho}_S(t)] - \mathrm{Tr}_E[\hat{\rho}_E(t)\log\hat{\omega}_\beta] \\ &= S(\hat{\rho}_S(t)) + S(\hat{\rho}_E(t)) - S(\hat{\rho}(t)) + D(\hat{\rho}_E(t)\|\hat{\omega}_\beta) - S(\hat{\rho}_E(t)) \\ &= I_{SE}(t) + D(\hat{\rho}_E(t)\|\hat{\omega}_\beta). \end{aligned} \tag{3.56}$$

This derivation confirms the equivalence between the two expressions for Σ.

3.3.3 Validity of the Global Energy Approach

The definitions of entropy production based on relative entropy play a central theoretical role. They offer a clear interpretation of the sources of irreversibility and provide a rigorous formulation of the second law. However, in practical applications it is often more convenient to use the expression

$$\Sigma = \Delta S - \beta Q, \tag{3.57}$$

especially in scenarios where the heat Q can be expressed in terms of currents. However, this formulation must be used with care, as it coincides with the relative entropy definition only when heat is defined as the energy lost by the environment, i.e.,

$$\dot{Q} = -\frac{\mathrm{d}}{\mathrm{d}t}\big\langle \hat{H}_E \big\rangle. \tag{3.58}$$

This condition is satisfied in the global energy approach, where internal energy includes both $\hat{H}_S$ and the interaction term $\hat{H}_{SE}$. As a result, the second law is guaranteed to hold:

$$\Sigma \geq 0. \tag{3.59}$$

In contrast, the bare Hamiltonian approach defines internal energy as $U^{\mathrm{bare}} = \big\langle \hat{H}_S \big\rangle$ and computes heat from the system alone:

$$\dot{Q}^{\mathrm{bare}} = \mathrm{Tr}\left[\frac{\mathrm{d}\hat{\rho}_S}{\mathrm{d}t}\hat{H}_S\right]. \tag{3.60}$$

Using the global energy balance, this quantity satisfies

$$\dot{Q}^{\mathrm{bare}} = -\frac{\mathrm{d}}{\mathrm{d}t}\big\langle \hat{H}_E \big\rangle + \frac{\mathrm{d}}{\mathrm{d}t}\big\langle \hat{H}_{SE} \big\rangle = \dot{Q} + \frac{\mathrm{d}}{\mathrm{d}t}\big\langle \hat{H}_{SE} \big\rangle. \tag{3.61}$$

Consequently, the corresponding entropy production is given by

$$\Sigma^{\mathrm{bare}} = \Sigma + \beta\frac{\mathrm{d}}{\mathrm{d}t}\big\langle \hat{H}_{SE} \big\rangle. \tag{3.62}$$

Because $\langle \hat{H}_{SE} \rangle$ may fluctuate—and even decrease—over time, the second term can be negative and outweigh Σ, leading to $\Sigma^{\text{bare}} < 0$.

This result highlights a key limitation of the bare Hamiltonian approach in the strong coupling regime. By defining heat using only the system's reduced dynamics, it overlooks the role of interaction energy, leading to potential violations of the second law. In contrast, the global energy approach explicitly includes the interaction term, ensuring consistency with both the first and second laws, even in the presence of strong coupling and system-environment correlations.

3.4 Generalized Setup: Multiple Baths, Chemical Potential and Currents

We consider now a generalization of the setup introduced earlier, in which the system is coupled to multiple reservoirs that are allowed to have a non-zero chemical potential. Each bath is labeled by the index α and is characterized by an inverse temperature β_α and chemical potential μ_α. The total Hamiltonian is taken to be of the form

$$\hat{H}(t) = \hat{H}_S(t) + \sum_\alpha \left(\hat{H}_\alpha + \hat{H}_{S\alpha} \right), \tag{3.63}$$

where $\hat{H}_S(t)$ is the (possibly time-dependent) Hamiltonian of the system, $\hat{H}_\alpha$ is the Hamiltonian of bath α and $H_{S\alpha}$ describes its interaction with the system.

We assume that the initial state of the full system is uncorrelated, with each reservoir prepared in a Gibbs state state. Explicitly, the initial state is

$$\hat{\rho}(0) = \hat{\rho}_S(0) \otimes \bigotimes_\alpha \hat{\omega}_\alpha, \quad \text{with} \quad \hat{\omega}_\alpha = \frac{e^{-\beta_\alpha(\hat{H}_\alpha - \mu_\alpha N_\alpha)}}{Z_\alpha}. \tag{3.64}$$

where $\hat{N}_\alpha$ is the particle number operator of bath α and $Z_\alpha = \text{Tr}[e^{-\beta_\alpha(\hat{H}_\alpha - \mu_\alpha \hat{N}_\alpha)}]$ is the corresponding partition function. Additionally, we assume that $[H_\alpha, N_\alpha] = 0$, ensuring that each bath preserves the number of particles in the absence of coupling.

Generalized Definitions of Work and Heat

The presence of reservoirs with nonzero chemical potentials introduces an additional contribution to the energy balance: chemical work. When reservoir α exchanges particles with the system, each particle transfer delivers an energy μ_α to it. The corresponding power input is given by

$$\dot{W}_{\text{chem}}(t) = -\sum_\alpha \mu_\alpha \frac{\mathrm{d}}{\mathrm{d}t} \langle \hat{N}_\alpha \rangle. \tag{3.65}$$

In addition to this term, the system may also be subject to external driving through a time-dependent Hamiltonian $\hat{H}_S(t)$. This is associated with mechanical work, defined as in the previous sections:

$$\dot{W}_{\text{mech}}(t) = \text{Tr}\left[\frac{dH_S(t)}{dt} \rho(t) \right]. \tag{3.66}$$

The total work performed on the system is then

$$\dot{W}(t) = \dot{W}_{\text{mech}}(t) + \dot{W}_{\text{chem}}(t). \tag{3.67}$$

The notion of heat must also be adapted to account for particle exchange. For each reservoir α, we define the heat flow into the system as the change in the reservoir's energy, excluding the contribution associated with particle transfer:

$$\dot{Q}_\alpha(t) = -\frac{\mathrm{d}}{\mathrm{d}t}\langle \hat{H}_\alpha \rangle - \mu_\alpha \frac{\mathrm{d}}{\mathrm{d}t}\langle \hat{N}_\alpha \rangle. \tag{3.68}$$

This definition can be understood as the rate of change of the expectation value of an effective Hamiltonian $\hat{H}_{\text{eff}} = \hat{H}_\alpha - \mu_\alpha \hat{N}_\alpha$, which explicitly corrects for the energy exchanged through particle transfer. The total heat flow is given by

$$\dot{Q}(t) = \sum_\alpha \dot{Q}_\alpha(t). \tag{3.69}$$

As before, we define the internal energy through the global energy approach, explicitly including the interaction term:

$$U(t) = \langle \hat{H}_S \rangle + \langle \hat{H}_{SE} \rangle. \tag{3.70}$$

With these definitions in place, the first law of thermodynamics retains its familiar structure:

$$\frac{dU(t)}{dt} = \dot{W}(t) + \dot{Q}(t). \tag{3.71}$$

3.4.1 Second law

The second law of thermodynamics admits a natural extension for the generalized setup. With the heat flow from each reservoir now defined to account for both energy and particle exchange, the entropy production over a process can be written as

$$\Sigma = \Delta S - \sum_\alpha \beta_\alpha Q_\alpha, \tag{3.72}$$

where ΔS is the change in the system's von Neumann entropy, and Q_α is the total heat received from reservoir α. This expression is fully consistent with the global energy approach and reflects the same physical content as the entropy balance derived earlier.

Indeed, the derivation proceeds in close analogy to that of Sec. 3.3, with the only modification being the use of a grand canonical thermal state for each environment. More precisely,

$$\log \hat{\omega}_\alpha = -\beta_\alpha \hat{H}_\alpha + \beta_\alpha \mu_\alpha \hat{N}_\alpha - \log Z_\alpha. \tag{3.73}$$

With this replacement, the argument follows as before, relying on the conservation of global entropy and the assumption of an initially factorized state.

The entropy production can equivalently be expressed as a quantum relative entropy,

$$\Sigma = D\left(\hat{\rho}(t) \,\middle\|\, \hat{\rho}_S(t) \otimes \bigotimes_\alpha \hat{\omega}_\alpha\right), \tag{3.74}$$

highlighting its interpretation as a measure of irreversibility arising from the buildup of system-environment correlations and deviations from equilibrium. This form ensures that $\Sigma \geq 0$ at all times, in agreement with the second law.

3.4.2 Particle and energy currents

While it is conceptually clear to define thermodynamic quantities via changes in the environment observables, this approach is not always practical from an operational or computational perspective. In many situations—especially in transport setups—it is more convenient to express thermodynamic quantities in terms of energy and particle *currents*. These currents not only provide an operational description of the thermodynamics but also connect directly to experimentally accessible quantities.

To define these currents, we consider the time evolution of observables in the Heisenberg picture, where an operator $\hat{\mathcal{O}}$ evolves according to

$$\frac{\mathrm{d}\hat{\mathcal{O}}}{\mathrm{d}t} = i[\hat{H}, \hat{\mathcal{O}}] \tag{3.75}$$

The energy current operator associated with bath α is then defined as

$$\hat{J}^E_\alpha(t) = -\frac{\mathrm{d}\hat{H}_\alpha}{\mathrm{d}t} = i[\hat{H}_\alpha, \hat{H}]. \tag{3.76}$$

Similarly, the particle current operator is defined as

$$\hat{J}^P_\alpha(t) = -\frac{\mathrm{d}\hat{N}_\alpha}{\mathrm{d}t} = i[\hat{N}_\alpha, \hat{H}]. \tag{3.77}$$

Under the assumptions that $[\hat{H}_\alpha, \hat{N}_\alpha] = 0$ and using $[\hat{H}_S, \hat{H}_E] = 0$, these expressions simplify to

$$\hat{J}^E_\alpha(t) = i[\hat{H}_\alpha, \hat{H}_{S\alpha}], \qquad \hat{J}^P_\alpha(t) = i[\hat{N}_\alpha, \hat{H}_{S\alpha}], \tag{3.78}$$

making explicit that the currents originate at the system-reservoir boundary.

The average energy and particle currents are obtained by taking the expectation value:

$$J^E_\alpha(t) = \mathrm{Tr}\big[\hat{\rho}(t)\hat{J}^E_\alpha(t)\big] = \langle \hat{J}^E_\alpha(t)\rangle \quad \text{and} \quad J^P_\alpha(t) = \mathrm{Tr}\big[\hat{\rho}(t)\hat{J}^P_\alpha(t)\big] = \langle \hat{J}^P_\alpha(t)\rangle. \tag{3.79}$$

The heat current from reservoir α is then defined as

$$J^Q_\alpha(t) = J^E_\alpha(t) - \mu_\alpha J^P_\alpha(t), \tag{3.80}$$

in direct correspondence with the definition introduced earlier. Total energy, particle, and heat currents are given by sums over reservoirs, e.g., $J^Q(t) = \sum_\alpha J^Q_\alpha(t)$.

In terms of these currents, the first law takes the form

$$\frac{\mathrm{d}U(t)}{\mathrm{d}t} = \dot{W}(t) + \sum_\alpha J^Q_\alpha(t), \tag{3.81}$$

where the total work rate is given by $\dot{W}(t) = \dot{W}_{\mathrm{mech}}(t) + \sum_\alpha \mu_\alpha J^P_\alpha(t)$.

To express the second law in terms of energy and particle currents, we rewrite it in differential form. Following standard convention, we define the *entropy production rate* as

$$\sigma(t) \equiv \dot{\Sigma}(t). \tag{3.82}$$

The second law then takes the compact form

$$\sigma(t) = \frac{\mathrm{d}S(t)}{\mathrm{d}t} - \sum_{\alpha} \beta_{\alpha} J_{\alpha}^{Q}(t). \tag{3.83}$$

Unlike the total entropy production $\Sigma(t)$, the entropy production rate $\sigma(t)$ can occasionally become negative. However, as discussed earlier, the integrated entropy production must satisfy

$$\Sigma(t) = \int_0^t \mathrm{d}\tau \sigma(\tau) \geq 0. \tag{3.84}$$

In the special case of Markovian dynamics—which requires the weak coupling assumption—it can be shown that the entropy production rate remains non-negative at all times [30]. We will focus on this regime in the following section.

A particularly important situation arises when a system coupled to multiple reservoirs reaches a *non-equilibrium steady state* (NESS). In this regime, the reduced state of the system becomes time-independent, so that $\frac{\mathrm{d}S(t)}{\mathrm{d}t} = 0$. Nevertheless, the system remains out of equilibrium, as steady-state currents continue to flow through it. In this case, the entropy production rate simplifies to

$$\sigma = \sum_{\alpha} \beta_{\alpha} J_{\alpha}^{Q}, \tag{3.85}$$

which is constant in time. As a result, the total entropy production grows linearly with time,

$$\Sigma(t) \sim \sigma t, \tag{3.86}$$

emphasizing that the currents required to maintain the NESS inevitably lead to continuous dissipation. This persistent entropy production is the hallmark of non-equilibrium steady states.

3.5 Example: Entropy Production in a Single Fermionic Mode

To illustrate the general formalism developed so far, we consider a minimal model that allows for transparent and complete thermodynamic analysis: a single fermionic mode coupled to a non-interacting fermionic reservoir. Our goals are to compute explicit expressions for energy and particle currents, analyze the entropy production decomposition, and demonstrate a second law violation under the bare Hamiltonian approach.

The total Hamiltonian is written in the standard form:

$$\hat{H}(t) = \hat{H}_S(t) + \hat{H}_E + \hat{H}_{SE}, \tag{3.87}$$

where the system Hamiltonian is

$$\hat{H}_S(t) = \epsilon(t)\hat{c}^\dagger\hat{c}, \tag{3.88}$$

and the bath Hamiltonian and interaction term are given by

$$\begin{aligned}\hat{H}_E &= \sum_k \omega_k \hat{b}_k^\dagger \hat{b}_k, \\ \hat{H}_{SE} &= \sum_k \lambda_k \left(\hat{c}^\dagger \hat{b}_k + \hat{b}_k^\dagger \hat{c}\right).\end{aligned} \tag{3.89}$$

Here, $\hat{c}$ and $\hat{b}_k$ are fermionic annihilation operators for the system and reservoir modes, respectively. The time-dependent parameter $\epsilon(t)$ controls the energy level of the system, while ω_k and λ_k denote the energies and coupling strengths of the reservoir modes.

As in previous sections, we assume that the system and reservoir are initially uncorrelated, with the environment prepared in a grand canonical Gibbs state:

$$\hat{\rho}(0) = \hat{\rho}_S \otimes \left[\frac{e^{-\beta(\hat{H}_E - \mu\hat{N}_E)}}{Z_E}\right], \tag{3.90}$$

where $Z_E = \mathrm{Tr}[e^{-\beta(\hat{H}_E - \mu\hat{N}_E)}]$.

3.5.1 Finite-Size Bath Approximation

To make the model numerically tractable, we approximate the fermionic reservoir using a finite number of modes N, chosen to reproduce a flat spectral density over a finite bandwidth [95]. Specifically, we assume a constant spectral density over the interval $[-W/2, W/2]$, given by

$$\mathcal{J}(\omega) = \begin{cases} \Gamma, & \omega \in [-\frac{W}{2}, \frac{W}{2}], \\ 0, & \text{otherwise.} \end{cases} \tag{3.91}$$

where Γ sets the overall coupling strength and W denotes the reservoir bandwidth.

The bath frequencies are sampled uniformly within this range as

$$\omega_k = (k-1)\Delta\omega - \frac{W}{2}, \quad \text{for} \quad k = 1, \ldots, N \tag{3.92}$$

where $\Delta\omega = W/(N-1)$ is the level spacing. The coupling strengths are then set to

$$\lambda_k = \sqrt{\frac{\Gamma\Delta\omega}{2\pi}}, \tag{3.93}$$

ensuring that the discretized reservoir reproduces the desired spectral density in the limit $N \to \infty$ [95]. With this choice, the couplings are frequency-independent, reflecting the assumption of a flat spectral density. A schematic representation of the setup is shown in Fig. 3.1

This finite-bath approximation captures the relevant short- and intermediate-time dynamics. However, due to the finite number of degrees of freedom, the system eventually exhibits Poincaré recurrences, leading to unphysical revivals. Consequently, this approach

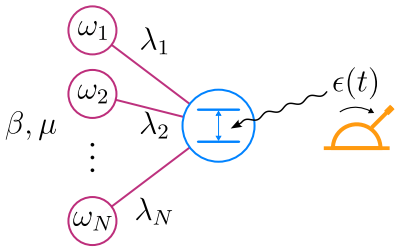

Figure 3.1: Schematic representation of a single fermionic mode interacting with a finite bath with N modes. The energy of the mode is controlled by a time-dependent protocol $\epsilon(t)$.

is valid only up to a finite time scale set by the number of modes N and the structure of the spectral density [31, 96, 97].

3.5.2 Time evolution

The system and environment considered here are both non-interacting, with a linear coupling between them. Consequently, the total Hamiltonian remains non-interacting. To see this explicit, we group the system and bath fermionic operators into a single vector:

$$\hat{\boldsymbol{d}} = (\hat{c}, \hat{b}_1, \hat{b}_2, \dots, \hat{b}_N), \tag{3.94}$$

so that the full Hamiltonian takes the compact form

$$\hat{H}(t) = \sum_{i,j} H_{ij}(t)\, \hat{d}_i^\dagger \hat{d}_j, \tag{3.95}$$

where $H_{ij}(t)$ denotes the elements of the single-particle Hamiltonian matrix. For the model introduced above, this matrix is given by

$$\boldsymbol{H}(t) = \begin{pmatrix} \epsilon(t) & \lambda_1 & \cdots & \lambda_N \\ \lambda_1 & \omega_1 & \cdots & 0 \\ \vdots & \vdots & \ddots & \vdots \\ \lambda_N & 0 & \cdots & \omega_N \end{pmatrix} \tag{3.96}$$

which is a Hermitian $(N+1) \times (N+1)$ matrix.

The Hamiltonian in Eq. (3.95) is quadratic in the modes $\hat{d}$, which implies that the dynamics is Gaussian-preserving. We discuss the theory of Gaussian systems in detail in Chapter 4. Here, we will simply use the relevant results. For a full treatment, we refer the reader to that chapter [4].

The key property of a Gaussian state is that is completely characterized by its two-point correlation functions. Accordingly, we define the covariance matrix

$$C_{ji} = \langle \hat{d}_j^\dagger \hat{c}_i \rangle, \tag{3.97}$$

which is a Hermitian $(N+1) \times (N+1)$ matrix that fully encodes the state of the system and environment.

Given that the reservoir is initially in a Gibbs state, the initial two-point correlations satisfy $\langle \hat{b}_k^\dagger \hat{b}_k \rangle = f(\omega_k)$, where $f(\omega) = (1+e^{\beta(\omega-\mu)})^{-1}$ is the Fermi-Dirac distribution. Therefore, the initial covariance matrix is diagonal:

$$\boldsymbol{C}(0) = \begin{pmatrix} n_0 & 0 & \cdots & 0 \\ 0 & f(\omega_1) & \cdots & 0 \\ \vdots & \vdots & \ddots & \vdots \\ 0 & 0 & \cdots & f(\omega_N), \end{pmatrix} \tag{3.98}$$

where $n_0 = \langle \hat{c}^\dagger \hat{c} \rangle_0$ is the initial occupation of the system mode.

The time evolution of the covariance matrix is then governed by the equation

$$\frac{\mathrm{d}\boldsymbol{C}(t)}{\mathrm{d}t} = -i[\boldsymbol{H}(t), \boldsymbol{C}(t)], \tag{3.99}$$

which closely resembles the von Neumann equation for an $(N+1)$-level system evolving under the single-particle Hamiltonian $\boldsymbol{H}(t)$. For further details, see Section 4.4.1 of Chapter 4.

Equation (3.99) can be integrated numerically using standard techniques, yielding the full time evolution of the covariance matrix and, consequently, of all physical observables.

3.5.3 Currents and Entropy Production: Numerical Results

The energy and particle currents can be computed using the definitions introduced earlier:

$$\hat{J}^P = i[\hat{N}_E, \hat{H}], \tag{3.100}$$

$$\hat{J}^E = i[\hat{H}_E, \hat{H}], \tag{3.101}$$

The explicit computation of these commutators involves a bit of algebra, which we carry out in detail in Chapter 4. The final result is

$$J^P(t) = \sum_k \lambda_k \left[\langle \hat{c}^\dagger \hat{b}_k \rangle - \langle \hat{b}_k^\dagger \hat{c} \rangle \right], \tag{3.102}$$

$$J^E(t) = \sum_k \lambda_k \omega_k \left[\langle \hat{c}^\dagger \hat{b}_k \rangle - \langle \hat{b}_k^\dagger \hat{c} \rangle \right], \tag{3.103}$$

which shows that both currents are encoded in the coherences of the covariance matrix.

These expressions have a clear physical interpretation. The term $\langle \hat{c}^\dagger \hat{b}_k \rangle$ corresponds to a particle transfer from bath mode k to the system, while $\langle \hat{b}_k^\dagger \hat{c} \rangle$ describes the reverse process. The total current reflects the net imbalance between these two processes, with each mode weighted by the corresponding tunneling rate λ_k. In the case of the energy current, the contributions are further weighted by the mode energies ω_k, accounting for the energy carried by each particle transfer.

The heat current is then defined as

$$J^Q(t) = J^E(t) - \mu J^P(t), \tag{3.104}$$

This is the quantity that enters the entropy balance and second law.

To compute the von Neumann entropy of the system, we draw on results from Chapter 4.

The von Neumann entropy of a Gaussian state can be computed directly from its covariance matrix. If ν_i are its eigenvalues, the entropy is given by

$$S = -\sum_i [\nu_i \log \nu_i + (1-\nu_i)\log(1-\nu_i)]. \tag{3.105}$$

The reduced covariance matrix of a subsystem is obtained by simply restricting the full covariance matrix $\boldsymbol{C}(t)$ to the corresponding rows and columns. In our case, the reduced covariance matrix is 1×1 and has eigenvalue $\nu = n(t)$, the mode occupation. The entropy therefore simplifies to

$$S(t) = -n(t)\log n(t) - (1-n(t))\log(1-n(t)). \tag{3.106}$$

In numerical simulations, the time derivative of the entropy is often computed using finite differences. However, in the single-mode case, $S(t)$ depends explicitly on the occupation number $n(t)$, allowing for an analytic expression. Since the total particle number is conserved, i.e., $[\hat{H}, \hat{N}_S + \hat{N}_E] = 0$, it follows that $\dot{n}(t) = -J^P(t)$. Substituting into the derivative of the entropy yields

$$\frac{\mathrm{d}S}{\mathrm{d}t} = -J^P(t)\log\left(\frac{n(t)}{1-n(t)}\right). \tag{3.107}$$

With the currents and entropy expressions in hand, the total entropy production reads

$$\Sigma(t) = \Delta S(t) - \beta Q(t). \tag{3.108}$$

Alternatively, as discussed in Sec. 3.3, the entropy production can be broken down into two components:

$$\Sigma(t) = D(\hat{\rho}_E(t) \,\|\, \hat{\rho}_E(0)) + I_{SE}(t), \tag{3.109}$$

where $I_{SE}(t)$ is the mutual information between system and environment.

Both $D_E(t)$ and $I_{SE}(t)$ can be computed efficiently from the covariance matrix using formulas provided in Section 7.2 of Chapter 4. This enables a numerical verification of the entropy production decomposition.

To illustrate the entropy dynamics, we consider a simple linear ramp protocol for the system energy level:

$$\epsilon(t) = \epsilon_0 + \alpha t. \tag{3.110}$$

We fix the overall energy scale by choosing $\Gamma = 1$, and discretize the reservoir with $N = 50$ modes. The bath is initialized at inverse temperature $\beta = 3$ and chemical potential $\mu = 1$. The protocol parameters are $\epsilon_0 = 0$ and $\alpha = 0.1$, corresponding to a slow drive that starts aligned with the chemical potential. To ensure the energy level remains well within the reservoir's frequency range throughout the evolution, we choose $W = 5$. The system is initially empty, with $n(0) = 0$.

As shown in Fig. 3.2(a), the entropy production rate $\sigma(t)$ can become temporarily negative due to system-bath coherences, a behavior allowed in the general non-Markovian regime. Nevertheless, the total entropy production $\Sigma(t)$ remains non-negative at all times, in accordance with the second law.

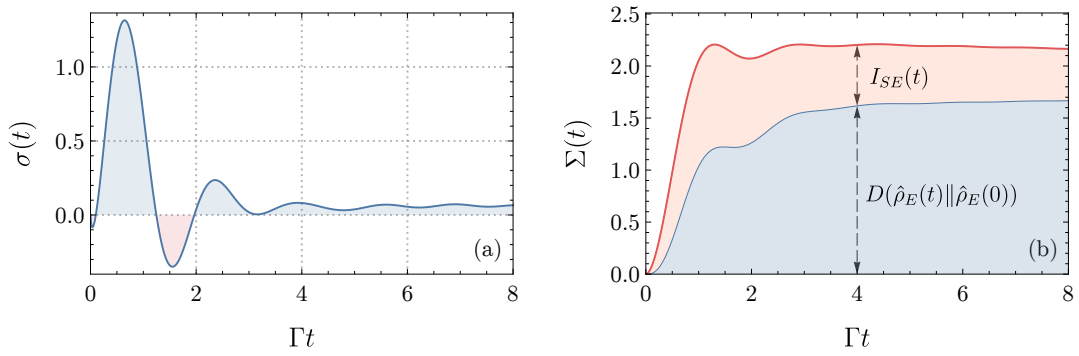

Figure 3.2: Entropy production and its decomposition for a driven single fermionic mode. (a) Entropy production rate $\sigma(t)$ as a function of time. Regions where $\sigma(t) > 0$ are shaded in blue, while regions where $\sigma(t) < 0$ are shaded in red. While $\sigma(t)$ can become temporarily negative due to non-Markovian effects, $\Sigma(t)$ remains non-negative, in accordance with the second law. (b) Total entropy production $\Sigma(t)$, decomposed into the relative entropy $D(\hat{\rho}_E(t)\|\hat{\rho}_E(0))$ and the mutual information $I_{SE}(t)$, as in Eq. (3.53). Both contributions are non-negative at all times, confirming the consistency of the decomposition. Simulation parameters: $\Gamma = 1$, $W = 5$,$N = 50$, $\beta = 3$, $\mu = 1$, $\epsilon_0 = 0$, $\alpha = 0.1$, and initial occupation $n(0) = 0$.

Figure 3.2(b) confirms the decomposition of $\Sigma(t)$ into the two non-negative contributions discussed in Eq. (3.53): the relative entropy $D(\hat{\rho}_E(t)\,\|\,\hat{\rho}_E(0))$ between the environment and its reference thermal state, and the mutual information $I_{SE}(t)$ between the system and environment. While neither term is guaranteed to increase monotonically, both contributions remain non-negative throughout the evolution.

3.5.4 Second law violation with the bare Hamiltonian approach

We now show that the bare Hamiltonian approach, introduced in Section 3.2, can lead to a violation of the second law of thermodynamics when applied beyond its regime of validity.

For simplicity, we consider a time-independent protocol $\epsilon(t) = \epsilon_0$ and set $\mu = 0$. In the bare Hamiltonian framework, the internal energy and heat rate are defined as

$$U^{\text{bare}}(t) = \mathrm{Tr}\left[\hat{\rho}_S(t)\hat{H}_S\right] \quad \text{and} \quad \dot{Q}^{\text{bare}}(t) = \mathrm{Tr}\left[\frac{\mathrm{d}\hat{\rho}_S}{\mathrm{d}t}\hat{H}_S\right], \tag{3.111}$$

which, by construction, satisfy the first law. However, as discussed in Section 3.2, the corresponding entropy production differs from the global definition. In particular, it obeys the relation

$$\Sigma^{\text{bare}}(t) = \Sigma(t) + \beta\Delta\langle\hat{H}_{SE}(t)\rangle, \tag{3.112}$$

which shows that a sufficiently negative change in the interaction energy $\langle\hat{H}_{SE}(t)\rangle$ can render $\Sigma^{\text{bare}}(t)$ negative—violating the second law.

To demonstrate this behavior, we carefully choose the initial conditions to emphasize the role of the interaction energy. We fix the parameters $\Gamma = 1$, $\beta = 3$, and $\mu = 0$, and set $\epsilon_0 = 1$. Since $\epsilon_0 \sim \Gamma$, this corresponds to a strong coupling regime. Crucially, the system is initialized with population

$$n_0 = \frac{1}{1 + e^{\beta(\epsilon_0 - \mu)}} \approx 0.0474, \tag{3.113}$$

which matches the equilibrium population set by the bath. If the system were decoupled from the reservoir, this choice would correspond to a thermal equilibrium configuration and the global state would remain stationary.

However, due to the strong system-reservoir coupling, the total initial state is not an equilibrium state of the full Hamiltonian. Although the dot population remains close to n_0 throughout the evolution, coherences between the system and the environment quickly develop. Importantly, these coherences induce significant fluctuations in the interaction energy $\langle \hat{H}_{SE}(t) \rangle$, even though the system's occupation barely changes.

This setting creates the ideal conditions for testing the bare Hamiltonian framework: while the population dynamics are essentially frozen, the neglected interaction energy dominates the evolution. As a result, the bare entropy production $\Sigma^{\text{bare}}(t)$ becomes negative throughout the process, as shown in Fig. 3.3. In contrast, the globally defined entropy production $\Sigma(t)$ remains strictly non-negative, in agreement with the second law.

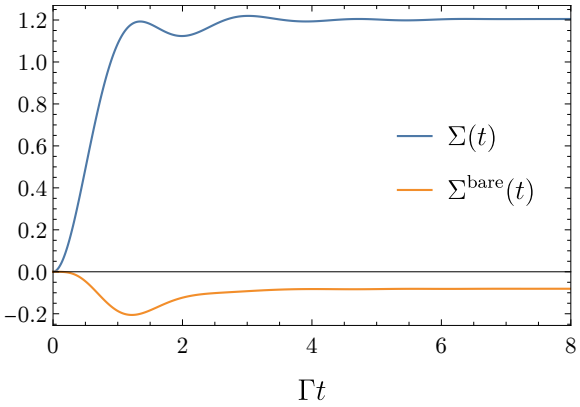

Figure 3.3: Comparison of the entropy production computed using the global and bare Hamiltonian approaches. The globally defined entropy production $\Sigma(t)$ (blue) remains non-negative throughout the evolution, consistent with the second law. In contrast, the bare entropy production $\Sigma^{\text{bare}}(t)$ (orange) becomes negative, demonstrating the failure of the bare approach in the strong coupling regime. Parameters: $\Gamma = 1$, $\beta = 3$, $\mu = 0$, $\epsilon_0 = 1$, and $n_0 = 1/(1 + e^{\beta\epsilon_0}) \approx 0.0474$.

This example highlights the importance of a consistent definition of heat in the application of the second law. In the strong coupling regime, where interaction energy plays a significant role, naively defining heat in terms of reduced system dynamics—such as in the bare Hamiltonian approach—can lead to apparent violations of fundamental thermodynamic principles.

3.6 Quantum Thermodynamics in the Markovian Regime

In this section, we study the thermodynamics of open quantum systems in the weak-coupling, Markovian regime. The dynamics of such systems are described by a Lindblad master equation, which constitutes a quantum dynamical semigroup. Within this setting, two theoretical frameworks are particularly significant: the formulation of the first law by Alicki [98], which connects the master equation to energy and particle currents, and Spohn's formulation of the second law [30], which provides a general expression for entropy production.

We consider a system with Hamiltonian $\hat{H}$ coupled to N reservoirs labeled by $\alpha = 1, \dots, N$. The dynamics of the system is described by a Lindblad master equation:

$$\frac{\mathrm{d}\hat{\rho}}{\mathrm{d}t} = \mathcal{L}(\hat{\rho}) \equiv -i[\hat{H}, \hat{\rho}] + \sum_{\alpha} \mathcal{D}_{\alpha}(\hat{\rho}), \tag{3.114}$$

where each dissipator $\mathcal{D}_{\alpha}$ models the effect of a single reservoir, characterized by an inverse temperature β_{α} and chemical potential μ_{α}. We define the partial generator

$$\mathcal{L}_{\alpha}(\hat{\rho}) \equiv -i[\hat{H}, \hat{\rho}] + \mathcal{D}_{\alpha}(\hat{\rho}), \tag{3.115}$$

which describes the dynamics under the effect of reservoir α alone.

We assume that each $\mathcal{L}_{\alpha}$ admits a thermal Gibbs state ω_{α} as a fixed point,

$$\mathcal{L}_{\alpha}(\hat{\omega}_{\alpha}) = 0, \tag{3.116}$$

with

$$\omega_{\alpha} = \frac{e^{-\beta_{\alpha}(\hat{H} - \mu_{\alpha}\hat{N})}}{Z_{\alpha}}, \quad \text{where} \quad Z_{\alpha} = \mathrm{Tr}\left[e^{-\beta_{\alpha}(\hat{H} - \mu_{\alpha}\hat{N})}\right] \tag{3.117}$$

and $\hat{N}$ is the system's particle number operator. We assume that $[\hat{H}, \hat{N}] = 0$, ensuring that changes in the average particle number occur only through particle exchange with the baths.

3.6.1 Alicki's Framework: Energy Balance and the First Law

In the Markovian regime, the first law of thermodynamics acquires a particularly transparent form. The effects of the environment are fully encoded in the dissipators, and interaction energy considerations no longer arise. Consequently, both particle and energy currents can be expressed solely in terms of system observables.

We begin by defining the internal energy of the system as

$$U(t) = \mathrm{Tr}\left[\rho(t)\hat{H}\right]. \tag{3.118}$$

To introduce the particle current, we consider the time derivative of the average particle number:

$$\begin{aligned} \frac{\mathrm{d}}{\mathrm{d}t}\langle \hat{N} \rangle &= \mathrm{Tr}\left[\frac{\mathrm{d}\hat{\rho}}{\mathrm{d}t}\hat{N}\right] && (3.119)\\ &= -i\,\mathrm{Tr}\left[\hat{\rho}[\hat{H}, \hat{N}]\right] + \sum_{\alpha} \mathrm{Tr}\left[\mathcal{D}_{\alpha}(\hat{\rho})\hat{N}\right] && (3.120)\\ &= \sum_{\alpha} \mathrm{Tr}\left[\hat{\rho}\,\mathcal{D}_{\alpha}^{\dagger}(\hat{N})\right], && (3.121) \end{aligned}$$

where we used that $[\hat{H}, \hat{N}] = 0$ and the definition of the dissipator $\mathcal{D}_{\alpha}^{\dagger}$, discussed in Chapter. 2.

This can be interpreted as a continuity equation, which motivates the definition of the particle current from reservoir α as

$$J_{\alpha}^{P} = \mathrm{Tr}\left[\hat{\rho}\,\mathcal{D}_{\alpha}^{\dagger}(\hat{N})\right], \tag{3.122}$$

representing the rate of particle exchange with this bath. Similarly, the energy current associated with bath α is defined as

$$J_\alpha^E = \mathrm{Tr}\left[\hat{\rho}\,\mathcal{D}_\alpha^\dagger(\hat{H})\right]. \tag{3.123}$$

The total particle and energy currents are obtained by summing over all contributions, yielding $J^P = \sum_\alpha J_\alpha^P$ and $J^E = \sum_\alpha J_\alpha^E$.

This brings us to the notion of work. While Alicki's original formulation [98] did not explicitly account for chemical potentials, it is natural to extend the framework by incorporating a chemical work contribution, as discussed in Section 3.2.

The mechanical work is associated with changes in the system Hamiltonian due to the external protocol,

$$\dot{W}_{\mathrm{mech}}(t) = \mathrm{Tr}\left[\hat{\rho}(t)\frac{\mathrm{d}\hat{H}}{\mathrm{d}t}\right], \tag{3.124}$$

whereas the chemical work accounts for the energy transferred through particle exchange:

$$\dot{W}_{\mathrm{chem}}(t) = \sum_\alpha \mu_\alpha J_\alpha^P. \tag{3.125}$$

The total power is then

$$\dot{W}(t) = \dot{W}_{\mathrm{mech}}(t) + \dot{W}_{\mathrm{chem}}(t). \tag{3.126}$$

To derive the first law, we consider the energy balance of the system. Differentiating Eq. (3.118) yields

$$\frac{\mathrm{d}U}{\mathrm{d}t} = \mathrm{Tr}\left[\rho(t)\frac{\mathrm{d}\hat{H}}{\mathrm{d}t}\right] + \mathrm{Tr}\left[\frac{\mathrm{d}\rho}{\mathrm{d}t}\hat{H}\right]. \tag{3.127}$$

The first term can be recognized as the mechanical work, while the second term corresponds to the total energy current:

$$\mathrm{Tr}\left[\frac{\mathrm{d}\rho}{\mathrm{d}t}\hat{H}\right] = \sum_\alpha \mathrm{Tr}\left[\mathcal{D}_\alpha(\hat{\rho})\hat{H}\right] = \sum_\alpha J_\alpha^E. \tag{3.128}$$

Therefore, we obtain the energy balance

$$\frac{\mathrm{d}U}{\mathrm{d}t} = \dot{W}_{\mathrm{mech}} + \sum_\alpha J_\alpha^E. \tag{3.129}$$

In this purely energetic formulation, the particle currents and chemical work do not appear explicitly. To connect with the conventional statement of the first law, we introduce the heat current associated with each bath as

$$J_\alpha^Q = J_\alpha^E - \mu_\alpha J_\alpha^P. \tag{3.130}$$

Substituting $J_\alpha^E = \mu_\alpha J_\alpha^P + J_\alpha^Q$ into the energy balance, we find

$$\frac{\mathrm{d}U}{\mathrm{d}t} = \dot{W}_{\mathrm{mech}}(t) + \sum_\alpha \mu_\alpha J_\alpha^P + \sum_\alpha J_\alpha^Q \tag{3.131}$$

$$= \dot{W}_{\mathrm{mech}}(t) + \dot{W}_{\mathrm{chem}}(t) + \sum_\alpha J_\alpha^Q \tag{3.132}$$

$$= \dot{W}(t) + \dot{Q}(t), \tag{3.133}$$

where we defined the total heat flow as

$$\dot{Q}(t) = \sum_\alpha J_\alpha^Q. \tag{3.134}$$

This completes the formulation of the first law in the Markovian regime. In the next section, we address the second law, which characterizes the irreversibility of the dynamics through the entropy production rate.

3.6.2 Spohn's framework: Entropy Production and the Second Law

In this section, we formulate the second law of thermodynamics for open quantum systems within the framework introduced by Spohn. The definition of entropy production in the quantum regime can sometimes lead to confusion, often due to subtle differences in conventions and formulations. However, in most cases, these differences are primarily semantic. To avoid any ambiguity, we will adopt a careful and systematic approach, explicitly analyzing different definitions and identifying the conditions under which they coincide.

Single bath case

For clarity, we begin by considering the simplest setting: a system coupled to a single reservoir, characterized by a temperature and chemical potential. This will allow us to establish the essential concepts before addressing the more complex case involving multiple reservoirs.

In this case, the master equation simplifies to

$$\frac{\mathrm{d}\hat{\rho}}{\mathrm{d}t} = \mathcal{L}(\hat{\rho}) = -i[\hat{H}, \hat{\rho}] + \mathcal{D}(\hat{\rho}) \tag{3.135}$$

where $\mathcal{D}$ models the coupling to a single environment characterized by an inverse temperature β and chemical potential μ. As before, we assume that the dynamics admits a Gibbs state as a stationary state,

$$\hat{\rho}_{\mathrm{ss}} = \frac{e^{-\beta(\hat{H}-\mu\hat{N})}}{Z}, \tag{3.136}$$

where $Z = \mathrm{Tr}\left[e^{-\beta(\hat{H}-\mu\hat{N})}\right]$ is the partition function.

As discussed in Chapter 2, the Liouvillian $\mathcal{L}$ is the generator of the dynamical map $\mathcal{V}_t = e^{t\mathcal{L}}$, which forms a quantum dynamical semigroup. That is, $\mathcal{V}_0 = \mathbb{1}$ and $\mathcal{V}_{t_1+t_2} = \mathcal{V}_{t_1}\mathcal{V}_{t_2}$, for all $t_1, t_2 \geq 0$.

In his seminal work [30], Spohn introduced the notion of *entropy production rate relative to the stationary state* for quantum dynamical semigroups. It is defined as

$$\sigma(t) = -\frac{\mathrm{d}}{\mathrm{d}t} D(\hat{\rho}(t) \| \hat{\rho}_{\mathrm{ss}}) \tag{3.137}$$

where $D(\rho\|\sigma)$ denotes the quantum relative entropy. As we will discuss shortly, $\sigma(t)$ is non-negative at all times.

In the single-reservoir case, it turns out that this definition coincides with the familiar thermodynamic expression

$$\sigma(t) = \frac{\mathrm{d}S(t)}{\mathrm{d}t} - \beta \dot{Q}(t), \tag{3.138}$$

where $S(t)$ is the von Neumann entropy of the system. To verify this, we compute the logarithm of the steady state, using the fact that it is a Gibbs state:

$$\log \hat{\rho}_{\mathrm{ss}} = -\beta(\hat{H} - \mu \hat{N}) - \log Z. \tag{3.139}$$

Substituting into the definition of the relative entropy yields

$$D(\hat{\rho}(t) \| \hat{\rho}_{\mathrm{ss}}) = -S(t) + \beta\Big(\mathrm{Tr}\left[\hat{\rho}(t)\hat{H}\right] - \mu\,\mathrm{Tr}\left[\hat{\rho}(t)\hat{N}\right]\Big) + \log Z, \tag{3.140}$$

thus

$$\begin{aligned} \sigma(t) &= -\frac{\mathrm{d}}{\mathrm{d}t} D(\hat{\rho}(t) \| \hat{\rho}_{\mathrm{ss}}) \\ &= \frac{\mathrm{d}S}{\mathrm{d}t} - \beta(J^E + \mu J^P) \\ &= \frac{\mathrm{d}S}{\mathrm{d}t} - \beta \dot{Q}, \end{aligned} \tag{3.141}$$

where we used the definitions of the particle and energy currents.

The non-negativity of the entropy production rate follows from a fundamental property of the quantum relative entropy: its monotonicity under completely positive trace-preserving (CPTP) maps. Specifically, for any CPTP map $\mathcal{E}$ and any pair of density matrices $\hat{\rho}$ and $\hat{\sigma}$, one has

$$D(\mathcal{E}\hat{\rho} \| \mathcal{E}\hat{\sigma}) \leq D(\hat{\rho} \| \hat{\sigma}), \tag{3.142}$$

as shown, for instance, in Refs. [99, 100, 101].

In our setting, the dynamics is generated by the quantum dynamical semigroup $\mathcal{V}_t = e^{t\mathcal{L}}$, and the steady state satisfies $\mathcal{V}_t(\hat{\rho}_{\mathrm{ss}}) = \hat{\rho}_{\mathrm{ss}}$ for all $t \geq 0$. Applying the monotonicity property with $\mathcal{E} = \mathcal{V}_\epsilon$, we obtain

$$D(\hat{\rho}(t+\epsilon) \| \hat{\rho}_{\mathrm{ss}}) \leq D(\hat{\rho}(t) \| \hat{\rho}_{\mathrm{ss}}). \tag{3.143}$$

Rearranging and dividing by ϵ, we find

$$\frac{D(\rho(t+\epsilon) \| \rho_{\mathrm{ss}}) - D(\hat{\rho}(t) \| \hat{\rho}_{\mathrm{ss}})}{\epsilon} \leq 0 \tag{3.144}$$

Thus, taking the limit $\epsilon \to 0$, we conclude that

$$\sigma(t) = -\frac{\mathrm{d}}{\mathrm{d}t} D(\hat{\rho}(t) \| \hat{\rho}_{\mathrm{ss}}) \geq 0, \tag{3.145}$$

as claimed.

It is important to emphasize that the non-negativity established here applies to the entropy production rate $\sigma(t)$ at each instant in time, not merely to its time-integrated value. This is a distinctive feature of Markovian dynamics. In contrast, non-Markovian dynamics can exhibit temporary negative entropy production rates.

The expression for the entropy production rate can be written in an alternative but equivalent form, known as *Spohn's inequality* [30]. Using the master equation $\dot{\hat{\rho}} = \mathcal{L}(\hat{\rho})$, we can write the entropy production rate as

$$\sigma(t) = -\operatorname{Tr}[\mathcal{L}(\hat{\rho}(t))(\log \hat{\rho}(t) - \log \hat{\rho}_{\mathrm{ss}})] \geq 0. \tag{3.146}$$

The unitary contribution vanishes due to the cyclic property of the trace, using the identity $\operatorname{Tr}[A[B, C]] = 0$. As a result, the same expression holds with $\mathcal{D}$ in place of $\mathcal{L}$:

$$\sigma(t) = -\operatorname{Tr}[\mathcal{D}(\hat{\rho}(t))(\log \hat{\rho}(t) - \log \hat{\rho}_{\mathrm{ss}})] \geq 0. \tag{3.147}$$

This quantity is non-negative at all times.

Entropy production as a free energy consumption rate

Before moving to the multiple-bath case, it is worth discussing an interesting thermodynamic interpretation of Spohn's entropy production rate in terms of free energy.

For a system in thermal equilibrium, the equilibrium free energy is defined as

$$F_{\mathrm{eq}}(\hat{\omega}_{\beta,\mu}) = \operatorname{Tr}\left[\hat{\omega}_{\beta,\mu}(\hat{H} - \mu\hat{N})\right] - \beta^{-1} S(\hat{\omega}_{\beta,\mu}), \tag{3.148}$$

where $\hat{\omega}_{\beta,\mu}$ is the corresponding Gibbs state.

For a general out-of-equilibrium state $\hat{\rho}(t)$, we define the non-equilibrium free energy as

$$F_{\mathrm{neq}}(\hat{\rho}(t)) = \operatorname{Tr}\left[\hat{\rho}(t)(\hat{H} - \mu\hat{N})\right] - \beta^{-1} S(\hat{\rho}(t)). \tag{3.149}$$

As shown in Eq. (3.139), the relative entropy with respect to a Gibbs state can be written as

$$\begin{aligned} D(\hat{\rho}(t) \| \hat{\omega}_{\beta,\mu}) &= \beta \left[\operatorname{Tr}\left[\hat{\rho}(t)(\hat{H} - \mu\hat{N})\right] - \beta^{-1} S(\hat{\rho}(t))\right] + \log Z \\ &= \beta F_{\mathrm{neq}}(\hat{\rho}(t)) + \log Z. \end{aligned} \tag{3.150}$$

On the other hand, since $\hat{\omega}_{\beta,\mu}$ is a Gibbs state,

$$\log Z = -\beta F_{\mathrm{eq}}(\hat{\omega}_{\beta,\mu}), \tag{3.151}$$

so we find

$$D(\hat{\rho}(t) \| \hat{\omega}_{\beta,\mu}) = \beta\left[F_{\mathrm{neq}}(\hat{\rho}(t)) - F_{\mathrm{eq}}(\hat{\omega}_{\beta,\mu})\right], \tag{3.152}$$

thereby interpreting the relative entropy as the excess free energy relative to equilibrium.

As a consequence, the entropy production rate admits a simple thermodynamic interpretation as the rate at which non-equilibrium free energy is dissipated:

$$\sigma(t) = -\beta \frac{\mathrm{d}F_{\mathrm{neq}}(t)}{\mathrm{d}t}, \tag{3.153}$$

where the factor β ensures that $\sigma(t)$ is dimensionless.

3.6.3 Multiple Reservoirs

We now generalize the previous analysis to the case where the system is coupled to multiple reservoirs. In this setting, the steady state $\hat{\rho}_{\mathrm{ss}}$ is in general no longer a Gibbs state. Nevertheless, one can still define the entropy production rate *relative to the steady state* as

$$\sigma_{\mathrm{Spohn}}(t) = -\frac{\mathrm{d}}{\mathrm{d}t} D(\hat{\rho}(t) \| \hat{\rho}_{\mathrm{ss}}), \tag{3.154}$$

which is guaranteed to be non-negative. This quantity will play a central role in our later discussion of the information geometry of nonequilibrium transitions.

However, this does not coincide in general with the *operational* definition of entropy production, which is determined by the heat flows exchanged with the reservoirs:

$$\sigma(t) = \frac{\mathrm{d}S(t)}{\mathrm{d}t} - \sum_{\alpha} \beta_{\alpha} J_{\alpha}^{Q}(t). \tag{3.155}$$

Here, the term operational is used in a non-standard but practical sense, referring to entropy production computed directly from currents. This convention is motivated by the fact that in the steady state, where $\mathrm{d}S/\mathrm{d}t = 0$, this quantity can be inferred from measurements, unlike the relative entropy, which requires full state tomography.

Fortunately, we can still prove that this operational entropy production rate is non-negative, using a generalization of Spohn's inequality that applies when multiple reservoirs are present.

We first note that the time derivative of the von Neumann entropy can be written as

$$\frac{\mathrm{d}S(t)}{\mathrm{d}t} = -\operatorname{Tr}\left[\frac{\mathrm{d}\hat{\rho}(t)}{\mathrm{d}t} \log \hat{\rho}(t)\right], \tag{3.156}$$

as shown in Appendix A.1. Using the master equation, we obtain

$$\frac{\mathrm{d}S(t)}{\mathrm{d}t} = -\sum_{\alpha} \operatorname{Tr}[\mathcal{D}_{\alpha}(\hat{\rho}) \log \hat{\rho}(t)]. \tag{3.157}$$

Each dissipator $\mathcal{D}_{\alpha}$ admits a Gibbs state $\hat{\omega}_{\alpha}$ as a fixed point. From the expression $\log \hat{\omega}_{\alpha} = -\beta_{\alpha}(\hat{H} - \mu_{\alpha}\hat{N}) - \log Z_{\alpha}$, we can similarly write the contribution from the heat flows as

$$\beta_{\alpha} J_{\alpha}^{Q} = -\operatorname{Tr}[\mathcal{D}_{\alpha}(\hat{\rho}) \log \hat{\omega}_{\alpha}]. \tag{3.158}$$

Combining these results, the entropy production rate becomes

$$\sigma(t) = \sum_{\alpha} \operatorname{Tr}[\mathcal{D}_{\alpha}(\hat{\rho})(\log \hat{\omega}_{\alpha} - \log \hat{\rho})]. \tag{3.159}$$

Using the identity $\mathrm{Tr}[A[B,C]] = 0$, each term remains unchanged if we replace $\mathcal{D}_\alpha$ by the partial generator $\mathcal{L}_\alpha = -i[\hat{H}, \cdot] + \mathcal{D}_\alpha$. Each contribution can thus be interpreted as the entropy production in the dynamics generated $\mathcal{L}_\alpha$. By Spohn's inequality, each term is non-negative. Therefore, we conclude that

$$\sigma(t) = \sum_\alpha \mathrm{Tr}[\mathcal{L}_\alpha(\hat{\rho})(\log \hat{\omega}_\alpha - \log \hat{\rho})] \geq 0, \tag{3.160}$$

thus establishing the non-negativity of the operational entropy production rate in the multiple-reservoir setting.

Part II

Gaussian Fermionic Systems

4 Gaussian fermionic systems

Gaussian states are a fundamental class of quantum systems that arise as ground and thermal states of non-interacting Hamiltonians. Their key property is that they are fully characterized by the two-point correlation functions of the creation and annihilation operators, which allows for a drastic simplification: instead of working with the exponentially large density matrix, one can describe Gaussian states using the covariance matrix, which scales only quadratically with system size. As a result, many problems involving Gaussian systems are analytically treatable, and numerical computations become significantly more efficient. A very common approach to deal with interacting systems, used extensively, for example, in optomechanics [102], is to perform a mean-field approximation that effectively renders the system Gaussian [102].

Beyond their computational advantages, Gaussian systems have great theoretical significance. Since spin chains can be mapped to fermionic systems via the Jordan–Wigner transformation, Gaussian fermionic states are very useful in quantum computation and condensed matter. This mapping has been widely used to study transport in non-interacting spin chains [103, 104, 105, 65]. Bosonic Gaussian states are equally important, as they form the backbone of quantum optics.

Here we focus specifically on fermionic systems. Fermionic Gaussian states have been extensively studied in the literature. A key reference is the seminal work by Bravyi [106], which lays much of the theoretical foundation for the study of these systems. Ref. [107] provides an introduction to numerical methods with Gaussian states. Quantum information with Gaussian states has also been widely explored. Notably, Peschel's formula [108] for the computation of the Von Neumann entropy using the covariance matrix, is a well-known result. However, when considering quantum information quantities that involve two states, such as the relative entropy or the trace distance, the results are less well-known, despite their presence in the literature [109, 110].

In this chapter, we provide a pedagogical introduction to fermionic Gaussian states, covering their fundamental properties, numerical methods and key quantum information quantities. These results will be essential in Chapter 5, when we discuss the mesoscopic leads approach applied to non-interacting systems.

◆

4.1 Quadratic Hamiltonians

Quadratic Hamiltonians play a fundamental role in the study of Gaussian states and will be central to our discussion. In this section, we introduce their formalism and establish the notation used throughout this chapter.

We consider a system of N fermionic modes described by the creation and annihilation operators $\{\hat{c}_i^\dagger\}_{i=1}^N$ and $\{\hat{c}_i\}_{i=1}^N$, which satisfy the *canonical anti-commutation relations*:

$$\{\hat{c}_i, \hat{c}_j^\dagger\} = \delta_{ij}\hat{\mathbb{1}}, \quad \{\hat{c}_i, \hat{c}_j\} = 0. \tag{4.1}$$

An important property of these operators is that a unitary transformation preserves the anti-commutation relations. To see this, consider the transformation $\hat{b}_k^\dagger = \sum_i U_{ij}\hat{c}_i^\dagger$, where $\boldsymbol{U}$ is an $N \times N$ unitary matrix, i.e., $\boldsymbol{U}^\dagger\boldsymbol{U} = \mathbb{1}$. We then have that

$$\begin{aligned}\{\hat{b}_k^\dagger, \hat{b}_q\} &= \sum_{ij} U_{ik}U_{jq}^*\{\hat{c}_i, \hat{c}_j^\dagger\} \\ &= \sum_i U_{ik}U_{iq}^* = \delta_{kq},\end{aligned} \tag{4.2}$$

where the last equality follows from the unitarity of $\boldsymbol{U}$.

A Hamiltonian is called *quadratic* (or non-interacting) if it contains only terms that are at most quadratic in the fermionic operators. While this definition, in principle, includes linear terms proportional to $\hat{c}_i^\dagger$ or $\hat{c}_i$, we focus exclusively on strictly quadratic Hamiltonians. The most general form of such a Hamiltonian is

$$\hat{H} = \sum_{ij}(A_{ij}\hat{c}_i^\dagger\hat{c}_j + B_{ij}\hat{c}_i\hat{c}_j^\dagger + C_{ij}\hat{c}_i\hat{c}_j + D_{ij}\hat{c}_i^\dagger\hat{c}_j^\dagger), \tag{4.3}$$

where $\boldsymbol{A}, \boldsymbol{B}, \boldsymbol{C}$, and $\boldsymbol{D}$ are $N \times N$ complex matrices.

This expression can be brought to a more convenient form without loss of generality. Requiring $\hat{H}$ to be Hermitian imposes the constraints $\boldsymbol{A} = \boldsymbol{A}^\dagger$, $\boldsymbol{B} = \boldsymbol{B}^\dagger$, and $\boldsymbol{C} = \boldsymbol{D}^\dagger$. Using these conditions along with Eq. (4.1), we can rewrite $\hat{H}$ in the symmetrized form:

$$\hat{H} = \sum_{ij}\left[(A_{ij} - B_{ji})\hat{c}_i^\dagger\hat{c}_j + \frac{1}{2}(D_{ij} - D_{ji})\hat{c}_i^\dagger\hat{c}_j^\dagger - \frac{1}{2}(D_{ij}^* - D_{ji}^*)\hat{c}_i\hat{c}_j\right] + \mathrm{tr}[\boldsymbol{B}]. \tag{4.4}$$

Disregarding the constant term and defining $\boldsymbol{H} = \boldsymbol{A} - \boldsymbol{B}$ and $\boldsymbol{G} = \boldsymbol{D} - \boldsymbol{D}^\top$, we see that the most generic quadratic Hamiltonian can be written as

$$\hat{H} = \sum_{ij}\left[H_{ij}\hat{c}_i^\dagger\hat{c}_j + \frac{1}{2}(G_{ij}\hat{c}_i^\dagger\hat{c}_j^\dagger - G_{ij}^*\hat{c}_i\hat{c}_j)\right], \tag{4.5}$$

where $\boldsymbol{H} \in \mathbb{C}^{N\times N}$ is Hermitian and $\boldsymbol{G} \in \mathbb{C}^{N\times N}$ is antisymmetric ($\boldsymbol{G} = -\boldsymbol{G}^\top$). The matrix $\boldsymbol{H}$ is known as the *single-particle Hamiltonian*, and should not be confused with the full many-body operator $\hat{H}$, which acts on the full Hilbert space. Here, we follow the notation of Refs. [111, 112].

In Eq. (4.5), the terms of the form $\hat{c}_i^\dagger\hat{c}_j$ preserve the total number of particles, since they commute with the total number operator $\hat{\mathcal{N}} = \sum_i \hat{c}_i^\dagger\hat{c}_i$, but the terms proportional $\hat{c}_i^\dagger\hat{c}_j^\dagger$ and $\hat{c}_i\hat{c}_j$ do not. The term $\hat{c}_i^\dagger\hat{c}_j^\dagger$ creates a pair of fermions, while $\hat{c}_i\hat{c}$ destroys a pair. For this reason, they are often referred to as *pairing* terms.

In what follows, we focus exclusively on Hamiltonians that conserve total particle number, i.e., those with $\boldsymbol{G} = 0$.

4.2 Diagonalization

The most general quadratic Hamiltonian that preserves the total particle number is obtained by setting $\boldsymbol{G} = 0$ in Eq. (4.5), yielding

$$\hat{H} = \sum_{ij} H_{ij} \hat{c}_i^\dagger \hat{c}_j. \tag{4.6}$$

Defining the column vector

$$\hat{\boldsymbol{c}} = \begin{pmatrix} \hat{c}_1 \\ \vdots \\ \hat{c}_N \end{pmatrix}, \tag{4.7}$$

we can express the Hamiltonian compactly as a quadratic form, $\hat{H} = \hat{\boldsymbol{c}}^\dagger \boldsymbol{H} \hat{\boldsymbol{c}}$.

The non-interacting nature of $\hat{H}$ allows it to be diagonalized by simply diagonalizing the single-particle Hamiltonian $\boldsymbol{H}$, whose dimension is exponentially smaller. To see this, suppose $\boldsymbol{H}$ admits the eigendecomposition

$$\boldsymbol{H} = \boldsymbol{S} \boldsymbol{\epsilon} \boldsymbol{S}^\dagger, \tag{4.8}$$

where $\boldsymbol{S}$ is unitary ($\boldsymbol{S}\boldsymbol{S}^\dagger = \mathbb{1}$) and $\boldsymbol{\epsilon} = \mathrm{diag}(\epsilon_1, \dots, \epsilon_N)$ contains the eigenvalues of $\boldsymbol{H}$. Using this decomposition, we rewrite the Hamiltonian as

$$\hat{H} = \hat{\boldsymbol{c}}^\dagger (\boldsymbol{S} \boldsymbol{\epsilon} \boldsymbol{S}^\dagger) \hat{\boldsymbol{c}} = (\boldsymbol{S}^\dagger \hat{\boldsymbol{c}})^\dagger \boldsymbol{\epsilon} (\boldsymbol{S}^\dagger \hat{\boldsymbol{c}}) = \hat{\boldsymbol{b}}^\dagger \boldsymbol{\epsilon} \hat{\boldsymbol{b}}, \tag{4.9}$$

where we defined the energy-basis fermionic modes

$$\hat{\boldsymbol{b}} = \boldsymbol{S}^\dagger \hat{\boldsymbol{c}}, \quad \text{or component-wise} \quad \hat{b}_k = \sum_i S_{ik}^* \hat{c}_i. \tag{4.10}$$

Since $\boldsymbol{S}$ is unitary, the new operators $\hat{\boldsymbol{b}}$ satisfy canonical anti-commutation relations. In terms of these new modes, the Hamiltonian takes the diagonal form

$$\hat{H} = \sum_k \epsilon_k \hat{b}_k^\dagger \hat{b}_k, \tag{4.11}$$

showing that a quadratic Hamiltonian is equivalent to a free-fermion system in a rotated basis.

The eigenvalues and eigenstates of the full many-body Hamiltonian $\hat{H}$ follow directly from this diagonal form. The eigenstates are number states in the $\hat{b}_k$ basis:

$$|E_{\boldsymbol{n}}\rangle = \prod_{k=1}^{N} (\hat{b}_k^\dagger)^{n_k} |0\rangle \qquad n_k \in \{0, 1\}, \tag{4.12}$$

where $\boldsymbol{n} = (n_1, \dots, n_N)$ denotes the fermionic occupation profile in the energy basis, with $n_k = \langle \hat{b}_k^\dagger \hat{b}_k \rangle$. The corresponding eigenvalues are

$$E_{\boldsymbol{n}} = \sum_k \epsilon_k n_k. \tag{4.13}$$

4.2.1 Canonical Transformations

The eigenstates $|E_{\boldsymbol{n}}\rangle$ obtained in the previous section form a complete basis of the Fock space. Thus, they must be related to the original number basis $|\boldsymbol{n}\rangle$ by a unitary transformation:

$$|E_{\boldsymbol{n}}\rangle = \hat{\mathcal{S}}|\boldsymbol{n}\rangle. \tag{4.14}$$

In this new basis, the Hamiltonian is given by $\hat{\mathcal{S}}^\dagger \hat{H} \hat{\mathcal{S}}$ and, as previously discussed, is diagonal:

$$\hat{\mathcal{S}}^\dagger(\hat{\boldsymbol{c}}^\dagger \boldsymbol{H} \hat{\boldsymbol{c}})\hat{\mathcal{S}} = (\boldsymbol{S}^\dagger \hat{\boldsymbol{c}})^\dagger \boldsymbol{\epsilon} (\boldsymbol{S}^\dagger \hat{\boldsymbol{c}}) = \hat{\boldsymbol{b}}^\dagger \boldsymbol{\epsilon} \hat{\boldsymbol{b}}. \tag{4.15}$$

This implies that $\hat{\mathcal{S}}$ acts on the fermionic operators as

$$\hat{\mathcal{S}}^\dagger \hat{\boldsymbol{c}}\, \hat{\mathcal{S}} = \boldsymbol{S}^\dagger \hat{\boldsymbol{c}}, \quad \text{and} \quad \hat{\mathcal{S}}^\dagger \hat{\boldsymbol{c}}^\dagger\, \hat{\mathcal{S}} = \hat{\boldsymbol{c}}^\dagger \boldsymbol{S}. \tag{4.16}$$

In other words, the unitary $\hat{\mathcal{S}}$ acting on the many-body Hilbert space implements the linear transformation $\hat{\boldsymbol{c}} \mapsto \boldsymbol{S}^\dagger \hat{\boldsymbol{c}}$ derived from the single-particle basis change.

This is an instance of a more general and foundational result in the theory of quadratic fermionic systems: *any* unitary transformation of the form

$$\hat{\boldsymbol{c}} \mapsto \boldsymbol{S}^\dagger \hat{\boldsymbol{c}}, \qquad \text{with} \quad \boldsymbol{S}^\dagger \boldsymbol{S} = \mathbb{1}, \tag{4.17}$$

can be implemented by a unitary operator $\hat{\mathcal{S}}$ acting on the Fock space, which is generated by a quadratic, Hermitian operator:

$$\hat{\mathcal{S}} = e^{-i\hat{K}}, \qquad \text{with} \quad \hat{K} = \hat{\boldsymbol{c}}^\dagger \boldsymbol{K} \hat{\boldsymbol{c}}, \tag{4.18}$$

where $\boldsymbol{K} \in \mathbb{C}^{N\times N}$ is Hermitian and satisfies $\boldsymbol{S} = e^{-i\boldsymbol{K}}$ [106, 113].

Note that, since $\boldsymbol{S}$ is unitary, it can always be written as $\boldsymbol{S} = e^{-i\boldsymbol{K}}$ for some Hermitian matrix $\boldsymbol{K}$. The operator $\hat{\mathcal{S}}$ then implements the transformation

$$\hat{\mathcal{S}}^\dagger \hat{\boldsymbol{c}}\, \hat{\mathcal{S}} = \boldsymbol{S}^\dagger \hat{\boldsymbol{c}} \quad \text{that is,} \quad e^{i\hat{\boldsymbol{c}}^\dagger \boldsymbol{K} \hat{\boldsymbol{c}}}\, \hat{\boldsymbol{c}}\, e^{-i\hat{\boldsymbol{c}}^\dagger \boldsymbol{K} \hat{\boldsymbol{c}}} = e^{-i\boldsymbol{K}} \hat{\boldsymbol{c}}. \tag{4.19}$$

We now present a proof of this result, following an argument adapted from Ref. [113]. We will use the Baker-Campbell-Hausdorff (BCH) formula:

$$e^{\hat{A}} \hat{B} e^{-\hat{A}} = \sum_{n=0}^{\infty} \frac{1}{n!} \hat{C}_n, \quad \text{with} \quad \hat{C}_0 = \hat{B}, \quad \hat{C}_n = [\hat{A}, \hat{C}_{n-1}], \tag{4.20}$$

setting $\hat{A} = i\hat{\boldsymbol{c}}^\dagger \boldsymbol{K} \hat{\boldsymbol{c}}$ and $\hat{B} = \hat{\boldsymbol{c}}$. Using the identity

$$[\hat{A}\hat{B}, \hat{C}] = \hat{A}\{\hat{B}, \hat{C}\} - \{\hat{A}, \hat{C}\}\hat{B}, \tag{4.21}$$

and the canonical anticommutation relations, one finds:

$$[\hat{c}_i^\dagger \hat{c}_j, \hat{c}_n] = -\delta_{in} \hat{c}_j, \quad [\hat{c}_i^\dagger \hat{c}_j, \hat{c}_n^\dagger] = \delta_{jn} \hat{c}_i^\dagger. \tag{4.22}$$

These expressions will be useful in later sections.

Applying these, we obtain

$$[i\hat{\boldsymbol{c}}^\dagger \boldsymbol{K}\hat{\boldsymbol{c}}, \hat{c}_i] = \sum_{kj} iK_{kj}[\hat{c}_k^\dagger \hat{c}_j, \hat{c}_i] = -\sum_j iK_{ij}\hat{c}_j, \tag{4.23}$$

or, in vector notation,

$$[i\hat{\boldsymbol{c}}^\dagger \boldsymbol{K}\hat{\boldsymbol{c}}, \hat{\boldsymbol{c}}] = -i\boldsymbol{K}\hat{\boldsymbol{c}}. \tag{4.24}$$

where the commutator is to be understood component-wise, i.e., $[\hat{\boldsymbol{c}}^\dagger \boldsymbol{K}\hat{\boldsymbol{c}}, \hat{\boldsymbol{c}}]_j = [\hat{\boldsymbol{c}}^\dagger \boldsymbol{K}\hat{\boldsymbol{c}}, \hat{c}_j]$.

Since each successive commutator introduces another factor of $-i\boldsymbol{K}$, we find

$$e^{i\hat{\boldsymbol{c}}^\dagger \boldsymbol{K}\hat{\boldsymbol{c}}}\hat{\boldsymbol{c}}\, e^{-i\hat{\boldsymbol{c}}^\dagger \boldsymbol{K}\hat{\boldsymbol{c}}} = \sum_{n=0}^{\infty} \frac{(-i\boldsymbol{K})^n}{n!}\hat{\boldsymbol{c}} = e^{-i\boldsymbol{K}}\hat{\boldsymbol{c}}, \tag{4.25}$$

which completes the proof.

This correspondence between unitary transformations and canonical transformations is central to the formalism of Gaussian states, as we will explore in later sections. A key consequence of this result is that time evolution under a quadratic Hamiltonian acts as a linear transformation on the fermionic modes. Specifically, let

$$\hat{U}_t = e^{-it\,\hat{\boldsymbol{c}}^\dagger \boldsymbol{H}\hat{\boldsymbol{c}}}. \tag{4.26}$$

In the Heisenberg picture, operators evolve according to $\hat{\mathcal{O}}_t = \hat{U}_t^\dagger \hat{\mathcal{O}}\hat{U}_t$. Applying this to the fermionic modes, we obtain

$$\hat{U}_t^\dagger\, \hat{\boldsymbol{c}}\, \hat{U}_t = e^{-i\boldsymbol{H}t}\hat{\boldsymbol{c}}, \qquad \hat{U}_t^\dagger\, \hat{\boldsymbol{c}}^\dagger\, \hat{U}_t = \hat{\boldsymbol{c}}^\dagger e^{i\boldsymbol{H}t}. \tag{4.27}$$

This result demonstrates that the single-particle Hamiltonian $\boldsymbol{H}$ fully determines the time evolution of the fermionic operators, highlighting the convenience of quadratic Hamiltonians.

4.3 Gaussian states

In this section, we introduce the definition of Gaussian states and discuss some important properties.

A Gaussian state (with no pairing terms) is a state of the form

$$\hat{\rho} = \frac{1}{Z}e^{-\sum_{ij} M_{ij}\hat{c}_i^\dagger \hat{c}_j} = \frac{1}{Z}e^{-\hat{\boldsymbol{c}}^\dagger \boldsymbol{M}\hat{\boldsymbol{c}}}, \quad \text{with} \quad Z = \operatorname{tr}\left[e^{-\hat{\boldsymbol{c}}^\dagger \boldsymbol{M}\hat{\boldsymbol{c}}}\right], \tag{4.28}$$

where Z is a normalization factor and $\boldsymbol{M} \in \mathbb{C}^{N\times N}$ is a Hermitian matrix. From this expression, we see that Gaussian states can be interpreted as thermal states (with $\beta = 1$) of a quadratic Hamiltonian $\hat{H}_{\boldsymbol{M}} = \hat{\boldsymbol{c}}^\dagger \boldsymbol{M}\hat{\boldsymbol{c}}$, which is known as the *entanglement* or *parent* Hamiltonian.

The key property of a Gaussian state is that it is entirely characterized by its second moments $\langle \hat{c}_j^\dagger \hat{c}_i \rangle$. Consequently, there is a one-to-one correspondence between $\hat{\rho}$ and the covariance matrix $\boldsymbol{C}$, which is an $N \times N$ Hermitian matrix collecting all the second moments:

$$C_{ij} = \operatorname{Tr}\left[\hat{\rho}\, \hat{c}_j^\dagger \hat{c}_i\right]. \tag{4.29}$$

Note that we define C_{ij} as $\langle \hat{c}_j^\dagger \hat{c}_i \rangle$ (rather than $\langle \hat{c}_i^\dagger \hat{c}_j \rangle$). This is simply a stylistic choice made to avoid transposes when discussing time evolution.

4.3.1 Diagonal Form of the Density Matrix

We now show that $\hat{\rho}$ can be fully expressed in terms of its second moments. To do so, we diagonalize the parent Hamiltonian using the procedure from Section 4.1. Let $\boldsymbol{M} = \boldsymbol{U}\boldsymbol{\Omega}\boldsymbol{U}^\dagger$, with $\boldsymbol{\Omega} = \mathrm{diag}(\omega_1, \dots, \omega_N)$ and $\boldsymbol{U}^\dagger\boldsymbol{U} = \mathbb{1}$. Setting

$$\hat{b}_k = \sum_i U_{ik}^* \, \hat{c}_i, \qquad \hat{H}_{\boldsymbol{M}} = \sum_k \omega_k \, \hat{b}_k^\dagger \hat{b}_k, \tag{4.30}$$

we can rewrite $\hat{\rho}$ in the convenient factorized form[1]

$$\hat{\rho} = \frac{1}{Z} e^{-\sum_k \omega_k \hat{b}_k^\dagger \hat{b}_k} = \bigotimes_{k=1}^{N} \frac{1}{Z_k} e^{-\omega_k \hat{b}_k^\dagger \hat{b}_k}, \tag{4.31}$$

where $Z_k = \mathrm{Tr}[e^{-\omega_k \hat{b}_k^\dagger \hat{b}_k}] = 1 + e^{-\omega_k}$ and $Z = \prod_k Z_k$. Alternatively, the normalization can be obtained from the trace–det formula for fermionic quadratic forms [114, 115]:

$$Z = \mathrm{Tr}[e^{-\hat{\boldsymbol{c}}^\dagger \boldsymbol{M} \hat{\boldsymbol{c}}}] = \det(\mathbb{1} + e^{-\boldsymbol{M}}). \tag{4.32}$$

The trace-det formulas are, in fact, a family of relations, which are extremely useful when dealing with quadratic fermionic systems [116]. We discuss these formulas in Appendix A.3.

Equation (4.31) shows that $\hat{\rho}$ is a product of single-mode thermal states with inverse temperature $\beta = 1$. Each such state is fully specified by its occupation number $f_k = \langle \hat{b}_k^\dagger \hat{b}_k \rangle = (1 + e^{\omega_k})^{-1}$. Thus, the state is completely characterized by the occupation profile $\{f_k\}_{k=1}^N$.

Since $(\hat{b}_k^\dagger \hat{b}_k)^2 = \hat{b}_k^\dagger \hat{b}_k$, each factor can be written as

$$\begin{aligned} e^{-\epsilon_k \hat{b}_k^\dagger \hat{b}_k} &= \sum_{n=0}^{\infty} \frac{(-\epsilon_k \hat{b}_k^\dagger \hat{b}_k)^n}{n!} = \mathbb{1}_2 + \hat{b}_k^\dagger \hat{b}_k \sum_{n=1}^{\infty} \frac{(-\epsilon_k)^n}{n!} \\ &= \mathbb{1}_2 + (e^{-\epsilon_k} - 1)\hat{b}_k^\dagger \hat{b}_k, \end{aligned} \tag{4.33}$$

where $\mathbb{1}_2$ is the 2×2 identity acting on the local mode. Substituting this into Eq. (4.31) yields

$$\hat{\rho} = \bigotimes_k \frac{1}{1 + e^{-\epsilon_k}} \left[\hat{\mathbb{1}}_2 + (e^{-\epsilon_k} - 1)\hat{b}_k^\dagger \hat{b}_k \right], \tag{4.34}$$

which explicitly shows that $\hat{\rho}$ can be written in terms of the second moments. Collecting terms, this can also be written the form

$$\hat{\rho} = \bigotimes_k \left[f_k \, \hat{b}_k^\dagger \hat{b}_k + (1 - f_k)(1 - \hat{b}_k^\dagger \hat{b}_k) \right], \tag{4.35}$$

making explicit that the state is diagonal in the energy eigenbasis, with eigenvalues determined by the mode occupations $f_k = \langle \hat{b}_k^\dagger \hat{b}_k \rangle$.

[1] We are making a slight abuse of notation: we use the same notation for $\hat{b}_k$ acting on the full Fock space and on the local two-level mode with basis $\{|0\rangle_k, |1\rangle_k\}$.

This discussion is a consequence of a simple result: since $\hat{\rho} = e^{-\hat{H}_M}/Z$, the same unitary $\hat{S}$ the diagonalizes $\hat{H}_M$ brings $\hat{\rho}$ to the factorized form in Eq. (4.31). Consequently, their eigenvalues are related by

$$\lambda_{\boldsymbol{n}} = \frac{1}{Z} e^{-E_{\boldsymbol{n}}}, \qquad E_{\boldsymbol{n}} = \sum_k \omega_k n_k, \quad n_k \in \{0, 1\}. \tag{4.36}$$

Substituting the expression for the partition function $Z = \prod_k (1 + e^{-\omega_k})$, we obtain

$$\lambda_{\boldsymbol{n}} = \prod_{k=1}^{N} \frac{e^{-\omega_k n_k}}{1 + e^{-\omega_k}}. \tag{4.37}$$

This expression will allow for a convenient computation of the von Neumann entropy in a later section.

4.3.2 Covariance Matrix in the Energy Basis

We can exploit the factorized form of $\hat{\rho}$ to derive the covariance matrix in terms of $\boldsymbol{M}$. Since the state is thermal, the two-point correlators in the energy basis satisfy

$$\langle \hat{b}_k^\dagger \hat{b}_q \rangle = f(\omega_k)\delta_{kq}. \tag{4.38}$$

Thus, the covariance matrix in the energy basis $\boldsymbol{B}$, defined via $B_{kq} = \langle \hat{b}_q^\dagger \hat{b}_k \rangle$ is diagonal:

$$B_{kq} = f(\omega_k)\delta_{kq}, \tag{4.39}$$

or, in matrix notation,

$$\boldsymbol{B} = (\mathbb{1} + e^{\boldsymbol{\Omega}})^{-1}. \tag{4.40}$$

Transforming back to the original basis via $\hat{b}_k = \sum_i U_{ik}^* \hat{c}_i$, we find

$$\boldsymbol{C} = \boldsymbol{U}\boldsymbol{B}\boldsymbol{U}^\dagger, \qquad \text{or} \qquad \boldsymbol{B} = \boldsymbol{U}^\dagger \boldsymbol{C} \boldsymbol{U}. \tag{4.41}$$

This shows that $\boldsymbol{C}$ and $\boldsymbol{M}$ are diagonalized by the same unitary:

$$\boldsymbol{M} = \boldsymbol{U} \begin{pmatrix} \omega_1 & & \\ & \ddots & \\ & & \omega_N \end{pmatrix} \boldsymbol{U}^\dagger \quad \text{and} \quad \boldsymbol{C} = \boldsymbol{U} \begin{pmatrix} f(\omega_1) & & \\ & \ddots & \\ & & f(\omega_N) \end{pmatrix} \boldsymbol{U}^\dagger \tag{4.42}$$

Hence, the eigenvalues of $\boldsymbol{C}$ and $\boldsymbol{M}$ are related by

$$\zeta_i = f(\omega_i) = \frac{1}{1 + e^{\omega_i}}, \tag{4.43}$$

where $\{\zeta_i\}$ are the eigenvalues of $\boldsymbol{C}$. In matrix notation:

$$\boldsymbol{C} = \frac{1}{\mathbb{1} + e^{\boldsymbol{M}}}, \qquad \boldsymbol{M} = \log\left(\frac{\mathbb{1} - \boldsymbol{C}}{\boldsymbol{C}}\right). \tag{4.44}$$

In terms of the covariance matrix, the normalization constant can be written as

$$Z = \frac{1}{\det(\mathbb{1} - \boldsymbol{C})}. \tag{4.45}$$

This parallel structure extends to the many-body level: just as $\boldsymbol{C}$ and $\boldsymbol{M}$ are diagonalized in the same basis by the unitary matrix $\boldsymbol{S}$, the density matrix $\hat{\rho}$ and its parent Hamiltonian $\hat{H}_M$ are diagonalized by a corresponding unitary operator $\hat{\mathcal{S}} = e^{-i\hat{\boldsymbol{c}}^\dagger \boldsymbol{K} \hat{\boldsymbol{c}}}$ acting on the Fock space, where $\boldsymbol{S} = e^{i\boldsymbol{K}}$. This sets up a useful structural analogy between the single-particle and many-body representations of Gaussian states.

4.3.3 Wick's Theorem

One of the most important properties of fermionic Gaussian states is that they satisfy *Wick's theorem*, which states that all higher-order correlation functions can be expressed entirely in terms of two-point functions.

Our goal is to evaluate expectation values of strings of creation and annihilation operators of the form $\langle \hat{c}_i^\dagger \hat{c}_j^\dagger \hat{c}_k \hat{c}_l \rangle$. We begin by noting that, In the absence of pairing terms, expectation values of operator strings with unequal numbers of creation and annihilation operators—such as $\langle \hat{c} \rangle$ or $\langle \hat{c}_i^\dagger c_j^\dagger \hat{c}_k \rangle$—vanish.

To see this, note that the Gaussian state defined in Eq. (4.28) commutes with the total number operator $\hat{\mathcal{N}} = \sum_i \hat{c}_i^\dagger \hat{c}_i$:

$$[\hat{\rho}, \hat{\mathcal{N}}] = 0. \tag{4.46}$$

As a result, $\hat{\rho}$ and $\hat{\mathcal{N}}$ can be simultaneously diagonalized. The spectral decomposition of $\hat{\rho}$ takes the form

$$\hat{\rho} = \sum_{n,\alpha} p_{n,\alpha} |n, \alpha\rangle\langle n, \alpha|, \qquad \hat{\mathcal{N}} |n, \alpha\rangle = n |n, \alpha\rangle, \tag{4.47}$$

where $n \in \{0, 1, \ldots, N\}$ and α labels states within each fixed-number sector. This decomposition shows that $\hat{\rho}$ has a block-diagonal structure, with each block supported entirely within a fixed particle-number sector.

Now consider an operator $\hat{\mathcal{O}}$ containing an unbalanced number of creation and annihilation operators. Such an operator only connects states in different number sectors, i.e., it satisfies

$$\langle n, \alpha | \hat{\mathcal{O}} | n, \alpha \rangle = 0. \tag{4.48}$$

Therefore, the expectation value vanishes:

$$\langle \hat{\mathcal{O}} \rangle = \mathrm{Tr}\left[\hat{\rho}\hat{\mathcal{O}}\right] = \sum_{n,\alpha} p_{n,\alpha} \langle n, \alpha | \hat{\mathcal{O}} | n, \alpha \rangle = 0. \tag{4.49}$$

In particular, this implies that

$$\langle \hat{c}_i \rangle = \langle \hat{c}_i^\dagger \rangle = 0. \tag{4.50}$$

Consequently, we can restrict our attention to correlation functions involving equal numbers of creation and annihilation operators of the form $\langle \hat{c}_{i_1}^\dagger \ldots \hat{c}_{i_n}^\dagger \hat{c}_{j_1} \ldots \hat{c}_{j_n} \rangle$.

In this case, Wick's theorem states that the expectation value computed over a Gaussian state is given by the sum over all possible pairings between creation and annihilation operators [106, 113, 117]:

$$\langle \hat{c}_{i_1}^\dagger \cdots \hat{c}_{i_n}^\dagger \hat{c}_{j_n} \cdots \hat{c}_{j_1} \rangle = \sum_\sigma \mathrm{sgn}(\sigma) \langle \hat{c}_{i_1}^\dagger \hat{c}_{j_{\sigma_1}} \rangle \cdots \langle \hat{c}_{i_n}^\dagger \hat{c}_{j_{\sigma_n}} \rangle, \tag{4.51}$$

where the sum runs over all the permutations of $\{1, ..., n\}$ and $\mathrm{sgn}(\sigma)$ denotes the signature of σ, which is +1 for even and -1 for odd permutations.

Alternatively, the result can be compactly expressed as a determinant:

$$\langle \hat{c}_{i_1}^\dagger \cdots \hat{c}_{i_n}^\dagger \hat{c}_{j_n} \cdots \hat{c}_{j_1} \rangle = \begin{vmatrix} \langle \hat{c}_{i_1}^\dagger \hat{c}_{j_1} \rangle & \cdots & \langle \hat{c}_{i_1}^\dagger \hat{c}_{j_n} \rangle \\ \vdots & \ddots & \vdots \\ \langle \hat{c}_{i_n}^\dagger \hat{c}_{j_1} \rangle & \cdots & \langle \hat{c}_{i_n}^\dagger \hat{c}_{j_n} \rangle \end{vmatrix}. \tag{4.52}$$

A particularly useful case is the four-point correlator:

$$\langle \hat{c}_i^\dagger \hat{c}_j^\dagger \hat{c}_k \hat{c}_l \rangle = \langle \hat{c}_i^\dagger \hat{c}_l \rangle \langle \hat{c}_j^\dagger \hat{c}_k \rangle - \langle \hat{c}_i^\dagger \hat{c}_k \rangle \langle \hat{c}_j^\dagger \hat{c}_l \rangle. \tag{4.53}$$

In the next few sections, we discuss some important properties of Gaussian states.

4.3.4 Reduced and product states

The definition of the partial trace over a subset of fermionic modes is inherently subtle. Unlike in quantum spin chain, for example, the fermionic Fock space does not admit a decomposition as a tensor product of single-mode Hilbert spaces. Instead, each sector of the Hilbert space with a fixed particle number is constructed as an anti-symmetrized tensor product of single-particle spaces. Due to this structure, the usual way of defining the partial trace as a sum over an orthonormal basis of the subspace results in a sign ambiguity [118].

Fortunately, however, for fermionic Gaussian states the problem is rather simple. Consider a subset of modes $A = \{i_1, ..., i_M\}$ of the N modes and let $\hat{\rho}_A$ be the reduced state of the system restricted to A. From a physical grounds, any definition of a reduced state must recover all expectation values within the subsystem. Since the global state satisfies Wick's theorem, any observable in A can be factorized as a combination of the second moments of the subsystem alone—specifically, expectation values of the form $\langle \hat{c}_j^\dagger \hat{c}_i \rangle$, where $i, j \in A$. This ensures that $\hat{\rho}_A$ also satisfies Wick's theorem and is therefore a Gaussian state. Moreover, its covariance matrix is simply the restriction of the global covariance matrix $\boldsymbol{C}$ to rows and columns in to A, denoted as $\boldsymbol{C}|_{\{i_1,...,i_M\}}$.

Operationally, the covariance matrix of a reduced state is obtained by removing the rows and columns corresponding to the modes being traced out. For instance, in a system with $N = 4$ modes, tracing out modes 2 and 4 results in:

$$\begin{pmatrix} C_{11} & \cancel{C_{12}} & C_{13} & \cancel{C_{14}} \\ \cancel{C_{21}} & \cancel{C_{22}} & \cancel{C_{23}} & \cancel{C_{24}} \\ C_{31} & \cancel{C_{32}} & C_{33} & \cancel{C_{34}} \\ \cancel{C_{41}} & \cancel{C_{42}} & \cancel{C_{43}} & \cancel{C_{44}} \end{pmatrix} \xrightarrow{\substack{\text{trace out modes} \\ \text{2 and 4}}} \begin{pmatrix} C_{11} & C_{13} \\ C_{31} & C_{33} \end{pmatrix}. \tag{4.54}$$

Conversely, the covariance matrix of a product state takes a block-diagonal form, where each block corresponds to the covariance matrix of an independent subsystem. Specifically, for a system composed of M independent subsystems, the global covariance matrix is given by the direct sum:

$$\boldsymbol{C} = \boldsymbol{C}_1 \oplus \boldsymbol{C}_2 \oplus \cdots \oplus \boldsymbol{C}_M = \begin{pmatrix} \boxed{\boldsymbol{C}_1} & & \\ & \boxed{\boldsymbol{C}_2} & \\ & & \ddots \\ & & \boxed{\boldsymbol{C}_M} \end{pmatrix}. \tag{4.55}$$

As a particularly relevant case, the covariance matrix of a pure state with a given occupation profile $\{n_i\}_{i=1}^N$, where $n_i = \langle \hat{c}_i^\dagger \hat{c}_i \rangle$, is a diagonal matrix of the form $\boldsymbol{C} = \mathrm{diag}(n_1, ..., n_N)$.

Expectation value of a quadratic operator

The covariance matrix representation of a Gaussian state provides a convenient framework for computing expectation values of quadratic operators. Consider an observable of the form

$$\hat{A} = \hat{\boldsymbol{c}}^\dagger \boldsymbol{A} \hat{\boldsymbol{c}}, \tag{4.56}$$

where $\boldsymbol{A}$ is a Hermitian matrix. The expectation value of $\hat{A}$ with respect to a Gaussian state $\hat{\rho}$ follows as:

$$\begin{aligned} \langle \hat{A} \rangle &= \mathrm{Tr}\big[\hat{\rho}\, \hat{\boldsymbol{c}}^\dagger \boldsymbol{A} \hat{\boldsymbol{c}}\big] \\ &= \sum_{ij} A_{ij} \,\mathrm{Tr}\big[\hat{\rho}\, \hat{c}_i^\dagger \hat{c}_j\big] \\ &= \sum_{ij} A_{ij} C_{ji} \\ &= \mathrm{Tr}[\boldsymbol{A}\boldsymbol{C}]. \end{aligned} \tag{4.57}$$

Therefore, the expectation value of any quadratic operator can be directly computed from the covariance matrix.

4.3.5 Von Neumann Entropy

One of the most convenient features of a Gaussian state is that the von Neumann entropy can be computed directly from the eigenvalues of the covariance matrix.

The von Neumann entropy of a quantum state $\hat{\rho}$ is defined as

$$S(\hat{\rho}) = -\,\mathrm{Tr}[\hat{\rho} \log \hat{\rho}]. \tag{4.58}$$

For a Gaussian state of the form $\hat{\rho} = e^{-\hat{\boldsymbol{c}}^\dagger \boldsymbol{M} \hat{\boldsymbol{c}}}/Z$, the entropy can be written as

$$S(\hat{\rho}) = \mathrm{Tr}\big[\hat{\rho}\, \hat{\boldsymbol{c}}^\dagger \boldsymbol{M} \hat{\boldsymbol{c}}\big] + \log Z \tag{4.59}$$

$$= \langle \hat{H}_{\boldsymbol{M}} \rangle + \log Z. \tag{4.60}$$

where $\hat{H}_{\boldsymbol{M}} = \hat{\boldsymbol{c}}^\dagger \boldsymbol{M} \hat{\boldsymbol{c}}$ is the parent Hamiltonian and $Z = \mathrm{Tr}[e^{-\hat{H}_{\boldsymbol{M}}}]$ is the normalization constant.

Using the expression for the expectation value of a quadratic operator (Eq. (4.57)), we obtain

$$\begin{aligned} \langle \hat{H}_{\boldsymbol{M}} \rangle &= \mathrm{Tr}[\boldsymbol{C}\boldsymbol{M}] \\ &= \mathrm{Tr}\left[\boldsymbol{C} \log\left(\frac{\mathbb{1} - \boldsymbol{C}}{\boldsymbol{C}}\right)\right] \\ &= \mathrm{Tr}[\boldsymbol{C} \log(\mathbb{1} - \boldsymbol{C})] - \mathrm{Tr}[\boldsymbol{C} \log \boldsymbol{C}], \end{aligned} \tag{4.61}$$

where we used the relation between $\boldsymbol{M}$ and $\boldsymbol{C}$ given in Eq. (4.44).

The contribution from the normalization factor is

$$\log Z = \log(\det(\mathbb{1} - \boldsymbol{C})) = \mathrm{Tr}[\log(\mathbb{1} - \boldsymbol{C})], \tag{4.62}$$

where we used the identity $\mathrm{Tr}[\log \boldsymbol{A}] = \log \det \boldsymbol{A}$.

Combining these results, the von Neumann entropy becomes

$$\begin{aligned} S(\hat{\rho}) &= -\mathrm{Tr}[\boldsymbol{C} \log \boldsymbol{C}] - \mathrm{Tr}[(\mathbb{1} - \boldsymbol{C}) \log(\mathbb{1} - \boldsymbol{C})] \\ &= -\sum_{k=1}^{N} [\zeta_k \log \zeta_k + (1 - \zeta_k) \log(1 - \zeta_k)]. \end{aligned} \tag{4.63}$$

where ζ_k are the eigenvalues of the covariance matrix $\boldsymbol{C}$.

This expression is often referred to as *Peschel's formula* [108], and shows that the von Neumann entropy of a Gaussian state reduces to the Shannon entropy of the eigenvalues of the covariance matrix. This provides an efficient and widely used method for entropy calculations in free fermion systems.

4.3.6 Covariance matrix of a thermal state

The procedure used in Section 4.3 to diagonalize the parent Hamiltonian can also be applied to compute the covariance matrix of a thermal state. Consider a quadratic Hamiltonian of the form $\hat{H} = \sum_{ij} H_{ij} \hat{c}_i^\dagger \hat{c}_j$. The corresponding thermal state at inverse temperature β is given by

$$\omega_\beta = \frac{1}{Z} e^{-\beta \hat{\boldsymbol{c}}^\dagger \boldsymbol{H} \hat{\boldsymbol{c}}}. \tag{4.64}$$

Viewing $\beta \hat{H}$ as the parent Hamiltonian of a Gaussian state, we immediately find that the covariance matrix is

$$\boldsymbol{C}_\beta = (\mathbb{1} + e^{\beta \boldsymbol{H}})^{-1}, \tag{4.65}$$

as given in Eq. (4.44).

Alternatively, the same result can be obtained by first diagonalizing the single-particle Hamiltonian, $\boldsymbol{H} = \boldsymbol{S} \boldsymbol{\epsilon} \boldsymbol{S}^\dagger$, and constructing the diagonal covariance matrix in the energy basis:

$$\boldsymbol{B} = (\mathbb{1} + e^{\beta \boldsymbol{\epsilon}})^{-1}. \tag{4.66}$$

Rotating back to the original basis yields

$$\begin{aligned} \boldsymbol{C} &= \boldsymbol{S}\boldsymbol{B}\boldsymbol{S}^\dagger \\ &= \boldsymbol{S}\cdot(\mathbb{1}+e^{\beta\boldsymbol{\epsilon}})^{-1}\cdot\boldsymbol{S}^\dagger \\ &= (\mathbb{1}+e^{\beta\boldsymbol{H}})^{-1}, \end{aligned} \tag{4.67}$$

reproducing the same expression for the thermal covariance matrix.

4.4 Time evolution

4.4.1 Unitary time evolution

As discussed in Section 4.2.1, the time-evolution operator generated by a quadratic Hamiltonian implements a linear transformation on the fermionic modes. A direct consequence of this fact is that an initially Gaussian state remains Gaussian at all times. To see this explicitly, consider the time evolution operator

$$\hat{U}_t = e^{-it\hat{\boldsymbol{c}}^\dagger\boldsymbol{H}\hat{\boldsymbol{c}}} \tag{4.68}$$

and let the initial state be the Gaussian density matrix $\hat{\rho}_0 = \frac{1}{Z}e^{-\hat{\boldsymbol{c}}^\dagger\boldsymbol{M}\hat{\boldsymbol{c}}}$. The time-evolved state is given by $\hat{\rho}_t = \hat{U}\hat{\rho}_0\hat{U}_t^\dagger$, so

$$\begin{aligned} \hat{\rho}_t &= \hat{U}_t\left(\frac{e^{-\hat{\boldsymbol{c}}^\dagger\boldsymbol{M}\hat{\boldsymbol{c}}}}{Z}\right)\hat{U}_t^\dagger \\ &= \frac{1}{Z}e^{-\hat{U}_t(\hat{\boldsymbol{c}}^\dagger\boldsymbol{M}\hat{\boldsymbol{c}})\hat{U}_t^\dagger} \\ &= \frac{1}{Z}\exp(-\hat{\boldsymbol{c}}^\dagger e^{i\boldsymbol{H}t}\boldsymbol{M}e^{-i\boldsymbol{H}t}\hat{\boldsymbol{c}}) \\ &= \frac{1}{Z}\exp(-\hat{\boldsymbol{c}}^\dagger\boldsymbol{M}_t\,\hat{\boldsymbol{c}}), \end{aligned} \tag{4.69}$$

where we defined $\boldsymbol{M}_t = e^{i\boldsymbol{H}t}\boldsymbol{M}e^{-i\boldsymbol{H}t}$. This shows that $\hat{\rho}_t$ remains Gaussian at all times, and its evolution is fully captured by $\boldsymbol{M}_t$, or equivalently, of the covariance matrix.

In the Heisenberg picture, operators evolve according to $\hat{\mathcal{O}}_t = \hat{U}_t^\dagger\hat{\mathcal{O}}\hat{U}_t$. Applying this to the covariance matrix elements, we find

$$C_{ij}(t) = \langle\hat{U}_t^\dagger\hat{c}_j^\dagger\hat{c}_i\hat{U}_t\rangle. \tag{4.70}$$

Since the evolution is unitary, we may insert the identity $\hat{U}_t\hat{U}_t^\dagger = \mathbb{1}$ between $\hat{c}_j^\dagger$ and $\hat{c}_i$:

$$C_{ij}(t) = \langle\hat{U}_t^\dagger\hat{c}_j^\dagger\hat{U}_t\cdot\hat{U}_t^\dagger\hat{c}_i\hat{U}_t\rangle \tag{4.71}$$

From Eq. (4.27), the explicit action of $\hat{U}_t$ on the fermionic modes is given by

$$\hat{U}_t^\dagger\hat{c}_i\hat{U}_t = \sum_n\left[e^{-i\boldsymbol{H}t}\right]_{in}\hat{c}_n, \qquad \hat{U}_t^\dagger\hat{c}_j^\dagger\hat{U}_t = \sum_m\hat{c}_m^\dagger\left[e^{i\boldsymbol{H}t}\right]_{mj} \tag{4.72}$$

Therefore,

$$C_{ij}(t) = \sum_{nm} \left[e^{-i\boldsymbol{H}t}\right]_{in} \langle \hat{c}_m^\dagger \hat{c}_n \rangle \left[e^{i\boldsymbol{H}t}\right]_{mj}, \tag{4.73}$$

which in matrix notation reads

$$\boldsymbol{C}(t) = e^{-i\boldsymbol{H}t} \boldsymbol{C}_0 e^{i\boldsymbol{H}t}. \tag{4.74}$$

Alternatively, the time evolution of $\boldsymbol{C}$ can be derived from the Heisenberg equation of motion,

$$\frac{\mathrm{d}\hat{\mathcal{O}}}{\mathrm{d}t} = i[\hat{H}, \hat{\mathcal{O}}]. \tag{4.75}$$

Applying this to $\hat{c}_j^\dagger \hat{c}_i$, and using the identity $[\hat{A}\hat{B}, \hat{C}] = [\hat{A}, \hat{C}]\hat{B} + \hat{A}[\hat{B}, \hat{C}]$, we obtain

$$\begin{aligned} \frac{\mathrm{d}}{\mathrm{d}t}\hat{c}_j^\dagger \hat{c}_i &= i[\hat{H}, \hat{c}_j^\dagger]\hat{c}_i + i\hat{c}_j^\dagger[\hat{H}, \hat{c}_i] \\ &= \sum_{nm} \left\{ iH_{nm}[\hat{c}_n^\dagger \hat{c}_m, \hat{c}_j^\dagger]\hat{c}_i + iH_{nm}\hat{c}_j^\dagger[\hat{c}_n^\dagger \hat{c}_m, \hat{c}_i] \right\} \\ &= \sum_n iH_{nj}\hat{c}_n^\dagger \hat{c}_i - \sum_m iH_{im}\hat{c}_j^\dagger \hat{c}_m. \end{aligned} \tag{4.76}$$

Taking the expectation value leads to the matrix equation

$$\frac{\mathrm{d}\boldsymbol{C}}{\mathrm{d}t} = -i[\boldsymbol{H}, \boldsymbol{C}], \tag{4.77}$$

which is the differential form of Eq. (4.74).

4.4.2 Quadratic Lindblad Master Equation

Consider an open fermionic system with a quadratic Hamiltonian $\hat{H} = \hat{\boldsymbol{c}}^\dagger \boldsymbol{H} \hat{\boldsymbol{c}}$, evolving under a Lindblad master equation:

$$\frac{\mathrm{d}\hat{\rho}}{\mathrm{d}t} = -i[\hat{H}, \hat{\rho}] + \sum_\mu \left(\hat{L}_\mu \hat{\rho} \hat{L}_\mu^\dagger - \frac{1}{2}\{\hat{L}_\mu^\dagger \hat{L}_\mu, \hat{\rho}\} \right), \tag{4.78}$$

where $\{\hat{L}_\mu\}$ are the jump operators.

From the structure of the Lindbladian, the dissipator includes quadratic terms such as $\hat{L}_\mu^\dagger \hat{L}_\mu$ and $\hat{L}_\mu \hat{\rho} \hat{L}_\mu^\dagger$, acting on both sides of $\hat{\rho}$. If the Hamiltonian is quadratic and the jump operators are linear in the fermionic modes, then the Liouvillian remains quadratic in the fermionic operators.

For example, consider the two jump operators

$$\hat{L}^+ = \sum_i \alpha_i \hat{c}_i \quad \text{and} \quad \hat{L}^- = \sum_i \beta_i \hat{c}_i^\dagger, \tag{4.79}$$

The corresponding master equation becomes:

$$\frac{\mathrm{d}\hat{\rho}}{\mathrm{d}t} = -i[\hat{H}, \hat{\rho}] + \sum_{ij} \left[\Gamma_{ij}^- f_i \left(\hat{c}_i \hat{\rho} \hat{c}_j^\dagger - \frac{1}{2}\{\hat{c}_j^\dagger \hat{c}_i, \hat{\rho}\} \right) + \Gamma_{ij}^+ \left(\hat{c}_i^\dagger \hat{\rho} \hat{c}_j - \frac{1}{2}\{\hat{c}_j \hat{c}_i^\dagger, \hat{\rho}\} \right) \right]. \tag{4.80}$$

where $\Gamma_{ij}^+ = \alpha_i \alpha_j^*$ and $\Gamma_{ij}^- = \beta_i \beta_j^*$.

When the Hamiltonian is quadratic and the jump operators are linear, Gaussianity is preserved throughout the evolution. A detailed proof of this result can be found in Ref. [119], and also via the third quantization formalism discussed in Ref. [120].

As a consequence, time evolution under such a quadratic Liouvillian defines a *Gaussian-preserving map*. In particular, if the Liouvillian admits a unique steady state, that steady state must be Gaussian—since any initial Gaussian state remains Gaussian under the dynamics.

4.4.3 The Lyapunov equation

We now consider the case in which the jump operators are $\{\hat{c}_i\}$ and $\{\hat{c}_i^\dagger\}$, modeling a chain coupled to thermal baths at each site. The master equation takes the form

$$\frac{\mathrm{d}\hat{\rho}}{\mathrm{d}t} = -i[\hat{H}, \hat{\rho}] + \sum_i \mathcal{D}_i(\hat{\rho}), \tag{4.81}$$

where each dissipator is given by

$$\mathcal{D}_i(\hat{\rho}) = \Gamma_i f_i \mathbb{D}[\hat{c}_i^\dagger] + \Gamma_i(1 - f_i)\mathbb{D}[\hat{c}], \tag{4.82}$$

with f_i the Fermi-Dirac occupation of bath i, and Γ_i the coupling strength. The superoperator $\mathbb{D}[\hat{L}]$ is shorthand for

$$\mathbb{D}[\hat{L}] = \hat{L}\hat{\rho}\hat{L}^\dagger - \frac{1}{2}\{\hat{L}^\dagger\hat{L}, \hat{\rho}\}. \tag{4.83}$$

For completeness, the full master equation reads

$$\frac{\mathrm{d}\hat{\rho}}{\mathrm{d}t} = -i[\hat{H}, \hat{\rho}] + \sum_i \left[\Gamma_i f_i \left(\hat{c}_i\hat{\rho}\hat{c}_i^\dagger - \frac{1}{2}\{\hat{c}_i^\dagger\hat{c}_i, \hat{\rho}\}\right) + \Gamma_i(1 - f_i)\left(\hat{c}_i^\dagger\hat{\rho}\hat{c}_i - \frac{1}{2}\{\hat{c}_i\hat{c}_i^\dagger, \hat{\rho}\}\right)\right]. \tag{4.84}$$

This master equation includes the important case of boundary-driven chains, where only the first and last sites are coupled to reservoirs. We return to this scenario in Section 4.7, where we discuss an example.

Since the jump operators are linear, the dynamics is Gaussian-preserving, and the evolution is fully captured by the covariance matrix. In the Heisenberg picture, the Lindblad equation becomes

$$\frac{\mathrm{d}\hat{\mathcal{O}}}{\mathrm{d}t} = i[\hat{H}, \mathcal{O}] + \sum_i \mathcal{D}_i^\dagger(\mathcal{O}), \tag{4.85}$$

where $\mathcal{D}_i^\dagger$ is the adjoint dissipator, given by

$$\mathcal{D}_i^\dagger(\hat{\mathcal{O}}) = \Gamma_i f_i \mathbb{D}^\dagger[\hat{c}_i^\dagger](\hat{\mathcal{O}}) + \Gamma_i(1 - f_i)\mathbb{D}^\dagger[\hat{c}_i](\hat{\mathcal{O}}), \tag{4.86}$$

with

$$\mathbb{D}^\dagger[\hat{L}](\hat{\mathcal{O}}) = \frac{1}{2}\hat{L}^\dagger[\hat{\mathcal{O}}, \hat{L}] + \frac{1}{2}[\hat{L}^\dagger, \hat{\mathcal{O}}]\hat{L}. \tag{4.87}$$

Unlike the unitary case, one cannot compute $\boldsymbol{C}_t$ by simply evolving the individual fermionic operators, since $e^{\mathcal{L}^\dagger t}(\hat{c}_j^\dagger\hat{c}_i) \neq e^{\mathcal{L}^\dagger t}(\hat{c}_j^\dagger)e^{\mathcal{L}^\dagger t}(\hat{c}_i)$. However, it can be obtained from the master

equation in the Heisenberg picture. Using the commutator identities from Eq. (4.22), one finds:

$$\begin{aligned}\mathbb{D}^\dagger[\hat{c}_n](\hat{c}_j^\dagger\hat{c}_i) &= \frac{1}{2}\hat{c}_n^\dagger[\hat{c}_j^\dagger\hat{c}_i,\hat{c}_n] + \frac{1}{2}[\hat{c}_n^\dagger,\hat{c}_j^\dagger\hat{c}_i]\hat{c}_n \\ &= -\frac{1}{2}\delta_{jn}\hat{c}_n^\dagger\hat{c}_i - \frac{1}{2}\delta_{in}\hat{c}_i^\dagger\hat{c}_n \\ &= -\frac{1}{2}(\delta_{jn}+\delta_{in})\hat{c}_j^\dagger\hat{c}_i\end{aligned} \tag{4.88}$$

Proceeding analogously for $\mathbb{D}^\dagger[\hat{c}_n^\dagger]$, we obtain

$$\mathbb{D}^\dagger[\hat{c}_n^\dagger](\hat{c}_j^\dagger\hat{c}_i) = \frac{1}{2}(\delta_{jn}+\delta_{in})\hat{c}_i\hat{c}_j^\dagger. \tag{4.89}$$

Combining all terms, the dissipator acting on site n is given by

$$\begin{aligned}\mathcal{D}_n^\dagger(\hat{c}_j^\dagger\hat{c}_i) &= \Gamma_n f_n\left[\frac{1}{2}(\delta_{jn}+\delta_{in})\hat{c}_j\hat{c}_i^\dagger\right] + \Gamma_n(1-f_n)\left[\frac{1}{2}(\delta_{jn}+\delta_{in})\hat{c}_j^\dagger\hat{c}_i\right] \\ &= -\frac{1}{2}\Gamma_i\delta_{in}\hat{c}_n^\dagger\hat{c}_i - \frac{1}{2}\Gamma_j\delta_{jn}\hat{c}_j^\dagger\hat{c}_n + \Gamma_i f_i\delta_{ij}.\end{aligned} \tag{4.90}$$

Substituting into Eq. (4.85), the Heisenberg equation of motion for $\hat{c}_j^\dagger\hat{c}_j$ becomes

$$\frac{\mathrm{d}}{\mathrm{d}t}\hat{c}_j^\dagger\hat{c}_i = -\sum_k\left(iH_{ik}+\frac{1}{2}\Gamma_i\delta_{ik}\right)\hat{c}_k^\dagger\hat{c}_i - \sum_k\hat{c}_j^\dagger\hat{c}_k\left(iH_{kj}+\frac{1}{2}\Gamma_j\delta_{jk}\right) + \Gamma_i f_i\delta_{ij}. \tag{4.91}$$

Taking the expectation value yields the equation of motion for the covariance matrix:

$$\frac{\mathrm{d}\boldsymbol{C}}{\mathrm{d}t} = -(\boldsymbol{W}\boldsymbol{C}+\boldsymbol{C}\boldsymbol{W}^\dagger)+\boldsymbol{F}, \tag{4.92}$$

where we defined the matrices

$$\boldsymbol{W} = i\boldsymbol{H}+\frac{\boldsymbol{\Gamma}}{2}, \quad \boldsymbol{\Gamma} = \mathrm{diag}(\Gamma_1,\dots,\Gamma_N) \quad \text{and} \quad \boldsymbol{F} = \mathrm{diag}(f_1\Gamma_1,\dots,f_N\Gamma_N). \tag{4.93}$$

Equation (4.92) is a linear differential equation in $\boldsymbol{C}$, known as the Lyapunov differential equation. It can be efficiently integrated numerically. In vectorized form, it reads

$$\frac{\mathrm{d}}{\mathrm{d}t}\mathrm{vec}(\boldsymbol{C}) = -(\mathbb{1}\otimes\boldsymbol{W}+\boldsymbol{W}^*\otimes\mathbb{1})\cdot\mathrm{vec}(\boldsymbol{C})+\mathrm{vec}(\boldsymbol{F}), \tag{4.94}$$

where $\mathrm{vec}(\cdot)$ denotes the vectorization described in Appendix A.2.

To find the steady-state covariance matrix $\boldsymbol{C}_{\mathrm{ss}}$, we set $\mathrm{d}\boldsymbol{C}/\mathrm{d}t = 0$ in Eq. (4.92), yielding

$$(\boldsymbol{W}\boldsymbol{C}_{\mathrm{ss}}+\boldsymbol{C}_{\mathrm{ss}}\boldsymbol{W}^\dagger) = \boldsymbol{F}. \tag{4.95}$$

This is the *continuous Lyapunov equation*, which plays a central role in control theory. Most numerical linear algebra libraries include efficient solvers based on the Bartels–Stewart algorithm [121], whose computational complexity scales as $\mathcal{O}(N^2)$. In Section 4.4.4, we present an alternative method based on the eigendecomposition of $\boldsymbol{W}$, which often performs better in practice.

Finally, the knowledge of the steady state allows us to convert Eq. (4.92) into a homogeneous equation. Define $\tilde{\boldsymbol{C}} = \boldsymbol{C} - \boldsymbol{C}_{\mathrm{ss}}$, which satisfies

$$\frac{\mathrm{d}\tilde{\boldsymbol{C}}}{\mathrm{d}t} = -(\boldsymbol{W}\tilde{\boldsymbol{C}} + \tilde{\boldsymbol{C}}\boldsymbol{W}^\dagger), \tag{4.96}$$

which can be verified by a direct differentiation:

$$\begin{aligned}
\frac{\mathrm{d}\tilde{\boldsymbol{C}}}{\mathrm{d}t} &= \frac{\mathrm{d}}{\mathrm{d}t}(\boldsymbol{C} - \boldsymbol{C}_{\mathrm{ss}}) \\
&= \frac{\mathrm{d}\boldsymbol{C}}{\mathrm{d}t} \\
&= -(\boldsymbol{W}\boldsymbol{C} + \boldsymbol{C}\boldsymbol{W}^\dagger) + \boldsymbol{F} \\
&= -[\boldsymbol{W}(\boldsymbol{C} + \boldsymbol{C}_{\mathrm{ss}}) + (\boldsymbol{C} + \boldsymbol{C}_{\mathrm{ss}})\boldsymbol{W}^\dagger] + \boldsymbol{F} \\
&= -(\boldsymbol{W}\tilde{\boldsymbol{C}} + \tilde{\boldsymbol{C}}\boldsymbol{W}^\dagger) - \underbrace{(\boldsymbol{W}\boldsymbol{C}_{\mathrm{ss}} + \boldsymbol{C}_{\mathrm{ss}}\boldsymbol{W}^\dagger)}_{=\boldsymbol{F}} + \boldsymbol{F} \\
&= -(\boldsymbol{W}\tilde{\boldsymbol{C}} + \tilde{\boldsymbol{C}}\boldsymbol{W}^\dagger).
\end{aligned} \tag{4.97}$$

The formal solution to Eq. (4.96) is $\tilde{\boldsymbol{C}}_t = e^{-\boldsymbol{W}t}\tilde{\boldsymbol{C}}_0 e^{-\boldsymbol{W}^\dagger t}$, which in terms of the original covariance matrix reads

$$\boldsymbol{C}_t = \boldsymbol{C}_{\mathrm{ss}} + e^{-\boldsymbol{W}t}(\boldsymbol{C}_0 - \boldsymbol{C}_{\mathrm{ss}})e^{-\boldsymbol{W}^\dagger t}. \tag{4.98}$$

This expression explicitly shows the relaxation of the covariance matrix towards the steady state.

4.4.4 Efficient steady-state solution

In this section, we present an efficient method for computing the steady-state covariance matrix when the matrix $\boldsymbol{W}$ is diagonalizable. This approach was first introduced in Ref. [122]. Although $\boldsymbol{W}$ is generally non-Hermitian and not guaranteed to be diagonalizable, many systems of interest satisfy this condition in practice.

The formal solution to Eq. (4.92) is given by [123]

$$\boldsymbol{C}_t = e^{-\boldsymbol{W}t}\boldsymbol{C}_0 e^{-\boldsymbol{W}^\dagger t} + \int_0^t \mathrm{d}t'\, e^{-\boldsymbol{W}(t-t')}\boldsymbol{F}e^{-W^\dagger(t-t')}. \tag{4.99}$$

Making the change of variables $t - t' \to t'$ and taking the limit $t \to \infty$, we obtain the steady-state solution:

$$\boldsymbol{C}_{\mathrm{ss}} = \int_0^\infty \mathrm{d}t\, e^{-\boldsymbol{W}t}\boldsymbol{F}e^{-\boldsymbol{W}^\dagger t}, \tag{4.100}$$

Assuming $\boldsymbol{W}$ is diagonalizable, it can be written as

$$\boldsymbol{W} = \boldsymbol{S}\boldsymbol{\Lambda}\boldsymbol{S}^{-1}, \tag{4.101}$$

where $\boldsymbol{\Lambda} = \mathrm{diag}(\lambda_1, \ldots, \lambda_N)$ contains the eigenvalues of $\boldsymbol{W}$ and $\boldsymbol{S}$ is the matrix of right eigenvectors. In general, $\boldsymbol{S}$ is not unitary.

Using this decomposition, the matrix exponentials become

$$e^{-\boldsymbol{W}t} = \boldsymbol{S}e^{-\boldsymbol{\Lambda}t}\boldsymbol{S}^{-1}, \qquad e^{-\boldsymbol{W}^\dagger t} = (\boldsymbol{S}^{-1})^\dagger e^{-\boldsymbol{\Lambda}^* t}\boldsymbol{S}^\dagger. \tag{4.102}$$

Substituting into Eq. (4.100), we obtain

$$\boldsymbol{C}_{\text{ss}} = \boldsymbol{S}\left[\int_0^\infty \mathrm{d}t\, e^{-\boldsymbol{\Lambda}t}\boldsymbol{S}^{-1}\boldsymbol{F}(\boldsymbol{S}^{-1})^\dagger e^{-\lambda^* t}\right]\boldsymbol{S}^\dagger. \tag{4.103}$$

Defining the matrix $\boldsymbol{Y}$ as

$$\boldsymbol{Y} = \int_0^\infty \mathrm{d}t\; e^{-\boldsymbol{\Lambda}t}\boldsymbol{S}^{-1}\boldsymbol{F}(\boldsymbol{S}^{-1})^\dagger e^{-\boldsymbol{\Lambda}^* t}, \tag{4.104}$$

we can write the solution compactly as

$$\boldsymbol{C}_{\text{ss}} = \boldsymbol{S}\boldsymbol{Y}\boldsymbol{S}^\dagger. \tag{4.105}$$

Element-wise, $\boldsymbol{Y}$ is given by

$$\begin{aligned} Y_{ij} &= \sum_k (S^{-1})_{ik}(S^{-1})^*_{jk}\Gamma_k f_k \int_0^\infty \mathrm{d}t\, e^{-(\lambda_i+\lambda_j^*)t} \\ &= \sum_k (S^{-1})_{ik}(S^{-1})^*_{jk}\frac{\Gamma_k f_k}{\lambda_i+\lambda_j^*}. \end{aligned} \tag{4.106}$$

This formulation provides a computationally efficient method for obtaining the steady-state covariance matrix, avoiding explicit solution of the Lyapunov equation and reducing the problem to matrix diagonalization and integration over exponentials.

4.5 Spin-chains and the Jordan–Wigner transformation

A chain of spin operators can be mapped to a fermionic chain via the Jordan–Wigner transformation [124], so that one may choose to work in whichever representation is more convenient. In particular, a non-interacting spin chain is mapped to a quadratic fermionic system, so the covariance matrix formalism can also be applied to the spin picture. In this section, we briefly describe the Jordan–Wigner transformation, focusing on a boundary-driven chains.

Boundary-driven chains

For a chain with N sites and open boundary conditions, the most general non-interacting spin Hamiltonian is

$$\hat{H} = \sum_{i=1}^{N-1}\left[J_x\hat{\sigma}_i^x\hat{\sigma}_{i+1}^x + J_y\hat{\sigma}_i^y\hat{\sigma}_{i+1}^y\right] + g\sum_{i=1}^{N}\hat{\sigma}_i^z, \tag{4.107}$$

where J_x and J_y are the nearest-neighbor coupling strengths in the x and y directions, and g is the magnetic field in the z-direction. The couplings are often written in the form

$$J_x = J\Big(\frac{1+\kappa}{2}\Big) \quad \text{and} \quad J_y = J\Big(\frac{1-\kappa}{2}\Big), \tag{4.108}$$

where $\kappa \in [-1, 1]$ is the anisotropy parameter and $J > 0$ sets the energy scale. When $0 < \kappa < 1$, the interaction is anisotropic and the model is known as the XY chain; for $\kappa = 0$, it reduces to the isotropic XX chain. When $\kappa = \pm 1$, the interaction vanishes in one direction and the model corresponds to the transverse-field Ising model (TFIM).

The system is driven out of equilibrium by two reservoirs coupled to each boundary, modeled by Lindblad dissipators. There are four jump operators, two corresponding to each bath, given by

$$\hat{L}_1^{\pm} = \sqrt{\frac{\Gamma(1 \pm \mu)}{2}}\hat{\sigma}_1^{\pm} \quad \text{and} \quad \hat{L}_N^{\pm} = \sqrt{\frac{\Gamma(1 \mp \mu)}{2}}\hat{\sigma}_N^{\pm}, \tag{4.109}$$

where Γ is the coupling strength and μ is the magnetization bias. The master equation reads

$$\frac{\mathrm{d}\hat{\rho}}{\mathrm{d}t} = -i[\hat{H}, \hat{\rho}] + \mathcal{D}_1(\hat{\rho}) + \mathcal{D}_N(\hat{\rho}), \tag{4.110}$$

where each dissipator is given by

$$\begin{aligned} \mathcal{D}_1(\hat{\rho}) &= \Gamma\Big(\frac{1-\mu}{2}\Big)\mathbb{D}[\hat{\sigma}_1^+] + \Gamma\Big(\frac{1+\mu}{2}\Big)\mathbb{D}[\hat{\sigma}_1^-], \\ \mathcal{D}_N(\hat{\rho}) &= \Gamma\Big(\frac{1+\mu}{2}\Big)\mathbb{D}[\hat{\sigma}_N^+] + \Gamma\Big(\frac{1-\mu}{2}\Big)\mathbb{D}[\hat{\sigma}_N^-]. \end{aligned} \tag{4.111}$$

The dissipator on the left tries to push the magnetization of the first site to μ, while the bath on the right tries to push the magnetization of the last site to $-\mu$.

Alternatively, this can be written as

$$\mathcal{D}_i(\hat{\rho}) = \Gamma f_i \mathbb{D}[\hat{\sigma}_i^+] + \Gamma(1 - f_i)\mathbb{D}[\hat{\sigma}_i^-], \tag{4.112}$$

with $f_1 = (1+\mu)/2$ and $f_N = (1-\mu)/2$.

Jordan–Wigner Transformation

Before applying the Jordan–Wigner transformation, it is convenient to rewrite the Hamiltonian in terms of the spin ladder operators:

$$\hat{\sigma}_i^{\pm} = \frac{\hat{\sigma}_i^x \pm i\hat{\sigma}_i^y}{2}, \tag{4.113}$$

resulting in

$$H = \sum_{i=1}^{N-1} \left\{ J(\hat{\sigma}_i^+\hat{\sigma}_{i+1}^- + \hat{\sigma}_i^-\hat{\sigma}_{i+1}^+) + J\gamma(\hat{\sigma}_i^+\hat{\sigma}_{i+1}^+ + \hat{\sigma}_i^-\hat{\sigma}_{i+1}^-) \right\} + g\sum_{i=1}^{N}\hat{\sigma}_i^z. \tag{4.114}$$

In terms of these operators, we have that $\hat{\sigma}_i^z = 2\hat{\sigma}_i^+\hat{\sigma}_i^- - 1$.

The Jordan–Wigner transformation maps spin operators to fermionic modes as follows:

$$\hat{c}_i = \left[\prod_{k=1}^{i-1}(-\hat{\sigma}_k^z)\right]\hat{\sigma}_i^- \quad \text{and} \quad \hat{c}_i^\dagger = \left[\prod_{k=1}^{i-1}(-\hat{\sigma}_k^z)\right]\hat{\sigma}_i^+. \tag{4.115}$$

The term $(-\hat{\sigma}_1^z)\cdots(-\hat{\sigma}_{i-1}^z)$ is known as a Jordan–Wigner string. Notice that all the operators in the string commute with each other. With this definition, the operators $\hat{c}_i$ and $\hat{c}_i^\dagger$ satisfy the anti-commutation relations [125]:

$$\{\hat{c}_i, \hat{c}_j^\dagger\} = \delta_{ij} \quad \text{and} \quad \{\hat{c}_i, \hat{c}_j\} = 0. \tag{4.116}$$

Moreover, one finds that $\hat{c}_i^\dagger\hat{c}_i = \hat{\sigma}_i^+\hat{\sigma}_i^-$, so

$$\hat{\sigma}_i^z = 2\hat{c}_i^\dagger\hat{c}_i - \mathbb{1}. \tag{4.117}$$

Applying this transformation to Eq. (4.114), we obtain the fermionic Hamiltonian:

$$H = \sum_{i=1}^{L-1}\left\{J(\hat{c}_i^\dagger\hat{c}_{i+1} + \hat{c}_{i+1}^\dagger\hat{c}_i) + J\gamma(\hat{c}_i^\dagger\hat{c}_{i+1}^\dagger + \hat{c}_{i+1}\hat{c}_i)\right\} + 2h\sum_{i=1}^{L}\hat{c}_i^\dagger\hat{c}_i. \tag{4.118}$$

Effect on Jump Operators and Parity Conservation

To analyze how the boundary jump operators transform under the Jordan–Wigner mapping, it is helpful to recast the transformation in an alternative, more convenient form. Using the identity $(-\hat{\sigma}_i^z) = e^{i\pi\hat{\sigma}_i^+\hat{\sigma}_i^-}$, the transformation and its inverse become

$$\hat{c}_i = \exp\left(i\pi\sum_{k=1}^{i-1}\hat{\sigma}_k^+\hat{\sigma}_k^-\right)\hat{\sigma}_i^-, \quad \hat{\sigma}_i^- = \exp\left(i\pi\sum_{k=1}^{i-1}\hat{c}_k^\dagger\hat{c}_k\right)\hat{c}_i. \tag{4.119}$$

Applying Euler's identity $e^{i\pi} = -1$, this can be written compactly as

$$\hat{\sigma}_i^- = (-1)^{\hat{\mathcal{N}}_{i-1}}\hat{c}_i, \tag{4.120}$$

where $\hat{\mathcal{N}}_{i-1} = \sum_{k=1}^{i-1}\hat{c}_k^\dagger\hat{c}_k$ is the number operator up to site $i-1$.

A useful trick here is that the string can be extended by one. Let $\hat{n}_i = \hat{c}_i^\dagger\hat{c}_i$, then $(-1)^{\hat{n}_i}\hat{c}_i = \hat{c}_i$, since the action of $\hat{c}_i$ ensures $\hat{n}_i = 0$ afterward, making the prefactor equal to one[2]. This allows us to insert the additional factor $(-1)^{\hat{n}_i}$ without modifying the operator:

$$\hat{\sigma}_i^- = (-1)^{\hat{\mathcal{N}}_{i-1}}\cdot(-1)^{n_i}\hat{c}_i = (-1)^{\hat{\mathcal{N}}_i}\hat{c}_i. \tag{4.121}$$

However, this extended string no longer commutes with $\hat{c}_i$, so when taking the Hermitian conjugate, the order must be reversed:

$$\hat{\sigma}_i^+ = \hat{c}_i^\dagger(-1)^{\hat{\mathcal{N}}_i}. \tag{4.122}$$

[2]This also follows from the identity $(-1)^{\hat{n}_i} = 1 - 2\hat{n}_i$.

We now examine how the jump operators transform. At the first site, the string is trivial: $\hat{\sigma}_1^- = \hat{c}_1$. Therefore, the left-bath jump operators map directly to fermionic operators:

$$\hat{L}_1^+ = \sqrt{\tfrac{\Gamma}{2}(1-\mu)}\,\hat{c}_1^\dagger, \quad \text{and} \quad \hat{L}_1^- = \sqrt{\tfrac{\Gamma}{2}(1+\mu)}\,\hat{c}_1. \tag{4.123}$$

However, the fermionic operator corresponding to the last site picks up a string:

$$\hat{\sigma}_N^- = (-1)^{\hat{\mathcal{N}}}\hat{c}_N, \tag{4.124}$$

with $\hat{\mathcal{N}} = \sum_{k=1}^N \hat{c}_k^\dagger \hat{c}_k$ the total particle number operator. Consequently, the right bath's jump operators become nonlocal and nonlinear:

$$\hat{L}_N^+ = \sqrt{\tfrac{\Gamma}{2}(1+\mu)}\,\hat{c}_1^\dagger \hat{P}, \quad \text{and} \quad \hat{L}_N^- = \sqrt{\tfrac{\Gamma}{2}(1-\mu)}\,\hat{P}\hat{c}_N. \tag{4.125}$$

where $\hat{P} = (-1)^{\hat{\mathcal{N}}}$ is the fermionic parity operator.

To determine whether this nonlocality affects the dynamics, we consider the dissipator acting on a density matrix $\hat{\rho}$. The fermionic operators $\hat{c}_i^\dagger$ and $\hat{c}_i$ change the particle number by one, so they flip the parity, which implies that they anticommute with $\hat{P}$:

$$\hat{P}\hat{c}_i = -\hat{c}_i\hat{P}, \qquad \hat{P}\hat{c}_i^\dagger = -\hat{c}_i^\dagger\hat{P}. \tag{4.126}$$

Thus, the action of the right-bath dissipator dissipator reads

$$\begin{aligned}\mathcal{D}(\hat{\rho}) &= \Gamma_-\left[\hat{P}\hat{c}_N\hat{\rho}\hat{c}_N^\dagger\hat{P} - \tfrac{1}{2}\{\hat{P}\hat{c}_N^\dagger\hat{c}_N\hat{P},\hat{\rho}\}\right] + \Gamma_+\left[\hat{c}_N^\dagger\hat{P}\hat{\rho}\hat{P}\hat{c}_N - \tfrac{1}{2}\{\hat{P}\hat{c}_N\hat{c}_N^\dagger\hat{P},\hat{\rho}\}\right] \\ &= \Gamma_-\left[\hat{c}_N(\hat{P}\hat{\rho}\hat{P})\hat{c}_N^\dagger - \tfrac{1}{2}\{\hat{c}_N^\dagger\hat{c}_N,\hat{\rho}\}\right] + \Gamma_+\left[\hat{c}_N^\dagger(\hat{P}\hat{\rho}\hat{P})\hat{c}_N - \tfrac{1}{2}\{\hat{c}_N\hat{c}_N^\dagger,\hat{\rho}\}\right],\end{aligned} \tag{4.127}$$

where $\Gamma_\pm = \Gamma(1\pm\mu)/2$, and we used $\hat{P}^2 = \mathbb{1}$. We observe that if the state $\hat{\rho}$ is parity symmetric, i.e., which implies that $[\hat{P},\hat{\rho}] = 0$, then the string has no dynamical effect. It remains to verify that the Lindblad evolution preserves parity.

Every quadratic operator commutes with the parity operator. Terms like $\hat{c}_i^\dagger\hat{c}_j$ commute with $\hat{\mathcal{N}}$, and pairing terms such as $\hat{c}_i\hat{c}_j$ or $\hat{c}_i^\dagger\hat{c}_j^\dagger$ destroy or create a pair of particles, preserving the parity. Since the Hamiltonian is quadratic, $\hat{P}\hat{H}\hat{P} = \hat{H}$. Therefore, the unitary term conserves parity:

$$\hat{P}[\hat{H},\hat{\rho}]\hat{P} = [\hat{H},(\hat{P}\hat{\rho}\hat{P})] \tag{4.128}$$

Consider now a jump operator $\hat{L}$ with well-defined parity:

$$\hat{P}\hat{L}\hat{P} = \hat{\eta}\hat{L}, \qquad \eta \in \{-1,+1\}. \tag{4.129}$$

Then the corresponding dissipator satisfies

$$\begin{aligned}\hat{P}\mathbb{D}[\hat{L}](\hat{\rho})\hat{P} &= \hat{P}\hat{L}\hat{\rho}\hat{L}^\dagger\hat{P} + \tfrac{1}{2}\hat{P}\{\hat{L}^\dagger\hat{L},\hat{\rho}\}\hat{P} \\ &= \hat{P}\hat{L}\hat{P}(\hat{P}\hat{\rho}\hat{P})\hat{P}\hat{L}^\dagger\hat{P} + \tfrac{1}{2}\{\hat{P}\hat{L}^\dagger\hat{P}\,\hat{P}\hat{L}\hat{P}, \hat{P}\hat{\rho}\hat{P}\} \\ &= \eta^2\hat{L}\hat{\rho}\hat{L}^\dagger + \tfrac{1}{2}\eta^2\{\hat{L}^\dagger\hat{L},\hat{\rho}\} \\ &= \mathbb{D}[\hat{L}](\hat{P}\hat{\rho}\hat{P}),\end{aligned} \tag{4.130}$$

Thus, the Lindblad dynamics preserves parity as long as the Hamiltonian commutes with $\hat{P}$ and the jump operators have a well-defined parity. A direct calculation shows that our right-bath jump operators are parity-odd:

$$\hat{P}(\hat{P}\hat{c}_n)\hat{P} = -\hat{P}\hat{c}_n, \qquad \hat{P}(\hat{c}_n^\dagger\hat{P})\hat{P} = -\hat{c}_n^\dagger\hat{P}. \tag{4.131}$$

In summary, although the Jordan–Wigner transformation introduces a nonlocal string at the final site, in boundary-driven quadratic fermionic systems. It is therefore equivalent to work with local jump operators in both the spin and fermionic pictures.

4.6 Dephasing noise

In the spin formulation, the presence of local dephasing noise acting on site i with coupling strength Γ can be modeled by the dissipator

$$\mathcal{D}_i^{\text{deph}}(\hat{\rho}) = \frac{\Gamma}{2}\mathbb{D}[\hat{\sigma}_i^z] = \frac{\Gamma}{2}(\hat{\sigma_i}^z\hat{\rho}\hat{\sigma}_i^z - \hat{\rho}). \tag{4.132}$$

In the fermionic language, this translates to

$$\begin{aligned}\mathcal{D}_i^{\text{deph}}(\hat{\rho}) = 2\Gamma\mathbb{D}[\hat{c}_i^\dagger\hat{c}_i] &= 2\Gamma\left(\hat{c}_i^\dagger\hat{c}_i\hat{\rho}\hat{c}_i^\dagger\hat{c}_i - \frac{1}{2}\left\{(\hat{c}_i^\dagger\hat{c}_i)^2,\hat{\rho}\right\}\right) \\ &= 2\Gamma\left(\hat{n}_i\hat{\rho}\hat{n}_i - \frac{1}{2}\{\hat{n}_i,\hat{\rho}\}\right)\end{aligned} \tag{4.133}$$

where $\hat{n}_i = \hat{c}_i^\dagger\hat{c}_i$, and we have used the identity $\hat{\sigma}_i^z = 2\hat{c}_i^\dagger\hat{c}_i - 1$. Since the jump operator is nonlinear in the fermionic operators, the resulting dissipator is not quadratic. As a result, the dynamics no longer preserve Gaussianity, even if the Hamiltonian is quadratic.

However, it can be shown that, due to the algebraic structure of the fermionic operators, the Heisenberg equations of motion for the second-moments $\hat{c}_j^\dagger\hat{c}_i$ remain closed, meaning they do not depend on higher moments [104, 120, 65]. Therefore, the equation of motion for the covariance matrix is still numerically tractable. Since the state is not guaranteed to be Gaussian, the covariance no longer reproduces all the expectation values of the system, and in particular cannot be used to compute the von Neumann entropy. Nonetheless, it still provides access to observables relevant for transport, such as the magnetization profile and particle or energy currents.

To compute the effect of dephasing on the covariance matrix, we evaluate the action of the adjoint dissipator:

$$\mathbb{D}^\dagger[\hat{n}_k](\bullet) = \hat{n}_k \bullet \hat{n}_k - \frac{1}{2}\{\hat{n}_k,\bullet\} \tag{4.134}$$

Using that $n_k \hat{c}_i^\dagger = \delta_{ik}\hat{c}_i^\dagger$ and $\hat{c}_i n_k = \delta_{ik}\hat{c}_i$, we find:

$$\mathbb{D}_k^\dagger[\hat{n}_k](\hat{c}_j^\dagger \hat{c}_i) = \left[\delta_{kj}\delta_{ki} - \frac{1}{2}(\delta_{kj} + \delta_{ki})\right]\hat{c}_j^\dagger \hat{c}_i. \tag{4.135}$$

The contribution of all the dephasing channels to the time evolution of $\hat{c}_j^\dagger \hat{c}_j$ is then

$$\sum_k \mathbb{D}_k^\dagger[\hat{n}_k](\hat{c}_j^\dagger \hat{c}_i) = \left(\sum_k \delta_{kj}\delta_{ki} - \frac{1}{2}\sum_k (\delta_{kj} + \delta_{ki})\right)\hat{c}_j^\dagger \hat{c}_i \tag{4.136}$$

$$= (\delta_{ij} - 1)\hat{c}_j^\dagger \hat{c}_i, \tag{4.137}$$

where we used the identity $\sum_k \delta_{kj}\delta_{ki} = \delta_{ij}$. Taking the expectation value and inserting into the Heisenberg equation for $\boldsymbol{C}$, we find that dephasing contributes:

$$\left.\frac{\mathrm{d}\boldsymbol{C}}{\mathrm{d}t}\right|_{\text{deph}} = -\Gamma\,\Delta(\boldsymbol{C}), \tag{4.138}$$

where $\Delta(\boldsymbol{C}) = \boldsymbol{C} - \mathrm{diag}(\boldsymbol{C})$. Thus, the presence of dephasing leads to a modified Lyapunov equation:

$$\frac{\mathrm{d}\boldsymbol{C}}{\mathrm{d}t} = -(\boldsymbol{W}\boldsymbol{C} + \boldsymbol{C}\boldsymbol{W}^\dagger) - \Gamma\Delta(\boldsymbol{C}) + \boldsymbol{F}, \tag{4.139}$$

where $\Delta(\boldsymbol{A}) = \boldsymbol{A} - \mathrm{diag}(\boldsymbol{A})$.

The steady state satisfies

$$(\boldsymbol{W}\boldsymbol{C} + \boldsymbol{C}\boldsymbol{W}^\dagger) + \Gamma\Delta(\boldsymbol{C}) = \boldsymbol{F}. \tag{4.140}$$

This equation is no longer of Lyapunov form, so it cannot be solved using specialized routines or the efficient method described in Section 4.4.4. However, since $\Delta(\cdot)$ is a linear operation, the equation remains a sparse linear system in the entries of $\boldsymbol{C}_{\text{ss}}$, and can be solved by vectorization.

The operation $\Delta(\boldsymbol{C})$ corresponds to a linear transformation on $\mathrm{vec}(\boldsymbol{C})$, so there exists an $N^2 \times N^2$ matrix $\mathcal{M}_\Delta$ such that

$$\mathcal{M}_\Delta \cdot \mathrm{vec}(\boldsymbol{C}) = \mathrm{vec}(\Delta(\boldsymbol{C})). \tag{4.141}$$

Using the vectorization notation, this matrix is given explicitly by

$$\mathcal{M}_\Delta = \mathbb{1}_{N^2} - \mathrm{diag}(\mathrm{Vec}(\mathbb{1}_{N^2})), \tag{4.142}$$

where $\mathbb{1}_{N^2}$ is the $N^2 \times N^2$ identity matrix in the vectorized space. Thus, the vectorized form of Eq. (4.140) becomes

$$(\boldsymbol{W} \otimes \mathbb{1} + \boldsymbol{W}^* \otimes \mathbb{1} + \Gamma\mathcal{M}_\Delta) \cdot \mathrm{vec}(\boldsymbol{C}) = \mathrm{vec}(\boldsymbol{F}). \tag{4.143}$$

4.7 Case study: dephasing enhanced transport in a tilted-lattice

In this section, we illustrate how the covariance matrix formalism can be employed to analyze transport in a boundary-driven chain with dephasing. As a case study, we discuss the results of Ref. [105], one of the works listed in the list of publications. In that work, we explored the interplay between dephasing and a tilted potential in the transport properties of an XX chain. Here, we reformulate the problem in the fermionic language and show how the steady-state properties, including magnetization and current profiles, can be efficiently computed using the covariance matrix approach.

Model and Observables

We consider a one-dimensional spin-$\frac{1}{2}$ chain of length L, governed by an XX Hamiltonian in the presence of a site-dependent magnetic field:

$$\hat{H} = J\sum_{j=1}^{L-1}\left(\hat{\sigma}_j^x\hat{\sigma}_{j+1}^x + \hat{\sigma}_j^y\hat{\sigma}_{j+1}^y\right) + \sum_{j=1}^{L}\epsilon_j\hat{\sigma}_j^z, \tag{4.144}$$

where $J > 0$ is the nearest-neighbor coupling strength and ϵ_j defines a linear magnetic potential:

$$\epsilon_j = -Uj, \tag{4.145}$$

with $U > 0$ representing the tilt strength. The linear field introduces an energy gradient across the chain, inducing Wannier–Stark localization in the coherent system.

The system is driven out of equilibrium by coupling the boundary spins to Markovian reservoirs that inject and remove spin excitations. The dynamics are described by a Lindblad master equation,

$$\frac{\mathrm{d}\hat{\rho}}{\mathrm{d}t} = -i[\hat{H},\hat{\rho}] + \mathcal{D}_L(\hat{\rho}) + \mathcal{D}_R(\hat{\rho}) + \mathcal{D}^{\mathrm{deph}}(\hat{\rho}), \tag{4.146}$$

where $\mathcal{D}_L$ and $\mathcal{D}_R$ describe the boundary dissipators, and $\mathcal{D}^{\mathrm{deph}}$ accounts for local dephasing noise. Each boundary is modeled by two jump operators acting on the first and last spins:

$$\hat{L}_1^{\pm} = \sqrt{\frac{\Gamma}{2}(1\pm f)}\,\hat{\sigma}_1^{\pm}, \qquad \hat{L}_L^{\pm} = \sqrt{\frac{\Gamma}{2}(1\mp f)}\,\hat{\sigma}_L^{\pm}, \tag{4.147}$$

where Γ is the system-bath coupling and $f \in [-1,1]$ sets the magnetization bias. Dephasing is modeled by local jump operators at each site j:

$$\hat{L}_j^{\mathrm{deph}} = \sqrt{\frac{\gamma}{2}}\,\hat{\sigma}_j^z, \tag{4.148}$$

with $\gamma \geq 0$ the dephasing rate.

The main observables of interest are the local magnetization and the spin current. The magnetization profile is given by the expectation values $\langle\hat{\sigma}_j^z\rangle$. In the bulk of the chain, the spin current is defined via the continuity equation:

$$\frac{\mathrm{d}\langle\hat{\sigma}_j^z\rangle}{\mathrm{d}t} = \langle\hat{I}_{j-1}\rangle - \langle\hat{I}_j\rangle, \quad 1 < j < L, \tag{4.149}$$

where $\hat{I}_j$ is the spin current operator flowing from site j to site $j+1$, defined as

$$\hat{I}_j = 2J(\hat{\sigma}_j^x \hat{\sigma}_{j+1}^y - \hat{\sigma}_j^y \hat{\sigma}_{j+1}^x). \tag{4.150}$$

At the boundaries, the magnetization change is governed by exchange with the baths. This leads to the continuity equations:

$$\begin{aligned} \frac{\mathrm{d}\langle \hat{\sigma}_1^z \rangle}{\mathrm{d}t} &= \mathrm{Tr}[\hat{\sigma}_1^z \, \mathcal{D}_L(\hat{\rho})] - \langle \hat{I}_1 \rangle \\ \frac{\mathrm{d}\langle \hat{\sigma}_L^z \rangle}{\mathrm{d}t} &= \langle \hat{I}_{L-1} \rangle + \mathrm{Tr}[\hat{\sigma}_L^z \, \mathcal{D}_R(\hat{\rho})], \end{aligned} \tag{4.151}$$

where

$$\mathrm{Tr}[\hat{\sigma}_1^z \, \mathcal{D}_L(\hat{\rho})] = \Gamma(f - \langle \sigma_1^z \rangle), \qquad \mathrm{Tr}[\hat{\sigma}_L^z \, \mathcal{D}_R(\hat{\rho})] = -\Gamma(f + \langle \sigma_L^z \rangle). \tag{4.152}$$

In the steady state, all time derivatives vanish and the current becomes spatially homogeneous. We define the stationary current $\langle I \rangle_\infty$ as

$$\langle I \rangle_\infty \equiv \langle \hat{I}_1 \rangle = \cdots = \langle \hat{I}_{L-1} \rangle. \tag{4.153}$$

This also matches the currents at the boundaries:

$$\langle I \rangle_\infty = \Gamma(f - \langle \hat{\sigma}_1^z \rangle) = \Gamma(f + \langle \hat{\sigma}_L^z \rangle) \tag{4.154}$$

Steady-State Solution: Lyapunov Equation

To solve for the non-equilibrium steady state, we map the spin model to a quadratic fermionic system using the Jordan–Wigner transformation. This mapping allows us to work within the covariance matrix formalism, which enables an efficient computation of steady-state observables for non-interacting or weakly interacting systems.

Under the Jordan–Wigner transformation, the Hamiltonian becomes

$$\hat{H} = 2J \sum_{j=1}^{L-1} \left(\hat{c}_j^\dagger \hat{c}_{j+1} + \hat{c}_{j+1}^\dagger \hat{c}_j \right) + \sum_{j=1}^{L} \epsilon_j (2\hat{c}_j^\dagger \hat{c}_j - 1), \tag{4.155}$$

where $\hat{c}_j$ and $\hat{c}_j^\dagger$ are fermionic annihilation and creation operators, and $\epsilon_j = -Uj$ is the linear potential.

The boundary jump operators transform as

$$\hat{L}_1^+ = \sqrt{\tfrac{\Gamma}{2}(1+f)}\, \hat{c}_1^\dagger, \qquad \hat{L}_1^- = \sqrt{\tfrac{\Gamma}{2}(1-f)}\, \hat{c}_1, \tag{4.156}$$

$$\hat{L}_L^+ = \sqrt{\tfrac{\Gamma}{2}(1-f)}\, \hat{c}_L^\dagger, \qquad \hat{L}_L^- = \sqrt{\tfrac{\Gamma}{2}(1+f)}\, \hat{c}_L. \tag{4.157}$$

As discussed in Section 4.5, the right-bath operators formally pick up a fermionic parity string under the Jordan–Wigner transformation. However, for systems with parity symmetry, this string has no effect on the dynamics of the second moments and can be safely omitted in the covariance matrix description.

The dephasing jump operators transform into nonlinear fermionic operators:

$$\hat{L}_j^{\text{deph}} = \sqrt{\gamma}\,\hat{n}_j, \qquad \text{with} \quad \hat{n}_j = \hat{c}_j^\dagger \hat{c}_j. \tag{4.158}$$

Although these operators are not linear, they preserve the closure of the Heisenberg equations for second moments due to the algebraic properties of fermions [104, 65, 120].

The system's steady-state correlations are encoded in the covariance matrix $\boldsymbol{C}$, with entries

$$C_{ij} = \langle \hat{c}_j^\dagger \hat{c}_i \rangle. \tag{4.159}$$

From this matrix, we can reconstruct the observables of interest using the Jordan–Wigner transformation. The magnetization profile is contained in the diagonal of $\boldsymbol{C}$:

$$\langle \sigma_j^z \rangle = 2\langle \hat{c}_j^\dagger \hat{c}_j \rangle - 1 = 2C_{jj} - 1. \tag{4.160}$$

In the fermionic picture, the spin current operator translates to

$$\hat{I}_j = 2J(\hat{\sigma}_j^x \hat{\sigma}_{j+1}^y - \hat{\sigma}_j^y \hat{\sigma}_{j+1}^x) = 4i(\hat{c}_j^\dagger \hat{c}_{j+1} - \hat{c}_{j+1}^\dagger \hat{c}_j) \tag{4.161}$$

Taking the expectation value, we find

$$\langle \hat{I}_j \rangle = 8J\,\mathrm{Im}(C_{j,j+1}). \tag{4.162}$$

The equation of motion for $\boldsymbol{C}$ takes the form of a modified Lyapunov equation:

$$\frac{\mathrm{d}\boldsymbol{C}}{\mathrm{d}t} = -(\boldsymbol{W}\boldsymbol{C} + \boldsymbol{C}\boldsymbol{W}^\dagger) - 2\gamma\Delta(\boldsymbol{C}) + \boldsymbol{F}, \tag{4.163}$$

where $\boldsymbol{W}$ is an effective non-Hermitian matrix determined by the Hamiltonian and boundary dissipators, $\boldsymbol{F}$ is a source matrix, and $\Delta(\boldsymbol{C}) = \boldsymbol{C} - \mathrm{diag}(\boldsymbol{C})$ removes the diagonal elements. In the steady state, $\mathrm{d}\boldsymbol{C}/\mathrm{d}t = 0$, so the equation reduces to:

$$\boldsymbol{W}\boldsymbol{C} + \boldsymbol{C}\boldsymbol{W}^\dagger + 2\gamma\Delta(\boldsymbol{C}) = \boldsymbol{F}. \tag{4.164}$$

Although this equation is no longer of strict Lyapunov form due to the $\Delta(\boldsymbol{C})$ term, it remains a sparse linear system in the entries of $\boldsymbol{C}$ and can be efficiently solved numerically.

The matrix $\boldsymbol{W}$ has tridiagonal structure, given explicitly by

$$W_{ij} = iH_{ij} + \frac{\Gamma}{2}\big(\delta_{i1}\delta_{j1} + \delta_{iL}\delta_{jL}\big), \tag{4.165}$$

where $\boldsymbol{H}$ is the single-particle Hamiltonian, given by

$$H_{ij} = 2J\big(\delta_{i,j+1} + \delta_{i,j-1}\big) + 2\epsilon_i\delta_{ij}. \tag{4.166}$$

The source matrix $\boldsymbol{F}$ is diagonal and nonzero only at the boundaries:

$$\boldsymbol{F} = \mathrm{diag}\big(\tfrac{\Gamma}{2}(1+f),\, 0,\, \ldots,\, 0,\, \tfrac{\Gamma}{2}(1-f)\big). \tag{4.167}$$

Wannier–Stark Localization

We now analyze the transport properties of the clean system in the absence of dephasing ($\gamma = 0$).

The linear field introduces an energy offset U between neighboring sites, so the total energy drop across the chain is $V = U(L-1)$. To ensure a well-defined thermodynamic limit, we hold V fixed as $L \to \infty$, implying $U \sim V/L \to 0$ as $L \to \infty$.

In the closed system, the model exhibits *Wannier–Stark localization* [126, 127]: the single-particle eigenstates become localized due to the linear potential, despite the absence of disorder. The energy spectrum forms a set of equally spaced levels $E_n = E_0 + nU$, known as the Wannier–Stark ladder.

This phenomenon is closely related to *Bloch oscillations* [128], where a wavepacket in a constant field (in our case, a constant energy offset U between neighboring sites) undergoes coherent periodic motion in momentum space, with a characteristic period $\tau_B \sim U^{-1}$.

In the boundary-driven setting, the interplay between the Wannier–Stark localization and external driving leads to the formation of a domain wall. The left reservoir attempts to impose a local magnetization $\langle \hat{\sigma}_1^z \rangle = +f$, while the right reservoir enforces $\langle \hat{\sigma}_L^z \rangle = -f$. In the strongly localized regime, the excitations injected at the boundaries fail to traverse the bulk. As a result, they accumulate near the edges, forming a non-equilibrium steady state with two nearly uniform polarization domains separated by a sharp domain wall at the center. From the boundary current relation, we find

$$\langle I \rangle = \Gamma(f - \langle \hat{\sigma}_1^z \rangle) \approx 0, \tag{4.168}$$

up to exponentially small corrections, and hence

$$\langle I \rangle \propto e^{-L/\xi}, \tag{4.169}$$

where ξ is a localization length that depends on V.

This behavior is illustrated in Fig. 4.1. Panel (a) shows the formation of the magnetization domain wall as L increases at fixed tilt V, while panel (b) confirms the exponential decay of the steady-state current.

4.7.1 Dephasing-assisted Transport

We now investigate the role of dephasing ($\gamma > 0$) in restoring transport in the tilted chain. While the clean system exhibits Wannier–Stark localization and an exponentially suppressed current, the introduction of bulk dephasing noise breaks quantum coherence and disrupts localization. As a result, spin excitations can propagate across the chain, leading to a finite steady-state current even in the presence of a large tilt.

This effect, known as *dephasing-enhanced transport*, arises from the interplay between coherent dynamics and incoherent noise. At small γ, the current grows rapidly with increasing dephasing. At large γ, however, incoherent scattering dominates and suppresses transport, giving rise to a non-monotonic current profile with a clear maximum at intermediate dephasing strength.

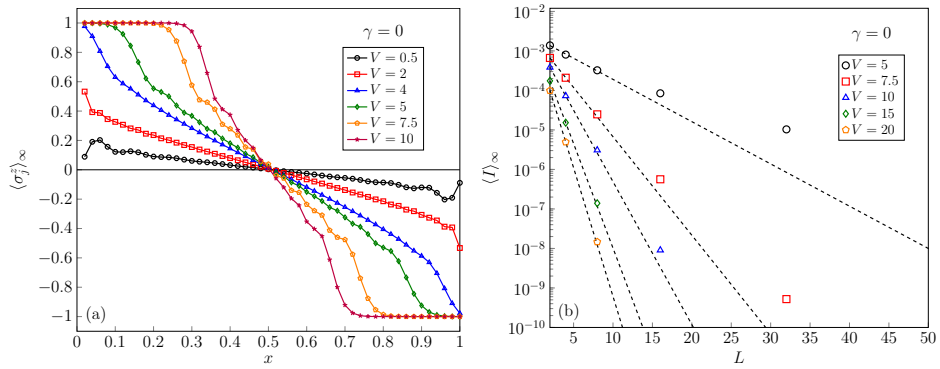

Figure 4.1: **Wannier–Stark localization in the absence of dephasing.** (**a**) Steady-state magnetization profiles for different system sizes at fixed total tilt V, showing the formation of flat polarization domains separated by a sharp domain wall. (**b**) Spin current as a function of system size L, showing exponential decay $\langle I\rangle \propto e^{-L/\xi}$. Both panels are reproduced from Fig. 2 of Ref. [105].

Exact Current for $L = 2$

To illustrate the mechanism of dephasing-assisted transport, we begin with the smallest nontrivial case: a two-site chain ($L = 2$). In this case, the steady-state current can be computed exactly as [105]:

$$\langle I\rangle = f \cdot \frac{16J^2\Gamma(2\gamma+\Gamma)}{16J^2(2\gamma+\Gamma)+4\Gamma U^2+\Gamma(2\gamma+\Gamma)^2}. \tag{4.170}$$

The optimal dephasing rate that maximizes the current is obtained by differentiating Eq. (22), yielding

$$\gamma_{\max} = U - \frac{\Gamma}{2} \geq 0. \tag{4.171}$$

This relation shows that dephasing-assisted transport occurs when the potential gradient U is sufficiently large compared to the boundary coupling Γ.

The full behavior of the current as a function of γ is shown in Fig. 4.2, which confirms the existence of a well-defined maximum at intermediate dephasing.

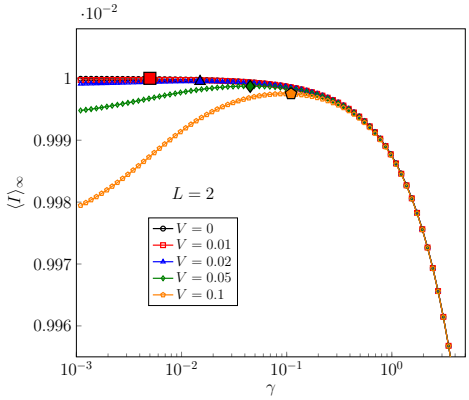

Figure 4.2: **Dephasing-enhanced transport in a minimal system.** Steady-state current as a function of dephasing rate γ for a chain of length $L = 2$, showing a pronounced maximum at intermediate dephasing. The curve corresponds to the exact expression in Eq. (4.170). Reproduced from Fig. 4 of Ref. [105].

Tridiagonal Approximation

To gain analytical traction for larger chains, we adopt a tridiagonal approximation for the steady-state covariance matrix. In the strongly localized regime ($V \gg 0$), correlations decay rapidly with distance, justifying the truncation of $\boldsymbol{C}$ to a tridiagonal form:

$$C_{ij} = \frac{1}{2}(\langle\hat{\sigma}_j^z\rangle + 1)\delta_{ij} + \left(\kappa_j + \frac{i\langle I\rangle}{4J}\right)\delta_{j,j+1} + \left(\kappa_j - \frac{i\langle I\rangle}{4J}\right)\delta_{j,j-1} \tag{4.172}$$

Here, the diagonal elements encode the local magnetization, while the imaginary part of the nearest-neighbor terms fixes the (homogeneous) current $\langle I\rangle$.

Substituting this ansatz into the steady-state Lyapunov equation and retaining only the equations corresponding to the main and first off-diagonals yields a closed system:

$$\begin{cases} \Gamma(f - \langle\hat{\sigma}_1^z\rangle) = \langle I\rangle \\ \Gamma(f + \langle\hat{\sigma}_L^z\rangle) = \langle I\rangle \\ \left[2\gamma + \dfrac{\Gamma}{2}\big(\delta_{j,1} + \delta_{j,L-1}\big)\right]\kappa_j = \dfrac{U\langle I\rangle}{4J} \\ J\big(\langle\hat{\sigma}_{j+1}^z\rangle - \langle\hat{\sigma}_j^z\rangle\big) + 2U\kappa_j + \dfrac{\gamma\langle I\rangle}{8J} + \dfrac{\Gamma\langle I\rangle}{16J}\big(\delta_{j,1} + \delta_{j,L-1}\big) = 0 \end{cases} \tag{4.173}$$

Summing the last equation from $j = 1$ to $L - 1$ yields a telescopic identity:

$$J(\langle\hat{\sigma}_L^z\rangle - \langle\hat{\sigma}_1^z\rangle) + 2\sum_{j=1}^{L-1} U\kappa_j + \frac{\gamma\langle I\rangle}{4J}(L-1) + \frac{\Gamma\langle I\rangle}{4J} = 0 \tag{4.174}$$

The difference $\langle\hat{\sigma}_L^z\rangle - \langle\hat{\sigma}_1^z\rangle$ is set by the continuity equation at the boundaries:

$$\langle\hat{\sigma}_L^z\rangle - \langle\hat{\sigma}_1^z\rangle = \frac{2\langle I\rangle}{\Gamma} - 2f \tag{4.175}$$

From the third equation, we obtain expression for κ_j, which reads

$$\kappa_j = \frac{U\langle I\rangle}{4J[2\gamma + \frac{\Gamma}{2}(\delta_{j,1} + \delta_{j,L-1})]}, \tag{4.176}$$

leading to the sum

$$\begin{aligned} \sum_{j=1}^{L-1} U\kappa_j &= \frac{U^2\langle I\rangle}{8J\gamma}(L-3) + \frac{U^2\langle I\rangle}{2J[2\gamma + \frac{\Gamma}{2}]} \\ &= \frac{U^2\langle I\rangle}{4J}\left[\frac{L-3}{2\gamma} + \frac{4}{4\gamma + \Gamma}\right] \end{aligned} \tag{4.177}$$

Substituting all the terms in Eq. (4.174) and solving for $\langle I\rangle$ yields

$$\langle I\rangle = \frac{16\Gamma J^2 f}{16J^2 + \Gamma[2\gamma(L-1) + \Gamma] + 4\Gamma U^2\left[\frac{L-3}{\gamma} + \frac{4}{4\gamma+\Gamma}\right]} \tag{4.178}$$

This expression captures the key features of dephasing-assisted transport, including its non-monotonic behavior as a function of γ. In particular, for fixed total tilt $V = U(L-1)$,

the current is maximized when $\gamma \sim U$, reflecting a resonance between the dephasing rate and the intrinsic Bloch frequency.

This behavior is illustrated in Fig. 4.3, which shows the finite-size diffusion coefficient $D = L\langle I\rangle/f$ as a function of γ for different values of V. Each curve exhibits a clear peak around $\gamma \approx U$, confirming that moderate dephasing enhances transport by suppressing Wannier–Stark localization. For larger γ, the current decreases as transport enters a diffusive regime, with $D \propto \gamma^{-1}$.

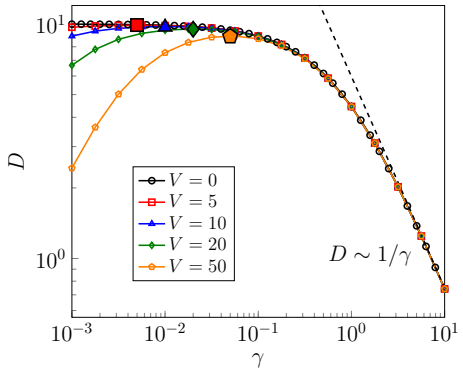

Figure 4.3: Finite-size diffusion coefficient $D = L\langle I\rangle/f$ as a function of the dephasing rate γ, for several values of the total tilt V. Each curve displays a clear maximum near $\gamma \approx U$, consistent with the resonance condition for optimal transport. For $\gamma \gg U$, transport becomes diffusive and $D \sim \gamma^{-1}$. Adapted from Fig. 6(a) of Ref. [105])

4.8 Quantum information with Gaussian states

A key advantage of Gaussian states is that quantum information measures—such as fidelity, relative entropy, and Rényi relative entropy—can be computed directly from their covariance matrices. In this section, we derive explicit expressions for these quantities between two Gaussian states.

To do so, we use several properties of Gaussian states. For a Gaussian state $\hat{\rho} = e^{-\hat{\boldsymbol{c}}^\dagger \boldsymbol{M} \hat{\boldsymbol{c}}}$, one can move freely between its density matrix and covariance matrix representations via the relations

$$\boldsymbol{C} = \frac{1}{\mathbb{1} + e^{\boldsymbol{M}}}, \qquad \boldsymbol{M} = \log\left(\frac{\mathbb{1} - \boldsymbol{C}}{\boldsymbol{C}}\right), \tag{4.179}$$

with normalization constant

$$Z = \frac{1}{\det(\mathbb{1} - \boldsymbol{C})} = \prod_{k=1}^{n} \frac{1}{1 - \zeta_k}, \tag{4.180}$$

where ζ_k are the eigenvalues of $\boldsymbol{C}$.

The logarithm of a Gaussian state, which appears in definitions of quantities such as the von Neumann entropy and relative entropy, takes the form

$$\log \hat{\rho} = -\hat{\boldsymbol{c}}^\dagger \boldsymbol{M} \hat{\boldsymbol{c}} - \log Z. \tag{4.181}$$

We also make use of trace-determinant identities for quadratic fermionic operators, which we review in Appendix A.3. For a quadratic operator of the form $\hat{A} = \hat{\boldsymbol{c}}^\dagger \boldsymbol{A} \hat{\boldsymbol{c}}$, the trace of the exponential is given by

$$\mathrm{Tr}\left[e^{\hat{A}}\right] = \det\left(\mathbb{1} + e^{\boldsymbol{A}}\right). \tag{4.182}$$

There is also a useful generalization to products of exponentials. Given another quadratic operator $\hat{B} = \hat{\boldsymbol{c}}^\dagger \boldsymbol{B} \hat{\boldsymbol{c}}$, one has

$$\mathrm{Tr}[e^{\hat{A}} e^{\hat{B}}] = \det\left(\mathbb{1} + e^{\boldsymbol{A}} e^{\boldsymbol{B}}\right). \tag{4.183}$$

It is also useful to recall the identity relating the trace and determinant of a square matrix:

$$\log\det(\boldsymbol{A}) = \mathrm{Tr}[\log \boldsymbol{A}]. \tag{4.184}$$

With these tools in hand, we now proceed to the explicit evaluation of quantum information measures.

4.8.1 Relative entropy

The relative entropy between two quantum states $\hat{\rho}$ and $\hat{\sigma}$ is defined as

$$\begin{aligned} D(\hat{\rho} \,\|\, \hat{\sigma}) &= \mathrm{Tr}[\hat{\rho}(\log\hat{\rho} - \log\hat{\sigma})] \\ &= S(\hat{\rho}) - \mathrm{Tr}[\hat{\rho}\log\hat{\sigma}]. \end{aligned} \tag{4.185}$$

Consider now two Gaussian states of the form

$$\hat{\rho} = \frac{1}{Z_\rho} e^{-\hat{\boldsymbol{c}}^\dagger \boldsymbol{M}_\rho \hat{\boldsymbol{c}}}, \qquad \hat{\sigma} = \frac{1}{Z_\sigma} e^{-\hat{\boldsymbol{c}}^\dagger \boldsymbol{M}_\sigma \hat{\boldsymbol{c}}}, \tag{4.186}$$

with associated covariance matrices $\boldsymbol{C}_\rho$ and $\boldsymbol{C}_\sigma$.

The first term in Eq. (4.185) is the von Neumann entropy of $\hat{\rho}$, as computed in Section 4.3.5. To evaluate the second term, we use the expression

$$\log\hat{\sigma} = -\hat{\boldsymbol{c}}^\dagger \boldsymbol{M}_\sigma \hat{\boldsymbol{c}} - \log Z_\sigma, \tag{4.187}$$

which gives

$$\begin{aligned} \mathrm{Tr}[\hat{\rho}\log\hat{\sigma}] &= -\mathrm{Tr}[\hat{\rho}\,\hat{\boldsymbol{c}}^\dagger \boldsymbol{M}_\sigma \hat{\boldsymbol{c}}] - \log Z_\sigma \\ &= -\mathrm{Tr}\left[\boldsymbol{M}_\sigma \boldsymbol{C}_\rho\right] - \log Z_\sigma, \end{aligned} \tag{4.188}$$

where we used the trace-det identity. Combining these expressions, the relative entropy becomes

$$D(\hat{\rho} \,\|\, \hat{\sigma}) = S(\hat{\rho}) + \mathrm{Tr}\left[\boldsymbol{M}_\sigma \boldsymbol{C}_\rho\right] + \log Z_\sigma \tag{4.189}$$

4.8.2 Rényi entropy

The Rényi-α entropy of a state $\hat{\rho}$ is defined as

$$S_\alpha(\hat{\rho}) = \frac{1}{1-\alpha} \log \mathrm{Tr}\,\hat{\rho}^\alpha. \tag{4.190}$$

Assuming $\hat{\rho}$ has the Gaussian form $\hat{\rho} = Z^{-1} e^{-\hat{\boldsymbol{c}}^\dagger \boldsymbol{M} \hat{\boldsymbol{c}}}$, we obtain

$$\begin{aligned} S_\alpha(\hat{\rho}) &= \frac{1}{1-\alpha} \log\Big(\frac{1}{Z^\alpha} \operatorname{Tr}\big[e^{-\alpha \hat{\boldsymbol{c}}^\dagger \boldsymbol{M} \hat{\boldsymbol{c}}} \big] \Big) \\ &= \frac{1}{1-\alpha} \big[\log\det(\mathbb{1} + e^{-\alpha \boldsymbol{M}}) - \alpha \log Z \big]. \end{aligned} \tag{4.191}$$

Using the identities $\log\det(\boldsymbol{A}) = \operatorname{Tr}[\log \boldsymbol{A}]$ and $\boldsymbol{e}^{-\boldsymbol{M}} = \boldsymbol{C}(\mathbb{1} - \boldsymbol{C})^{-1}$, the entropy simplifies to

$$S_\alpha(\hat{\rho}) = \frac{1}{1-\alpha} \operatorname{Tr}\left[\log\left(\mathbb{1} + \left(\frac{\boldsymbol{C}}{\mathbb{1} - \boldsymbol{C}} \right)^\alpha \right) \right] - \frac{\alpha}{1-\alpha} \log Z. \tag{4.192}$$

This expression can be conveniently evaluated in terms of the eigenvalues $\{\zeta_k\}$ of the covariance matrix $\boldsymbol{C}$:

$$\operatorname{Tr}\left[\log\left(\mathbb{1} + \left(\frac{\boldsymbol{C}}{\mathbb{1} - \boldsymbol{C}} \right)^\alpha \right) \right] = \sum_{k=1}^{N} \log\left(1 + \left(\frac{\zeta_k}{1 - \zeta_k} \right)^\alpha \right) \tag{4.193}$$

4.8.3 Rényi relative entropy

The Rényi relative entropy of order α between two quantum states $\hat{\rho}$ and $\hat{\sigma}$ is defined as

$$S_\alpha(\hat{\rho} \,\|\, \hat{\sigma}) = -\frac{1}{1-\alpha} \log \operatorname{Tr}\Big[\big(\hat{\sigma}^{\frac{1-\alpha}{2\alpha}} \hat{\rho} \hat{\sigma}^{\frac{1-\alpha}{2\alpha}} \big)^\alpha \Big] \tag{4.194}$$

Assuming both $\hat{\rho}$ and $\hat{\sigma}$ are Gaussian states, the operator inside the trace becomes

$$\hat{\sigma}^{\frac{1-\alpha}{2\alpha}} \hat{\rho} \hat{\sigma}^{\frac{1-\alpha}{2\alpha}} = \frac{1}{Z_\rho Z_\sigma^{2\nu}} e^{-\nu \hat{\boldsymbol{c}}^\dagger \boldsymbol{M}_\sigma \hat{\boldsymbol{c}}} e^{-\hat{\boldsymbol{c}}^\dagger \boldsymbol{M}_\rho \hat{\boldsymbol{c}}} e^{-\nu \hat{\boldsymbol{c}}^\dagger \boldsymbol{M}_\sigma \hat{\boldsymbol{c}}}, \quad \text{with} \quad \nu = \frac{1-\alpha}{2\alpha}. \tag{4.195}$$

As shown in Appendix A.3, a product of exponentials of quadratic operators remains of Gaussian form:

$$e^{-\hat{\boldsymbol{c}}^\dagger \boldsymbol{A}_1 \hat{\boldsymbol{c}}} e^{-\hat{\boldsymbol{c}}^\dagger \boldsymbol{A}_2 \hat{\boldsymbol{c}}} e^{-\hat{\boldsymbol{c}}^\dagger \boldsymbol{A}_3 \hat{\boldsymbol{c}}} = e^{-\hat{\boldsymbol{c}}^\dagger \boldsymbol{Q} \hat{\boldsymbol{c}}}, \quad \text{where} \quad e^{-\boldsymbol{Q}} = e^{-\boldsymbol{A}_1} e^{-\boldsymbol{A}_2} e^{-\boldsymbol{A}_3}. \tag{4.196}$$

Applying this to our case yields

$$e^{-\nu \hat{\boldsymbol{c}}^\dagger \boldsymbol{M}_\sigma \hat{\boldsymbol{c}}} e^{-\hat{\boldsymbol{c}}^\dagger \boldsymbol{M}_\rho \hat{\boldsymbol{c}}} e^{-\nu \hat{\boldsymbol{c}}^\dagger \boldsymbol{M}_\sigma \hat{\boldsymbol{c}}} = e^{-\hat{\boldsymbol{c}}^\dagger \boldsymbol{Q}_\alpha \hat{\boldsymbol{c}}}, \qquad \boldsymbol{Q}_\alpha = -\log(e^{-\nu \boldsymbol{M}_\sigma} e^{-\boldsymbol{M}_\rho} e^{-\nu \boldsymbol{M}_\sigma}). \tag{4.197}$$

Therefore,

$$\big(\hat{\sigma}^{\frac{1-\alpha}{2\alpha}} \hat{\rho} \hat{\sigma}^{\frac{1-\alpha}{2\alpha}} \big)^\alpha = \frac{1}{Z_\rho^\alpha Z_\sigma^{1-\alpha}} e^{-\alpha \hat{\boldsymbol{c}}^\dagger \boldsymbol{Q}_\alpha \hat{\boldsymbol{c}}}. \tag{4.198}$$

Using the trace-determinant identity, we obtain

$$\log \operatorname{Tr}\big[e^{-\alpha \hat{\boldsymbol{c}}^\dagger \boldsymbol{Q}_\alpha \hat{\boldsymbol{c}}} \big] = \log\det(\mathbb{1} + e^{-\alpha \boldsymbol{Q}_\alpha}) \tag{4.199}$$

$$= \operatorname{Tr} \log(\mathbb{1} + e^{-\alpha \boldsymbol{Q}_\alpha}). \tag{4.200}$$

The Rényi relative entropy then becomes

$$S_\alpha(\hat{\rho} \,\|\, \hat{\sigma}) = -\frac{1}{1-\alpha} \operatorname{Tr} \log(\mathbb{1} + e^{-\alpha \boldsymbol{Q}_\alpha}) + \frac{\alpha}{1-\alpha} \log Z_\rho + \log Z_\sigma. \tag{4.201}$$

To express this in terms of the covariance matrices, we use the identities

$$e^{-\nu \boldsymbol{M}_\sigma} = \left(\frac{\boldsymbol{C}_\sigma}{\mathbb{1} - \boldsymbol{C}_\sigma}\right)^{\frac{1-\alpha}{2\alpha}}, \quad e^{-\boldsymbol{M}_\rho} = \left(\frac{\boldsymbol{C}_\rho}{\mathbb{1} - \boldsymbol{C}_\rho}\right), \tag{4.202}$$

so that

$$\begin{aligned} S_\alpha(\hat{\rho} \,\|\, \hat{\sigma}) = &- \frac{1}{1-\alpha} \operatorname{Tr} \log \left[\mathbb{1} + \left(\left(\frac{\boldsymbol{C}_\sigma}{\mathbb{1} - \boldsymbol{C}_\sigma}\right)^{\frac{1-\alpha}{2\alpha}} \left(\frac{\boldsymbol{C}_\rho}{\mathbb{1} - \boldsymbol{C}_\rho}\right) \left(\frac{\boldsymbol{C}_\sigma}{\mathbb{1} - \boldsymbol{C}_\sigma}\right)^{\frac{1-\alpha}{2\alpha}}\right)^\alpha\right] \\ &+ \frac{\alpha}{1-\alpha} \log Z_\rho + \log Z_\sigma. \end{aligned} \tag{4.203}$$

Note that due to non-commutativity, the exponent α cannot be distributed across the product of the three matrices. A convenient way to evaluate this expression is by diagonalizing the covariance matrices:

$$\boldsymbol{C}_\rho = \boldsymbol{S}_\rho \boldsymbol{\zeta}_\rho \boldsymbol{S}_\rho^\dagger, \qquad \boldsymbol{C}_\sigma = \boldsymbol{S}_\sigma \boldsymbol{\zeta}_\sigma \boldsymbol{S}_\sigma^\dagger, \tag{4.204}$$

where $\boldsymbol{\zeta}_\rho$ and $\boldsymbol{\zeta}_\sigma$ are diagonal matrices containing the eigenvalues of $\boldsymbol{C}_\rho$ and $\boldsymbol{C}_\sigma$, respectively. Then, we define the matrix

$$\begin{aligned} \boldsymbol{G} &= e^{-\boldsymbol{Q}_\alpha} \\ &= \boldsymbol{S}_\sigma \left(\frac{\boldsymbol{\zeta}_\sigma}{\mathbb{1} - \boldsymbol{\zeta}_\sigma}\right)^\nu \boldsymbol{S}_\sigma^\dagger \cdot \boldsymbol{S}_\rho \left(\frac{\boldsymbol{\zeta}_\rho}{\mathbb{1} - \boldsymbol{\zeta}_\rho}\right) \boldsymbol{S}_\rho^\dagger \cdot \boldsymbol{S}_\sigma \left(\frac{\boldsymbol{\zeta}_\sigma}{\mathbb{1} - \boldsymbol{\zeta}_\sigma}\right)^\nu \boldsymbol{S}_\sigma^\dagger. \end{aligned} \tag{4.205}$$

Finally, we diagonalize $\boldsymbol{G}$ to obtain its eigenvalues $\{g_k\}$. The final expression for the Rényi relative entropy becomes

$$S_\alpha(\hat{\rho} \,\|\, \hat{\sigma}) = \frac{\alpha}{1-\alpha} \log Z_\rho + \log Z_\sigma - \frac{1}{1-\alpha} \sum_{k=1}^{N} \log(1 + g_k^\alpha). \tag{4.206}$$

4.8.4 Fidelity

The Uhlmann fidelity between two quantum states $\hat{\rho}$ and $\hat{\sigma}$ is defined as

$$F(\hat{\rho}, \hat{\sigma}) = \left(\operatorname{Tr}\left[\sqrt{\sqrt{\hat{\sigma}} \hat{\rho} \sqrt{\hat{\sigma}}}\right]\right)^2. \tag{4.207}$$

It satisfies $0 \leq F(\hat{\rho}, \hat{\sigma}) \leq 1$, with equality $F(\hat{\rho}, \hat{\sigma}) = 1$ if and only if $\hat{\rho} = \hat{\sigma}$.

Setting $\alpha = \frac{1}{2}$ in the definition of the Rényi-α relative entropy, we obtain

$$S_{1/2}(\hat{\rho} \,\|\, \hat{\sigma}) = -2 \log \operatorname{Tr}\left[\left(\hat{\sigma}^{\frac{1}{2}} \hat{\rho} \hat{\sigma}^{\frac{1}{2}}\right)^{\frac{1}{2}}\right] = -\log F(\hat{\rho}, \hat{\sigma}). \tag{4.208}$$

Hence, the fidelity can be computed using the results derived in the previous section:

$$F(\hat{\rho}, \hat{\sigma}) = e^{-S_{1/2}(\hat{\rho} \,\|\, \hat{\sigma})} \tag{4.209}$$

Alternatively, the fidelity can also be expressed in the symmetric form [129]

$$F(\hat{\rho},\hat{\sigma}) = \Big(\mathrm{Tr}\Big[\sqrt{\hat{\rho}\hat{\sigma}}\Big]\Big)^2, \tag{4.210}$$

Using the fact that exponentials of quadratic operators remain Gaussian under multiplication, we write

$$\hat{\rho}\hat{\sigma} = e^{-\hat{\boldsymbol{c}}^\dagger \boldsymbol{M}_\rho \hat{\boldsymbol{c}}} e^{-\hat{\boldsymbol{c}}^\dagger \boldsymbol{M}_\sigma \hat{\boldsymbol{c}}} = e^{-\hat{\boldsymbol{c}}\boldsymbol{Q}\hat{\boldsymbol{c}}} \quad \text{with} \quad e^{\boldsymbol{Q}} = e^{\boldsymbol{M}_\rho} e^{\boldsymbol{M}_\sigma}. \tag{4.211}$$

The fidelity then becomes

$$F(\hat{\rho},\hat{\sigma}) = \frac{1}{Z_\rho Z_\sigma}\Big(\mathrm{Tr}\Big[e^{-\frac{1}{2}\hat{\boldsymbol{c}}^\dagger \boldsymbol{Q}\hat{\boldsymbol{c}}}\Big]\Big)^2. \tag{4.212}$$

In terms of the matrices $\boldsymbol{M}_\rho$ and $\boldsymbol{M}_\sigma$, the fidelity becomes

$$F(\hat{\rho},\hat{\sigma}) = \frac{\det\Big(\mathbb{1} + \sqrt{e^{-\boldsymbol{M}_\rho}\cdot e^{-\boldsymbol{M}_\sigma}}\Big)^2}{\det\big(\mathbb{1}+e^{-\boldsymbol{M}_\rho}\big)\cdot\det\big(\mathbb{1}+e^{-\boldsymbol{M}_\sigma}\big)}, \tag{4.213}$$

while in terms of the covariance matrices it reads

$$F(\hat{\rho},\hat{\sigma}) = \frac{1}{\det\big(\mathbb{1}-\boldsymbol{C}_\rho\big)\det\big(\mathbb{1}-\boldsymbol{C}_\sigma\big)}\det\left(\mathbb{1}+\left[\left(\frac{\boldsymbol{C}_\rho}{\mathbb{1}-\boldsymbol{C}_\rho}\right)\left(\frac{\boldsymbol{C}_\sigma}{\mathbb{1}-\boldsymbol{C}_\sigma}\right)\right]^{\frac{1}{2}}\right)^2. \tag{4.214}$$

Part III

The mesoscopic leads approach

5 The mesoscopic approach to quantum thermodynamics

Modeling quantum systems in contact with an environment is essential for understanding real-world phenomena across quantum optics, condensed matter, and quantum information. As discussed in the Introduction and in Chapter 2, one of the central tools in this context is the Lindblad master equation, which describes the most general form of completely positive and trace-preserving (CPTP) Markovian evolution [63]. The Lindblad framework offers both theoretical and numerical advantages: from a computational perspective, it eliminates the need to track the state of the environment, enabling significant simplifications in both memory and time. In particular, it provides access to the quantum jump method, which is especially efficient in terms of memory usage [29, 28].

Despite its versatility, the Lindblad description has important limitations. The underlying assumptions—especially the Markov approximation—break down in a number of physically relevant scenarios. For instance, strong system-environment coupling, structured reservoirs with non-flat spectral densities (as encountered in photonic crystals or nanocavities), low-temperature environments, or finite-size baths (such as in ion trap experiments or mesoscopic quantum dots) can all induce memory effects that invalidate a Markovian treatment. Additionally, in systems driven on timescales comparable to or faster than the bath correlation time, non-Markovian behavior naturally emerges [34].

To address these limitations, various techniques have been developed to model non-Markovian dynamics. These include the hierarchical equations of motion (HEOM) [69, 130], the TEMPO algorithm [73], and other tensor-network-based approaches. Each comes with trade-offs in terms of computational cost, scalability, and physical transparency. Among the most elegant approaches in the context of quantum transport is the Landauer–Büttiker formalism [131, 132], which is particularly well-suited to steady-state transport through mesoscopic systems. However, generalizing this framework to time-dependent driving remains challenging. While periodic driving can sometimes be handled using Floquet theory, capturing transient dynamics and short-time current behavior is significantly more difficult. Furthermore, computing the transmission function—the central quantity in Landauer–Büttiker theory—becomes highly nontrivial when interactions are present.

A promising alternative for treating non-Markovian dynamics is the mesoscopic leads formalism, also known in various contexts as the pseudomodes method [40], the extended reservoir approach [133, 134], or, in related fashion, the driven Liouville–von Neumann (DLvN) method [135, 136]. The central idea is to embed the system within a larger structure: one couples the system to a finite auxiliary subsystem—the "lead"—which is in turn subject to Markovian dissipation. The dynamics of the combined system (system + lead) then follow a Lindblad equation, even though the reduced dynamics of the system alone can display

non-Markovian features. This so-called Markovian embedding enables one to recover memory effects while retaining the numerical advantages of Lindblad dynamics. Importantly, it also permits the use of the quantum jump method in non-Markovian settings, offering a computationally efficient route to simulate open quantum systems [37, 46].

This technique has seen important theoretical development in recent years. An important step was taken by Brenes *et al.* [44], who demonstrated how the method can be used to study thermodynamics in interacting systems, using a tensor-network approach, focusing on the steady-state. Building on this, we extended the thermodynamic analysis to the time-dependent case, without requiring perturbation theory in the driving speed [45]. In parallel, Ref. [137] investigated unravelings of the dynamics within this framework, exploring the role of quantum trajectories.

The present work contributes to this growing literature by extending the thermodynamic analysis within the mesoscopic leads formalism to *fully time-dependent driving scenarios*. This generalization is crucial for addressing realistic quantum thermodynamic protocols where systems are subject to strong driving or evolve far from equilibrium. The approach retains thermodynamic consistent defintion, thereby providing a flexible and efficient tool for studying energy flows, entropy production, and irreversibility in dynamically evolving quantum systems.

This chapter focuses on the development, application, and extension of the mesoscopic leads framework to quantum thermodynamics beyond the weak-coupling and adiabatic limits. It is based on Ref. [45], which is on the main contributions of this thesis.

The present work contributes to this growing literature by extending the thermodynamic analysis within the mesoscopic leads formalism to fully time-dependent driving scenarios. This generalization is crucial for addressing realistic quantum thermodynamic protocols where systems are subject to strong driving or evolve far from equilibrium. The approach retains thermodynamically consistent definitions of work, heat and entropy production and accommodates strong coupling, thereby providing a flexible tool for studying thermodynamics beyond the weak-coupling regime.

This chapter is structured as follows. In Section 5.1, we discuss the main system-bath setup and introduce the necessary notation. In Section 5.2, we provide a pedagogically-oriented introduction to the technique and provide a prescription for a numerical implementation. Then, In Section 5.3, we discuss its relationship to the reaction coordinate (RC) mapping. In particular, we provide a formal justification of the mesoscopic leads framework via the RC mapping. While this connection is acknowledged in the literature, here we present it in details. In Section 5.4, we discuss the thermodynamics within the framework, deriving consistent definitions of particle and energy currents from first principles. In Section 5.5, we discuss implementation details of the technique when the central system is non-interacting, via the Lyapunov equation formalism. In Section 5.6 we benchmark the technique using the resonant-level model. Finally, in Section 5.7, we use the method to study rectification in a driven-double dot system, which exhibits rectification despite being quadratic.

◆

5.1 The Target Problem: Fermionic System Coupled to Thermal Reservoirs

In this section, we present the main setup we want to approximate with the mesoscopic leads approach: a fermionic system coupled to non-interacting fermionic baths. For future reference, we will refer to this setup as the *original* or *target problem*.

We consider a fermionic system S, possibly interacting and time-dependent, described by N fermionic modes $\{\hat{c}_i\}_{i=1}^{N}$. The system is coupled to M reservoirs, indexed by α. The total Hamiltonian of the setup takes the form

$$\hat{H}_{\text{tot}}(t) = \hat{H}_S(t) + \sum_{\alpha} \left(\hat{H}_{S\alpha} + \hat{H}_{\alpha}\right). \tag{5.1}$$

Throughout this chapter, we denote by $\hat{H}_{\text{tot}}$ the full microscopic Hamiltonian, encompassing the system, the baths and their interactions.

Each bath is described by a continuum of non-interacting modes with annihilation operators $\hat{b}_{m\alpha}$:

$$\hat{H}_{\alpha} = \sum_{m=1}^{\infty} \omega_{m\alpha} \hat{b}_{m\alpha}^{\dagger} \hat{b}_{m\alpha}. \tag{5.2}$$

We assume that each reservoir couples to a single system site p_α. In a one-dimensional chain, these would typically correspond to the first and last site. The system-bath coupling terms are modeled as tunneling Hamiltonians:

$$\hat{H}_{S\alpha} = \sum_{m=1}^{\infty} \left(\lambda_{m\alpha} \hat{c}_{p_\alpha}^{\dagger} \hat{b}_{m\alpha} + \lambda_{m\alpha}^{*} \hat{b}_{m\alpha}^{\dagger} \hat{c}_{p_\alpha}\right). \tag{5.3}$$

A schematic illustration of this setup is shown in Fig. 5.1.

Both $\hat{H}_\alpha$ and $\hat{H}_{S\alpha}$ conserve the particle number $\hat{N}_\alpha = \sum_m \hat{b}_{m\alpha}^{\dagger}\hat{b}_{m\alpha}$. Additionally, we will assume that the total particle number is also conserved, i.e., $[\hat{H}_{\text{tot}}, \hat{N}_S + \sum_\alpha \hat{N}_\alpha] = 0$, where $\hat{N}_S = \sum_i \hat{c}_i^{\dagger}\hat{c}_i$.

At $t = 0$, each bath is prepared in a Gibbs state with inverse temperature β_α and chemical potential μ_α, and the full system is initialized as a product state:

$$\hat{\rho}(0) = \hat{\rho}_{\text{S}}(0) \otimes \bigotimes_{\alpha} \hat{\omega}_{\alpha}, \quad \hat{\omega}_{\alpha} = \frac{e^{-\beta_\alpha(\hat{H}_\alpha - \mu_\alpha \hat{N}_\alpha)}}{Z_\alpha}, \tag{5.4}$$

which implies that the initial occupation of the bath modes is given by the Fermi–Dirac distribution, $\langle \hat{b}_{m\alpha}^{\dagger}\hat{b}_{m\alpha}\rangle = f_\alpha(\omega_{m\alpha}) = (e^{\beta_\alpha(\omega_{m\alpha}-\mu_\alpha)}+1)^{-1}$.

We focus on an average description of thermodynamics, without account for fluctuations or stochastic effects. Within this framework, the particle and energy currents are sufficient to express the first law. For the second law, a fully time-dependent formulation requires the time-derivative of the von Neumann entropy, which depends on the full state of the system. However, in the steady-state regime, the entropy becomes time-independent, and its derivative vanishes. As a result, the entropy production can be expressed entirely in terms of particle and energy currents. Accordingly, these currents become the central quantities in our thermodynamic analysis.

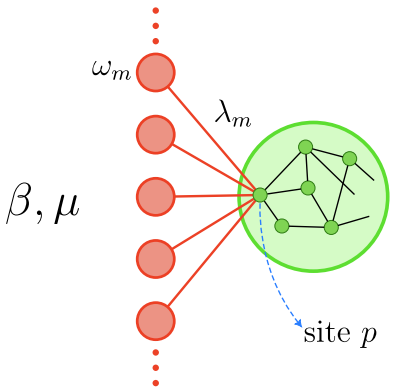

Figure 5.1: Schematic of the target problem: a fermionic system (green) is coupled at site p to a reservoir composed of non-interacting modes ω_m (red), with coupling strengths λ_m. Insets illustrate the Fermi–Dirac distribution $f(\omega)$ with thermal width $\sim 1/\beta$, and the reservoir's spectral density $\mathcal{J}(\omega)$, supported over a bandwidth W.

The definitions of the currents were introduced in Section 3.4.2 of Chapter 3. For completeness, we recall them here. The average energy current flowing out of reservoir α is defined by

$$J_\alpha^E = -\frac{\mathrm{d}\langle \hat{H}_\alpha \rangle}{\mathrm{d}t} = i\langle [\hat{H}_\alpha, \hat{H}_{S\alpha}] \rangle, \tag{5.5}$$

where we used $[\hat{H}_{\mathrm{tot}}, \hat{H}_\alpha] = [\hat{H}_{S\alpha}, \hat{H}_\alpha]$. The particle current is given by

$$J_\alpha^P = -\frac{\mathrm{d}\langle \hat{N}_\alpha \rangle}{\mathrm{d}t} = i\langle [\hat{N}_\alpha, \hat{H}_{S\alpha}] \rangle, \tag{5.6}$$

since $[\hat{H}_{\mathrm{tot}}, \hat{N}_\alpha] = [\hat{H}_{S\alpha}, \hat{N}_\alpha]$. The heat current is then naturally defined as

$$J_\alpha^Q = J_\alpha^E - \mu_\alpha J_\alpha^P. \tag{5.7}$$

Together with the assumption that baths are initially thermal states, the effect of reservoir α on the system is fully characterized by its spectral density:

$$\mathcal{J}_\alpha(\omega) = 2\pi \sum_{m=1}^{\infty} |\lambda_{m\alpha}|^2 \delta(\omega - \omega_{m\alpha}), \tag{5.8}$$

which encodes both mode density and coupling strength. A common measure of total coupling strength is

$$\Gamma_\alpha = \frac{1}{2W_\alpha} \int \mathrm{d}\omega \, \mathcal{J}_\alpha(\omega), \tag{5.9}$$

assuming $\mathcal{J}_\alpha(\omega)$ is supported on some frequency interval with half-bandwidth W_α.

When the system Hamiltonian is non-interacting and time-independent, the steady-state currents can be computed from the Landauer–Büttiker formalism. For a system coupled to two reservoirs—denoted left (L) and right (R)—the steady-state particle current is given by the Landauer–Büttiker formula:

$$J^P = \int \frac{d\omega}{2\pi} \mathcal{T}(\omega)[f_{\mathrm{L}}(\omega) - f_{\mathrm{R}}(\omega)], \tag{5.10}$$

where $f_\alpha(\omega) = \left(e^{\beta_\alpha(\omega-\mu_\alpha)}+1\right)^{-1}$ is the Fermi–Dirac distribution of reservoir α, and $\mathcal{T}(\omega)$ is the transmission function, computable from the system's non-equilibrium Green's functions. The corresponding energy current is

$$J^E = \int \frac{\mathrm{d}\omega}{2\pi}\,\omega\mathcal{T}(\omega)[f_{\mathrm{L}}(\omega) - f_{\mathrm{R}}(\omega)], \tag{5.11}$$

with heat current $J_L^Q = J_L^E - \mu_L J_L^P$.

This framework provides an elegant description of coherent transport in mesoscopic systems and has been foundational in quantum thermoelectrics [131, 132]. However, it relies critically on assumptions of non-interacting dynamics, time-translational invariance, and a well-defined steady state. These assumptions break down in the presence of time-dependent driving or strong coupling, where memory effects and reservoir back-action become important. This motivates the development of alternative approaches—such as the mesoscopic leads formalism—capable of treating strongly coupled, dynamically driven open systems in a thermodynamically consistent manner.

5.2 The Mesoscopic Leads Approach

In this section, we present the mesoscopic leads formalism. We begin with a unitary description of the setup, which serves as the foundation for the Markovian embedding developed in the next subsection.

5.2.1 Unitary description

To clarify the construction, we begin by considering the case of a single reservoir. The total Hamiltonian then simplifies to

$$\hat{H}_{\mathrm{tot}} = \hat{H}_S + \hat{H}_B + \hat{H}_{SB}, \tag{5.12}$$

where $\hat{H}_B$ is the reservoir Hamiltonian, and $\hat{H}_{SB}$ represents the system-bath coupling:

$$\begin{aligned}\hat{H}_B &= \sum_{m=1}^{\infty} \omega_m \hat{b}_m^\dagger \hat{b}_m,\\ \hat{H}_{SB} &= \sum_{m=1}^{\infty} \left(\lambda_m \hat{c}_p^\dagger \hat{b}_m + \lambda_m^* \hat{b}_m^\dagger \hat{c}_p\right),\end{aligned} \tag{5.13}$$

where the reservoir is coupled locally to a given site p. This environment is described by some spectral density $\mathcal{J}(\omega)$, which we seek to approximate.

The mesoscopic leads approach replaces this continuum bath with a finite set of L modes $\{\hat{a}_k\}_{k=1}^L$, collectively referred to as the *lead*. The Hamiltonian of the lead and its coupling to the system are given by

$$\hat{H}_L = \sum_{k=1}^{L} \epsilon_k \hat{a}_k^\dagger \hat{a}_k, \tag{5.14}$$

$$\hat{H}_{SL} = \sum_{k=1}^{L} \left(\kappa_k \hat{c}_p^\dagger \hat{a}_k + \kappa_k^* \hat{a}_k^\dagger \hat{c}_p\right). \tag{5.15}$$

The energies ϵ_k are chosen to sample the frequency range of the original bath's spectral density, typically over a finite energy window where the system–reservoir coupling is significant. We return to this point below.

Replacing an infinite reservoir with a finite lead having a discrete spectrum has important consequences for the dynamics. In particular, the system will inevitably exhibit recurrence behavior on long time scales, with a Poincaré recurrence time set by the inverse of the minimal level spacing [63, 138].

To restore the irreversible behavior, each lead mode $\hat{a}_k$ is coupled to its own auxiliary reservoir, modeled as a collection of non-interacting modes $\hat{b}_{kq}$ with energies ω_{kq}. The total Hamiltonian of these auxiliary baths, which we collectively denote as $\mathcal{E}$, is

$$\hat{H}_{\mathcal{E}} = \sum_{k=1}^{L} \sum_{q} \omega_{kq} \hat{b}_{kq}^{\dagger} \hat{b}_{kq}, \tag{5.16}$$

$$\hat{H}_{L\mathcal{E}} = \sum_{k=1}^{L} \sum_{q} \left(\nu_{kq} \hat{a}_k^{\dagger} \hat{b}_{kq} + \nu_{kq}^{*} \hat{b}_{kq}^{\dagger} \hat{a}_k \right). \tag{5.17}$$

The role of these auxiliary environments is to induce dissipation on the lead modes.

The lead interacts directly with the system, while the external environment couples only to the lead modes. This yields a total Hamiltonian with a natural hierarchical structure:

$$\hat{H}_{\text{tot}} = \hat{H}_S + \hat{H}_{SL} + \hat{H}_L + \hat{H}_{L\mathcal{E}} + \hat{H}_{\mathcal{E}}. \tag{5.18}$$

Crucially, we assume that each auxiliary environment has a flat spectral density over a wide energy range,

$$\mathcal{J}_k(\omega) = 2\pi \sum_{q} |\nu_{kq}|^2 \delta(\omega - \omega_{kq}) = \Gamma_k, \tag{5.19}$$

where Γ_k is taken to be constant and independent of ω. Under this assumption, as we will show in the next section, the effective spectral density seen by the system through the damped lead modes becomes

$$\mathcal{J}_{\text{eff}}(\omega) = \sum_{k=1}^{L} \frac{|\kappa_k|^2 \Gamma_k}{(\omega - \epsilon_k)^2 + (\Gamma_k/2)^2}. \tag{5.20}$$

This expression corresponds to a sum of Lorentzians centered at the lead mode energies ϵ_k, each broadened by the corresponding damping rate Γ_k.

To determine the lead couplings κ_k and damping rates Γ_k, we divide the relevant frequency window into L energy bins of width $\Delta\epsilon_k$, each centered at ϵ_k. Each Lorentzian is constructed to approximate the local spectral weight of $\mathcal{J}(\omega)$ within its corresponding bin. This leads to a natural identification of the damping rate with the bin width, $\Gamma_k = \Delta\epsilon_k$. We then require that the integrated weight of the Lorentzian matches that of the true spectral density over the same interval:

$$\int_{-\infty}^{\infty} \mathrm{d}\omega \, \frac{|\kappa_k|^2 \Gamma_k}{(\omega - \epsilon_k)^2 + (\Gamma_k/2)^2} = \int_{\epsilon_k - \frac{1}{2}\Delta\epsilon_k}^{\epsilon_k + \frac{1}{2}\Delta\epsilon_k} \mathrm{d}\omega \, \mathcal{J}(\omega). \tag{5.21}$$

Assuming that $\mathcal{J}(\omega)$ varies slowly across each bin, we approximate the right-hand side using the midpoint rule:

$$\int_{\epsilon_k-\frac{1}{2}\Delta\epsilon_k}^{\epsilon_k+\frac{1}{2}\Delta\epsilon_k} \mathrm{d}\omega\, \mathcal{J}(\omega) \approx \mathcal{J}(\epsilon_k)\,\Delta\epsilon_k. \tag{5.22}$$

The left-hand side evaluates to

$$\int_{-\infty}^{\infty} \mathrm{d}\omega\, \frac{\Gamma_k}{(\omega-\epsilon_k)^2+(\Gamma_k/2)^2} = 2\pi, \tag{5.23}$$

yielding the identification

$$2\pi|\kappa_k|^2 = \mathcal{J}(\epsilon_k)\,\Delta\epsilon_k. \tag{5.24}$$

Therefore, if we take κ_k to be real, we arrive at the parameter prescription

$$\Gamma_k = \Delta\epsilon_k, \quad \kappa_k = \sqrt{\frac{\mathcal{J}(\epsilon_k)\Delta\epsilon_k}{2\pi}}. \tag{5.25}$$

To verify that this choice yields a faithful approximation of $\mathcal{J}(\omega)$, we recall that a Lorentzian provides a representation of the δ-function:

$$\delta_\Gamma(\omega-\epsilon) = \frac{1}{2\pi}\cdot\frac{\Gamma}{(\omega-\epsilon)^2+\Gamma^2} \quad \xrightarrow{\Gamma\to 0} \quad \delta(\omega-\epsilon), \tag{5.26}$$

in the distributional sense. With the parameters defined in Eq. (5.25), the effective spectral density can be written as

$$\mathcal{J}_{\mathrm{eff}}(\omega) = \sum_k \mathcal{J}(\epsilon_k)\,\Delta\epsilon_k\cdot\delta_{\Gamma_k}(\omega-\epsilon_k), \tag{5.27}$$

which is a Riemann sum approximation to the convolution of $\mathcal{J}(\omega)$ with a sequence of normalized Lorentzians. Therefore, assuming that $\mathcal{J}(\omega)$ is continuous and slowly varying on the scale of $\Delta\epsilon_k$, we find

$$\mathcal{J}_{\mathrm{eff}}(\omega) \xrightarrow{\Gamma\to 0} \int \mathrm{d}\epsilon\, \mathcal{J}(\epsilon)\,\delta(\omega-\epsilon) = \mathcal{J}(\omega). \tag{5.28}$$

As mentioned above, the lead mode energies ϵ_k are chosen to sample the relevant frequency window where the system–bath coupling is significant. Suppose this window is symmetric around zero, $\omega\in[-W,W]$. A simple and widely used choice is uniform (linear) discretization, where the ϵ_k are evenly spaced across the interval. In this case, the spacings are constant, $\Delta\epsilon_k = 2W/L$, leading to uniform damping rates $\Gamma_k = 2W/L$ and coupling amplitudes

$$\kappa_k = \sqrt{\frac{\mathcal{J}(\epsilon_k)\,(2W/L)}{2\pi}}. \tag{5.29}$$

An alternative is the so-called linear-logarithmic (lin-log) discretization, which uses finer resolution near a reference energy—typically the chemical potential—and coarser resolution away from it. This is particularly advantageous when modeling transport near sharp features in $\mathcal{J}(\omega)$, such as the Fermi edge or localized resonances. Lin-log schemes have been used in various contexts, including pseudomode constructions [39], reaction coordinate mappings [139, 88], and numerical renormalization group approaches [140].

5.2.2 Markovian embedding

The structure of the mesoscopic leads setup naturally enables a Markovian description of dissipation. As the number of lead modes L increases, the energy resolution of the discretization improves. The energy bin widths scale as $\Delta\epsilon_k \sim 1/L$, and the corresponding damping rates and couplings satisfy

$$\Gamma_k \sim \frac{1}{L}, \quad \kappa_k \sim \frac{1}{\sqrt{L}}. \tag{5.30}$$

This ensures that the total spectral density remains finite in the limit $L \to \infty$, even though the coupling to each individual mode becomes weak. Importantly, even though the coupling to each lead mode κ_k becomes small, the overall system–lead coupling can still be strong.

In this regime, the conditions for a Born–Markov approximation are met at the level of each lead–environment pair: (i) the coupling ν_{qk} to each reservoir is weak, and (ii) the reservoir correlation functions decay rapidly, which follows from the fact that a flat spectral density corresponds to white-noise correlations:

$$\langle \hat{b}^\dagger_{kq}(t)\hat{b}_{kq}(t')\rangle \propto \delta(t-t'). \tag{5.31}$$

Moreover, since the individual system-lead couplings κ_k are small, the *local* master equation approach is well-justified.

The full environment $\mathcal{E}$ can thus be replaced by a set of independent Lindblad operators acting on the lead. The dynamics of the system and lead is governed by a local, Markovian master equation:

$$\frac{\mathrm{d}\hat{\rho}}{\mathrm{d}t} = -i[\hat{H},\hat{\rho}] + \sum_{k=1}^{L} \mathcal{D}_k[\hat{\rho}], \tag{5.32}$$

where $\hat{H}$ is the Hamiltonian of the extended system:

$$\hat{H} = \hat{H}_S + \hat{H}_{SL} + \hat{H}_L, \tag{5.33}$$

Throughout this chapter, we use $\hat{H}$ exclusively to denote the Hamiltonian of the extended system, to distinguish it from the full microscopic Hamiltonian H_{tot}.

Each dissipator $\mathcal{D}_k$ acts only on lead mode $\hat{a}_k$ and takes the form

$$\mathcal{D}_k[\hat{\rho}] = \Gamma_k(1-f_k)\mathbb{D}[\hat{a}_k](\hat{\rho}) + \Gamma_k f_k \mathbb{D}[\hat{a}^\dagger_k](\hat{\rho}), \tag{5.34}$$

with the standard Lindblad superoperator

$$\mathbb{D}[\hat{L}](\hat{\rho}) = \hat{L}\hat{\rho}\hat{L}^\dagger - \frac{1}{2}\{\hat{L}^\dagger\hat{L},\hat{\rho}\}. \tag{5.35}$$

Here, $f_k = (e^{\beta(\epsilon_k-\mu)}+1)^{-1}$ is the Fermi–Dirac distribution of the fictitious environment at inverse temperature β and chemical potential μ.

The resulting master equation describes a Markovian embedding of the original open system problem: the true reservoir is replaced by a finite auxiliary system (the lead) coupled to idealized, memoryless environments. While the full dynamics of the original system is

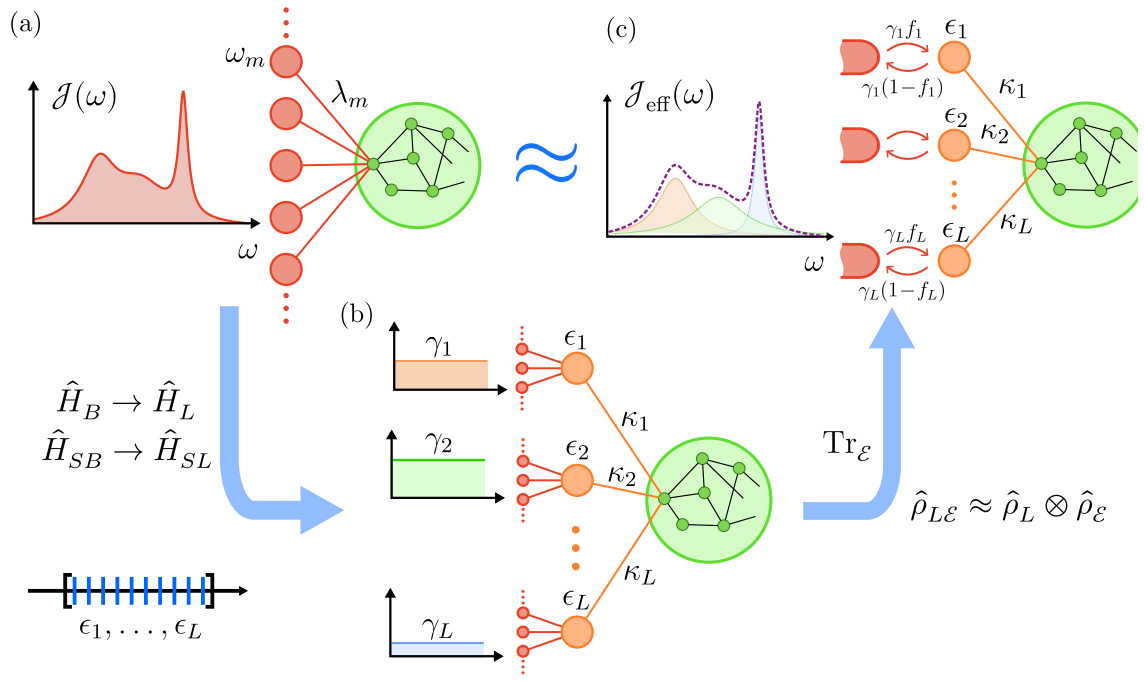

Figure 5.2: **Construction of the mesoscopic leads formalism.** (a) In the original model, the system (green graph) is coupled to a continuum reservoir described by a spectral density $\mathcal{J}(\omega)$ and coupling amplitudes λ_m. (b) In the mesoscopic leads approach, the bath is replaced by a finite set of discrete lead modes with energies ϵ_k and couplings κ_k, each broadened by a damping rate γ_k through coupling to an auxiliary environment with flat spectral density. (c) The auxiliary environments are then traced out under the Born–Markov approximation, $\hat{\rho}_{L\mathcal{E}} \approx \hat{\rho}_L \otimes \hat{\rho}_{\mathcal{E}}$, yielding an effective Lindblad dissipator for each lead mode that enforces a local Fermi distribution f_k. The resulting effective spectral density $\mathcal{J}_{\text{eff}}(\omega)$ approximates the original continuum.

non-Markovian, the inclusion of the lead degrees of freedom explicitly accounts for nontrivial environmental correlations, thereby restoring a Markovian structure in the enlarged space. This perspective has deep implications. It allows the use of the extensive theoretical and numerical machinery developed for Lindblad master equations, including quantum trajectory methods, tensor-network simulations, and steady-state solvers.

Indeed, one of the original motivations for this type of embedding was to enable a quantum jump description of open fermionic systems [37, 38], by shifting non-Markovian memory effects into coherent degrees of freedom. Once the dynamics is cast in Lindblad form, stochastic unravelings and trajectory-based methods become applicable, even in regimes of strong coupling and structured environments.

Furthermore, if one is interested only in the steady-state properties, there exist efficient techniques to compute the stationary solution of Eq. (5.32) directly—without explicit time evolution. In the non-interacting case, the problem reduces to solving a quadratic equation for the covariance matrix [65, 120], while in the interacting case, iterative and variational methods remain tractable due to the locality and structure of the Lindblad generators.

Figure 5.2 summarizes the mesoscopic leads construction and its Markovian embedding.

Initial state of the lead

In the target open system, the reservoir is assumed to be initially in a thermal state,

$$\hat{\rho}_B(0) \propto e^{-\beta(\hat{H}_B+\mu\hat{N}_B)}. \tag{5.36}$$

This assumption is necessary for the correct thermodynamic interpretation of the entropy production. See, for example, our discussion of the second law in Section 3.3.2 of Chapter 2.

In the mesoscopic leads formalism, the original reservoir B is replaced by the composite $L+\mathcal{E}$, where L is the finite lead and $\mathcal{E}$ represents the collection of auxiliary environments. To preserve consistency with the original setup, the composite system must also be initialized in a thermal state,

$$\hat{\rho}_{L\mathcal{E}}(0) \propto e^{-\beta(\hat{H}_L+\hat{H}_\mathcal{E}+\hat{H}_{L\mathcal{E}}-\mu(\hat{N}_L+\hat{N}_\mathcal{E}))}. \tag{5.37}$$

On the other hand, the microscopic derivation of the Lindblad equation—obtained by tracing out the auxiliary environments—requires that $\mathcal{E}$ alone is initially thermal:

$$\hat{\rho}_\mathcal{E}(0) \propto e^{-\beta(\hat{H}_\mathcal{E}-\mu\hat{N}_\mathcal{E})}. \tag{5.38}$$

This assumption is necessary to ensure the resulting reduced dynamics takes Lindblad form, as discussed in Chapter 2.

These two requirements are reconciled by the fact that the derivation also invokes the Born approximation at the level of the lead–environment coupling, which imposes

$$\hat{\rho}_{L\mathcal{E}}(t) \approx \hat{\rho}_L(t) \otimes \hat{\rho}_\mathcal{E}(t) \tag{5.39}$$

at all times. In particular, the initial global state must be uncorrelated. Since the total Hamiltonian $\hat{H}_L + \hat{H}_\mathcal{E}$ is non-interacting, the thermal state of the composite system factorizes:

$$\hat{\rho}_{L\mathcal{E}}(0) \propto e^{-\beta(\hat{H}_L-\mu\hat{N}_L)} \otimes e^{-\beta(\hat{H}_\mathcal{E}-\mu\hat{N}_\mathcal{E})}. \tag{5.40}$$

This implies that the lead must also be initialized in a thermal state:

$$\hat{\rho}_L(0) = \frac{1}{Z_L} e^{-\beta(\hat{H}_L-\mu\hat{N}_L)}, \qquad Z_L = \mathrm{Tr}\left[e^{-\beta(\hat{H}_L-\mu\hat{N}_L)}\right]. \tag{5.41}$$

Thus, the thermal initialization of the lead is required to maintain consistency between the assumptions of the microscopic derivation and the thermodynamic structure of the full model.

5.2.3 Time Resolution

In this section, we examine the temporal resolution of the mesoscopic leads method and its implications for dynamical accuracy. The central object in this analysis is the reservoir *correlation function*, which governs the influence of the environment on the system through both dissipation and memory.

For a continuum reservoir with spectral density $\mathcal{J}(\omega)$, the correlation function takes the form

$$C(t) = \int_{-\infty}^{\infty} \frac{\mathrm{d}\omega}{2\pi}\, \mathcal{J}(\omega)\, f(\omega)\, e^{-i\omega t}, \tag{5.42}$$

where $f(\omega)$ is the Fermi–Dirac distribution. The structure of $C(t)$ directly determines the memory kernel in the system's effective dynamics.

In the mesoscopic leads approach, each lead mode $\hat{a}_k$ is coupled to an auxiliary environment with flat spectral density. The Heisenberg equations of motion for the lead modes yield a quantum Langevin equation [44, 38]:

$$\frac{\mathrm{d}\hat{a}_k}{\mathrm{d}t} = -i\epsilon_k \hat{a}_k - i\kappa_k \hat{c}_p - \frac{\Gamma_k}{2}\hat{a}_k + \hat{\xi}_k(t), \tag{5.43}$$

where $\hat{\xi}_k(t)$ is a quantum noise operator with delta-correlated fluctuations. Solving this equation and substituting the result into the Heisenberg dynamics of the system yields an integro-differential equation of the form

$$\frac{\mathrm{d}\hat{c}_p}{\mathrm{d}t} = \ldots - \int_0^t \mathrm{d}\tau C_{\mathrm{eff}}(t-\tau)\, \hat{c}_p(\tau) + \text{noise}, \tag{5.44}$$

with an effective bath correlation function

$$C_{\mathrm{eff}}(t) = \sum_k |\kappa_k|^2\, f(\epsilon_k)\, e^{-i\epsilon_k t} e^{-\Gamma_k t/2}. \tag{5.45}$$

This expression shows that the system interacts with its environment through a convolution with $C_{\mathrm{eff}}(t)$, which encodes the accessible memory time scales.

Since $C_{\mathrm{eff}}(t)$ is constructed from a finite set of discretized frequencies ϵ_k, it lacks fine-grained spectral structure. In particular, it cannot resolve features in the true correlation function $C(t)$ that occur on timescales shorter than the inverse of the average level spacing:

$$\delta t_{\min} \sim \frac{1}{\Delta\epsilon}. \tag{5.46}$$

This limitation reflects a general time–frequency uncertainty principle and is closely related to the Shannon–Nyquist theorem [141, 142], which states that sampling a function in frequency with resolution $\Delta\epsilon$ restricts the shortest resolvable timescale to $t \gtrsim 1/\Delta\epsilon$. Consequently, if the target spectral density $\mathcal{J}(\omega)$ contains fine spectral features on scales narrower than $\Delta\epsilon$, these cannot be faithfully reproduced by the mesoscopic leads construction. However, when $\mathcal{J}(\omega)$ is smooth and already well approximated by a sum of a few Lorentzian components, accurate results can be obtained even with a small number of lead modes.

Generalization to Multiple Reservoirs

The mesoscopic leads formalism naturally extends to the case where the system is coupled to multiple reservoirs, indexed by α. For each reservoir, we introduce a corresponding finite lead L_α, composed of L_α discrete modes with annihilation operators $\hat{a}_{k\alpha}$, energies $\epsilon_{k\alpha}$, and couplings $\kappa_{k\alpha}$ to the system. Each lead mode is further coupled to its own auxiliary environment with a flat spectral density, inducing a damping rate $\Gamma_{k\alpha}$.

The extended Hamiltonian, encompassing the system and all mesoscopic leads, takes the form

$$\hat{H} = \hat{H}_S + \sum_\alpha \big(\hat{H}_{SL_\alpha} + \hat{H}_{L_\alpha}\big), \tag{5.47}$$

with the lead and coupling Hamiltonians given by

$$\begin{aligned} \hat{H}_{L_\alpha} &= \sum_{k=1}^{L_\alpha} \epsilon_{k\alpha} \hat{a}^\dagger_{k\alpha} \hat{a}_{k\alpha}, \\ \hat{H}_{SL_\alpha} &= \sum_{k=1}^{L_\alpha} \big(\kappa_{k\alpha} \hat{c}^\dagger_{p_\alpha} \hat{a}_{k\alpha} + \kappa^*_{k\alpha} \hat{a}^\dagger_{k\alpha} \hat{c}_{p_\alpha}\big). \end{aligned} \tag{5.48}$$

Each lead mode is subject to a local Lindblad dissipator enforcing relaxation toward a Fermi–Dirac distribution characterized by the temperature β_α and chemical potential μ_α of the corresponding reservoir. The full dynamics is governed by the master equation

$$\frac{\mathrm{d}\hat{\rho}}{\mathrm{d}t} = -i[\hat{H}, \hat{\rho}] + \sum_\alpha \sum_{k=1}^{L_\alpha} \mathcal{D}_{k\alpha}[\hat{\rho}], \tag{5.49}$$

with dissipators

$$\mathcal{D}_{k\alpha}[\hat{\rho}] = \Gamma_{k\alpha}(1 - f_{k\alpha})\mathbb{D}[\hat{a}_{k\alpha}](\hat{\rho}) + \Gamma_{k\alpha} f_{k\alpha} \mathbb{D}[\hat{a}^\dagger_{k\alpha}](\hat{\rho}), \tag{5.50}$$

where $f_{k\alpha} = (e^{\beta_\alpha(\epsilon_{k\alpha} - \mu_\alpha)} + 1)^{-1}$ is the Fermi–Dirac occupation of lead mode k in reservoir α.

This modular structure enables the straightforward simulation of setups with arbitrary reservoir configurations, including thermal machines and multi-terminal transport settings.

5.3 Mesoscopic Leads and Reaction Coordinate Mapping

The mesoscopic leads construction introduced above is conceptually and mathematically related to the reaction coordinate (RC) mapping, a technique developed to address non-Markovian environments. In this section, we clarify this connection by presenting the RC transformation in the fermionic setting. We demonstrate how it gives rise to Lorentzian spectral densities and how the mesoscopic leads structure naturally emerges as a multi-mode generalization. We also discuss the chain mapping technique, which iteratively applies the RC procedure to recast the bath as a one-dimensional tight-binding chain—a representation that has proven particularly effective in numerical simulations of open quantum systems.

5.3.1 The Reaction Coordinate Transformation

We begin by reviewing the RC mapping for a fermionic system linearly coupled to a reservoir. Consider a system Hamiltonian $\hat{H}_S$, coupled via a single site p to a bath of non-interacting fermionic modes. The total Hamiltonian is

$$\begin{aligned} \hat{H}_{\mathrm{tot}} &= \hat{H}_S + \hat{H}_{SB} + \hat{H}_B \\ &= \hat{H}_S + \sum_k \big(\lambda_k \hat{c}^\dagger_p \hat{b}_k + \lambda^*_k \hat{b}^\dagger_k \hat{c}_p\big) + \sum_k \omega_k \hat{b}^\dagger_k \hat{b}_k, \end{aligned} \tag{5.51}$$

where ω_k are reservoir frequencies and λ_k are coupling amplitudes. The influence of the reservoir is fully encoded in the spectral density

$$\mathcal{J}^{(0)}(\omega) = 2\pi \sum_k |\lambda_k|^2 \delta(\omega - \omega_k). \tag{5.52}$$

The core idea of the RC mapping is to isolate a collective degree of freedom of the reservoir—the *reaction coordinate*—that mediates the system-bath interaction. The system couples only to this mode, which in turn interacts with a residual environment. This structure closely resembles the mesoscopic leads construction. The hope is that the residual bath is weakly coupled to the RC, enabling a Markovian description.

To perform the mapping, we apply a unitary transformation of the bath operators into a new set of modes $\hat{f}_n = \sum_k \Lambda_{nk} \hat{b}_k$, with $\boldsymbol{\Lambda}^\dagger \boldsymbol{\Lambda} = \mathbb{1}$. As discussed in Section 4.2.1 of Chapter 4, such transformations preserve the canonical anticommutation relations $\{\hat{f}_n, \hat{f}_m^\dagger\} = \delta_{nm}$. We designate the first mode of this new set, $\hat{f}_1$. Specifically, we want the interaction term to transform as

$$\hat{H}_{SB} = \sum_k \left(\lambda_k \hat{c}_p^\dagger \hat{b}_k + \lambda_k^* \hat{b}_k^\dagger \hat{c}_p\right) \to g \hat{c}_p^\dagger \hat{f}_1 + g^* \hat{f}_1^\dagger \hat{c}_p. \tag{5.53}$$

This is achieved by choosing the first row of $\boldsymbol{\Lambda}$ as

$$\Lambda_{1k} = \frac{\lambda_k}{g}, \quad \text{so that} \quad g\hat{f}_1 = \sum_k \lambda_k \hat{b}_k. \tag{5.54}$$

The anticommutation relation $\{\hat{f}_1, \hat{f}_1^\dagger\} = 1$ then determines the system–RC coupling strength:

$$|g|^2 = \sum_k |\lambda_k|^2 = \int \frac{\mathrm{d}\omega}{2\pi} \mathcal{J}^{(0)}(\omega), \tag{5.55}$$

where the sum has been replaced by an integral in the continuum limit.

To ensure that the residual bath remains diagonal in the new basis, we impose that $\boldsymbol{\Lambda}$ also diagonalizes the bath Hamiltonian in the subspace orthogonal to $\hat{f}_1$:

$$\sum_k \Lambda_{nk} \omega_k \Lambda_{mk}^* = \delta_{nm} \varepsilon_n \quad \text{for all } n, m \neq 1, \tag{5.56}$$

Under this transformation, the bath Hamiltonian becomes

$$\hat{H}_B = \sum_k \omega_k \hat{b}_k^\dagger \hat{b}_k = \varepsilon_1 \hat{f}_1^\dagger \hat{f}_1 + \sum_{n>1} \left(t_n \hat{f}_1^\dagger \hat{f}_n + t_n^* \hat{f}_n^\dagger \hat{f}_1\right) + \sum_{n>1} \varepsilon_n \hat{f}_n^\dagger \hat{f}_n, \tag{5.57}$$

with

$$t_n = \sum_k \frac{\omega_k \lambda_k \Lambda_{nk}^*}{g}, \quad \varepsilon_n = \sum_k \omega_k |\Lambda_{nk}|^2. \tag{5.58}$$

In particular, the energy of the RC is

$$\varepsilon_1 = \sum_k \frac{\omega_k |\lambda_k|^2}{|g|^2} = \frac{1}{2\pi |g|^2} \int \mathrm{d}\omega\, \omega \mathcal{J}^{(0)}(\omega). \tag{5.59}$$

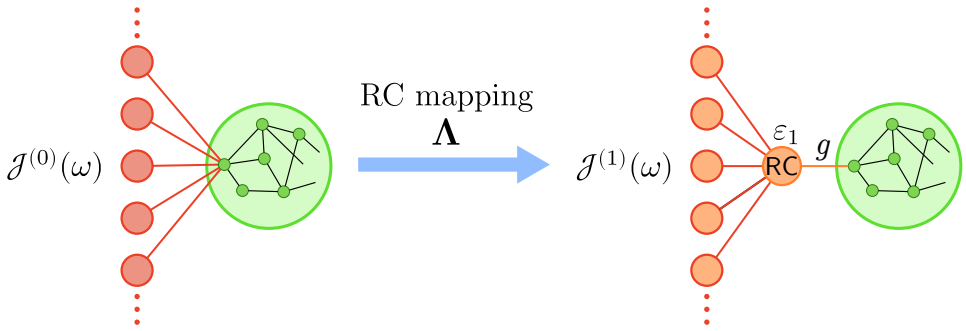

Figure 5.3: **Schematic representation of the reaction coordinate (RC) mapping.** The original bath, characterized by the spectral density $\mathcal{J}^{(0)}(\omega)$, is shown on the left as a collection of modes (red) coupled to the system (green). The RC mapping Λ transforms the environment by isolating a collective mode (orange node labeled "RC") with energy ε_1 and coupling strength g. The remaining modes define a residual environment with a new spectral density $\mathcal{J}^{(1)}(\omega)$. The system now couples only to the RC mode, which in turn mediates the interaction with the residual bath.

The full Hamiltonian after the RC transformation thus reads

$$\hat{H}'_{\text{tot}} = \hat{H}_S + g\hat{c}_p^\dagger \hat{f}_1 + g^* \hat{f}_1^\dagger \hat{c}_p + \varepsilon_1 \hat{f}_1^\dagger \hat{f}_1 + \sum_{n>1}^{\infty} \left(t_n \hat{f}_1^\dagger \hat{f}_n + t_n^* \hat{f}_n^\dagger \hat{f}_1 \right) + \sum_{n>1}^{\infty} \varepsilon_n \hat{f}_n^\dagger \hat{f}_n. \tag{5.60}$$

From a linear algebra perspective, the unitary matrix $\boldsymbol{\Lambda}$ can always be constructed. Once the first row $\boldsymbol{\Lambda}_1 = (\lambda_1/g, \dots)$ is fixed, the remaining rows can be chosen to diagonalize the matrix $\boldsymbol{W} = \text{diag}(\boldsymbol{\omega})$ restricted to the orthogonal subspace $\boldsymbol{\Lambda}_1^\perp$. Explicitly, this corresponds to diagonalizing $\boldsymbol{V}\boldsymbol{W}\boldsymbol{V}^\dagger$, where the rows of $\boldsymbol{V}$ form an orthonormal basis for $\boldsymbol{\Lambda}_1^\perp$.

Figure 5.3 provides a schematic illustration of the transformation.

Residual Spectral Density

The influence of the residual bath on the reaction coordinate is described by the spectral density

$$\mathcal{J}^{(1)}(\omega) = 2\pi \sum_n |t_n|^2 \delta(\omega - \varepsilon_n). \tag{5.61}$$

We now aim to express $\mathcal{J}^{(0)}(\omega)$ as a functional of $\mathcal{J}^{(1)}(\omega)$ by comparing the system dynamics before and after the mapping. This is done by matching the system's effective dynamics before and after the RC transformation, allowing us to relate the two self-energies via the equations of motion.

Under the original Hamiltonian, the Heisenberg equations of motion for the system operator $\hat{c}_p$ and bath modes $\hat{b}_k$ are

$$\begin{cases} \dfrac{\mathrm{d}}{\mathrm{d}t}\hat{c}_p(t) = i[\hat{H}_S(t), \hat{c}_p(t)] - i\displaystyle\sum_k \lambda_k \hat{b}_k(t) \\ \dfrac{\mathrm{d}}{\mathrm{d}t}\hat{b}_k(t) = -i\omega_k \hat{b}_k(t) - i\lambda_k^* \hat{c}_p(t). \end{cases} \tag{5.62}$$

To proceed, we define the transformation for $z \in \mathbb{C}$ with $\text{Im}\, z > 0$:

$$\tilde{f}(z) = \int_0^\infty \mathrm{d}t\, e^{izt} f(t). \tag{5.63}$$

Note this is not exactly a Fourier transform, but rather a hybrid between a Fourier and a Laplace transform, owing to the complex nature of z. The condition $\operatorname{Im} z > 0$ is necessary for the convergence of the integral. While this terminology is not standard, we will refer to it as a *Fourier-Laplace transform*.

Similarly to the conventional Fourier transform, it satisfies the identity

$$\widetilde{\frac{\mathrm{d}f}{\mathrm{d}t}} = -iz\,\tilde{f}(z). \tag{5.64}$$

Applying this transformation to Eq. (5.62), we obtain

$$\begin{cases} -iz\tilde{c}_p(z) = i\widetilde{[\hat{H}_S, \hat{c}_p]}(z) - i\sum_k \lambda_k \tilde{b}_k(z), \\ -iz\tilde{b}_k(z) = -i\omega_k \tilde{b}_k(z) - i\lambda_k^* \tilde{c}_p(z). \end{cases} \tag{5.65}$$

Solving for $\tilde{b}_k(z)$ and substituting into the equation for $\tilde{c}_p(z)$ yields

$$\tilde{b}_k(z) = \frac{\lambda_k^*}{z-\omega_k}\tilde{c}_p(z), \qquad z\tilde{c}_p(z) = -\widetilde{[\hat{H}_S, \hat{c}_p]}(z) + \sum_k \frac{|\lambda_k|^2}{z-\omega_k}\tilde{c}_p(z). \tag{5.66}$$

We now define the reservoir (retarded) self-energy as

$$\Sigma^{(0)}(z) = \sum_k \frac{|\lambda_k|^2}{z-\omega_k} = \frac{1}{2\pi}\int \mathrm{d}\omega'\, \frac{\mathcal{J}^{(0)}(\omega')}{z-\omega'}, \tag{5.67}$$

which is the Cauchy transform of the spectral density $\mathcal{J}^{(0)}(\omega)$. It satisfies the Sokhotski–Plemelj theorem [143, 144]:

$$\Sigma^{(0)}(\omega + i0^+) = -\frac{i}{2}\mathcal{J}^{(0)}(\omega) + \frac{1}{2\pi}\mathcal{P}\int \mathrm{d}\omega'\, \frac{\mathcal{J}^{(0)}(\omega')}{\omega'-\omega}, \tag{5.68}$$

where the limit is defined as $\Sigma(\omega + i0^+) = \lim_{\epsilon\to 0^+}\Sigma(\omega + i\epsilon)$.

The second term in Eq. (5.68) is an instance of the *Hilbert transform* [145], a singular integral operator defined as

$$\mathcal{H}[f](\omega) = \frac{1}{\pi}\mathcal{P}\int \mathrm{d}\omega'\, \frac{f(\omega')}{\omega'-\omega}. \tag{5.69}$$

This operation plays an important role in signal processing theory.

Hence, the equation of motion for the system mode becomes

$$z\tilde{c}_p(z) = -\widetilde{[\hat{H}_S, \hat{c}_p]}(z) + \Sigma^{(0)}(z)\tilde{c}_p(z). \tag{5.70}$$

Now consider the equations of motion after the RC transformation:

$$\begin{cases} \dfrac{\mathrm{d}}{\mathrm{d}t}\hat{c}_p(t) = i[\hat{H}_S(t), \hat{c}_p(t)] - ig\hat{f}_1(t), \\ \dfrac{\mathrm{d}}{\mathrm{d}t}\hat{f}_1(t) = -i\varepsilon_1\hat{f}_1(t) - ig^*\hat{c}_p(t) - i\sum_{n>1} t_n^*\hat{f}_n(t), \\ \dfrac{\mathrm{d}}{\mathrm{d}t}\hat{f}_n(t) = -i\varepsilon_n\hat{f}_n(t) - it_n\hat{f}_1(t), \qquad n>1. \end{cases} \tag{5.71}$$

Applying the Fourier-Laplace transform, we obtain:

$$\begin{cases} -iz\tilde{c}_p(z) = i\widetilde{[\hat{H}_S, \hat{c}_p]}(z) - ig\tilde{f}_1(z), \\ -iz\tilde{f}_1(z) = -i\varepsilon_1\tilde{f}_1(z) - ig^*\tilde{c}_p(z) - i\sum_{n>1} t_n^*\tilde{f}_n(z), \\ -iz\tilde{f}_n(z) = -i\varepsilon_n\tilde{f}_n(z) - it_n\tilde{f}_1(z), \qquad n > 1. \end{cases} \tag{5.72}$$

Solving hierarchically, we first eliminate the residual bath modes:

$$\tilde{f}_n(z) = \frac{t_n}{z - \varepsilon_n}\tilde{f}_1(z), \tag{5.73}$$

and substitute into the equation for $\tilde{f}_1(z)$:

$$\tilde{f}_1(z) = \frac{g^*}{z - \varepsilon_1 - \sum_{n>1} \frac{|t_n|^2}{z-\varepsilon_n}}\,\tilde{c}_p(z). \tag{5.74}$$

Here, we recognize the self-energy of the residual bath:

$$\Sigma^{(1)}(z) = \sum_{n>1} \frac{|t_n|^2}{z - \varepsilon_n}. \tag{5.75}$$

The resulting equation of motion for the system mode then becomes

$$z\tilde{c}_p(z) = -i\widetilde{[\hat{H}_S, \hat{c}_p]}(z) + \frac{|g|^2}{z - \varepsilon_1 - \Sigma^{(1)}(z)}\tilde{c}_p(z). \tag{5.76}$$

Since the reaction coordinate mapping is an exact unitary transformation of the bath degrees of freedom, the dynamics of the system mode must remain unchanged. This allows us to equate the two expressions for $\tilde{c}_p(z)$ and directly compare the corresponding self-energies. Matching with Eq. (5.70) gives

$$\Sigma^{(0)}(z) = \frac{|g|^2}{z - \varepsilon_1 + \Sigma^{(1)}(z)} \quad \Rightarrow \quad \Sigma^{(1)}(z) = (z - \varepsilon_1) - \frac{|g|^2}{\Sigma^{(0)}(z)}. \tag{5.77}$$

Finally, using the Sokhotski–Plemelj relation and the identity $\mathrm{Im}(1/x) = -\mathrm{Im}(x)/|x|^2$, we obtain the transformed spectral density:

$$\mathcal{J}^{(1)}(\omega) = \frac{2|g|^2\,\mathrm{Re}\,\Sigma^{(0)}(\omega + i0^+)}{|\Sigma^{(0)}(\omega + i0^+)|^2} = \frac{4|g|^2\mathcal{J}^{(0)}(\omega)}{\left[\frac{1}{\pi}\mathcal{P}\int \mathrm{d}\omega' \frac{\mathcal{J}^{(0)}(\omega')}{\omega' - \omega}\right]^2 + \left[\mathcal{J}^{(0)}(\omega)\right]^2}. \tag{5.78}$$

This completes the formal derivation of the RC-transformed spectral density.

Interpretation and Example

The RC mapping is formally exact: it involves a unitary transformation on the bath degrees of freedom and introduces no approximation. Its practical value lies in the fact that, for many spectral densities of physical interest, the residual bath couples more weakly to the RC than the original bath did to the system. This can make the setup more amenable to

Markovian treatments, even though the dynamics of the reduced state of the system remains non-Markovian.

A useful heuristic, discussed in Ref. [146], helps explain why this often occurs. If the original spectral density is scaled as $\mathcal{J}^{(0)}(\omega) \to \alpha\mathcal{J}^{(0)}(\omega)$ for some $\alpha > 0$, the system–RC coupling becomes $g \to \sqrt{\alpha}\, g$, while the residual spectral density $\mathcal{J}^{(1)}(\omega)$ remains unchanged. Thus, even in the strong-coupling limit, the non-Markovianity is absorbed into the system–RC interaction, while the residual bath remains weakly coupled.

While the RC mapping often leads to a reduction in coupling strength, this behavior is not guaranteed and depends on the form of the initial spectral density. Table 5.1 presents several representative spectral densities along with the resulting system–RC coupling strength, RC frequency, and residual spectral density following a single RC mapping. These examples, adapted from Ref. [146], demonstrate how certain forms lead to dramatic simplifications, while others retain significant structure in the residual bath.

Table 5.1: Examples of initial spectral densities $\mathcal{J}^{(0)}(\omega)$, corresponding system–RC coupling strengths $|g|^2$, RC frequencies ε_1, and residual spectral densities $\mathcal{J}^{(1)}(\omega)$ after a single reaction coordinate mapping. Adapted from Ref. [146].

$\mathcal{J}^{(0)}(\omega)$	$\lvert g\rvert^2$	ε_1	$\mathcal{J}^{(1)}(\omega)$
$\dfrac{\Gamma\delta^2}{(\omega-\epsilon)^2+\delta^2}$	$\dfrac{\Gamma\delta}{2}$	ϵ	2δ
$\Gamma e^{-\frac{(\omega-\epsilon)^2}{\delta^2}}$	$\dfrac{\Gamma\delta\sqrt{\pi}}{2}$	ϵ	$\dfrac{2\Gamma\delta\sqrt{\pi}\left[1+\left(\frac{\omega-\epsilon}{\delta}\right)^2\right]}{1-\operatorname{erf}(i\frac{\omega-\epsilon}{\delta})}$
$\Gamma\Theta(\omega,\epsilon-\delta,\epsilon+\delta)$	$\dfrac{\Gamma\delta}{\pi}$	ϵ	$\dfrac{4\pi\Gamma\delta\,\operatorname{atanh}^2\left(\frac{\omega-\epsilon}{\delta}\right)}{\pi^2+4\,\operatorname{atanh}^2\left(\frac{\omega-\epsilon}{\delta}\right)}\Theta(\omega,\epsilon-\delta,\epsilon+\delta)$
$\Gamma\sqrt{1-\left(\dfrac{\omega-\epsilon}{\delta}\right)^2}\Theta(\omega,\epsilon-\delta,\epsilon+\delta)$	$\dfrac{\Gamma\delta}{4}$	ϵ	$\dfrac{\Gamma\delta}{4}\sqrt{1-\left(\dfrac{\omega-\epsilon}{\delta}\right)^2}\Theta(\omega,\epsilon-\delta,\epsilon+\delta)$

One particularly simple and widely used case is the Lorentzian spectral density:

$$\mathcal{J}^{(0)}(\omega) = \frac{\kappa^2\gamma}{(\omega-\epsilon)^2+(\gamma/2)^2}, \tag{5.79}$$

which is centered at frequency ϵ, with width γ, and coupling strength κ.

The coupling between the system and the RC, denoted $|g|$, follows from the general identity

$$|g|^2 = \int_{-\infty}^{\infty}\frac{\mathrm{d}\omega}{2\pi}\,\mathcal{J}^{(0)}(\omega) = \int_{-\infty}^{\infty}\frac{\mathrm{d}\omega}{2\pi}\,\frac{\kappa^2\gamma}{(\omega-\epsilon)^2+(\gamma/2)^2} = \kappa^2, \tag{5.80}$$

where the final equality follows from the normalization of the Lorentzian function.

To compute the residual spectral density, we make use of the Hilbert transform of the Lorentzian [145]:

$$\mathcal{H}\left[\frac{1}{(x-a)^2+b^2}\right] = \frac{(x-a)}{b[(x-a)^2+b^2]}. \tag{5.81}$$

Applying this to Eq. (5.79), we obtain:

$$\mathcal{H}\left[\mathcal{J}^{(0)}\right](\omega) = \frac{2\kappa^2(\omega-\epsilon)}{(\omega-\epsilon)^2+(\gamma/2)^2}. \tag{5.82}$$

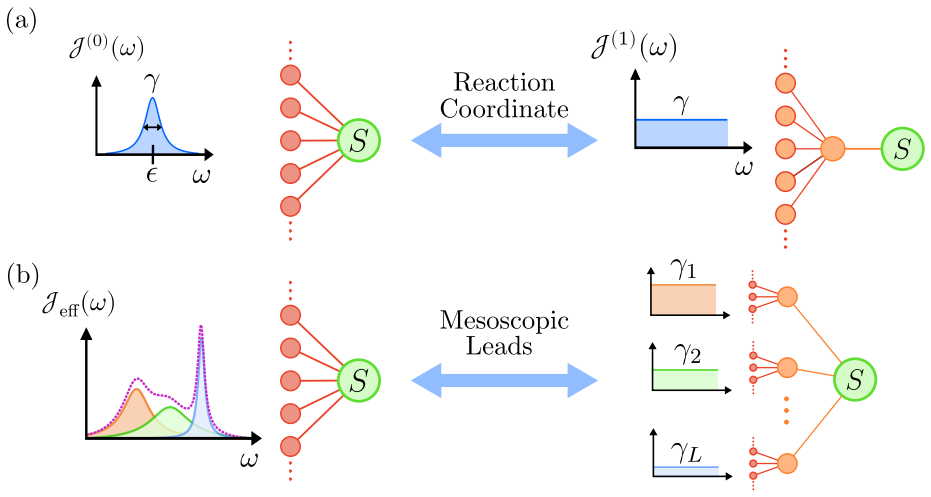

Figure 5.4: (a) The reaction coordinate (RC) mapping isolates a single mode from an initial Lorentzian spectral density $\mathcal{J}^{(0)}(\omega)$, resulting in a flat residual spectral density $\mathcal{J}^{(1)}(\omega)$. (b) In the mesoscopic leads construction, the system couples to multiple discrete modes, each connected to a flat auxiliary reservoir. The resulting effective spectral density is a sum of Lorentzians, generalizing the RC mapping to a multi-mode setting.

We now substitute the explicit forms of $\mathcal{J}^{(0)}(\omega)$ and its Hilbert transform into Eq. (5.78) to obtain the residual spectral density. For compactness, define $D = (\omega - \epsilon)^2 + (\gamma/2)^2$. Then,

$$\mathcal{J}^{(1)}(\omega) = \frac{4\kappa^2 \cdot \dfrac{\kappa^2\gamma}{D}}{\left(\dfrac{2\kappa^2(\omega-\epsilon)}{D}\right)^2 + \left(\dfrac{\kappa^2\gamma}{D}\right)^2} \tag{5.83}$$

$$= \frac{4\kappa^4\gamma D}{4\kappa^4(\omega-\epsilon)^2 + \kappa^4\gamma^2} \tag{5.84}$$

$$= \gamma \cdot \frac{D}{(\omega-\epsilon)^2 + \gamma^2/4} = \gamma. \tag{5.85}$$

We conclude that the residual spectral density is a constant:

$$\mathcal{J}^{(1)}(\omega) = \gamma. \tag{5.86}$$

This shows that when a discrete mode is coupled to a flat reservoir, the resulting effective spectral density seen by the system takes a Lorentzian form. This observation forms the conceptual bridge to the mesoscopic leads formalism, which we now examine.

5.3.2 Connection to the Mesoscopic Leads Approach

In the mesoscopic leads picture, the system couples to L discrete modes, each of which is connected to an independent auxiliary bath with a flat spectral density. The intuition from the RC mapping suggests that the resulting effective spectral density should be a sum of Lorentzians. This analogy is summarized visually in Fig. 5.4. In this section, we make this correspondence explicit by directly analyzing the equations of motion.

We first observe that the mesoscopic leads setup can be recast into the standard form of a system linearly coupled to a quadratic environment. The Hamiltonian reads

$$\hat{H}_{\text{tot}} = \hat{H}_S + \sum_{k=1}^{L} \left(\kappa_k \hat{c}_p^\dagger \hat{a}_k + \text{h.c.} \right) + \sum_{k=1}^{L} \epsilon_k \hat{a}_k^\dagger \hat{a}_k + \sum_q \left(\nu_{kq} \hat{a}_k^\dagger \hat{b}_{kq} + \text{h.c.} \right) + \sum_q \Omega_{kq} \hat{b}_{kq}^\dagger \hat{b}_{kq}. \quad (5.87)$$

Our goal is to bring the hierarchical environment (lead plus auxiliary baths) into the standard form $\hat{H}_B = \sum_k \omega_k \hat{\psi}_k^\dagger \hat{\psi}_k$, where the system couples to a diagonalized bath. In principle, this requires diagonalizing a hybrid environment composed of discrete modes ($\hat{a}_k$) coupled to a continuum ($\hat{b}_{kq}$). The procedure of diagonalizing such composite systems is known as *Fano diagonalization* [147], and underlies the pseudomode formalism developed by Garraway [39, 148].

In our case, however, we work with fermionic baths whose spectral densities have finite support. This allows us to treat the auxiliary reservoirs as effectively finite-dimensional by discretizing them into K modes with $K \to \infty$. Within this approximation, the diagonalization becomes a standard unitary transformation on a large but finite single-particle Hamiltonian. This discretized picture retains the physical intuition of the Fano framework while allowing us to focus on the connection with the RC mapping.

To simplify the notation, we define a composite basis $\{\hat{f}_n\}$, where the first L elements correspond to the lead modes $\hat{a}_k$, and the remaining elements span the auxiliary reservoirs:

$$\{\hat{f}_n\} = \{\hat{a}_1, \dots, \hat{a}_L, \hat{b}_{11}, \hat{b}_{12}, \dots\}.$$

The full Hamiltonian can then be expressed as

$$\hat{H}_{\text{tot}} = \hat{H}_S + \sum_{n=1}^{L} \left(\kappa_n \hat{c}_p^\dagger \hat{f}_n + \text{h.c.} \right) + \sum_{nm} h_{nm} \hat{f}_n^\dagger \hat{f}_m, \quad (5.88)$$

where h_{nm} is the single-particle Hamiltonian of the hierarchical environment.

To recover the standard form, we diagonalize this matrix as $\sum_{nm} S_{jn} h_{nm} S_{km}^* = \omega_j \delta_{jk}$. We denote the corresponding normal modes

$$\hat{f}_n = \sum_k S_{kn}^* \hat{\psi}_k, \quad (5.89)$$

which yields the standard system–bath form

$$\hat{H}_{\text{tot}} = \hat{H}_S + \sum_k \omega_k \hat{\psi}_k^\dagger \hat{\psi}_k + \sum_k \left(g_k \hat{c}_p^\dagger \hat{\psi}_k + \text{h.c.} \right). \quad (5.90)$$

This result is not surprising: it simply reflects the fact that, although the environment in the mesoscopic leads formalism is hierarchically structured, the system ultimately couples to an effective spectral density.

Having established this connection, we now derive the effective spectral density seen by the system, following the same approach used in the RC mapping. The coupled Heisenberg equations of motion are

$$\begin{aligned}
\frac{\mathrm{d}}{\mathrm{d}t}\hat{c}_p &= i[\hat{H}_S, \hat{c}_p] - i\sum_{k=1}^{L} \kappa_k \hat{a}_k, \\
\frac{\mathrm{d}}{\mathrm{d}t}\hat{a}_k &= -i\epsilon_k \hat{a}_k - i\kappa_k^* \hat{c}_p - i\sum_q \nu_{kq}\hat{b}_{kq}, \\
\frac{\mathrm{d}}{\mathrm{d}t}\hat{b}_{kq} &= -i\Omega_{kq}\hat{b}_{kq} - i\nu_{kq}^* \hat{a}_k,
\end{aligned} \tag{5.91}$$

where we have suppressed the explicit time dependence for clarity.

Applying the Fourier–Laplace transform, we obtain

$$\begin{aligned}
-iz\tilde{c}_p &= i\widetilde{[\hat{H}_S, \hat{c}_p]} - i\sum_k \kappa_k \tilde{a}_k, \\
-iz\tilde{a}_k &= -i\epsilon_k \tilde{a}_k - i\kappa_k^* \tilde{c}_p - i\sum_q \nu_{kq}\tilde{b}_{kq}, \\
-iz\tilde{b}_{kq} &= -i\Omega_{kq}\tilde{b}_{kq} - i\nu_{kq}^* \tilde{a}_k.
\end{aligned} \tag{5.92}$$

Solving the last equation gives

$$\tilde{b}_{kq}(z) = \frac{\nu_{kq}}{z - \Omega_{kq}}\tilde{a}_k(z), \tag{5.93}$$

and substituting into the equation for $\tilde{a}_k(z)$, we find

$$\tilde{a}_k(z) = \frac{\kappa_k^*}{z - \epsilon_k - \Sigma_k(z)}\tilde{c}_p(z), \tag{5.94}$$

where

$$\Sigma_k(z) = \sum_q \frac{|\nu_{kq}|^2}{z - \Omega_{kq}} = \frac{1}{2\pi}\int \mathrm{d}\omega\, \frac{\mathcal{J}_k(\omega)}{z - \omega} \tag{5.95}$$

is the self-energy due to the reservoir coupled to $\hat{a}_k$.

Substituting back, the equation of motion for $\tilde{c}_p(z)$ becomes

$$z\tilde{c}_p(z) = i\widetilde{[\hat{H}_S, \hat{c}_p]}(z) + \sum_{k=1}^{L} \frac{|\kappa_k|^2}{z - \epsilon_k - \Sigma_k(z)}\tilde{c}_p(z). \tag{5.96}$$

Now, we assume that each auxiliary reservoir has a *flat spectral density*:

$$\mathcal{J}_k(\omega) = \Gamma_k, \tag{5.97}$$

supported over a broad frequency interval $[-W_k, W_k]$ with $W_k \gg \Gamma_k$. In this case, the principal value integral diverges logarithmically as $W_k \to \infty$, but its imaginary part converges to

$$\operatorname{Im}\Sigma_k(\omega + i0^+) = -\frac{\Gamma_k}{2}, \tag{5.98}$$

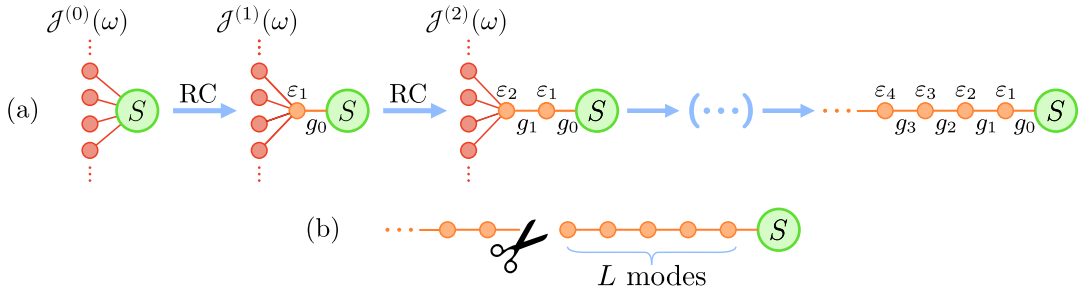

Figure 5.5: (a) Iterative application of the reaction coordinate (RC) mapping. Starting from an original environment characterized by the spectral density $\mathcal{J}^{(0)}(\omega)$, the first RC (with energy ε_1 and coupling g_0) is extracted, yielding a residual spectral density $\mathcal{J}^{(1)}(\omega)$. This process is repeated, resulting in a semi-infinite tight-binding chain with on-site energies ε_n and hoppings g_n, where the system S couples only to the first site. (b) In practical simulations, the chain is truncated after L modes, introducing finite-size effects that limit simulation time.

and the real part can be absorbed into a redefinition of ϵ_k. Thus, in the so-called *wide band limit*, we approximate

$$\Sigma_k(z) \approx -i\frac{\Gamma_k}{2}. \tag{5.99}$$

The effective self-energy is then

$$\Sigma_{\text{eff}}(z) = \sum_k \frac{|\kappa_k|^2}{z - \epsilon_k + i\Gamma_k/2}, \tag{5.100}$$

and the corresponding spectral density is

$$\mathcal{J}_{\text{eff}}(\omega) = 2\,\text{Im}\,\Sigma_{\text{eff}}(\omega + i0^+) = \sum_k \frac{|\kappa_k|^2\Gamma_k}{(\omega - \epsilon_k)^2 + (\Gamma_k/2)^2}, \tag{5.101}$$

which is a sum of Lorentzians centered at the lead mode energies ϵ_k, each broadened by Γ_k.

5.3.3 Chain Mapping

The reaction coordinate (RC) mapping can be iteratively applied to derive a powerful technique known as *chain mapping*. After a single RC transformation, the original bath is replaced by a single mode (the RC) coupled to a residual environment. One can then apply the RC mapping again, this time to the residual bath, resulting in a chain of two modes coupled to a residual bath at the end. Repeating this process L times results in an L-mode tight binding chain, with only the last one coupled to a residual bath.

The total Hamiltonian after L such transformations takes the form

$$\hat{H}_{\text{tot}} = \hat{H}_S + (g_0\hat{c}_p^\dagger\hat{f}_1 + \text{h.c}) + \hat{H}_{\text{chain}}^{(L)} + \sum_{k>L}(t_k\hat{f}_L^\dagger\hat{f}_k + \text{h.c.}) + \sum_{k>L}\varepsilon_k\hat{f}_k^\dagger\hat{f}_k, \tag{5.102}$$

where

$$\hat{H}_{\text{chain}}^{(L)} = \sum_{n=1}^{L}\varepsilon_n\hat{f}_n^\dagger\hat{f}_n + \sum_{n=1}^{L-1}\left(g_n\hat{f}_n^\dagger\hat{f}_{n+1} + \text{h.c.}\right). \tag{5.103}$$

The parameters $\{\varepsilon_n, g_n\}$ defining the chain are obtained by recursively applying the RC map. Starting with the original bath spectral density $\mathcal{J}_0(\omega)$, the recursion relations are given by

$$|g_n|^2 = \int \frac{\mathrm{d}\omega}{2\pi}\, \mathcal{J}_n(\omega), \tag{5.104}$$

$$\varepsilon_{n+1} = \frac{1}{|g_n|^2} \int \frac{\mathrm{d}\omega}{2\pi}\, \omega \mathcal{J}_n(\omega), \tag{5.105}$$

$$\mathcal{J}_{n+1}(\omega) = \frac{4|g_n|^2 \mathcal{J}_n(\omega)}{\left[\frac{1}{\pi}\mathcal{P}\int \mathrm{d}\omega' \frac{\mathcal{J}_n(\omega')}{\omega'-\omega}\right]^2 + [\mathcal{J}_n(\omega)]^2}. \tag{5.106}$$

This iterative procedure is illustrated schematically in Fig. 5.5, where each RC transformation converts a residual bath into an additional site in a growing tight-binding chain, ultimately yielding an exact representation of the environment as a semi-infinite lattice.

While this is not guaranteed in general, if the coupling to the residual reservoir decays with n, the Markovian approximation may become justified for the dynamics of the system plus a finite-length chain.

Significant theoretical effort has been devoted to analyzing the asymptotic behavior of the chain parameters $\{g_n, \varepsilon_n\}$ and the residual spectral densities $\mathcal{J}_n(\omega)$ as $n \to \infty$ [149].

In the limit $n \to \infty$, the environment is mapped exactly onto a semi-infinite tight-binding chain. The full Hamiltonian becomes

$$\hat{H}_{\mathrm{tot}} = \hat{H}_S + (g_0 \hat{c}_p^\dagger \hat{f}_1 + \mathrm{h.c.}) + \sum_{n=1}^{\infty} \left(g_n \hat{f}_n^\dagger \hat{f}_{n+1} + \mathrm{h.c.}\right) + \sum_{n=1}^{\infty} \varepsilon_n \hat{f}_n^\dagger \hat{f}_n. \tag{5.107}$$

This transformation belongs to a family of methods known as *chain mapping*, and has become a foundational tool in the simulation of open quantum systems [150, 97, 74, 149].

The chain mapping is formally exact: it is implemented by a unitary transformation that preserves all dynamical properties of the original system–bath model. Importantly, although it maps a continuum bath to a discrete semi-infinite chain, this transformation is not a discretization in the conventional sense.

Each mode in the chain is constructed as a carefully weighted average over the original bath modes, preserving the full spectral information. Essentially, the mapping consists in transforming the diagonal bath into a tridiagonal form. This ensures that no frequency resolution is lost, unlike standard discretization techniques based on mode sampling.

A thermal state of the bath is mapped into a thermal state of the chain via the unitary transformation. Since the original bath is assumed to be initially thermal, the initial state of the chain is given by

$$\hat{\rho}_B(0) = \frac{e^{-\beta(\hat{H}_{\mathrm{chain}} - \mu \hat{N}_{\mathrm{chain}})}}{Z} \tag{5.108}$$

where $\hat{H}_{\mathrm{chain}}$ and $\hat{N}_{\mathrm{chain}}$ are the Hamiltonian and particle number of the semi-infinite chain and Z is the corresponding partition function.

In practice, simulations based on the chain mapping require truncating the semi-infinite chain to a finite length L. This approximation introduces important finite size effects: after a finite time, the dynamics will inevitably exhibit recurrences due to the reflection of excitations at the end of the truncated chain. These effects are analogous to Poincaré

recurrences, with a characteristic timescale that scales inversely with the chain length, $t_{\text{rec}} \sim 1/L$ [31].

A useful perspective comes from causality: information propagates along the chain with a finite velocity, so it takes a finite time for any influence from the end of the chain to travel back to the system. This idea is formalized by the Lieb–Robinson bound [151], which sets an effective light cone for information propagation in local quantum systems. Consequently, the simulation remains faithful up to a maximum time

$$t_{\max} \sim \frac{L}{v}, \tag{5.109}$$

where v is the Lieb–Robinson velocity. Ref. [152] provides rigorous bounds for error introduced in this truncation in a bosonic chain, using a closely related chain mapping method (TEDOPA).

An additional subtlety arises in how the initial state of the truncated chain is prepared. In practice, one typically initializes the finite chain in a Gibbs state of the truncated chain Hamiltonian:

$$\hat{\rho}^{(L)}_{\text{chain}}(0) = \frac{e^{-\beta\left(\hat{H}^{(L)}_{\text{chain}} - \mu \hat{N}^{(L)}_{\text{chain}}\right)}}{Z_L}. \tag{5.110}$$

where $\hat{H}^{(L)}_{\text{chain}}$ and $\hat{N}^{(L)}_{\text{chain}}$ refer to the Hamiltonian and number operator of the truncated chain, and Z_L is the corresponding partition function.

This differs from the true reduced state obtained by tracing out the remainder of the semi-infinite chain:

$$\hat{\rho}^{(L)}_{\text{chain}}(0) \neq \text{Tr}_{N>L}[\hat{\rho}_{\text{chain}}(0)], \tag{5.111}$$

where $\text{Tr}_{n>L}$ denotes the partial trace over the discarded modes. However, the error introduced by this approximation vanishes as $L \to \infty$, particularly when the coupling to the residual environment becomes negligible.

One way to circumvent this issue is by applying a thermofield transformation, which maps the finite-temperature chain to two coupled zero-temperature chains with temperature-dependent couplings [150, 153].

5.4 Thermodynamics in the Mesoscopic Leads Approach

As we briefly discussed in Section 5.1, the main ingredients for the description of the thermodynamics are the particle and energy currents, as well as the entropy production rate.

Let us consider the case of a system coupled to multiple baths. In the mesoscopic leads approach, the extended system Hamiltonian takes the form

$$\hat{H} = \hat{H}_S + \sum_{\alpha} \left(\hat{H}_{SL_\alpha} + \hat{H}_{L_\alpha}\right), \tag{5.112}$$

where $\hat{H}_{L_\alpha}$ is the Hamiltonian of lead α and $\hat{H}_{SL_\alpha}$ describes its coupling to the system.

The dynamics of the extended state (system + leads), denoted simply by $\hat{\rho}$, follows a Lindblad master equation:

$$\frac{\mathrm{d}\hat{\rho}}{\mathrm{d}t} = -i[\hat{H}, \hat{\rho}] + \sum_{\alpha} \mathcal{D}_\alpha[\hat{\rho}], \tag{5.113}$$

where $\hat{H}$ is the Hamiltonian of the extended system, and $\mathcal{D}_\alpha$ is the collective dissipator acting on lead α.

Within this Lindblad framework, the thermodynamic formalism developed by Alicki (see Chapter 3, Section 3.6) provides operational definitions for the energy and particle currents:

$$I_\alpha^E = \mathrm{Tr}\big[\hat{H}\mathcal{D}_\alpha(\hat{\rho})\big], \qquad I_\alpha^P = \mathrm{Tr}\big[\hat{N}\mathcal{D}_\alpha(\hat{\rho})\big], \tag{5.114}$$

where $\hat{N}$ denotes the particle number operator of the extended system.

Since the dissipator $\mathcal{D}_\alpha$ is local and acts only on operators of lead α, the particle current simplifies to

$$I_\alpha^P = \mathrm{Tr}\big[\hat{N}\mathcal{D}_\alpha(\hat{\rho})\big] = \mathrm{Tr}\big[\hat{N}_\alpha\mathcal{D}_\alpha(\hat{\rho})\big], \tag{5.115}$$

which reflects the rate at which particles are injected into lead α. The energy current, on the other hand, accounts for the injection of energy into both the lead and the interaction term:

$$I_\alpha^E = \mathrm{Tr}\big[(\hat{H}_{L_\alpha} + \hat{H}_{SL_\alpha})\mathcal{D}_\alpha(\hat{\rho})\big], \tag{5.116}$$

since $\hat{H}_{SL_\alpha}$ includes operators acting on the lead.

However, a subtle distinction arises in the mesoscopic leads construction: the currents defined above describe the flow of energy and particles into the *full extended system*. We refer to these quantities as the *external currents*, reflecting flows from the auxiliary baths into the extended system. They do not necessarily coincide with the currents flowing from the leads into the original system, which also include coherent contributions from the unitary part of the evolution. We refer to these as the *internal currents*.

In the steady state, this distinction becomes irrelevant: conservation of energy and particle number ensures that internal and external currents are equal. Outside the steady state, however, this equivalence no longer holds. The lead modes may accumulate or release energy and particles, and the external currents no longer reflect the net exchange with the system.

Ultimately, our goal is to define currents that recover those of the *original setup* in the limit $L_\alpha \to \infty$. A schematic distinction between internal and external currents in the mesoscopic leads framework is shown in Fig. 5.6.

In the remainder of this section, we examine this question in detail. We begin with the steady-state case, deriving explicit expressions for the particle and energy currents. We then turn to the transient regime, where we rely on the unitary structure of the mesoscopic leads model to define the internal currents.

5.4.1 Steady-State Currents

If the system Hamiltonian is time-independent, the extended system relaxes to a non-equilibrium steady state (NESS), where the external and internal currents coincide.

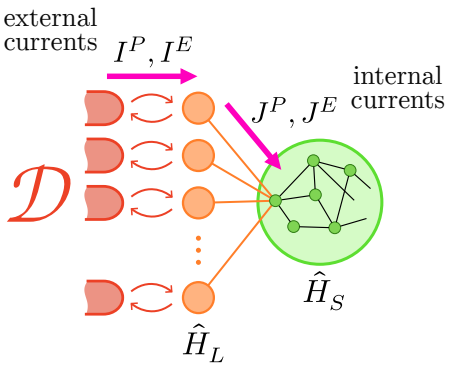

Figure 5.6: **Internal vs external currents in the mesoscopic leads approach.** The auxiliary reservoirs (red) inject energy and particles into the lead modes (orange) via local dissipators $\mathcal{D}_\alpha$, collectively denoted by the large red $\mathcal{D}$. These define the *external* energy and particle currents, I^E and I^P, entering the extended system (leads + system). In turn, the lead modes exchange energy and particles with the system (green), giving rise to the *internal* currents J^E and J^P. At steady state, internal and external currents coincide, but they differ during transients due to finite lead occupation.

To illustrate this, consider the paradigmatic setup of a system coupled to two baths—denoted left (L) and right (R)—held at different temperatures or chemical potentials. The master equation governing the dynamics takes the form

$$\frac{\mathrm{d}\hat{\rho}}{\mathrm{d}t} = -i[\hat{H}, \hat{\rho}] + \mathcal{D}_L(\hat{\rho}) + \mathcal{D}_R(\hat{\rho}), \tag{5.117}$$

where $\mathcal{D}_{L(R)}$ are the dissipators associated with the left (right) auxiliary environments.

From this, the time evolution of the average particle number $\langle \hat{N} \rangle$ follows:

$$\frac{\mathrm{d}\langle \hat{N} \rangle}{\mathrm{d}t} = -i\,\mathrm{Tr}\big([\hat{H}, \hat{N}]\hat{\rho}\big) + \mathrm{Tr}\big[\hat{N}\mathcal{D}_L(\hat{\rho})\big] + \mathrm{Tr}\big[\hat{N}\mathcal{D}_R(\hat{\rho})\big]. \tag{5.118}$$

Assuming global particle-number conservation, $[\hat{H}, \hat{N}] = 0$, we obtain a continuity equation:

$$\frac{\mathrm{d}\langle \hat{N} \rangle}{\mathrm{d}t} = I_L^P + I_R^P, \quad \text{where} \quad I_\alpha^P = \mathrm{Tr}\big[\hat{N}_\alpha \mathcal{D}_\alpha(\hat{\rho})\big], \quad \alpha = L, R. \tag{5.119}$$

Explicit expressions for the external currents can be obtained using the adjoint master equation formalism introduced in Section 2.4. Acting on the operator $\hat{N}_\alpha = \sum_{k=1}^{N_\alpha} \hat{a}_{k\alpha}^\dagger \hat{a}_{k\alpha}$ with the adjoint dissipator $\mathcal{D}_\alpha^\dagger$, we find

$$I_\alpha^P = \sum_{k=1}^{N_\alpha} \gamma_{k\alpha} \left\langle f_{k\alpha} - \hat{a}_{k\alpha}^\dagger \hat{a}_{k\alpha} \right\rangle, \tag{5.120}$$

where $\gamma_{k\alpha}$ is the damping rate and $f_{k\alpha}$ is the thermal occupation of mode k in bath α.

In the steady state, particle number is conserved, so Eq. (5.119) reduces to

$$\frac{\mathrm{d}}{\mathrm{d}t}\langle \hat{N} \rangle = 0 \quad \Rightarrow \quad I_L^P + I_R^P = 0. \tag{5.121}$$

In this regime, the system supports a unique steady-state particle current:

$$J_{\mathrm{ss}}^P \equiv I_L^P = -I_R^P. \tag{5.122}$$

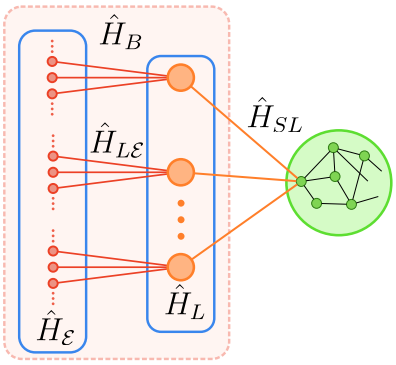

Figure 5.7: **Structure of the hierarchical environment in the mesoscopic leads framework.** Each lead mode (orange) is coupled to a system site (green, right) via the Hamiltonian $\hat{H}_{SL}$. The lead modes themselves form part of a larger environment (shaded red region) composed of the lead Hamiltonian $\hat{H}_L$, auxiliary reservoirs $\mathcal{E}$ (red), and their couplings $\hat{H}_{L\mathcal{E}}$. The full bath Hamiltonian is given by $\hat{H}_B = \hat{H}_L + \hat{H}_{L\mathcal{E}} + \hat{H}_{\mathcal{E}}$. This structure underlies the definition of internal currents (between system and lead) and external currents (from the auxiliary environments into the lead).

Moreover, since $\hat{H}_S$ conserves particle number, any particle current defined at an internal bond within the system must match the steady-state value J^P_{ss}, as there is no accumulation in the system bulk

An analogous argument holds for the energy current. The total energy continuity equation is

$$\frac{\mathrm{d}}{\mathrm{d}t}\langle \hat{H}\rangle = I^E_L + I^E_R \quad \text{where} \quad I^E_\alpha = \mathrm{Tr}\big[\hat{H}\mathcal{D}_\alpha(\hat{\rho})\big], \quad \alpha = L, R. \tag{5.123}$$

Since the dissipators act only on the lead modes, and the interaction term $\hat{H}_{SL_\alpha}$ involves lead operators, the energy current simplifies to

$$I^E_\alpha = \mathrm{Tr}\big[(\hat{H}_{L_\alpha} + \hat{H}_{SL_\alpha})\mathcal{D}_\alpha(\hat{\rho})\big]. \tag{5.124}$$

Acting with the adjoint dissipator $\mathcal{D}^\dagger_\alpha$ on the lead and interaction Hamiltonians given in Eq. (5.48), we obtain:

$$I^E_\alpha = \sum_{k=1}^{N_\alpha} \gamma_{k\alpha}\epsilon_{k\alpha}\left\langle f_{k\alpha} - \hat{a}^\dagger_{k\alpha}\hat{a}_{k\alpha}\right\rangle - \frac{1}{2}\sum_{k=1}^{N_\alpha}\gamma_{k\alpha}\left\langle \kappa_{k\alpha}\hat{c}^\dagger_{p_\alpha}\hat{a}_{k\alpha} + \kappa^*_{k\alpha}\hat{a}^\dagger_{k\alpha}\hat{c}_{p_\alpha}\right\rangle. \tag{5.125}$$

5.4.2 Internal Currents

In this section, we construct definitions of the internal particle and energy currents—those flowing between the system and the leads—which remain consistent with the original microscopic model, both in the steady state and in the transient regime. Our derivation relies on the unitary picture of the setup, which is illustrated schematically in Fig. 5.7.

For clarity, we focus on the single-bath case. In the original model, the total Hamiltonian reads

$$\hat{H}_{\mathrm{tot}} = \hat{H}_S + \hat{H}_{SB} + \hat{H}_B. \tag{5.126}$$

The particle and energy currents are then defined as

$$\begin{aligned} J^P &= -\frac{\mathrm{d}}{\mathrm{d}t}\langle \hat{N}_B \rangle = i\Big\langle [\hat{N}_B, \hat{H}] \Big\rangle, \\ J^E &= -\frac{\mathrm{d}}{\mathrm{d}t}\langle \hat{H}_B \rangle = i\Big\langle [\hat{H}_B, \hat{H}] \Big\rangle. \end{aligned} \tag{5.127}$$

As discussed in Chapter 3, this definition of the energy current is consistent with the first and second laws, provided the interaction term is included in the definition of internal energy, i.e., $U(t) = \langle \hat{H}_S + \hat{H}_{SB} \rangle$.

Because $[\hat{H}_B, \hat{N}_B] = 0$ and $[\hat{H}_S, \hat{H}_B] = 0$, these expressions simplify to

$$J^P = i\langle [\hat{N}_B, \hat{H}_{SB}] \rangle, \qquad J^E = -i\langle [\hat{H}_B, \hat{H}_{SB}] \rangle. \tag{5.128}$$

In the unitary picture of mesoscopic leads, the bath is replaced by a hierarchical structure:

$$\hat{H}_B \to \hat{H}_L + \hat{H}_{L\mathcal{E}} + \hat{H}_{\mathcal{E}}, \qquad \hat{H}_{SB} \to \hat{H}_{SL}. \tag{5.129}$$

Since $\hat{H}_{SL}$ acts only on the system and lead degrees of freedom, it commutes with all operators acting solely on $\mathcal{E}$:

$$[\hat{N}_{\mathcal{E}}, \hat{H}_{SL}] = [\hat{H}_{\mathcal{E}}, \hat{H}_{SL}] = 0. \tag{5.130}$$

Let us begin with the particle current. In the new setting, the bath number operator becomes $\hat{N}_B = \hat{N}_L + \hat{N}_{\mathcal{E}}$, so Eq. (5.128) becomes

$$J^P = i\langle [\hat{N}_L + \hat{N}_{\mathcal{E}}, \hat{H}_{SL}] \rangle = i\langle [\hat{N}_L, \hat{H}_{SL}] \rangle, \tag{5.131}$$

where we used $[\hat{N}_{\mathcal{E}}, \hat{H}_{SL}] = 0$. This expression depends only on operators of the extended system (system + lead), and thus remains valid when the environment $\mathcal{E}$ is traced out under the Born–Markov approximation. It can therefore be computed from the reduced state $\hat{\rho}$.

We now turn to the energy current. From Eq. (5.127), and using the identifications above, we write

$$J^E = i\langle [\hat{H}_L + \hat{H}_{L\mathcal{E}}, \hat{H}_{SL}] \rangle. \tag{5.132}$$

However, since $[\hat{H}_{L\mathcal{E}}, \hat{H}_{SL}] \neq 0$, this expression involves operators outside the extended system and cannot be used directly once $\mathcal{E}$ is traced out.

To eliminate these external terms, we consider the time derivative of the interaction energy. From the Heisenberg equation under the full Hamiltonian $\hat{H}_{\mathrm{tot}}$, we have

$$\begin{aligned} \frac{\mathrm{d}}{\mathrm{d}t}\langle \hat{H}_{SL} \rangle &= i\langle [\hat{H}_{\mathrm{tot}}, \hat{H}_{SL}] \rangle \\ &= i\langle [\hat{H}_L + \hat{H}_{L\mathcal{E}}, \hat{H}_{SL}] \rangle + i\langle [\hat{H}_S, \hat{H}_{SL}] \rangle \\ &= J^E + i\langle [\hat{H}_S, \hat{H}_{SL}] \rangle \end{aligned} \tag{5.133}$$

Rearranging terms gives a convenient expression for the internal energy current:

$$J^E = \frac{\mathrm{d}}{\mathrm{d}t}\langle \hat{H}_{SL} \rangle - i\langle [\hat{H}_S, \hat{H}_{SL}] \rangle \tag{5.134}$$

Crucially, both terms depend only on operators acting within the extended system, and therefore remain valid after tracing out the environment $\mathcal{E}$.

The time derivative of $\langle \hat{H}_{SL} \rangle$ can now be evaluated using the master equation:

$$\begin{aligned} \frac{\mathrm{d}}{\mathrm{d}t}\langle \hat{H}_{SL} \rangle &= i\langle [\hat{H}, \hat{H}_{SL}] \rangle + \mathrm{Tr}[\hat{H}_{SL}\mathcal{D}(\hat{\rho})] \\ &= i\langle [\hat{H}_S, \hat{H}_{SL}] \rangle + i\langle [\hat{H}_L, \hat{H}_{SL}] \rangle + \mathrm{Tr}[\hat{H}_{SL}\mathcal{D}(\hat{\rho})]. \end{aligned} \tag{5.135}$$

Substituting into the previous expression for J^E, we arrive at:

$$J^E = i\langle [\hat{H}_L, \hat{H}_{SL}] \rangle + \mathrm{Tr}[\hat{H}_{SL}\mathcal{D}(\hat{\rho})]. \tag{5.136}$$

The expressions above generalize straightforwardly to multiple baths. For each lead L_α, the internal particle and energy currents are given by:

$$J^P_\alpha = i\langle [\hat{N}_{L_\alpha}, \hat{H}_{SL_\alpha}] \rangle \tag{5.137}$$

$$J^E_\alpha = i\langle [\hat{H}_{L_\alpha}, \hat{H}_{SL_\alpha}] \rangle + \mathrm{Tr}[\hat{H}_{SL_\alpha}\mathcal{D}_\alpha(\hat{\rho})]. \tag{5.138}$$

In terms of creation and annihilation operators, these become:

$$J^P_\alpha = \sum_{k=1}^{N_\alpha} i\langle \kappa_{k\alpha}\hat{c}^\dagger_{p_\alpha}\hat{a}_{k\alpha} - \kappa^*_{k\alpha}\hat{a}^\dagger_{k\alpha}\hat{c}_{p_\alpha} \rangle \tag{5.139}$$

$$J^E_\alpha = \sum_{k=1}^{N_\alpha} \Big[i\omega_{k\alpha}\langle \kappa_{k\alpha}\hat{c}^\dagger_{p_\alpha}\hat{a}_{k\alpha} - \kappa^*_{k\alpha}\hat{a}^\dagger_{k\alpha}\hat{c}_{p_\alpha} \rangle - \frac{\gamma_{k\alpha}}{2}\langle \kappa_{k\alpha}\hat{c}^\dagger_{p_\alpha}\hat{a}_{k\alpha} + \kappa^*_{k\alpha}\hat{a}^\dagger_{k\alpha}\hat{c}_{p_\alpha} \rangle \Big]. \tag{5.140}$$

Equivalence in the Steady State

As we mentioned, the internal and external currents coincide in the steady state. To see this explicitly, we consider the energy and charge balance in the lead L_α. From the master equation, the time evolution of the lead particle number $\hat{N}_{L_\alpha}$ is given by

$$\begin{aligned} \frac{\mathrm{d}}{\mathrm{d}t}\langle \hat{N}_{L_\alpha} \rangle &= \mathrm{Tr}[\hat{N}_{L_\alpha}\mathcal{D}_\alpha(\hat{\rho})] + i\langle [\hat{H}, \hat{N}_{L_\alpha}] \rangle \\ &= I^P_\alpha - J^P_\alpha, \end{aligned} \tag{5.141}$$

where in the second equality we used that $[\hat{H}_S, \hat{N}_{L_\alpha}] = [\hat{H}_{L_\alpha}, \hat{N}_{L_\alpha}] = 0$, so that only the commutator with $\hat{H}_{SL_\alpha}$ contributes. This explicitly shows that any mismatch between the internal and external particle currents corresponds to a net accumulation of charge in the lead. In the steady state, the left-hand side vanishes, and we recover the equality

$$I^P_{\alpha,\mathrm{ss}} = J^P_{\alpha,\mathrm{ss}}, \tag{5.142}$$

as claimed.

A similar analysis applies to the energy current. From the master equation, the time evolution of the lead energy is given by

$$\frac{\mathrm{d}}{\mathrm{d}t}\langle \hat{H}_{L_\alpha} \rangle = i\langle [\hat{H}, \hat{H}_{L_\alpha}] \rangle + \mathrm{Tr}[\hat{H}_{L_\alpha}\mathcal{D}_\alpha(\hat{\rho})]. \tag{5.143}$$

To interpret the dissipative term, we note that $\hat{H}_{L_\alpha} = \hat{H} - \hat{H}_S - \hat{H}_{SL_\alpha}$, so that

$$\begin{aligned} \mathrm{Tr}[\hat{H}_{L_\alpha}\mathcal{D}_\alpha(\hat{\rho})] &= \mathrm{Tr}[(\hat{H} - \hat{H}_S - \hat{H}_{SL_\alpha})\mathcal{D}_\alpha(\hat{\rho})] \\ &= I_\alpha^E - \mathrm{Tr}[\hat{H}_{SL_\alpha}\mathcal{D}_\alpha(\hat{\rho})], \end{aligned} \tag{5.144}$$

where we have used the definition of the external energy current $I_\alpha^E = \mathrm{Tr}[\hat{H}\mathcal{D}_\alpha(\hat{\rho})]$ and the fact that the system Hamiltonian does not couple directly to the dissipator.

Substituting back, we find

$$\begin{aligned} \frac{\mathrm{d}}{\mathrm{d}t}\langle \hat{H}_{L_\alpha}\rangle &= I_\alpha^E - \big(i\langle[\hat{H}_{L_\alpha}, \hat{H}_{SL_\alpha}]\rangle + \mathrm{Tr}[\hat{H}_{SL_\alpha}\mathcal{D}_\alpha(\hat{\rho})]\big) \\ &= I_\alpha^E - J_\alpha^E, \end{aligned} \tag{5.145}$$

which again shows that any difference between the internal and external energy currents corresponds to energy accumulation in the lead. In the steady state, the derivative vanishes, and we obtain

$$I_{\alpha,\mathrm{ss}}^E = J_{\alpha,\mathrm{ss}}^E. \tag{5.146}$$

5.5 Mesoscopic Leads with Non-Interacting Systems

In this section, we describe the implementation of the mesoscopic leads method when the central system is non-interacting. For clarity, we begin by considering a single reservoir and later generalize to multiple baths.

5.5.1 Single-Particle Hamiltonian

The system is assumed to be non-interacting and governed by a general quadratic Hamiltonian,

$$\hat{H}_S = \sum_{ij} [\boldsymbol{H}_S]_{ij} \hat{c}_i^\dagger \hat{c}_j, \tag{5.147}$$

where $\boldsymbol{H}_S \in \mathbb{C}^{N\times N}$ is a Hermitian matrix representing the single-particle Hamiltonian of the system.

The lead is also non-interacting, with a diagonal single-particle Hamiltonian:

$$\hat{H}_L = \sum_k \epsilon_k \hat{a}_k^\dagger \hat{a}_k. \tag{5.148}$$

It couples linearly to the system via a specific site p:

$$\hat{H}_{SL} = \sum_k \big(\kappa_k \hat{c}_p^\dagger \hat{a}_k + \kappa_k^* \hat{a}_k^\dagger \hat{c}_p\big). \tag{5.149}$$

As a consequence, the Hamiltonian of the extended system $\hat{H} = \hat{H}_S + \hat{H}_L + \hat{H}_{SL}$ remains quadratic in the modes $\{\hat{c}_i\}$ and $\{\hat{a}_k\}$.

It is then convenient to collect the modes of the system and leads into a single set of $N + L$ modes:

$$\{\hat{d}_i\} = \{\hat{c}_1, \dots, \hat{c}_N, \hat{a}_1, \dots, \hat{a}_L\} \tag{5.150}$$

so that the full Hamiltonian takes the compact quadratic form

$$\hat{H} = \sum_{ij} H_{ij} \hat{d}_i^\dagger \hat{d}_j, \tag{5.151}$$

where $\boldsymbol{H} \in \mathbb{C}^{(N+L)\times(N+L)}$ is the single-particle Hamiltonian of the extended system.

This matrix naturally inherits a block structure from the decomposition into system and lead:

$$\boldsymbol{H} = \begin{pmatrix} \boldsymbol{H}_S & \boldsymbol{H}_{SL} \\ \boldsymbol{H}_{SL}^\dagger & \boldsymbol{H}_L \end{pmatrix}. \tag{5.152}$$

Here, $\boldsymbol{H}_L = \mathrm{diag}(\epsilon_1, \dots, \epsilon_L)$ is the single-particle Hamiltonian of the lead, and the off-diagonal term $\boldsymbol{H}_{SL} \in \mathbb{C}^{N\times L}$ encodes the system-lead coupling. It is a rectangular matrix whose only non-zero row is the pth, containing the system-lead coupling via site p:

$$[\boldsymbol{H}_{SL}]_{ik} = \kappa_k \delta_{ip}. \tag{5.153}$$

This structure generalizes naturally to the case of multiple leads. If the system is coupled to K independent reservoirs, the full single-particle Hamiltonian becomes

$$\boldsymbol{H} = \begin{pmatrix} \boldsymbol{H}_S & \boldsymbol{H}_{SL_1} & \cdots & \boldsymbol{H}_{SL_K} \\ \boldsymbol{H}_{SL_1}^\dagger & \boldsymbol{H}_{L_1} & & \\ \vdots & & \ddots & \\ \boldsymbol{H}_{SL_K}^\dagger & & & \boldsymbol{H}_{L_K} \end{pmatrix}, \tag{5.154}$$

where each $\boldsymbol{H}_{L_\alpha}$ is diagonal and each $\boldsymbol{H}_{SL_\alpha}$ contains nonzero entries only in the row corresponding to the system site p_α coupled to lead α.

5.5.2 Covariance Matrix

The Hamiltonian $\hat{H}$ is quadratic, and the dissipators introduced by the mesoscopic leads construction are linear in the lead modes. As a result, the full Liouvillian is quadratic in fermionic operators.

As discussed in Chapter 4, a quadratic Lindbladian generates Gaussian-preserving dynamics. That is, if the initial state is Gaussian–i.e., fully characterized by its second moments—it will remain Gaussian throughout the evolution. Importantly, this implies that the steady state is Gaussian.

The leads are initialized in thermal states, which are Gaussian by construction. If the system is also initialized in a Gaussian state—which includes a wide range of physically relevant states such as thermal or uncorrelated product states—then the full initial state is Gaussian.

This significantly reduces the computational complexity: instead of solving for the full density matrix, one can work entirely at the level of the *covariance matrix*. We define the covariance matrix $\boldsymbol{C} \in \mathbb{C}^{(N+L)\times(N+L)}$ as

$$C_{ij} = \langle \hat{d}_j^\dagger \hat{d}_i \rangle, \tag{5.155}$$

This particular ordering of the indices leads to a cleaner equation of motion.

For Gaussian states, there is a one-to-one correspondence between the state and the covariance matrix:

$$\boldsymbol{C} \leftrightarrow \hat{\rho} \tag{5.156}$$

The structure of Gaussian states also simplifies the treatment of reduced states and tensor products. Like the single-particle Hamiltonian, the covariance matrix inherits a natural block structure:

$$\boldsymbol{C} = \begin{pmatrix} \boldsymbol{C}_S & \boldsymbol{C}_{SL} \\ \boldsymbol{C}_{SL}^\dagger & \boldsymbol{C}_L, \end{pmatrix}. \tag{5.157}$$

where the diagonal blocks represent the reduced covariance matrices of the system and lead:

$$[\boldsymbol{C}_S]_{ij} = \langle \hat{c}_j^\dagger \hat{c}_i \rangle, \qquad [\boldsymbol{C}_L]_{kq} = \langle \hat{a}_q^\dagger \hat{a}_k \rangle, \tag{5.158}$$

and the off-diagonal block encodes system-lead correlations:

$$[\boldsymbol{C}_{SL}]_{ki} = \langle \hat{a}_k^\dagger \hat{c}_i \rangle. \tag{5.159}$$

The covariance matrices of the reduced states $\hat{\rho}_S = \mathrm{Tr}_L[\hat{\rho}]$ and $\hat{\rho}_L = \mathrm{Tr}_S[\hat{\rho}]$ are then obtained by extracting the corresponding diagonal blocks:

$$\boldsymbol{C}_S \leftrightarrow \hat{\rho}_S, \qquad \boldsymbol{C}_L \leftrightarrow \hat{\rho}_L. \tag{5.160}$$

Since the system and lead are initially uncorrelated, the off-diagonal block vanishes: $\boldsymbol{C}_{SL}(0) = 0$. The lead is prepared in a Gibbs state at inverse temperature β and chemical potential μ, resulting in a diagonal covariance matrix:

$$\left\langle \hat{b}_q^\dagger \hat{b}_k \right\rangle = f_k \delta_{kq} \quad \Rightarrow \quad \boldsymbol{C}_L(0) = (\mathbb{1} + e^{\beta \boldsymbol{H}_L})^{-1} = \begin{pmatrix} f_1 & & \\ & \ddots & \\ & & f_L \end{pmatrix}, \tag{5.161}$$

where $f_k = (e^{-\beta \epsilon_k} + 1)^{-1}$ is the Fermi occupation of mode $\hat{a}_k$.

The full initial covariance matrix of the extended system then reads

$$\boldsymbol{C} = \left(\begin{array}{c|ccc} \boldsymbol{C}_S(0) & & & \\ \hline & f_1 & & \\ & & \ddots & \\ & & & f_L \end{array}\right). \tag{5.162}$$

In the presence of multiple leads, each prepared in its own thermal state, the initial covariance matrix is constructed by simply adding the corresponding diagonal blocks. That is, if the system is coupled to K leads, the initial covariance matrix takes the form

$$\boldsymbol{C}(0) = \begin{pmatrix} \boldsymbol{C}_S(0) & & & \\ & \boldsymbol{C}_{L_1}(0) & & \\ & & \ddots & \\ & & & \boldsymbol{C}_{L_K}(0) \end{pmatrix}, \tag{5.163}$$

where each $\boldsymbol{C}_{L_\alpha}(0) = \mathrm{diag}(f_{1,\alpha}, \ldots, f_{L_\alpha,\alpha})$ contains the thermal occupations of the αth lead.

5.5.3 Dynamics: Lyapunov Equation

As discussed in Chapter 4, when the Liouvillian is quadratic, the covariance matrix $\boldsymbol{C}(t)$ evolves according to a Lyapunov differential equation

$$\frac{\mathrm{d}\boldsymbol{C}}{\mathrm{d}t} = -(\boldsymbol{W}\boldsymbol{C} + \boldsymbol{C}\boldsymbol{W}^\dagger) + \boldsymbol{F}, \tag{5.164}$$

where $\boldsymbol{W} \in \mathbb{C}^{(N+L)\times(N+L)}$ is a non-Hermitian matrix—often called the *drift matrix*—given by

$$\boldsymbol{W}(t) = i\boldsymbol{H}(t) + \frac{\boldsymbol{\Gamma}}{2}. \tag{5.165}$$

Here, $\boldsymbol{H}$ is the Hermitian single-particle Hamiltonian of the extended system introduced earlier, while $\boldsymbol{\Gamma}$ is a diagonal matrix collecting the damping rates:

$$\boldsymbol{\Gamma} = \mathrm{diag}(0, \dots, 0, \Gamma_1, \dots, \Gamma_L) \tag{5.166}$$

where the first N zeros indicate the absence of dissipation on the system modes. The matrix $\boldsymbol{F} \in \mathbb{R}^{(N+L)\times(N+L)}$, often called the *diffusion matrix*, is a diagonal matrix given by

$$\boldsymbol{F} = \mathrm{diag}(0, \dots, 0, f_1\Gamma_1, \dots, f_L\Gamma_L). \tag{5.167}$$

The Lyapunov equation provides an efficient numerical framework for simulating the time evolution of the extended system. Since it is linear in $\boldsymbol{C}(t)$, standard integration routines for matrix differential equations can be used, and no truncation of the Hilbert space is required.

In particular, the steady state is obtained by setting the left-hand side to zero. This yields a continuous Lyapunov equation for the stationary covariance matrix $\boldsymbol{C}_{\mathrm{ss}}$:

$$\boldsymbol{W}\boldsymbol{C}_{\mathrm{ss}} + \boldsymbol{C}_{\mathrm{ss}}\boldsymbol{W}^\dagger = \boldsymbol{F}. \tag{5.168}$$

This equation defines a linear system that can be solved using standard numerical techniques. Its solution characterizes the non-equilibrium steady state reached by the extended system in the long-time limit.

This structure generalizes naturally to the case of multiple baths. If the system is coupled to K leads, with the αth lead having L_α modes, then the dissipation matrices take the form

$$\boldsymbol{\Gamma} = \begin{pmatrix} 0 & & & \\ & \boldsymbol{\Gamma}_1 & & \\ & & \ddots & \\ & & & \boldsymbol{\Gamma}_K \end{pmatrix}, \qquad \boldsymbol{F} = \begin{pmatrix} 0 & & & \\ & \boldsymbol{F}_1 & & \\ & & \ddots & \\ & & & \boldsymbol{F}_K \end{pmatrix}, \tag{5.169}$$

where $\boldsymbol{\Gamma_\alpha} = \mathrm{diag}(\Gamma_{1,\alpha}, \dots, \Gamma_{L_\alpha,\alpha})$ and $\boldsymbol{F}_\alpha = \mathrm{diag}(f_{1,\alpha}\Gamma_{1,\alpha}, \dots, f_{L_\alpha,\alpha}\Gamma_{L_\alpha,\alpha})$. Here, $f_{k\alpha}$ denotes the thermal occupation of mode k in lead α, and $\Gamma_{k\alpha}$ its damping rate. All matrices are defined over the $N + \sum_\alpha L_\alpha$ modes of the extended system.

5.5.4 Floquet Solution of the Periodically-Driven Lyapunov Equation

We now consider the case where the single-particle Hamiltonian $\boldsymbol{H}(t)$ of the extended system is periodic in time, satisfying $\boldsymbol{H}(t+T) = \boldsymbol{H}(t)$, with $T = 2\pi/\omega$. This leads to a time-dependent Lyapunov equation for the covariance matrix $\boldsymbol{C}(t)$:

$$\frac{d\boldsymbol{C}}{dt} = -(\boldsymbol{W}(t)\boldsymbol{C} + \boldsymbol{C}\boldsymbol{W}^{\dagger}(t)) + \boldsymbol{F}, \tag{5.170}$$

where $\boldsymbol{F}$ is constant, while $\boldsymbol{W}(t)$ is periodic with frequency ω, i.e., $\boldsymbol{W}(t+T) = \boldsymbol{W}(t)$, with $T = 2\pi/\omega$. Since the Liouvillian is periodic, the system is expected to reach a limit cycle in the long-time limit. That is, after a transient time, the covariance matrix itself becomes periodic:

$$\boldsymbol{C}(t+T) = \boldsymbol{C}(t). \tag{5.171}$$

We now describe an efficient method to compute this limit-cycle solution without directly integrating the Lyapunov equation over time.

We assume the drift matrix admits a Fourier expansion

$$\boldsymbol{W}(t) = \sum_{m=-M}^{M} \boldsymbol{W}_m e^{im\omega t}, \tag{5.172}$$

where M is the number of harmonics, which ideally is small. We seek a time-periodic solution with the same period T, which we represent as a Fourier series:

$$\boldsymbol{C}(t) = \sum_{n=-\infty}^{\infty} \boldsymbol{C}_n e^{in\omega t}, \tag{5.173}$$

where the Hermiticity of $\boldsymbol{C}(t)$ implies $\boldsymbol{C}_{-n} = \boldsymbol{C}_n^{\dagger}$.

Substituting into Eq. (5.170), the left-hand side becomes

$$\frac{\mathrm{d}\boldsymbol{C}(t)}{\mathrm{d}t} = \sum_n (in\omega)\boldsymbol{C}_n e^{in\omega t}. \tag{5.174}$$

while the right-hand side yields

$$\begin{aligned} \boldsymbol{W}(t)\boldsymbol{C} + \boldsymbol{C}\boldsymbol{W}^{\dagger}(t) &= \sum_{lm} \boldsymbol{W}_m \boldsymbol{C}_l e^{i(m+l)\omega t} + \sum_{lm} \boldsymbol{C}_l \boldsymbol{W}_m^{\dagger} e^{i(l+m)\omega t} \\ &= \sum_n e^{in\omega t} \left[\sum_m \boldsymbol{W}_m \boldsymbol{C}_{n-m} + \boldsymbol{C}_{n-m} \boldsymbol{W}_m^{\dagger} \right], \end{aligned} \tag{5.175}$$

where we changed the summation index to $n = m + l$.

Equating both sides and comparing Fourier coefficients, we obtain the set of equations

$$in\omega \boldsymbol{C}_n = -\sum_{m=-M}^{M} \left(\boldsymbol{W}_m \boldsymbol{C}_{n-m} + \boldsymbol{C}_{n-m} \boldsymbol{W}_m^{\dagger} \right) + \boldsymbol{F}\delta_{n,0}. \tag{5.176}$$

Isolating the $\boldsymbol{C}_n$ term, we obtain the recursive equation

$$(in\omega\mathbb{1} + \boldsymbol{W}_0)\boldsymbol{C}_n + \boldsymbol{C}_n\boldsymbol{W}_0^\dagger = -\sum_{\substack{m=-M \\ m\neq 0}}^{M} \left(\boldsymbol{W}_m\boldsymbol{C}_{n-m} + \boldsymbol{C}_{n-m}\boldsymbol{W}_m^\dagger\right) + \boldsymbol{F}\delta_{n,0}. \tag{5.177}$$

This set of equations can be solved iteratively using a procedure analogous to the Gauss–Seidel method. Given an initial guess $\boldsymbol{C}_n^{(k)}$, the coefficients are updated by solving

$$(in\omega\,\mathbb{1} + \boldsymbol{W}_0)\boldsymbol{C}_n^{(k+1)} + \boldsymbol{C}_n^{(k+1)}\boldsymbol{W}_0^\dagger = \boldsymbol{R}_n^{(k)}, \tag{5.178}$$

where the right-hand side is

$$\boldsymbol{R}_n^{(k)} = -\sum_{\substack{m=-M \\ m\neq 0}}^{M} \left(\boldsymbol{W}_m\boldsymbol{C}_{n-m}^{(k)} + \boldsymbol{C}_{n-m}^{(k)}\boldsymbol{W}_m^\dagger\right) + \boldsymbol{F}\delta_{n,0}. \tag{5.179}$$

The initial guess is taken as a static solution:

$$\boldsymbol{C}_n^{(0)} = \begin{cases} \boldsymbol{C}_0^{(0)} & \text{if } n = 0, \\ 0 & \text{otherwise,} \end{cases} \tag{5.180}$$

where $\boldsymbol{C}_0^{(0)}$ solves the time-independent Lyapunov equation:

$$\boldsymbol{W}_0\boldsymbol{C}_0^{(0)} + \boldsymbol{C}_0^{(0)}\boldsymbol{W}_0^\dagger = \boldsymbol{F}. \tag{5.181}$$

The iteration proceeds until convergence is reached within some precision ϵ, which can be measured by monitoring the norm of the update

$$\|\boldsymbol{C}_n^{(k+1)} - \boldsymbol{C}_n^{(k)}\| < \epsilon, \tag{5.182}$$

for all n.

The recursion relation couples each coefficient $\boldsymbol{C}_n^{(k+1)}$ to its $2M$ neighbors, namely $\boldsymbol{C}_{n-M}^{(k)}, \ldots, \boldsymbol{C}_{n+M}^{(k)}$. As a result, the number of nonzero coefficients increases by $2M$ with each iteration. After k steps, the support of the solution extends to Fourier modes satisfying $|n| \leq kM$. In practice, the amplitudes $\boldsymbol{C}_n$ typically decay with increasing $|n|$, allowing us to introduce a finite cutoff $n_{\max}$ beyond which the coefficients are neglected. The time-dependent solution is then approximated by the truncated Fourier series

$$\boldsymbol{C}^{(k)}(t) = \sum_{n=-n_{\max}}^{n_{\max}} \boldsymbol{C}_n^{(k)} e^{in\omega t}. \tag{5.183}$$

The matrix equation solved at each iteration has the form

$$\boldsymbol{A}\boldsymbol{X} + \boldsymbol{X}\boldsymbol{B} = \boldsymbol{R}, \tag{5.184}$$

with $\boldsymbol{A} = in\omega\,\mathbb{1} + \boldsymbol{W}_0$, $\boldsymbol{B} = \boldsymbol{W}_0^\dagger$, and $\boldsymbol{X} = \boldsymbol{C}_n^{(k+1)}$. This system is known as the *Sylvester equation*, and it can be efficiently solved using standard numerical routines.

A further simplification occurs when $\boldsymbol{W}_0$ is diagonalizable. Let $\boldsymbol{W}_0 = \boldsymbol{S}\boldsymbol{\Lambda}\boldsymbol{S}^{-1}$, with $\boldsymbol{\Lambda}$ diagonal. In this basis, the Sylvester equation becomes diagonal in component form. Defining

$$\tilde{\boldsymbol{C}}_n = \boldsymbol{S}^{-1}\boldsymbol{C}_n\boldsymbol{S}^{-\dagger}, \qquad \tilde{\boldsymbol{R}}_n = \boldsymbol{S}^{-1}\boldsymbol{R}_n\boldsymbol{S}^{-\dagger}, \tag{5.185}$$

each matrix element satisfies

$$[\tilde{\boldsymbol{C}}_n]_{ij} = \frac{[\tilde{\boldsymbol{R}}_n]_{ij}}{in\omega + \lambda_i + \lambda_j^*}, \tag{5.186}$$

where λ_i is the i-th eigenvalue of $\boldsymbol{W}_0$. After solving, the original coefficients are recovered as $\boldsymbol{C}_n = \boldsymbol{S}\tilde{\boldsymbol{C}}_n\boldsymbol{S}^\dagger$. This approach significantly reduces computational cost by avoiding repeated solutions of the Sylvester equation.

5.6 Example: Thermodynamics of a Driven Resonant-Level

5.6.1 Model and Implementation

In this section, we apply the formalism to the driven resonant-level model—a minimal setup for studying thermodynamics in driven open quantum systems [154, 155, 156, 157, 158, 159, 136]. This model allows us to benchmark our results against a range of methods previously used in the literature. The presentation here is adapted from Ref. [45], included in the list of publications.

The system consists of a single fermionic mode—representing a quantum dot—with an externally modulated energy $\epsilon(t)$, coupled to two thermal baths. The Hamiltonian of the system is

$$\hat{H}_{\mathrm{S}}(t) = \epsilon(t)\hat{c}^\dagger\hat{c}, \tag{5.187}$$

where $\hat{c}^\dagger$ and $\hat{c}$ are fermionic creation and annihilation operators for the dot. We take the dot energy to be driven by a sinusoidal protocol of the form

$$\epsilon(t) = A\sin(\omega t), \tag{5.188}$$

with driving amplitude A and frequency ω.

The system is coupled to two fermionic baths, labeled by $\alpha = L, R$. While the mesoscopic leads formalism can accommodate arbitrary, structured spectral densities, we focus here on a simplified case in which both baths are described by the same flat spectral density:

$$\mathcal{J}(\omega) = \begin{cases} \Gamma, & \omega \in [-W, W] \\ 0, & \text{otherwise}, \end{cases} \tag{5.189}$$

where Γ is the system-bath coupling strength and W is a hard cut-off.

Following the mesoscopic leads prescription, each bath is replaced by a finite lead. We take both leads to contain the same number of modes L and use a linear-logarithmic discretization for the lead energies $\{\epsilon_{k\alpha}\}$. Specifically, L_{lin} modes are spaced linearly within a central window $[-W^*, W^*]$, while the remaining L_{log} modes are logarithmically spaced within the

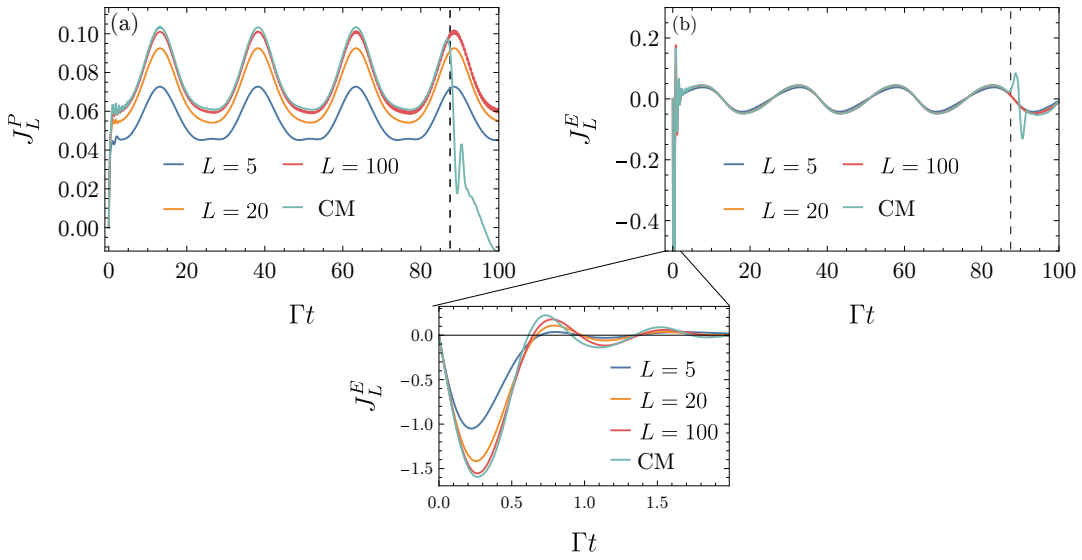

Figure 5.8: (a) Particle current and (b) energy current in the driven resonant-level model. Solid lines show results obtained using the mesoscopic leads method for increasing numbers of lead modes L. The dashed line shows numerically exact results from the chain-mapping approach, valid up to a finite time. Parameters: $\Gamma = 1$, $A = 1$, $\omega = 0.25$, $\mu_{\mathrm{L}} = -\mu_{\mathrm{R}} = 0.5$, $T_{\mathrm{L}} = T_{\mathrm{R}} = 1$, $p_0 = 0.5$.

outer intervals $[-W, -W^*]$ and $[W^*, W]$. This yields a total of $L = L_{\mathrm{lin}} + 2L_{\mathrm{log}}$ modes per lead, with symmetric sampling about zero. Throughout this section, we set $\Gamma = 1$ to define the energy scale and use $W = 8$, $W^* = 4$ as standard parameters unless otherwise noted.

Since the system is non-interacting, the dynamics is fully encoded in the covariance matrix $\boldsymbol{C}(t)$, which evolves according to the Lyapunov equation introduced in Section 5.5.

To test the accuracy of the mesoscopic leads formalism, we compute the particle and energy currents from the left bath, J_L^P and J_L^E, and compare them to results obtained using the chain-mapping method, discussed in Section 5.3.3.

Figure 5.8 shows the particle and energy currents as functions of time for increasing values of the lead size L. We observe rapid convergence with increasing L, indicating that even a modest number of lead modes is sufficient to accurately capture the system dynamics. For reference, we also include results from the chain-mapping method, which are numerically exact up to a finite time set by the length of the chain. An estimate of this time threshold is indicated by a vertical dashed line.

The agreement with chain-mapping illustrates an important conceptual point: physical observables are insensitive to the microscopic details of the baths, provided the effective spectral densities are matched. However, this invariance relies on using a consistent definition of currents—specifically, the internal currents. Figure 5.9 highlights the difference by comparing internal and external current expressions.

5.6.2 Entropy production

A key advantage of the mesoscopic leads framework is that it provides complete access to the state of the system at all times. Such time-resolved quantities are generally inaccessible in methods based on Floquet or scattering theory, which typically yield only cycle-averaged

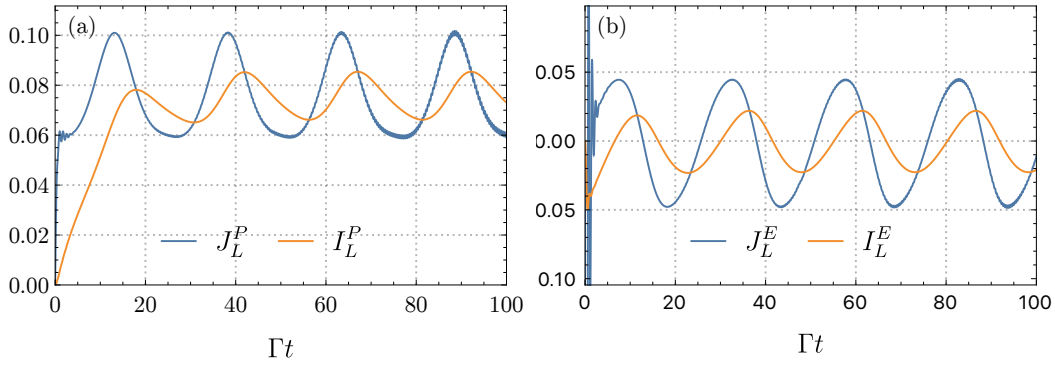

Figure 5.9: Comparison between internal and external currents in the driven resonant-level model. (a) Particle current from the left lead into the system, computed using the internal current expression (solid) and the residual bath expression (dashed). (b) Same comparison for the energy current. Both leads have $L = 100$ modes, with parameters $\Gamma = 1$, $W = 8$, $W^* = 4$, $T_L = T_R = 1$, $\mu_L = -\mu_R = 0.5$, $A = 1$, $\omega = 0.25$, $p_0 = 0.5$, and $L_{\text{lin}}/L_{\log} = 0.1$.

results. In particular, this enables the computation of time-dependent thermodynamic quantities such as entropy and entropy production at all times.

In the resonant-level model, the system consists of a single fermionic mode. Its state is fully described by the occupation probability $p_t = \langle \hat{c}^\dagger \hat{c} \rangle$, corresponding to the single entry of the system's covariance matrix. The von Neumann entropy of the system is then given by the binary entropy function:

$$S(t) = -p_t \log p_t - (1 - p_t) \log(1 - p_t). \tag{5.190}$$

For this single-mode system, the time derivative of the entropy can be computed analytically as:

$$\dot{S}(t) = -\dot{p}_t \log\left(\frac{p_t}{1 - p_t}\right). \tag{5.191}$$

The instantaneous entropy production rate is obtained from the second law:

$$\dot{\Sigma}(t) = \dot{S}(t) - \sum_{\alpha=L,R} \beta_\alpha J_\alpha^Q(t), \tag{5.192}$$

where $J_\alpha^Q(t)$ is the heat current flowing from reservoir α into the system, and $\beta_\alpha = 1/T_\alpha$ is the inverse temperature.

Figure 5.10 shows the entropy production rate $\dot{\Sigma}(t)$ computed using the mesoscopic leads framework for increasing numbers of lead modes. For reference, we also include results obtained from the chain-mapping approach. The curves exhibit rapid convergence with increasing L, and demonstrate excellent agreement with the numerically exact result within its time window of validity.

5.6.3 High-Temperature Limit

As a final benchmark, we test whether the mesoscopic leads approach correctly reproduces the classical dynamics expected in the high-temperature regime. In the limit $T \gg \Gamma$,

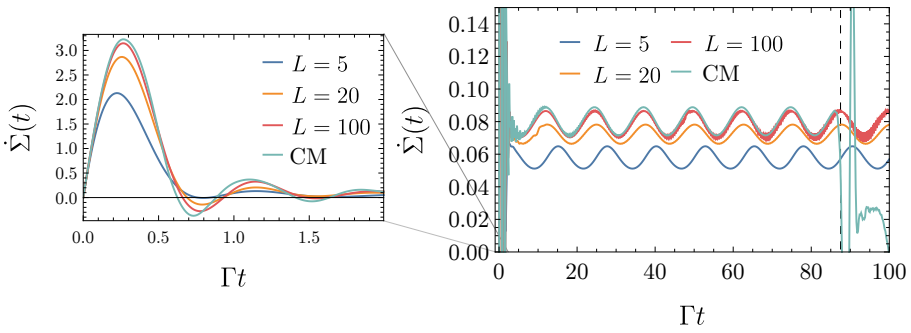

Figure 5.10: Instantaneous entropy production rate $\dot{\Sigma}(t)$ for the driven resonant-level model. The curves show convergence of the mesoscopic leads method with increasing L, compared against exact results from chain mapping (black dashed). Same parameters as in Fig. 5.8.

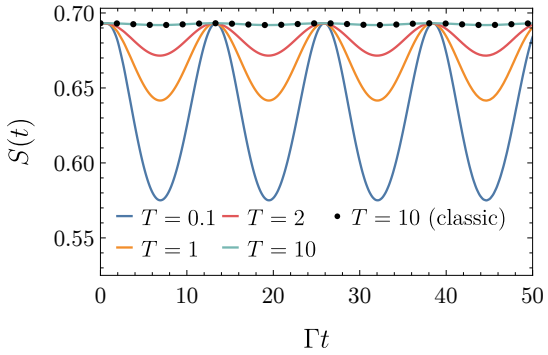

Figure 5.11: Convergence of the entropy of the dot in the driven resonant-level model as the temperature increases. Solid lines correspond to the mesoscopic leads approach; black dots represent the solution of the classical Pauli master equation [Eq. (5.193)]. Parameters: $A = 1$, $\omega = 0.25$, $W = 8$, $W^* = 4$, $L = 100$, $L_{\log}/L_{\text{lin}} = 0.1$, $\Gamma = 1$, $p_0 = 0.5$.

the occupation probability of the dot becomes well-described by a classical Pauli master equation:

$$\dot{p}_t = \sum_{\alpha=L,R} \Gamma[f_\alpha(t) - p_t], \tag{5.193}$$

where $f_\alpha(t) = [e^{(\epsilon(t)-\mu_\alpha)/T} + 1]^{-1}$ is the instantaneous Fermi–Dirac distribution for reservoir α.

In Fig. 5.11, we compare the entropy of the dot computed using the mesoscopic leads method to the result obtained from numerically integrating the classical master equation (5.193). As the temperature increases, the two results converge, demonstrating that the mesoscopic leads formalism correctly recovers the high-temperature limit, providing further support for the consistency of the approach.

5.7 Case Study: Rectification in a Driven Double Dot

We now demonstrate the capabilities of the mesoscopic leads formalism by investigating heat rectification in a periodically driven, non-interacting system. Inspired by Ref. [160], which examined the bosonic version of this problem, we consider instead a chain of two coupled fermionic modes, where only the first site is driven. Similar problems have been addressed in Refs. [161, 162], though with focus on particle currents. Our framework enables a natural extension to energy transport, allowing us to study heat rectification [163].

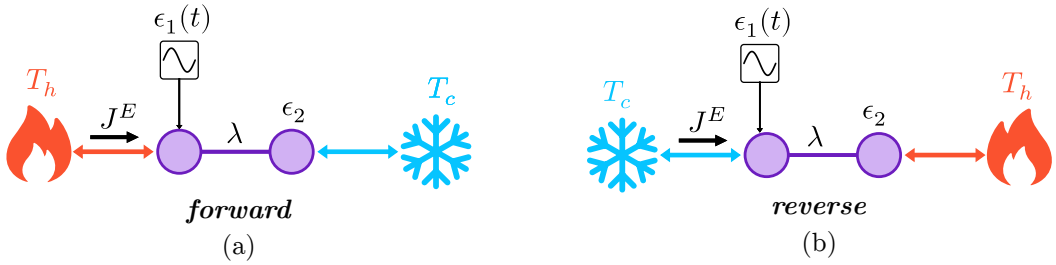

Figure 5.12: Schematic of the rectification model. Two coupled quantum dots are connected to separate thermal baths. Only the left dot is subject to a periodic drive at frequency ω. Heat rectification is studied by comparing the energy current in the forward configuration—where the left bath is hotter—with the reverse configuration, in which the baths are swapped.

The Hamiltonian of the system is given by

$$\hat{H}_{\mathrm{S}}(t) = \epsilon_1(t)\hat{c}_1^\dagger\hat{c}_1 + \epsilon_2\hat{c}_2^\dagger\hat{c}_2 + \lambda\left(\hat{c}_1^\dagger\hat{c}_2 + \hat{c}_2^\dagger\hat{c}_1\right), \tag{5.194}$$

where λ is the tunneling amplitude between the two dots, and $\epsilon_1(t) = A\sin(\omega t)$ is a time-dependent onsite energy applied only to the first dot. In simulations, we set $\epsilon_1(0) = \epsilon_2 = 0$.

Each dot is coupled to an independent thermal bath, modeled via mesoscopic leads with flat spectral densities as in Eq. (5.189). We fix $\Gamma = 1$ to set the energy scale and take $\mu_L = \mu_R = 0$, so that energy and heat currents coincide.

To investigate rectification, we consider two configurations. In the *forward* configuration, the left bath is hot and the right bath is cold: $T_L = T_h$, $T_R = T_c$, with $T_h > T_c$. In the *reverse* configuration, the baths are swapped: $T_L = T_c$, $T_R = T_h$.

Because the system is time-dependent, care is needed when defining rectification: the heat flowing through the system is not uniquely defined. In particular, due to the driving, the time-averaged energy currents into the left and right baths are generally not equal, even in the long-time limit. They differ precisely by the time-averaged power supplied by the driving protocol. Consequently, we restrict attention to the energy current into the left mode, which is the one directly driven.

Figure 5.13 shows the energy current into the left bath as a function of time for both configurations, across increasing values of the driving frequency ω, with fixed coupling $\lambda = 3$. In all simulations, we set the driving amplitude to $A = 1$, and the bath temperatures to $T_h = 2$ and $T_c = 1$. We use $L = 100$ modes in each lead, which was verified to ensure convergence. We denote by J_L^E the energy current from the left bath in the forward configuration, and by $-\tilde{J}_L^E$ the energy current into the left bath in the reverse configuration (see Fig. 5.12).

Both currents settle into limit cycles that exhibit periodic oscillations at the driving frequency. The horizontal dashed lines represent the cycle-averaged energy currents in the steady state, computed using the method described in Sec. 5.5.4. The results demonstrate that the magnitudes of the forward and reverse currents differ in the limit cycle, and that the gap between them depends on the driving frequency. Notably, we have found that such rectification effects are absent in the particle current for this setup.

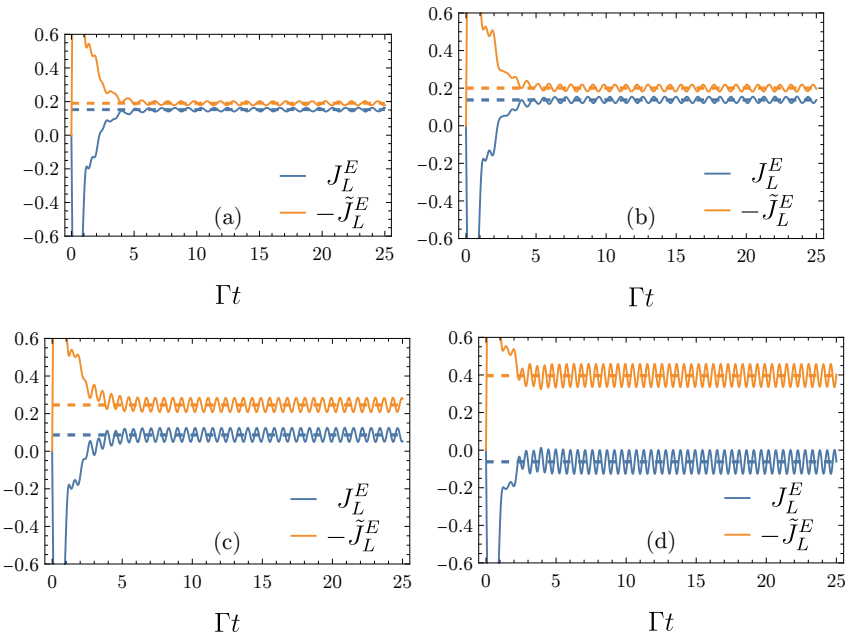

Figure 5.13: Energy current from the left bath in the forward configuration (blue) and the negative of the current in the reverse configuration (orange), plotted for increasing values of the driving frequency: (a) $\omega = 3$, (b) $\omega = 4$, (c) $\omega = 5$, (d) $\omega = 6$. Dashed lines indicate the corresponding cycle-averaged values in the limit cycle. Parameters: $\lambda = 3$, $T_h = 2$, $T_c = 1$, $A = 1$, $\Gamma = 1$, $\mu_L = \mu_R = 0$, $W = 8$, $W^* = 4$, $L = 100$, $L_{\text{lin}}/L_{\log} = 0.1$.

To quantify rectification, we define the rectification coefficient as

$$R = \frac{|J + \tilde{J}|}{|J - \tilde{J}|}, \tag{5.195}$$

where, for compactness, we denote the cycle-averaged energy current from the left bath in the forward (reverse) configuration by

$$J = \frac{1}{\tau}\int_{t_0}^{t_0+\tau} \mathrm{d}t\, J_L^E(t), \qquad \tilde{J} = \frac{1}{\tau}\int_{t_0}^{t_0+\tau} \mathrm{d}t\, \tilde{J}_L^E(t), \tag{5.196}$$

with $\tau = 2\pi/\omega$ the driving period, and t_0 chosen sufficiently late so that the system has reached the limit cycle. If the system acts as a perfect diode, i.e., one configuration yields current while the other yields none, then $R = 1$. If both configurations give equal and opposite currents, $R = 0$. In driven systems, R can exceed 1 if both J and $\tilde{J}$ have the same sign, as seen in Fig. 5.13(d).

In Fig. 5.14(a), we plot R as a function of ω/λ for various values of λ. Rectification is suppressed at both low and high frequencies and reaches a maximum at intermediate values of ω/λ. For $\lambda > 1$, the location of this maximum occurs around the same value of ω/λ.

In the limit cycle, the average entropy production rate is given by

$$\overline{\sigma} = \sum_\alpha \beta_\alpha \overline{J_\alpha^Q}, \tag{5.197}$$

where $\overline{J}_\alpha$ is the cycle-averaged heat current from reservoir α, and $\beta_\alpha = 1/T_\alpha$. Interestingly, although the energy current into the left bath differs between forward and reverse setups,

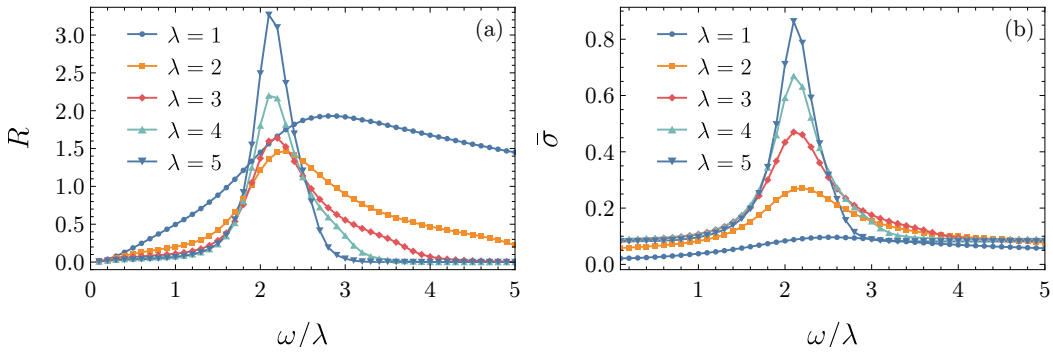

Figure 5.14: (a) Rectification coefficient R as a function of ω/λ for increasing values of the inter-dot coupling λ. (b) Corresponding cycle-averaged entropy production rate $\overline{\sigma}$, showing a peak aligned with maximal rectification. Parameters: $T_h = 2$, $T_c = 1$, $A = 1$, $\Gamma = 1$, $\mu_L = \mu_R = 0$, $W = 8$, $W^* = 4$, $L = 100$, $L_{\text{lin}}/L_{\text{log}} = 0.1$.

the entropy production rate $\overline{\sigma}$ is identical in both cases. As shown in Fig. 5.14(b), the entropy production exhibits a pronounced peak at the same frequency where rectification is maximized, suggesting that stronger rectification comes at the cost of greater irreversibility.

These results would be difficult to obtain using standard methods. The regime explored here lies well beyond the validity of Markovian master equations and perturbative expansions. Our approach enables non-perturbative, time-resolved access to thermodynamic observables across a broad range of parameters.

Even in this minimal setup, many interesting directions remain open. The dependence of rectification on temperature, chemical bias, or the shape of the driving protocol can all be explored within our framework. These topics merit dedicated investigation in future work.

6 Entropy production in the mesoscopic-leads formalism

Computing entropy production in open quantum systems strongly coupled to their environment remains a central challenge in quantum thermodynamics. Standard techniques often rely on weak-coupling and Markovian approximations, which break down in this regime.

In Chapter 5, we introduced the *Markovian embedding* provided by the mesoscopic leads approach: a discretized representation of a thermal bath in which each mode is weakly coupled to an external reservoir. This construction enables a Lindblad evolution for the extended system (system + leads), even though the system's reduced dynamics is generally non-Markovian. A schematic illustration of the embedding is shown in Fig. 6.1.

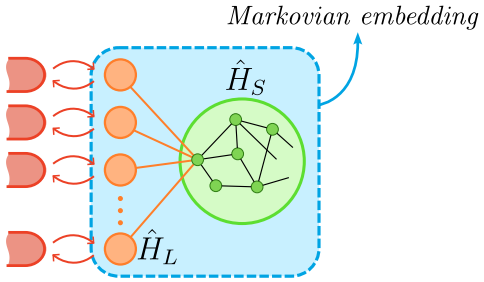

Figure 6.1: Markovian embedding in the mesoscopic leads framework. The system $\hat{H}_S$ is coupled to a lead $\hat{H}_L$, which is locally damped by Markovian reservoirs (red). The extended system (system + lead) evolves under a Lindblad equation.

One appealing feature of this approach—discussed throughout the thesis—is that it allows us to import results from the theory of quantum dynamical semigroups, including Spohn's framework for entropy production [30]. This raises a natural question: *Can we compute the entropy production of the original system using Spohn's definition, applied at the level of the embedding?* This is the central goal of this chapter.

If the extended system reaches a thermal stationary state, then Spohn's formula defines the entropy production as the relative entropy between the evolving state and this thermal fixed point. However, in our setting, the dissipators act only on the lead modes, so thermalization of the full extended system is not guaranteed. Nevertheless, we present strong numerical evidence—both for non-interacting and interacting systems—that the extended system becomes approximately thermal as the number of lead modes increases.

Once this thermalization property is established, Spohn's definition of entropy production can be applied at the level of the embedding. We show that this definition agrees with the standard thermodynamic expression based on external particle and energy currents in the limit of large lead modes.

Finally, we analyze the relationship between the entropy production computed from the system alone and that obtained from the full embedding.

◆

6.1 Entropy production in Markovian systems

In this section, we briefly review the definition of entropy production in Markovian open quantum systems. A more detailed discussion, including derivations and thermodynamic interpretations, can be found in Chapter 3, Section 3.6.2.

For a system coupled to a single thermal reservoir at inverse temperature β and chemical potential μ, and whose dynamics is described by a quantum dynamical semigroup with generator $\mathcal{L}$, the entropy production rate is defined by Spohn as

$$\sigma(t) = -\frac{\mathrm{d}}{\mathrm{d}t} D(\hat{\rho}(t) \| \hat{\rho}_{\mathrm{ss}}), \tag{6.1}$$

where $D(\hat{\rho}\|\hat{\sigma}) = \mathrm{Tr}[\hat{\rho}(\log\hat{\rho} - \log\hat{\sigma})]$ denotes the quantum relative entropy and $\hat{\rho}_{\mathrm{ss}}$ is the stationary state of the dynamics. This quantity is non-negative at all times, a consequence of the monotonicity of the relative entropy under completely positive, trace-preserving (CPTP) maps.

Equivalently, the entropy production rate can be expressed in terms of the dissipator $\mathcal{D}$ as

$$\sigma(t) = -\mathrm{Tr}[\mathcal{D}(\hat{\rho}(t))(\log\hat{\rho}(t) - \log\hat{\rho}_{\mathrm{ss}})] \geq 0, \tag{6.2}$$

a form known as *Spohn's inequality* [30].

This framework generalizes naturally to systems coupled to multiple reservoirs. In that case, assuming each partial generator $\mathcal{L}_\alpha = -i[\hat{H}, \cdot] + \mathcal{D}_\alpha$ has a Gibbs state $\hat{\omega}_\alpha$ as its fixed point, the entropy production rate becomes

$$\sigma(t) = \sum_\alpha \mathrm{Tr}[\mathcal{D}_\alpha(\hat{\rho}(t))(\log\hat{\rho}(t) - \log\hat{\omega}_\alpha)] \geq 0. \tag{6.3}$$

Each term in the sum is non-negative and can be interpreted as the entropy production due to the individual reservoir α.

These expressions will serve as the benchmark for the entropy production computed within the Markovian embedding introduced in the following sections.

6.2 Model and Setup

To study entropy production in the mesoscopic leads framework, we focus on a paradigmatic example: a fermionic lattice system coupled to a thermal reservoir. The system consists of N sites with nearest-neighbour hopping, and may include nearest-neighbour density-density interactions. Its Hamiltonian is given by

$$\hat{H}_S = \sum_{j=1}^{N} \epsilon_j \hat{c}_j^\dagger \hat{c}_j - g \sum_{j=1}^{N-1} \left(\hat{c}_j^\dagger \hat{c}_{j+1} + \hat{c}_{j+1}^\dagger \hat{c}_j \right) + U \sum_{j=1}^{N-1} \hat{n}_j \hat{n}_{j+1}, \tag{6.4}$$

where $\hat{c}_j$ is the fermionic annihilation operator on site j, and $\hat{n}_j = \hat{c}_j^\dagger \hat{c}_j$.

We assume the system is coupled to a thermal reservoir at inverse temperature β and chemical potential μ, characterized by a spectral function $\mathcal{J}(\omega)$. To model this coupling, we use the approach introduced in Chapter 5, where the bath is approximated by a finite set of fermionic modes (the lead), each locally damped by a residual environment. The residual reservoirs are assumed to be Markovian and weakly coupled, allowing the full dynamics to be captured by a Lindblad master equation.

For simplicity, we take the spectral density to be flat:

$$\mathcal{J}(\omega) = \begin{cases} \Gamma, & \omega \in [-W, W], \\ 0, & \text{otherwise}, \end{cases} \tag{6.5}$$

where Γ is the effective coupling strength and W is a cutoff energy. The reservoir is discretized into L equally spaced energy modes $\{\epsilon_k\}$ in the range $[-W, W]$, with each mode weakly coupled to a local residual bath. We choose the couplings κ_k such that

$$\kappa_k = \sqrt{\frac{\Gamma \Delta\epsilon}{2\pi}}, \tag{6.6}$$

where $\Delta\epsilon = \epsilon_{k+1} - \epsilon_k = 2W/L$ is the mode spacing. We also take the damping rates γ_k of the residual reservoirs to match the spacing: $\gamma_k = \Delta\epsilon = 2W/L$. This ensures that the mesoscopic representation becomes an accurate approximation to the original continuum bath in the limit $L \to \infty$.

The total Hamiltonian of the extended system (system + lead) is then given by

$$\hat{H} = \hat{H}_S + \hat{H}_L + \hat{H}_{SL}, \tag{6.7}$$

where

$$\hat{H}_L = \sum_{k=1}^{L} \epsilon_k \hat{a}_k^\dagger \hat{a}_k, \tag{6.8}$$

$$\hat{H}_{SL} = \sum_{k=1}^{L} \kappa_k \left(\hat{c}_1^\dagger \hat{a}_k + \hat{a}_k^\dagger \hat{c}_1 \right), \tag{6.9}$$

with $\hat{a}_k$ the fermionic annihilation operator for the k-th lead mode.

The dynamics of the extended state $\hat{\rho}_{SL}(t)$ is governed by a Lindblad master equation of the form

$$\frac{\mathrm{d}\hat{\rho}_{SL}(t)}{\mathrm{d}t} = -i[\hat{H}, \hat{\rho}_{SL}(t)] + \mathcal{D}(\hat{\rho}_{SL}(t)), \tag{6.10}$$

where the dissipator encodes the coupling of each lead mode to its residual bath:

$$\mathcal{D}[\hat{\rho}] = \sum_{k=1}^{L} \gamma_k (1 - f_k) \left(\hat{a}_k \hat{\rho} \hat{a}_k^\dagger - \tfrac{1}{2} \{ \hat{a}_k^\dagger \hat{a}_k, \hat{\rho} \} \right) + \gamma_k f_k \left(\hat{a}_k^\dagger \hat{\rho} \hat{a}_k - \tfrac{1}{2} \{ \hat{a}_k \hat{a}_k^\dagger, \hat{\rho} \} \right), \tag{6.11}$$

with $f_k = (e^{\beta(\epsilon_k - \mu)} + 1)^{-1}$ the Fermi-Dirac distribution.

The analysis of the system dynamics depends on whether interactions are present. In what follows, we consider both the non-interacting and interacting regimes separately.

6.3 Thermalization of the extended system steady state

We now investigate whether the extended system reaches a thermal steady state when coupled to a single mesoscopic lead. In particular, we ask whether the long-time state $\hat{\rho}_{SL}(t \to \infty)$ approximates a thermal Gibbs state $\hat{\rho}_\beta \propto e^{-\beta \hat{H}}$, where $\hat{H}$ is the full Hamiltonian of system plus lead. The analysis is carried out separately for the non-interacting and interacting cases, as they require different numerical and analytical tools.

6.3.1 Non-interacting systems ($U = 0$)

In the absence of interactions ($U = 0$), the total Hamiltonian is quadratic and the dynamics remains Gaussian. In this regime, the full state $\hat{\rho}_{SL}(t)$ is entirely determined by its two-point correlation functions.

We define a total of $N + L$ fermionic modes,

$$\hat{d}_i = \begin{cases} \hat{c}_i, & \text{for } i = 1, \dots, N \quad \text{(system modes)}, \\ \hat{a}_{i-N}, & \text{for } i = N+1, \dots, N+L \quad \text{(lead modes)}, \end{cases} \tag{6.12}$$

and rewrite the full Hamiltonian as

$$\hat{H} = \sum_{ij} H_{ij}\, \hat{d}_i^\dagger \hat{d}_j, \tag{6.13}$$

where $\boldsymbol{H} \in \mathbb{C}^{(N+L)\times(N+L)}$ is the single-particle Hamiltonian of the extended system.

The state is characterized by its covariance matrix $\boldsymbol{C}(t)$, with entries

$$C_{ij}(t) = \mathrm{Tr}[\hat{\rho}_{SL}(t)\, \hat{d}_j^\dagger \hat{d}_i]. \tag{6.14}$$

Its time evolution is governed by the Lyapunov equation

$$\frac{\mathrm{d}\boldsymbol{C}(t)}{\mathrm{d}t} = -(\boldsymbol{W}\boldsymbol{C}(t) + \boldsymbol{C}(t)\boldsymbol{W}^\dagger) + \boldsymbol{F}, \tag{6.15}$$

with $\boldsymbol{W} = i\boldsymbol{H} + \boldsymbol{\Gamma}/2$, and

$$\boldsymbol{\Gamma} = \mathrm{diag}(0, \dots, 0, \gamma_1, \dots, \gamma_L), \quad \boldsymbol{F} = \mathrm{diag}(0, \dots, 0, f_1\gamma_1, \dots, f_L\gamma_L). \tag{6.16}$$

In the long-time limit, the system reaches a unique steady state $\hat{\rho}_{\mathrm{ss}}$, whose covariance matrix satisfies

$$\boldsymbol{W}\boldsymbol{C}_{\mathrm{ss}} + \boldsymbol{C}_{\mathrm{ss}}\boldsymbol{W}^\dagger = \boldsymbol{F}. \tag{6.17}$$

To test whether the steady state is approximately thermal, we compare $\hat{\rho}_{\mathrm{ss}}$ with the thermal reference state

$$\hat{\rho}_\beta = \frac{1}{Z} e^{-\beta \hat{H}}, \tag{6.18}$$

where $\hat{H}$ is the Hamiltonian of the extended system and $Z = \mathrm{Tr}\left[e^{-\beta\hat{H}}\right]$ is the partition function. As a measure of closeness, we use the quantum fidelity

$$F(\hat{\rho}_1, \hat{\rho}_2) = \mathrm{Tr}\left[\sqrt{\sqrt{\hat{\rho}_1}\,\hat{\rho}_2\,\sqrt{\hat{\rho}_1}}\right]^2, \tag{6.19}$$

which can be efficiently computed for fermionic Gaussian states in terms of their covariance matrices.

This result was derived in Section 4.8 of Chapter 4; we recall it here for completeness. Given two Gaussian states with covariance matrices $\boldsymbol{C}_1$ and $\boldsymbol{C}_2$, the corresponding density operators can be written as

$$\hat{\rho}_j = \frac{1}{Z_j} e^{-\hat{\boldsymbol{d}}^\dagger \boldsymbol{M}_j \hat{\boldsymbol{d}}}, \quad \boldsymbol{M}_j = \log\left(\frac{\mathbb{1} - \boldsymbol{C}_j}{\boldsymbol{C}_j}\right).$$

for $j = 1, 2$. The fidelity is then given by

$$F(\hat{\rho}_1, \hat{\rho}_2) = \frac{\det\left(\mathbb{1} + \sqrt{e^{-\boldsymbol{M}_1} e^{-\boldsymbol{M}_2}}\right)^2}{\det(\mathbb{1} + e^{-\boldsymbol{M}_1}) \cdot \det(\mathbb{1} + e^{-\boldsymbol{M}_2})}. \tag{6.20}$$

In our case, we take $\hat{\rho}_1 = \hat{\rho}_{\mathrm{ss}}$ and $\hat{\rho}_2 = \hat{\rho}_\beta$. The covariance matrix of a thermal state is given by

$$\boldsymbol{C}_\beta = (\mathbb{1} + e^{\beta \boldsymbol{H}})^{-1}. \tag{6.21}$$

so that $\boldsymbol{M}_2 = \beta \boldsymbol{H}$.

Figure 6.2 shows the infidelity $1 - F(\hat{\rho}_{\mathrm{ss}}, \hat{\rho}_\beta)$ as a function of the number of lead modes L, for different system sizes and temperatures. As L increases, the infidelity decreases monotonically, indicating convergence of the steady state toward a thermal state. We also observe that larger systems require more lead modes to reach the same level of agreement, consistent with the fact that a finite-size reservoir can only approximate thermalization up to a certain precision.

6.3.2 Interacting systems ($U \neq 0$)

In the presence of interactions ($U \neq 0$), the system is no longer Gaussian, and the covariance matrix formalism no longer applies. To compute both thermal and steady states in this regime, we use a matrix product state (MPS) approach based on the superfermion representation of the entire Markovian embedding [44, 164]. In this framework, the density matrix of the $N + L$ site system is mapped to a pure state on a doubled Hilbert space with $2N + 2L$ sites, where each physical fermionic site is paired with an ancilla. This method offers the advantage of incorporating fermionic correlations without introducing cumbersome long-range Jordan-Wigner strings [44].

To generate a thermal state $\hat{\rho}_\beta$, we employ imaginary time evolution using the time-dependent variational principle (TDVP). The evolution is performed with a time step $\Delta\beta = 0.001$, a truncation cutoff of 10^{-6}, a maximum bond dimension of 80, and a minimum bond dimension of 15. For a fixed Hamiltonian, the thermal state is obtained in a single sweep from infinite temperature, progressing from the highest temperature state to the lowest. A brief

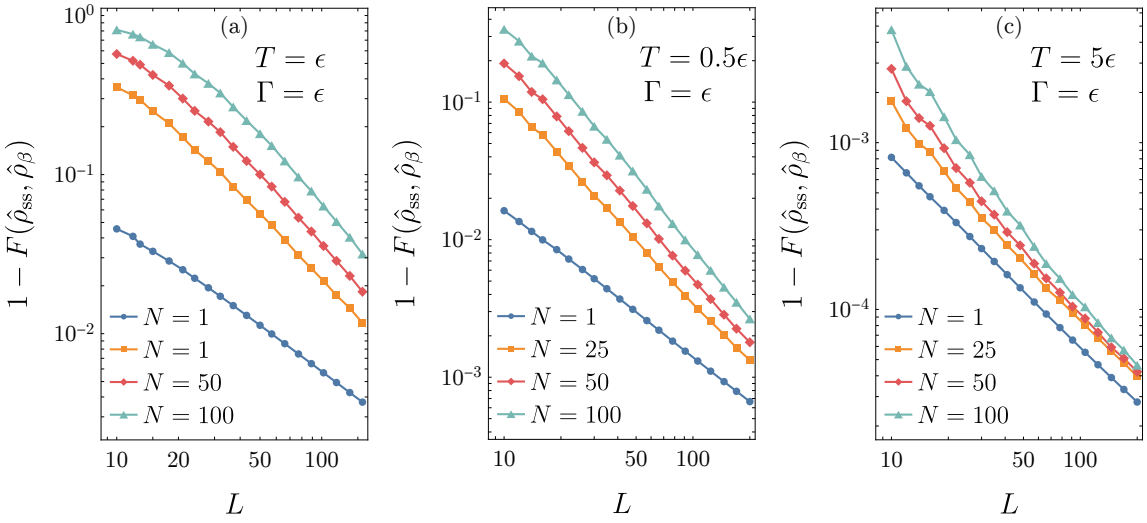

Figure 6.2: Infidelity, $1 - F(\hat{\rho}_{\rm ss}, \hat{\rho}_\beta)$, between the steady state and thermal state of the extended system, as a function of the number of lead modes L. The system consists of a chain of N fermionic sites with nearest-neighbour hopping and on-site energies $\epsilon_j = \epsilon$, and the lead is coupled to the first site. We set $g = \epsilon = 1$, and consider temperatures $T = 0.5\epsilon$, ϵ, and 5ϵ in panels (a), (b), and (c), respectively. The infidelity is computed using Eq. (6.18) and the fidelity formula above.

summary of the superfermion formalism and of the TDVP-based thermal-state preparation is provided in Appendix A.5.

In tensor network simulations, quantities that involve high powers or matrix square roots of the density matrix, such as the quantum fidelity, are generally difficult to compute, as they require access to nonlocal operations that are not readily available in MPS representations. In contrast, linear and quadratic functionals of $\hat{\rho}$, such as expectation values and Hilbert-Schmidt norms, can be efficiently evaluated. For this reason, to assess whether a thermal state $\hat{\rho}_\beta \propto e^{-\beta \hat{H}}$ is a good approximation to the steady state, we compute its *variability*, defined as

$$v(\hat{\rho}_\beta) = \sqrt{\mathrm{Tr}\big[\mathcal{L}(\hat{\rho}_\beta)^\dagger \mathcal{L}(\hat{\rho}_\beta)\big]}. \tag{6.22}$$

This measure is motivated by the fact that $\mathcal{L}(\hat{\rho}_{\rm ss}) = 0$, where $\hat{\rho}_{\rm ss}$ is the steady state. Therefore, if $v(\hat{\rho}_\beta) \approx 0$, then $\hat{\rho}_\beta$ is approximately a fixed point of the dissipative dynamics. This approach has the significant advantage that it only requires knowledge of the thermal state and does not require a separate calculation of the steady state. We assume throughout that the steady state is unique, which is justified by the absence of known strong symmetries [165] and the fact that we consider ergodic models in the interacting case. A discussion of the error estimate for $v(\hat{\rho}_\beta)$ and the robustness of its computation, including convergence with bond dimension, is provided in Appendix A.6.

Figure 6.3 shows the variability $v(\hat{\rho}_\beta)$ as a function of the number of lead modes L, for a fixed system size $N = 3$, and for various interaction strengths and temperatures. As in the non-interacting case (cf. Fig. 6.2), the variability decreases monotonically with L, indicating that the extended system approaches a thermal fixed point as the number of lead modes increases—even in the presence of strong system-lead coupling and local interactions. This supports the conclusion that the mesoscopic lead construction faithfully

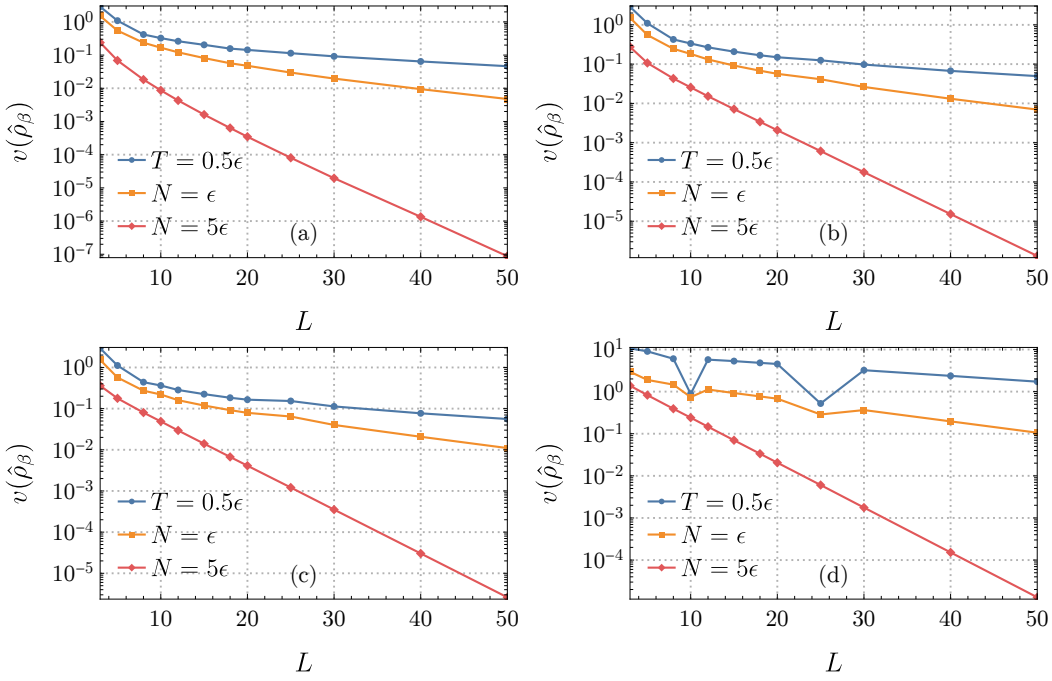

Figure 6.3: Variability $v(\hat{\rho}_\beta)$ as a function of the number of lead modes L for different temperatures $T = 0.5\epsilon, \epsilon, 5\epsilon$ (blue, orange, green) and interaction strengths $U = 0, 0.5\epsilon, \epsilon, 5\epsilon$ [panels (a)–(d)]. Parameters: $\epsilon = 1$, $W = 10$, $\Gamma = 1$, system size $N = 3$.

captures thermalization behavior, even for systems with non-quadratic interactions and non-trivial system-bath correlations.

6.4 Entropy production

We now investigate how the entropy production (defined over the entire extended system) behaves for a single bath in the transient regime before reaching the steady state. To this end, we begin by defining the currents flowing between the lead modes and their respective residual reservoirs—quantities we refer to as *external currents*. The external energy and particle currents are given by

$$\begin{aligned} I^E(t) &= \mathrm{Tr}\big[\hat{H}\mathcal{L}(\hat{\rho}_{SL}(t))\big], \\ I^P(t) &= \mathrm{Tr}\big[\hat{N}\mathcal{L}(\hat{\rho}_{SL}(t))\big], \end{aligned} \tag{6.23}$$

and the corresponding heat current is defined as

$$I^Q(t) = I^E(t) - \mu I^P(t)\,. \tag{6.24}$$

Following Refs. [166, 167, 168, 169, 45], we define the entropy production rate at the level of the extended system as

$$\sigma_{SL}(t) = \dot{S}_{SL}(t) - \beta I^Q(t), \tag{6.25}$$

where $S_{SL}(t) \equiv S(\hat{\rho}_{SL}(t))$ is the von Neumann entropy of the extended system and $\dot{S}_{SL}(t)$ is its time derivative. Importantly, this definition does not assume that the steady state is thermal [103].

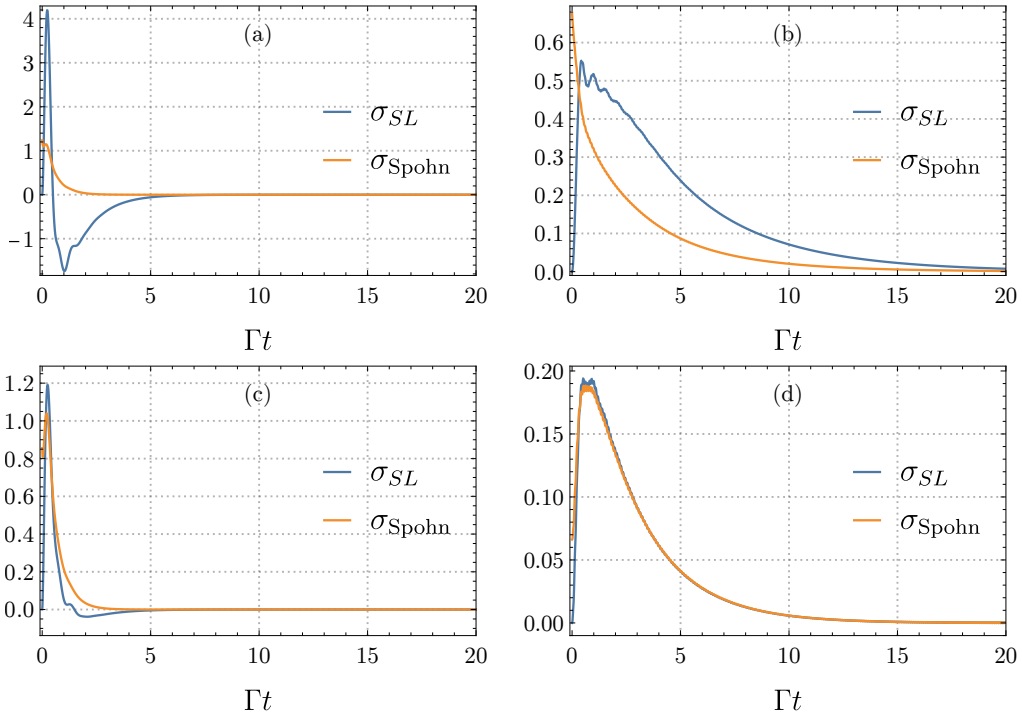

Figure 6.4: Comparison of the two different definitions of the entropy production rate, $\sigma_{SL}(t)$ and $\sigma_{\text{Spohn}}(t)$, for the resonant level model at different temperatures and lead sizes. We set $\epsilon = 1$, $\Gamma = 1$, and $W = 10$ in all plots. The temperatures and lead sizes are as follows: (a) $T = 0.1\epsilon$, $L = 5$; (b) $T = \epsilon$, $L = 5$; (c) $T = 0.1\epsilon$, $L = 100$; (d) $T = \epsilon$, $L = 100$. Panel (d) corresponds to the high-temperature, large-lead limit, where agreement between the two definitions is expected and observed.

Since the extended system obeys Lindblad dynamics, we also consider Spohn's definition of the entropy production rate [30]

$$\sigma_{\text{Spohn}}(t) = -\frac{\mathrm{d}}{\mathrm{d}t} D(\hat{\rho}_{SL}(t) \| \hat{\rho}_{\text{ss}}) \geq 0, \tag{6.26}$$

where $\hat{\rho}_{\text{ss}}$ is the fixed point of the dynamics. As we discussed in Section 3.6.2, this quantity is non-negative, which follows from the contractivity of quantum relative entropy under CPTP maps. Moreover, in Section 3.6.2, we also show that if the steady state is thermal, $\hat{\rho}_{\text{ss}} = \hat{\rho}_\beta \propto e^{-\beta \hat{H}}$, the two definitions coincide, i.e., $\sigma_{\text{Spohn}}(t) = \sigma_{SL}(t)$.

As discussed in the previous section, the steady state of the extended system approaches a thermal state when the number of lead modes is large. Therefore, we expect the two definitions in Eqs. (6.25) and (6.26) to agree in the limit of large L or high temperature.

To demonstrate this, we consider the resonant-level model with $N = 1$, as defined in Eq. (6.4). Figure 6.4 compares $\sigma_{\text{Spohn}}(t)$ and $\sigma_{SL}(t)$ for different lead sizes and temperatures, assuming a flat spectral density as in Eq. (6.5). Agreement improves with increasing L, and is particularly strong at higher temperature, consistent with expectations: the mesoscopic leads approximation becomes more accurate as $L \to \infty$, though convergence requires more modes at low temperature [44, 45].

It is worth noting that we restrict to moderate values of L in Fig. 6.4, since the numerical computation of $\dot{S}_{SL}(t)$ becomes ill-conditioned for large systems. This limitation does not

affect entropy production computations at the level of the system alone, which we explore in the next subsection.

6.4.1 Entropic discrepancy with a single bath

So far, we have studied the thermalization of the extended system $\hat{\rho}_{SL}(t)$ and analyzed the entropy production rate during the transient regime in the presence of a single bath. It is important to emphasize, however, that while the extended dynamics is Markovian by construction, the reduced dynamics of the central system is generally non-Markovian.

In the limit of a large number of lead modes, we have seen that the two definitions of entropy production rate, σ_{Spohn} and σ_{SL}, become equivalent for the full system. The question we now address is how this global entropy production relates to that of the reduced system, defined as $\sigma_S(t)$, with $\hat{\rho}_S(t) = \text{Tr}_L[\hat{\rho}_{SL}(t)]$.

As discussed in Section 5.4 of Chapter 5, the internal particle and energy currents are defined as

$$\begin{aligned} J^E(t) &= i\langle[\hat{H}_L, \hat{H}_{SL}]\rangle + \text{Tr}[\hat{H}_{SL}\,\mathcal{D}(\hat{\rho}_{SL})], \\ J^P(t) &= i\langle[\hat{N}_L, \hat{H}_{SL}]\rangle, \end{aligned} \tag{6.27}$$

where $\mathcal{D}(\cdot)$ is the dissipator acting on the lead modes. These currents define the heat flow as

$$J^Q(t) = J^E(t) - \mu J^P(t) \tag{6.28}$$

The entropy production rate at the system level is then given by

$$\sigma_S(t) = \dot{S}_S(t) - \beta J^Q(t), \tag{6.29}$$

where $S_S(t)$ is the von Neumann entropy of the reduced system state $\hat{\rho}_S(t) = \text{Tr}_L[\hat{\rho}_{SL}(t)]$.

In the single bath case, both $\sigma_S(t)$ and $\sigma_{SL}(t)$ vanish in the steady state. However, they may differ in the transient regime. This is expected: information is thrown away when tracing out the lead, which should be reflected in the entropy production rate. In particular, while $\sigma_{SL}(t) \geq 0$ by construction, $\sigma_S(t)$ can become negative due to the non-Markovianity of the reduced dynamics.

To analyze this difference, we introduce the integrated entropy productions

$$\Sigma_S(t) = \int_0^t \mathrm{d}t'\, \sigma_S(t'), \quad \Sigma_{SL}(t) = \int_0^t \mathrm{d}t'\, \sigma_{SL}(t'). \tag{6.30}$$

Subtracting the definitions of $\sigma_S(t)$ and $\sigma_{SL}(t)$, we find

$$\Sigma_S(t) - \Sigma_{SL}(t) = \int_0^t \mathrm{d}t' \left[(\dot{S}_S - \dot{S}_{SL}) - \beta\{(J^E - I^E) + \mu(J^P - I^P)\}\right] \tag{6.31}$$

We now evaluate the three terms in this expression. First, consider the difference in entropy production rates. Since system and lead are initially uncorrelated, the initial entropy is additive, $S_{SL}(0) = S_L(0) + S_S(0)$. We can then write

$$\begin{aligned}\int_0^t \mathrm{d}t' \, (\dot{S}_S - \dot{S}_{SL}) &= S_S(t) - S_S(0) - S_{SL}(t) + S_{SL}(0) \\ &= S_S(t) - S_{SL}(t) + S_L(0).\end{aligned} \tag{6.32}$$

Adding and subtracting $S_L(t)$, we obtain

$$\int_0^t \mathrm{d}t' \, (\dot{S}_S - \dot{S}_{SL}) = I_{SL}(t) - \Delta S_L, \tag{6.33}$$

where $I_{SL}(t) = S_S(t) + S_L(t) - S_{SL}(t)$ is the mutual information between system and lead and $\Delta S_L = S_L(t) - S_L(0)$ is the change in the entropy of the lead. Next, consider the particle current terms. From the master equation, we find

$$\begin{aligned}\int_0^t \mathrm{d}t' \, (I^P - J^P) &= \int_0^t \mathrm{d}t' \left(\mathrm{Tr}[\hat{N}_L \mathcal{D}(\hat{\rho})] + i\langle [\hat{H}, \hat{N}_L] \rangle \right) \\ &= \int_0^t \mathrm{d}t' \, \partial_{t'} \langle \hat{N}_L \rangle \\ &= \Delta N_L\end{aligned} \tag{6.34}$$

where $\Delta N_L = \langle \hat{N}_L \rangle_t - \langle \hat{N}_L \rangle_0$. A similar argument holds for the energy current difference,

$$\int_0^t \mathrm{d}t' \, (I^E - J^E) = \int_0^t \mathrm{d}t' \partial_{t'} \langle \hat{H}_L \rangle = \Delta E_L, \tag{6.35}$$

where $\Delta E_L = \langle \hat{H}_L \rangle_t - \langle \hat{H}_L \rangle_0$. Bringing everything together, we obtain an expression for the difference in the entropy production of the central and extended systems,

$$\Sigma_S(t) - \Sigma_{SL}(t) = \beta \Delta F_L + I_{SL}(t) \tag{6.36}$$

where $\Delta F_L = F_L(t) - F_L(0)$ is the change in the non-equilibrium free energy of the lead, which is defined as

$$F_L(t) = \langle \hat{H}_L \rangle_t - \mu \langle \hat{N}_L \rangle_t - T S_L(t) \tag{6.37}$$

This expression reveals that the difference between system-level and extended entropy production comes from two contributions: the change in the lead's nonequilibrium free energy and the correlations built up between system and lead. Both terms are non-negative. Moreover, since the initial state of the lead is thermal, its free energy cannot decrease. Indeed, as we show in Section 3.6.2, the change in free energy can be written as a relative entropy [170]:

$$\Delta F_L = \frac{1}{\beta} D\left(\hat{\rho}_L \,\middle\|\, \frac{e^{-\beta(\hat{H}_L - \mu \hat{N}_L)}}{Z_L} \right) \geq 0, \tag{6.38}$$

where we used the fact that $F_L(0) = -T \log Z_L$.

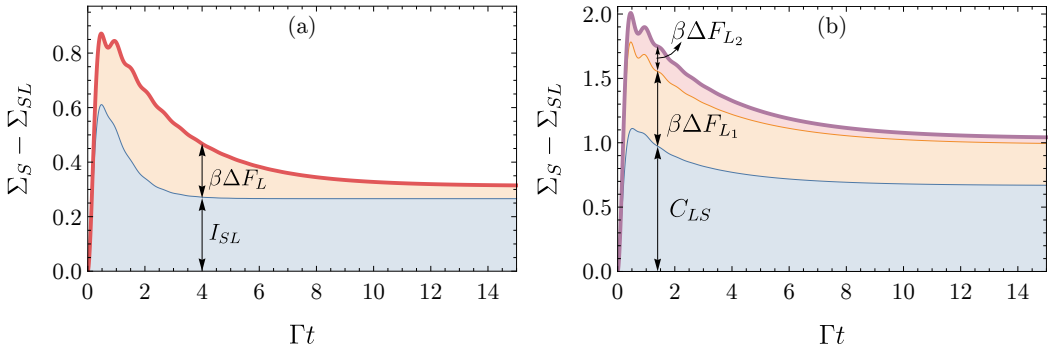

Figure 6.5: Difference between system-level and extended entropy production, $\Sigma_S(t) - \Sigma_{SL}(t)$, for a resonant-level model with $N = 1$, illustrating the contributions from correlations and lead free energy. (a) Single-bath setup with flat spectral density, showing the decomposition into mutual information I_{SL} and nonequilibrium free energy $\beta\Delta F_L$; (b) Two-bath configuration with leads at different temperatures $T_1 = 0.5\epsilon$ and $T_2 = \epsilon$, showing the total correlation term $C_{LS}(t)$ and the contributions $\beta\Delta F_1$, $\beta\Delta F_2$ from each lead. In both panels, shaded regions represent the terms on the right-hand side of Eq. (6.36) and Eq. (6.55), respectively. Parameters: $\Gamma = \epsilon$, $\mu = 0$, $L = 100$, $W = 10\epsilon$, and time step $\Delta t = 0.01$.

Therefore, we conclude that

$$\Sigma_S(t) \geq \Sigma_{SL}(t). \tag{6.39}$$

This inequality holds regardless of whether the system is interacting or not. It expresses the fact that focusing on the central system (i.e. tracing out the lead) represents a kind of coarse-graining, under which the entropy production can only increase [171].

We can also identify two conditions which together suffice to ensure that $\Sigma_S(t) \approx \Sigma_{SL}(t)$ in the steady-state: (i) the lead returns to its initial state, i.e., $\Delta F_L \approx 0$; (ii) the correlations between system and lead are negligible, i.e., $I_{SL} \approx 0$.

This result is illustrated in Fig. 6.5(a), which shows a numerical evaluation of both sides of Eq. (6.36) for the resonant-level model ($N = 1$). We observe excellent agreement between the left- and right-hand sides of the equation, with the mutual information I_{SL} contributing the dominant share of the difference. This reflects the significant system-lead correlations that arise due to the strong coupling between them.

6.4.2 Entropic differences with multiple baths

We now extend the analysis to the case where the central system is coupled to K distinct baths. In the mesoscopic leads framework, each reservoir is modeled by an independent damped lead. The joint state of the system and all leads is denoted by $\hat{\rho}_{SL}$, and its dynamics is governed by a Lindblad equation of the form

$$\frac{\mathrm{d}\hat{\rho}_{SL}}{\mathrm{d}t} = -i[\hat{H}, \hat{\rho}_{SL}] + \sum_{\alpha=1}^{K} \mathcal{D}_\alpha(\hat{\rho}_{SL}), \tag{6.40}$$

where $\mathcal{D}_\alpha$ is the dissipator associated with lead α.

The internal energy and particle currents from each lead α into the system are defined as

$$\begin{aligned} J_\alpha^E(t) &= i\langle[\hat{H}_{L_\alpha}, \hat{H}_{SL_\alpha}]\rangle + \mathrm{Tr}\big[\hat{H}_{SL_\alpha}\,\mathcal{D}_\alpha(\hat{\rho}_{SL})\big], \\ J_\alpha^P(t) &= i\langle[\hat{N}_{L_\alpha}, \hat{H}_{SL_\alpha}]\rangle, \end{aligned} \tag{6.41}$$

where $\hat{H}_{SL_\alpha}$ is the interaction between system and lead α, and $\hat{H}_{L_\alpha}$, $\hat{N}_{L_\alpha}$ are the lead's Hamiltonian and number operator, respectively.

The entropy production rate at the system level is then

$$\sigma_S(t) = \dot{S}_S(t) - \sum_{\alpha=1}^{K} \beta_\alpha J_\alpha^Q(t), \tag{6.42}$$

where $J_\alpha^Q(t) = J_\alpha^E(t) - \mu_\alpha J_\alpha^P(t)$ is the internal heat current associated with lead α.

To define the entropy production at the level of the extended system, the relevant currents are the external ones:

$$\begin{aligned} I_\alpha^E(t) &= \mathrm{Tr}\big[\hat{H}\,\mathcal{D}_\alpha(\hat{\rho}_{SL})\big], \\ I_\alpha^P(t) &= \mathrm{Tr}\big[\hat{N}\,\mathcal{D}_\alpha(\hat{\rho}_{SL})\big]. \end{aligned} \tag{6.43}$$

leading to external heat currents $I_\alpha^Q(t) = I_\alpha^E(t) - \mu_\alpha I_\alpha^P(t)$. The corresponding entropy production rate for the extended system is

$$\sigma_{SL}(t) = \frac{\mathrm{d}S_{SL}(t)}{\mathrm{d}t} - \sum_{\alpha=1}^{K} \beta_\alpha I_\alpha^Q(t). \tag{6.44}$$

The non-negativity of $\sigma_{SL}(t)$ follows from the generalization of Spohn's inequality to multi-terminal setups [172], which we discussed in Section 3.6.2. Let $\hat{\rho}_\alpha$ denote the steady state for that lead acting in isolation, i.e.

$$\mathcal{L}_\alpha(\hat{\rho}_\alpha) \equiv -i[\hat{H}, \hat{\rho}_\alpha] + \mathcal{D}_\alpha(\hat{\rho}_\alpha) = 0, \tag{6.45}$$

where $\mathcal{L}_\alpha(\cdot) = -i[\hat{H}, \cdot] + \mathcal{D}_\alpha(\cdot)$ is the partial generator associated with bath α. The contractivity of the relative entropy implies

$$\mathrm{Tr}[\mathcal{L}_\alpha(\hat{\rho}_{SL})(\log\hat{\rho}_\alpha - \log\hat{\rho}_{SL})] \geq 0. \tag{6.46}$$

Assuming $\hat{\rho}_\alpha \propto \exp[-\beta_\alpha(\hat{H} - \mu_\alpha\hat{N})]$ is a thermal state, σ_{SL} can be rewritten as

$$\sigma_{SL}(t) = \sum_{\alpha=1}^{K} \mathrm{Tr}[\mathcal{L}_\alpha(\hat{\rho}_{SL})(\log\hat{\rho}_\alpha - \log\hat{\rho}_{SL})] \geq 0. \tag{6.47}$$

See Section 3.6.2 of Chapter 3 for details.

We now derive an explicit expression for the difference between the integrated entropy productions Σ_S and Σ_{SL}. Subtracting the two definitions yields

$$\Sigma_S(t) - \Sigma_{SL}(t) = \int_0^t \mathrm{d}t'(\dot{S}_S(t') - \dot{S}_{SL}(t')) - \sum_{\alpha=1}^{K}\int_0^t \mathrm{d}t'\,\beta_\alpha(J_\alpha^Q(t') - I_\alpha^Q(t')). \tag{6.48}$$

We begin by evaluating the current differences. The heat current term decomposes as

$$\begin{aligned}\int_0^t \mathrm{d}t' \left[J_\alpha^Q(t') - I_\alpha^Q(t')\right] &= \int_0^t \mathrm{d}t' \left[J_\alpha^E(t') - I_\alpha^E(t') - \mu_\alpha (J_\alpha^P(t') - I_\alpha^P(t'))\right] \\ &= -\Delta E_\alpha + \mu_\alpha \Delta N_\alpha,\end{aligned} \tag{6.49}$$

where $\Delta E_\alpha = \langle \hat{H}_{L_\alpha} \rangle_t - \langle \hat{H}_{L_\alpha} \rangle_0$ and $\Delta N_\alpha = \langle \hat{N}_{L_\alpha} \rangle_t - \langle \hat{N}_{L_\alpha} \rangle_0$. These relations follow from particle and energy conservation, and mirror the arguments given for the single-bath case.

Next, we compute the entropy difference term. Since the system and leads are initially uncorrelated, the total initial entropy is additive:

$$S_{SL}(0) = S_S(0) + \sum_{\alpha=1}^{K} S_{L_\alpha}(0). \tag{6.50}$$

It follows that

$$\begin{aligned}\int_0^t \mathrm{d}t' (\dot{S}_S(t') - \dot{S}_{SL}(t')) &= S_S(t) - S_S(0) - (S_{SL}(t) - S_{SL}(0)) \\ &= S_S(t) - S_{SL}(t) + S_{SL}(0) - S_S(0) \\ &= S_S(t) - S_{SL}(t) + \sum_{\alpha=1}^{K} S_{L_\alpha}(0),\end{aligned} \tag{6.51}$$

Adding and subtracting $\sum_\alpha S_{L_\alpha}(t)$, we obtain

$$\int_0^t \mathrm{d}t' (\dot{S}_S(t') - \dot{S}_{SL}(t')) = \sum_{\alpha=1}^{K} (S_{L_\alpha}(t) - S_{L_\alpha}(0)) + S_S(t) + \sum_{\alpha=1}^{K} S_{L_\alpha}(t) - S_{SL}(t) \tag{6.52}$$

$$= \sum_{\alpha=1}^{K} \Delta S_{L_\alpha} - C_{LS}(t), \tag{6.53}$$

where $\Delta S_{L_\alpha} = S_{L_\alpha}(t) - S_{L_\alpha}(0)$, and

$$C_{LS}(t) = S_S(t) + \sum_{\alpha=1}^{K} S_{L_\alpha}(t) - S_{SL}(t) \tag{6.54}$$

denotes the total correlation between the system and all the leads. Combining everything, we find

$$\Sigma_S(t) - \Sigma_{SL}(t) = \sum_{\alpha=1}^{K} \beta_\alpha \Delta F_{L_\alpha} + C_{LS}(t), \tag{6.55}$$

where ΔF_{L_α} is the change in nonequilibrium free energy of lead α, defined as

$$\Delta F_{L_\alpha} = \Delta E_\alpha - \mu_\alpha \Delta N_\alpha - T_\alpha \Delta S_{L_\alpha}. \tag{6.56}$$

This generalizes Eq. (6.36) to the multi-terminal case. As in the single-bath scenario, the coarse-grained entropy production is always greater than or equal to that of the full system:

$$\Sigma_S(t) \geq \Sigma_{SL}(t), \tag{6.57}$$

with equality achieved when both the leads return to their initial equilibrium state ($\Delta F_{L_\alpha} \approx 0$) and correlations vanish ($C_{LS} \approx 0$).

To illustrate this, we consider the resonant level model connected to two leads at different temperatures. Figure 6.5 (b) shows a numerical evaluation of both sides of Eq. (6.55). As in the single-bath case (cf. Fig. 6.5(a)), the largest contribution to the difference comes from correlations. Importantly, the difference between $\Sigma_S(t)$ and $\Sigma_{SL}(t)$ saturates in the steady state, while both entropy productions grow linearly in time. Hence, either formulation provides a consistent thermodynamic description in the long-time limit.

Part IV

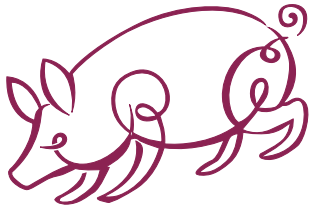

Information Geometry

7 Information Geometry in Thermodynamics

Information geometry provides a powerful mathematical framework for studying families of probability distributions using tools from differential geometry. In this approach, probability distributions are treated as points on a manifold endowed with a Riemannian metric derived from the Fisher information. This geometric structure allows one to quantify statistical distinguishability, define geodesics, and analyze curvature from an information-theoretic perspective. The Fisher information plays a central role in classical estimation theory, where it determines the precision limits of unbiased estimators through the Cramér–Rao [173, 174]. In the quantum domain, it forms the backbone of quantum metrology, where it sets fundamental limits on parameter estimation under constraints imposed by quantum mechanics [175, 176].

Beyond statistics and metrology, the geometric perspective offered by Fisher information has proven remarkably fruitful in thermodynamics. When thermodynamic states are interpreted as probability distributions (or density matrices), the Fisher metric acquires thermodynamic significance: it quantifies the distinguishability between nearby equilibrium states and encodes the system's linear response to external driving. Many thermodynamic quantities—such as work and entropy production—can be interpreted geometrically, and bounds on irreversibility often take the form of geometric inequalities involving distances or actions on the space of control parameters [177, 54, 55]. This geometric approach unifies diverse results in nonequilibrium thermodynamics and provides a powerful toolset for identifying optimal driving protocols, particularly in the slow-driving or near-equilibrium regime.

The aim of this chapter is to develop the foundations of information geometry and explore its applications in thermodynamics, with particular emphasis on quantum systems. In the first part, we introduce the Fisher information as a Riemannian metric on the space of probability distributions. Then, we extend this framework to quantum states. Unlike the classical case, the quantum Fisher information is not unique; the noncommutativity of quantum states leads to a family of monotone Riemannian metrics classified by operator monotone functions [178]. We examine several important choices—including the symmetric logarithmic derivative (SLD) and the Kubo–Mori–Bogoliubov (KMB) metrics—and highlight their operational roles in quantum thermodynamics.

The second part of the chapter focuses on the concept of *thermodynamic length*, which arises by integrating the Fisher metric along a path in parameter space. We trace the historical development of this idea, beginning with the work of Weinhold and Ruppeiner on thermodynamic metrics [179, 180], and continuing through its information-geometric reformulation by Crooks [54]. We conclude with the recent quantum generalization of thermody-

namic length for open quantum systems evolving under Lindblad dynamics [59], where the KMB metric plays a central role.

This chapter is structured as follows. Section 7.1 introduces the classical Fisher information and its interpretation as a Riemannian metric on the space of probability distributions. Section 7.2 extends this framework to quantum systems, highlighting the ambiguities introduced by noncommutativity and the resulting family of monotone Riemannian metrics. Section 7.4 presents a historical overview of thermodynamic geometry, tracing the development of thermodynamic length and its connection to dissipation in both classical and quantum regimes. Finally, Section 7.4.6 summarizes the main insights and prepares the ground for the next chapter, where we study the geometry of transitions between nonequilibrium steady states.

◆

7.1 Classical Fisher Information

In this section, we review the concept of classical Fisher information, which quantifies the sensitivity of probability distributions to changes in external parameters. We then show how this quantity gives rise to a natural geometric structure on the space of probability distributions.

7.1.1 Single Parameter Case

Consider a parametric family of probability distributions $p(x|\theta)$, where $\theta \in \mathbb{R}$ is a real parameter. When θ is varied, the probability distribution changes accordingly. A natural way to measure the sensitivity of the distribution with respect to θ is through the *score function*, defined as

$$\ell(x,\theta) = \frac{\partial}{\partial\theta} \log p(x|\theta).^{1} \tag{7.1}$$

From the chain rule, it follows that the score function can also be written as

$$\ell(x,\theta) = \frac{1}{p(x|\theta)} \frac{\partial p(x|\theta)}{\partial\theta}. \tag{7.2}$$

The score function measures the rate of change of the log-likelihood at a given point x. To quantify the global sensitivity of the distribution, one might consider taking the expectation value of $\ell(x,\theta)$ with respect to $p(x|\theta)$. However, a direct calculation shows that this quantity vanishes:

$$\begin{aligned} \langle \ell(x,\theta) \rangle &= \int \mathrm{d}x\, p(x|\theta)\ell(x,\theta) \\ &= \frac{\partial}{\partial\theta}\left(\int \mathrm{d}x\, p(x|\theta) \right) \\ &= 0 \end{aligned} \tag{7.3}$$

[1] Physically, the score function measures the relative change of $p(x|\theta)$ under an infinitesimal variation of θ, as $(p(x|\theta+\mathrm{d}\theta) - p(x|\theta))/p(x|\theta) \approx \ell(x,\theta)\mathrm{d}\theta$ for small $\mathrm{d}\theta$.

where $\langle\cdot\rangle$ denotes the expectation value with respect to $p(x|\theta)$, and we used that $\int \mathrm{d}x\, p(x|\theta) = 1$.

Since the mean of the score function vanishes, a more informative quantity to consider is its variance, which defines the *Fisher information*:

$$\mathcal{J}(\theta) = \langle \ell(x,\theta)^2 \rangle = \int \mathrm{d}x\, p(x|\theta) \left(\frac{\partial \log p(x|\theta)}{\partial \theta} \right)^2. \tag{7.4}$$

The Fisher information plays a central role in statistical inference: it sets a lower bound on the variance of any unbiased estimator of θ via the celebrated Cramér-Rao inequality, thereby quantifying the fundamental limits of precision in estimation tasks [174, 173]. More intuitively, Fisher information measures the amount of information that the random variable x carries about the parameter θ. When the Fisher information is large, small changes in θ induce significant, distinguishable changes in the probability distribution $p(x|\theta)$, enabling more precise estimation of the underlying parameter.

Beyond its interpretation in estimation theory, the Fisher information also introduces a natural geometric structure on the space of probability distributions. Specifically, it defines a Riemannian metric on the manifold of probability densities parametrized by θ, allowing one to measure infinitesimal distances between infinitesimally close distributions [181, 173, 182]. This geometric viewpoint will prove particularly powerful when we later extend these ideas to quantum systems.

To make the connection with geometry more precise, we observe that the Fisher information can be expressed as the squared norm of the score function under a weighted inner product. Specifically, given two functions $f(x)$ and $g(x)$ of the random variable x, we define their weighted inner product with respect to $p(x|\theta)$ as

$$\langle f, g \rangle_p = \int \mathrm{d}x\, p(x|\theta) f(x) g(x), \tag{7.5}$$

so that

$$\mathcal{J}(\theta) = \langle \ell(x,\theta), \ell(x,\theta) \rangle_p. \tag{7.6}$$

This formulation highlights how the Fisher information captures the "length" of the score function, thereby setting the stage for its geometric interpretation.

7.1.2 Classical Fisher Information from the Relative Entropy

Another fundamental connection between Fisher information and geometry emerges through the local expansion of the relative entropy between nearby distributions. Given a parametric family $p(x|\theta)$, the relative entropy between $p(x|\theta)$ and $p(x|\theta+\epsilon)$ is defined as

$$D_{\mathrm{KL}}(p(x|\theta) \,\|\, p(x|\theta+\epsilon)) = \int \mathrm{d}x\, p(x|\theta) \log \frac{p(x|\theta)}{p(x|\theta+\epsilon)}. \tag{7.7}$$

Expanding $\log p(x|\theta+\epsilon)$ around θ to second order, we find

$$\log p(x|\theta+\epsilon) = \log p(x|\theta) + \epsilon \frac{\partial}{\partial\theta} \log p(x|\theta) + \frac{1}{2}\epsilon^2 \frac{\partial^2}{\partial\theta^2} \log p(x|\theta) + \mathcal{O}(\epsilon^3). \tag{7.8}$$

Substituting this into the definition of D_{KL} and keeping terms up to second order, we obtain

$$\begin{aligned} D_{\mathrm{KL}}(p(x|\theta) \,\|\, p(x|\theta+\epsilon)) &= -\epsilon \int \mathrm{d}x\, p(x|\theta) \frac{\partial}{\partial\theta} \log p(x|\theta) \\ &\quad - \frac{1}{2}\epsilon^2 \int \mathrm{d}x\, p(x|\theta) \frac{\partial^2}{\partial\theta^2} \log p(x|\theta) + \mathcal{O}(\epsilon^3) \\ &= -\epsilon \langle \ell(x,\theta) \rangle - \frac{1}{2}\epsilon^2 \left\langle \frac{\partial^2}{\partial\theta^2} \log p(x|\theta) \right\rangle + \mathcal{O}(\epsilon^3). \end{aligned} \tag{7.9}$$

The first term vanishes because $\langle \ell(x,\theta) \rangle = 0$. To evaluate the second term, we use the identity

$$\frac{\partial^2}{\partial\theta^2} \log p(x|\theta) = \frac{1}{p(x|\theta)} \frac{\partial^2}{\partial\theta^2} p(x|\theta) - \left(\frac{\partial \log p(x|\theta)}{\partial\theta} \right)^2, \tag{7.10}$$

which follows from applying the chain rule to $\log p(x|\theta)$. Taking the expectation of both sides, we obtain

$$\begin{aligned} \left\langle \frac{\partial^2}{\partial\theta^2} \log p(x|\theta) \right\rangle &= \frac{\partial^2}{\partial\theta^2} \int \mathrm{d}x\, p(x|\theta) - \int \mathrm{d}x\, p(x|\theta) \left(\frac{\partial \log p(x|\theta)}{\partial\theta} \right)^2 \\ &= -\mathcal{I}(\theta), \end{aligned} \tag{7.11}$$

where the first term vanishes due to normalization of the probability distribution. Using this expression in Eq. (7.9) we obtain,

$$D_{\mathrm{KL}}(p(x|\theta) \,\|\, p(x|\theta+\epsilon)) = \frac{1}{2}\epsilon^2\, \mathcal{I}(\theta) + \mathcal{O}(\epsilon^3). \tag{7.12}$$

This result shows that, to leading order, the Fisher information quantifies the infinitesimal divergence between neighboring probability distributions. The second-order expansion of the relative entropy thereby defines a Riemannian metric structure on the statistical manifold, with $\mathcal{I}(\theta)$ playing the role of the metric tensor in parameter space. For the single-parameter family, the infinitesimal squared distance between distributions is given by

$$\mathrm{d}s^2 = \mathcal{I}(\theta)(\mathrm{d}\theta)^2. \tag{7.13}$$

This metric quantifies the local distinguishability of nearby distributions in parameter space.

As a consequence of the second-order expansion, we find that the KL divergence becomes locally symmetric. Although the KL divergence is not symmetric in general (i.e., $D_{\mathrm{KL}}(p\|q) \neq D_{\mathrm{KL}}(q\|p)$), this asymmetry appears only at third order when $p(x|\theta)$ and $p(x|\theta+\epsilon)$ are infinitesimally close. Indeed, reparametrizing $\theta' = \theta + \epsilon$ shows that

$$D_{\mathrm{KL}}(p(x|\theta+\epsilon) \,\|\, p(x|\theta)) = \frac{1}{2}\epsilon^2 \mathcal{I}(\theta) + \mathcal{O}(\epsilon^3), \tag{7.14}$$

where we used that $\mathcal{I}(\theta+\epsilon) = \mathcal{I}(\theta) + \mathcal{O}(\epsilon)$. This local symmetry validates the use of the second-order expansion of the KL divergence as a Riemannian metric.

7.1.3 Multiparameter Generalization

We now generalize to the case where $\boldsymbol{\theta} = (\theta^1, \theta^2, \dots, \theta^n) \in \mathbb{R}^n$ is a vector of real parameters. For each parameter component, we define the corresponding logarithmic derivative (or score function) as

$$\ell_i(x, \boldsymbol{\theta}) = \frac{\partial}{\partial \theta^i} \log p(x|\boldsymbol{\theta}), \quad i = 1, \dots, n. \tag{7.15}$$

Each $\ell_i(x, \boldsymbol{\theta})$ is a random variable depending on x.

The *Fisher information matrix* is then defined as the covariance matrix of the logarithmic derivatives [174, 181]:

$$g_{ij}(\boldsymbol{\theta}) = \big\langle \ell_i(x, \boldsymbol{\theta}), \ell_j(x, \boldsymbol{\theta}) \big\rangle_p = \int \mathrm{d}x\, p(x|\boldsymbol{\theta})\, \ell_i(x, \boldsymbol{\theta})\, \ell_j(x, \boldsymbol{\theta}). \tag{7.16}$$

As a covariance matrix, $g_{ij}(\boldsymbol{\theta})$ is symmetric and positive semi-definite by construction.

In analogy with the single-parameter case, the Fisher information matrix defines a Riemannian metric on the parameter space. The infinitesimal squared distance $\mathrm{d}s^2$ between two nearby distributions $p(x|\boldsymbol{\theta})$ and $p(x|\boldsymbol{\theta} + \mathrm{d}\boldsymbol{\theta})$ is given by

$$\mathrm{d}s^2 = g_{ij}(\boldsymbol{\theta})\, \mathrm{d}\theta^i \mathrm{d}\theta^j. \tag{7.17}$$

Thus, the parameter space is endowed with a natural geometric structure where the Fisher information matrix plays the role of the metric tensor.

The Fisher information matrix provides a natural metric that quantifies the distinguishability of nearby probability distributions. However, in quantum systems, the objects of interest are density operators rather than classical distributions, and observables do not necessarily commute. In the next section, we extend this geometric framework to the quantum domain, making the necessary modifications to account for the noncommutative structure.

7.2 Quantum Fisher Information

In this section, we extend the notion of Fisher information to the quantum setting. This requires generalizing two key ingredients: the classical score function, which is replaced by a *logarithmic derivative* operator, and the classical weighted inner product, which must be adapted to incorporate the density matrix.

In the quantum setting, we replace the probability distribution by a smooth family of density matrices $\{\hat{\rho}_\theta\}$ parametrized by $\theta \in \mathbb{R}$. Expectation values of observables $\hat{A}$ are then given by $\langle A \rangle_\theta = \mathrm{Tr}[\hat{\rho}_\theta \hat{A}]$.

The direct analog of the classical score function $\ell(x, \theta)$ is the operator $\partial_\theta \log \hat{\rho}_\theta$. As long as $\hat{\rho}_\theta$ is full rank, this quantity is well-defined and unique. However, our primary objective is not to generalize $\ell(x, \theta)$ itself, but rather its *operational properties* that tie the Fisher information to an underlying geometric structure.

To motivate this approach, let us first recall the key operational properties of the classical score function. In particular, it satisfies the identity

$$\partial_\theta p(x|\theta) = p(x|\theta) \ell(x, \theta). \tag{7.18}$$

Given a smooth test function $f(x)$, multiplying both sides by $f(x)$ and integrating yields

$$\langle f, \ell \rangle_p = \int \mathrm{d}x \, f(x) \, \partial_\theta p(x|\theta), \tag{7.19}$$

which we can write compactly as

$$\langle f, \ell \rangle_p = \partial_\theta \langle f \rangle_p, \tag{7.20}$$

where $\langle \cdot, \cdot \rangle_p$ denotes the p-weighted inner product defined previously, and $\langle f \rangle_p$ the expectation value of f under $p(x|\theta)$.[2]

Thus, the score function plays a central operational role: it governs how expectation values of observables change under infinitesimal variations of the underlying parameter.

To preserve this operational structure in the quantum setting, we seek an operator $\hat{L}_\theta$, referred to as a *quantum logarithmic derivative*, such that, for all observables $\hat{A}$,

$$\partial_\theta \langle \hat{A} \rangle_\theta = \langle \hat{A}, \hat{L}_\theta \rangle_{\hat{\rho}}, \tag{7.21}$$

where $\langle \cdot, \cdot \rangle_{\hat{\rho}}$ denotes a generalized inner product weighted by $\hat{\rho}$, to be precisely defined below.

However, an important distinction from the classical case emerges. Although $\partial_\theta \hat{\rho}_\theta$ is well-defined, it generally does not commute with $\hat{\rho}_\theta$,

$$[\hat{\rho}_\theta, \partial_\theta \hat{\rho}_\theta] \neq 0, \tag{7.22}$$

which prevents a straightforward quantum analog of the classical relation $\partial_\theta p(x|\theta) = p(x|\theta)\ell(x, \theta)$, as the order of operator multiplication now matters.

The non-commutativity also complicates the choice of inner product. In the classical setting, there is only one natural choice for the p-weighted inner product $\langle \cdot, \cdot \rangle_p$, as it involves a product of real numbers. In the quantum case, however, there is no canonical way to "weight" an observable with the density matrix $\hat{\rho}_\theta$, since the order of operator multiplication becomes significant. For instance, one may consider different expressions such as

$$\mathrm{Tr}\big[\hat{A}^\dagger \hat{\rho}_\theta \hat{B}\big], \quad \mathrm{Tr}\big[\hat{A}^\dagger \hat{B} \hat{\rho}_\theta\big], \quad \text{or} \quad \mathrm{Tr}\big[\hat{A}^\dagger \hat{\rho}_\theta^s \hat{B} \hat{\rho}_\theta^{1-s}\big], \tag{7.23}$$

where $0 < s < 1$. These forms are generally distinct due to the non-commutativity of the operators involved.

To unify such expressions, we introduce a linear, positive map $\mathbb{J}_{\hat{\rho}}$ that generalizes the classical notion of weighting by $p(x|\theta)$:

$$\mathbb{J}_{\hat{\rho}}(\hat{B}) = \int_0^1 \mathrm{d}s \, \mu(s) \, \hat{\rho}^s \hat{B} \hat{\rho}^{1-s}, \tag{7.24}$$

[2] In functional-analytic terms, $\ell(x, \theta)$ is the Riesz representation of the linear functional $f \mapsto \int dx \, f(x) \, \partial_\theta p(x|\theta)$ on $L^2(p)$. Geometrically, it describes the infinitesimal deformation of the distribution as a vector in the same Hilbert space as the observables.

where $\mu(s)$ is a probability distribution on $[0,1]$. For example, setting $\mu(s) = \delta(s)$ yields $\mathbb{J}_{\hat{\rho}}(\hat{B}) = \hat{B}\hat{\rho}$, while a uniform distribution recovers the symmetrized form $\int_0^1 \mathrm{d}s\, \hat{\rho}^s \hat{B} \hat{\rho}^{1-s}$. Importantly, for any such choice of $\mu(s)$, the cyclic property of the trace ensures

$$\mathrm{Tr}\left[\mathbb{J}_{\hat{\rho}}(\hat{B})\right] = \mathrm{Tr}\left[\hat{\rho}\hat{B}\right], \tag{7.25}$$

preserving the interpretation of $\mathbb{J}_{\hat{\rho}}$ as a generalized quantum weighting operation.

Using this map, we define a $\hat{\rho}$-weighted inner product between operators $\hat{A}$ and $\hat{B}$ as

$$\langle \hat{A}, \hat{B} \rangle_{\hat{\rho}} = \mathrm{Tr}\left[\hat{A}^\dagger\, \mathbb{J}_{\hat{\rho}}(\hat{B})\right]. \tag{7.26}$$

This construction mirrors the classical p-weighted inner product, with the map $\mathbb{J}_{\hat{\rho}}$ encoding the choice of operator weighting.

We then define the quantum logarithmic derivative $\hat{L}_\theta$ implicitly through the relation

$$\partial_\theta \hat{\rho}_\theta = \mathbb{J}_{\hat{\rho}}(\hat{L}_\theta), \tag{7.27}$$

which generalizes the classical identity (7.18), supporting the interpretation of $\hat{L}_\theta$ as the quantum analog of the score function. Moreover, by the cyclic property of the trace, it immediately follows that

$$\mathrm{Tr}\left[\mathbb{J}_{\hat{\rho}}(\hat{L}_\theta)\right] = \mathrm{Tr}\left[\hat{\rho}_\theta \hat{L}_\theta\right] = \partial_\theta\, \mathrm{Tr}[\hat{\rho}_\theta] = 0, \tag{7.28}$$

in direct analogy with the classical property $\langle \ell(x,\theta) \rangle = 0$.

The quantum Fisher information associated with this choice of logarithmic derivative is defined by

$$\mathcal{I}(\theta) = \langle \hat{L}_\theta, \hat{L}_\theta \rangle_{\hat{\rho}} = \mathrm{Tr}\left[\hat{L}_\theta^\dagger \mathbb{J}_{\hat{\rho}}(\hat{L}_\theta)\right], \tag{7.29}$$

which extends the classical expression given in Eq. (7.6). Using Eq. (7.27), the Fisher information can also be expressed as

$$\mathcal{I}(\theta) = \mathrm{Tr}\left[\hat{L}_\theta^\dagger\, \partial_\theta \hat{\rho}_\theta\right], \tag{7.30}$$

mirroring the classical Fisher information as a measure of sensitivity to parameter changes.

Different choices for the map $\mathbb{J}_{\hat{\rho}}$ give rise to distinct generalizations of the classical Fisher information. For example, a simple choice is to define the *right logarithmic derivative* (RLD) via

$$\partial_\theta \hat{\rho}_\theta = \hat{\rho}_\theta \hat{L}_\theta^{(\mathrm{RLD})}, \tag{7.31}$$

which corresponds to the map

$$\mathbb{J}_{\hat{\rho}}^{(\mathrm{RLD})}(\hat{B}) = \hat{\rho}\hat{B}. \tag{7.32}$$

Similarly, one may define a *left logarithmic derivative* (LLD) through the choice $\mathbb{J}_{\hat{\rho}}(\hat{B}) = \hat{B}\hat{\rho}_\theta$.

A particularly important choice that is widely used in quantum metrology is the *symmetric logarithmic derivative* (SLD), in which the weighting is performed symmetrically on both sides:

$$\mathbb{J}_{\hat{\rho}}^{(\mathrm{SLD})}(\hat{B}) = \frac{1}{2}\big(\hat{B}\hat{\rho}_\theta + \hat{\rho}_\theta \hat{B}\big). \tag{7.33}$$

The associated operator $\hat{L}_\theta^{(\mathrm{SLD})}$ satisfies

$$\partial_\theta \hat{\rho}_\theta = \frac{1}{2}\{\hat{\rho}_\theta, \hat{L}_\theta^{(\mathrm{SLD})}\}, \tag{7.34}$$

where $\{\cdot,\cdot\}$ denotes the anticommutator. The corresponding Fisher information then takes a particularly simple form:

$$\mathcal{J}^{(\mathrm{SLD})}(\theta) = \mathrm{Tr}\big[\hat{\rho}_\theta (\hat{L}_\theta^{(\mathrm{SLD})})^2\big]. \tag{7.35}$$

Another prominent example, which arises naturally in quantum statistical mechanics, is the *Kubo–Mori–Bogoliubov* (KMB) Fisher information [183, 184]. It is defined through the KMB operator:

$$\mathbb{J}_{\hat{\rho}}^{(\mathrm{KMB})}(\hat{B}) = \int_0^1 \mathrm{d}s\, \hat{\rho}^s \hat{B} \hat{\rho}^{1-s}. \tag{7.36}$$

The corresponding logarithmic derivative operator $\hat{L}_\theta^{(\mathrm{KMB})}$ satisfies the integral identity

$$\partial_\theta \hat{\rho}_\theta = \int_0^1 \mathrm{d}s\, \hat{\rho}_\theta^s\, \hat{L}_\theta^{(\mathrm{KMB})}\, \hat{\rho}_\theta^{1-s}. \tag{7.37}$$

Notably, the KMB logarithmic derivative coincides with the natural quantum generalization of the classical score function $\ell(x,\theta)$ introduced in Eq. (7.1):

$$\hat{L}_\theta^{(\mathrm{KMB})} = \frac{\partial \log \hat{\rho}_\theta}{\partial \theta}. \tag{7.38}$$

Since $\hat{\rho}_\theta$ is Hermitian, this implies that $\hat{L}_\theta^{(\mathrm{KMB})}$ is also Hermitian.

This identity follows from a general formula for differentiating operator exponentials. Specifically, if $A(\theta)$ is a differentiable family of operators, then [185]

$$\frac{d}{d\theta} e^{A(\theta)} = \int_0^1 \mathrm{d}s\, e^{sA(\theta)} \frac{dA}{d\theta} e^{(1-s)A(\theta)}. \tag{7.39}$$

Applying this result to the identity $\hat{\rho}_\theta = e^{\log \hat{\rho}_\theta}$ yields

$$\partial_\theta \hat{\rho}_\theta = \int_0^1 \mathrm{d}s\, \hat{\rho}_\theta^s \frac{\partial \log \hat{\rho}_\theta}{\partial \theta} \hat{\rho}_\theta^{1-s}, \tag{7.40}$$

which precisely matches the integral definition of the KMB logarithmic derivative. In terms of the associated superoperator, this expression can be compactly written as

$$\partial_\theta \hat{\rho}_\theta = \mathbb{J}_{\hat{\rho}}^{(\mathrm{KMB})}\big(\hat{L}_\theta^{(\mathrm{KMB})}\big). \tag{7.41}$$

This connection helps to explain why the KMB logarithmic derivative arises naturally in quantum statistical mechanics. It frequently appears in the context of differentiating

thermal states of the form $\hat{\rho}_\theta \propto e^{-\beta \hat{H}(\theta)}$. Moreover, as will be discussed in the next section, the KMB Fisher information emerges naturally as the second-order term in the expansion of quantum relative entropy, further reinforcing its thermodynamic and information-theoretic significance.

7.3 Quantum Fisher Information from Relative Entropy

In this section, we show how KMB quantum Fisher information naturally arises from the second-order expansion of the relative entropy between nearby states. The proof closely mirrors the classical case.

The quantum relative entropy between two density matrices $\hat{\rho}_\theta$ and $\hat{\rho}_{\theta+\epsilon}$ is defined as

$$D(\hat{\rho}_\theta \,\|\, \hat{\rho}_{\theta+\epsilon}) = \mathrm{Tr}[\hat{\rho}_\theta(\log \hat{\rho}_\theta - \log \hat{\rho}_{\theta+\epsilon})]. \tag{7.42}$$

Expanding $\log \hat{\rho}_{\theta+\epsilon}$ to second order, we find

$$\log \hat{\rho}_{\theta+\epsilon} = \log \hat{\rho}_\theta + \epsilon \frac{\partial}{\partial \theta} \log \hat{\rho}_\theta + \frac{1}{2}\epsilon^2 \frac{\partial^2}{\partial \theta^2} \log \hat{\rho}_\theta + \mathcal{O}(\epsilon^3). \tag{7.43}$$

Substituting into the definition of the relative entropy and keeping terms up to second order, we find

$$D(\hat{\rho}_\theta \,\|\, \hat{\rho}_{\theta+\epsilon}) = -\epsilon \,\mathrm{Tr}\left[\hat{\rho}_\theta \hat{L}_\theta\right] - \frac{1}{2}\epsilon^2 \,\mathrm{Tr}\left[\hat{\rho}_\theta \frac{\partial^2 \log \hat{\rho}_\theta}{\partial \theta^2}\right] + \mathcal{O}(\epsilon^3). \tag{7.44}$$

The first term is zero, since $\langle \hat{L}_\theta \rangle = 0$. To evaluate the second term, we use the product rule to expand the second derivative:

$$\begin{aligned} \mathrm{Tr}\left[\hat{\rho}_\theta \frac{\partial^2 \log \hat{\rho}_\theta}{\partial \theta^2}\right] &= \frac{\partial}{\partial \theta} \mathrm{Tr}\left[\hat{\rho}_\theta \frac{\partial \log \hat{\rho}_\theta}{\partial \theta}\right] - \mathrm{Tr}\left[\frac{\partial \hat{\rho}_\theta}{\partial \theta} \frac{\partial \log \hat{\rho}_\theta}{\partial \theta}\right] \\ &= -\mathrm{Tr}\left[\frac{\partial \hat{\rho}_\theta}{\partial \theta} \hat{L}_\theta\right] \\ &= -\mathcal{J}(\theta) \end{aligned} \tag{7.45}$$

where we have used the identity $\mathcal{J}(\theta) = \mathrm{Tr}[\hat{L}_\theta^\dagger \, \partial_\theta \hat{\rho}_\theta]$. Substituting back into Eq. (7.44), we obtain

$$D(\hat{\rho}_\theta \,\|\, \hat{\rho}_{\theta+\epsilon}) = \frac{1}{2}\epsilon^2 \, \mathcal{J}(\theta) + \mathcal{O}(\epsilon^3). \tag{7.46}$$

This result shows that the KMB quantum Fisher information quantifies the local distinguishability of nearby quantum states. As in the classical case, the second-order expansion of the quantum relative entropy defines a Riemannian metric structure on the space of quantum states, with $\mathcal{J}(\theta)$ playing the role of the metric tensor. For single-parameter families, the infinitesimal squared distance is given by

$$\mathrm{d}s^2 = \mathcal{J}(\theta)(\mathrm{d}\theta)^2. \tag{7.47}$$

7.3.1 Multiparameter Generalization

We now extend the formalism to the case where $\boldsymbol{\theta} = (\theta^1, \theta^2, \dots, \theta^n) \in \mathbb{R}^n$ is a vector of real parameters. For each parameter component, we define the corresponding logarithmic derivative operator $\hat{L}_i$ via the relation

$$\partial_{\theta^i} \langle \hat{A} \rangle_{\boldsymbol{\theta}} = \langle \hat{A}, \hat{L}_i \rangle_{\hat{\rho}}, \tag{7.48}$$

for all observables $\hat{A}$, where $\langle \cdot, \cdot \rangle_{\hat{\rho}}$ denotes the generalized inner product associated with the choice of weighting map $\mathbb{J}_{\hat{\rho}}$.

The *quantum Fisher information matrix* is then defined as the covariance matrix of the logarithmic derivatives:

$$g_{ij}(\boldsymbol{\theta}) = \langle \hat{L}_i, \hat{L}_j \rangle_{\hat{\rho}}. \tag{7.49}$$

The matrix $g_{ij}(\boldsymbol{\theta})$ is Hermitian and positive semi-definite, reflecting the statistical distinguishability structure induced by the choice of inner product.

In analogy with the classical case, the quantum Fisher information matrix defines a Riemannian metric on the parameter space. The infinitesimal squared distance $\mathrm{d}s^2$ between two nearby quantum states $\hat{\rho}_{\boldsymbol{\theta}}$ and $\hat{\rho}_{\boldsymbol{\theta}+\mathrm{d}\boldsymbol{\theta}}$ is given by

$$\mathrm{d}s^2 = g_{ij}(\boldsymbol{\theta})\, d\theta^i d\theta^j. \tag{7.50}$$

Thus, the parameter space is endowed with a natural geometric structure, where the quantum Fisher information matrix plays the role of the metric tensor.

7.4 Historical Development of Thermodynamic Geometry

The idea of introducing geometric structures into thermodynamics has a long and rich history, motivated by the desire to quantify the distinguishability between macroscopic equilibrium states and the costs associated with finite-time transformations.

A summary of the major developments in the concept of thermodynamic length is provided in Table 7.1 at the end of this chapter, which may serve as a reference as we review the individual contributions in detail.

7.4.1 Weinhold: Geometric Structure from Thermodynamic Potentials (1975)

The first formal attempt to introduce a Riemannian geometric structure into thermodynamics was made by Weinhold [179]. Motivated by analogies with differential geometry and classical mechanics, Weinhold proposed equipping the thermodynamic state space with a metric structure derived from second derivatives of thermodynamic potentials.

In Weinhold's formulation, each equilibrium state is represented by a point in the space of extensive variables $(X^1, \dots, X^n)$, which serve as coordinates on the thermodynamic state manifold. These variables typically include quantities such as entropy, volume, and particle

number. A Riemannian metric on this manifold is then defined by taking the Hessian of the internal energy U:

$$g_{\mu\nu} = \frac{\partial^2 U}{\partial X^\mu \partial X^\nu}. \tag{7.51}$$

This construction endowed the thermodynamic state space with notions of distance and curvature. However, at this stage, the interpretation of the metric remained largely formal and lacked a clear physical or statistical interpretation. Weinhold's metric was not explicitly connected to statistical mechanics or fluctuations, and its operational meaning in thermodynamic processes was not yet clarified.

Nevertheless, this initial proposal laid the groundwork for later developments that provided physical content to thermodynamic geometry.

7.4.2 Ruppeiner: Metric from Fluctuation Theory (1979)

Building on Weinhold's geometric formulation, Ruppeiner [180] introduced a thermodynamic metric grounded in fluctuation theory and statistical mechanics. His approach begins with the entropy function S, expressed in terms of extensive variables X^i, and draws on Einstein's theory of thermodynamic fluctuations.

Near equilibrium, spontaneous fluctuations occur around a macrostate, and the probability of a fluctuation is given by

$$P \propto \exp(\Delta S), \tag{7.52}$$

where ΔS is the entropy difference relative to equilibrium. For small deviations δX^i, a second-order expansion yields

$$\Delta S \approx -\frac{1}{2} g_{ij}\, \delta X^i \delta X^j, \tag{7.53}$$

which corresponds to a Gaussian distribution over fluctuation space. The coefficients g_{ij} are defined as the negative Hessian of the entropy:

$$g_{ij} = -\frac{\partial^2 S}{\partial X^i \partial X^j}. \tag{7.54}$$

This matrix defines a Riemannian metric on the manifold of equilibrium states. The associated line element,

$$\mathrm{d}s^2 = g_{ij}\, \mathrm{d}X^i \mathrm{d}X^j, \tag{7.55}$$

measures the statistical distance between neighboring macrostates and quantifies the system's susceptibility to fluctuations.

Ruppeiner's metric encodes how sensitively entropy responds to changes in macroscopic variables, and thus reflects the underlying correlations in the system. It differs from Weinhold's in the choice of thermodynamic potential—entropy rather than internal energy—but the two are conformally related via temperature:

$$g^{\text{Ruppeiner}}_{\mu\nu} = \frac{1}{T} g^{\text{Weinhold}}_{\mu\nu}. \tag{7.56}$$

This formulation introduced a clear physical interpretation to thermodynamic geometry and laid the foundation for its application to diverse systems, including black holes [186, 187, 188, 189].

7.4.3 Salamon and Berry: Thermodynamic Length (1983)

Following the establishment of a geometric structure in thermodynamics, Salamon and Berry [177] introduced the concept of *thermodynamic length*. Their work shifted attention from static geometric structures to the dynamics of transformations between equilibrium states, particularly focusing on finite-time processes.

Thermodynamic length was defined as the integrated distance along a path according to the Weinhold metric:

$$\mathcal{L} = \int_\gamma \mathrm{d}\xi \sqrt{g_{\mu\nu} \frac{\mathrm{d}X^\mu}{\mathrm{d}\xi} \frac{\mathrm{d}X^\nu}{\mathrm{d}\xi}}, \tag{7.57}$$

where ξ parametrizes the trajectory γ through the space of extensive variables, and $g_{\mu\nu}$ is the metric tensor derived from the Hessian of internal energy.

It was demonstrated that, under near-equilibrium conditions and assuming linear response, thermodynamic length provides a lower bound on the dissipation incurred during a finite-time transformation. In particular, minimizing thermodynamic length corresponds to minimizing the *dissipated availability*, a quantity closely related to irreversible entropy production, when moving between states at a finite rate.

This insight connected geometric ideas directly to thermodynamic optimization, opening a new perspective on nonequilibrium thermodynamics in which geometric concepts such as distance and curvature influence the efficiency of real transformations.

7.4.4 Crooks: Thermodynamic Divergence and Information Geometry (2007)

A major conceptual advance in thermodynamic geometry came with its reformulation through information geometry, particularly in the work of Crooks [54]. By identifying thermodynamic length with the Fisher information metric, Crooks established a direct link between the geometry of equilibrium distributions and the energetic costs of driving a system through parameter space.

In Crooks' framework, a classical system is in contact with a thermal bath at inverse temperature β. The system is described by a time-dependent Hamiltonian of the form

$$\beta H(x, \lambda(t)) = \lambda_i(t) X^i(x), \tag{7.58}$$

where x denotes a microstate, $\lambda_i(t)$ are externally controlled parameters and $X^i(x)$ are the corresponding observables. Here, the factor of β is absorbed into λ_i, rendering the product $\lambda_i X^i$ dimensionless.

For fixed λ_i, the corresponding equilibrium distribution is given by

$$p(x|\lambda) = \frac{1}{Z(\lambda)} e^{-\lambda_i X^i(x)}. \tag{7.59}$$

This formulation moves the focus from the space of extensive variables to the manifold of control parameters λ, building on earlier work by Schlögl [190].

The metric is then constructed from the Massieu potential $\psi(\lambda) = \ln Z(\lambda)$, whose first derivatives yield expectation values of the observables: $\partial\psi/\partial\lambda_i = -\langle X_i\rangle$. The second derivatives generate the covariance matrix:

$$g_{ij}(\lambda) = \frac{\partial^2\psi}{\partial\lambda^i\partial\lambda^j} = \langle (X_i - \langle X_i\rangle)(X_j - \langle X_j\rangle)\rangle. \tag{7.60}$$

As highlighted by Crooks, this metric coincides with the Fisher information matrix for the family of equilibrium distributions:

$$g_{ij}(\lambda) = \int \mathrm{d}x\, p(x|\lambda) \frac{\partial \ln p(x|\lambda)}{\partial\lambda_i} \frac{\partial \ln p(x|\lambda)}{\partial\lambda_j}. \tag{7.61}$$

It quantifies the statistical distinguishability of nearby thermal states and is equivalent to the Fisher–Rao metric in information geometry.

Using this metric, the thermodynamic length of a path in parameter space is defined as

$$\mathcal{L} = \int_0^\tau \mathrm{d}t \sqrt{\frac{\mathrm{d}\lambda^i}{\mathrm{d}t}\, g_{ij}\, \frac{\mathrm{d}\lambda^j}{\mathrm{d}t}}, \tag{7.62}$$

where τ is the protocol time. Crooks also introduced the notion of *thermodynamic divergence*, which is given by the action of the metric along the path, scaled by τ:

$$\mathcal{J} = \tau \int_0^\tau \mathrm{d}t\, \frac{\mathrm{d}\lambda^i}{\mathrm{d}t}\, g_{ij}\, \frac{\mathrm{d}\lambda^j}{\mathrm{d}t}. \tag{7.63}$$

These quantities satisfy the inequality

$$\mathcal{J} \geq \mathcal{L}^2, \tag{7.64}$$

which follows from the Cauchy–Schwarz inequality $\int_0^\tau u^2\,\mathrm{d}t \int_0^\tau v^2\,\mathrm{d}t \geq (\int_0^\tau uv\,\mathrm{d}t)^2$ by taking $u = \sqrt{g_{ij}\dot\lambda^i\dot\lambda^j}$ and $v = 1$.

To assign operational meaning to these geometric quantities, Crooks proposed a discretized protocol that drives the system from $\lambda(0)$ to $\lambda(\tau)$ in a sequence of quenches. At each step, the control parameters are quenched from λ_t to λ_{t+1}, and the system is allowed to reequilibrate. Once the final state is reached, the protocol is reversed, returning to the initial configuration.

It is then shown that, in the continuum limit, the total entropy produced over the complete forward-reverse process—referred to as the *hysteresis*—converges to the thermodynamic divergence:

$$\Sigma \to \mathcal{J}. \tag{7.65}$$

Combining this with the inequality $\mathcal{J} \geq \mathcal{L}^2$ yields a geometric bound on total entropy production:

$$\Sigma \geq \mathcal{L}^2. \tag{7.66}$$

This result has a compelling interpretation: the irreversibility of a finite-time process, measured by entropy production, is bounded from below by a purely geometric quantity. This suggests that minimally dissipative protocols can be designed by minimizing thermodynamic length—that is, by identifying geodesics in the space of control parameters. This principle laid the foundation for later work by Sivak and Crooks [55], who related thermodynamic divergence to excess work in slowly driven processes.

The identification of thermodynamic length with the Fisher information metric has since influenced a wide range of developments in nonequilibrium thermodynamics, optimal control, and quantum thermodynamics. It offers a useful perspective for understanding energetic costs in systems undergoing nonequilibrium transformations.

7.4.5 Scandi and Perarnau-Llobet: Thermodynamic Length in Open Quantum Systems (2019)

Building on classical results, Scandi and Perarnau-Llobet [59] extended the concept of thermodynamic length to the quantum domain. They considered open quantum systems evolving under Lindblad dynamics and showed that, in a slow transition between thermal states, the dissipation can be expressed as the action of a Riemannian metric naturally related to the Kubo–Mori–Bogoliubov (KMB) quantum Fisher information.

More specifically, they considered a system with a time-dependent Hamiltonian $\hat{H}_t$ coupled to a reservoir at inverse temperature β, assuming the dynamics is governed by a Lindblad master equation,

$$\dot{\hat{\rho}}_t = \mathcal{L}_t \hat{\rho}_t. \tag{7.67}$$

If $\hat{H}_t$ is fixed, the system is assumed to relax to the instantaneous thermal state:

$$\hat{\omega}_\beta(\hat{H}_t) = \frac{e^{-\beta \hat{H}_t}}{\mathrm{Tr}[e^{-\beta \hat{H}_t}]}. \tag{7.68}$$

As in Crooks' framework, the Hamiltonian is taken to be a linear combination of control observables:

$$\hat{H}_t = \lambda^i(t) \hat{X}_i, \tag{7.69}$$

where $\lambda^i(t)$ are externally controlled parameters and $\hat{X}_i$ are system observables.

The total work extracted over a protocol γ is given by

$$W[\gamma] = -\int_\gamma dt\, \mathrm{Tr}\left[\hat{\rho}_t \dot{\hat{H}}_t\right]. \tag{7.70}$$

As they discuss, the total work can be split into two components: a reversible part, which depends only on the endpoints, and an irreversible part, which is path-dependent. The latter, referred to as *dissipative work*, is given by the integrated entropy production rate:

$$W_{\mathrm{diss}} = \int_\gamma \mathrm{d}t\, \sigma_t, \tag{7.71}$$

To obtain a geometric structure, the authors consider the slow-driving limit, expanding the state $\hat{\rho}_t$ perturbatively in powers of the driving speed and substituting into the expression

for W_{diss}. This yields a Riemannian metric on the space of control parameters, and the dissipative work takes the form of a quadratic action:

$$W_{\mathrm{diss}} = \beta \int_{\gamma} \mathrm{d}t\, \dot{\lambda}^i_t\, g_{ij}(\lambda)\, \dot{\lambda}^j_t. \tag{7.72}$$

The metric tensor is given by

$$g_{ij} = -\frac{1}{2}\,\mathrm{Tr}\Big[\hat{X}_i \mathcal{L}^{+}[\mathbb{J}_{\hat{\omega}_\beta}(\hat{X}_j)] + \hat{X}_j \mathcal{L}^{+}[\mathbb{J}_{\hat{\omega}_\beta}(\hat{X}_i)]\Big], \tag{7.73}$$

where $\mathcal{L}^{+}$ denotes the Drazin inverse of the Lindblad generator, and $\mathbb{J}_{\hat{\omega}_\beta}[\cdot]$ is the KMB operator introduced in Section 7.2.

We will return to this formalism in greater detail in Chapter 9, where it will be applied to transitions between nonequilibrium steady states. For now, we emphasize that this result provides a natural extension of thermodynamic length to the quantum regime.

7.4.6 Summary

In this chapter, we traced the development of information geometry in thermodynamics, from its origin as a formal metric on the space of extensive variables to its modern role in characterizing dissipation and irreversibility in finite-time processes. A central theme has been the reinterpretation of thermodynamic quantities—such as entropy production and work—as geometric path integrals over the space of control parameters. In the next chapter, we extend these ideas to nonequilibrium steady-state transitions.

Table 7.1 summarizes the key milestones in this conceptual evolution, highlighting how the notion of thermodynamic length has emerged and expanded over time.

Table 7.1: Historical development of the concept of thermodynamic length.

Year	Authors	Contribution
1975	Weinhold [179]	Introduced a Riemannian metric in thermodynamics via the Hessian of internal energy with respect to extensive variables.
1979 / 1995	Ruppeiner [180, 186]	Related the thermodynamic metric to fluctuation theory, connecting metric distance to statistical distinguishability between equilibrium states.
1983	Salamon and Berry [177]	Defined thermodynamic length along paths in thermodynamic space and linked it to dissipation in finite-time processes.
2007	Crooks [54]	Provided an information-theoretic foundation for thermodynamic length using relative entropy and Fisher information geometry; introduced thermodynamic divergence.
2012	Sivak and Crooks [55]	Demonstrated that excess work in near-equilibrium transformations is approximately proportional to thermodynamic divergence, giving it operational meaning.
2019	Scandi and Perarnau-Llobet [59]	Generalized thermodynamic length to open quantum systems described by Lindblad dynamics, using the Kubo–Mori–Bogoliubov metric.

8 Entropy production in nonequilibrium steady states

Entropy production is a fundamental quantity in nonequilibrium thermodynamics, capturing the irreversibility of physical processes and setting the direction of time's arrow. In the context of nonequilibrium steady states (NESS), where systems are continuously driven by external forces or boundary conditions, entropy production becomes a central object of study. While the total entropy production satisfies the second law in the form of a non-negative average, recent developments have emphasized that it can be usefully decomposed into two distinct contributions: the *adiabatic* and *nonadiabatic* components [57, 60, 191]. The adiabatic term accounts for steady-state dissipation, while the nonadiabatic term captures transient relaxation toward or between steady states. This decomposition provides a refined understanding of irreversibility in both classical and quantum nonequilibrium systems and underpins the derivation of multiple fluctuation theorems.

This chapter is structured in two main parts. In the first part, we review the trajectory-level formulation of entropy production in classical Markov jump processes. We define the dual and dual-reversed processes and derive fluctuation theorems for the total, adiabatic, and nonadiabatic entropy production. Special attention is given to the role of steady-state structure and local detailed balance in enabling a physically meaningful decomposition.

In the second part, we turn to the quantum setting, focusing on systems governed by Lindblad master equations. We develop a consistent trajectory-level thermodynamics within the quantum jump formalism [29, 28, 192], construct the time-reversed and dual processes, and derive quantum analogues of the fluctuation theorems. From an experimental standpoint, this trajectory-level formulation is not merely a mathematical convenience: it matches the level at which many platforms are probed, namely through continuous monitoring of the system's output channels. Different unravellings of a given Lindblad dynamics correspond to different measurement schemes on the environment, for instance photon counting versus homodyne or heterodyne detection, and the resulting stochastic state updates represent conditioning on the observed record, while the master equation is recovered upon averaging over records [193, 192, 32].

The mathematical subtleties of the quantum dual dynamics, including its non-uniqueness and relation to modular theory [194], are addressed. Under appropriate assumptions—notably, the existence of a privileged representation of the jump operators—we recover a clear operational interpretation of the adiabatic and nonadiabatic entropy components in the quantum regime.

Throughout the chapter, we emphasize conceptual continuity between classical and quantum frameworks, while highlighting key differences that arise due to non-commutativity in the quantum case.

Classical Case

8.1 Entropy Production in Classical Markovian Systems

In this section, we introduce the framework of stochastic thermodynamics for classical continuous-time Markov processes. Classical Markovian systems serve as a foundational setting in stochastic thermodynamics, already exhibiting the essential structural features we aim to generalize: the emergence of steady states, the distinction between equilibrium and nonequilibrium regimes, and the production of entropy through stochastic dynamics. Our goal is to establish notation and concepts that will guide our later analysis of entropy production in open quantum systems. For background and comprehensive treatments, see Refs. [17, 60, 195].

We consider a continuous-time Markov chain on a discrete set of states $i = 1, \dots, N$, described by a time-dependent probability distribution $\mathbf{p}(t) = (p_1(t), \dots, p_N(t))$. The dynamics is governed by the Pauli master equation,

$$\frac{\mathrm{d}p_i}{\mathrm{d}t} = \sum_{j:j\neq i} \left[W_{ij}p_j - W_{ji}p_i\right], \tag{8.1}$$

where $W_{ij} \geq 0$ denotes the transition rate from state j to state i. The first term accounts for probability flowing into state i, while the second describes probability leaving it.

To make the probability flow more transparent, we define the net probability current between states i and j as

$$J_{ij} = W_{ij}p_j - W_{ji}p_i, \tag{8.2}$$

which satisfies the antisymmetry relation $J_{ji} = -J_{ij}$. We set $J_{ii} = 0$ by convention. In terms of these currents, the master equation becomes

$$\frac{\mathrm{d}p_i}{\mathrm{d}t} = \sum_j J_{ij}, \tag{8.3}$$

emphasizing its role as a continuity equation for probability flow.

This formulation is particularly convenient for computing the time derivative of expectation values. For any observable $A = \{A_i\}$ defined in the network, the average $\langle A\rangle = \sum_i A_i p_i$ evolves as

$$\frac{\mathrm{d}}{\mathrm{d}t}\langle A\rangle = \sum_i A_i \frac{\mathrm{d}p_i}{\mathrm{d}t} = \sum_{ij} J_{ij}A_i. \tag{8.4}$$

To express the dynamics in matrix form, we assign the total escape rate from each state to the diagonal elements of the rate matrix: $W_{ii} = -\sum_{j:j\neq i} W_{ji}$. With this convention, the columns of the matrix $\boldsymbol{W}$ sum to zero, $\sum_i W_{ij} = 0$, ensuring conservation of total probability:

$$\frac{\mathrm{d}}{\mathrm{d}t}\sum_i p_i = \sum_{ij} W_{ij}p_j = \sum_j p_j \left(\sum_i W_{ij}\right) = 0. \tag{8.5}$$

The master equation can thus be written compactly as

$$\frac{\mathrm{d}\boldsymbol{p}}{\mathrm{d}t} = \boldsymbol{W}\boldsymbol{p}. \tag{8.6}$$

From this equation, we see that the steady-state distributions, for which $\mathrm{d}\boldsymbol{p}/\mathrm{d}t = 0$, lie in the kernel of $\boldsymbol{W}$:

$$\boldsymbol{W}\boldsymbol{p} = 0, \tag{8.7}$$

which implies that the net inflow of probability vanishes at every state: $\sum_j J_{ij} = 0$. This condition admits two physically distinct scenarios, depending on the structure of the individual currents J_{ij}. If each current vanishes independently, $J_{ij} = 0$ for all i, j, the system is said to satisfy *detailed balance*, which characterizes equilibrium. Using Eq. (8.2), this condition reads

$$W_{ij}\pi_j = W_{ji}\pi_i, \quad \forall i, j, \tag{8.8}$$

which implies that balance holds at the level of each pairwise transition—hence the term *detailed* balance.

A canonical example of detailed balance arises when the system is coupled to a thermal reservoir at inverse temperature β, and each state i is assigned an energy E_i. This is typically modeled by imposing that the transition rates satisfy the local detailed balance condition[1]

$$\frac{W_{ij}}{W_{ji}} = e^{-\beta(E_i - E_j)}, \quad \forall i, j. \tag{8.9}$$

The resulting steady state is the Boltzmann distribution,

$$\pi_i = \frac{e^{-\beta E_i}}{Z}, \qquad Z = \sum_j e^{-\beta E_j}, \tag{8.10}$$

which satisfies the detailed balance condition $W_{ij}\pi_j = W_{ji}\pi_i$ for all i, j. We return to the interpretation of the local detailed balance condition in the next section.

In contrast, many systems evolve toward *nonequilibrium steady states* (NESS), where the stationary condition $\boldsymbol{W}\boldsymbol{\pi} = 0$ still holds, but some individual currents J_{ij}^{ss} do not vanish. This typically occurs when probability flows form closed loops, leading to persistent circulation in state space. As we will see, these steady-state currents are intimately connected to sustained entropy production, even in the absence of time-dependent driving.

Figure 8.1 summarizes the structural distinction between equilibrium and nonequilibrium steady states.

8.1.1 Local vs. Global Detailed Balance

Before introducing the framework of entropy production, it is useful to clarify the distinction between two related concepts: *local* and *global detailed balance*. This distinction is not merely terminological, but plays a key functional role: local detailed balance will later enable a thermodynamic interpretation of the entropy balance.

[1] This is a stronger version of local detailed balance than the more general form $W_{ij}/W_{ji} = e^{\Delta S_{j\to i}}$, which allows for arbitrary entropy flow assignments. We return to this point in the next section.

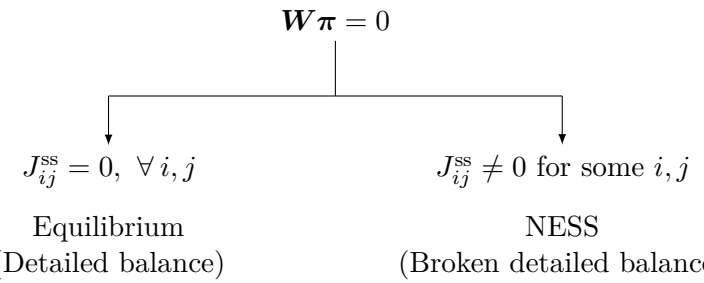

Figure 8.1: Classification of steady states according to the structure of probability currents. All steady states satisfy $\boldsymbol{W}\boldsymbol{\pi} = 0$, but only those with vanishing currents J_{ij} satisfy detailed balance and represent equilibrium.

In the previous section, we introduced the detailed balance condition

$$W_{ij}\pi_j = W_{ji}\pi_i \quad \forall\, i,j, \tag{8.11}$$

which characterizes equilibrium steady states. This condition is sometimes referred to as *global detailed balance* to distinguish it from the more microscopic notion of *local detailed balance*.

Global detailed balance is a property of both the transition matrix $\boldsymbol{W}$ and the steady-state distribution $\boldsymbol{\pi}$: it asserts that every pairwise transition is exactly balanced in steady state, and implies the absence of probability currents.

By contrast, local detailed balance refers to a condition on the transition rates alone. It takes the general form

$$\frac{W_{ij}}{W_{ji}} = e^{\Delta S_{j\to i}}, \tag{8.12}$$

where $\Delta S_{j\to i}$ denotes the entropy transferred to the environment during the transition $j \to i$. This relation implies that each transition is associated with a well-defined entropy flow.

In the case of a thermal reservoir at inverse temperature β, the entropy flow is determined by the heat $Q_{j\to i} = E_i - E_j$ absorbed by the system, yielding the Clausius relation

$$\Delta S_{j\to i} = -\beta(E_i - E_j). \tag{8.13}$$

Substituting this into Eq. (8.12) recovers the familiar form $W_{ij}/W_{ji} = e^{-\beta(E_i - E_j)}$, as discussed in the previous section.

When the entropy change $\Delta S_{j\to i}$ arises from an energy difference of the form $-\beta(E_i - E_j)$, the local detailed balance condition implies global detailed balance, with the steady-state given by the Boltzmann distribution $\pi_i \propto e^{-\beta E_i}$. Indeed, from Eq. (8.13), one finds

$$\frac{W_{ij}}{W_{ji}} = \frac{e^{-\beta E_i}}{e^{-\beta E_j}} = \frac{\pi_i}{\pi_j}, \tag{8.14}$$

which ensures that $W_{ij}\pi_j = W_{ji}\pi_i$ holds for all i,j.

By contrast, the more general local detailed balance condition in Eq. (8.12) does not necessarily imply global detailed balance. The converse direction also does not hold in general: a system may satisfy global detailed balance without any clear local interpretation of the rates in terms of entropy exchange.

In some contexts, the term "local detailed balance" is also used in systems coupled to multiple environments—such as thermal reservoirs at different temperatures—where the transition rates associated with each environment separately satisfy local detailed balance. In such settings, the total rate matrix can be decomposed as

$$\boldsymbol{W} = \sum_{\alpha} \boldsymbol{W}^{(\alpha)}, \tag{8.15}$$

where each $\boldsymbol{W}^{(\alpha)}$ describes the transitions mediated by a specific reservoir α, and satisfies

$$\frac{W_{ij}^{(\alpha)}}{W_{ji}^{(\alpha)}} = e^{\Delta S_{j\to i}^{(\alpha)}}. \tag{8.16}$$

While global detailed balance is generally broken in such systems, the local structure allows one to assign entropy flows to individual reservoirs. This is the typical setting for nonequilibrium steady states and underlies models of thermal machines and transport phenomena.

8.1.2 Schnakenberg Entropy Production

We now discuss the entropic balance in classical Markovian systems and introduce the notion of irreversibility. A natural starting point is the Shannon entropy of the probability distribution $\boldsymbol{p}(t)$, defined as

$$S(t) = -\sum_{i} p_i(t) \log p_i(t). \tag{8.17}$$

Its time derivative is given by

$$\frac{\mathrm{d}S}{\mathrm{d}t} = -\sum_{i} \frac{\mathrm{d}p_i}{\mathrm{d}t} \log p_i, \tag{8.18}$$

as shown in Appendix A.1. Using the continuity equation $\dot{p}_i = \sum_j J_{ij}$, this becomes

$$\frac{\mathrm{d}S}{\mathrm{d}t} = -\sum_{ij} J_{ij} \log p_i. \tag{8.19}$$

To obtain a more symmetric expression, we exploit the antisymmetry of the probability currents, $J_{ij} = -J_{ji}$, and rewrite the entropy change rate as

$$\begin{aligned} \frac{\mathrm{d}S}{\mathrm{d}t} &= -\frac{1}{2}\sum_{ij} J_{ij} \log p_i - \frac{1}{2}\sum_{ij} J_{ji} \log p_j \\ &= \frac{1}{2}\sum_{ij} J_{ij} \log\left(\frac{p_j}{p_i}\right). \end{aligned} \tag{8.20}$$

This expression reflects the internal redistribution of probability within the system. However, it does not, by itself, characterize thermodynamic irreversibility: the entropy can increase or decrease depending on how the distribution evolves, and no information is yet included about interactions with the environment. In particular, this is not the quantity that enters the second law.

To quantify irreversibility, we seek a decomposition of the form

$$\frac{dS}{dt} = \dot{\Sigma} - \dot{\Pi}, \tag{8.21}$$

where $\dot{\Pi}$ describes the reversible entropy exchange rate with the environment, and $\dot{\Sigma} \geq 0$ is *entropy production rate*, which characterizes the spontaneous, irreversible entropy change.

To motivate the structure of this decomposition, consider the case where the transition rates satisfy local detailed balance:

$$\log\left(\frac{W_{ij}}{W_{ji}}\right) = \Delta S_{j\to i}, \tag{8.22}$$

where $\Delta S_{j\to i}$ denotes the entropy exchanged with the environment in the transition $j \to i$. Since J_{ij} gives the net transition rate from $j \to i$, the total entropy flux is

$$\dot{\Pi} = \sum_{ij} J_{ij} \Delta S_{j\to i} = \frac{1}{2} \sum_{ij} J_{ij} \log\left(\frac{W_{ij}}{W_{ji}}\right). \tag{8.23}$$

If the environment is thermal, the entropy flux $\dot{\Pi}$ admits a particularly transparent interpretation. In this case, local detailed balance takes the form $\Delta S_{j\to i} = \beta Q_{j\to i}$, where $Q_{j\to i}$ is the heat released to the environment. The entropy flux then becomes $\dot{\Pi} = \beta \dot{Q}$, with

$$\dot{Q} = \sum_{ij} J_{ij} Q_{j\to i} = \frac{1}{2\beta} \sum_{ij} J_{ij} \log\left(\frac{W_{ij}}{W_{ji}}\right). \tag{8.24}$$

To obtain the entropy production rate $\dot{\Sigma}$, we substitute this expression into the entropy balance (8.21), yielding

$$\begin{aligned} \dot{\Sigma} &= \frac{\mathrm{d}S}{\mathrm{d}t} + \dot{\Pi} \\ &= \frac{1}{2} \sum_{ij} J_{ij} \log\left(\frac{p_j}{p_i}\right) + \frac{1}{2} \sum_{ij} J_{ij} \log\left(\frac{W_{ij}}{W_{ji}}\right) \\ &= \frac{1}{2} \sum_{ij} J_{ij} \log\left(\frac{W_{ij} p_j}{W_{ji} p_i}\right), \end{aligned} \tag{8.25}$$

which is the celebrated Schnakenberg expression for entropy production [195].

In the absence of local detailed balance, the decomposition in Eq. (8.21) is still mathematically well-defined, since it follows directly from separating logarithmic terms. However, its interpretation becomes more subtle. In this general setting, the entropy flux $\dot{\Pi}$ may no longer correspond to a physical current—such as heat—but the decomposition remains operationally meaningful.

This structure is not arbitrary. It remains physically motivated by analogy with systems that do obey local detailed balance, including Langevin dynamics, as pointed out in Ref. [17]. More importantly, the quantity $\dot{\Sigma}$ defined in this way satisfies the essential properties expected of an entropy production rate. We now examine these properties in more detail.

The most fundamental of these properties is non-negativity:

$$\dot{\Sigma} \geq 0, \tag{8.26}$$

which encodes the second law of thermodynamics.

This result follows from the inequality

$$(x-y)\log\left(\frac{x}{y}\right) \geq 0 \quad \text{for all } x, y > 0, \tag{8.27}$$

with equality if and only if $x = y$. This relation plays an important role in information theory (see, e.g., Ref. [173]).

Recalling that $J_{ij} = W_{ij}p_j - W_{ji}p_i$, the Schnakenberg expression can be written as

$$\dot{\Sigma} = \frac{1}{2}\sum_{ij}(W_{ij}p_j - W_{ji}p_i)\log\left(\frac{W_{ij}p_j}{W_{ji}p_i}\right). \tag{8.28}$$

Applying the inequality to each term in the sum, with $x = W_{ij}p_j$ and $y = W_{ji}p_i$, establishes that $\dot{\Sigma} \geq 0$.

Importantly, equality holds if and only if the detailed balance condition $W_{ij}p_j = W_{ji}p_i$ holds for all i, j, which corresponds to thermodynamic equilibrium. Therefore, $\dot{\Sigma} = 0$ if and only if the system is at equilibrium.

To further clarify the structure of entropy production, it is useful to introduce the *thermodynamic affinity*

$$\mathcal{A}_{ij} = \log\left(\frac{W_{ij}p_j}{W_{ji}p_i}\right), \tag{8.29}$$

which measures the deviation from the detailed balance condition $W_{ij}p_j = W_{ji}p_i$. This quantity plays the role of a generalized force driving the probability current along the transition $j \to i$. The entropy production then takes the compact form

$$\dot{\Sigma} = \frac{1}{2}\sum_{ij} J_{ij}\mathcal{A}_{ij}, \tag{8.30}$$

making explicit that entropy is produced when probability flows along nonzero thermodynamic forces.

This formulation highlights that $\dot{\Sigma} = 0$ at equilibrium: when detailed balance holds, both J_{ij}^{ss} and $\mathcal{A}_{ij}$ vanish identically.

By contrast, in a NESS, the probability distribution $\boldsymbol{p}^{\text{ss}}$ is time-independent, so $\dot{S} = 0$, but detailed balance is violated. This leads to sustained probability currents $J_{ij}^{\text{ss}} \neq 0$ and nonzero affinities $\mathcal{A}_{ij}^{\text{ss}} \neq 0$, resulting in a strictly positive entropy production:

$$\dot{\Sigma}^{\text{ss}} = \frac{1}{2}\sum_{ij} J_{ij}^{\text{ss}}\mathcal{A}_{ij}^{\text{ss}} > 0. \tag{8.31}$$

This persistent entropy production is a hallmark of nonequilibrium steady states: although the system is stationary, it is continuously dissipating energy and generating entropy.

In the special case where the steady state $\boldsymbol{\pi}$ satisfies detailed balance—such as for a system coupled to a thermal reservoir—the entropy production reduces to the negative time derivative of the relative entropy between $\boldsymbol{p}(t)$ and $\boldsymbol{\pi}$:

$$\dot{\Sigma}(t) = -\frac{\mathrm{d}}{\mathrm{d}t} D(\boldsymbol{p}(t) \| \boldsymbol{\pi}), \tag{8.32}$$

where $D(p\|\pi) = \sum_i p_i \log(p_i/\pi_i)$ is the Kullback–Leibler divergence. This expression reflects the idea that entropy production quantifies relaxation toward equilibrium and vanishes if and only if $\boldsymbol{p}(t) = \boldsymbol{\pi}$.

To see this, we compute the time derivative

$$\frac{\mathrm{d}}{\mathrm{d}t} D(p(t)\|\pi) = \sum_i \dot{p}_i(t) \log\left(\frac{p_i(t)}{\pi_i}\right), \tag{8.33}$$

and substitute the master equation $\dot{p}_i = \sum_j W_{ij} p_j$, yielding

$$\frac{\mathrm{d}}{\mathrm{d}t} D(p\|\pi) = \sum_{ij} W_{ij} p_j \log\left(\frac{p_i}{\pi_i}\right). \tag{8.34}$$

Using the antisymmetry of the probability current $J_{ij} = W_{ij}p_j - W_{ji}p_i$, we symmetrize the sum:

$$-\frac{\mathrm{d}}{\mathrm{d}t} D(p\|\pi) = -\frac{1}{2} \sum_{ij} J_{ij} \log\left(\frac{p_i/\pi_i}{p_j/\pi_j}\right) = \frac{1}{2} \sum_{ij} J_{ij} \log\left(\frac{\pi_i p_j}{\pi_j p_i}\right). \tag{8.35}$$

This matches the Schnakenberg formula for entropy production when the rates satisfy detailed balance, i.e., $W_{ij}/W_{ji} = \pi_i/\pi_j$.

Beyond equilibrium, this identification no longer holds: if $\boldsymbol{\pi}$ does not satisfy detailed balance, the expression $-\frac{\mathrm{d}}{\mathrm{d}t} D(p(t)\|\pi)$ no longer coincides with the entropy production. In the next section, we will see how this structure can be generalized by introducing a time-dependent protocol.

8.1.3 Time-Dependent Driving and the Adiabatic/Nonadiabatic Decomposition

When a system coupled to a thermal bath is driven out of equilibrium by an external protocol, dissipation arises from the currents induced by the system's deviation from equilibrium. In such cases, entropy production is entirely due to the system's lag behind the instantaneous equilibrium state.

As we discussed, a nonequilibrium steady state exhibits non-zero entropy production even in the absence of external driving. The total entropy production has two distinct physical sources: an intrinsic contribution associated with the steady-state currents, and another other arising from the system's response to the time-dependent driving.

In this section, we introduce a formalism that separates the total entropy production into two non-negative components, corresponding to these two mechanisms. This decomposition, into *adiabatic* and *nonadiabatic* contributions, provides a refined understanding of irreversibility in driven nonequilibrium systems.

We consider a classical Markov process governed by a time-dependent master equation,

$$\frac{\mathrm{d}\boldsymbol{p}}{\mathrm{d}t} = \boldsymbol{W}(\lambda_t)\,\boldsymbol{p}(t), \tag{8.36}$$

where λ_t denotes an externally controlled parameter. For each fixed value of λ, the rate matrix $\boldsymbol{W}(\lambda)$ is assumed to admit a unique instantaneous steady state $\boldsymbol{\pi}^\lambda$, satisfying $\boldsymbol{W}(\lambda)\,\boldsymbol{\pi}^\lambda = 0$. This reference distribution may correspond to an equilibrium state (if detailed balance holds) or to a nonequilibrium steady state (NESS) with nonvanishing steady-state currents.

Even in the presence of time-dependent driving, the time derivative of the Shannon entropy retains the same structure as in the time-independent case:

$$\dot{S}(t) = -\sum_i \frac{\mathrm{d}p_i}{\mathrm{d}t}\log p_i(t) = \frac{1}{2}\sum_{ij} J_{ij}(t)\log\left(\frac{p_j(t)}{p_i(t)}\right), \tag{8.37}$$

with the probability currents given $J_{ij}(t) = W_{ij}(\lambda_t)p_j(t) - W_{ji}(\lambda_t)p_i(t)$. Using the identity

$$\log\left(\frac{p_j}{p_i}\right) = \log\left(\frac{W_{ij}(\lambda_t)p_j}{W_{ji}(\lambda_t)p_i}\right) + \log\left(\frac{W_{ij}(\lambda_t)}{W_{ji}(\lambda_t)}\right), \tag{8.38}$$

we can again decompose $\dot{S}(t)$ into an entropy production rate and an entropy flow rate. This yields the total entropy production rate in the form:

$$\dot{\Sigma}(t) = \frac{1}{2}\sum_{ij} J_{ij}(t)\log\left(\frac{W_{ij}(\lambda_t)p_j(t)}{W_{ji}(\lambda_t)p_i(t)}\right), \tag{8.39}$$

which is a time-dependent version of the Schnakenberg formula.

The remaining term from the logarithmic splitting defines the entropy flux into the environment:

$$\dot{\Pi}(t) = \frac{1}{2}\sum_{ij} J_{ij}(t)\log\left(\frac{W_{ij}(\lambda_t)}{W_{ji}(\lambda_t)}\right), \tag{8.40}$$

which quantifies the reversible entropy exchange with the environment. We return to this term in the next section.

In the driven-NESS case, the Schnakenberg formula gives the *total* entropy production, accounting for both the intrinsic NESS dissipation and the response to the driving. To isolate these distinct contributions, we follow Refs. [57, 60] and decompose the total entropy production rate into two non-negative parts:

$$\dot{\Sigma}(t) = \dot{\Sigma}_{\mathrm{ad}}(t) + \dot{\Sigma}_{\mathrm{na}}(t). \tag{8.41}$$

where the *adiabatic* term $\dot{\Sigma}_{\mathrm{ad}}$ quantifies entropy production associated with persistent steady-state currents, while the *nonadiabatic* term $\dot{\Sigma}_{\mathrm{na}}$ captures irreversibility due to the system's deviation from the evolving steady state.

To motivate the definition of the nonadiabatic entropy production, consider the special case in which the instantaneous steady states satisfy detailed balance. In this equilibrium setting, the steady-state currents vanish, and the Schnakenberg formula coincides with the

nonadiabatic contribution. Inserting the detailed balance conditions $W_{ij}(\lambda_t)/W_{ji}(\lambda_t) = \pi_i^{\lambda_t}/\pi_j^{\lambda_t}$ into the Schnakenberg expression, one finds

$$\begin{aligned}\dot{\Sigma}_{\mathrm{na}}(t) &= \frac{1}{2}\sum_{ij} J_{ij}(t)\log\left(\frac{\pi_i^{\lambda_t} p_j(t)}{\pi_j^{\lambda_t} p_i(t)}\right) \\ &= -\frac{\partial}{\partial s} D(\boldsymbol{p}(s)\|\boldsymbol{\pi}^{\lambda_t})\big|_{s=t},\end{aligned} \tag{8.42}$$

where the second line follows from the same symmetrization argument used in Eq. (8.35), now applied to the time-dependent reference distribution $\boldsymbol{\pi}^{\lambda_t}$. Note that the derivative is taken with respect to the first argument of the relative entropy, while the reference $\boldsymbol{\pi}^{\lambda_t}$ is held fixed.

In the general case—without assuming detailed balance—it is natural to retain this definition:

$$\dot{\Sigma}_{\mathrm{na}}(t) \equiv -\frac{\partial}{\partial s} D(\boldsymbol{p}(s)\|\boldsymbol{\pi}^{\lambda_t})\big|_{s=t} \geq 0. \tag{8.43}$$

This expression quantifies the irreversibility due to the system's deviation from the instantaneous steady state. In the quasistatic limit, where $\boldsymbol{p}(t) \approx \boldsymbol{\pi}^{\lambda_t}$ at all times, this contribution vanishes. As we will show in the next section, $\dot{\Sigma}_{\mathrm{na}}(t)$ is always non-negative. The non-negativity follows from the fact that it is the (negative) time derivative of a relative entropy, which is known to decrease monotonically under Markovian dynamics—a result closely related to the H-theorem discussed in Ref. [5].

The complementary *adiabatic* entropy production is defined by subtracting the nonadiabatic component from the total entropy production:

$$\dot{\Sigma}_{\mathrm{ad}}(t) \equiv \dot{\Sigma}(t) - \dot{\Sigma}_{\mathrm{na}}(t). \tag{8.44}$$

Substituting the expressions for each term, we obtain

$$\dot{\Sigma}_{\mathrm{ad}}(t) = \frac{1}{2}\sum_{ij} J_{ij}(t)\log\left(\frac{W_{ij}(\lambda_t)\pi_j^{\lambda_t}}{W_{ji}(\lambda_t)\pi_i^{\lambda_t}}\right). \tag{8.45}$$

To interpret this expression, we define the *steady-state affinities* as

$$\mathcal{A}_{ij}^{\mathrm{ss}}(\lambda_t) = \log\left(\frac{W_{ij}(\lambda_t)\pi_j^{\lambda_t}}{W_{ji}(\lambda_t)\pi_i^{\lambda_t}}\right), \tag{8.46}$$

which act as thermodynamic forces and vanish precisely when detailed balance holds. Using this notation, the adiabatic entropy production becomes:

$$\dot{\Sigma}_{\mathrm{ad}}(t) = \frac{1}{2}\sum_{ij} J_{ij}(t)\,\mathcal{A}_{ij}^{\mathrm{ss}}(\lambda_t), \tag{8.47}$$

which makes explicit its interpretation as the entropy produced by steady-state currents flowing against instantaneous thermodynamic forces.

The terminology *adiabatic* and *nonadiabatic* finds its justification in a timescale separation argument. As explained in Ref. [191], if the system relaxes much faster than the timescale of

the driving protocol λ_t, then it remains arbitrarily close to the instantaneous steady state throughout the evolution. In this quasistatic limit, the nonadiabatic contribution vanishes and the total entropy production reduces to its adiabatic component. It is thus natural to interpret the adiabatic term as the cost of maintaining the instantaneous nonequilibrium structure, and the nonadiabatic term as a measure of the lag induced by finite-time driving. We emphasize that the term "adiabatic" is not used here in the thermodynamic sense of zero heat exchange, but rather to describe an evolution in which the system stays in its instantaneous steady state.

We now show that the adiabatic entropy production $\dot{\Sigma}_{\mathrm{ad}}(t)$ is non-negative at all times, following Ref. [191]. The key ingredient is the inequality

$$-\log x \geq 1 - x \qquad \text{for all } x > 0, \tag{8.48}$$

with equality if and only if $x = 1$.

We begin by writing $\dot{\Sigma}_{\mathrm{ad}}(t)$ in the unsymmetrized form

$$\dot{\Sigma}_{\mathrm{ad}}(t) = \sum_{ij} W_{ij}(\lambda_t) p_j(t) \log\left(\frac{W_{ji}(\lambda_t)\pi_i^{\lambda_t}}{W_{ij}(\lambda_t)\pi_j^{\lambda_t}}\right). \tag{8.49}$$

Since $W_{ij}(\lambda_t)p_j(t) \geq 0$, we can apply the inequality term by term. Applying the inequality with $x = W_{ji}(\lambda_t)\pi_i^{\lambda_t}/W_{ij}(\lambda_t)\pi_j^{\lambda_t}$, we find

$$\begin{aligned}
\sum_{ij} W_{ij}(\lambda_t) p_j(t) \log\left(\frac{W_{ji}(\lambda_t)\pi_i^{\lambda_t}}{W_{ij}(\lambda_t)\pi_j^{\lambda_t}}\right) &\geq \sum_{ij} W_{ij}(\lambda_t) p_j(t) \left(1 - \frac{W_{ji}(\lambda_t)\pi_i^{\lambda_t}}{W_{ij}(\lambda_t)\pi_j^{\lambda_t}}\right) \\
&= \sum_i p_i \sum_j W_{ij} - \sum_j \frac{p_j(t)}{\pi_j^{\lambda_t}} \sum_i W_{ji}\pi_i^{\lambda_t} \\
&= 0,
\end{aligned} \tag{8.50}$$

where we used that $\sum_j W_{ij} = 0$ and $\boldsymbol{W}(\lambda_t)\,\boldsymbol{\pi}^{\lambda_t} = 0$.

Therefore,

$$\dot{\Sigma}_{\mathrm{ad}}(t) \geq 0, \tag{8.51}$$

with equality if and only if the instantaneous steady state satisfies detailed balance, i.e., $W_{ij}(\lambda_t)\pi_j^{\lambda_t} = W_{ji}(\lambda_t)\pi_i^{\lambda_t}$.

8.1.4 The Nonequilibrium Potential and the Housekeeping/Excess Decomposition

In parallel with the decomposition of entropy production, the entropy exchange with the environment can be separated into two distinct contributions. This leads to the *housekeeping/excess* decomposition of the entropy flux, which is closely tied to the concept of nonequilibrium potential—a central tool for describing how systems respond to time-dependent driving.

The entropy flux $\dot{\Pi}(t)$ can be decomposed into two contributions:

$$\dot{\Pi}(t) = \dot{\Pi}_{\mathrm{ex}}(t) + \dot{\Pi}_{\mathrm{hk}}(t), \tag{8.52}$$

where $\dot{\Pi}_{\mathrm{hk}}$ is the *housekeeping* entropy flux required to maintain the nonequilibrium steady-state, and $\dot{\Pi}_{\mathrm{ex}}$ is the *excess* flux arising from deviations from it. These terms mirror the adiabatic and nonadiabatic components of entropy production introduced earlier.

With this decomposition, the full entropy balance becomes

$$\frac{\mathrm{d}S}{\mathrm{d}t} = \big(\dot{\Sigma}_{\mathrm{ad}}(t) + \dot{\Sigma}_{\mathrm{na}}(t)\big) - \big(\dot{\Pi}_{\mathrm{ex}}(t) + \dot{\Pi}_{\mathrm{hk}}(t)\big). \tag{8.53}$$

In a nonequilibrium steady state, the Shannon entropy remains constant, $\dot{S}(t) = 0$, and the nonadiabatic entropy production vanishes by definition, $\dot{\Sigma}_{\mathrm{na}}(t) = 0$. If we additionally require that the excess entropy flux vanishes in steady state, $\dot{\Pi}_{\mathrm{ex}}(t) = 0$, then the entropy balance simplifies to

$$\dot{\Pi}_{\mathrm{hk}}(t) = \dot{\Sigma}_{\mathrm{ad}}(t). \tag{8.54}$$

This motivates defining the housekeeping entropy flux to have the same structure as the adiabatic entropy production:

$$\begin{aligned}\dot{\Pi}_{\mathrm{hk}}(t) &\equiv \dot{\Sigma}_{\mathrm{ad}}(t) \\ &= \frac{1}{2}\sum_{ij} J_{ij}(t) \log\left(\frac{W_{ij}(\lambda_t)\pi_j^{\lambda_t}}{W_{ji}(\lambda_t)\pi_i^{\lambda_t}}\right).\end{aligned} \tag{8.55}$$

This quantity vanishes if the instantaneous steady state satisfies detailed balance, $W_{ij}(\lambda_t)\,\pi_j^{\lambda_t} = W_{ji}(\lambda_t)\,\pi_i^{\lambda_t}$, and admits the same current-force interpretation as $\dot{\Sigma}_{\mathrm{ad}}(t)$, introduced in Eq. (8.47).

The excess entropy flux is then obtained by the complement $\dot{\Pi}_{\mathrm{ex}}(t) \equiv \dot{\Pi}(t) - \dot{\Pi}_{\mathrm{hk}}(t)$. Using the expression for the total entropy flux in Eq. (8.40), this yields

$$\dot{\Pi}_{\mathrm{ex}}(t) = \frac{1}{2}\sum_{ij} J_{ij}(t) \log\left(\frac{\pi_j^{\lambda_t}}{\pi_i^{\lambda_t}}\right). \tag{8.56}$$

An equivalent, unsymmetrized expression for this quantity is

$$\dot{\Pi}_{\mathrm{ex}}(t) = \sum_{ij} W_{ij} p_j(t) \log\big(\pi_i^{\lambda_t}\big). \tag{8.57}$$

In thermal systems obeying detailed balance, where the steady-state distribution takes the Boltzmann form $\pi_i^{\lambda_t} = e^{-\beta E_i(\lambda_t)}/Z$, this becomes

$$\begin{aligned}\dot{\Pi}_{\mathrm{ex}}(t) &= \sum_{ij} W_{ij} p_j(t)(-\beta E_i - \log Z) \\ &= -\beta \sum_i \dot{p}_i(t) E_i \\ &= -\beta \frac{\mathrm{d}}{\mathrm{d}t}\langle E\rangle,\end{aligned} \tag{8.58}$$

where $\langle E\rangle$ denotes the average energy of the system, and we have used the fact that $\sum_j W_{ij} = 0$ to eliminate the $\log Z$ term. In this setting, the excess entropy flux corresponds precisely to the reversible heat current into the environment, that is, $\dot{\Pi}_{\mathrm{ex}}(t) = \beta\dot{Q}$.

Beyond the thermal case, $\dot{\Pi}_{\rm ex}(t)$ generally loses a direct interpretation in terms of heat. Nevertheless, it retains a meaningful structure when expressed in terms of the so-called *nonequilibrium potential*,

$$\Phi_i(\lambda_t) \equiv -\log \pi_i^{\lambda_t}. \tag{8.59}$$

This quantity, introduced by Hatano and Sasa in the context of Langevin dynamics [57], captures the "energy-like" landscape associated with the instantaneous steady state. In terms of Φ_i, the excess entropy flux becomes

$$\dot{\Pi}_{\rm ex}(t) = -\sum_{ij} W_{ij} p_j(t)\, \Phi_i = -\sum_i \dot{p}_i(t)\, \Phi_i(\lambda_t), \tag{8.60}$$

where the second equality follows from the master equation. In thermal systems, the nonequilibrium potential reduces to $\Phi_i = \beta E_i + \log Z$, recovering the earlier result.

The excess flux can also be written in the symmetrized form

$$\dot{\Pi}_{\rm ex}(t) = -\frac{1}{2}\sum_{ij} J_{ij}(t)[\Phi_i(\lambda_t) - \Phi_j(\lambda_t)], \tag{8.61}$$

which reveals its structure as an entropy flux arising from differences in the nonequilibrium potential across transitions.

With the identification $\dot{\Pi}_{\rm hk}(t) = \dot{\Sigma}_{\rm ad}(t)$, the full entropy balance in Eq. (8.53) simplifies to

$$\frac{{\rm d}S}{{\rm d}t} = \dot{\Sigma}_{\rm na}(t) - \dot{\Pi}_{\rm ex}(t), \tag{8.62}$$

which is known as the *Hatano–Sasa relation* [57].

This relation provides a refined version of the second law that isolates the effects of time-dependent driving. In nonequilibrium steady states, dissipation arises continuously from persistent probability currents, even in the absence of external driving. These contributions are intrinsic to the steady-state structure and cannot be eliminated. The Hatano–Sasa relation effectively renormalizes the second law by accounting for this baseline dissipation, focusing instead on the additional irreversibility generated by the protocol itself.

Integrating over a finite protocol of duration τ, one obtains

$$\Delta S + \int_0^\tau {\rm d}t\, \dot{\Pi}_{\rm ex}(t) = \int_0^\tau {\rm d}t\, \dot{\Sigma}_{\rm na}(t) \geq 0, \tag{8.63}$$

which generalizes the Clausius inequality to nonequilibrium conditions. Here, the total change in Shannon entropy is bounded below by the negative of the excess entropy flux, reflecting the thermodynamic cost of driving the system away from its instantaneous steady state. This relation becomes an equality in the quasistatic limit, where the system remains arbitrarily close to the evolving steady state and the nonadiabatic entropy production vanishes.

8.1.5 Trajectory-Level Description of Markov Dynamics

In stochastic thermodynamics, the entropy production defined at the ensemble level admits a natural refinement at the level of individual realizations, or *trajectories*, of the stochastic process. This trajectory-level formulation is central for expressing fluctuation theorems.

A single realization of a continuous-time Markov process is specified by the sequence of visited states and the times at which transitions occur:

$$\gamma = \{(i_0, 0), (i_1, t_1), \dots, (i_n, t_n), (i_n, \tau)\}, \tag{8.64}$$

indicating that the system starts in state i_0, jumps to i_1 at time t_1, and so on, eventually reaching state i_n at time t_n, where it remains until the final time τ.

The probability of observing a given trajectory γ can be written as[2]

$$\mathbb{P}[\gamma] = p_{i_0}(0) \cdot \mathbb{P}(\text{no jump in } [0, t_1) \mid i_0) \cdot \prod_{k=1}^{n} \Big[W_{i_k i_{k-1}}(\lambda_{t_k}) \cdot \mathbb{P}(\text{no jump in } [t_k, t_{k+1}) \mid i_k) \Big], \tag{8.65}$$

where we define $t_{n+1} \equiv \tau$ for convenience. For each interval $[t_k, t_{k+1})$, the probability of observing no jump is given by [17, 60]

$$\mathbb{P}(\text{no jump in } [t_k, t_{k+1}) \mid i_k) = \exp\left(- \int_{t_k}^{t_{k+1}} \mathrm{d}t \, r_{i_k}(t) \right), \tag{8.66}$$

where $r_i(t) = \sum_{j \neq i} W_{ji}(\lambda_t)$ is the total escape rate from state i at time t.

Substituting into Eq. (8.65), we obtain

$$\begin{aligned} \mathbb{P}[\gamma] &= p_{i_0}(0) \cdot \exp\left(- \int_0^{t_1} \mathrm{d}t \, r_{i_0}(t) \right) \cdot \prod_{k=1}^{n} \left[W_{i_k i_{k-1}}(\lambda_{t_k}) \cdot \exp\left(- \int_{t_k}^{t_{k+1}} \mathrm{d}t \, r_{i_k}(t) \right) \right] \\ &= p_{i_0}(0) \cdot \prod_{k=1}^{n} W_{i_k i_{k-1}}(\lambda_{t_k}) \cdot \exp\left(- \int_0^{\tau} \mathrm{d}t \, r_{i(t)}(t) \right), \end{aligned} \tag{8.67}$$

where in the last equality we combined all waiting-time contributions into a single integral, denoting by $i(t)$ the system's state at time t.

At the trajectory level, we define the *stochastic entropy* of the system at time t as

$$s(t) = -\log p_{i(t)}(t), \tag{8.68}$$

where $p_i(t)$ is the probability of the system being in state i at that time.

Taking the average of $s(t)$ over all realizations recovers the ensemble-level Shannon entropy:

$$\langle s(t) \rangle = -\sum_i p_i(t) \log p_i(t) = S(t). \tag{8.69}$$

[2] Strictly speaking, $\mathbb{P}[\gamma]$ is a product of discrete probabilities over state sequences and continuous probability densities over jump times. Nonetheless, it is commonly referred to as the "probability" or "weight" of a trajectory [17, 60].

The total change in stochastic entropy along a trajectory γ is then given by

$$\Delta s[\gamma] = s(\tau) - s(0) = \log\left(\frac{p_{i_0}(0)}{p_{i_n}(\tau)}\right), \tag{8.70}$$

where i_0 and i_n are the initial and final states of the trajectory, respectively.

We now introduce the total entropy flux exchanged with the environment along the trajectory γ, denoted $\Pi[\gamma]$. In the special case where the transition rates satisfy a local detailed balance condition, each jump $j \to i$ is associated with a well-defined entropy change,

$$\Delta S_{j\to i} = \log\left(\frac{W_{ij}}{W_{ji}}\right). \tag{8.71}$$

Accordingly, the total entropy flux is given by the sum of these contributions over all jumps in the trajectory:

$$\Pi[\gamma] = \sum_{k=1}^{n} \log\left(\frac{W_{i_k i_{k-1}}(\lambda_{t_k})}{W_{i_{k-1} i_k}(\lambda_{t_k})}\right). \tag{8.72}$$

Even when detailed balance does not hold, Eq. (8.72) can still be interpreted as the entropy flux to the environment. This is justified by the same reasoning discussed in the previous section: the expression coincides with the expected result under local detailed balance, and—crucially—the corresponding entropy production, introduced below, obeys all expected thermodynamic properties, including positivity and fluctuation relations [17].

8.1.6 Trajectory-Level Entropy Production

The entropy production along a trajectory is intimately connected to the concept of microscopic reversibility. To define entropy production at this level—and to derive fluctuation theorems—we must introduce the notion of a time-reversed process. This process corresponds to observing the system as it evolves backward in time, retracing the original sequence of transitions in reverse order. Throughout this chapter, we use a tilde to denote time-reversed quantities.

Given a trajectory γ generated by the forward process, the corresponding time-reversed trajectory is defined as

$$\tilde{\gamma} = \{(i_n, 0), (i_{n-1}, \tau - t_n), \ldots, (i_0, \tau - t_1)\}, \tag{8.73}$$

where the system starts in the final state i_n and undergoes transitions in the reverse order.

The time-reversed process is defined by reversing the driving protocol, so that $\tilde{\lambda}_t = \lambda_{\tau - t}$. The initial distribution of the reversed process is taken to be $\tilde{p}_i(0) = p_i(\tau)$, i.e., the final distribution of the forward process.

The probability weight of the time-reversed trajectory $\tilde{\gamma}$ under the reversed dynamics is then given by [60]

$$\tilde{\mathbb{P}}[\tilde{\gamma}] = p_{i_n}(\tau) \cdot \prod_{k=1}^{n} W_{i_{k-1} i_k}(\tilde{\lambda}_{\tau - t_k}) \cdot \exp\left(-\int_0^\tau \mathrm{d}t\, r_{i(t)}(t)\right), \tag{8.74}$$

where $i(t)$ denotes the state occupied at time t along the original trajectory. Notice that the waiting-time contribution is unchanged under time reversal, since $\int_0^\tau \mathrm{d}t\, r_{i(\tau-t)}(\tau-t) = \int_0^\tau \mathrm{d}t\, r_{i(t)}(t)$,.

We now define the total entropy production along a trajectory as the log-ratio between the probability of observing a given trajectory in the forward process and the probability of observing its time-reversed counterpart under the reversed dynamics:

$$\Sigma[\gamma] = \log \frac{\mathbb{P}[\gamma]}{\tilde{\mathbb{P}}[\tilde{\gamma}]}. \tag{8.75}$$

This expression captures the fundamental asymmetry between the forward and backward dynamics. Physically, it quantifies how distinguishable the process is from its time reversal, thereby serving as a trajectory-level measure of irreversibility. It was first introduced in the context of stochastic thermodynamics by Crooks [21], and further developed by Seifert [58], who identified the log-ratio of path probabilities as the natural definition of stochastic entropy production.

Substituting the expressions for $\mathbb{P}[\gamma]$ and $\tilde{\mathbb{P}}[\tilde{\gamma}]$, and using the assumption $\tilde{p}_i(0) = p_i(\tau)$, one finds

$$\Sigma[\gamma] = \log \frac{p_{i_0}(0)}{p_{i_n}(\tau)} + \sum_{k=1}^{n} \log \frac{W_{i_k i_{k-1}}(\lambda_{t_k})}{W_{i_{k-1} i_k}(\lambda_{t_k})}. \tag{8.76}$$

The first term can be recognized as the change in stochastic system entropy, given in Eq. (8.70), while the second term corresponds to the total entropy flux to the environment along the trajectory γ, as defined in Eq. (8.72). This confirms the trajectory-level entropy balance:

$$\Sigma[\gamma] = \Delta s[\gamma] + \Pi[\gamma]. \tag{8.77}$$

Averaging over all possible trajectories yields[3]

$$\langle \Sigma \rangle = \sum_{\gamma} \mathbb{P}[\gamma] \log \frac{\mathbb{P}[\gamma]}{\tilde{\mathbb{P}}[\tilde{\gamma}]} = D(\mathbb{P} \,\|\, \tilde{\mathbb{P}}), \tag{8.78}$$

where $D(\mathbb{P} \,\|\, \tilde{\mathbb{P}})$ denotes the Kullback–Leibler divergence between the forward and time-reversed trajectory distributions. Since the relative entropy is non-negative, this confirms that $\langle \Sigma \rangle \geq 0$, with equality if and only if the process is microscopically reversible. For a detailed derivation, see Ref. [60].

Moreover, this definition leads directly to the integral fluctuation theorem. Taking the expectation value of $e^{-\Sigma[\gamma]}$, we find

$$\left\langle e^{-\Sigma[\gamma]} \right\rangle = \sum_{\gamma} \mathbb{P}[\gamma] \, \exp\left(- \log \frac{\mathbb{P}[\gamma]}{\tilde{\mathbb{P}}[\tilde{\gamma}]} \right) \tag{8.79}$$

$$= \sum_{\gamma} \tilde{\mathbb{P}}[\tilde{\gamma}] \tag{8.80}$$

$$= 1, \tag{8.81}$$

[3] The average over trajectories $\sum_\gamma \mathbb{P}[\gamma](\cdot)$ serves as a compact notation for a path integral over all possible realizations, following the convention of Ref. [60].

where we used the normalization of $\tilde{\mathbb{P}}$. Therefore, we obtain the integral fluctuation theorem

$$\left\langle e^{-\Sigma[\gamma]} \right\rangle = 1. \tag{8.82}$$

This identity has a profound physical interpretation. While the entropy production $\Sigma[\gamma]$ is non-negative on average, individual trajectories can exhibit negative values. The fluctuation theorem implies that such trajectories are exponentially rare. To see how this follows from Eq. (8.82), it is useful to partition the space of trajectories into three disjoint subsets:

$$\Gamma_+ = \{\gamma : \Sigma[\gamma] > 0\}, \quad \Gamma_0 = \{\gamma : \Sigma[\gamma] = 0\}, \quad \Gamma_- = \{\gamma : \Sigma[\gamma] < 0\}. \tag{8.83}$$

In terms of this decomposition, the integral fluctuation theorem becomes

$$\left\langle e^{-\Sigma[\gamma]} \right\rangle = \sum_{\gamma \in \Gamma_+} \mathbb{P}[\gamma]\, e^{-\Sigma[\gamma]} + \sum_{\gamma \in \Gamma_0} \mathbb{P}[\gamma] + \sum_{\gamma \in \Gamma_-} \mathbb{P}[\gamma]\, e^{-\Sigma[\gamma]}. \tag{8.84}$$

Since $e^{-\Sigma[\gamma]} < 1$ on Γ_+ and $e^{-\Sigma[\gamma]} > 1$ on Γ_-, the only way for the total to equal 1 is if there is nonzero probability weight assigned to Γ_-. Moreover, this balance also implies that the total probability mass on Γ_+ must be larger than that on Γ_-. In other words, trajectories with negative entropy production must exist, even though they are exponentially suppressed.

The ensemble-level second law also follows directly from the fluctuation theorem via Jensen's inequality. For any convex function f and random variable X, the inequality

$$\langle f(X) \rangle \geq f(\langle X \rangle) \tag{8.85}$$

holds [173]. Since $f(x) = e^{-x}$ is a convex function, applying Jensen's inequality to $\Sigma[\gamma]$ and using Eq. (8.82), we find

$$1 = \left\langle e^{-\Sigma} \right\rangle \geq e^{-\langle \Sigma \rangle} \quad \Rightarrow \quad \langle \Sigma \rangle \geq 0, \tag{8.86}$$

which recovers the ensemble version of the second law.

8.1.7 Trajectory-Level Adiabatic and Nonadiabatic Contributions

In this section, we discuss the adiabatic/nonadiabatic decomposition of entropy production at the level of individual trajectories. In analogy with the ensemble-level decomposition, the total entropy production along a trajectory γ can be split into two contributions:

$$\Sigma[\gamma] = \Sigma_{\mathrm{na}}[\gamma] + \Sigma_{\mathrm{ad}}[\gamma]. \tag{8.87}$$

We begin with the adiabatic term $\Sigma_{\mathrm{ad}}[\gamma]$. Recall that at the ensemble level, the adiabatic entropy production rate is given by

$$\dot{\Sigma}_{\mathrm{ad}}(t) = \frac{1}{2} \sum_{i,j} J_{ij}(t) \log \left(\frac{W_{ij}(\lambda_t) \pi_j^{\lambda_t}}{W_{ji}(\lambda_t) \pi_i^{\lambda_t}} \right), \tag{8.88}$$

where $J_{ij}(t)$ is the probability current from state j to i, and $\pi_i^{\lambda_t}$ denotes the instantaneous steady-state distribution. The trajectory-level counterpart is defined as

$$\Sigma_{\mathrm{ad}}[\gamma] = \sum_{k=1}^{n} \log\left(\frac{W_{i_k i_{k-1}}(\lambda_{t_k})\pi_{i_{k-1}}^{\lambda_{t_k}}}{W_{i_{k-1} i_k}(\lambda_{t_k})\pi_{i_k}^{\lambda_{t_k}}}\right), \tag{8.89}$$

where the summation runs over all jumps in the trajectory. Each term quantifies the entropy produced in maintaining the system's steady-state currents during a transition at time t_k.

We now turn to the nonadiabatic component $\Sigma_{\mathrm{na}}[\gamma]$, defined via the difference $\Sigma_{\mathrm{na}}[\gamma] \equiv \Sigma[\gamma] - \Sigma_{\mathrm{ad}}[\gamma]$. Substituting the explicit expressions for each term, we find

$$\Sigma_{\mathrm{na}}[\gamma] = \log\left(\frac{p_{i_0}(0)}{p_{i_n}(\tau)}\right) + \sum_{k=1}^{n} \log\left(\frac{\pi_{i_k}^{\lambda_{t_k}}}{\pi_{i_{k-1}}^{\lambda_{t_k}}}\right). \tag{8.90}$$

The first term can be recognized as the total change in stochastic entropy $\Delta s[\gamma]$, introduced in Eq. (8.70).

From the definition of the nonequilibrium potential, $\Phi_i(\lambda_t) = -\log \pi_i^{\lambda_t}$, we see that the second term corresponds to the trajectory-level version of the excess entropy flux, defined in Eq. (8.61), but with a minus sign:

$$\Pi_{\mathrm{ex}}[\gamma] = -\sum_{k=1}^{n} [\Phi_{i_k}(\lambda_{t_k}) - \Phi_{i_{k-1}}(\lambda_{t_k})] = -\sum_{k=1}^{n} \log\left(\frac{\pi_{i_k}^{\lambda_{t_k}}}{\pi_{i_{k-1}}^{\lambda_{t_k}}}\right). \tag{8.91}$$

This quantity corresponds to the Hatano–Sasa functional, often denoted $Y[\gamma]$ in the literature [57].

Combining the terms, we recover the Hatano–Sasa relation at the trajectory level:

$$\Delta s[\gamma] = \Sigma_{\mathrm{na}}[\gamma] - \Pi_{\mathrm{ex}}[\gamma]. \tag{8.92}$$

8.2 Three Fluctuation Theorems: the Dual and Dual-Reversed Processes

Remarkably, each component of the entropy production—adiabatic and nonadiabatic—satisfies its own fluctuation theorem [191, 60]. Just as the total entropy production can be written as the log-ratio between the probability of a trajectory and that of its time-reversed counterpart [Eq. (8.75)], each contribution admits a similar expression involving suitably constructed auxiliary dynamics:

$$\Sigma_{\mathrm{ad}}[\gamma] = \log\frac{\mathbb{P}[\gamma]}{\mathbb{P}^{+}[\gamma]}, \qquad \Sigma_{\mathrm{na}}[\gamma] = \log\frac{\mathbb{P}[\gamma]}{\widetilde{\mathbb{P}}^{+}[\tilde{\gamma}]}, \tag{8.93}$$

where $\mathbb{P}^{+}[\gamma]$ denotes the probability of a trajectory under the so-called *dual process*, and $\widetilde{\mathbb{P}}^{+}[\gamma]$ denotes the probability of the reversed trajectory under the *dual-reverse process*.

These identities have two immediate consequences. First, taking the expectation over all trajectories yields ensemble-level expressions in terms of Kullback–Leibler divergences, which are manifestly non-negative:

$$\begin{aligned}\langle \Sigma_{\mathrm{ad}}[\gamma] \rangle &= D(\mathbb{P} \,\|\, \mathbb{P}^+) \geq 0, \\ \langle \Sigma_{\mathrm{na}}[\gamma] \rangle &= D(\mathbb{P} \,\|\, \tilde{\mathbb{P}}^+) \geq 0.\end{aligned} \tag{8.94}$$

Second, applying the same reasoning used to derive the fluctuation theorem for the total entropy production [Eq. (8.79)] leads to a family of *three fluctuation theorems* [60]:

$$\left\langle e^{-\Sigma[\gamma]} \right\rangle = 1, \qquad \left\langle e^{-\Sigma_{\mathrm{ad}}[\gamma]} \right\rangle = 1, \qquad \left\langle e^{-\Sigma_{\mathrm{na}}[\gamma]} \right\rangle = 1. \tag{8.95}$$

Our goal in this section is to define the dual and dual-reversed processes $\mathbb{P}^+$ and $\tilde{\mathbb{P}}^+$ and interpret their structure, preparing the ground for the quantum generalization.

The reverse process, introduced earlier, is constructed by running the external protocol λ_t in reverse while keeping the transition governed by the same family of rate matrices $\boldsymbol{W}(\lambda_t)$. However, even for a fixed protocol λ, Markovian dynamics can break time-reversal symmetry in two distinct ways. First, the relaxation toward a steady state is inherently time-asymmetric: the state evolves toward the fixed point, not away from it. Second, when detailed balance is broken, the steady state itself supports persistent probability currents that circulate in fixed directions through state space.

In equilibrium, where detailed balance holds, this asymmetry disappears: the time-reversal of stationary dynamics coincides with the forward one. More generally, the time-reversal of a Markov chain with time-independent rates can be constructed via the *dual rate matrix*. For a fixed λ, the dual rate matrix $\boldsymbol{W}^+(\lambda)$ with respect to the steady state $\boldsymbol{\pi}^\lambda$ of $\boldsymbol{W}(\lambda)$ is defined as

$$W^+_{ij}(\lambda) = \frac{\pi^\lambda_i}{\pi^\lambda_j} W_{ji}(\lambda). \tag{8.96}$$

In matrix form, the dual rate matrix can be written as

$$\boldsymbol{W}^+ = \mathrm{diag}(\boldsymbol{\pi}) \cdot \boldsymbol{W}^\top \cdot \mathrm{diag}(\boldsymbol{\pi})^{-1}. \tag{8.97}$$

This definition ensures that the dual rate matrix $\boldsymbol{W}^+(\lambda)$ shares the same steady state as the original:

$$\sum_j W^+_{ij}(\lambda)\pi^\lambda_j = \sum_j \frac{\pi^\lambda_i}{\pi^\lambda_j} W_{ji}(\lambda)\pi^\lambda_j \tag{8.98}$$

$$= \pi^\lambda_i \sum_j W_{ji}(\lambda) = 0, \tag{8.99}$$

where we used the fact that the columns of $\boldsymbol{W}$ sum to zero.

However, the steady-state currents are reversed. Recall that the steady-state currents associated with $\boldsymbol{W}$ and π^λ are given by

$$J^{\mathrm{ss}}_{ij} = W_{ij}(\lambda)\pi^\lambda_j - W_{ji}(\lambda)\pi^\lambda_i. \tag{8.100}$$

For the dual Markov chain, the corresponding expression becomes

$$J_{ij}^{+,\mathrm{ss}} = W_{ij}^{+}(\lambda)\pi_j^{\lambda} - W_{ji}^{+}(\lambda)\pi_i^{\lambda} \tag{8.101}$$

$$= W_{ji}(\lambda)\pi_i^{\lambda} - W_{ij}(\lambda)\pi_j^{\lambda} = -J_{ij}^{\mathrm{ss}}. \tag{8.102}$$

Thus, the dual process generator inverts the direction of intrinsic steady-state currents, while the steady-state distribution remains unchanged.

In the special case of detailed balance, where $W_{ij}(\lambda)\pi_j^{\lambda} = W_{ji}(\lambda)\pi_i^{\lambda}$ for all i, j, the dual rate matrix coincides with the original: $\boldsymbol{W}^{+}(\lambda) = \boldsymbol{W}(\lambda)$. This condition defines equilibrium as the unique situation in which the Markovian dynamics is invariant under time reversal.

It is important to clarify the terminology. In the classical Markov chain literature, the Markov chain associated with $\boldsymbol{W}^{+}$ is often referred to as the *time-reversed* chain. Here, we adopt the term *dual*, more common in stochastic thermodynamics, to distinguish it from the actual *reverse process*, which refers to the dynamics generated by running the protocol λ_t in reverse, while keeping the original transition matrix $\boldsymbol{W}(\lambda)$. This distinction is essential: the reverse process inverts the protocol, while the dual generator inverts the dynamics itself, relative to a fixed steady state.

However, since $\boldsymbol{W}^{+}(\lambda)$ defines a valid rate matrix for every λ, it can also be used to define a time-dependent *dual process* by applying the instantaneous dual generator at each time:

$$\frac{\mathrm{d}\boldsymbol{p}(t)}{\mathrm{d}t} = \boldsymbol{W}^{+}(\lambda_t)\boldsymbol{p}(t). \tag{8.103}$$

This process runs the protocol λ_t forward in time, but with transition rates given by the dual generator $\boldsymbol{W}^{+}(\lambda_t)$. We denote the probability of observing a trajectory γ under the dual process by $\mathbb{P}^{+}[\gamma]$.

In the same way, we also define the *dual-reversed process*, in which the dual generator is applied in reverse protocol order: that is, the system evolves under $\boldsymbol{W}^{+}(\tilde{\lambda}_t)$, where $\tilde{\lambda}_t = \lambda_{\tau-t}$. The probability of observing a reversed trajectory $\tilde{\gamma}$ under this process is denoted $\tilde{\mathbb{P}}^{+}[\tilde{\gamma}]$.

To compute these log-ratios explicitly, consider a trajectory $\gamma = \{(i_0, 0), \ldots, (i_n, \tau)\}$. Following the same steps as in Eq. (8.67), the probability of observing γ under the dual process is given by

$$\begin{aligned}
\mathbb{P}^{+}[\gamma] &= p_{i_0}(0) \cdot \prod_{k=1}^{n} W_{i_k i_{k-1}}^{+}(\lambda_{t_k}) \cdot \exp\left(-\int_0^{\tau} \mathrm{d}t\, r_{i(t)}^{+}(t)\right) \\
&= p_{i_0}(0) \cdot \prod_{k=1}^{n} W_{i_{k-1} i_k}(\lambda_{t_k}) \cdot \frac{\pi_{i_k}^{\lambda_{t_k}}}{\pi_{i_{k-1}}^{\lambda_{t_k}}} \cdot \exp\left(-\int_0^{\tau} \mathrm{d}t\, r_{i(t)}^{+}(t)\right)
\end{aligned} \tag{8.104}$$

where $r_{i(t)}^{+} = \sum_{j \neq i} W_{ji}^{+}(\lambda_t)$ denotes the escape rate from state $i(t)$ under the dual process. By construction, the dual generator $\boldsymbol{W}^{+}$ has the same diagonal entries as the original: $W_{ii}^{+} = W_{ii}$. Consequently, the escape rates are identical:

$$r_{i(t)}^{+} = r_{i(t)}. \tag{8.105}$$

Thus, when computing the log-ratio $\log(\mathbb{P}[\gamma]/\mathbb{P}^+[\gamma])$, the initial condition $p_{i_0}(0)$ and the exponential cancel, leaving

$$\log \frac{\mathbb{P}[\gamma]}{\mathbb{P}^+[\gamma]} = \sum_{k=1}^{n} \log\left(\frac{W_{i_k i_{k-1}}(\lambda_{t_k}) \pi_{i_{k-1}}^{\lambda_{t_k}}}{W_{i_{k-1} i_k}(\lambda_{t_k}) \pi_{i_k}^{\lambda_{t_k}}} \right), \tag{8.106}$$

which matches exactly the expression for the stochastic adiabatic entropy production defined in Eq. (8.89). We thus confirm the identity

$$\Sigma_{\mathrm{ad}}[\gamma] = \log \frac{\mathbb{P}[\gamma]}{\mathbb{P}^+[\gamma]}, \tag{8.107}$$

leading directly to a fluctuation theorem.

In the equilibrium case, the dynamics is time-reversal symmetric, in the sense that $\mathbb{P}[\gamma \mid \boldsymbol{p}(0) = \boldsymbol{\pi}] = \mathbb{P}^+[\gamma \mid \boldsymbol{p}(0) = \boldsymbol{\pi}]$ for all trajectories. It follows that the adiabatic entropy production vanishes identically: $\Sigma_{\mathrm{ad}}[\gamma] = 0$. This aligns with its interpretation as the entropy generated by steady-state currents, which are absent in equilibrium.

Proceeding similarly, we compute the probability of the time-reversed trajectory $\tilde{\gamma}$ under the dual-reversed process. By definition, this process evolves under the time-reversed protocol $\tilde{\lambda}_t = \lambda_{\tau - t}$ using the dual generator $\boldsymbol{W}^+$. The path probability is then

$$\begin{aligned} \tilde{\mathbb{P}}^+[\tilde{\gamma}] &= p_{i_n}(\tau) \cdot \prod_{k=1}^{n} W^+_{i_{k-1} i_k}(\tilde{\lambda}_{\tau - t_k}) \cdot \exp\left(- \int_0^\tau \mathrm{d}t \, r^+_{i(t)}(t) \right) \\ &= p_{i_n}(\tau) \cdot \prod_{k=1}^{n} W_{i_k i_{k-1}}(\lambda_{t_k}) \cdot \frac{\pi_{i_{k-1}}^{\lambda_t}}{\pi_{i_k}^{\lambda_t}} \cdot \exp\left(- \int_0^\tau \mathrm{d}t \, r_{i(t)}(t) \right) \\ &= p_{i_n} \cdot \prod_{k=1}^{n} \frac{\pi_{i_{k-1}}^{\lambda_t}}{\pi_{i_k}^{\lambda_t}} \cdot \mathbb{P}[\gamma]. \end{aligned} \tag{8.108}$$

where in the second line we used the definition of the dual rates and the equality $r^+_{i(t)} = r_{i(t)}$, and in the third line we grouped terms to factor out the original trajectory probability $\mathbb{P}[\gamma]$.

Taking the logarithm of the ratio then yields

$$\begin{aligned} \log \frac{\mathbb{P}[\gamma]}{\tilde{\mathbb{P}}^+[\tilde{\gamma}]} &= \log \frac{p_{i_0}}{p_{i_n}} + \sum_{k=1}^{n} \log\left(\frac{\pi_{i_k}^{\lambda_t}}{\pi_{i_{k-1}}^{\lambda_t}} \right) \\ &= \Sigma_{\mathrm{na}}[\gamma]. \end{aligned} \tag{8.109}$$

which confirms the expression for the stochastic nonadiabatic entropy production given in Eq. (8.93).

Now that we have explicit expressions for the probability of observing a trajectory under each process, we can directly verify the interpretation of the dual rate matrix $\boldsymbol{W}^+$ as generating a time-reversed Markov chain. At the level of trajectory probabilities, this interpretation is captured by the identity

$$\tilde{\mathbb{P}}^+_{\lambda, \boldsymbol{\pi}^\lambda}[\tilde{\gamma}] = \mathbb{P}_{\lambda, \boldsymbol{\pi}^\lambda}[\gamma], \tag{8.110}$$

where both processes evolve under the fixed protocol $\lambda_t = \lambda$, and are initialized in the corresponding steady state $\boldsymbol{p}(0) = \boldsymbol{\pi}^\lambda$.

Fixing $\lambda_t = \lambda$ allows us to simplify the expression for the dual-reversed process probability of the reversed trajectory $\tilde{\gamma}$:

$$\begin{aligned}\tilde{\mathbb{P}}^+_{\lambda,\boldsymbol{\pi}^\lambda}[\tilde{\gamma}] &= \pi^\lambda_{i_n} \cdot \prod_{k=1}^{n} W^+_{i_{k-1}i_k}(\lambda) \cdot \exp\left(-\int_0^\tau \mathrm{d}t\, r^+_{i(t)}(t)\right) \\ &= \pi^\lambda_{i_n} \prod_{k=1}^{n} \frac{\pi^\lambda_{i_{k-1}}}{\pi^\lambda_{i_k}} \cdot \prod_{k=1}^{n} W_{i_k i_{k-1}}(\lambda) \cdot \exp\left(-\int_0^\tau \mathrm{d}t\, r^+_{i(t)}(t)\right).\end{aligned} \tag{8.111}$$

Using the telescoping identity

$$\prod_{k=1}^{n} \frac{\pi^\lambda_{i_{k-1}}}{\pi^\lambda_{i_k}} = \frac{\pi^\lambda_{i_0}}{\pi^\lambda_{i_n}}, \tag{8.112}$$

we obtain

$$\begin{aligned}\tilde{\mathbb{P}}^+_{\lambda,\boldsymbol{\pi}^\lambda}[\tilde{\gamma}] &= \pi^\lambda_{i_0} \prod_{k=1}^{n} W_{i_k i_{k-1}}(\lambda) \cdot \exp\left(-\int_0^\tau \mathrm{d}t\, r^+_{i(t)}(t)\right) \\ &= \mathbb{P}_{\lambda,\boldsymbol{\pi}^\lambda}[\gamma],\end{aligned} \tag{8.113}$$

which confirms the identity.

This equality confirms that the dual-reversed generator $\boldsymbol{W}^+$ reproduces the time-reversed statistics of the original Markov process, provided the system is initialized in its steady state. This result will serve as the starting point for constructing the dual process in the quantum case, discussed in a later section.

Quantum Case

8.3 Entropy Production in Time-Dependent Lindblad Dynamics

Having reviewed the classical framework for Markovian dynamics, we now extend the analysis of entropy production to open quantum systems governed by time-dependent Lindblad dynamics. Our goal is to generalize the adiabatic/nonadiabatic and housekeeping/excess decompositions to the quantum regime, both at the ensemble and trajectory levels. Although originally developed for classical Markov processes, these ideas carry over naturally to quantum systems under suitable conditions.

We consider a quantum system $\hat{\rho}_t$ evolving under a time-dependent Lindblad master equation:

$$\frac{\mathrm{d}\hat{\rho}_t}{\mathrm{d}t} = \mathcal{L}_{\lambda_t}[\hat{\rho}_t], \tag{8.114}$$

where λ_t is a time-dependent control parameter governed by an external protocol. The Liouvillian superoperator $\mathcal{L}_\lambda$ takes the standard Lindblad form:

$$\mathcal{L}_\lambda[\hat{\rho}] = -i[\hat{H}(\lambda), \hat{\rho}] + \sum_k \left(\hat{L}_k(\lambda)\hat{\rho}\hat{L}_k^\dagger(\lambda) - \frac{1}{2}\left\{\hat{L}_k^\dagger(\lambda)\hat{L}_k(\lambda), \hat{\rho}\right\}\right), \tag{8.115}$$

where $\hat{H}(\lambda)$ is the system Hamiltonian and $\{\hat{L}_k(\lambda)\}$ are Lindblad jump operators representing dissipative interactions with the environment.

We assume that for each fixed value of λ, the system relaxes to a unique steady state $\hat{\pi}_\lambda$, satisfying

$$\mathcal{L}_\lambda[\hat{\pi}_\lambda] = 0. \tag{8.116}$$

At this stage, we do not require any specific thermodynamic interpretation of $\hat{\pi}_\lambda$; in particular, it may not correspond to a thermal equilibrium state.

8.3.1 Entropy Production and Entropy Flux

As in the classical case, our starting point for analyzing entropy production is the time derivative of the von Neumann entropy:

$$\frac{\mathrm{d}S(t)}{\mathrm{d}t} = -\operatorname{Tr}\left[\dot{\hat{\rho}}_t \log \hat{\rho}_t\right]. \tag{8.117}$$

We aim to decompose this quantity into two contributions,

$$\frac{\mathrm{d}S(t)}{\mathrm{d}t} = \dot{\Sigma}(t) - \dot{\Pi}(t), \tag{8.118}$$

where $\dot{\Sigma}(t)$ denotes the irreversible entropy production rate, and $\dot{\Pi}(t)$ corresponds to the reversible entropy flux exchanged with the environment.

In certain settings, there is only one natural way of performing this splitting. The clearest example is that of a system coupled to a single thermal reservoir, whose steady state is a Gibbs state, $\hat{\pi}_\lambda \propto e^{-\beta \hat{H}(\lambda)}$. As shown in Chapter 3.6, the entropy production rate in this case is given by

$$\dot{\Sigma}(t) = -\frac{\mathrm{d}}{\mathrm{d}t} D\big(\hat{\rho}_t \| \hat{\pi}_{\lambda_t}\big) = \frac{\mathrm{d}S(t)}{\mathrm{d}t} - \beta \dot{Q}(t), \tag{8.119}$$

where $\dot{Q}(t)$ is the heat current from the bath and $D(\cdot\|\cdot)$ denotes the quantum relative entropy. Here, the flux term is naturally identified as $\dot{\Pi}(t) = \beta \dot{Q}(t)$, and Spohn's expression for entropy production serves as a direct quantum analogue of the classical Schnakenberg formula.

This framework also extends naturally to systems coupled to multiple thermal reservoirs. Each reservoir is modeled by a dissipative term $\mathcal{D}_\alpha$ in the master equation, associated with an inverse temperature β_α. In this setting, the entropy production rate is given by a sum of Spohn-like terms:

$$\dot{\Sigma}(t) = \sum_\alpha \operatorname{Tr}[\mathcal{D}_\alpha(\hat{\rho}_t)(\log \hat{\rho}_t - \log \hat{\omega}_\alpha)], \tag{8.120}$$

where $\hat{\omega}_\alpha$ is the thermal state associated with bath α. This generalized expression, derived in Chapter 3.6, remains non-negative and coincides with the operational notion of entropy production, $\dot{\Sigma} = \dot{S} - \sum_\alpha \dot{Q}_\alpha$. The corresponding entropy flux is given by $\dot{\Pi}(t) = \sum_\alpha \beta_\alpha \dot{Q}_\alpha$, thus preserving the structure of Eq. (8.118).

However, beyond these settings, the decomposition becomes more subtle. In open quantum systems—especially those coupled to non-thermal or structured environments—the splitting of $\dot{S}(t)$ into entropy flux and production is no longer unique. In particular, there is no universal analogue of the Schnakenberg expression [61]. The interpretation of entropy

flux becomes model-dependent, and identifying a physically meaningful entropy production rate often requires additional assumptions about the system–environment interaction [196, 197].

Even when a unique instantaneous steady state $\hat{\pi}_{\lambda_t}$ exists, the lack of a thermal interpretation introduces ambiguity. A notable intermediate case involves systems obeying *local detailed balance*, which will be briefly discussed in the next section.

Several strategies have been proposed to address these issues. One approach is to express the entropy production in the instantaneous eigenbasis of the system's state, treating the dynamics as effectively classical in that basis. While this can offer insights—especially in the presence of strong decoherence—it introduces basis dependence and may overlook coherent contributions [198, 199].

An alternative is to define entropy production at the trajectory level using quantum jump unravellings of the Lindblad equation. In this framework, the division into flux and production is performed along individual realizations of the stochastic dynamics [200, 201]. However, the resulting expressions are sensitive to the choice of measurement scheme or unravelling, leading again to non-uniqueness at the ensemble level [202].

8.3.2 Ensemble-Level Adiabatic/nonadiabatic Splitting

In this section, we extend the adiabatic/nonadiabatic decomposition of entropy production at the ensemble level to time-dependent Lindblad dynamics. As a starting point, we assume that the total entropy production rate $\dot{\Sigma}(t)$ is defined via the entropy balance introduced in the previous section. While the decomposition is generally not unique, it is well-defined for many physically relevant scenarios, including systems with a thermal steady state or those satisfying local detailed balance. Taking $\dot{\Sigma}(t)$ as given, we focus on its further division into two components with distinct physical interpretations.

As we discussed in Section 8.1, in classical Markov processes the adiabatic/nonadiabatic splitting is well-defined at both the ensemble level and along individual trajectories. Both contributions are non-negative and satisfy fluctuation theorems. In the quantum setting, the situation is more nuanced.

At the level of individual trajectories—defined via a quantum jump unravelling of the Lindblad equation, which we revisit shortly—the adiabatic/nonadiabatic splitting is only meaningful if the jump operators satisfy a specific structural condition [203, 61, 204]:

$$[\hat{\Phi}_\lambda, \hat{L}_k(\lambda)] = \Delta\phi_k(\lambda)\hat{L}_k(\lambda) \quad \text{with } \hat{\Phi}_\lambda = -\log\hat{\pi}_\lambda, \tag{8.121}$$

which ensures that each jump induces a well-defined change in the nonequilibrium potential, enabling a consistent definition of trajectory-level stochastic entropy production. Under this condition, both components of the decomposition are non-negative and satisfy fluctuation relations. We return to this point in the next section.

If these conditions are not met, a trajectory-level decomposition becomes ill-defined. Nevertheless, the decomposition can still be carried out at the ensemble level, without additional assumptions. While the resulting adiabatic term is not guaranteed to be non-negative, the decomposition remains operationally meaningful and retains the expected physical interpretation.

Most importantly, the nonadiabatic component is always non-negative and quantifies the dissipation due to the system being out of instantaneous steady state. In contrast with the adiabatic contribution—which reflects intrinsic steady-state dissipation and is often determined by the environment—the nonadiabatic term depends directly on the external protocol. As such, it is typically the component over which one has the most control, making it central to thermodynamic optimization and driving efficiency.

We now construct the decomposition of the total entropy production rate into adiabatic and nonadiabatic components at the ensemble level. The structure closely parallels the classical setting discussed in Section 8.1.3.

We begin by defining the nonadiabatic entropy production as the negative time derivative of the quantum relative entropy between the system state $\hat{\rho}_t$ and the instantaneous steady state $\hat{\pi}_{\lambda_t}$, with the derivative acting only on the first argument:

$$\dot{\Sigma}_{\mathrm{na}}(t) \equiv -\frac{\partial}{\partial s} D(\hat{\rho}_s \| \hat{\pi}_{\lambda_t})\Big|_{s=t}. \tag{8.122}$$

It quantifies the dissipation arising from the system's failure to remain in the instantaneous steady state. It vanishes in the quasistatic limit, where $\hat{\rho}_t = \hat{\pi}_{\lambda_t}$.

Taking the derivative explicitly and using the master equation yields the equivalent expression:

$$\dot{\Sigma}_{\mathrm{na}}(t) = -\operatorname{Tr}\big[\dot{\hat{\rho}}_t \big(\log \hat{\rho}_t - \log \hat{\pi}_{\lambda_t}\big)\big]. \tag{8.123}$$

This form emphasizes the dynamical origin of the nonadiabatic contribution and coincides with the entropy production rate with respect to a reference state $\hat{\pi}_{\lambda_t}$ introduced by Spohn [30] for quantum dynamical semigroups. Its non-negativity follows from the contractivity of quantum relative entropy under completely positive trace-preserving (CPTP) maps, and was discussed in detail in Chapter 3.

The adiabatic entropy production is then defined as the residual:

$$\dot{\Sigma}_{\mathrm{ad}}(t) \equiv \dot{\Sigma}(t) - \dot{\Sigma}_{\mathrm{na}}(t). \tag{8.124}$$

This term quantifies the entropy production that would persist even if the system were always in its instantaneous steady state. It typically arises from steady-state currents or irreversible processes intrinsic to the system–environment coupling and is not necessarily non-negative. In many practical settings, $\dot{\Sigma}_{\mathrm{ad}}(t)$ captures dissipation due to coupling with the environment and is often outside direct control. Nevertheless, it remains important for understanding the thermodynamic cost of maintaining nonequilibrium conditions.

8.3.3 Ensemble-Level Housekeeping/Excess Decomposition

In parallel with the adiabatic/nonadiabatic decomposition of entropy production, the entropy flux can be split into two contributions: a *housekeeping* part, associated with steady-state dissipation, and an *excess* part, arising from the time-dependent driving. Specifically, we introduce the decomposition

$$\dot{\Pi}(t) = \dot{\Pi}_{\mathrm{hk}}(t) + \dot{\Pi}_{\mathrm{ex}}(t), \tag{8.125}$$

where $\dot{\Pi}_{\mathrm{hk}}(t)$ is the *housekeeping* entropy flux required to maintain the nonequilibrium steady state, and $\dot{\Pi}_{\mathrm{ex}}(t)$ is the *excess* entropy flux induced by the protocol. This mirrors the classical decomposition introduced in Section 8.1.4.

As in the classical case, we motivate the definition of the housekeeping term by examining the steady-state behavior of the global entropy balance:

$$\frac{\mathrm{d}S}{\mathrm{d}t} = \big(\dot{\Sigma}_{\mathrm{ad}}(t) + \dot{\Sigma}_{\mathrm{na}}(t)\big) - \big(\dot{\Pi}_{\mathrm{hk}}(t) + \dot{\Pi}_{\mathrm{ex}}(t)\big). \tag{8.126}$$

In a NESS, the system entropy remains constant, and the only non-vanishing contributions are the adiabatic entropy production and the housekeeping flux. This motivates the identification

$$\dot{\Pi}_{\mathrm{hk}}(t) \equiv \dot{\Sigma}_{\mathrm{ad}}(t). \tag{8.127}$$

Unlike in the classical Markovian setting, however, there is no universal closed-form expression for the housekeeping flux in the quantum case.

The excess entropy flux is then defined as the complement:

$$\dot{\Pi}_{\mathrm{ex}}(t) \equiv \dot{\Pi}(t) - \dot{\Pi}_{\mathrm{hk}}(t). \tag{8.128}$$

To derive an explicit expression for this quantity, we use the identification $\dot{\Pi}_{\mathrm{hk}}(t) = \dot{\Sigma}_{\mathrm{ad}}(t)$ in the entropy balance equation (8.126), which yields

$$\dot{\Pi}(t) = \dot{S}(t) + \dot{\Sigma}_{\mathrm{ad}}(t). \tag{8.129}$$

Substituting the definition for each term, we find

$$\begin{aligned} \dot{\Pi}_{\mathrm{ex}}(t) &= \mathrm{Tr}\big[\dot{\hat{\rho}}_t \log \hat{\rho}_t\big] - \mathrm{Tr}\big[\dot{\hat{\rho}}_t (\log \hat{\rho}_t - \log \hat{\pi}_{\lambda_t})\big] \\ &= \mathrm{Tr}\big[\dot{\hat{\rho}}_t \log \hat{\pi}_{\lambda_t}\big]. \end{aligned} \tag{8.130}$$

This leads naturally to the introduction of the *nonequilibrium potential* [57], a Hermitian operator defined as

$$\hat{\Phi}_{\lambda_t} \equiv -\log \hat{\pi}_{\lambda_t}, \tag{8.131}$$

in terms of which the excess entropy flux becomes

$$\dot{\Pi}_{\mathrm{ex}}(t) = -\mathrm{Tr}\big[\dot{\hat{\rho}}_t \hat{\Phi}_{\lambda_t}\big]. \tag{8.132}$$

Rearranging Eq. (8.129), we obtain the quantum version of the Hatano–Sasa relation:

$$\frac{\mathrm{d}S}{\mathrm{d}t} = \dot{\Sigma}_{\mathrm{na}}(t) - \dot{\Pi}_{\mathrm{ex}}(t), \tag{8.133}$$

Integrating over the protocol duration τ yields the generalized Clausius inequality:

$$\Delta S + \int_0^\tau \mathrm{d}t\ \dot{\Pi}_{\mathrm{ex}}(t) = \int_0^\tau \mathrm{d}t\ \dot{\Sigma}_{\mathrm{na}}(t) \geq 0, \tag{8.134}$$

which refines the second law by isolating the contribution due to time-dependent driving. The left-hand side represents the total reversible entropy exchange, while the right-hand

side quantifies the irreversible dissipation. Equality holds in the quasistatic limit, where the system remains arbitrarily close to the instantaneous steady state at all times.

8.3.4 Quantum Trajectories and Jump Unraveling

In the following sections, we study entropy production at the level of individual trajectories. For systems governed by Lindblad dynamics, such trajectory-level descriptions are provided by the quantum jump formalism. This section provides a brief introduction to the method, presenting the key ingredients needed to define stochastic entropy production and formulate fluctuation theorems. For comprehensive treatments, see Refs. [193, 192, 205].

The key idea is to interpret the Lindblad master equation as the ensemble average over many realizations of a stochastic process. Each realization—or *trajectory*—consists of a sequence of random quantum jumps interspersed with coherent evolution generated by a non-Hermitian effective Hamiltonian.

To make this interpretation precise, consider a small time step of the Lindblad master equation, expanded to first order as

$$\hat{\rho}_{t+\delta t} = \hat{\rho}_t + \delta t\, \mathcal{L}[\hat{\rho}_t] + \mathcal{O}(\delta t^2), \tag{8.135}$$

where, for notational simplicity, we temporarily suppress the dependence on the control parameter λ_t. Using the explicit form of the Lindblad generator, we can rewrite the right-hand side as

$$\begin{aligned}\hat{\rho}_{t+\delta t} &= \hat{\rho}_t - \delta t\Big(i\hat{H} - \frac{1}{2}\sum_k \hat{L}_k^\dagger \hat{L}_k\Big)\hat{\rho}_t - \delta t\hat{\rho}_t\Big(-i\hat{H} - \frac{1}{2}\sum_k \hat{L}_k^\dagger \hat{L}_k\Big) + \delta t\sum_k \hat{L}_k\hat{\rho}_t\hat{L}_k^\dagger + \mathcal{O}(\delta t^2)\\ &= \hat{\rho}(t) - \delta t(\hat{H}_{\text{eff}}\hat{\rho}_t + \hat{\rho}_t\hat{H}_{\text{eff}}^\dagger) + \delta t\sum_k \hat{L}_k\hat{\rho}_t\hat{L}_k^\dagger + \mathcal{O}(\delta t^2),\end{aligned} \tag{8.136}$$

where we introduced the non-Hermitian effective Hamiltonian

$$\hat{H}_{\text{eff}} = \hat{H} - \frac{i}{2}\sum_k \hat{L}_k^\dagger \hat{L}_k. \tag{8.137}$$

This decomposition naturally leads to an operator-sum representation. Using the identity

$$(\hat{\mathbb{1}} - \delta t\,\hat{H}_{\text{eff}})\hat{\rho}_t(\hat{\mathbb{1}} - \delta t\,\hat{H}_{\text{eff}}^\dagger) = \hat{\rho}_t + \delta t\,(\hat{H}_{\text{eff}}\hat{\rho}_t + \hat{\rho}_t\hat{H}_{\text{eff}}^\dagger) + \mathcal{O}(\delta t^2), \tag{8.138}$$

we can write the time evolution step as

$$\hat{\rho}(t+\delta t) = \hat{\Omega}_0\hat{\rho}_t\hat{\Omega}_0^\dagger + \sum_k \hat{\Omega}_k\hat{\rho}_t\hat{\Omega}_k^\dagger + \mathcal{O}(\delta t^2), \tag{8.139}$$

where the Kraus operators are given by

$$\hat{\Omega}_0 = \hat{\mathbb{1}} - \delta t(i\hat{H} + \frac{1}{2}\sum_k \hat{L}_k^\dagger \hat{L}_k), \tag{8.140}$$

$$\hat{\Omega}_k = \sqrt{\delta t}\,\hat{L}_k. \tag{8.141}$$

To leading order in δt, these operators satisfy the completeness relation $\hat{\Omega}_0^\dagger \hat{\Omega}_0 + \sum_k \hat{\Omega}_k^\dagger \hat{\Omega}_k = \hat{\mathbb{1}} + \mathcal{O}(\delta t^2)$.

This operator-sum decomposition admits a natural stochastic interpretation. At each time step, the ensemble-level state evolves as a mixture of different possible outcomes. With probability $\mathbb{P}_0 \approx 1 - \delta t$, no jump occurs, and the system evolves under the non-Hermitian effective Hamiltonian:

$$\hat{\Omega}_0 = \hat{\mathbb{1}} - \delta t \hat{H}_{\text{eff}} + \mathcal{O}(\delta t^2) \approx e^{-i\hat{H}_{\text{eff}}\delta t}. \tag{8.142}$$

Alternatively, with probability $\mathbb{P}_k \approx \delta t$, a jump of type k occurs, and the system collapses to

$$\hat{\rho}_{t+\delta t} \mapsto \frac{\hat{L}_k \hat{\rho}_t \hat{L}_k^\dagger}{\text{Tr}[\hat{L}_k \hat{\rho}_t \hat{L}_k^\dagger]}. \tag{8.143}$$

In this way, the Lindblad evolution can be interpreted as a stochastic process in which the system undergoes periods of continuous, non-unitary evolution interrupted by discrete quantum jumps. This picture forms the basis of the quantum jump formalism, which we now use to construct trajectory-level descriptions of entropy production.

To proceed, we assume that the jump operators come in pairs $\{\hat{L}_k, \hat{L}_{\tilde{k}}\}$, where each pair corresponds to a single physical process occurring in two opposite directions, such as excitation/relaxation or absorption/emission. We use the notation $\tilde{k}$ to denote the jump in the opposite direction of k. However, we do not impose local detailed balance at this stage: these forward and backward processes need not be thermodynamically equilibrated.

To formulate the trajectory, we adopt the two-point measurement (TPM) scheme, in which projective measurements are carried out at the beginning and end of the protocol. For simplicity, we assume that the projective measurements at $t = 0$ and $t = \tau$ are performed in the eigenbases of $\hat{\rho}_0$ and $\hat{\rho}_\tau$, respectively. Specifically, we assume that $\hat{\rho}_0$ has spectral decomposition

$$\hat{\rho}_0 = \sum_n p_n^0 |n\rangle\langle n|, \tag{8.144}$$

and that the initial projective measurement at time $t = 0$ is performed in this eigenbasis. The measurement yields outcome n with probability $p_n^0 = \langle n|\hat{\rho}_0|n\rangle$, collapsing the state to the pure state $|n\rangle\langle n|$.

Following this initialization, the system then evolves stochastically under the quantum jump dynamics associated with a time-dependent protocol λ_t, undergoing a sequence of jumps $\{(k_j, t_j)\}_{j=1}^K$. At time $t = \tau$, a second projective measurement is performed in the eigenbasis of $\hat{\rho}_\tau$, yielding outcome m.

The full trajectory γ is then defined by the initial measurement outcome, the sequence of jumps, and the final measurement outcome:

$$\gamma = (n, \{(k_1, t_1), \dots, (k_K, t_K)\}, m). \tag{8.145}$$

Between jumps, the system evolves under the non-Hermitian effective Hamiltonian according to the map

$$\mathcal{U}_{t_b,t_a}[\hat{\rho}] = \hat{U}_{t_b,t_a} \hat{\rho}\, \hat{U}_{t_b,t_a}^\dagger, \quad \text{with} \quad \hat{U}_{t_b,t_a} = \mathcal{T} \exp\left(-i \int_{t_a}^{t_b} \mathrm{d}s\ \hat{H}_{\text{eff}}(s)\right), \tag{8.146}$$

where $\mathcal{T}$ denotes time-ordering. Each jump is represented by the superoperator

$$\mathcal{J}_k[\hat{\rho}] = \hat{L}_k \hat{\rho} \hat{L}_k^\dagger. \tag{8.147}$$

Given a record of jump events $\{(k_j, t_j)\}$, the unnormalized state at the end of the protocol, before the final measurement, is

$$\bar{\rho}_\gamma(\tau) = \mathcal{U}_{\tau,t_K} \circ \mathcal{J}_{k_K} \circ \cdots \circ \mathcal{J}_{k_1} \circ \mathcal{U}_{t_1,0}[|n\rangle\langle n|]. \tag{8.148}$$

The conditional probability density for observing this trajectory, given the initial state $|n\rangle$, is obtained by projecting $\bar{\rho}_\gamma(\tau)$ onto the final outcome $|m\rangle$:

$$\begin{aligned} \mathbb{P}[\gamma \mid n] &= \langle m|\bar{\rho}_\gamma(\tau)|m\rangle \\ &= \left|\langle m|\hat{U}_{\tau,t_K} \hat{L}_{k_K}(\lambda_{t_K}) \cdots \hat{L}_{k_1}(\lambda_{t_1}) \hat{U}_{t_1,0}|n\rangle\right|^2. \end{aligned} \tag{8.149}$$

The total probability of observing the trajectory γ is then

$$\mathbb{P}[\gamma] = p_n^0 \cdot \mathbb{P}[\gamma \mid n]. \tag{8.150}$$

We refer to this evolution—starting from the initial measurement, proceeding through stochastic quantum jumps, and ending with a final measurement at time τ—as the *forward process*.

8.3.5 Trajectory-Level Entropy Production

Entropy production at the level of individual trajectories provides a microscopic measure of irreversibility. As in the classical case, it is defined by comparing the probability of a trajectory in the forward process with that of its time-reversed counterpart. A positive entropy production indicates that the trajectory is more likely in the forward direction, consistent with the second law.

In the classical setting, the reversed process is typically constructed by time-reversing the protocol and transposing the rate matrix. In the quantum setting, it is implemented through the *time-reversal operator* $\hat{\Theta}$, which is an anti-unitary operator. This means it satisfies $\hat{\Theta}\hat{\Theta}^\dagger = \hat{\mathbb{1}}$, preserving inner products, but it acts anti-linearly on superpositions:

$$\hat{\Theta}(\alpha|\psi\rangle + \beta|\phi\rangle) = \alpha^* \hat{\Theta}|\psi\rangle + \beta^* \hat{\Theta}|\phi\rangle, \tag{8.151}$$

which can equivalently be written as the operator identity $\hat{\Theta} i = -i\hat{\Theta}$. These properties ensure that both the dynamics and observables transform correctly under time reversal, particularly in the presence of time-odd quantities such as momentum or magnetic fields.

To define the reverse process, we first time-reverse the protocol: $\tilde{\lambda}_t = \lambda_{\tau-t}$. While one could attempt to directly time-reverse the Lindblad master equation, it is more natural in this setting to apply time reversal at the level of the operator-sum decomposition used in the quantum jump formalism.

Recall from the previous section that the state update over a small time step δt admits the form

$$\hat{\rho}_{t+\delta t} = \hat{\Omega}_0(\lambda_t)\,\hat{\rho}_t\,\hat{\Omega}_0^\dagger(\lambda_t) + \sum_k \hat{\Omega}_k(\lambda_t)\,\hat{\rho}_t\,\hat{\Omega}_k^\dagger(\lambda_t) + \mathcal{O}(\delta t^2). \tag{8.152}$$

Applying the time-reversal transformation $\hat{\Theta}(\cdot)\hat{\Theta}^\dagger$ to both sides and substituting $t \mapsto \tau - t$, we obtain the operator-sum representation for a time step in the reversed dynamics:

$$\begin{aligned}
\tilde{\rho}_{t+\delta t} &= \hat{\Theta}\hat{\rho}_{\tau-t+\delta t}\hat{\Theta}^\dagger \\
&= \hat{\Theta}\left[\hat{\Omega}_0(\lambda_{\tau-t})\,\hat{\rho}_{\tau-t}\,\hat{\Omega}_0^\dagger(\lambda_{\tau-t}) + \sum_k \hat{\Omega}_k(\lambda_{\tau-t})\,\hat{\rho}_{\tau-t}\,\hat{\Omega}_k^\dagger(\lambda_{\tau-t})\right]\hat{\Theta}^\dagger + \mathcal{O}(\delta t^2) \\
&= \widetilde{\Omega}_0(\tilde{\lambda}_t)\,\tilde{\rho}_t\,\widetilde{\Omega}_0^\dagger(\tilde{\lambda}_t) + \sum_k \widetilde{\Omega}_k(\tilde{\lambda}_t)\,\tilde{\rho}_t\,\widetilde{\Omega}_k^\dagger(\tilde{\lambda}_t) + \mathcal{O}(\delta t^2),
\end{aligned} \tag{8.153}$$

where $\tilde{\rho}_t = \hat{\Theta}\hat{\rho}_{\tau-t}\hat{\Theta}^\dagger$ is the time-reversed state, and the reversed Kraus operators are defined as

$$\widetilde{\Omega}_0(\tilde{\lambda}_t) = \hat{\mathbb{1}} - \delta t\,\widetilde{H}_{\text{eff}}(\tilde{\lambda}_t), \tag{8.154}$$

$$\widetilde{\Omega}_k(\tilde{\lambda}_t) = \sqrt{\delta t}\,\widetilde{L}_k(\tilde{\lambda}_t), \tag{8.155}$$

with the time-reversed Hamiltonian and jump operators given by

$$\widetilde{H}(\tilde{\lambda}_t) = \hat{\Theta}\hat{H}(\lambda_{\tau-t})\hat{\Theta}^\dagger, \qquad \widetilde{L}_k(\tilde{\lambda}_t) = \hat{\Theta}\hat{L}_k(\lambda_{\tau-t})\hat{\Theta}^\dagger. \tag{8.156}$$

This yields a full quantum jump description of the reversed process. The no-jump propagator becomes

$$\widetilde{U}_{t_b,t_a} = \hat{\Theta}\hat{U}^\dagger_{\tau-t_a,\tau-t_b}\hat{\Theta}^\dagger, \qquad \widetilde{\mathcal{U}}_{t_b,t_a}[\hat{\rho}] = \widetilde{U}_{t_b,t_a}\hat{\rho}\widetilde{U}^\dagger_{t_b,t_a}, \tag{8.157}$$

and each jump of type k in the reverse process is represented by

$$\widetilde{\mathcal{J}}_k[\hat{\rho}] = \widetilde{L}_k(\tilde{\lambda}_t)\,\hat{\rho}\,\widetilde{L}_k^\dagger(\tilde{\lambda}_t). \tag{8.158}$$

It is important to emphasize that while the operator $\widetilde{L}_k$ is the time-reversed version of $\hat{L}_k$, it still corresponds to a jump of the same type k within the reversed dynamics. Consequently, constructing a reversed trajectory requires more than simply applying time reversal operator: we must also reverse the direction of each jump. This is where the assumption of paired jump operators $\{\hat{L}_k, \hat{L}_{\tilde{k}}\}$ proves useful: reversing the direction of a jump amounts to swapping $k \leftrightarrow \tilde{k}$. We note, however, that it is possible to define a reverse process even in more general settings where such a pairing is not available [61, 203].

To define the reverse process, we take its initial state to be the time-reversed final state of the forward process, $\tilde{\rho}_0 = \hat{\Theta}\hat{\rho}_\tau\hat{\Theta}^\dagger$. The initial projective measurement is performed in the basis $\{|\widetilde{m}\rangle = \hat{\Theta}|m\rangle\}$, which diagonalizes $\tilde{\rho}_0$. The probability of obtaining outcome $\widetilde{m}$ is

$$p_m^\tau = \langle\widetilde{m}|\tilde{\rho}_0|\widetilde{m}\rangle = \langle m|\hat{\rho}_\tau|m\rangle. \tag{8.159}$$

Crucially, this is the same as the probability of measuring $\hat{\rho}_\tau$ in its own eigenbasis. After the measurement, the state collapses to $|\widetilde{m}\rangle\langle\widetilde{m}|$.

The system then evolves under the reversed protocol $\tilde{\lambda}_t = \lambda_{\tau-t}$, undergoing a sequence of reversed jumps in reverse temporal order. At the end of the protocol, a final projective measurement is performed in the basis $\{|\tilde{n}\rangle = \hat{\Theta}|n\rangle\}$. The final state $\tilde{\rho}_\tau$ is not, in general, diagonal in this basis, but the projectors $\{|\tilde{n}\rangle\langle\tilde{n}|\}$ still form a complete set, so the measurement statistics remain well-defined.

The full reversed trajectory is thus

$$\tilde{\gamma} = (\widetilde{m}, \{(\tilde{k}_K, \tau - t_K), \dots, (\tilde{k}_1, \tau - t_1)\}, \tilde{n}), \tag{8.160}$$

where each $\tilde{k}_j$ denotes a jump of the type opposite to k_j occurring at time t_j.

Given a record of jump events, the unnormalized final state is

$$\bar{\rho}_{\tilde{\gamma}}(\tau) = \widetilde{\mathcal{U}}_{0,\tau-t_1} \circ \widetilde{\mathcal{J}}_{\tilde{k}_1} \circ \cdots \circ \widetilde{\mathcal{J}}_{\tilde{k}_K} \circ \widetilde{\mathcal{U}}_{\tau-t_K,0}[|\widetilde{m}\rangle\langle\widetilde{m}|]. \tag{8.161}$$

The conditional probability of observing $\tilde{\gamma}$ under the reverse process, given the initial state $|\widetilde{m}\rangle$, is then

$$\begin{aligned}
\tilde{\mathbb{P}}[\tilde{\gamma} \mid \widetilde{m}] &= \langle\tilde{n}|\bar{\rho}_{\tilde{\gamma}}(\tau)|\tilde{n}\rangle \\
&= \left|\langle\tilde{n}|\, \widetilde{U}_{\tau,\tau-t_1} \widetilde{L}_{\tilde{k}_1}(\tilde{\lambda}_{\tau-t_1}) \cdots \widetilde{L}_{\tilde{k}_K}(\tilde{\lambda}_{\tau-t_K}) \widetilde{U}_{\tau-t_K,0} |\widetilde{m}\rangle\right|^2 \\
&= \left|\langle\tilde{n}|\, \widetilde{U}_{\tau,\tau-t_1} \left(\prod_{j=1}^{K} \widetilde{L}_{\tilde{k}_j}(\tilde{\lambda}_{\tau-t_j})\, \widetilde{U}_{\tau-t_j,\tau-t_{j+1}}\right) |\widetilde{m}\rangle\right|^2,
\end{aligned} \tag{8.162}$$

where we set $t_{K+1} \equiv \tau$ for convenience. The total trajectory probability is then

$$\tilde{\mathbb{P}}[\tilde{\gamma}] = p^\tau_m \cdot \tilde{\mathbb{P}}[\tilde{\gamma} \mid \widetilde{m}]. \tag{8.163}$$

Finally, the entropy production along a single trajectory γ is defined as

$$\Sigma[\gamma] = \log \frac{\mathbb{P}[\gamma]}{\tilde{\mathbb{P}}[\tilde{\gamma}]}, \tag{8.164}$$

quantifying the extent to which the trajectory breaks microscopic reversibility. A positive value implies the trajectory is more likely in the forward process than in reverse, in line with the second law.

To proceed, we impose the assumption of *local detailed balance* (LDB), which encodes the thermodynamic structure of the environment and allows entropy changes to be consistently assigned to individual quantum jumps. For each pair of jump operators $\{\hat{L}_k(\lambda), \hat{L}_{\tilde{k}}(\lambda)\}$, we assume the existence of a well-defined entropy change $\Delta s_k(\lambda)$ such that

$$\hat{L}_k(\lambda) = \hat{L}^\dagger_{\tilde{k}}(\lambda)\, e^{\frac{1}{2}\Delta s_k(\lambda)}. \tag{8.165}$$

By consistency, this implies $\Delta s_{\tilde{k}}(\lambda) = -\Delta s_k(\lambda)$.

This relation allows us to express the time-reversed jump operators $\widetilde{L}_k(\tilde{\lambda}_t)$, defined earlier via time-reversal conjugation, in terms of the forward ones:

$$\widetilde{L}_k(\tilde{\lambda}_t) = \hat{\Theta}\hat{L}_k(\lambda_{\tau-t})\hat{\Theta}^\dagger = \hat{\Theta}\hat{L}^\dagger_{\tilde{k}}(\lambda_{\tau-t})\hat{\Theta}^\dagger\, e^{\frac{1}{2}\Delta s_k(\lambda_{\tau-t})}. \tag{8.166}$$

Using this expression in Eq. (8.162), along with the facts that $|\tilde{n}\rangle = \hat{\Theta}|n\rangle$ and $\langle\tilde{m}| = \langle m|\hat{\Theta}^\dagger$, we obtain

$$\begin{aligned}\tilde{\mathbb{P}}[\tilde{\gamma} \mid \widetilde{m}] &= \left|\langle\tilde{n}|\,\widetilde{U}_{\tau,\tau-t_1}\left(\prod_{j=1}^{K}\widetilde{L}_{\tilde{k}_j}(\tilde{\lambda}_{\tau-t_j})\,\widetilde{U}_{\tau-t_j,\tau-t_{j+1}}\right)|\widetilde{m}\rangle\right|^2 \\ &= \left|\langle n|\hat{\Theta}^\dagger\cdot\hat{\Theta}\hat{U}^\dagger_{0,t_1}\hat{\Theta}^\dagger\cdot\left(\prod_{j=1}^{K}e^{\frac{1}{2}\Delta s_{k_j}(\lambda_{t_j})}\hat{\Theta}\hat{L}^\dagger_{k_j}(\lambda_{t_j})\hat{\Theta}^\dagger\cdot\hat{\Theta}\hat{U}^\dagger_{t_j,t_{j+1}}\hat{\Theta}^\dagger\right)\cdot\hat{\Theta}|m\rangle\right|^2.\end{aligned} \tag{8.167}$$

Noting that each $\hat{\Theta}$ is followed by its adjoint and using the anti-unitarity condition $\hat{\Theta}\hat{\Theta}^\dagger = \hat{\mathbb{1}}$, the conditional probability simplifies to

$$\tilde{\mathbb{P}}[\tilde{\gamma} \mid \widetilde{m}] = e^{\sum_j \Delta s_{k_j}(\lambda_{t_j})}\cdot\left|\langle n|\hat{U}^\dagger_{0,t_1}\hat{L}^\dagger_{k_1}\cdots\hat{L}^\dagger_{k_K}\hat{U}^\dagger_{t_K,\tau}|m\rangle\right|^2. \tag{8.168}$$

Finally, using the identity $|\langle n|\hat{A}^\dagger|m\rangle|^2 = |\langle m|\hat{A}|n\rangle|^2$, which follows from the definition of the Hermitian adjoint, we recognize the resulting amplitude as that of the forward process, yielding

$$\tilde{\mathbb{P}}[\tilde{\gamma} \mid \widetilde{m}] = e^{\sum_j \Delta s_{k_j}(\lambda_{t_j})}\cdot\mathbb{P}[\gamma \mid n]. \tag{8.169}$$

Therefore, by Eq. (8.164), the total stochastic entropy production along the trajectory is

$$\begin{aligned}\Sigma[\gamma] &= \log\left(\frac{\mathbb{P}[\gamma \mid n]\cdot p^0_n}{\tilde{\mathbb{P}}[\tilde{\gamma} \mid \widetilde{m}]\cdot p^\tau_m}\right) \\ &= \log\frac{p^0_n}{p^\tau_m} + \log\frac{\mathbb{P}[\gamma \mid n]}{\tilde{\mathbb{P}}[\tilde{\gamma} \mid \widetilde{m}]} \\ &= -\log\frac{p^\tau_m}{p^0_n} + \sum_{j=1}^{K}\Delta s_{k_j}(\lambda_{t_j}).\end{aligned} \tag{8.170}$$

The first term can be identified as the *stochastic entropy* along the trajectory [17, 204]:

$$\Delta s[\gamma] = \log p^\tau_m - \log p^0_n = -\log\frac{p^\tau_m}{p^0_n}. \tag{8.171}$$

This quantity measures the change in the system's surprisal between the initial and final measurement outcomes, as determined by the TPM scheme.

The second term in Eq. (8.170) corresponds to the total entropy exchanged with the environment through quantum jumps. Each jump of type k_j contributes an entropy increment $\Delta s_{k_j}(\lambda_{t_j})$, so that the cumulative entropy *flux* is

$$\Pi[\gamma] = \sum_{j=1}^{K}\Delta s_{k_j}(\lambda_{t_j}). \tag{8.172}$$

Thus, the total stochastic entropy production admits the trajectory-level decomposition

$$\Sigma[\gamma] = \Delta s[\gamma] + \Pi[\gamma], \tag{8.173}$$

which parallels the classical thermodynamic structure and gives a clear operational meaning to irreversibility in the quantum setting.

As in the classical case, Eq. (8.164) immediately leads to an integral fluctuation theorem. Taking the average over all trajectories yields

$$\left\langle e^{-\Sigma[\gamma]} \right\rangle = \sum_{\gamma} \mathbb{P}[\gamma]\, e^{-\Sigma[\gamma]} = 1. \tag{8.174}$$

This identity encapsulates the statistical symmetry between forward and time-reversed dynamics. It implies that while individual trajectories can exhibit negative entropy production, these are balanced in such a way that the ensemble average remains non-negative. In particular, applying Jensen's inequality recovers the second law in the form $\langle \Sigma \rangle \geq 0$, confirming the consistency of the trajectory-level description with macroscopic thermodynamic irreversibility.

8.3.6 The Dual Dynamics

As in the classical case, deriving fluctuation theorems for the adiabatic and nonadiabatic components requires the introduction of the *dual dynamics*. This is defined by time-reversing the generator $\mathcal{L}_\lambda$ itself, at fixed λ, and is thus distinct from the reverse process, which involves inverting the full protocol. However, in contrast to the classical setting, the definition of the dual Lindblad generator is more subtle: it may not be unique and, crucially, may fail to generate a valid quantum dynamical semigroup.

The mathematical framework underpinning dual quantum dynamics has been rigorously established by Fagnola and Umanità [194], using tools from modular theory. In this formulation, the dual process is closely tied to the concept of quantum detailed balance. Here, we summarize the essential definitions and conditions for when a valid dual semigroup exists.

In the Heisenberg picture, the time evolution of observables is generated by the adjoint map $\mathcal{V}_t^\dagger = e^{\mathcal{L}^\dagger t}$, where $\mathcal{L}^\dagger$ is the adjoint Liouvillian. Given a fixed steady state $\hat{\pi}$, the s-dual of $\mathcal{V}_t^\dagger$, denoted $\mathcal{V}_t^{(s)}$, is defined as the adjoint with respect to the weighted inner product

$$\langle \hat{A}, \hat{B} \rangle_{\hat{\pi},s} = \mathrm{Tr}\left[\hat{\pi}^{1-s} \hat{A}^\dagger \hat{\pi}^s \hat{B}\right], \quad s \in [0,1]. \tag{8.175}$$

That is, $\mathcal{V}_t^{(s)}$ satisfies the identity

$$\langle \mathcal{V}_t^{(s)}(\hat{A}), \hat{B} \rangle_{\hat{\pi},s} = \langle \hat{A}, \mathcal{V}_t^\dagger(\hat{B}) \rangle_{\hat{\pi},s}. \tag{8.176}$$

Each value of $s \in [0,1]$ defines a different dual map $\mathcal{V}_t^{(s)}$. For $s = 1/2$, the map is always a quantum dynamical semigroup [194], but for other values of s, the dual may fail to be completely positive or trace-preserving.

The necessary and sufficient condition for $\mathcal{V}_t^{(0)}$ to define a quantum dynamical semigroup is the commutation of the generator with the modular automorphism associated with the steady state [194, Theorem 3.1]:

$$[\mathcal{L}^\dagger, \mathcal{M}_{\hat{\pi}}] = 0, \qquad \text{where} \quad \mathcal{M}_{\hat{\pi}}(\cdot) = \hat{\pi}(\cdot)\hat{\pi}^{-1}. \tag{8.177}$$

When this condition holds, the dual maps for all $s \in [0,1]$ coincide:

$$\mathcal{V}_t^{(s)} = \mathcal{V}_t^{(0)} \quad \forall s \in [0,1], \tag{8.178}$$

and one obtains a unique dual semigroup $\mathcal{V}_t^\star$, generated by a Liouvillian $\mathcal{L}^\star$.

To switch to the Schrödinger picture, we take the adjoint of $\mathcal{L}^\star$ under the Hilbert–Schmidt inner product:

$$\mathrm{Tr}\big[\hat{A}\mathcal{L}^+(\hat{B})\big] = \mathrm{Tr}\big[\mathcal{L}^\star(\hat{A})^\dagger \hat{B}\big]. \tag{8.179}$$

The resulting generator $\mathcal{L}^+$ can be expressed as [194, Remark 3.1, Prop. 3.2]:

$$\mathcal{L}^+(\hat{\rho}) = \hat{\pi}^s \mathcal{L}^\dagger(\hat{\pi}^{1-s}\hat{\rho}\hat{\pi}^s)\hat{\pi}^{1-s}, \quad \forall s \in [0,1]. \tag{8.180}$$

For the symmetric case $s = 1/2$, this reduces to a similarity transformation:

$$\mathcal{L}^+(\hat{\rho}) = \mathbb{J}_{\hat{\pi}} \circ \mathcal{L}^\dagger \circ \mathbb{J}_{\hat{\pi}}^{-1}(\hat{\rho}), \quad \text{with} \quad \mathbb{J}_{\hat{\pi}}(\cdot) = \hat{\pi}^{1/2}(\cdot)\hat{\pi}^{1/2}, \tag{8.181}$$

which closely mirrors the classical dual generator in Eq. (8.97) and coincides with the expression introduced by Crooks [206].

A central result of Ref. [194] concerns the representation of the generator. The Lindblad form of a quantum Markov semigroup is not unique: one may, for instance, apply unitary transformations to the jump operators without affecting the dynamics [31]. In particular, Fagnola and Umanità show that if the commutation condition

$$[\mathcal{L}^\dagger, \mathcal{M}_{\hat{\pi}}] = 0 \tag{8.182}$$

holds, then there exists a special representation—called the *privileged representation*—in which the jump operators $\hat{L}'_k$ and the Hamiltonian $\hat{H}'$ satisfy

$$\begin{aligned} \hat{\pi}\hat{L}'_k &= \alpha_k \hat{L}'_k \hat{\pi}, \\ [\hat{H}', \hat{\pi}] &= \sum_k \big[\hat{L}'^\dagger_k \hat{L}'_k, \hat{\pi}\big] = 0, \end{aligned} \tag{8.183}$$

where $\alpha_k > 0$. The constants α_k are determined by the eigenvalues of $\hat{\pi}$: given the eigendecomposition $\hat{\pi} = \sum_n \pi_n |\pi_n\rangle\langle\pi_n|$, they satisfy

$$\alpha_k = \frac{\pi_n}{\pi_m} \quad \text{for all pairs } n, m \text{ such that} \quad \langle \pi_n | \hat{L}_k | \pi_m \rangle \neq 0. \tag{8.184}$$

In other words, each jump operator $\hat{L}_k$ only connects eigenstates of $\hat{\pi}$ whose stationary probabilities are related by fixed ratio α_k, as noted in Ref. [207].

The first relation in Eq. (8.183) implies[4]

$$[\hat{L}'_k, \hat{\Phi}] = -\Delta\phi_k \, \hat{L}'_k, \tag{8.185}$$

where $\hat{\Phi} = -\log \hat{\pi}$ is the nonequilibrium potential and $\Delta\phi_k = -\log \alpha_k$ is the associated change. Thus, in the privileged representation, each jump operator $\hat{L}'_k$ corresponds to a transition with a well-defined change in nonequilibrium potential, enabling a trajectory-level decomposition of entropy production.

If the original operators $(\hat{H}, \{\hat{L}_k\})$ satisfy the conditions in Eq. (8.183), then they are already in the privileged representation. In this case, the dual quantum dynamics is guaranteed to be a Markovian semigroup, and its trajectory-level interpretation remains physically meaningful: each jump operator corresponds directly to an identifiable microscopic process with a well-defined change in nonequilibrium potential.

If this is not the case—i.e., if the original representation does not satisfy Eq. (8.183)—the dual dynamics may still form a valid quantum dynamical semigroup, provided the commutation condition (8.177) holds. While a privileged representation always exists under this condition, the resulting jump operators may involve linear combinations or transformations of the original operators and thus may not correspond to physical or experimentally meaningful trajectories. In such cases, the dual remains mathematically well-defined, but its operational interpretation becomes ambiguous.

Accordingly, in the following section we assume that the original Lindblad operators $\hat{H}$ and $\hat{L}_k$ already satisfy Eq. (8.183). This assumption enables a consistent thermodynamic interpretation and allows us to derive fluctuation theorems for the adiabatic and nonadiabatic entropy components.

8.3.7 Dual and Dual-Reverse Processes

We now derive explicit expressions for the dual jump operators $\hat{L}_k^+(\lambda)$ and no-jump propagator $\hat{U}^+_{t_b,t_a}$, and define the associated *dual* and *dual-reverse* processes.

The dual process corresponds to running the forward protocol λ_t, but evolving under the dual generator $\mathcal{L}^+(\lambda_t)$ at each time. The dual-reverse process is constructed by time-reversing the dual process:

$$\widetilde{U}^+_{t_a,t_b} = \hat{\Theta}(U^+_{\tau-t_a,\tau-t_b})^\dagger, \quad \widetilde{L}^+(\tilde{\lambda}_t) = \hat{\Theta}\hat{L}_k^+(\lambda_{\tau-t})\hat{\Theta}^\dagger. \tag{8.186}$$

We denote by $\mathbb{P}^+[\gamma]$ the probability of observing a trajectory γ under the dual process, and by $\tilde{\mathbb{P}}^+[\tilde{\gamma}]$ the probability of its time-reversal $\tilde{\gamma}$ under the dual-reverse process.

[4] This follows from the identity $e^{\hat{\Phi}}\hat{L}_k e^{-\hat{\Phi}} = e^{\mathrm{ad}_{\hat{\Phi}}}(\hat{L}_k)$, where $\mathrm{ad}_{\hat{\Phi}}(\cdot) := [\hat{\Phi}, \cdot]$. This is an important relation in Lie theory that expresses conjugation by an exponential as the exponential of the commutator map [208].

As before, we assume that the Lindblad jump operators come in conjugate pairs $\{\hat{L}_k, \hat{L}_{\tilde{k}}\}$, representing opposite directions of the same physical process. We also assume that the privileged representation conditions hold:

$$\begin{aligned} [\hat{L}_k, \hat{\Phi}] &= -\Delta\phi_k \, \hat{L}_k \quad (\text{or equivalently } \hat{\pi}\hat{L}_k = e^{\Delta\phi_k}\hat{L}_k\hat{\pi}) \\ [\hat{H}, \hat{\Phi}] &= [\sum_k \hat{L}_k^\dagger \hat{L}_k, \hat{\Phi}] = 0, \end{aligned} \tag{8.187}$$

where $\hat{\Phi} = -\log\hat{\pi}$ is the nonequilibrium potential. The second condition ensures that both the Hamiltonian $\hat{H}$ and the effective no-jump Hamiltonian $\hat{H}_{\text{eff}}$ commute with the steady state.

Additionally, we impose the *local detailed balance* condition:

$$\hat{L}_k(\lambda) = \hat{L}_{\tilde{k}}^\dagger(\lambda)\, e^{\frac{1}{2}\Delta s_k(\lambda)}. \tag{8.188}$$

which associates an entropy change Δs_k with each jump of type k. This condition implies that $\hat{L}_{\tilde{k}} \propto \hat{L}_k^\dagger$. Consequently, if $\hat{L}_k$ connects eigenstates $|\pi_m\rangle \to |\pi_n\rangle$, then $\hat{L}_{\tilde{k}}$ connects $|\pi_n\rangle \to |\pi_m\rangle$. Since $\Delta\phi_k$ reflects the logarithmic ratio of the corresponding eigenvalues, we find

$$\Delta\phi_{\tilde{k}} = -\Delta\phi_k. \tag{8.189}$$

Thus, local detailed balance ensures that conjugate jumps produce opposite changes in potential.

To determine the dual operators, we impose the condition [206, 207]

$$\tilde{\mathbb{P}}^+_{\lambda,\tilde{\pi}^\lambda}[\tilde{\gamma}] = \mathbb{P}_{\lambda,\hat{\pi}^\lambda}[\gamma], \tag{8.190}$$

which equates the probabilities of a trajectory γ under the forward process with its time-reversal $\tilde{\gamma}$ under the dual-reverse process. Here, the subscript λ indicates that the control parameter is held fixed throughout the evolution, and the initial state is taken to be the corresponding stationary state. For clarity, we suppress the explicit dependence on λ.

To illustrate the implications of this requirement, consider a quantum trajectory $\gamma = \{n, (k, t_1), m\}$ consisting of a single jump of type k occurring at time t_1, along with initial and final projective measurements in the eigenbasis of $\hat{\pi} = \sum_i \pi_i |\pi_i\rangle$. The probability of observing this trajectory under the forward process is given by

$$\mathbb{P}_{\hat{\pi}}[\gamma] = \left|\langle\pi_m|\hat{U}_{\tau,t_1}\hat{L}_k\hat{U}_{t_1,0}|\pi_n\rangle\right|^2 \cdot \pi_n. \tag{8.191}$$

We now seek expressions for the dual-reverse operators $\widetilde{L}^+_{\tilde{k}}$ and $\widetilde{U}^+_{t_b,t_a}$ such that the time-reversed trajectory $\tilde{\gamma} = \{\widetilde{m}, (\tilde{k}, \tau - t_1), \tilde{n}\}$ occurs under the dual-reverse process with the same probability. This probability is given by

$$\begin{aligned} \tilde{\mathbb{P}}^+_{\tilde{\pi}}[\tilde{\gamma}] &= \left|\langle\tilde{\pi}_n|\widetilde{U}^+_{\tau,\tau-t_1}\widetilde{L}^+_{\tilde{k}}\widetilde{U}^+_{\tau-t_1,0}|\tilde{\pi}_m\rangle\right|^2 \cdot \pi_m \\ &= \left|\langle\pi_m|\hat{U}^+_{\tau,t_1}(\hat{L}^+_{\tilde{k}})^\dagger\hat{U}^+_{t_1,0}|\pi_n\rangle\right|^2 \cdot \pi_m, \end{aligned} \tag{8.192}$$

where we inserted the identity $\hat{\mathbb{1}} = \hat{\Theta}\hat{\Theta}^\dagger$ between each operator and used the relation $|\langle n|\hat{A}^\dagger|m\rangle|^2 = |\langle m|\hat{A}|n\rangle|^2$, as in the derivation of Eq. (8.168).

To reconcile the different prefactors π_n and π_m, we can write $|\pi_n\rangle = \pi_n^{-1/2}\hat{\pi}^{1/2}|\pi_n\rangle$ and $\langle\pi_m| = \pi_m^{1/2}\langle\pi_m|\hat{\pi}^{-1/2}$, which gives

$$\mathbb{P}_{\hat{\pi}}[\gamma] = \left|\langle\pi_m|\hat{\pi}^{-1/2}\hat{U}_{\tau,t_1}\hat{L}_k\hat{U}_{t_1,0}\hat{\pi}^{1/2}|\pi_n\rangle\right|^2 \cdot \pi_m. \tag{8.193}$$

Next, we insert identities of the form $\hat{\mathbb{1}} = \hat{\pi}^{1/2}\hat{\pi}^{-1/2}$ between each operator, yielding

$$\mathbb{P}_{\hat{\pi}}[\gamma] = \left|\langle\pi_m|\,\hat{\pi}^{\frac{1}{2}}\hat{U}_{\tau,t_1}\hat{\pi}^{\frac{1}{2}}\,\hat{\pi}^{-\frac{1}{2}}\hat{L}_k\hat{\pi}^{\frac{1}{2}}\,\hat{\pi}^{-\frac{1}{2}}\hat{U}_{t_1,0}\hat{\pi}^{-\frac{1}{2}}\,|\pi_n\rangle\right|^2 \cdot \pi_m. \tag{8.194}$$

Comparing with Eq. (8.192), we identify the dual jump operators and the dual no-jump propagator:

$$\hat{L}^+_{\tilde{k}}(\lambda) = \hat{\pi}^{\frac{1}{2}}\hat{L}_k^\dagger(\lambda)\hat{\pi}^{-\frac{1}{2}}, \qquad \hat{U}^+_{t_b,t_a} = \hat{\pi}^{\frac{1}{2}}\hat{U}_{t_a,t_b}\hat{\pi}^{-\frac{1}{2}}. \tag{8.195}$$

Using the commutation $[\hat{\pi}, \hat{H}_{\text{eff}}] = 0$, we find that $\hat{U}^+_{t,t_0}$ satisfies the same differential equation as $\hat{U}_{t,t_0}$:

$$\begin{aligned}\frac{\partial\hat{U}^+_{t,t_0}}{\partial t} &= \hat{\pi}^{\frac{1}{2}}\frac{\partial\hat{U}_{t,t_0}}{\partial t}\hat{\pi}^{-\frac{1}{2}} \\ &= -i\hat{H}_{\text{eff}}\hat{\pi}^{\frac{1}{2}}\hat{U}_{t,t_0}\hat{\pi}^{-\frac{1}{2}} \\ &= -i\hat{H}_{\text{eff}}\hat{U}_{t,t_0},\end{aligned} \tag{8.196}$$

Therefore, since they share the same initial condition, $\hat{U}^+_{t_0,t_0} = \hat{U}_{t_0,t_0}$, it follows that

$$\hat{U}^+_{t_b,t_a} = \hat{U}_{t_b,t_a}. \tag{8.197}$$

From the privileged representation condition (8.187), we have $\hat{\pi}\hat{L}_k = e^{\Delta\phi_k}\hat{L}_k\hat{\pi}$, which implies that the similarity transformation by $\hat{\pi}^{1/2}$ acts as a scaling:

$$\hat{\pi}^{1/2}\hat{L}_k^\dagger\hat{\pi}^{-1/2} = e^{\frac{1}{2}\Delta\phi_k}\hat{L}_k^\dagger. \tag{8.198}$$

Using the local detailed balance condition (8.188), we then find

$$\hat{L}^+_{\tilde{k}}(\lambda_t) = e^{\Delta\phi_k(\lambda_t)}\hat{L}_k^\dagger(\lambda_t) = e^{-\frac{1}{2}(\Delta s_k(\lambda_t) - \Delta\phi_k(\lambda_t))}\hat{L}_{\tilde{k}}(\lambda_t). \tag{8.199}$$

Finally, the dual-reversed jump operators take the form:

$$\widetilde{L}^+_{\tilde{k}}(\lambda_t) = \hat{\Theta}\hat{L}^+_{\tilde{k}}(\lambda_{\tau-t})\hat{\Theta}^\dagger = e^{\Delta\phi_k(\lambda_{\tau-t})}\hat{\Theta}\hat{L}_k^\dagger(\lambda_{\tau-t})\hat{\Theta}^\dagger. \tag{8.200}$$

8.3.8 Fluctuation Theorems for the Adiabatic and Nonadiabatic Components

We now have all the necessary ingredients to define the adiabatic and nonadiabatic components of the entropy production at the trajectory level, and to derive the corresponding fluctuation theorems. As discussed previously, these components are associated with two distinct processes: the dual process and the dual-reversed process.

In analogy with the classical case, we define the trajectory-level adiabatic and nonadiabatic entropy productions as [207, 204]:

$$\Sigma_{\mathrm{ad}}[\gamma] = \log \frac{\mathbb{P}[\gamma]}{\mathbb{P}^{+}[\gamma]}, \qquad \Sigma_{\mathrm{na}}[\gamma] = \log \frac{\mathbb{P}[\gamma]}{\tilde{\mathbb{P}}^{+}[\tilde{\gamma}]}, \tag{8.201}$$

where $\mathbb{P}^{+}[\gamma]$ denotes the probability of observing the trajectory γ under the dual process, and $\tilde{\mathbb{P}}^{+}[\tilde{\gamma}]$ is the probability of its time-reversal $\tilde{\gamma}$ under the dual-reversed process.

We now derive explicit expressions for these quantities. Using the definition of the dual-reversed jump operators, we can write

$$\begin{aligned}
\tilde{\mathbb{P}}^{+}[\tilde{\gamma} \mid \pi_m] &= \left| \langle \tilde{\pi}_n | \widetilde{U}^{+}_{\tau,\tau-t_1} \widetilde{L}^{+}_{\tilde{k}_1}(\tilde{\lambda}_{\tau-t_1}) \cdots \widetilde{L}^{+}_{\tilde{k}_K}(\tilde{\lambda}_{\tau-t_K}) \widetilde{U}^{+}_{\tau-t_K,0} | \tilde{\pi}_m \rangle \right|^2 \\
&= e^{-\sum_{j=1}^{K} \Delta\phi_{k_j}} \cdot \left| \langle \pi_m | \hat{U}_{\tau,t_K} \hat{L}_{k_K}(\lambda_{t_K}) \cdots \hat{L}_{k_1}(\lambda_{t_1}) \hat{U}_{t_1,0} | \pi_n \rangle \right|^2 . \\
&= e^{-\sum_{j=1}^{K} \Delta\phi_{k_j}} \cdot \mathbb{P}[\gamma \mid \pi_n].
\end{aligned} \tag{8.202}$$

Therefore, the nonadiabatic entropy production becomes

$$\Sigma_{\mathrm{na}}[\gamma] = -\log \frac{\pi_m}{\pi_n} + \sum_{j=1}^{K} \Delta\phi_j = \Delta s[\gamma] + \Pi_{\mathrm{ex}}[\gamma], \tag{8.203}$$

where $\Delta s[\gamma] = -\log(\pi_m/\pi_n)$ is the stochastic entropy change along the trajectory. The term $\Pi_{\mathrm{ex}}[\gamma] = \sum_j \Delta\phi_{k_j}$ can be viewed as the trajectory-level counterpart of the excess flux $\dot{\Pi}_{\mathrm{ex}} = -\operatorname{Tr}[\dot{\hat{\rho}}_t \hat{\Phi}]$, thereby recovering the Hatano–Sasa relation at the trajectory level.

To obtain the adiabatic component, we apply the generalized local detailed balance condition from Eq. (8.199). The probability under the dual process is

$$\begin{aligned}
\mathbb{P}^{+}[\gamma|\pi_n] &= \left| \langle \pi_m | \hat{U}^{+}_{\tau,t_K} \hat{L}^{+}_{k_K}(\lambda_{t_K}) \cdots \hat{L}^{+}_{k_1}(\lambda_{t_1}) \hat{U}^{+}_{t_1,0} | \pi_n \rangle \right|^2 \\
&= e^{-\sum_j [\Delta s_j(\lambda_{t_j}) - \Delta\phi_{k_j}(\lambda_{t_j})]} \cdot \left| \langle \pi_m | \hat{U}_{\tau,t_K} \hat{L}_{k_K}(\lambda_{t_K}) \cdots \hat{L}_{k_1}(\lambda_{t_1}) \hat{U}_{t_1,0} | \pi_n \rangle \right|^2 \\
&= e^{-\sum_j [\Delta s_j(\lambda_{t_j}) - \Delta\phi_{k_j}(\lambda_{t_j})]} \cdot \mathbb{P}[\gamma|\pi_n]
\end{aligned} \tag{8.204}$$

from which we obtain

$$\Sigma_{\mathrm{ad}}[\gamma] = \sum_{j=1}^{K} [\Delta s_{k_j}(\lambda_{t_j}) - \Delta\phi_{k_j}(\lambda_{t_j})] = \Pi[\gamma] - \Pi_{\mathrm{ex}}[\gamma]. \tag{8.205}$$

Importantly, the sum of the adiabatic and nonadiabatic components recovers the total entropy production:

$$\Sigma[\gamma] = \Sigma_{\mathrm{ad}}[\gamma] + \Sigma_{\mathrm{na}}[\gamma] = \Delta s[\gamma] + \Pi[\gamma], \tag{8.206}$$

in agreement with Eq. (8.173).

Finally, each component satisfies a detailed fluctuation theorem:

$$\left\langle e^{-\Sigma_{\mathrm{ad}}[\gamma]} \right\rangle = 1, \qquad \left\langle e^{-\Sigma_{\mathrm{na}}[\gamma]} \right\rangle = 1, \tag{8.207}$$

which directly implies $\langle \Sigma_{\mathrm{ad}}[\gamma] \rangle \geq 0$ and $\langle \Sigma_{\mathrm{na}}[\gamma] \rangle \geq 0$. Thus, under the privileged representation conditions, both the adiabatic and nonadiabatic entropy productions are non-negative and satisfy fluctuation theorems.

9 Information geometry of transitions between quantum nonequilibrium steady states

Nonequilibrium steady states (NESS) arise in systems that are continuously driven by external forces or gradients, resulting in persistent flows of energy, particles, or entropy [209]. Unlike equilibrium states, NESS embody dynamic stability, balancing inflows and outflows while breaking detailed balance, making them central to understanding dissipation, irreversibility, and entropy production [210]. These states are central to understanding a wide range of phenomena, from classical transport to quantum thermodynamic processes, and they play a crucial role in technologies such as quantum heat engines, thermoelectric devices, and nanoscale machines [17, 211, 212].

In quantum systems, NESS offer a natural framework for studying dissipation, coherence, and transport beyond equilibrium. They are particularly important in the context of quantum technologies, where they underpin efforts to harness quantum resources for energy conversion and information processing [213, 214]. In condensed matter physics, they provide a foundation for understanding quantum transport [215, 216], emergent diffusion [217], and nonequilibrium quantum critical phenomena [49, 218].

While significant progress has been made in characterizing steady states themselves, the *transitions between* NESS remain less well understood—especially in the quantum domain. Such transitions occur naturally when external control parameters are modulated in time, as in the operation of quantum thermal machines or during driven open-system dynamics. In classical stochastic thermodynamics, these processes have been thoroughly explored through frameworks such as the Hatano–Sasa relation [219, 57, 220, 221, 222, 60, 56], which decomposes entropy production into relaxation and excess contributions, providing a deep connection between dissipation and information geometry. In contrast, the quantum case introduces additional conceptual and technical challenges, owing to coherence, noncommutativity, and the lack of a straightforward analog of detailed balance [223, 203, 61, 204].

In this chapter, we develop a geometric approach to characterize dissipation in quantum NESS-to-NESS transitions. This approach both builds on and extends classical results [56], providing a unified quantum framework for understanding and optimizing dissipation in NESS transitions. We show that the leading term of the excess entropy flux is given by the integral of a Riemannian metric along a path plus a boundary term. This boundary term is, as we discuss, precisely the excess flux of a pure relaxation process to the final NESS and the change in von Neumann entropy between initial and final NESS. In addition, we provide a completely general upper bound on the excess entropy flux in NESS transitions

which is based on recent works that explore the Fisher information with respect to time as applied to classical and quantum dynamics [224, 225, 226, 227, 228, 229, 230].

The remainder of this chapter is structured as follows. We begin by reviewing the general setup of nonequilibrium steady states in Lindblad dynamics and introduce the basic definitions of entropy production. We then derive the geometric structure associated with slow transitions, including the friction tensor, thermodynamic metric, and generalized relaxation time. Finally, we apply this formalism to a concrete example: a three-level quantum thermal machine undergoing a slow driving protocol. This example illustrates how geometric considerations can guide the design of low-dissipation protocols even in simple quantum systems.

This chapter is based on results of Ref. [62].

◆

9.1 Housekeeping/excess decomposition

In this section, we summarize the main results of Ref. [62], which studied the thermodynamic cost of driving a quantum system between nonequilibrium steady states (NESS) using slow, time-dependent control. The focus is on characterizing the entropy production, particularly the excess component, incurred during such transitions.

We begin by summarizing the decomposition of entropy flux into *housekeeping* and *excess* components, which plays a central role in the thermodynamics of nonequilibrium steady states (NESS). A more detailed discussion is provided in Chapter 8.

Consider a quantum system governed by a time-dependent Lindblad master equation,

$$\dot{\hat{\rho}}_t = \mathcal{L}_\lambda[\hat{\rho}_t], \tag{9.1}$$

where λ_t denotes a set of externally controlled parameters. For each fixed λ, we assume the existence of a unique instantaneous steady state $\hat{\pi}_\lambda$, defined by $\mathcal{L}_\lambda[\hat{\pi}_\lambda] = 0$.

We assume that the change in the system's von Neumann entropy can be decomposed as

$$\dot{S}(t) = \dot{\Sigma}(t) - \dot{\Pi}(t), \tag{9.2}$$

where $\dot{\Sigma}(t)$ is the entropy production rate and $\dot{\Pi}(t)$ is the entropy flux to the environment. For example, when the environment consists of multiple thermal baths at inverse temperatures β_α, the flux takes the form $\dot{\Pi} = \sum_\alpha \beta_\alpha \langle \hat{J}^Q_\alpha \rangle$, where $\langle \hat{J}^Q_\alpha \rangle$ is the average heat current into bath α.

As discussed in Chapter 8, the entropy production can be further decomposed into adiabatic and non-adiabatic components:

$$\dot{\Sigma}(t) = \dot{\Sigma}_{\rm ad}(t) + \dot{\Sigma}_{\rm na}(t), \tag{9.3}$$

where the non-adiabatic part captures dissipation due to deviations from the instantaneous steady state:

$$\dot{\Sigma}_{\rm na}(t) = -\frac{\partial}{\partial s} D(\hat{\rho}_s \| \hat{\pi}_{\lambda_t})\Big|_{s=t} = -\operatorname{Tr}\big[\dot{\hat{\rho}}_t (\log \hat{\rho}_t - \log \hat{\pi}_{\lambda_t})\big]. \tag{9.4}$$

The adiabatic term $\dot{\Sigma}_{\rm ad} = \dot{\Sigma} - \dot{\Sigma}_{\rm na}$ accounts for the persistent dissipation required to maintain the NESS itself.

Equivalently, this decomposition can be expressed in terms of the entropy flux. The *housekeeping* component is operationally defined as $\dot{\Pi}_{\rm hk}(t) := \dot{\Sigma}_{\rm ad}(t)$, ensuring that it is the only nonzero contribution in the steady state. The *excess* entropy flux is then defined by the remainder, $\dot{\Pi}_{\rm ex}(t) := \dot{\Pi}(t) - \dot{\Pi}_{\rm hk}(t)$. As shown in Section 8.3.3, it can be written as

$$\dot{\Pi}_{\rm ex} = \operatorname{Tr}[\dot{\hat{\rho}}_t \log \hat{\pi}_\lambda]. \tag{9.5}$$

This motivates the definition of the *nonequilibrium potential*, the Hermitian operator

$$\hat{\Phi}_\lambda = -\log \hat{\pi}_\lambda, \tag{9.6}$$

so that the excess entropy flux becomes

$$\dot{\Pi}_{\rm ex} = -\operatorname{Tr}[\dot{\hat{\rho}}_t \hat{\Phi}_\lambda]. \tag{9.7}$$

In the special case where the steady state is thermal, $\hat{\pi}_\lambda = Z_\lambda^{-1} e^{-\beta \hat{H}_\lambda}$, the nonequilibrium potential reduces to $\hat{\Phi}_\lambda = \beta \hat{H}_\lambda + \log Z_\lambda$, and the excess flux becomes $\dot{\Pi}_{\rm ex} = \beta \operatorname{Tr}[\dot{\hat{\rho}}_t \hat{H}_\lambda]$, which is the standard expression for the heat current with a factor of β.

With these definitions, we arrive at the Hatano–Sasa relation:

$$\dot{S}(t) + \dot{\Pi}_{\rm ex}(t) = \dot{\Sigma}_{\rm na}(t) \geq 0, \tag{9.8}$$

which generalizes the Clausius inequality to transitions between nonequilibrium steady states. This can be interpreted as a modified second law, renormalized by the baseline dissipation required to maintain the NESS.

9.2 Geometry of Slow NESS-to-NESS Transitions

In this section, we develop a perturbative and geometric framework for analyzing slow transitions between quantum nonequilibrium steady states, with a focus on the associated excess entropy flux. The material is based on Ref. [62].

9.2.1 Protocol

We consider a protocol in which the control parameters $\lambda_t \in \mathbb{R}^d$ are slowly varied from an initial value λ_i to a final value λ_f over a finite time interval $t \in [0, T]$. The system is initially prepared in the steady state $\hat{\pi}_{\lambda_i}$, and evolves under the time-dependent Lindblad equation as λ_t is varied. The driving stage ends at time T, after which the system is allowed to relax under the fixed Liouvillian $\mathcal{L}_{\lambda_f}$ until it reaches the final steady state $\hat{\pi}_{\lambda_f}$.

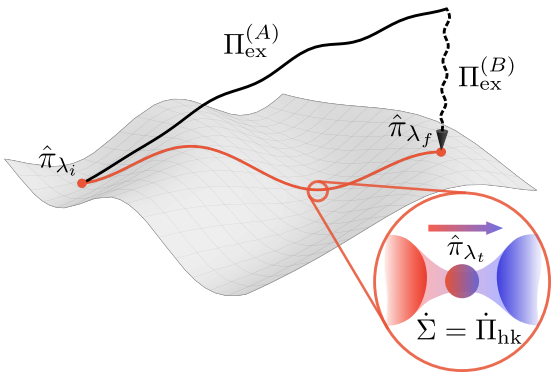

Figure 9.1: Geometric representation of a slow transition between nonequilibrium steady states (NESS). The system is initialized in the steady state $\hat{\pi}_{\lambda_i}$, and the control parameters λ_t are slowly varied (red trajectory) toward λ_f. The black curve represents the actual state trajectory $\hat{\rho}_t$, which lags behind the instantaneous NESS. The total excess entropy flux Π_{ex} splits into a driving contribution $\Pi_{\mathrm{ex}}^{(A)}$ accumulated along the protocol, and a relaxation contribution $\Pi_{\mathrm{ex}}^{(B)}$ incurred after the driving ends. The inset shows the persistent entropy production $\dot{\Sigma} = \dot{\Pi}_{\mathrm{hk}}$ required to maintain a fixed NESS.

The total excess entropy flux generated during this process naturally splits into two contributions: one accumulated during the driving stage, denoted $\Pi_{\mathrm{ex}}^{(A)}$, and one due to the final relaxation phase, denoted $\Pi_{\mathrm{ex}}^{(B)}$. This decomposition is illustrated in Fig. 9.1. The total is then

$$\Pi_{\mathrm{ex}} = \Pi_{\mathrm{ex}}^{(A)} + \Pi_{\mathrm{ex}}^{(B)}. \tag{9.9}$$

To analyze this decomposition, we examine how each term relates to the nonequilibrium potential. Taking the derivative of $\langle \hat{\Phi}_\lambda \rangle = \mathrm{Tr}[\hat{\rho}_t \hat{\Phi}_\lambda]$, we obtain

$$\begin{aligned} \frac{\mathrm{d}}{\mathrm{d}t}\langle \hat{\Phi}_\lambda \rangle &= \mathrm{Tr}\left[\frac{\mathrm{d}\hat{\rho}_t}{\mathrm{d}t}\hat{\Phi}_\lambda\right] + \mathrm{Tr}\left[\hat{\rho}_t \frac{\mathrm{d}\hat{\Phi}_\lambda}{\mathrm{d}t}\right] \\ &= -\dot{\Pi}_{\mathrm{ex}} - \mathrm{Tr}\left[\hat{\rho}_t \frac{\mathrm{d}\log\hat{\pi}_\lambda}{\mathrm{d}t}\right], \end{aligned} \tag{9.10}$$

Rearranging terms, we obtain the useful decomposition:

$$\dot{\Pi}_{\mathrm{ex}} = -\frac{\mathrm{d}}{\mathrm{d}t}\langle \hat{\Phi}_\lambda \rangle - \mathrm{Tr}\left[\hat{\rho}_t \frac{\mathrm{d}\log\hat{\pi}_\lambda}{\mathrm{d}t}\right]. \tag{9.11}$$

During the final relaxation stage, the control parameter λ_t is held fixed at λ_f, so the second term vanishes. The excess flux accumulated in the relaxation stage then becomes

$$\Pi_{\mathrm{ex}}^{(B)} = -\int_T^\infty \mathrm{d}t' \, \frac{\mathrm{d}\langle \hat{\Phi}_\lambda \rangle}{\mathrm{d}t'} = \mathrm{Tr}\left[\left(\hat{\pi}_{\lambda_f} - \hat{\rho}_T\right)\hat{\Phi}_{\lambda_f}\right]. \tag{9.12}$$

We now turn to the driving stage and develop the tools necessary to compute the path-dependent contribution $\Pi_{\mathrm{ex}}^{(A)}$, which will require a perturbative expansion around the instantaneous steady state.

9.2.2 Slow-driving Expansion

We now analyze the system's evolution during the driving stage, where the control parameters $\lambda(t)$ vary slowly from λ_i to λ_f. Although the system does not remain in a steady state at each instant, the slow variation ensures that the true state $\hat{\rho}_t$ stays close to the instantaneous steady state $\hat{\pi}_\lambda$. This motivates a perturbative expansion around $\hat{\pi}_\lambda$, which allows us to compute the path-dependent contribution $\Pi_{\rm ex}^{\rm drive}$ to the excess entropy flux.

To formalize the notion of slow driving, we introduce a small parameter $\epsilon > 0$ that characterizes the speed of the protocol:

$$\epsilon \propto \left|\frac{\mathrm{d}\lambda}{\mathrm{d}t}\right| \sim \frac{1}{T}, \tag{9.13}$$

where T is the total duration of the protocol. We assume that all components of the velocity vector $\dot{\lambda}(t)$ scale uniformly with ϵ, i.e., $\dot{\lambda}^i(t) = \mathcal{O}(\epsilon)$ for each i.

In the limit $\epsilon \to 0$, corresponding to infinitely slow driving, the system remains arbitrarily close to the instantaneous steady state $\hat{\pi}_\lambda$. For finite ϵ, however, the actual state $\hat{\rho}_t$ deviates from $\hat{\pi}_\lambda$. To characterize this deviation, we define the *lag*:

$$\hat{\rho}_t = \hat{\pi}_\lambda + \delta\hat{\rho}_t, \tag{9.14}$$

with $\mathrm{Tr}[\delta\hat{\rho}_t] = 0$ by trace preservation.

Substituting this decomposition into the master equation $\dot{\hat{\rho}}_t = \mathcal{L}_\lambda[\hat{\rho}_t]$, we find:

$$\frac{\mathrm{d}}{\mathrm{d}t}\hat{\pi}_\lambda + \frac{\mathrm{d}}{\mathrm{d}t}\delta\hat{\rho}_t = \mathcal{L}_\lambda[\hat{\pi}_\lambda] + \mathcal{L}_\lambda[\delta\hat{\rho}_t]. \tag{9.15}$$

Using $\mathcal{L}_\lambda[\hat{\pi}_\lambda] = 0$, this simplifies to

$$\left(\mathcal{L}_\lambda - \frac{\mathrm{d}}{\mathrm{d}t}\right)[\delta\hat{\rho}_t] = \frac{\mathrm{d}\hat{\pi}_\lambda}{\mathrm{d}t}. \tag{9.16}$$

In Ref. [62], we introduced an iterative solution to this equation. Here, we adopt an equivalent approach based on a perturbative expansion in the driving speed.

Specifically, we consider an expansion of the state in powers of ϵ:

$$\hat{\rho}_t = \hat{\rho}_t^{(0)} + \epsilon\hat{\rho}_t^{(1)} + \epsilon^2\hat{\rho}_t^{(2)} + \cdots, \tag{9.17}$$

where each $\hat{\rho}_t^{(n)}$ is $\mathcal{O}(1)$.

In the limit $\epsilon \to 0$, only the leading-order term $\hat{\rho}_t^{(0)}$ survives, which implies

$$\hat{\rho}_t^{(0)} = \hat{\pi}_\lambda. \tag{9.18}$$

Comparing this with Eq. (9.14), we identify the lag as the sum of higher-order corrections:

$$\delta\hat{\rho}_t = \epsilon\hat{\rho}_t^{(1)} + \epsilon^2\hat{\rho}_t^{(2)} + \cdots. \tag{9.19}$$

To compute the corrections $\hat{\rho}^{(n)}$, we substitute the expansion (9.17) into the master equation $\dot{\hat{\rho}}_t = \mathcal{L}_\lambda[\hat{\rho}_t]$ and collect terms by powers of ϵ. This step requires special attention to

the time derivatives, which raise the order in ϵ by one. While $\hat{\rho}^{(n)}$ is $\mathcal{O}(1)$, its derivative $\dot{\hat{\rho}}^{(n)}$ is $\mathcal{O}(\epsilon)$. To make this explicit, it is convenient to introduce a rescaled time variable $s = \epsilon t$, so that

$$\frac{\mathrm{d}}{\mathrm{d}t} = \epsilon \frac{\mathrm{d}}{\mathrm{d}s}.$$

In terms of the rescaled time, the master equation becomes

$$\mathcal{L}_\lambda \hat{\rho}(s) = \frac{\mathrm{d}\hat{\rho}(s)}{\mathrm{d}s} \tag{9.20}$$

Substituting the expansion (9.14) yields

$$\epsilon \frac{\mathrm{d}}{\mathrm{d}s}\big(\hat{\rho}^{(0)} + \epsilon\hat{\rho}^{(1)} + \cdots\big) = \mathcal{L}_\lambda\big[\hat{\rho}^{(0)} + \epsilon\hat{\rho}^{(1)} + \cdots\big]. \tag{9.21}$$

Matching powers of ϵ, we find:

$$\epsilon^0: \quad \mathcal{L}_\lambda \hat{\rho}^{(0)} = 0, \tag{9.22}$$

$$\epsilon^1: \quad \mathcal{L}_\lambda \hat{\rho}^{(1)} = \frac{\mathrm{d}}{\mathrm{d}s}\hat{\rho}^{(0)}, \tag{9.23}$$

$$\epsilon^2: \quad \mathcal{L}_\lambda \hat{\rho}^{(2)} = \frac{\mathrm{d}}{\mathrm{d}s}\hat{\rho}^{(1)}, \quad \text{and so on.} \tag{9.24}$$

This confirms that the zeroth-order term corresponds to the steady state:

$$\mathcal{L}_\lambda \hat{\rho}^{(0)} = 0 \quad \Rightarrow \quad \hat{\rho}^{(0)} = \hat{\pi}_\lambda. \tag{9.25}$$

The higher-order terms obey the recursive relation:

$$\mathcal{L}_\lambda \hat{\rho}^{(n)} = \frac{\mathrm{d}}{\mathrm{d}s}\hat{\rho}^{(n-1)} \qquad \text{for } n \geq 1. \tag{9.26}$$

In principle, Eq. (9.26) can be solved order by order to construct all corrections, starting from $\hat{\rho}^{(0)} = \hat{\pi}_\lambda$. However, each step involves inverting the Liouvillian $\mathcal{L}_\lambda$, which is not invertible in the usual sense: it has a non-trivial kernel containing the steady state $\hat{\pi}_\lambda$. To address this, we employ the *Drazin inverse* $\mathcal{L}_\lambda^{\mathrm{D}}$, which acts as a generalized inverse on the image of $\mathcal{L}_\lambda$. It satisfies

$$\mathcal{L}_\lambda \mathcal{L}_\lambda^{\mathrm{D}} = \mathbb{1} - \mathcal{P}_\lambda \quad \text{and} \quad \mathcal{L}_\lambda^{\mathrm{D}} \mathcal{L}_\lambda = \mathbb{1} - \mathcal{P}_\lambda, \tag{9.27}$$

where $\mathcal{P}_\lambda[\,\cdot\,] = \hat{\pi}_\lambda \operatorname{Tr}[\,\cdot\,]$ is the projection superoperator on the kernel of $\mathcal{L}_\lambda$.

We now summarize the essential properties of the Drazin inverse. For any operator $\hat{A}$, it satisfies

(i) **Partial inversion:** $\mathcal{L}_\lambda \mathcal{L}_\lambda^{\mathrm{D}}[\hat{A}] = \hat{A} - \hat{\pi}_\lambda \operatorname{Tr}\big[\hat{A}\big]$,

(ii) **Annihilation of the steady state:** $\mathcal{L}_\lambda^{\mathrm{D}}[\hat{\pi}_\lambda] = 0$,

(iii) **Traceless image:** $\operatorname{Tr}[\mathcal{L}_\lambda^{\mathrm{D}}[\hat{A}]] = 0$.

These properties ensure that $\mathcal{L}_\lambda^{\mathrm{D}}$ yields a unique solution to equations of the form $\mathcal{L}_\lambda[X] = Y$, provided that Y lies in the image of $\mathcal{L}_\lambda$, which is guaranteed when $\mathrm{Tr}[Y] = 0$. This condition is satisfied by each source term in the perturbative hierarchy.

Importantly, the Drazin inverse admits the integral representation:

$$\mathcal{L}_\lambda^{\mathrm{D}}[\hat{A}] := \int_0^\infty \mathrm{d}\tau e^{\tau\mathcal{L}_\lambda}\left(\hat{\pi}_\lambda \,\mathrm{Tr}\left[\hat{A}\right] - \hat{A}\right), \tag{9.28}$$

which will prove useful when deriving the geometric structure.

Applying $\mathcal{L}_\lambda^{\mathrm{D}}$ recursively to the hierarchy (9.26), each correction can be written as:

$$\hat{\rho}^{(n)}(s) = \left(\mathcal{L}_\lambda^{\mathrm{D}}\frac{\mathrm{d}}{\mathrm{d}s}\right)^n \hat{\pi}_\lambda, \tag{9.29}$$

so that the full state expansion becomes

$$\hat{\rho}(s) = \sum_{n=0}^{\infty} \epsilon^n \left(\mathcal{L}_\lambda^{\mathrm{D}}\frac{\mathrm{d}}{\mathrm{d}s}\right)^n \hat{\pi}_\lambda. \tag{9.30}$$

Returning to the original time variable $t = s/\epsilon$, we find:

$$\hat{\rho}_t = \hat{\pi}_\lambda + \sum_{n=1}^{\infty}\left(\mathcal{L}_\lambda^{\mathrm{D}}\frac{\mathrm{d}}{\mathrm{d}t}\right)^n \hat{\pi}_\lambda, \tag{9.31}$$

where the zeroth-order term has been written explicitly to emphasize that it corresponds to the instantaneous steady state.

This expansion expresses the lag as a series of nested derivatives and Drazin inverses acting on the instantaneous steady state. It will serve as the basis for the geometric analysis in the sections that follow.

9.2.3 Quasistatic Limit

We now use the slow-driving expansion to recover an expression for the excess entropy flux in the quasistatic limit, providing a key consistency check. We begin by analyzing the boundary contribution $\Pi_{\mathrm{ex}}^{(B)}$, which quantifies the entropy flux during the final relaxation stage. According to Eq. (9.12), this term is given by

$$\Pi_{\mathrm{ex}}^{(B)} = \mathrm{Tr}\left[(\hat{\rho}_T - \hat{\pi}_{\lambda_f})\log\hat{\pi}_{\lambda_f}\right] = \mathrm{Tr}\left[\delta\hat{\rho}_T \log\hat{\pi}_{\lambda_f}\right]. \tag{9.32}$$

At the final time, the slow-driving expansion gives $\hat{\rho}_T = \hat{\pi}_{\lambda_f} + \epsilon\,\hat{\rho}_T^{(1)} + \mathcal{O}(\epsilon^2)$. Substituting into Eq. (9.32), we find

$$\Pi_{\mathrm{ex}}^{(B)} = \epsilon\,\mathrm{Tr}\left[\hat{\rho}_T^{(1)}\log\hat{\pi}_{\lambda_f}\right] + \mathcal{O}(\epsilon^2). \tag{9.33}$$

Thus, in the quasistatic limit $\epsilon \to 0$, this contribution vanishes: $\Pi_{\mathrm{ex}}^{(B)} \to 0$. This agrees with physical intuition: as the protocol becomes infinitely slow, the system remains arbitrarily close to the instantaneous steady state at all times. In particular, the final state already coincides with $\hat{\pi}_{\lambda_f}$, and no additional relaxation is required.

It follows that in the quasistatic limit, the total excess entropy flux is entirely due to the driving stage, $\Pi_{\mathrm{ex}} = \Pi_{\mathrm{ex}}^{(A)}$. To compute this, we note that to first order, the expansion gives $\hat{\rho}_t = \hat{\pi}_\lambda + \epsilon\,\hat{\rho}_t^{(1)} + \mathcal{O}(\epsilon^2)$. Taking the time derivative yields

$$\dot{\hat{\rho}}_t = \dot{\hat{\pi}}_\lambda + \mathcal{O}(\epsilon^2). \tag{9.34}$$

Substituting into the definition of the excess entropy flux, $\dot{\Pi}_{\mathrm{ex}}(t) = \mathrm{Tr}\left[\dot{\hat{\rho}}_t \log \hat{\pi}_\lambda\right]$, we obtain

$$\begin{aligned} \dot{\Pi}_{\mathrm{ex}}(t) &= \mathrm{Tr}\left[\dot{\hat{\pi}}_\lambda \log \hat{\pi}_\lambda\right] + \mathcal{O}(\epsilon) \\ &= -\frac{\mathrm{d}}{\mathrm{d}t} S(\hat{\pi}_\lambda) + \mathcal{O}(\epsilon), \end{aligned} \tag{9.35}$$

where $S(\hat{\pi}_\lambda) = -\mathrm{Tr}[\hat{\pi}_\lambda \log \hat{\pi}_\lambda]$ is the von Neumann entropy of the instantaneous steady state. Integrating over time, we obtain the generalized Clausius equality:

$$\Delta S + \int_0^T \mathrm{d}t\, \dot{\Pi}_{\mathrm{ex}}(t) \overset{\mathrm{qs}}{=} 0, \tag{9.36}$$

where the label "qs" emphasizes that this equality holds in the quasistatic limit $\epsilon \to 0$.

This result mirrors the familiar equilibrium case, where quasistatic processes are reversible and the system entropy change is exactly balanced by the entropy exchange with the environment. Here, even though the system evolves through nonequilibrium steady states, an analogous balance holds: the excess entropy flux equals the net change in steady-state entropy. However, the process is not thermodynamically reversible in the strict sense, as the total entropy production, including the ongoing dissipation required to maintain each NESS, diverges in the quasistatic limit. Still, the system remains arbitrarily close to the instantaneous steady state at all times, and a time-reversed protocol would retrace the same trajectory of NESS in reverse order [56]. In this sense, such transitions are the nonequilibrium analogues of reversible processes, despite ongoing entropy production from steady-state maintenance.

This analogy is appealing, but it conceals a subtlety in the definition of the quasistatic limit. One might argue that if the system is always in a steady state, then no excess entropy flux should occur. Indeed, using the master equation, we can write

$$\dot{\Pi}_{\mathrm{ex}}(t) = \mathrm{Tr}[\mathcal{L}_\lambda[\hat{\rho}_t] \log \hat{\pi}_\lambda]. \tag{9.37}$$

Taking the limit $\epsilon \to 0$ directly at the level of the state gives $\hat{\rho}_t \to \hat{\pi}_\lambda$, and since $\mathcal{L}_\lambda[\hat{\pi}_\lambda] = 0$, this yields

$$\dot{\Pi}_{\mathrm{ex}}(t) \to \mathrm{Tr}[\mathcal{L}_\lambda[\hat{\pi}_\lambda] \log \hat{\pi}_\lambda] = 0, \tag{9.38}$$

which appears to contradict the earlier result.

The resolution lies in the *order of limits*. Taking the quasistatic limit before computing $\dot{\Pi}_{\mathrm{ex}}$ eliminates the first-order corrections that are responsible for the leading contribution to entropy flux. The correct procedure is to first expand $\hat{\rho}_t$ to leading order in ϵ, evaluate the observable, and only then take the limit $\epsilon \to 0$, as done in Ref. [56]. While the instantaneous

flux vanishes in this limit, it integrates to a finite value because the protocol duration scales as $T \sim \epsilon^{-1}$.

In the next subsection, we show that the next-order correction introduces a geometric structure on the space of parameters. As we will show, this structure defines a Riemannian metric on the space of control parameters, quantifying the dissipation incurred during slow transitions between nonequilibrium steady states.

9.2.4 Geometric Structure and the Friction Tensor

To go beyond the quasistatic approximation, we now include the next-order term in the slow-driving expansion. Using Eq. (9.11), the excess entropy flux rate during the driving stage is given by

$$\dot{\Pi}_{\rm ex}^{(A)} = -\frac{\mathrm{d}}{\mathrm{d}t}\langle\hat{\Phi}_\lambda\rangle - \mathrm{Tr}\Big[\hat{\rho}_t \frac{\mathrm{d}\log\hat{\pi}_\lambda}{\mathrm{d}t}\Big], \tag{9.39}$$

for $t \in [0, T]$. Substituting the slow-driving expansion, Eq. (9.31), we find

$$\dot{\Pi}_{\rm ex}^{(A)} = -\frac{\mathrm{d}}{\mathrm{d}t}\langle\hat{\Phi}_\lambda\rangle - \sum_{n=1}^{\infty}\mathrm{Tr}\left[\frac{\mathrm{d}\log\hat{\pi}_\lambda}{\mathrm{d}t}\left(\mathcal{L}_\lambda^{\rm D}\frac{\mathrm{d}}{\mathrm{d}t}\right)^n\hat{\pi}_\lambda\right], \tag{9.40}$$

where we used $\mathrm{Tr}[\hat{\pi}_\lambda\,\partial_t\log\hat{\pi}_\lambda] = 0$, as shown in Appendix A.1, to eliminate the $n = 0$ term.

Integrating over the protocol duration and keeping only the leading-order term in ϵ, we obtain

$$\Pi_{\rm ex}^{(A)} = -\langle\hat{\Phi}_\lambda\rangle\Big|_0^T - \int_0^T \mathrm{d}t\ \mathrm{Tr}\left[\frac{\mathrm{d}\log\hat{\pi}_\lambda}{\mathrm{d}t}\mathcal{L}_\lambda^{\rm D}\frac{\mathrm{d}\hat{\pi}_\lambda}{\mathrm{d}t}\right] + \mathcal{O}(\epsilon^2), \tag{9.41}$$

where the boundary contribution is given by

$$\langle\hat{\Phi}_\lambda\rangle\Big|_0^T = -\mathrm{Tr}\big[\hat{\rho}_T\log\hat{\pi}_{\lambda_f}\big] + \mathrm{Tr}\big[\hat{\pi}_{\lambda_i}\log\hat{\pi}_{\lambda_i}\big]. \tag{9.42}$$

This term naturally splits into a change in steady-state entropy and the excess contribution from the final relaxation stage. Expanding the final state as $\hat{\rho}_T = \hat{\pi}_{\lambda_f} + \delta\hat{\rho}_T$, we find

$$\begin{aligned}\langle\hat{\Phi}_\lambda\rangle\Big|_0^T &= -\mathrm{Tr}\big[\hat{\pi}_{\lambda_f}\log\hat{\pi}_{\lambda_f}\big] - \mathrm{Tr}\big[\delta\hat{\rho}_T\log\hat{\pi}_{\lambda_f}\big] + \mathrm{Tr}\big[\hat{\pi}_{\lambda_i}\log\hat{\pi}_{\lambda_i}\big]\\ &= S(\hat{\pi}_{\lambda_f}) - S(\hat{\pi}_{\lambda_i}) - \mathrm{Tr}\big[\delta\hat{\rho}_T\log\hat{\pi}_{\lambda_f}\big]\\ &= \Delta S(\hat{\pi}_\lambda) + \Pi_{\rm ex}^{(B)}.\end{aligned} \tag{9.43}$$

Substituting into Eq. (9.41), we obtain the total excess entropy flux:

$$\Pi_{\rm ex} = -\Delta S(\hat{\pi}_\lambda) - \int_0^T \mathrm{d}t\ \mathrm{Tr}\left[\frac{\mathrm{d}\log\hat{\pi}_\lambda}{\mathrm{d}t}\mathcal{L}_\lambda^{\rm D}\frac{\mathrm{d}\hat{\pi}_\lambda}{\mathrm{d}t}\right] + \mathcal{O}(\epsilon^2). \tag{9.44}$$

This formulation allows us to relax the assumption that the protocol has vanishing velocity at the endpoints, thereby generalizing the treatment in Ref. [56].

To proceed, we use the chain rule to express the time derivative in terms of the protocol velocity:

$$\frac{\mathrm{d}}{\mathrm{d}t} = \sum_\mu \dot{\lambda}^\mu \frac{\partial}{\partial\lambda_\mu}$$

Substituting into the integrand of Eq. (9.44) yields

$$\mathrm{Tr}\left[\frac{\mathrm{d}\log\hat{\pi}_\lambda}{\mathrm{d}t}\mathcal{L}_\lambda^\dagger\frac{\mathrm{d}\hat{\pi}_\lambda}{\mathrm{d}t}\right] = -\sum_{\mu\nu}\dot{\lambda}^\mu\dot{\lambda}^\nu\,\mathrm{Tr}\left[\frac{\partial\log\hat{\pi}_\lambda}{\partial\lambda_\nu}\mathcal{L}_\lambda^\dagger\frac{\partial\hat{\pi}_\lambda}{\partial\lambda_\mu}\right]. \tag{9.45}$$

We define the (generally asymmetric) tensor

$$\xi_{\mu\nu} = -\,\mathrm{Tr}\left[\frac{\partial\log\hat{\pi}_\lambda}{\partial\lambda_\nu}\mathcal{L}_\lambda^\dagger\frac{\partial\hat{\pi}_\lambda}{\partial\lambda_\mu}\right], \tag{9.46}$$

so that the integrand becomes

$$\mathrm{Tr}\left[\frac{\mathrm{d}\log\hat{\pi}_\lambda}{\mathrm{d}t}\mathcal{L}_\lambda^\dagger\frac{\mathrm{d}\hat{\pi}_\lambda}{\mathrm{d}t}\right] = -\sum_{\mu\nu}\dot{\lambda}^\mu\xi_{\mu\nu}\dot{\lambda}^\nu. \tag{9.47}$$

Since the quadratic form $\sum_{\mu\nu}\dot{\lambda}^\mu\xi_{\mu\nu}\dot{\lambda}^\nu$ is symmetric under exchange of indices $\mu\leftrightarrow\nu$, only the symmetric part of $\xi_{\mu\nu}$ contributes to the sum:

$$\sum_{\mu\nu}\dot{\lambda}^\mu\xi_{\mu\nu}\dot{\lambda}^\nu = \frac{1}{2}\sum_{\mu\nu}\dot{\lambda}^\mu\xi_{\mu\nu}\dot{\lambda}^\nu + \frac{1}{2}\sum_{\mu\nu}\dot{\lambda}^\nu\xi_{\nu\mu}\dot{\lambda}^\mu \tag{9.48}$$

$$= \frac{1}{2}\sum_{\mu\nu}\dot{\lambda}^\mu(\xi_{\mu\nu}+\xi_{\nu\mu})\dot{\lambda}^\nu. \tag{9.49}$$

This motivates the definition of the *friction tensor* as the symmetric part of $\xi_{\mu\nu}$:

$$\zeta_{\mu\nu} := \frac{1}{2}(\xi_{\mu\nu}+\xi_{\nu\mu}), \tag{9.50}$$

With this definition, the excess entropy flux takes the form

$$\Pi_{\mathrm{ex}} = -\Delta S(\hat{\pi}_\lambda) + \sum_{\mu\nu}\int_0^T \mathrm{d}t\,\dot{\lambda}^\mu\zeta_{\mu\nu}\dot{\lambda}^\nu + \mathcal{O}(\epsilon^2). \tag{9.51}$$

9.3 Positivity of the friction tensor

In this section, we prove that the friction tensor $\zeta_{\mu\nu}(\lambda)$ is positive semidefinite for any value of the control parameters λ. To do so, we first show that it determines the leading-order contribution to the non-adiabatic entropy production rate $\dot{\Sigma}_{\mathrm{na}}$:

$$\dot{\Sigma}_{\mathrm{na}} = \sum_{\mu\nu}\dot{\lambda}_\mu\zeta_{\mu\nu}\dot{\lambda}_\nu + \mathcal{O}(\epsilon^3). \tag{9.52}$$

We begin with the leading-order expression for the excess entropy flux rate during the driving stage:

$$\dot{\Pi}_{\mathrm{ex}}^{(A)} = -\frac{\mathrm{d}\langle\hat{\Phi}_\lambda\rangle}{\mathrm{d}t} + \sum_{\mu\nu}\dot{\lambda}_\mu\zeta_{\mu\nu}\dot{\lambda}_\nu + \mathcal{O}(\epsilon^3) \tag{9.53}$$

Using the Hatano–Sasa decomposition from Eq. (9.8), we write

$$\dot{\Pi}_{\mathrm{ex}}^{(A)} = \dot{\Sigma}_{\mathrm{na}} - \dot{S}.$$

Inserting this into Eq. (9.53) and rearranging terms, we find

$$\dot{\Sigma}_{\mathrm{na}} = \sum_{\mu\nu} \dot{\lambda}_\mu \zeta_{\mu\nu} \dot{\lambda}_\nu - \frac{\mathrm{d}}{\mathrm{d}t}\big(\langle \hat{\Phi}_\lambda \rangle - S(\hat{\rho}_t)\big) + \mathcal{O}(\epsilon^3). \tag{9.54}$$

The difference $\langle \hat{\Phi}_\lambda \rangle - S(\hat{\rho}_t)$ is, in fact, the relative entropy between $\hat{\rho}_t$ and the instantaneous steady state $\hat{\pi}_\lambda$:

$$D(\hat{\rho}_t \| \hat{\pi}_\lambda) = \mathrm{Tr}[\hat{\rho}_t(\log \hat{\rho}_t - \log \hat{\pi}_\lambda)] = -S(\hat{\rho}_t) + \langle \hat{\Phi}_\lambda \rangle. \tag{9.55}$$

Therefore, we have

$$\dot{\Sigma}_{\mathrm{na}} = \sum_{\mu\nu} \dot{\lambda}_\mu \zeta_{\mu\nu} \dot{\lambda}_\nu - \frac{\mathrm{d}}{\mathrm{d}t} D(\hat{\rho} || \hat{\pi}_\lambda) + \mathcal{O}(\epsilon^3). \tag{9.56}$$

To complete the argument, we show that $\frac{\mathrm{d}}{\mathrm{d}t} D(\hat{\rho}_t \| \hat{\pi}_\lambda) = \mathcal{O}(\epsilon^3)$, and is therefore negligible to leading order. The operator logarithm admits the expansion [185]

$$\log(\hat{\pi}_\lambda + \delta\hat{\rho}_t) = \log \hat{\pi}_\lambda + \mathbb{J}_{\hat{\pi}}^{-1}(\delta\hat{\rho}_t) + \mathcal{O}(\epsilon^2), \tag{9.57}$$

where $\mathbb{J}_{\hat{\pi}}^{-1}$ is the super-operator

$$\mathbb{J}_{\hat{\pi}}^{-1}(\cdot) = \int_0^\infty \mathrm{d}s\, (\hat{\pi} + s\mathbb{1})^{-1}(\cdot)(\hat{\pi} + s\mathbb{1})^{-1}, \tag{9.58}$$

which is the inverse of the Kubo–Mori operator we introduced in Chapter 7: [185]

$$\mathbb{J}_{\hat{\pi}}(\cdot) = \int_0^1 \mathrm{d}s\, \hat{\pi}_\lambda^s(\cdot)\hat{\pi}_\lambda^{1-s}, \tag{9.59}$$

so that $\mathbb{J}_{\hat{\pi}}\mathbb{J}_{\hat{\pi}}^{-1}(\hat{X}) = \hat{X}$ for all $\hat{X}$. In particular, since $\mathbb{J}_{\hat{\pi}}(\hat{\mathbb{1}}) = \hat{\pi}_\lambda$, it follows that

$$\mathbb{J}_{\hat{\pi}}^{-1}(\hat{\pi}_\lambda) = \hat{\mathbb{1}}. \tag{9.60}$$

Substituting the expansion into the definition of the relative entropy, we obtain

$$\begin{aligned} D(\hat{\pi}_\lambda + \delta\hat{\rho}_t \| \hat{\pi}_\lambda) &= \mathrm{Tr}[(\hat{\pi}_\lambda + \delta\hat{\rho}_t)(\log \hat{\pi}_\lambda + \mathbb{J}_{\hat{\pi}}^{-1}(\delta\hat{\rho}_t) - \log \hat{\pi}_\lambda)] + \mathcal{O}(\epsilon^3) && (9.61)\\ &= \mathrm{Tr}[\hat{\pi}_\lambda\, \mathbb{J}_{\hat{\pi}}^{-1}(\delta\hat{\rho}_t)] + \mathrm{Tr}[\delta\hat{\rho}_t\, \mathbb{J}_{\hat{\pi}}^{-1}(\delta\hat{\rho}_t)] + \mathcal{O}(\epsilon^3). && (9.62) \end{aligned}$$

The Kubo–Mori inverse $\mathbb{J}_{\hat{\pi}}^{-1}$ is self-adjoint with respect to the Hilbert–Schmidt inner product [185]. As a result, the first term in the expansion vanishes:

$$\begin{aligned} \mathrm{Tr}[\hat{\pi}_\lambda\, \mathbb{J}_{\hat{\pi}}^{-1}(\delta\hat{\rho}_t)] &= \mathrm{Tr}[\mathbb{J}_{\hat{\pi}}^{-1}(\hat{\pi}_\lambda)\, \delta\hat{\rho}_t] \\ &= \mathrm{Tr}[\delta\hat{\rho}_t] = 0, \end{aligned} \tag{9.63}$$

since $\mathbb{J}_{\hat{\pi}}^{-1}(\hat{\pi}_\lambda) = \mathbb{1}$ and $\delta\hat{\rho}_t$ is traceless. Therefore,

$$D(\hat{\pi}_\lambda + \delta\hat{\rho}_t \| \hat{\pi}_\lambda) = \mathrm{Tr}[\delta\hat{\rho}_t\, \mathbb{J}_{\hat{\pi}}^{-1}(\delta\hat{\rho}_t)] + \mathcal{O}(\epsilon^3). \tag{9.64}$$

Since $\delta\hat{\rho}_t = \mathcal{O}(\epsilon)$, the relative entropy is $\mathcal{O}(\epsilon^2)$, and its time derivative is $\mathcal{O}(\epsilon^3)$:

$$\frac{\mathrm{d}}{\mathrm{d}t} D(\hat{\rho}_t \| \hat{\pi}_\lambda) = \mathcal{O}(\epsilon^3). \tag{9.65}$$

Substituting this result into Eq. (9.56) gives

$$\dot{\Sigma}_{\mathrm{na}} = \sum_{\mu\nu} \dot{\lambda}_\mu \zeta_{\mu\nu} \dot{\lambda}_\nu + \mathcal{O}(\epsilon^3), \tag{9.66}$$

and integrating over the path yields

$$\int_0^T \mathrm{d}t\, \dot{\Sigma}_{\mathrm{na}} = \int_0^T \mathrm{d}t \sum_{\mu\nu} \dot{\lambda}_\mu \zeta_{\mu\nu} \dot{\lambda}_\nu + \mathcal{O}(\epsilon^2), \tag{9.67}$$

We now turn to the main claim of this section: the friction tensor $\zeta_{\mu\nu}(\lambda)$ is positive semidefinite for all values of the control parameters λ. To prove this, it suffices to show that for any real vector $x \in \mathbb{R}^d$,

$$\sum_{\mu\nu} x_\mu\, \zeta_{\mu\nu}(\lambda)\, x_\nu \geq 0. \tag{9.68}$$

To show this, fix an arbitrary point λ_0 in parameter space and consider a linear protocol of the form $\lambda_t = \lambda_0 + \epsilon x t$, where x is a constant vector and ϵ is a small parameter. Substituting into Eq. (9.66), we find

$$\dot{\Sigma}_{\mathrm{na}} = \epsilon^2 \sum_{\mu\nu} x_\mu\, \zeta_{\mu\nu}(\lambda_0)\, x_\nu + \mathcal{O}(\epsilon^3). \tag{9.69}$$

Since $\dot{\Sigma}_{\mathrm{na}} \geq 0$ for all protocols and ϵ can be made arbitrarily small, the leading-order term must also be non-negative.

This establishes that the friction tensor $\zeta_{\mu\nu}(\lambda)$ defines a positive semidefinite, symmetric bilinear form, and thus constitutes a Riemannian metric on the space of control parameters.

9.3.1 Green-Kubo Relations and the Quantum Fisher Information

We now derive an alternative representation of the friction tensor $\zeta_{\mu\nu}$ in terms of steady-state correlation functions. This Green–Kubo-type expression reveals how $\zeta_{\mu\nu}$ captures the system's linear response to slow driving and connects it to the quantum Fisher information.

We begin by recalling the unsymmetrized expression:

$$\xi_{\mu\nu} = -\operatorname{Tr}\left[\frac{\partial \log \hat{\pi}_\lambda}{\partial \lambda^\nu}\, \mathcal{L}_\lambda^{\mathrm{D}}\left(\frac{\partial \hat{\pi}_\lambda}{\partial \lambda^\mu}\right)\right], \tag{9.70}$$

where $\mathcal{L}_\lambda^{\mathrm{D}}$ denotes the Drazin inverse of the Liouvillian $\mathcal{L}_\lambda$. This structure already suggests a connection to the Kubo–Mori–Bogoliubov (KMB) quantum Fisher information introduced in Chapter 7. To make this connection precise, we first recall that the logarithmic derivative of the steady state is given by

$$\hat{F}^\mu = \frac{\partial \log \hat{\pi}_\lambda}{\partial \lambda^\mu}. \tag{9.71}$$

As discussed in that chapter, the derivative of the steady state with respect to a control parameter can be expressed as

$$\frac{\partial \hat{\pi}_\lambda}{\partial \lambda^\mu} = \int_0^1 \mathrm{d}s\, \hat{\pi}_\lambda^s \hat{F}^\mu \hat{\pi}_\lambda^{1-s} = \mathbb{J}_{\hat{\pi}_\lambda}[\hat{F}^\mu], \tag{9.72}$$

where $\mathbb{J}_{\hat{\pi}_\lambda}[\,\cdot\,] = \int_0^1 \mathrm{d}s\, \hat{\pi}_\lambda^s(\cdot)\,\hat{\pi}_\lambda^{1-s}$ is the KMB weighting operator. The corresponding Fisher information matrix is then defined via the KMB inner product:

$$\mathcal{I}_{\mu\nu} = \langle \hat{F}^\mu, \hat{F}^\nu \rangle_{\hat{\pi}_\lambda} = \mathrm{Tr}\Big[\hat{F}^\mu\, \mathbb{J}_{\hat{\pi}_\lambda}[\hat{F}^\nu]\Big]. \tag{9.73}$$

Using this notation, we can rewrite the unsymmetrized friction tensor as

$$\xi_{\mu\nu} = -\,\mathrm{Tr}\Big[\hat{F}^\mu\, \mathcal{L}_\lambda^{\mathrm{D}}\Big(\mathbb{J}_{\hat{\pi}_\lambda}[\hat{F}^\nu]\Big)\Big]. \tag{9.74}$$

This expression closely resembles the KMB inner product, except that the presence of the Drazin inverse introduces dynamical dependence that goes beyond the static geometry encoded in $\mathcal{I}_{\mu\nu}$.

To bring this into the form of a Green–Kubo relation, we invoke the integral representation of the Drazin inverse:

$$\mathcal{L}_\lambda^{\mathrm{D}}[\hat{A}] = \int_0^\infty \mathrm{d}\tau e^{\tau\mathcal{L}_\lambda}\Big(\hat{\pi}_\lambda\,\mathrm{Tr}\Big[\hat{A}\Big] - \hat{A}\Big). \tag{9.75}$$

Since $\mathrm{Tr}[\partial_{\lambda^\mu}\hat{\pi}_\lambda] = 0$, the trace term vanishes, and we find

$$\begin{aligned}\xi_{\mu\nu} &= \int_0^\infty \mathrm{d}\tau\,\mathrm{Tr}\Big[\frac{\partial \log\hat{\pi}_\lambda}{\partial\lambda^\nu}\, e^{\tau\mathcal{L}_\lambda}\Big(\frac{\partial\hat{\pi}_\lambda}{\partial\lambda^\mu}\Big)\Big] \\ &= \int_0^\infty \mathrm{d}\tau\,\mathrm{Tr}\Big[\hat{F}^\nu\, e^{\tau\mathcal{L}_\lambda}\Big(\frac{\partial\hat{\pi}_\lambda}{\partial\lambda^\mu}\Big)\Big].\end{aligned} \tag{9.76}$$

We now switch to the Heisenberg picture, where observables evolve under the adjoint Liouvillian $\mathcal{L}_\lambda^\dagger$:

$$\hat{\mathcal{O}}(\tau) = e^{\tau\mathcal{L}_\lambda^\dagger}\hat{\mathcal{O}}, \qquad \text{with} \quad \mathrm{Tr}[\hat{A}\,\mathcal{L}_\lambda(\hat{B})] = \mathrm{Tr}[\mathcal{L}_\lambda^\dagger(\hat{A})\,\hat{B}]. \tag{9.77}$$

This allows us to move the time-evolution operator to the left:

$$\mathrm{Tr}\Big[\hat{F}^\nu\, e^{\tau\mathcal{L}_\lambda}\Big(\frac{\partial\hat{\pi}_\lambda}{\partial\lambda^\mu}\Big)\Big] = \mathrm{Tr}\Big[e^{\tau\mathcal{L}_\lambda^\dagger}(\hat{F}^\nu)\,\frac{\partial\hat{\pi}_\lambda}{\partial\lambda^\mu}\Big]. \tag{9.78}$$

The symmetrized friction tensor is obtained by averaging $\xi_{\mu\nu}$ and $\xi_{\nu\mu}$:

$$\zeta_{\mu\nu} = \frac{1}{2}(\xi_{\mu\nu} + \xi_{\nu\mu}). \tag{9.79}$$

Each term corresponds to a one-sided integral of a time correlation function. Combining them, we obtain:

$$\zeta_{\mu\nu} = \frac{1}{2}\int_0^\infty \mathrm{d}\tau\langle\hat{F}^\mu(0),\hat{F}^\nu(\tau)\rangle_{\hat{\pi}_\lambda} + \frac{1}{2}\int_0^\infty \mathrm{d}\tau\langle\hat{F}^\nu(0),\hat{F}^\mu(\tau)\rangle_{\hat{\pi}_\lambda}, \tag{9.80}$$

where the correlation function is defined with respect to the KMB inner product.

To isolate the geometric and dynamical content more cleanly, we define the generalized integral relaxation time:

$$\tau_{\mu\nu} = \int_0^\infty \mathrm{d}\tau \frac{\langle \hat{F}^\mu(0), \hat{F}^\nu(\tau)\rangle_{\hat{\pi}_\lambda}}{\langle \hat{F}^\mu, \hat{F}^\nu\rangle_{\hat{\pi}_\lambda}}. \tag{9.81}$$

With this, the friction tensor takes the form

$$\zeta_{\mu\nu} = \frac{1}{2}\big(\tau_{\mu\nu}\mathcal{J}_{\mu\nu} + \tau_{\nu\mu}\mathcal{J}_{\nu\mu}\big), \tag{9.82}$$

expressing it as a symmetrized product of dynamical and geometric quantities.

In the special case of systems satisfying detailed balance, the steady-state correlation functions are symmetric under time reversal:

$$\langle \hat{F}^\mu(0), \hat{F}^\nu(\tau)\rangle = \langle \hat{F}^\nu(0), \hat{F}^\mu(\tau)\rangle.$$

In this case, both $\tau_{\mu\nu}$ and $\mathcal{J}_{\mu\nu}$ are symmetric, and the friction tensor reduces to

$$\zeta_{\mu\nu} = \tau_{\mu\nu}\mathcal{J}_{\mu\nu} = \frac{1}{2}\int_{-\infty}^{\infty} \mathrm{d}\tau \,\langle \hat{F}^\mu(0), \hat{F}^\nu(\tau)\rangle_{\hat{\pi}_\lambda}.$$

We note that in such equilibrium settings, the positivity of $\zeta_{\mu\nu}$ follows directly from the time symmetry of the correlation function [56].

9.3.2 Optimization: Geodesics in Parameter Space

Having established that the leading-order excess entropy flux in a slow-driving protocol is given by the action of a Riemannian metric $\zeta_{\mu\nu}$, we now focus on the optimization problem: finding protocols that minimize this dissipation. Throughout this section, we adopt Einstein's summation convention.

The connection to geometry becomes explicit through the identification of the friction tensor $\zeta_{\mu\nu}$ with a Riemannian metric on the space of control parameters. The action associated with this metric is given by

$$\int_0^T \mathrm{d}t\, \dot{\lambda}^\mu \zeta_{\mu\nu} \dot{\lambda}^\nu = \int_0^T \mathrm{d}t\, \dot{\Sigma}_{\mathrm{na}} + \mathcal{O}(\epsilon^2), \tag{9.83}$$

so that the geometric action approximates the total nonadiabatic entropy production up to higher-order corrections. By the Cauchy–Schwarz inequality, this action is bounded from below by the square of the thermodynamic length ℓ divided by the protocol duration T,

$$\Sigma_{\mathrm{na}} \geq \frac{\ell^2}{T}, \qquad \ell = \int_0^T \mathrm{d}t \sqrt{\dot{\lambda}^\mu \zeta_{\mu\nu} \dot{\lambda}^\nu} \tag{9.84}$$

Equality holds if and only if the protocol traces a geodesic at constant speed. This observation motivates searching for geodesic paths as a means to identify minimally dissipative protocols.

The optimal protocol corresponds to the path $\lambda(t)$ that minimizes the geometric action

$$\mathcal{S}[\lambda(t)] = \int_0^T \mathrm{d}t\, \dot{\lambda}^\mu \zeta_{\mu\nu} \dot{\lambda}^\nu, \tag{9.85}$$

subject to fixed boundary conditions $\lambda(0) = \lambda_i$ and $\lambda(T) = \lambda_f$. This is a standard problem in Riemannian geometry, and its solution is given by the geodesics of the metric $\zeta_{\mu\nu}$.

The geodesic path is defined as the solution to the second-order differential equation

$$\frac{\mathrm{d}^2\lambda^\mu}{\mathrm{d}t^2} + \Gamma^\mu{}_{\alpha\beta} \frac{\mathrm{d}\lambda^\alpha}{\mathrm{d}t} \frac{\mathrm{d}\lambda^\beta}{\mathrm{d}t} \tag{9.86}$$

where $\Gamma^\alpha_{\mu\nu}$ are the Christoffel symbols associated with the metric ζ, given by

$$\Gamma^\mu{}_{\alpha\beta} = \frac{1}{2}\zeta^{\mu\nu}\left(\frac{\partial \zeta_{\beta\nu}}{\partial \lambda^\alpha} + \frac{\partial \zeta_{\alpha\nu}}{\partial \lambda^\beta} - \frac{\partial \zeta_{\alpha\beta}}{\partial \lambda^\nu}\right) \tag{9.87}$$

where $\zeta^{\mu\nu}$ denotes the inverse of the metric tensor $\zeta_{\mu\nu}$.

In the special case where the protocol involves only a single control parameter $\lambda(t) \in \mathbb{R}$, the problem simplifies considerably. The action becomes

$$\mathcal{S} = \int_0^T \mathrm{d}t\, \zeta(\lambda)\dot{\lambda}^2, \tag{9.88}$$

and the optimal protocol is one that proceeds at constant speed with respect to the thermodynamic length element $\mathrm{d}s = \sqrt{\zeta(\lambda)}\, d\lambda$. Explicitly, the optimal trajectory satisfies

$$\frac{\mathrm{d}\lambda}{\mathrm{d}t} = \frac{\ell}{T\sqrt{\zeta(\lambda)}}, \tag{9.89}$$

where $\ell = \int_{\lambda_i}^{\lambda_f} \sqrt{\zeta(\lambda)}\, d\lambda$ is the thermodynamic length of the path. Separating variables, we can write

$$\mathrm{d}t = \frac{T\sqrt{\zeta(\lambda)}}{\ell}\mathrm{d}\lambda. \tag{9.90}$$

Integrating from the initial condition yields

$$t(\lambda) = \frac{T}{\ell}\int_{\lambda_i}^{\lambda} \sqrt{\zeta(\lambda')}\, \mathrm{d}\lambda', \tag{9.91}$$

which can be evaluated numerically. Inverting this relation yields the optimal protocol $\lambda_{\mathrm{opt}}(t)$. This approach avoids solving a differential equation directly and provides an explicit construction of the minimal-dissipation trajectory for arbitrary $\zeta(\lambda)$.

On the Role of Nonadiabatic Optimization

One might reasonably ask why the focus is placed on minimizing the nonadiabatic entropy production Σ_{na}, especially when the adiabatic term Σ_{ad} can dominate the total dissipation in the slow-driving limit. Under the assumption that the steady-state entropy production

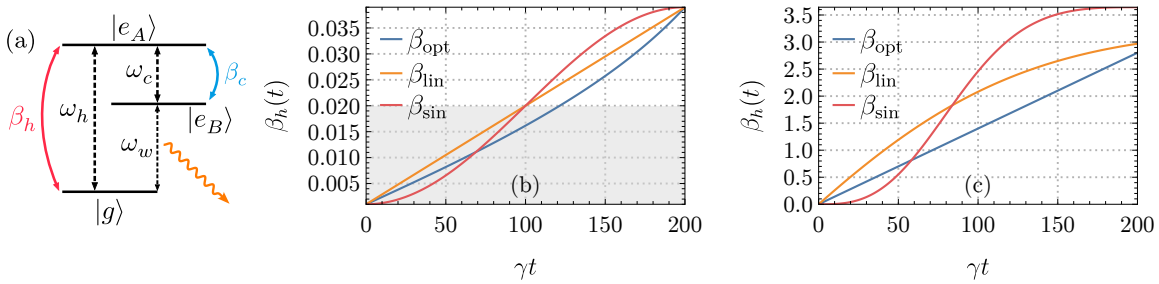

Figure 9.2: (a) Schematic of the three-level maser operating as a quantum thermal machine. The system is coupled to three baths: hot (β_h), cold (β_c), and work ($\beta_w = 0$). (b) Three protocols for driving $\beta_h(t)$ from β_0 to β_f in time T: the optimal protocol obtained from the geodesic equation, a linear interpolation $\beta_{\rm lin}(t) = \beta_0 + (\beta_f - \beta_0)t/T$, and a smooth protocol $\beta_{\rm sin}(t) = \beta_0 + (\beta_f - \beta_0)\sin^2(\pi t/2T)$. The system operates as heat engine when $\omega_c/\omega_h > \beta_h/\beta_c$ (shaded region), and as a refrigerator in the complementary regime. (c) Exact (solid lines) and slow-driving approximation (dashed lines) of the nonadiabatic entropy production for the three protocols. The geodesic protocol minimizes dissipation, with excellent agreement between the slow-driving approximation and exact results. Parameters: $\gamma_h = \gamma_c = \gamma_w = \gamma$, $\omega_h = 50\gamma$, $\omega_c = 10\gamma$, $\gamma\beta_c = 0.1$, $\gamma\beta_0 = 0.001$, $\gamma\beta_f = 0.039$, and $\gamma T = 200$.

rate $\dot{\Sigma}_{\rm ad}(t)$ varies slowly in time and remains relatively uniform across parameter space, the integrated adiabatic contribution is expected to scale linearly with the protocol duration,

$$\Sigma_{\rm ad} \sim \mathcal{O}(T). \tag{9.92}$$

Our focus on $\Sigma_{\rm na}$ is motivated by the specific regime considered: slow transformations between fixed initial and final nonequilibrium steady states, carried out over a fixed protocol duration. In this setting, $\Sigma_{\rm ad}$ reflects the baseline cost of maintaining the system close to a steady state and is not sensitive to the protocol velocity. It depends primarily on the locations in parameter space traversed by the protocol, rather than on the rate at which they are visited.

By contrast, the nonadiabatic entropy production is explicitly shaped by the time dependence of the control parameters. As seen in Eq. (9.66), it depends quadratically on the driving speed $\dot{\lambda}^\mu \sim \mathcal{O}(1/T)$, and thus scales as $\Sigma_{\rm na} \sim \mathcal{O}(1/T)$ in the slow-driving limit. Minimizing $\Sigma_{\rm na}$ therefore provides a well-defined and operationally meaningful strategy for reducing the additional dissipation incurred by finite-time driving, within the linear-response regime.

It is worth emphasizing, however, that this optimization does not necessarily minimize the total entropy production. A protocol with slightly higher $\Sigma_{\rm na}$ but lower cumulative $\Sigma_{\rm ad}$ could, in principle, be more efficient overall. Our approach aims instead to isolate and minimize the portion of the dissipation that is both controllable and universal in the slow-driving limit.

9.4 Example: Three-Level Maser

To illustrate the geometric framework introduced in the previous section, we consider a concrete example: a three-level quantum thermal machine operating as a maser. This

model provides a minimal yet analytically tractable setting for studying dissipation in driven nonequilibrium quantum dynamics.

The working medium consists of three energy eigenstates, denoted $\{|g\rangle, |e_A\rangle, |e_B\rangle\}$, with corresponding energies $\epsilon_g < \epsilon_B < \epsilon_A$. The system is coupled to three thermal reservoirs. The first is a hot bath at inverse temperature β_h, which drives transitions between the ground state $|g\rangle$ and the excited state $|e_A\rangle$. The second is a cold bath at fixed inverse temperature β_c, which induces transitions between $|e_B\rangle$ and $|e_A\rangle$. The third reservoir acts as a work bath and is assumed to be at infinite temperature ($\beta_w = 0$) , enabling transitions between $|g\rangle$ and $|e_B\rangle$. Because of the infinite temperature assumption, there is no entropy flux associated with this transition.

The master equation for the three-level system is given by

$$\frac{\mathrm{d}\hat{\rho}}{\mathrm{d}t} = -i[\hat{H}, \hat{\rho}] + \hat{\mathcal{D}}_h(\hat{\rho}) + \hat{\mathcal{D}}_c(\hat{\rho}) + \hat{\mathcal{D}}_w(\hat{\rho}), \tag{9.93}$$

where the system Hamiltonian is $\hat{H} = \epsilon_g|g\rangle\langle g| + \epsilon_A|e_A\rangle\langle e_A| + \epsilon_B|e_B\rangle\langle e_B|$, and the dissipators take the standard Lindblad form:

$$\mathcal{D}_x(\hat{\rho}) = \gamma_x\Big(\hat{L}_x\hat{\rho}\hat{L}_x^\dagger - \tfrac{1}{2}\{\hat{L}_x^\dagger\hat{L}_x, \hat{\rho}\}\Big) + \gamma_x e^{-\beta_x\omega_x}\Big(\hat{L}_x^\dagger\hat{\rho}\hat{L}_x - \tfrac{1}{2}\{\hat{L}_x\hat{L}_x^\dagger, \hat{\rho}\}\Big), \tag{9.94}$$

where $x \in \{h, c, w\}$. The corresponding jump operators are $\hat{L}_h = |g\rangle\langle e_A|$, $\hat{L}_c = |e_B\rangle\langle e_A|$, and $\hat{L}_w = |g\rangle\langle e_B|$, and the transition frequencies are defined as $\omega_h = \epsilon_A - \epsilon_g$, $\omega_c = \epsilon_A - \epsilon_B$, and $\omega_w = \epsilon_B - \epsilon_g$.

The mode of operation of the machine depends on the ratio ω_c/ω_h relative to β_h/β_c. When $\omega_c/\omega_h > \beta_h/\beta_c$, the system operates as a heat engine, exhibiting population inversion between $|g\rangle$ and $|e_B\rangle$, and producing net work via stimulated emission. In the complementary regime, the system operates as a refrigerator, consuming work to transfer heat from the cold to the hot bath [231].

We now consider finite-time driving protocols in which $\beta_h(t)$ is varied slowly while all other parameters remain fixed. In this setting, the friction tensor reduces to a scalar function $\zeta(\beta_h) \geq 0$, which can be computed analytically:

$$\zeta(\beta_h) = \frac{\omega_h^2\, e^{2\beta_h(\epsilon_g+\epsilon_A)}\big(e^{\beta_c\epsilon_B} + e^{\beta_c\epsilon_A}\big)}{\gamma\big(e^{\beta_h\epsilon_g} + 2e^{\beta_h\epsilon_A}\big)^3\big(e^{\beta_h\epsilon_g+\beta_c\epsilon_B} + e^{\beta_h\epsilon_g+\beta_c\epsilon_A} + e^{\beta_h\epsilon_A+\beta_c\epsilon_B}\big)}, \tag{9.95}$$

Similarly, the KMB Fisher information matrix reduces to a scalar function, corresponding to the KMB Fisher information:

$$\mathcal{J}(\beta_h) = \frac{\omega_h^2\, e^{(2\epsilon_g+\epsilon_A)\beta_h}\big(e^{\beta_c\epsilon_B} + e^{\beta_c\epsilon_A}\big)}{\big(e^{\beta_h\epsilon_g} + 2e^{\beta_h\epsilon_A}\big)^2\big(e^{\beta_h\epsilon_g+\beta_c\epsilon_B} + e^{\beta_h\epsilon_g+\beta_c\epsilon_A} + e^{\beta_h\epsilon_A+\beta_c\epsilon_B}\big)} \tag{9.96}$$

The analytical expression for the generalized time $\tau(\beta_h)$ is

$$\tau(\beta_h) = \frac{1}{\gamma(2 + e^{-\beta_h\omega_h})}. \tag{9.97}$$

confirming the factorization $\zeta(\beta_h) = \tau(\beta_h) \cdot \mathcal{J}(\beta_h)$.

Notably, the relaxation time depends only on γ, which sets the time scale of the dynamics, and the Boltzmann factor $e^{-\beta_h \omega_h}$ associated with transitions in the central system induced by interactions with the bath. In the infinite temperature limit, $\beta_h \to 0$, $\tau_0 = \frac{1}{3\gamma}$, whereas in the zero temperature limit, $\beta_h \to \infty$, $\tau_\infty = \frac{1}{2\gamma}$.

We compare three protocols for $\beta_h(t)$: (i) the optimal protocol $\beta_{\rm opt}(t)$, obtained by solving the geodesic equation corresponding to the friction tensor $\zeta(\beta_h)$; (ii) a linear protocol $\beta_{\rm lin}(t) = \beta_0 + (\beta_f - \beta_0)t/T$; and (iii) a smooth sinusoidal protocol $\beta_{\rm sin}(t) = \beta_0 + (\beta_f - \beta_0)\sin^2(\pi t/2T)$. The geodesic protocol minimizes the thermodynamic length $\int \sqrt{\zeta(\beta_h)}\,\mathrm{d}\beta_h$, and hence the leading-order contribution to the nonadiabatic entropy production in the slow-driving regime.

We choose β_0 and β_f such that the protocol drives the system from a regime in which it functions as a heat engine into one where it operates as a refrigerator, as shown in Fig. 9.2(b).

Figure 9.2(b) shows the three protocols. In Fig. 9.2(c), we compare the exact nonadiabatic entropy production $\Sigma_{\rm na}(t)$ with the slow-driving approximation $\Sigma_{\rm na}(t) \approx \int_0^T \dot{\lambda}^\top \zeta \lambda \mathrm{d}t,$. The dashed lines indicate the slow-driving predictions, while the solid lines are computed from the full quantum master equation. The excellent agreement between the two confirms the validity of the geometric approximation in this regime.

As expected, the total nonadiabatic entropy production is minimized by the geodesic protocol. This example demonstrates the practical utility of the geometric approach. Even in a relatively simple system, the structure of the metric ζ encodes nontrivial information about the underlying dynamics and dissipation mechanisms.

9.5 Beyond Slow Driving: Arbitrary-Speed Transitions

The geometric framework developed in the previous sections relies on the assumption that the driving is slow, such that the system remains close to its instantaneous nonequilibrium steady state at all times. While this regime is analytically tractable and yields valuable insights, it is important to address more general scenarios in which the driving may be fast or strongly nonadiabatic. In this section, we present a complementary geometric approach that applies to arbitrary-speed protocols.

The key idea is to shift from a geometry defined on the control parameter space to one parametrized by time. In this formulation, time plays the role of a curve parameter, and the relevant metric structure is provided by quantum Fisher information (QFI) defined with respect to time [224, 225, 226, 227, 228, 229, 230].

Let $\hat{\rho}_t$ be the time-dependent state of the system evolving under a general Lindblad equation. We consider QFI-based metrics of the form [232, 178]

$$\mathcal{J}_f(t) = \sum_{x,y} \frac{|\partial_t \rho_{xy}(t)|^2}{p_x(t) f(p_y(t)/p_x(t))}, \tag{9.98}$$

where $\hat{\rho}_t = \sum_x p_x(t)|x\rangle\langle x|$ is the spectral decomposition of the state, and f is an operator monotone function that defines a contractive quantum information metric. Well-known examples include the symmetric logarithmic derivative (SLD), the Wigner-Yanase metric, and the Kubo-Mori-Bogoliubov metric.

These metrics define a statistical line element

$$ds_f^2 = \frac{1}{4}\mathcal{J}_f(t)\,dt^2, \tag{9.99}$$

which allows us to interpret the evolution as a trajectory in state space with an associated speed $v_f = \sqrt{\mathcal{J}_f}$.

Building on this geometric connection, Refs. [233, 229] established a generalized speed limit on an arbitrary observable $\hat{A}$ in terms of v_f, resembling the celebrated Mandelstam-Tamm time-energy uncertainty relation [234],

$$|\dot{a}| \leq \sigma_{\hat{\rho}}^f[\hat{A}]v_f, \tag{9.100}$$

where $\dot{a} = \mathrm{Tr}[A\dot{\rho}]$, $\sigma_{\hat{\rho}}^2[\hat{A}] = \mathrm{Tr}\left[\hat{A}_0 L_{\hat{\rho}} f(L_{\hat{\rho}}^{-1}R_{\hat{\rho}})(\hat{A}_0)\right]$, with $\hat{A}_0 = \hat{A} - \mathrm{Tr}\left[\hat{\rho}\hat{A}\right]$, is a generalized variance that reduces to the standard one for the commonly used QFI based on the symmetric logarithmic derivative (SLD), and super-operators $L_{\hat{\rho}}(\cdot) = \hat{\rho}(\cdot)$ and $R_{\hat{\rho}}(\cdot) = (\cdot)\hat{\rho}$.

We apply this bound to the nonequilibrium potential $\hat{\Phi}_\lambda = -\log\hat{\pi}_\lambda$, which governs the excess entropy flux:

$$\dot{\Pi}_{\mathrm{ex}}(t) = -\,\mathrm{Tr}\left[\dot{\hat{\rho}}_t\,\hat{\Phi}_\lambda\right]. \tag{9.101}$$

Using the speed limit, we obtain

$$|\dot{\Pi}_{\mathrm{ex}}(t)| \leq \sigma_f[\hat{\Phi}_\lambda]\,v_f(t). \tag{9.102}$$

Upon integration, one finds

$$\int_0^T \mathrm{d}t\,|\dot{\Pi}_{\mathrm{ex}}| \leq \int_0^T \mathrm{d}t\,\sigma_{\hat{\rho}}^f[\hat{\Phi}]\,v_f, \tag{9.103}$$

Alternatively, dividing both sides by the generalized variance and integrating gives a bound in terms of the statistical length:

$$\int_0^T \mathrm{d}t\,\frac{|\dot{\Pi}_{\mathrm{ex}}(t)|}{\sigma_f[\hat{\Phi}_\lambda]} \leq 2\ell_f, \tag{9.104}$$

where $\ell_f = \int_0^T \mathrm{d}t\,v_f(t)$ is the path length traversed in state space under the metric defined by f.

These results provide general, model-independent constraints on entropy production that hold beyond the slow-driving limit. Importantly, they remain valid for arbitrary Lindblad dynamics with a unique steady state, and they reveal how both the geometry of state space and the statistical properties of observables constrain the dissipation incurred during fast processes.

10 Conclusion

This thesis has examined the thermodynamics of quantum systems beyond equilibrium, with a focus on nonequilibrium steady states and strong system-bath coupling. Structured around four original research papers, it aims not only to present new results, but also to provide clear and pedagogically motivated discussions of foundational and advanced topics in quantum thermodynamics. By integrating theoretical development, critical review and methodological innovation, this work aspires to contribute both to ongoing research and to the accessibility of the field for a broader audience.

The foundational chapters on open quantum systems and quantum thermodynamics provide (mostly) self-contained introductions to each topic, with a particular emphasis on their later application within the mesoscopic leads framework. The discussion of quantum thermodynamics pays special attention to the challenges that arise in the strong-coupling regime, examining different approaches proposed in the literature. This point is illustrated by an example in which inconsistent definitions of heat, work, and entropy production in the strong-coupling regime lead to an apparent violation of the second law.

Chapter 4, Gaussian Fermionic Systems, presents a collection of tools, tricks and references related to non-interacting fermionic models, gathered during the development of this work. The chapter aims to be a concise "handbook", covering topics such as the covariance matrix formalism, the Lyapunov equation, and aspects of quantum information theory for Gaussian states, including the computation of distinguishability measures like fidelity, relative entropy, and Rényi divergences. The chapter concludes with an application drawn from one of the thesis papers: a study of dephasing-assisted transport in a tilted lattice exhibiting Stark localization [105]. While the chapter focuses on the number-conserving case (i.e., without pairing terms), a natural extension would be to reformulate the material in the Majorana representation and incorporate the third quantization method—an effort that could potentially lead to a tutorial-style publication.

The next part of the thesis focuses on the mesoscopic leads formalism. The original motivation for this line of work was to extend the thermodynamic analysis presented in Ref. [44], which was limited to nonequilibrium steady states (NESS), to time-dependent scenarios. Chapter 5 offers a pedagogical introduction to the method, followed by a formal justification via the reaction coordinate transformation. While the connection between mesoscopic leads and reaction coordinate mappings has been acknowledged in the literature, this thesis presents a detailed account of that relationship. Building on this foundation, we develop a consistent formulation of thermodynamics within the mesoscopic leads framework, one that remains valid under conditions of strong coupling and rapid driving [45].

This development is further extended through an analysis of entropy production in the mesoscopic leads setting. As emphasized throughout the thesis, the mesoscopic leads method implements a *Markovian embedding*: by incorporating additional degrees of freedom (the

leads), the extended system follows a Lindblad-type Markovian evolution. This enables the application of tools from the theory of quantum dynamical semigroups, particularly Spohn's inequality [30, 172], to study entropy production. We show how these tools can be adapted to extract physically meaningful interpretations of entropy production in the original, non-Markovian system, and how the resulting decomposition admits both thermodynamic and information-theoretic interpretations. This approach provides a practical and rigorous method for quantifying entropy production in regimes where standard techniques break down.

The chapters dedicated to the mesoscopic leads method are closely aligned with the overarching theme of this thesis: the thermodynamics of quantum systems out of equilibrium, especially in steady-state regimes. Although the method is applicable in single-bath scenarios, it is particularly well suited to the prototypical NESS setting—a system coupled to two or more thermal reservoirs. This makes the mesoscopic leads framework a flexible and powerful tool for investigating quantum transport and thermodynamic processes beyond weak coupling and Markovian limits.

Looking ahead, one natural direction for future work is the application of the mesoscopic leads formalism to systems where the standard Lindblad master equation fails, and structured environments must be taken into account. Particularly challenging applications are the Anderson impurity model and Kondo phenomena. These systems feature strong correlations and non-trivial bath structures, especially at low temperatures, which require a large number of modes for accurate simulation. The mesoscopic leads framework, with its ability to resolve spectral features and handle memory, offers a promising route to modeling such systems beyond the weak-coupling, high-temperature limit.

From a methodological standpoint, there are several possible directions. One promising approach is the application of a thermofield transformation, which maps finite-temperature reservoirs into two zero-temperature chains, with the temperature information encoded in the couplings [235]. This representation may reduce the number of modes required for simulation at low temperatures and has connections to the concept of Markovian closure, as recently explored in the context of fermionic environments [236, 237].

On the practical side, the development of a Julia-based library implementing the mesoscopic leads tools is a potential direction of interest. Recent advances in many-body simulation techniques, such as Pauli string truncation methods [238], could enable efficient simulations even in the presence of interactions.

The final part of the thesis explores the role of information geometry in understanding entropy production during transitions between NESS. Chapter 7 begins with an introduction to quantum Fisher information, offering a geometrical perspective on how it generalizes the classical Fisher information. This is followed by a historical review of the concept of thermodynamic length, tracing its origins in the work of Ruppeiner and Weinhold, through its development in classical stochastic thermodynamics, and into recent quantum formulations.

In Chapter 8, we present a modern review of the Hatano–Sasa framework for entropy production in NESS. The discussion begins in the classical setting, using Markov processes as a starting point, and then proceeds to the quantum generalization within the Lindblad master equation formalism, where several technical challenges arise. While the framework is

well established in classical stochastic thermodynamics [58, 60, 222], and has been explored in the quantum context [207, 203, 61], it remains relatively underutilized within the quantum thermodynamics community. We hope that the perspective provided in this chapter contributes to making it more accessible.

The final chapter presents original work on the information geometry of slow transitions between NESS [62]. Within the Hatano–Sasa framework, we show that in the slow-driving regime, the non-adiabatic entropy production is governed by a Riemannian metric on the space of control parameters. This metric is related to the quantum Fisher information, but incorporates dynamical features that reflect the system's evolution. The result generalizes previous findings in classical and quantum thermodynamics [55, 54, 59], and further advances the geometric formulation of nonequilibrium thermodynamics in the context of open quantum systems.

Looking ahead, there are several promising directions for extending this work. A central motivation of this research has been to apply the geometric formalism to the study of dissipative phase transitions, which are characterized by the closing of the Liouvillian gap. These transitions arise in models such as the dissipative Dicke model, the Kerr model, and the boundary-driven XY model. Understanding these transitions from a thermodynamic perspective remains a significant open challenge. In particular, the concept of adiabaticity—and its breakdown near critical points—in open quantum systems is still not well understood. The tools developed in this thesis may offer new insights into these unresolved questions.

Additionally, there is potential to extend the formalism beyond the slow-driving regime. Preliminary results based on the quantum Fisher information with respect to time suggest the existence of a more general structure that may remain valid under fast driving and in more general nonequilibrium settings.

The study of nonequilibrium steady states lies at the forefront of quantum thermodynamics. As experimental capabilities advance and strong coupling becomes the rule rather than the exception, the tools and ideas developed in this thesis are intended to meet that emerging challenge. Beyond contributing to the technical understanding of quantum irreversibility, this work aspires to help shape the conceptual foundations of future research in open-system dynamics, thermodynamic control, and information geometry.

Appendix

A

A.1 Time Derivative of the von Neumann

In this appendix, we show that the time derivative of the von Neumann entropy can be expressed as

$$\frac{\mathrm{d}S(t)}{\mathrm{d}t} = -\operatorname{Tr}\left[\frac{\mathrm{d}\hat{\rho}_t}{\mathrm{d}t}\log\hat{\rho}_t\right]. \tag{A.1}$$

Recall that the von Neumann entropy is defined by

$$S(t) = -\operatorname{Tr}[\hat{\rho}_t \log\hat{\rho}_t]. \tag{A.2}$$

Differentiating with respect to time yields

$$\frac{\mathrm{d}S(t)}{\mathrm{d}t} = -\operatorname{Tr}\left[\frac{\mathrm{d}\hat{\rho}_t}{\mathrm{d}t}\log\hat{\rho}_t\right] - \operatorname{Tr}\left[\hat{\rho}_t\frac{\mathrm{d}\log\hat{\rho}_t}{\mathrm{d}t}\right]. \tag{A.3}$$

We now show that the second term vanishes. To do so, we expand the density matrix $\hat{\rho}_t$ in terms of its instantaneous eigenbasis, $\hat{\rho}_t = \sum_n p_n(t)|n_t\rangle\langle n_t|$. Using this decomposition, the time derivative of $\log\hat{\rho}_t$ becomes

$$\frac{\mathrm{d}\log\hat{\rho}_t}{\mathrm{d}t} = \sum_n\left[\frac{\dot{p}_n(t)}{p_n(t)}|n_t\rangle\langle n_t| + \log p_n(t)\Big(|\dot{n}_t\rangle\langle n_t| + |n_t\rangle\langle\dot{n}_t|\Big)\right]. \tag{A.4}$$

Substituting into the trace term, we obtain

$$\begin{aligned}
\operatorname{Tr}\left[\hat{\rho}_t\frac{\mathrm{d}\log\hat{\rho}_t}{\mathrm{d}t}\right] &= \sum_n p_n(t)\frac{\dot{p}_n(t)}{p_n(t)} + \sum_n \log p_n(t)\left[\langle n_t|\hat{\rho}_t|\dot{n}_t\rangle + \langle\dot{n}_t|\hat{\rho}_t|n_t\rangle\right] \\
&= \sum_n \dot{p}_n(t) + \sum_n p_n(t)\log p_n(t)\Big(\langle\dot{n}_t|n_t\rangle + \langle n_t|\dot{n}_t\rangle\Big) \\
&= \frac{\mathrm{d}}{\mathrm{d}t}\sum_n p_n(t) + \sum_n p_n(t)\log p_n(t)\frac{\mathrm{d}}{\mathrm{d}t}\langle n_t|n_t\rangle \\
&= 0,
\end{aligned}$$

where we used that $\sum_n p_n = 1$ and $\langle n_t|n_t\rangle = 1$. This completes the proof.

A.2 Vectorization

In this appendix, we briefly discuss the vectorization operation and how it can be used to solve the Lyapunov equation introduced in Section 4.4.3

The *vectorization* operator (denoted vec) maps a matrix $\boldsymbol{X} \in \mathbb{C}^{m\times n}$ to a column vector $\mathrm{vec}(\boldsymbol{X}) \in \mathbb{C}^{mn}$ by stacking the columns of $\boldsymbol{X}$ on top of each other:

$$\mathrm{vec}(\boldsymbol{X}) = \begin{bmatrix} X_{:,1} \\ X_{:,2} \\ \vdots \\ X_{:,n} \end{bmatrix} \tag{A.5}$$

For example, the vectorization of a 2×2 matrix is

$$\mathrm{vec} \begin{pmatrix} a & b \\ c & d \end{pmatrix} = \begin{pmatrix} a \\ c \\ b \\ d \end{pmatrix}. \tag{A.6}$$

A key identity involves the vectorization of a product of three matrices:

$$\mathrm{vec}(\boldsymbol{AXB}) = (\boldsymbol{B}^\top \otimes \boldsymbol{A})\,\mathrm{vec}(\boldsymbol{X}), \tag{A.7}$$

where $\boldsymbol{A}$, $\boldsymbol{X}$, and $\boldsymbol{B}$ have compatible dimensions, and $\otimes$ denotes the Kronecker product. Two important special cases follow immediately. If $\boldsymbol{X}$ is multiplied only from the left (i.e., $\boldsymbol{B} = \mathbb{1}$), we obtain

$$\mathrm{vec}(\boldsymbol{AX}) = (\mathbb{1} \otimes \boldsymbol{A})\,\mathrm{vec}(\boldsymbol{X}), \tag{A.8}$$

and if it is multiplied only from the right (i.e., $\boldsymbol{A} = \mathbb{1}$),

$$\mathrm{vec}(\boldsymbol{XB}) = (\boldsymbol{B}^\top \otimes \mathbb{1})\,\mathrm{vec}(\boldsymbol{X}), \tag{A.9}$$

where $\mathbb{1}$ denotes the identity matrix of appropriate size.

These identities allow matrix equations to be recast in the standard linear form $\boldsymbol{Ax} = \boldsymbol{b}$. For example, consider the Lyapunov equation

$$\boldsymbol{WC} + \boldsymbol{CW}^\dagger = \boldsymbol{F}. \tag{A.10}$$

Applying vectorization yields

$$(\mathbb{1} \otimes \boldsymbol{W} + \boldsymbol{W}^* \otimes \mathbb{1})\,\mathrm{vec}(\boldsymbol{C}) = \mathrm{vec}(\boldsymbol{F}), \tag{A.11}$$

where we used the identity $(\boldsymbol{W}^\dagger)^\top = \boldsymbol{W}^*$.

A.3 Trace-Determinant Identities for Fermionic Quadratic Forms

In this appendix we derive two important trace-determinant identities for fermionic Gaussian operators that conserve particle number. These formulas are widely used in the theory of Gaussian states. Key references include Klich (2003) [114] and Blankenbecler, Scalapino, and Sugar (1981) [115]. Ref. [116] discusses applications and further generalizations.

A.3.1 Basic Trace-Determinant Formula

Let $\hat{A}$ be a quadratic operator of the form

$$\hat{A} = \hat{\boldsymbol{c}}^\dagger \boldsymbol{A} \hat{\boldsymbol{c}}, \tag{A.12}$$

where $\hat{\boldsymbol{c}}$ and $\hat{\boldsymbol{c}}^\dagger$ are fermionic annihilation and creation operators.

The trace over the full fermionic Fock space satisfies

$$\mathrm{Tr}[e^{\hat{A}}] = \det\bigl(1 + e^{\boldsymbol{A}}\bigr). \tag{A.13}$$

Proof. We start by diagonalizing $\boldsymbol{A}$ via a unitary transformation: $\boldsymbol{A} = \boldsymbol{S}\boldsymbol{\epsilon}\boldsymbol{S}^\dagger$, where $\boldsymbol{\epsilon} = \mathrm{diag}(\varepsilon_1, \dots, \varepsilon_N)$. Let $\hat{b}_k = \sum_j S^*_{jk} \hat{c}_j$ be the new modes in the energy basis. In this basis, the operator becomes diagonal:

$$\hat{A} = \sum_k \varepsilon_k \, \hat{b}_k^\dagger \hat{b}_k. \tag{A.14}$$

The operator $e^{\hat{A}}$ then factorizes as a tensor product:

$$e^{\hat{A}} = \bigotimes_{k=1}^{N} e^{\varepsilon_k \hat{b}_k^\dagger \hat{b}_k}, \tag{A.15}$$

where each factor acts independently on a two-dimensional mode Fock space. Therefore, the trace becomes

$$\mathrm{Tr}[e^{\hat{A}}] = \prod_{k=1}^{N} \mathrm{Tr}_k[e^{\varepsilon_k \hat{b}_k^\dagger \hat{b}_k}] = \prod_{k=1}^{N} (1 + e^{\varepsilon_k}) = \det(1 + e^{\boldsymbol{\epsilon}}). \tag{A.16}$$

Finally, since $\boldsymbol{\epsilon}$ is unitarily equivalent to $\boldsymbol{A}$, we conclude

$$\mathrm{Tr}[e^{\hat{\boldsymbol{c}}^\dagger \boldsymbol{A} \hat{\boldsymbol{c}}}] = \det\bigl(1 + e^{\boldsymbol{A}}\bigr). \tag{A.17}$$

A.3.2 Generalized Trace-Determinant Formula

Consider two quadratic operators $\hat{A} = \hat{\boldsymbol{c}}^\dagger \boldsymbol{A} \hat{\boldsymbol{c}}$ and $\hat{B} = \hat{\boldsymbol{c}}^\dagger \boldsymbol{B} \hat{\boldsymbol{c}}$. Then

$$\mathrm{Tr}[e^{\hat{A}} e^{\hat{B}}] = \det\bigl(1 + e^{\boldsymbol{A}} e^{\boldsymbol{B}}\bigr). \tag{A.18}$$

This identity generalizes the basic formula to a product of Gaussian operators.

Proof. We begin by verifying the identity

$$[\hat{\boldsymbol{c}}^\dagger \boldsymbol{A} \hat{\boldsymbol{c}}, \, \hat{\boldsymbol{c}}^\dagger \boldsymbol{B} \hat{\boldsymbol{c}}] = \hat{\boldsymbol{c}}^\dagger [\boldsymbol{A}, \boldsymbol{B}] \hat{\boldsymbol{c}}. \tag{A.19}$$

Writing the operators explicitly,

$$\hat{A} = \sum_{ij} A_{ij} \, \hat{c}_i^\dagger \hat{c}_j, \quad \hat{B} = \sum_{kl} B_{kl} \, \hat{c}_k^\dagger \hat{c}_l, \tag{A.20}$$

we compute

$$[\hat{A}, \hat{B}] = \sum_{ij,kl} A_{ij} B_{kl} [\hat{c}_i^\dagger \hat{c}_j, \hat{c}_k^\dagger \hat{c}_l]. \tag{A.21}$$

Using the canonical anticommutation relations, one finds

$$[\hat{c}_i^\dagger \hat{c}_j, \hat{c}_k^\dagger \hat{c}_l] = \delta_{jk}\hat{c}_i^\dagger \hat{c}_l - \delta_{il}\hat{c}_k^\dagger \hat{c}_j. \tag{A.22}$$

Substituting and rearranging indices gives

$$[\hat{A}, \hat{B}] = \sum_{il}[AB]_{il}\, \hat{c}_i^\dagger \hat{c}_l - \sum_{kj}[BA]_{kj}\, \hat{c}_k^\dagger \hat{c}_j = \hat{\boldsymbol{c}}^\dagger [\boldsymbol{A}, \boldsymbol{B}]\hat{\boldsymbol{c}}. \tag{A.23}$$

Now apply the Baker–Campbell–Hausdorff formula to the product $e^{\hat{A}}e^{\hat{B}}$. Since all commutators remain quadratic by Eq. (A.19), the series yields another quadratic operator:

$$e^{\hat{A}}e^{\hat{B}} = \exp\Big(\hat{A} + \hat{B} + \tfrac{1}{2}[\hat{A}, \hat{B}] + \tfrac{1}{12}[\hat{A}, [\hat{A}, \hat{B}]] + \tfrac{1}{12}[\hat{B}, [\hat{A}, \hat{B}]] + \cdots\Big). \tag{A.24}$$

The result is again of the form $e^{\hat{\boldsymbol{c}}^\dagger \boldsymbol{C}\hat{\boldsymbol{c}}}$, where the matrix $\boldsymbol{C}$ is given by the BCH expansion:

$$\boldsymbol{C} = \boldsymbol{A} + \boldsymbol{B} + \tfrac{1}{2}[\boldsymbol{A}, \boldsymbol{B}] + \tfrac{1}{12}[\boldsymbol{A}, [\boldsymbol{A}, \boldsymbol{B}]] + \tfrac{1}{12}[\boldsymbol{B}, [\boldsymbol{A}, \boldsymbol{B}]] + \cdots = \log\big(e^{\boldsymbol{A}}e^{\boldsymbol{B}}\big). \tag{A.25}$$

Therefore, the product is again Gaussian:

$$e^{\hat{A}}e^{\hat{B}} = e^{\hat{\boldsymbol{c}}^\dagger \boldsymbol{C}\hat{\boldsymbol{c}}}, \qquad \boldsymbol{C} = \log\big(e^{\boldsymbol{A}}e^{\boldsymbol{B}}\big). \tag{A.26}$$

Applying the basic trace-determinant formula yields the result:

$$\mathrm{Tr}[e^{\hat{A}}e^{\hat{B}}] = \det(1 + e^{\boldsymbol{C}}) = \det\big(1 + e^{\boldsymbol{A}}e^{\boldsymbol{B}}\big). \tag{A.27}$$

This identity extends naturally to products of more than two exponentials. Let $\hat{A}_k = \hat{\boldsymbol{c}}^\dagger \boldsymbol{A}_k \hat{\boldsymbol{c}}$ for $k = 1, \ldots, M$. Then by iteratively applying the same logic, one finds

$$e^{\hat{A}_1}e^{\hat{A}_2}\cdots e^{\hat{A}_M} = \exp(\hat{\boldsymbol{c}}^\dagger \boldsymbol{Q}\hat{\boldsymbol{c}}), \qquad \boldsymbol{Q} = \log\big(e^{\boldsymbol{A}_1}e^{\boldsymbol{A}_2}\cdots e^{\boldsymbol{A}_M}\big). \tag{A.28}$$

Applying the basic formula once more yields

$$\mathrm{Tr}\Big[e^{\hat{A}_1}e^{\hat{A}_2}\cdots e^{\hat{A}_M}\Big] = \det\big(1 + e^{\boldsymbol{A}_1}e^{\boldsymbol{A}_2}\cdots e^{\boldsymbol{A}_M}\big). \tag{A.29}$$

This generalization follows by induction, using the closure of quadratic fermionic operators under commutation.

A.4 Action of the Inverse Kubo–Mori Operator on the Steady State

In this appendix, we show that the inverse Kubo–Mori operator satisfies

$$\mathbb{J}_{\hat{\pi}}^{-1}(\hat{\pi}) = \hat{\mathbb{1}}, \tag{A.30}$$

where $\hat{\pi}$ is a full-rank density operator and $\hat{\mathbb{1}}$ is the identity.

Recall that the inverse Kubo–Mori operator is defined as

$$\mathbb{J}_{\hat{\pi}}^{-1}(X) := \int_0^\infty \mathrm{d}s\, (\hat{\pi} + s\hat{\mathbb{1}})^{-1} X (\hat{\pi} + s\hat{\mathbb{1}})^{-1}. \tag{A.31}$$

We compute its action on $\hat{\pi}$ directly. Using the spectral decomposition

$$\hat{\pi} = \sum_i p_i |i\rangle\langle i|, \qquad p_i > 0, \tag{A.32}$$

we find

$$\mathbb{J}_{\hat{\pi}}^{-1}(\hat{\pi}) = \int_0^\infty \mathrm{d}s \sum_i \frac{p_i}{(p_i + s)^2} |i\rangle\langle i| \tag{A.33}$$

$$= \sum_i \left(\int_0^\infty \frac{p_i}{(p_i + s)^2} \mathrm{d}s \right) |i\rangle\langle i|. \tag{A.34}$$

Evaluating the integral,

$$\int_0^\infty \frac{p_i}{(p_i + s)^2} \mathrm{d}s = \left[-\frac{p_i}{p_i + s} \right]_0^\infty = 1, \tag{A.35}$$

so we obtain

$$\mathbb{J}_{\hat{\pi}}^{-1}(\hat{\pi}) = \sum_i |i\rangle\langle i| = \hat{\mathbb{1}}, \tag{A.36}$$

which completes the proof.

A.5 Superfermion formalism and TDVP implementation

A.5.1 Superfermion formalism

In this appendix we briefly outline the superfermion formalism used for thermal-state preparation with TDVP in Sec. 6.2. The construction is closely related to third quantization and vectorization techniques for open quantum systems [44, 164].

Consider a fermionic system with Fock basis $|\boldsymbol{n}\rangle$. The key step is to *double* the system by introducing an ancillary Fock space (the "tilde" space of Ref. [164]), with basis $|\tilde{\boldsymbol{n}}\rangle$. Our goal is to define fermionic operators on this *global* Fock space such that Liouvillian superoperators can be represented as ordinary operators.

A naive definition of "superfermions" as tensor products, i.e., $\hat{c}_i \otimes \hat{\mathbb{1}}$ and $\hat{\mathbb{1}} \otimes \hat{c}_i$, is inadequate: although these operators anticommute within each Fock space, they commute between the physical and tilde sectors and therefore do not satisfy the canonical anticommutation relations on the doubled space. Instead, we define the superfermions by specifying their action directly on basis states of the joint Fock space. We adopt an interleaved ordering of physical and ancillary modes[1]:

$$|\boldsymbol{n}|\tilde{\boldsymbol{m}}\rangle = \prod_{j=1}^{N} (\hat{c}_j^\dagger)^{n_j} (\tilde{c}_j^\dagger)^{m_j} |0\rangle, \tag{A.37}$$

[1] This is equivalent to attaching a parity operator to the tensor-product representation: $\hat{c}_j = \hat{c}_j \otimes \hat{\mathbb{1}}$ and $\tilde{c}_j = (-1)^{\hat{N}_{\mathrm{phys}}} \otimes c_j$, where $\hat{N}_{\mathrm{phys}}$ is the total physical number operator.

where $n_j, m_j \in \{0,1\}$ and $|0\rangle$ is the vacuum of both chains. Here, there is a mild abuse of notation: we use $\hat{c}_j$ and $\tilde{c}_j$ both for the original annihilation operators and for their representations on the doubled space.

On the doubled Fock space we define the (unnormalized) left vacuum

$$|I\rangle := \sum_{\boldsymbol{n}} |\boldsymbol{n}|\boldsymbol{n}\rangle, \tag{A.38}$$

where the sum runs over all configurations $\boldsymbol{n}$ of the physical modes. A density operator $\hat{\rho}(t)$ on the original Fock space is mapped to a state on the doubled space as

$$|\hat{\rho}(t)\rangle = \hat{\rho}(t)|I\rangle, \tag{A.39}$$

so that expectation values of physical operators $\hat{A}$ become

$$\left\langle \hat{A}(t) \right\rangle = \mathrm{Tr}\left[\hat{A}\hat{\rho}(t)\right] = \langle I|\hat{A}|\hat{\rho}(t)\rangle. \tag{A.40}$$

With the interleaved ordering one finds the following key identities on the left vacuum, the so-called *tilde conjugation rules* [164, 44]:

$$\tilde{c}_j^\dagger |I\rangle = -\hat{c}_j |I\rangle, \qquad \langle I|\,\tilde{c}_j = -\langle I|\,\hat{c}_j^\dagger, \tag{A.41}$$

$$\tilde{c}_j |I\rangle = \hat{c}_j^\dagger |I\rangle, \qquad \langle I|\,\tilde{c}_j^\dagger = \langle I|\,\hat{c}_j. \tag{A.42}$$

An important property of fermionic density matrices is that, when expanded in the operators $\{\hat{c}_j, \hat{c}_j^\dagger\}$, any physical $\hat{\rho}(t)$ contains only even terms [2]. As a consequence, $\hat{\rho}(t)$ commutes with all tilde operators, $[\hat{\rho}(t), \tilde{c}_j] = 0$. Combining this with the tilde-conjugation rules above, we can move all operators acting on the right of $\hat{\rho}$ to the left. For example,

$$\hat{c}_i \hat{\rho} \hat{c}_i^\dagger |I\rangle = \hat{c}_i \hat{\rho}\, \tilde{c}_i |I\rangle = -\tilde{c}_i \hat{c}_i |\hat{\rho}\rangle, \tag{A.43}$$

so the superoperator $\hat{\rho} \mapsto \hat{c}_i \hat{\rho} \hat{c}_i^\dagger$ corresponds to the action of $-\tilde{c}_i \hat{c}_i$ on the state $|\hat{\rho}\rangle$. Applying the same reasoning to all terms in the master equation, the Lindblad dynamics can be written in the compact form

$$\frac{\mathrm{d}}{\mathrm{d}t}|\hat{\rho}(t)\rangle = \hat{\mathcal{L}}|\hat{\rho}(t)\rangle, \tag{A.44}$$

where $\hat{\mathcal{L}}$ is an operator acting on the doubled Fock space.

As a simple illustration, consider a single fermionic mode with Hamiltonian

$$\hat{H} = \omega \hat{c}^\dagger \hat{c} \tag{A.45}$$

and jump operators

$$\hat{L}_1 = \sqrt{\Gamma_1}\,\hat{c}, \qquad \hat{L}_2 = \sqrt{\Gamma_2}\,\hat{c}^\dagger. \tag{A.46}$$

[2] Equivalently, physical states commute with the fermion-parity operator, so that $\hat{\rho}(t)$ is even under fermion parity and has no matrix elements between sectors of different parity; see Sec. 4.5 and, e.g., standard discussions of fermion-parity superselection rules [239].

The corresponding Lindblad master equation reads

$$\frac{\mathrm{d}\hat{\rho}}{\mathrm{d}t} = -i\omega[\hat{c}^\dagger\hat{c},\hat{\rho}] + \frac{\Gamma_1}{2}(2\hat{c}\hat{\rho}\hat{c}^\dagger - \{\hat{c}^\dagger\hat{c},\hat{\rho}\}) + \frac{\Gamma_2}{2}(2\hat{c}^\dagger\hat{\rho}\hat{c} - \{\hat{c}\hat{c}^\dagger,\hat{\rho}\}). \tag{A.47}$$

Multiplying from the right by $|I\rangle$ and using $|\hat{\rho}\rangle = \hat{\rho}|I\rangle$ together with the tilde conjugation rules, each term can be written as an operator acting on $|\hat{\rho}\rangle$, and we obtain

$$\frac{\mathrm{d}}{\mathrm{d}t}|\hat{\rho}\rangle = \Big[-i\omega(\hat{c}^\dagger\hat{c} - \tilde{c}^\dagger\tilde{c}) + \frac{\Gamma_1}{2}(-2i\,\tilde{c}\,\hat{c} - \tilde{c}^\dagger\hat{c} - \tilde{c}^\dagger\tilde{c}) + \frac{\Gamma_2}{2}(-2i\,\tilde{c}^\dagger\hat{c}^\dagger - \hat{c}\hat{c}^\dagger - \tilde{c}\tilde{c}^\dagger)\Big]|\hat{\rho}\rangle. \tag{A.48}$$

This identifies the Liouvillian as a quadratic operator acting on the doubled Fock space of the physical and tilde mode.

A.5.2 Vectorized Liouvillian and TDVP thermal-state preparation

Applying the superfermion formalism described above to the master equation of the extended system, Eq. (6.10), the dynamics is generated by a Liouvillian operator acting on the doubled Fock space of physical and tilde modes,

$$\begin{aligned}\hat{\mathcal{L}} = -i(\hat{H} - \tilde{H}) - \sum_{k=1}^{L}\Bigg[&i\,\gamma_k(1-f_k)\,\tilde{a}_k\hat{a}_k + \frac{\gamma_k(1-f_k)}{2}(\hat{a}_k^\dagger\hat{a}_k + \tilde{a}_k^\dagger\tilde{a}_k)\\ &+ i\,\gamma_k f_k\,\tilde{a}_k^\dagger\hat{a}_k^\dagger + \frac{\gamma_k f_k}{2}(\hat{a}_k\hat{a}_k^\dagger + \tilde{a}_k\tilde{a}_k^\dagger)\Bigg].\end{aligned} \tag{A.49}$$

Here $\hat{H} = \hat{H}_S + \hat{H}_L + \hat{H}_{SL}$ is the Hamiltonian of the extended system, and $\tilde{H} = \tilde{H}_S + \tilde{H}_L + \tilde{H}_{SL}$ denotes its representation on the tilde space. The operators $\tilde{H}_{S,L,SL}$ are obtained from $\hat{H}_{S,L,SL}$ by the replacements $\hat{c}_j \to \tilde{c}_j$, $\hat{a}_k \to \tilde{a}_k$, and similarly for their adjoints. Note that for $U \neq 0$ the term $-i(\hat{H} - \tilde{H})$ contains quartic contributions inherited from $\hat{H}_S$, while the lead dissipator contributes only quadratic terms, shown explicitly in Eq. (A.49).

To prepare thermal states, we use time-dependent variational principle (TDVP) evolution on the vectorized density matrix $|\hat{\rho}\rangle$. The unnormalized infinite-temperature state corresponds to the left vacuum $|I\rangle$, which is an equal-weight superposition of all physical-tilde occupation number configurations. Owing to the interleaved ordering of physical and ancillary modes, this state admits an efficient matrix product state (MPS) representation and can be prepared with bond dimension one.

A thermal state at inverse temperature β is then obtained by imaginary-time evolution,

$$|\hat{\rho}(\beta)\rangle \propto e^{\beta\hat{\mathcal{L}}/2}|I\rangle, \tag{A.50}$$

implemented using standard TDVP techniques for non-Hermitian generators. All simulations were carried out within the `ITensor` ecosystem, which provides efficient support for MPS-based real- and imaginary-time evolution on the doubled Fock space.

A.6 Uncertainty estimate for the variability

In Sec. 6.3.2 we quantify how close the thermal reference state $\hat{\rho}_\beta$ is to the fixed point through the *variability*,

$$v(\hat{\rho}_\beta) \equiv \sqrt{\mathrm{Tr}\big[\mathcal{L}(\hat{\rho}_\beta)^\dagger \mathcal{L}(\hat{\rho}_\beta)\big]} = \|\mathcal{L}(\hat{\rho}_\beta)\|_2, \tag{A.51}$$

where $\|\cdot\|_2$ is the Hilbert–Schmidt norm. In practice, $\hat{\rho}_\beta$ is represented as an MPS $|\hat{\rho}_\beta\rangle\!\rangle$ in the superfermion formalism (Appendix A.5) and obtained by imaginary-time TDVP with a finite bond dimension and a finite truncation cutoff. This appendix explains how we obtain a conservative numerical uncertainty δv on $v(\hat{\rho}_\beta)$.

Let $\hat{\rho}^*_\beta$ denote the exact thermal state and define the (unknown) error $\delta\hat{\rho} \equiv \hat{\rho}_\beta - \hat{\rho}^*_\beta$. Using the linearity of $\mathcal{L}$ and the reverse triangle inequality,

$$\begin{aligned} \big|v(\hat{\rho}^*_\beta) - v(\hat{\rho}_\beta)\big| &= \Big|\|\mathcal{L}(\hat{\rho}_\beta - \delta\hat{\rho})\|_2 - \|\mathcal{L}(\hat{\rho}_\beta)\|_2\Big| \le \|\mathcal{L}(\delta\hat{\rho})\|_2 \\ &\le \|\mathcal{L}\|_{2\to 2} \cdot \|\delta\hat{\rho}\|_2, \end{aligned} \tag{A.52}$$

where $\|\mathcal{L}\|_{2\to 2}$ is the induced norm associated with the Hilbert–Schmidt norm:

$$\|\mathcal{L}\|_{2\to 2} := \sup_{\hat{X}\neq 0} \frac{\|\mathcal{L}(\hat{X})\|_2}{\|\hat{X}\|_2}. \tag{A.53}$$

Therefore the problem reduces to bounding $\|\mathcal{L}\|_{2\to 2}$ and $\|\delta\hat{\rho}\|_2$.

A conservative bound for $\|\mathcal{L}\|_{2\to 2}$ follows by treating the unitary and dissipative parts of $\mathcal{L}(\cdot) = -i[\hat{H}, \cdot] + \mathcal{D}(\cdot)$ separately. For the Hamiltonian contribution we use the commutator inequality

$$\|[\hat{H}, \hat{X}]\|_2 \le 2\|\hat{H}\|_\infty \, \|\hat{X}\|_2, \tag{A.54}$$

which follows from $\|\hat{H}\hat{X}\|_2 \le \|H\|_\infty \|\hat{X}\|_2$ and $\|\hat{X}\hat{H}\|_2 \le \|\hat{H}\|_\infty \|\hat{X}\|_2$. Hence $\|-i[\hat{H}, \cdot]\|_{2\to 2} \le 2\|\hat{H}\|_\infty$.

For the dissipator, consider a single-jump channel of the form

$$\mathcal{D}(\hat{X}) = \gamma\Big(\hat{L}\,\hat{X}\,\hat{L}^\dagger - \tfrac{1}{2}\{\hat{L}^\dagger\hat{L}, \hat{X}\}\Big), \tag{A.55}$$

with $\hat{L} \in \{\hat{a}, \hat{a}^\dagger\}$. Using the bounds $\|\hat{L}\hat{X}\hat{L}^\dagger\|_2 \le \|\hat{L}\|^2_\infty \|\hat{X}\|_2$ and $\|\{\hat{A}, \hat{X}\}\|_2 \le 2\|\hat{A}\|_\infty \|\hat{X}\|_2$, one finds

$$\|\mathcal{D}(\hat{X})\|_2 \le \gamma\Big(\|\hat{L}\|^2_\infty + \|\hat{L}^\dagger\hat{L}\|_\infty\Big)\|\hat{X}\|_2. \tag{A.56}$$

For fermionic mode operators, $\|\hat{a}\|_\infty = \|\hat{a}^\dagger\|_\infty = 1$ and $\|\hat{a}^\dagger\hat{a}\|_\infty \le 1$, hence $\|\mathcal{D}\|_{2\to 2} \le 2\gamma$. Since the full dissipator is a sum of independent single-mode channels with rates γ_k, we obtain the coarse estimate $\|\mathcal{D}\|_{2\to 2} \le 2\sum_k \gamma_k$. In the wide-band discretization used throughout this chapter, $\gamma_k = 2W/L$ and therefore $\sum_k \gamma_k = 2W$, which leads to the practical bound

$$\|\mathcal{L}\|_{2\to 2} \;\le\; 2\|\hat{H}\|_\infty + 4W. \tag{A.57}$$

Numerically, $\|\hat{H}\|_\infty$ is itself upper bounded by a triangle inequality over the MPO coefficients, that is, by the sum of absolute local coupling strengths. This further increases conservativeness but is inexpensive and stable for large MPOs.

To estimate $\|\delta\hat{\rho}\|_2$, we use truncation diagnostics produced during the imaginary-time TDVP evolution. At each truncation step, the algorithm compresses the MPS back to the target bond dimension and reports a discarded weight ϵ_k, defined as the sum of discarded squared singular values at that truncation. Standard MPS error estimates [240] imply that, after a sequence of truncations, the deviation between the exact and truncated vectorized state obeys the bound

$$\|\delta\psi\|_2^2 = \big\||\psi\rangle - |\psi_{\text{trunc}}\rangle\big\|_2^2 \;\le\; 2\sum_{k=1}^{N_{\text{trunc}}} \epsilon_k, \tag{A.58}$$

where N_{trunc} is the total number of truncation events during the evolution and $|\psi\rangle$ denotes the unnormalized vectorized state produced by TDVP.

The physical density operator is obtained by trace normalization,

$$\big|\hat{\rho}_\beta\big\rangle = \frac{|\psi\rangle}{Z}, \qquad Z = \langle I|\psi\rangle, \tag{A.59}$$

where $|I\rangle$ is the left vacuum introduced in App. A.5. Propagating the perturbation $\delta\psi$ through this normalization yields the conservative estimate

$$\|\delta\hat{\rho}\|_2 \;\lesssim\; \frac{\|\delta\psi\|_2}{|Z|} + \frac{\|\psi\|_2\,\|I\|_2}{|Z|^2}\,\|\delta\psi\|_2, \tag{A.60}$$

which captures both the direct scaling of the state by the trace factor and the sensitivity of the normalization itself to perturbations in $|\psi\rangle$.

Combining Eqs. (A.52)–(A.60) defines the truncation-based uncertainty estimate

$$\delta v_{\text{TDVP}} \;:=\; \|\mathcal{L}\|_{2\to 2}\,\|\delta\hat{\rho}\|_2. \tag{A.61}$$

Finally, evaluating $v(\hat{\rho}_\beta)$ requires forming the state $|\eta\rangle = \mathcal{L}\big|\hat{\rho}_\beta\big\rangle$ by applying the MPO representation of $\mathcal{L}$ to the MPS $\big|\hat{\rho}_\beta\big\rangle$, followed by the contraction $v = \sqrt{\langle\eta|\eta\rangle}$. The MPO–MPS product generally increases the bond dimension of $|\eta\rangle$ beyond the target one and therefore involves an additional compression step, controlled by a cutoff ε and a maximum bond dimension χ (singular values below ε are discarded and bonds are truncated to at most χ). This truncation does not affect the prepared thermal state itself, but only the numerical evaluation of v, and its discarded weight is not reported in a form suitable for an analytical bound.

We therefore estimate this contribution empirically by recomputing v in two regimes. In the baseline regime we use $\varepsilon = 10^{-10}$ and $\chi = 400$, obtaining v_{base}. In the strict regime we use $\varepsilon = 10^{-14}$ and $\chi = 1200$, obtaining v_{strict}. We then compute the estimated uncertainty as

$$\delta v_{\text{apply}} \equiv \big|v_{\text{strict}} - v_{\text{base}}\big|. \tag{A.62}$$

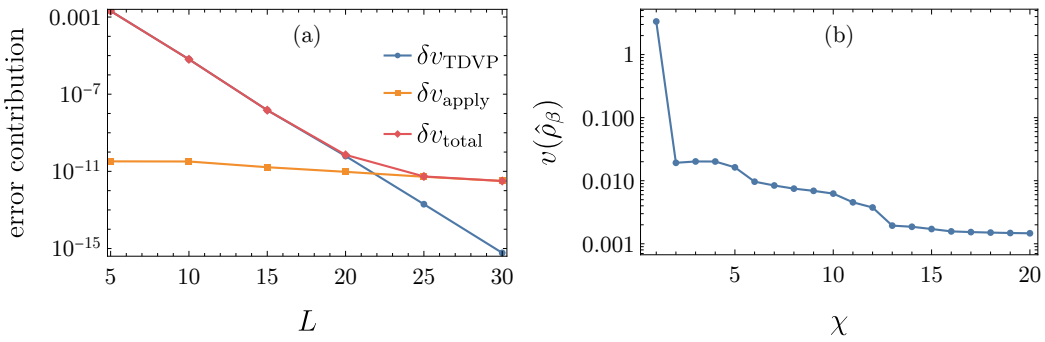

Figure A.1: Numerical uncertainty estimate for the variability. (a) Decomposition of the total error bar δv into the TDVP contribution δv_{TDVP} and the contraction contribution $\delta v_{\mathrm{apply}}$ as a function of the lead size L at $\beta = 0.5$ and fixed bond dimension. (b) Bond-dimension convergence of the variability $v(\hat{\rho}_\beta)$ at fixed $\beta = 0.5$ and $L = 30$.

The total uncertainty reported is taken as the sum of the TDVP error bound and the numerical uncertainty associated with evaluating v,

$$\delta v \equiv \delta v_{\mathrm{TDVP}} + \delta v_{\mathrm{apply}}. \tag{A.63}$$

Figure A.1 summarizes the uncertainty analysis. Panel (a) shows the decomposition of δv into δv_{TDVP} and $\delta v_{\mathrm{apply}}$ as a function of the lead size L at fixed $\beta = 0.5$ and fixed bond dimension. We additionally verify convergence with respect to the bond dimension used to represent $\hat{\rho}_\beta$. Fixing $\beta = 0.5$ and $L = 30$, we compute $v(\hat{\rho}_\beta)$ for increasing bond dimension (with the minimum and maximum bond dimensions set equal). Figure A.1 (b) shows that $v(\hat{\rho}_\beta)$ converges rapidly: beyond a modest bond dimension the successive differences $|v_\chi - v_{\chi'}|$ become negligible, and the values agree with those obtained at the parameters used in Fig. 6.3. This confirms that the reported variability is not limited by an insufficient bond dimension in the thermal-state preparation.

Bibliography

1. S. Carnot. *Réflexions sur la puissance motrice du feu et sur les machines propres à développer cette puissance*. Translated as *Reflections on the Motive Power of Fire*. Bachelier, Paris, 1824.
2. R. Clausius. "Über die bewegende Kraft der Wärme und die Gesetze, welche sich daraus für die Wärmelehre selbst ableiten lassen". *Annalen der Physik* 79, 1850. English translation available as *On the Moving Force of Heat*, pp. 368–397, 500–524.
3. W. Thomson. "On the Dynamical Theory of Heat, with Numerical Results Deduced from Mr. Joule's Equivalent of a Thermal Unit, and M. Regnault's Observations on Steam". *Transactions of the Royal Society of Edinburgh* 20, 1851, pp. 261–288.
4. L. Boltzmann. "Weitere Studien über das Wärmegleichgewicht unter Gasmolekülen". German. *Sitzungsberichte der Akademie der Wissenschaften Wien, Mathematisch-Naturwissenschaftliche Klasse* 66, 1872, pp. 275–370.
5. N. van Kampen. *Stochastic Processes in Physics and Chemistry*. 3rd. North-Holland, Amsterdam, 2007. ISBN: 9780444529657.
6. L. Onsager. "Reciprocal Relations in Irreversible Processes. I". *Physical Review* 37:4, 1931, pp. 405–426. DOI: 10.1103/PhysRev.37.405.
7. L. Onsager. "Reciprocal Relations in Irreversible Processes. II". *Physical Review* 38:12, 1931, pp. 2265–2279. DOI: 10.1103/PhysRev.38.2265.
8. I. Prigogine. *Introduction to Thermodynamics of Irreversible Processes*. 3rd. Interscience Publishers, New York, 1967.
9. I. Prigogine. *From Being to Becoming: Time and Complexity in the Physical Sciences*. W.H. Freeman, San Francisco, 1980.
10. I. Prigogine and I. Stengers. *Order Out of Chaos: Man's New Dialogue with Nature*. Bantam Books, New York, 1984.
11. I. Prigogine and R. Lefever. "Symmetry Breaking Instabilities in Dissipative Systems. II". *The Journal of Chemical Physics* 48:4, 1968, pp. 1695–1700. ISSN: 1089-7690. DOI: 10.1063/1.1668896. URL: http://dx.doi.org/10.1063/1.1668896.
12. B. Alberts, A. Johnson, J. Lewis, M. Raff, K. Roberts, and P. Walter. *Molecular Biology of the Cell*. 7th. W. W. Norton & Company, New York, 2022.
13. H. Qian. "Phosphorylation energy hypothesis: Open chemical systems and their biological functions". *Annual Review of Physical Chemistry* 58, 2007, pp. 113–142. DOI: 10.1146/annurev.physchem.58.032806.104550.
14. I. R. Epstein and J. A. Pojman. *An Introduction to Nonlinear Chemical Dynamics: Oscillations, Waves, Patterns, and Chaos*. Oxford University Press, New York, 1998.

15. H. J. Goldsmid. *Thermoelectric Refrigeration*. Plenum Press, New York, 1964.

16. E. Schrödinger. *What Is Life? The Physical Aspect of the Living Cell*. Cambridge University Press, Cambridge, 1944.

17. U. Seifert. "Stochastic Thermodynamics, Fluctuation Theorems, and Molecular Machines". *Reports on Progress in Physics* 75:12, 2012, p. 126001. DOI: 10.1088/0034-4885/75/12/126001. URL: https://doi.org/10.1088/0034-4885/75/12/126001.

18. D. J. Evans, E. G. D. Cohen, and G. P. Morriss. "Probability of second law violations in shearing steady states". *Physical Review Letters* 71:15, 1993, pp. 2401–2404. DOI: 10.1103/PhysRevLett.71.2401.

19. G. Gallavotti and E. G. D. Cohen. "Dynamical ensembles in nonequilibrium statistical mechanics". *Physical Review Letters* 74:14, 1995, pp. 2694–2697. DOI: 10.1103/PhysRevLett.74.2694.

20. C. Jarzynski. "Nonequilibrium equality for free energy differences". *Physical Review Letters* 78:14, 1997, pp. 2690–2693. DOI: 10.1103/PhysRevLett.78.2690.

21. G. E. Crooks. "Entropy production fluctuation theorem and the nonequilibrium work relation for free energy differences". *Physical Review E* 60:3, 1999, pp. 2721–2726. DOI: 10.1103/PhysRevE.60.2721.

22. J. Gemmer, M. Michel, and G. Mahler. *Quantum Thermodynamics: Emergence of Thermodynamic Behavior Within Composite Quantum Systems*. Springer Berlin Heidelberg, 2009. ISBN: 9783540705109. DOI: 10.1007/978-3-540-70510-9. URL: http://dx.doi.org/10.1007/978-3-540-70510-9.

23. J. Goold, M. Huber, A. Riera, L. d. Rio, and P. Skrzypczyk. "The role of quantum information in thermodynamics—a topical review". *Journal of Physics A: Mathematical and Theoretical* 49:14, 2016, p. 143001. ISSN: 1751-8121. DOI: 10.1088/1751-8113/49/14/143001. URL: http://dx.doi.org/10.1088/1751-8113/49/14/143001.

24. S. Vinjanampathy and J. Anders. "Quantum thermodynamics". *Contemporary Physics* 57:4, 2016, pp. 545–579. DOI: 10.1080/00107514.2016.1201896. URL: https://doi.org/10.1080/00107514.2016.1201896.

25. F. Binder, L. A. Correa, C. Gogolin, J. Anders, and G. Adesso, eds. *Thermodynamics in the Quantum Regime: Fundamental Aspects and New Directions*. Vol. 195. Fundamental Theories of Physics. Springer International Publishing, 2018. ISBN: 9783319990460. DOI: 10.1007/978-3-319-99046-0. URL: http://dx.doi.org/10.1007/978-3-319-99046-0.

26. V. Gorini, A. Kossakowski, and E. Sudarshan. "Completely Positive Dynamical Semigroups of N-Level Systems". *Journal of Mathematical Physics* 17:5, 1976, pp. 821–825. DOI: 10.1063/1.522979. URL: https://doi.org/10.1063/1.522979.

27. G. Lindblad. "On the Generators of Quantum Dynamical Semigroups". *Communications in Mathematical Physics* 48:2, 1976, pp. 119–130. DOI: 10.1007/BF01608499. URL: https://doi.org/10.1007/BF01608499.

28. M. B. Plenio and P. L. Knight. "The quantum-jump approach to dissipative dynamics in quantum optics". *Reviews of Modern Physics* 70:1, 1998, pp. 101–144. ISSN: 1539-0756. DOI: 10.1103/revmodphys.70.101. URL: http://dx.doi.org/10.1103/RevModPhys.70.101.

29. J. Dalibard, Y. Castin, and K. Mølmer. "Wave-function approach to dissipative processes in quantum optics". *Physical Review Letters* 68:5, 1992, pp. 580–583. ISSN: 0031-9007. DOI: 10.1103/physrevlett.68.580. URL: http://dx.doi.org/10.1103/PhysRevLett.68.580.

30. H. Spohn. "Entropy production for quantum dynamical semigroups". *Journal of Mathematical Physics* 19:5, 1978, pp. 1227–1230. DOI: 10.1063/1.523789.

31. H.-P. Breuer and F. Petruccione. *The Theory of Open Quantum Systems*. Oxford University Press, Oxford, 2002. ISBN: 978-0-19-852063-4.

32. C. W. Gardiner and P. Zoller. *Quantum Noise: A Handbook of Markovian and Non-Markovian Quantum Stochastic Methods with Applications to Quantum Optics*. 2nd. Vol. 56. Springer Series in Synergetics. Springer-Verlag, 2004. DOI: 10.1007/978-3-662-09174-5. URL: https://doi.org/10.1007/978-3-662-09174-5.

33. Á. Rivas, S. F. Huelga, and M. B. Plenio. "Quantum non-Markovianity: characterization, quantification and detection". *Reports on Progress in Physics* 77:9, 2014, p. 094001. ISSN: 1361-6633. DOI: 10.1088/0034-4885/77/9/094001. URL: http://dx.doi.org/10.1088/0034-4885/77/9/094001.

34. I. de Vega and D. Alonso. "Dynamics of non-Markovian open quantum systems". *Reviews of Modern Physics* 89:1, 2017. ISSN: 1539-0756. DOI: 10.1103/revmodphys.89.015001. URL: http://dx.doi.org/10.1103/RevModPhys.89.015001.

35. Á. Rivas and S. F. Huelga. *Open Quantum Systems: An Introduction*. SpringerBriefs in Physics. Springer, Berlin, Heidelberg, 2012. ISBN: 978-3-642-23354-8. DOI: 10.1007/978-3-642-23354-8. URL: https://link.springer.com/book/10.1007/978-3-642-23354-8.

36. D. Chruściński and S. Maniscalco. "Degree of Non-Markovianity of Quantum Evolution". *Physical Review Letters* 112:12, 2014. ISSN: 1079-7114. DOI: 10.1103/physrevlett.112.120404. URL: http://dx.doi.org/10.1103/PhysRevLett.112.120404.

37. A. Imamoglu. "Stochastic wave-function approach to non-Markovian systems". *Physical Review A* 50:5, 1994, pp. 3650–3653. DOI: 10.1103/PhysRevA.50.3650.

38. P. Stenius and A. Imamoglu. "Stochastic wavefunction methods beyond the Born - Markov and rotating-wave approximations". *Quantum and Semiclassical Optics: Journal of the European Optical Society Part B* 8:1, 1996, pp. 283–295. ISSN: 1361-6625. DOI: 10.1088/1355-5111/8/1/021. URL: http://dx.doi.org/10.1088/1355-5111/8/1/021.

39. B. M. Garraway and P. L. Knight. "Cavity modified quantum beats". *Physical Review A* 54:4, 1996, pp. 3592–3602. ISSN: 1094-1622. DOI: 10.1103/physreva.54.3592. URL: http://dx.doi.org/10.1103/PhysRevA.54.3592.

40. B. M. Garraway. "Nonperturbative decay of an atomic system in a cavity". *Physical Review A* 55:3, 1997, pp. 2290–2303. ISSN: 1094-1622. DOI: 10.1103/physreva.55.2290. URL: http://dx.doi.org/10.1103/PhysRevA.55.2290.

41. S. Datta. *Electronic Transport in Mesoscopic Systems*. Cambridge University Press, 1995. ISBN: 9780511805776. DOI: 10.1017/cbo9780511805776. URL: http://dx.doi.org/10.1017/CBO9780511805776.

42. M. Galperin, M. A. Ratner, and A. Nitzan. "Molecular transport junctions: vibrational effects". *Journal of Physics: Condensed Matter* 19:10, 2007, p. 103201. ISSN: 1361-648X. DOI: 10.1088/0953-8984/19/10/103201. URL: http://dx.doi.org/10.1088/0953-8984/19/10/103201.

43. K. Sun, M. Kang, H. Nuomin, G. Schwartz, D. N. Beratan, K. R. Brown, and J. Kim. "Quantum simulation of spin-boson models with structured bath". *Nature Communications* 16:1, 2025. ISSN: 2041-1723. DOI: 10.1038/s41467-025-59296-y. URL: http://dx.doi.org/10.1038/s41467-025-59296-y.

44. M. Brenes, J. J. Mendoza-Arenas, A. Purkayastha, M. T. Mitchison, S. R. Clark, and J. Goold. "Tensor-Network Method to Simulate Strongly Interacting Quantum Thermal Machines". *Physical Review X* 10:3, 2020. ISSN: 2160-3308. DOI: 10.1103/physrevx.10.031040. URL: http://dx.doi.org/10.1103/PhysRevX.10.031040.

45. A. M. Lacerda, A. Purkayastha, M. Kewming, G. T. Landi, and J. Goold. "Quantum thermodynamics with fast driving and strong coupling via the mesoscopic leads approach". *Physical Review B* 107:19, 2023. ISSN: 2469-9969. DOI: 10.1103/physrevb.107.195117. URL: http://dx.doi.org/10.1103/PhysRevB.107.195117.

46. L. P. Bettmann, M. J. Kewming, G. T. Landi, J. Goold, and M. T. Mitchison. *Quantum stochastic thermodynamics in the mesoscopic-leads formulation*. 2024. DOI: 10.48550/ARXIV.2404.06426. URL: https://arxiv.org/abs/2404.06426.

47. A. M. Lacerda, M. J. Kewming, M. Brenes, C. Jackson, S. R. Clark, M. T. Mitchison, and J. Goold. "Entropy production in the mesoscopic-leads formulation of quantum thermodynamics". *Physical Review E* 110:1, 2024. ISSN: 2470-0053. DOI: 10.1103/physreve.110.014125. URL: http://dx.doi.org/10.1103/PhysRevE.110.014125.

48. P. Strasberg, G. Schaller, T. Brandes, and M. Esposito. "Quantum and Information Thermodynamics: A Unifying Framework Based on Repeated Interactions". *Physical Review X* 7:2, 2017. ISSN: 2160-3308. DOI: 10.1103/physrevx.7.021003. URL: http://dx.doi.org/10.1103/PhysRevX.7.021003.

49. F. Minganti, A. Biella, N. Bartolo, and C. Ciuti. "Spectral theory of Liouvillians for dissipative phase transitions". *Physical Review A* 98:4, 2018, p. 042118. DOI: 10.1103/PhysRevA.98.042118. URL: https://doi.org/10.1103/PhysRevA.98.042118.

50. K. Hepp and E. H. Lieb. "On the superradiant phase transition for molecules in a quantized radiation field: the dicke maser model". *Annals of Physics* 76:2, 1973, pp. 360–404. ISSN: 0003-4916. DOI: 10.1016/0003-4916(73)90039-0. URL: http://dx.doi.org/10.1016/0003-4916(73)90039-0.

51. P. Kirton, M. M. Roses, J. Keeling, and E. G. Dalla Torre. "Introduction to the Dicke Model: From Equilibrium to Nonequilibrium, and Vice Versa". *Advanced Quantum Technologies* 2:1–2, 2018. ISSN: 2511-9044. DOI: 10.1002/qute.201800043. URL: http://dx.doi.org/10.1002/qute.201800043.

52. K. Baumann, C. Guerlin, F. Brennecke, and T. Esslinger. "Dicke quantum phase transition with a superfluid gas in an optical cavity". *Nature* 464:7293, 2010, pp. 1301–1306. ISSN: 1476-4687. DOI: 10.1038/nature09009. URL: http://dx.doi.org/10.1038/nature09009.

53. M. Brunelli, L. Fusco, R. Landig, W. Wieczorek, J. Hoelscher-Obermaier, G. Landi, F. L. Semião, A. Ferraro, N. Kiesel, T. Donner, G. De Chiara, and M. Paternostro. "Experimental Determination of Irreversible Entropy Production in out-of-Equilibrium Mesoscopic Quantum Systems". *Physical Review Letters* 121:16, 2018. ISSN: 1079-7114. DOI: 10.1103/physrevlett.121.160604.

54. G. E. Crooks. "Measuring thermodynamic length". *Physical Review Letters* 99:10, 2007, p. 100602. DOI: 10.1103/PhysRevLett.99.100602.

55. D. A. Sivak and G. E. Crooks. "Thermodynamic Metrics and Optimal Paths". *Physical Review Letters* 108:19, 2012, p. 190602. DOI: 10.1103/PhysRevLett.108.190602.

56. D. Mandal and C. Jarzynski. "Analysis of slow transitions between nonequilibrium steady states". *Journal of Statistical Mechanics: Theory and Experiment* 6, 2016, p. 063204. DOI: 10.1088/1742-5468/2016/06/063204. URL: https://doi.org/10.1088/1742-5468/2016/06/063204.

57. T. Hatano and S.-i. Sasa. "Steady-state thermodynamics of Langevin systems". *Physical Review Letters* 86:16, 2001, pp. 3463–3466. DOI: 10.1103/PhysRevLett.86.3463.

58. U. Seifert. "Entropy production along a stochastic trajectory and an integral fluctuation theorem". *Physical Review Letters* 95:4, 2005, p. 040602. DOI: 10.1103/PhysRevLett.95.040602.

59. M. Scandi and M. Perarnau-Llobet. "Thermodynamic length in open quantum systems". *Quantum* 3, 2019, p. 197. DOI: 10.22331/q-2019-10-24-197.

60. M. Esposito and C. V. den Broeck. "Three Detailed Fluctuation Theorems". *Physical Review Letters* 104:9, 2010, p. 090601. DOI: 10.1103/PhysRevLett.104.090601. URL: https://doi.org/10.1103/PhysRevLett.104.090601.

61. G. Manzano, J. M. Horowitz, and J. M. R. Parrondo. "Quantum Fluctuation Theorems for Arbitrary Environments: Adiabatic and Nonadiabatic Entropy Production". *Phys. Rev. X* 8:3, 2018, p. 031037. DOI: 10.1103/PhysRevX.8.031037. URL: https://link.aps.org/doi/10.1103/PhysRevX.8.031037.

62. A. M. Lacerda, L. P. Bettmann, and J. Goold. "Information geometry of transitions between quantum nonequilibrium steady states". *Physical Review E* 112:2, 2025. ISSN: 2470-0053. DOI: 10.1103/9f6l-d766. URL: http://dx.doi.org/10.1103/9f6l-d766.

63. H.-P. Breuer, E.-M. Laine, J. Piilo, and B. Vacchini. "Colloquium: Non-Markovian dynamics in open quantum systems". *Rev. Mod. Phys.* 88, 2 2016, p. 021002. DOI: 10.1103/RevModPhys.88.021002. URL: https://link.aps.org/doi/10.1103/RevModPhys.88.021002.

64. A. Purkayastha. "Lyapunov equation in open quantum systems and non-Hermitian physics". *Physical Review B* 105:17, 2022, p. 174207. DOI: 10.1103/PhysRevB.105.174207. arXiv: 2201.00677 [quant-ph]. URL: https://doi.org/10.1103/PhysRevB.105.174207.

65. T. Prosen. "Third quantization: a general method to solve master equations for quadratic open Fermi systems". *New Journal of Physics* 10:4, 2008, p. 043026. ISSN: 1367-2630. DOI: 10.1088/1367-2630/10/4/043026. URL: https://dx.doi.org/10.1088/1367-2630/10/4/043026 (visited on 02/26/2025).

66. J. Cui, J. I. Cirac, and M. C. Bañuls. "Variational matrix product operators for the steady state of dissipative quantum systems". *Physical Review Letters* 114, 2015, p. 220601. DOI: 10.1103/PhysRevLett.114.220601. URL: https://doi.org/10.1103/PhysRevLett.114.220601.

67. A. H. Werner, D. Jaschke, P. Silvi, M. Kliesch, T. Calarco, J. Eisert, and S. Montangero. "Positive tensor network approach for simulating open quantum many-body systems". *Physical Review Letters* 116, 2016, p. 237201. DOI: 10.1103/PhysRevLett.116.237201. URL: https://doi.org/10.1103/PhysRevLett.116.237201.

68. D. Jaschke, S. Montangero, and L. D. Carr. "One-dimensional many-body entangled open quantum systems with tensor network methods". *arXiv preprint arXiv:1804.09796*, 2018. URL: https://arxiv.org/abs/1804.09796.

69. Y. Tanimura and R. Kubo. "Time evolution of a quantum system in contact with a nearly Gaussian-Markoffian noise bath". *Journal of the Physical Society of Japan* 58:1, 1989, pp. 101–114. URL: https://doi.org/10.1143/JPSJ.58.101.

70. Y. Tanimura. "Numerically "exact" approach to open quantum dynamics: The hierarchical equations of motion (HEOM)". *The Journal of Chemical Physics* 153:2, 2020, p. 020901. URL: https://doi.org/10.1063/5.0011599.

71. R. P. Feynman and F. L. Vernon. "The theory of a general quantum system interacting with a linear dissipative system". *Annals of Physics* 24:1, 1963, pp. 118–173. URL: https://doi.org/10.1016/0003-4916(63)90068-X.

72. N. Makri and D. E. Makarov. "Tensor propagator for iterative quantum time evolution of reduced density matrices. I. Theory". *The Journal of Chemical Physics* 102:11, 1995, pp. 4600–4610. URL: https://doi.org/10.1063/1.469508.

73. A. Strathearn, P. Kirton, D. Kilda, J. Keeling, and B. W. Lovett. "Efficient non-Markovian quantum dynamics using time-evolving matrix product operators". *Nature Communications* 9:1, 2018, p. 3322. URL: https://doi.org/10.1038/s41467-018-05617-3.

74. J. Prior, A. W. Chin, S. F. Huelga, and M. B. Plenio. "Efficient simulation of strong system-environment interactions". *Physical Review Letters* 105:5, 2010, p. 050404. URL: https://doi.org/10.1103/PhysRevLett.105.050404.

75. K. Kraus. *States, Effects, and Operations: Fundamental Notions of Quantum Theory*. Vol. 190. Lecture Notes in Physics. Springer, Berlin, Heidelberg, 1983. ISBN: 978-3-540-12732-1. DOI: 10.1007/3-540-12732-1.

76. R. Alicki and K. Lendi. *Quantum Dynamical Semigroups and Applications*. Vol. 286. Lecture Notes in Physics. Springer-Verlag, 1987. DOI: 10.1007/3-540-18276-4. URL: https://doi.org/10.1007/3-540-18276-4.

77. P. P. Potts. *Quantum Thermodynamics*. Lecture notes. 2024. arXiv: 2406.19206 [quant-ph]. URL: https://arxiv.org/abs/2406.19206.

78. C. Cohen-Tannoudji, J. Dupont-Roc, and G. Grynberg. *Atom—Photon Interactions: Basic Process and Appilcations*. Wiley, 1998. ISBN: 9783527617197. DOI: 10.1002/9783527617197. URL: http://dx.doi.org/10.1002/9783527617197.

79. G. T. Landi. *Quantum Information and Quantum Noise*. Lecture notes. 2019. URL: https://www.fmt.if.usp.br/~gtlandi/courses/lecture-notes_v2-18.pdf.

80. M. Cattaneo, G. L. Giorgi, S. Maniscalco, and R. Zambrini. "Local vs global master equation with common and separate baths: superiority of the global approach in partial secular approximation". *New Journal of Physics* 21:11, 2019, p. 113045. DOI: 10.1088/1367-2630/ab54ac. URL: https://iopscience.iop.org/article/10.1088/1367-2630/ab54ac.

81. W. Rudin. *Real and Complex Analysis*. 3rd. McGraw-Hill, New York, 1987.

82. G. Schaller. *Open Quantum Systems Far from Equilibrium*. Vol. 881. Lecture Notes in Physics. Springer, 2014. ISBN: 978-3-319-03876-6. DOI: 10.1007/978-3-319-03877-3.

83. H. Wichterich, M. J. Henrich, H.-P. Breuer, J. Gemmer, and M. Michel. "Modeling heat transport through completely positive maps". *Physical Review E* 76:3, 2007, p. 031115. DOI: 10.1103/PhysRevE.76.031115. URL: https://journals.aps.org/pre/abstract/10.1103/PhysRevE.76.031115.

84. H. B. Callen. *Thermodynamics and an Introduction to Thermostatistics*. 2nd. Wiley, New York, 1985. ISBN: 9780471862567.

85. F. Reif. *Fundamentals of Statistical and Thermal Physics*. McGraw-Hill, New York, 1965. ISBN: 9780070518001.

86. A. Colla and H.-P. Breuer. "Open-system approach to nonequilibrium quantum thermodynamics at arbitrary coupling". *Physical Review A* 105:5, 2022. ISSN: 2469-9934. DOI: 10.1103/physreva.105.052216. URL: http://dx.doi.org/10.1103/PhysRevA.105.052216.

87. U. Seifert. "First and Second Law of Thermodynamics at Strong Coupling". *Physical Review Letters* 116:2, 2016, p. 020601. DOI: 10.1103/PhysRevLett.116.020601. URL: https://doi.org/10.1103/PhysRevLett.116.020601.

88. P. Strasberg, G. Schaller, N. Lambert, and T. Brandes. "Nonequilibrium thermodynamics in the strong coupling and non-Markovian regime based on a reaction coordinate mapping". *New Journal of Physics* 18:7, 2016, p. 073007. DOI: 10.1088/1367-2630/18/7/073007.

89. Á. Rivas. "Strong Coupling Thermodynamics of Open Quantum Systems". *Physical Review Letters* 124:16, 2020, p. 160601. DOI: 10.1103/PhysRevLett.124.160601. URL: https://doi.org/10.1103/PhysRevLett.124.160601.

90. M. F. Gelin and M. Thoss. "Thermodynamics of a subensemble of a canonical ensemble". en. *Phys. Rev. E Stat. Nonlin. Soft Matter Phys.* 79:5 Pt 1, 2009, p. 051121.

91. M. Campisi, P. Talkner, and P. Hänggi. "Thermodynamics and fluctuation theorems for a strongly coupled open quantum system: An exactly solvable case". *Physical Review E* 80:6, 2009, p. 061143. DOI: 10.1103/PhysRevE.80.061143.

92. P. Talkner and P. Hänggi. "Colloquium: Statistical mechanics and thermodynamics at strong coupling: Quantum and classical". *Reviews of Modern Physics* 92:4, 2020, p. 041002. DOI: 10.1103/RevModPhys.92.041002. URL: https://doi.org/10.1103/RevModPhys.92.041002.

93. M. A. Nielsen and I. L. Chuang. *Quantum Computation and Quantum Information*. Cambridge University Press, Cambridge, 2000. ISBN: 9780521635035.

94. M. Esposito, U. Harbola, and S. Mukamel. "Nonequilibrium fluctuations, fluctuation theorems, and counting statistics in quantum systems". *Reviews of Modern Physics* 81:4, 2009, pp. 1665–1702. ISSN: 15390756. DOI: 10.1103/RevModPhys.81.1665. arXiv: 0811.3717.

95. K. Ptaszyński and M. Esposito. "Entropy Production in Open Systems: The Predominant Role of Intraenvironment Correlations". *Phys. Rev. Lett.* 123, 20 2019, p. 200603. DOI: 10.1103/PhysRevLett.123.200603. URL: https://link.aps.org/doi/10.1103/PhysRevLett.123.200603.

96. U. Weiss. *Quantum Dissipative Systems*. 4th. Vol. 13. Series in Modern Condensed Matter Physics. World Scientific, Singapore, 2012. DOI: 10.1142/8334.

97. A. W. Chin, Á. Rivas, S. F. Huelga, and M. B. Plenio. "Exact mapping between system-reservoir quantum models and semi-infinite discrete chains using orthogonal polynomials". *Journal of Mathematical Physics* 51:9, 2010, p. 092109. DOI: 10.1063/1.3490188.

98. R. Alicki. "The quantum open system as a model of the heat engine". *J. Phys. A Math. Gen.* 12:5, 1979, pp. L103–L107.

99. G. Lindblad. "Completely positive maps and entropy inequalities". *Communications in Mathematical Physics* 40:2, 1975, pp. 147–151. DOI: 10.1007/BF01609396. URL: https://doi.org/10.1007/BF01609396.

100. A. Uhlmann. "Relative entropy and the Wigner-Yanase-Dyson-Lieb concavity in an interpolation theory". *Communications in Mathematical Physics* 54:1, 1977, pp. 21–32. DOI: 10.1007/BF01609834. URL: https://doi.org/10.1007/BF01609834.

101. M. A. Nielsen and D. Petz. "A simple proof of the strong subadditivity inequality". *Quantum Information and Computation* 5, 2005, pp. 507–513.

102. M. Aspelmeyer, T. J. Kippenberg, and F. Marquardt. "Cavity optomechanics". *Reviews of Modern Physics* 86:4, 2014, pp. 1391–1452. ISSN: 1539-0756. DOI: 10.1103/revmodphys.86.1391. URL: http://dx.doi.org/10.1103/RevModPhys.86.1391.

103. A. M. Lacerda, J. Goold, and G. T. Landi. "Dephasing enhanced transport in boundary-driven quasiperiodic chains". *Physical Review B* 104:17, 2021. ISSN: 2469-9969. DOI: 10.1103/physrevb.104.174203. URL: http://dx.doi.org/10.1103/PhysRevB.104.174203.

104. M. Žnidarič. "Exact solution for a diffusive nonequilibrium steady state of an open quantum chain". *Journal of Statistical Mechanics: Theory and Experiment* 2010:05, 2010, p. L05002. ISSN: 1742-5468. DOI: 10.1088/1742-5468/2010/05/l05002. URL: http://dx.doi.org/10.1088/1742-5468/2010/05/L05002.

105. S. L. Jacob, L. P. Bettmann, A. M. Lacerda, K. Zawadzki, S. R. Clark, J. Goold, and J. J. Mendoza-Arenas. "Dephasing-assisted transport in a tight-binding chain with a linear potential". *Frontiers in Physics* 12, 22, 2024. Publisher: Frontiers. ISSN: 2296-424X. DOI: 10.3389/fphy.2024.1474018. URL: https://www.frontiersin.org/journals/physics/articles/10.3389/fphy.2024.1474018/full.

106. S. Bravyi. "Lagrangian representation for fermionic linear optics". *Quantum Inf. Comput.* 5:3, 2005, pp. 216–238.

107. J. Surace and L. Tagliacozzo. "Fermionic Gaussian states: an introduction to numerical approaches". *SciPost Phys. Lect. Notes*, 2022, p. 54. DOI: 10.21468/SciPostPhysLectNotes.54. URL: https://scipost.org/10.21468/SciPostPhysLectNotes.54.

108. I. Peschel. "Calculation of reduced density matrices from correlation functions". *Journal of Physics A: Mathematical and General* 36:14, 2003, p. L205. ISSN: 0305-4470. DOI: 10.1088/0305-4470/36/14/101. URL: https://dx.doi.org/10.1088/0305-4470/36/14/101 (visited on 02/26/2025).

109. L. Banchi, P. Giorda, and P. Zanardi. "Quantum information-geometry of dissipative quantum phase transitions". *Physical Review E* 89:2, 2014. ISSN: 1550-2376. DOI: 10.1103/physreve.89.022102. URL: http://dx.doi.org/10.1103/PhysRevE.89.022102.

110. H. Casini, R. Medina, I. S. Landea, and G. Torroba. "Renyi relative entropies and renormalization group flows". *Journal of High Energy Physics* 2018:9, 2018. ISSN: 1029-8479. DOI: 10.1007/jhep09(2018)166. URL: http://dx.doi.org/10.1007/JHEP09(2018)166.

111. M. Coppola, D. Karevski, and G. T. Landi. "Conditional no-jump dynamics of non-interacting quantum chains". *Phys. Rev. B* 110, 9 2024, p. 094315. DOI: 10.1103/PhysRevB.110.094315. URL: https://link.aps.org/doi/10.1103/PhysRevB.110.094315.

112. M. Coppola. “Quantum correlations and non-equilibrium quantum transport”. Thèse soutenue le 17 novembre 2023. PhD thesis. Nancy, France: Université de Lorraine, 2023.

113. M. Fabrizio. *A Course in Quantum Many-Body Theory: From Conventional Fermi Liquids to Strongly Correlated Systems*. Graduate Texts in Physics. Springer International Publishing, Cham, Switzerland, 2022. ISBN: 978-3-031-16304-3. DOI: 10.1007/978-3-031-16305-0.

114. I. Klich. “A note on the full counting statistics of paired fermions”. *J. Stat. Mech.* 2014:11, 2014, P11006.

115. R. Blankenbecler, D. J. Scalapino, and R. L. Sugar. “Monte Carlo calculations of coupled boson-fermion systems. I”. *Physical Review D* 24:8, 1981, pp. 2278–2286. ISSN: 0556-2821. DOI: 10.1103/physrevd.24.2278. URL: http://dx.doi.org/10.1103/PhysRevD.24.2278.

116. G. T. Landi. “Waiting time statistics in boundary-driven free fermion chains”. *Phys. Rev. B* 104, 19 2021, p. 195408. DOI: 10.1103/PhysRevB.104.195408. URL: https://link.aps.org/doi/10.1103/PhysRevB.104.195408.

117. M. Gaudin. “Une démonstration simplifiée du théorème de wick en mécanique statistique”. *Nuclear Physics* 15, 1960, pp. 89–91. ISSN: 0029-5582. DOI: 10.1016/0029-5582(60)90285-6. URL: http://dx.doi.org/10.1016/0029-5582(60)90285-6.

118. N. Friis, A. R. Lee, and D. E. Bruschi. “Fermionic mode entanglement in quantum information”. *Physical Review A* 87:2, 25, 2013, p. 022338. ISSN: 1050-2947, 1094-1622. DOI: 10.1103/PhysRevA.87.022338. arXiv: 1211.7217[quant-ph]. URL: http://arxiv.org/abs/1211.7217 (visited on 02/26/2025).

119. S. Bravyi and R. Konig. “Classical simulation of dissipative fermionic linear optics”. *Quantum Information and Computation* 12:11–12, 2012, pp. 925–943. ISSN: 1533-7146. DOI: 10.26421/qic12.11-12-2. URL: http://dx.doi.org/10.26421/QIC12.11-12-2.

120. T. Barthel and Y. Zhang. “Solving quasi-free and quadratic Lindblad master equations for open fermionic and bosonic systems”. *Journal of Statistical Mechanics: Theory and Experiment* 2022:11, 2022, p. 113101. ISSN: 1742-5468. DOI: 10.1088/1742-5468/ac8e5c. URL: http://dx.doi.org/10.1088/1742-5468/ac8e5c.

121. R. H. Bartels and G. W. Stewart. “Algorithm 432 [C2]: Solution of the matrix equation AX + XB = C [F4]”. *Communications of the ACM* 15:9, 1972, pp. 820–826. ISSN: 1557-7317. DOI: 10.1145/361573.361582. URL: http://dx.doi.org/10.1145/361573.361582.

122. V. K. Varma, C. de Mulatier, and M. Žnidarič. “Fractality in nonequilibrium steady states of quasiperiodic systems”. *Physical Review E* 96:3, 2017. ISSN: 2470-0053. DOI: 10.1103/physreve.96.032130. URL: http://dx.doi.org/10.1103/PhysRevE.96.032130.

123. M. Behr, P. Benner, and J. Heiland. "Solution formulas for differential Sylvester and Lyapunov equations". *Calcolo* 56:4, 2019. ISSN: 1126-5434. DOI: 10.1007/s10092-019-0348-x. URL: http://dx.doi.org/10.1007/s10092-019-0348-x.

124. P. Jordan and E. Wigner. "Über das Paulische Äquivalenzverbot". German. *Zeitschrift für Physik* 47:9-10, 1928. Original paper introducing the Jordan–Wigner transformation, pp. 631–651. DOI: 10.1007/BF01331938. URL: https://doi.org/10.1007/BF01331938.

125. P. Coleman. *Introduction to Many-Body Physics*. Cambridge University Press, 2015. ISBN: 9781139020916. DOI: 10.1017/cbo9781139020916. URL: http://dx.doi.org/10.1017/CBO9781139020916.

126. G. H. Wannier. "Dynamics of Band Electrons in Electric and Magnetic Fields". *Reviews of Modern Physics* 34:4, 1, 1962. Publisher: American Physical Society, pp. 645–655. DOI: 10.1103/RevModPhys.34.645. URL: https://link.aps.org/doi/10.1103/RevModPhys.34.645 (visited on 02/26/2025).

127. M. Glück. "Wannier–Stark resonances in optical and semiconductor superlattices". *Physics Reports* 366:3, 2002, pp. 103–182. ISSN: 0370-1573. DOI: 10.1016/s0370-1573(02)00142-4. URL: http://dx.doi.org/10.1016/S0370-1573(02)00142-4.

128. T. Hartmann, F. Keck, H. J. Korsch, and S. Mossmann. "Dynamics of Bloch oscillations". *New J. Phys.* 6, 2004, pp. 2–2. DOI: 10.1088/1367-2630/6/1/002.

129. A. J. Baldwin and J. A. Jones. "Efficiently computing the Uhlmann fidelity for density matrices". *Physical Review A* 107:1, 2023. ISSN: 2469-9934. DOI: 10.1103/physreva.107.012427. URL: http://dx.doi.org/10.1103/PhysRevA.107.012427.

130. Y. Tanimura. "Stochastic Liouville, Langevin, Fokker–Planck, and Master Equation Approaches to Quantum Dissipative Systems". *Journal of the Physical Society of Japan* 75:8, 2006, p. 082001. ISSN: 1347-4073. DOI: 10.1143/jpsj.75.082001. URL: http://dx.doi.org/10.1143/JPSJ.75.082001.

131. R. Landauer. "Spatial Variation of Currents and Fields Due to Localized Scatterers in Metallic Conduction". *IBM Journal of Research and Development* 1:3, 1957, pp. 223–231. ISSN: 0018-8646. DOI: 10.1147/rd.13.0223. URL: http://dx.doi.org/10.1147/rd.13.0223.

132. M. Büttiker. "Four-Terminal Phase-Coherent Conductance". *Physical Review Letters* 57:14, 1986, pp. 1761–1764. ISSN: 0031-9007. DOI: 10.1103/physrevlett.57.1761. URL: http://dx.doi.org/10.1103/PhysRevLett.57.1761.

133. M. Zwolak. "Analytic expressions for the steady-state current with finite extended reservoirs". *The Journal of Chemical Physics* 153:22, 2020. ISSN: 1089-7690. DOI: 10.1063/5.0029223. URL: http://dx.doi.org/10.1063/5.0029223.

134. B. De, G. Wójtowicz, J. Zakrzewski, M. Zwolak, and M. M. Rams. "Transport in a periodically driven tilted lattice via the extended reservoir approach: Stability criterion for recovering the continuum limit". *Physical Review B* 107:23, 2023. ISSN: 2469-9969. DOI: 10.1103/physrevb.107.235148. URL: http://dx.doi.org/10.1103/PhysRevB.107.235148.

135. T. Zelovich, L. Kronik, and O. Hod. "State Representation Approach for Atomistic Time-Dependent Transport Calculations in Molecular Junctions". *Journal of Chemical Theory and Computation* 10:8, 2014, pp. 2927–2941. ISSN: 1549-9626. DOI: 10.1021/ct500135e. URL: http://dx.doi.org/10.1021/ct500135e.

136. A. Oz, O. Hod, and A. Nitzan. "Numerical Approach to Nonequilibrium Quantum Thermodynamics: Nonperturbative Treatment of the Driven Resonant Level Model Based on the Driven Liouville von-Neumann Formalism". *Journal of Chemical Theory and Computation* 16:2, 2019, pp. 1232–1248. DOI: 10.1021/acs.jctc.9b00999. URL: https://doi.org/10.1021%2Facs.jctc.9b00999.

137. L. P. Bettmann, M. J. Kewming, G. T. Landi, J. Goold, and M. T. Mitchison. *Quantum stochastic thermodynamics in the mesoscopic-leads formulation*. 2024. DOI: 10.48550/ARXIV.2404.06426. URL: https://arxiv.org/abs/2404.06426.

138. P. Bocchieri and A. Loinger. "Quantum Recurrence Theorem". *Physical Review* 107:2, 1957, pp. 337–338. DOI: 10.1103/PhysRev.107.337.

139. J. Iles-Smith, N. Lambert, and A. Nazir. "Environmental dynamics, correlations, and the emergence of noncanonical equilibrium states in open quantum systems". *Physical Review A* 90:3, 2014. ISSN: 1094-1622. DOI: 10.1103/physreva.90.032114. URL: http://dx.doi.org/10.1103/PhysRevA.90.032114.

140. R. Bulla, T. A. Costi, and T. Pruschke. "Numerical renormalization group method for quantum impurity systems". *Reviews of Modern Physics* 80:2, 2008, pp. 395–450. ISSN: 1539-0756. DOI: 10.1103/revmodphys.80.395. URL: http://dx.doi.org/10.1103/RevModPhys.80.395.

141. C. Shannon. "Communication in the Presence of Noise". *Proceedings of the IRE* 37:1, 1949, pp. 10–21. ISSN: 0096-8390. DOI: 10.1109/jrproc.1949.232969. URL: http://dx.doi.org/10.1109/JRPROC.1949.232969.

142. R. N. Bracewell. *The Fourier Transform and Its Applications*. Circuits and Systems. McGraw-Hill, 2000. ISBN: 9780071160438.

143. G. D. Mahan. *Many-Particle Physics*. 3rd. Springer, New York, 2000. ISBN: 978-0306463389.

144. W. Rudin. *Real and Complex Analysis*. 3rd. McGraw-Hill, New York, 1986. ISBN: 978-0070542341.

145. F. W. King. *Hilbert Transforms. Volume 1*. Vol. 124. Encyclopedia of Mathematics and its Applications. Cambridge University Press, Cambridge, 2009. ISBN: 978-0-521-88762-5.

146. A. Nazir and G. Schaller. "The Reaction Coordinate Mapping in Quantum Thermodynamics". In: *Quantum Thermodynamics*. Ed. by F. Binder, L. A. Correa, C. Gogolin, J. Anders, and G. Adesso. Springer, 2019, pp. 551–577. DOI: 10.1007/978-3-319-99046-0_22. URL: https://doi.org/10.1007/978-3-319-99046-0_22.

147. U. Fano. "Effects of Configuration Interaction on Intensities and Phase Shifts". *Physical Review* 124:6, 1961, pp. 1866–1878. ISSN: 0031-899X. DOI: 10.1103/physrev.124.1866. URL: http://dx.doi.org/10.1103/PhysRev.124.1866.

148. B. J. Dalton, S. M. Barnett, and B. M. Garraway. "Theory of pseudomodes in quantum optical processes". *Physical Review A* 64:5, 2001. ISSN: 1094-1622. DOI: 10.1103/physreva.64.053813. URL: http://dx.doi.org/10.1103/PhysRevA.64.053813.

149. M. P. Woods, R. Groux, A. W. Chin, S. F. Huelga, and M. B. Plenio. "Mappings of open quantum systems onto chain representations and Markovian embeddings". *Journal of Mathematical Physics* 55:3, 2014. ISSN: 1089-7658. DOI: 10.1063/1.4866769. URL: http://dx.doi.org/10.1063/1.4866769.

150. I. de Vega and M.-C. Bañuls. "Thermofield-based chain-mapping approach for open quantum systems". *Physical Review A* 92:5, 2015. ISSN: 1094-1622. DOI: 10.1103/physreva.92.052116. URL: http://dx.doi.org/10.1103/PhysRevA.92.052116.

151. E. H. Lieb and D. W. Robinson. "The finite group velocity of quantum spin systems". *Communications in Mathematical Physics* 28:3, 1972, pp. 251–257. ISSN: 1432-0916. DOI: 10.1007/bf01645779. URL: http://dx.doi.org/10.1007/BF01645779.

152. M. P. Woods, M. Cramer, and M. B. Plenio. "Simulating Bosonic Baths with Error Bars". *Physical Review Letters* 115:13, 2015. ISSN: 1079-7114. DOI: 10.1103/physrevlett.115.130401. URL: http://dx.doi.org/10.1103/PhysRevLett.115.130401.

153. D. Tamascelli, A. Smirne, J. Lim, S. F. Huelga, and M. B. Plenio. "Efficient Simulation of Finite-Temperature Open Quantum Systems". *Physical Review Letters* 123:9, 2019. ISSN: 1079-7114. DOI: 10.1103/physrevlett.123.090402. URL: http://dx.doi.org/10.1103/PhysRevLett.123.090402.

154. M. Esposito, M. A. Ochoa, and M. Galperin. "Quantum Thermodynamics: A Nonequilibrium Green's Function Approach". *Physical Review Letters* 114:8, 2015. DOI: 10.1103/physrevlett.114.080602. URL: https://doi.org/10.1103%2Fphysrevlett.114.080602.

155. M. Esposito, M. A. Ochoa, and M. Galperin. "Nature of heat in strongly coupled open quantum systems". *Phys. Rev. B* 92, 23 2015, p. 235440. DOI: 10.1103/PhysRevB.92.235440. URL: https://link.aps.org/doi/10.1103/PhysRevB.92.235440.

156. M. F. Ludovico, M. Moskalets, D. Sánchez, and L. Arrachea. "Dynamics of energy transport and entropy production in ac-driven quantum electron systems". *Physical Review B* 94:3, 2016. DOI: 10.1103/physrevb.94.035436. URL: https://doi.org/10.1103%2Fphysrevb.94.035436.

157. M. F. Ludovico, L. Arrachea, M. Moskalets, and D. Sánchez. "Periodic Energy Transport and Entropy Production in Quantum Electronics". *Entropy 2016, Vol. 18, Page 419* 18:11, 2016, p. 419. ISSN: 1099-4300. DOI: 10.3390/E18110419. eprint: 1610.05143. URL: https://www.mdpi.com/1099-4300/18/11/419/htm%20https://www.mdpi.com/1099-4300/18/11/419.

158. A. Bruch, M. Thomas, S. Viola Kusminskiy, F. von Oppen, and A. Nitzan. "Quantum thermodynamics of the driven resonant level model". *Phys. Rev. B* 93, 11 2016, p. 115318. DOI: 10.1103/PhysRevB.93.115318. URL: https://link.aps.org/doi/10.1103/PhysRevB.93.115318.

159. P. Haughian, M. Esposito, and T. L. Schmidt. "Quantum thermodynamics of the resonant-level model with driven system-bath coupling". *Physical Review B* 97:8, 2018. DOI: 10.1103/physrevb.97.085435. URL: https://doi.org/10.1103%2Fphysrevb.97.085435.

160. A. Riera-Campeny, M. Mehboudi, M. Pons, and A. Sanpera. "Dynamically induced heat rectification in quantum systems". *Phys. Rev. E* 99, 3 2019, p. 032126. DOI: 10.1103/PhysRevE.99.032126. URL: https://link.aps.org/doi/10.1103/PhysRevE.99.032126.

161. S. Kohler, S. Camalet, M. Strass, J. Lehmann, G.-L. Ingold, and P. Hänggi. "Charge transport through a molecule driven by a high-frequency field". *Chemical Physics* 296:2-3, 2004, pp. 243–249. DOI: 10.1016/j.chemphys.2003.09.023. URL: https://doi.org/10.1016%2Fj.chemphys.2003.09.023.

162. L. Chen, T. Hansen, and I. Franco. "Simple and Accurate Method for Time-Dependent Transport along Nanoscale Junctions". *The Journal of Physical Chemistry C* 118:34, 2014, pp. 20009–20017. DOI: 10.1021/jp505771f. URL: https://doi.org/10.1021%2Fjp505771f.

163. N. Li, J. Ren, L. Wang, G. Zhang, P. Hänggi, and B. Li. "Colloquium: Phononics: Manipulating heat flow with electronic analogs and beyond". *Reviews of Modern Physics* 84:3, 2012, pp. 1045–1066. DOI: 10.1103/revmodphys.84.1045. URL: https://doi.org/10.1103%2Frevmodphys.84.1045.

164. A. A. Dzhioev and D. S. Kosov. "Super-fermion representation of quantum kinetic equations for the electron transport problem". *The Journal of Chemical Physics* 134:4, 2011, p. 044121. DOI: 10.1063/1.3548065. URL: https://doi.org/10.1063%2F1.3548065.

165. B. Buča and T. Prosen. "A Note on Symmetry Reductions of the Lindblad Equation: Transport in Constrained Open Spin Chains". *New Journal of Physics* 14:7, 2012, p. 073007. ISSN: 1367-2630. DOI: 10.1088/1367-2630/14/7/073007.

166. M. Esposito, K. Lindenberg, and C. V. den Broeck. "Entropy production as correlation between system and reservoir". *New Journal of Physics* 12:1, 2010, p. 013013. DOI: 10.1088/1367-2630/12/1/013013. URL: https://doi.org/10.1088%2F1367-2630%2F12%2F1%2F013013.

167. D. Reeb and M. M. Wolf. "An improved Landauer principle with finite-size corrections". *New Journal of Physics* 16:10, 2014, p. 103011. DOI: 10.1088/1367-2630/16/10/103011. URL: https://doi.org/10.1088/1367-2630/16/10/103011.

168. G. T. Landi and M. Paternostro. "Irreversible entropy production: From classical to quantum". *Rev. Mod. Phys.* 93, 3 2021, p. 035008. DOI: 10.1103/RevModPhys.93.035008. URL: https://link.aps.org/doi/10.1103/RevModPhys.93.035008.

169. P. Strasberg and A. Winter. "First and Second Law of Quantum Thermodynamics: A Consistent Derivation Based on a Microscopic Definition of Entropy". *PRX Quantum* 2:3, 2021, p. 030202. DOI: 10.1103/PRXQuantum.2.030202. URL: https://doi.org/10.1103/PRXQuantum.2.030202.

170. M. J. Donald. "Free energy and the relative entropy". *Journal of Statistical Physics* 49:1-2, 1987, pp. 81–87. DOI: 10.1007/bf01009955. URL: https://doi.org/10.1007%5C%2Fbf01009955.

171. M. Esposito. "Stochastic thermodynamics under coarse graining". *Phys. Rev. E* 85, 4 2012, p. 041125. DOI: 10.1103/PhysRevE.85.041125. URL: https://link.aps.org/doi/10.1103/PhysRevE.85.041125.

172. H. Spohn and J. L. Lebowitz. *Irreversible Thermodynamics for Quantum Systems Weakly Coupled to Thermal Reservoirs*. 1978. DOI: 10.1002/9780470142578.ch2. URL: http://dx.doi.org/10.1002/9780470142578.ch2.

173. T. M. Cover and J. A. Thomas. *Elements of Information Theory*. 2nd. Wiley-Interscience, Hoboken, NJ, 2006. ISBN: 978-0-471-24195-9.

174. G. Casella and R. Berger. *Statistical Inference*. Chapman and Hall/CRC, 2024. ISBN: 9781003456285. DOI: 10.1201/9781003456285. URL: http://dx.doi.org/10.1201/9781003456285.

175. C. W. Helstrom. *Quantum Detection and Estimation Theory*. Vol. 123. Mathematics in Science and Engineering. Academic Press, 1976. ISBN: 9780123400505.

176. M. G. A. Paris. "Quantum Estimation for Quantum Technology". *International Journal of Quantum Information* 7:supp01, 2009, pp. 125–137. DOI: 10.1142/S0219749909004839.

177. P. Salamon and R. S. Berry. "Thermodynamic length and dissipated availability". *Physical Review Letters* 51:13, 1983, pp. 1127–1130. DOI: 10.1103/PhysRevLett.51.1127.

178. D. Petz. "Monotone Metrics on Matrix Spaces". *Linear Algebra and its Applications* 244, 1996, pp. 81–96. DOI: 10.1016/0024-3795(94)00211-8.

179. F. Weinhold. "Metric geometry of equilibrium thermodynamics". *The Journal of Chemical Physics* 63:6, 1975, pp. 2479–2483. DOI: 10.1063/1.431689.

180. G. Ruppeiner. "Thermodynamics: A Riemannian geometric model". *Physical Review A* 20:4, 1979, pp. 1608–1613. DOI: 10.1103/PhysRevA.20.1608.

181. S.-i. Amari and H. Nagaoka. *Methods of Information Geometry*. Vol. 191. Translations of Mathematical Monographs. American Mathematical Society and Oxford University Press, Providence, RI, 2000. ISBN: 978-0-8218-0531-2.

182. D. Petz. *Quantum Information Theory and Quantum Statistics*. Theoretical and Mathematical Physics. Springer Berlin Heidelberg, Berlin, 2008. ISBN: 9783540746348. DOI: 10.1007/978-3-540-74636-2. URL: http://dx.doi.org/10.1007/978-3-540-74636-2.

183. R. Kubo. "Statistical-Mechanical Theory of Irreversible Processes. I. General Theory and Simple Applications to Magnetic and Conduction Problems". *Journal of the Physical Society of Japan* 12:6, 1957, pp. 570–586. DOI: 10.1143/JPSJ.12.570.

184. H. Mori. "Transport, Collective Motion, and Brownian Motion". *Progress of Theoretical Physics* 33:3, 1965, pp. 423–455. DOI: 10.1143/PTP.33.423.

185. F. Hiai and D. Petz. *Introduction to Matrix Analysis and Applications*. Universitext. Springer, 2014. ISBN: 978-3-319-04041-7. DOI: 10.1007/978-3-319-04042-4.

186. G. Ruppeiner. "Riemannian geometry in thermodynamic fluctuation theory". *Reviews of Modern Physics* 67:3, 1995, pp. 605–659. DOI: 10.1103/RevModPhys.67.605.

187. J. E. Aman, I. Bengtsson, and N. Pidokrajt. "Geometry of black hole thermodynamics". *General Relativity and Gravitation* 35, 2003, pp. 1733–1743. DOI: 10.1023/A:1026058111582.

188. H. Quevedo. "Geometrothermodynamics". *Journal of Mathematical Physics* 48:1, 2007, p. 013506. DOI: 10.1063/1.2409524.

189. G. Ruppeiner. "Thermodynamic curvature and phase transitions in Kerr–Newman black holes". *Physical Review D* 78:2, 2008, p. 024016. DOI: 10.1103/PhysRevD.78.024016.

190. F. Schlögl. "Thermodynamic metric and stochastic measures". en. *Z. Physik B - Condensed Matter* 59:4, 1985, pp. 449–454.

191. M. Esposito and C. Van den Broeck. "The three faces of the second law. I. Master equation formulation". *Physical Review E* 82:1, 2010, p. 011143. DOI: 10.1103/PhysRevE.82.011143.

192. H. J. Carmichael. *An Open Systems Approach to Quantum Optics*. Vol. m18. Lecture Notes in Physics. Springer, 1993. ISBN: 9783540561392.

193. H. M. Wiseman and G. J. Milburn. *Quantum Measurement and Control*. Cambridge University Press, 2010. ISBN: 9780521804424.

194. F. Fagnola and V. Umanità. "Generators of Detailed Balance Quantum Markov Semigroups". *Infinite Dimensional Analysis, Quantum Probability and Related Topics* 10:3, 2007, pp. 335–363. DOI: 10.1142/S0219025707002762. arXiv: arXiv:0707.2147 [math-ph].

195. J. Schnakenberg. "Network theory of microscopic and macroscopic behavior of master equation systems". *Reviews of Modern Physics* 48:4, 1976, pp. 571–585. DOI: 10.1103/RevModPhys.48.571.

196. S. Deffner and E. Lutz. "Nonequilibrium entropy production for open quantum systems". *Physical Review Letters* 107:14, 2011, p. 140404.

197. J. P. Santos, L. C. Céleri, and G. T. Landi. "Role of quantum coherence in the thermodynamics of energy transfer". *npj Quantum Information* 5:1, 2019, p. 23.

198. T. V. Vu and K. Saito. "Thermodynamic Unification of Optimal Transport: Thermodynamic Uncertainty Relation, Minimum Dissipation, and Thermodynamic Speed Limits". *Phys. Rev. X* 13:1, 2023, p. 011013. DOI: 10.1103/PhysRevX.13.011013. URL: https://link.aps.org/doi/10.1103/PhysRevX.13.011013.

199. L. P. Bettmann and J. Goold. "Information Geometry Approach to Quantum Stochastic Thermodynamics". *Physical Review E* 111:1, 2025, p. 014133. DOI: 10.1103/PhysRevE.111.014133. URL: https://doi.org/10.1103/PhysRevE.111.014133.

200. D. Manzano. "A short introduction to the Lindblad master equation". *AIP Advances* 10:2, 2020, p. 025106.

201. J. P. Garrahan and I. Lesanovsky. "Therodynamics of quantum jump trajectories". *Physical Review Letters* 104:16, 2010, p. 160601.

202. F. Carollo, A. Di Biagio, S. F. Huelga, and M. B. Plenio. "Trajectory-based versus ensemble definitions of entropy production in quantum systems". *Physical Review Research* 2:2, 2020, p. 023011.

203. G. Manzano, J. M. Horowitz, and J. M. R. Parrondo. "Nonequilibrium potential and fluctuation theorems for quantum maps". *Physical Review E* 92:3, 2015. ISSN: 1550-2376. DOI: 10.1103/physreve.92.032129. URL: http://dx.doi.org/10.1103/PhysRevE.92.032129.

204. G. Manzano and R. Zambrini. "Quantum thermodynamics under continuous monitoring: A general framework". *AVS Quantum Science* 4:2, 2022. ISSN: 2639-0213. DOI: 10.1116/5.0079886. URL: http://dx.doi.org/10.1116/5.0079886.

205. J. Dalibard, Y. Castin, and K. Mølmer. "Wave-function approach to dissipative processes in quantum optics". *Physical Review Letters* 68:5, 1992, pp. 580–583. DOI: 10.1103/PhysRevLett.68.580.

206. G. E. Crooks. "Quantum operation time reversal". *Physical Review A* 77:3, 2008, p. 034101. DOI: 10.1103/PhysRevA.77.034101.

207. J. M. Horowitz and J. M. R. Parrondo. "Entropy production along nonequilibrium quantum jump trajectories". *New Journal of Physics* 15:8, 2013, p. 085028. DOI: 10.1088/1367-2630/15/8/085028. URL: https://dx.doi.org/10.1088/1367-2630/15/8/085028.

208. B. C. Hall. *Lie Groups, Lie Algebras, and Representations: An Elementary Introduction*. 2nd. Springer, 2015.

209. D. J. Evans and G. P. Morriss. *Statistical Mechanics of Nonequilibrium Liquids*. 2nd. Cambridge University Press, Cambridge, UK, 2008. ISBN: 9780521857918. DOI: 10.1017/CBO9780511535307. URL: https://doi.org/10.1017/CBO9780511535307.

210. P. Gaspard. *The Statistical Mechanics of Irreversible Phenomena*. Cambridge University Press, Cambridge, UK, 2022. ISBN: 9781108473729. DOI: 10.1017/9781108563055. URL: https://doi.org/10.1017/9781108563055.

211. G. Benenti, G. Casati, K. Saito, and R. S. Whitney. "Fundamental aspects of steady-state conversion of heat to work at the nanoscale". *Physics Reports* 694, 2017, pp. 1–124. DOI: 10.1016/j.physrep.2017.05.008. URL: https://doi.org/10.1016/j.physrep.2017.05.008.

212. A. I. Brown and D. A. Sivak. "Theory of Nonequilibrium Free Energy Transduction by Molecular Machines". *Chemical Reviews* 120:1, 2020, pp. 434–459. ISSN: 0009-2665. DOI: 10.1021/acs.chemrev.9b00254. URL: https://doi.org/10.1021/acs.chemrev.9b00254.

213. J. P. Pekola. "Towards quantum thermodynamics in electronic circuits". *Nature Physics* 11, 2015, pp. 118–123. DOI: 10.1038/nphys3169. URL: https://doi.org/10.1038/nphys3169.

214. M. T. Mitchison. "Quantum thermal absorption machines: refrigerators, engines and clocks". *Contemporary Physics* 60:2, 2019, pp. 164–187. DOI: 10.1080/00107514.2019.1631555. URL: https://doi.org/10.1080/00107514.2019.1631555.

215. J. P. Pekola and B. Karimi. "Colloquium: Quantum heat transport in condensed matter systems". *Reviews of Modern Physics* 93:4, 2021, p. 041001. DOI: 10.1103/RevModPhys.93.041001. URL: https://doi.org/10.1103/RevModPhys.93.041001.

216. G. T. Landi, D. Poletti, and G. Schaller. "Nonequilibrium boundary-driven quantum systems: Models, methods, and properties". *Rev. Mod. Phys.* 94, 4 2022, p. 045006. DOI: 10.1103/RevModPhys.94.045006. URL: https://link.aps.org/doi/10.1103/RevModPhys.94.045006.

217. B. Bertini, F. Heidrich-Meisner, C. Karrasch, T. Prosen, R. Steinigeweg, and M. Žnidarič. "Finite-temperature transport in one-dimensional quantum lattice models". *Reviews of Modern Physics* 93:2, 2021, p. 025003. DOI: 10.1103/RevModPhys.93.025003. URL: https://doi.org/10.1103/RevModPhys.93.025003.

218. R. Fazio, J. Keeling, L. Mazza, and M. Schirò. "Many-Body Open Quantum Systems". *arXiv preprint arXiv:2409.10300*, 2024. URL: https://arxiv.org/abs/2409.10300.

219. Y. Oono and M. Paniconi. "Steady State Thermodynamics". *Progress of Theoretical Physics Supplement* 130, 1998, pp. 29–44. ISSN: 0375-9687. DOI: 10.1143/PTPS.130.29. eprint: https://academic.oup.com/ptps/article-pdf/doi/10.1143/PTPS.130.29/5213770/130-29.pdf. URL: https://doi.org/10.1143/PTPS.130.29.

220. T. Speck and U. Seifert. "Integral fluctuation theorem for the housekeeping heat". *Journal of Physics A: Mathematical and General* 38:34, 2005, p. L581. DOI: 10.1088/0305-4470/38/34/L03. URL: https://dx.doi.org/10.1088/0305-4470/38/34/L03.

221. H. Ge. "Extended forms of the second law for general time-dependent stochastic processes". *Phys. Rev. E* 80, 2 2009, p. 021137. DOI: 10.1103/PhysRevE.80.021137. URL: https://link.aps.org/doi/10.1103/PhysRevE.80.021137.

222. H. Ge and H. Qian. "Physical origins of entropy production, free energy dissipation, and their mathematical representations". *Phys. Rev. E* 81, 5 2010, p. 051133. DOI: 10.1103/PhysRevE.81.051133. URL: https://link.aps.org/doi/10.1103/PhysRevE.81.051133.

223. J. M. Horowitz and T. Sagawa. "Equivalent definitions of the quantum nonadiabatic entropy production". en. *J. Stat. Phys.* 156:1, 2014, pp. 55–65.

224. D. P. Pires, M. Cianciaruso, L. C. Céleri, G. Adesso, and D. O. Soares-Pinto. "Generalized Geometric Quantum Speed Limits". *Phys. Rev. X* 6, 2 2016, p. 021031. DOI: 10.1103/PhysRevX.6.021031. URL: https://link.aps.org/doi/10.1103/PhysRevX.6.021031.

225. S. B. Nicholson, A. del Campo, and J. R. Green. "Nonequilibrium uncertainty principle from information geometry". *Phys. Rev. E* 98, 3 2018, p. 032106. DOI: 10.1103/PhysRevE.98.032106. URL: https://link.aps.org/doi/10.1103/PhysRevE.98.032106.

226. S. Ito. "Stochastic Thermodynamic Interpretation of Information Geometry". *Phys. Rev. Lett.* 121, 3 2018, p. 030605. DOI: 10.1103/PhysRevLett.121.030605. URL: https://link.aps.org/doi/10.1103/PhysRevLett.121.030605.

227. S. B. Nicholson, L. P. García-Pintos, A. del Campo, and J. R. Green. "Time–information uncertainty relations in thermodynamics". *Nature Physics* 16, 2020, pp. 1211–1215. DOI: 10.1038/s41567-020-0981-y. URL: https://doi.org/10.1038/s41567-020-0981-y.

228. L. P. García-Pintos, S. B. Nicholson, J. R. Green, A. del Campo, and A. V. Gorshkov. "Unifying Quantum and Classical Speed Limits on Observables". *Phys. Rev. X* 12, 1 2022, p. 011038. DOI: 10.1103/PhysRevX.12.011038. URL: https://link.aps.org/doi/10.1103/PhysRevX.12.011038.

229. J. Bringewatt, Z. Steffen, M. A. Ritter, A. Ehrenberg, H. Wang, B. S. Palmer, A. J. Kollár, A. V. Gorshkov, and L. P. García-Pintos. *Generalized geometric speed limits for quantum observables*. 2024. arXiv: 2409.04544 [quant-ph]. URL: https://arxiv.org/abs/2409.04544.

230. L. P. Bettmann and J. Goold. "Information geometry approach to quantum stochastic thermodynamics". *Phys. Rev. E* 111, 1 2025, p. 014133. DOI: 10.1103/PhysRevE.111.014133. URL: https://link.aps.org/doi/10.1103/PhysRevE.111.014133.

231. L. M. Cangemi, C. Bhadra, and A. Levy. "Quantum engines and refrigerators". *Physics Reports* 1087, 2024. Quantum engines and refrigerators, pp. 1–71. ISSN: 0370-1573. DOI: https://doi.org/10.1016/j.physrep.2024.07.001. URL: https://www.sciencedirect.com/science/article/pii/S0370157324002710.

232. D. Petz and C. Ghinea. "Introduction to quantum Fisher information". In: *Quantum Probability and Related Topics*. 2011, pp. 261–281. DOI: 10.1142/9789814338745_0015. URL: http://arxiv.org/abs/1008.2417 (visited on 06/20/2024).

233. L. P. García-Pintos, S. B. Nicholson, J. R. Green, A. del Campo, and A. V. Gorshkov. "Unifying Quantum and Classical Speed Limits on Observables". *Phys. Rev. X* 12, 1 2022, p. 011038. DOI: 10.1103/PhysRevX.12.011038. URL: https://link.aps.org/doi/10.1103/PhysRevX.12.011038.

234. L. Mandelstam and I. Tamm. "The Uncertainty Relation Between Energy and Time in Non-relativistic Quantum Mechanics". In: *Selected Papers*. Ed. by B. M. Bolotovskii, V. Y. Frenkel, and R. Peierls. Springer Berlin Heidelberg, Berlin, Heidelberg, 1991, pp. 115–123. ISBN: 978-3-642-74626-0. DOI: 10.1007/978-3-642-74626-0_8. URL: https://doi.org/10.1007/978-3-642-74626-0_8.

235. F. Schwarz, I. Weymann, J. von Delft, and A. Weichselbaum. "Nonequilibrium Steady-State Transport in Quantum Impurity Models: A Thermofield and Quantum Quench Approach Using Matrix Product States". *Physical Review Letters* 121:13, 2018. ISSN: 1079-7114. DOI: 10.1103/physrevlett.121.137702. URL: http://dx.doi.org/10.1103/PhysRevLett.121.137702.

236. D. Ferracin, A. Smirne, S. F. Huelga, M. B. Plenio, and D. Tamascelli. "Spectral density modulation and universal Markovian closure of fermionic environments". *The Journal of Chemical Physics* 161:17, 2024. ISSN: 1089-7690. DOI: 10.1063/5.0226723. URL: http://dx.doi.org/10.1063/5.0226723.

237. A. Nüßeler, D. Tamascelli, A. Smirne, J. Lim, S. F. Huelga, and M. B. Plenio. "Fingerprint and Universal Markovian Closure of Structured Bosonic Environments". *Physical Review Letters* 129:14, 2022. ISSN: 1079-7114. DOI: 10.1103/physrevlett.129.140604. URL: http://dx.doi.org/10.1103/PhysRevLett.129.140604.

238. J. Dehaene and B. De Moor. "Clifford group, stabilizer states, and linear and quadratic operations over GF(2)". *Physical Review A* 68:4, 2003. ISSN: 1094-1622. DOI: 10.1103/physreva.68.042318. URL: http://dx.doi.org/10.1103/PhysRevA.68.042318.

239. G. C. Wick, A. S. Wightman, and E. P. Wigner. "The Intrinsic Parity of Elementary Particles". *Physical Review* 88:1, 1952, pp. 101–105. ISSN: 0031-899X. DOI: 10.1103/physrev.88.101. URL: http://dx.doi.org/10.1103/PhysRev.88.101.

240. U. Schollwöck. "The density-matrix renormalization group". *Reviews of Modern Physics* 77:1, 2005, pp. 259–315. ISSN: 1539-0756. DOI: 10.1103/revmodphys.77.259. URL: http://dx.doi.org/10.1103/RevModPhys.77.259.